TECHNISCHE
UNIVERSITÄT
DARMSTADT

Physik

In-Medium No-Core Shell Model for Ab Initio Nuclear Structure Calculations

Vom Fachbereich Physik
der Technischen Universität Darmstadt

zur Erlangung des Grades
eines Doktors der Naturwissenschaften
(Dr. rer. nat.)

genehmigte Dissertation von
Eskendr Gebrerufael, M.Sc.
aus Asmara (Eritrea)

Darmstadt 2017
D17

In-Medium No-Core Shell Model for Ab Initio Nuclear Structure Calculations
In-Medium Schalenmodel für ab initio Kernstruktur-Rechnungen

Referent:	Prof. Dr. Robert Roth
Korreferent:	Prof. Dr. Jens Braun

Tag der Einreichung:	18.07.2017
Tag der Prüfung:	23.10.2017

Bitte zitieren Sie dieses Dokument als:
URN: urn:nbn:de:tuda-tuprints-69100
URL: http://tuprints.ulb.tu-darmstadt.de/id/eprint/6910

Dieses Dokument wird bereitgestellt von tuprints,
E-Publishing-Service der TU Darmstadt
http://tuprints.ulb.tu-darmstadt.de
tuprints@ulb.tu-darmstadt.de

Abstract

In this work, we merge two successful *ab initio* nuclear-structure methods, the no-core shell model (NCSM) and the multi-reference in-medium similarity renormalization group (IM-SRG), to define a novel many-body approach for the comprehensive description of ground and excited states of closed- and open-shell medium-mass nuclei.

Building on the key advantages of the two methods—the decoupling of excitations at the many-body level in the IM-SRG, and the exact diagonalization in the NCSM applicable up to medium-light nuclei—their combination enables fully converged no-core calculations for an unprecedented range of nuclei and observables at moderate computational cost. The efficiency and rapid model-space convergence of the new approach make it ideally suited for *ab initio* studies of ground and low-lying excited states of nuclei up to the medium-mass regime.

Interactions constructed within the framework of chiral effective field theory provide an excellent opportunity to describe properties of nuclei from first principles, i.e., rooted in quantum chromodynamics, they overcome the lack of predictive power of phenomenological potentials. The hard core of these interactions causes strong short-range correlations, which we soften by using the similarity-renormalization-group transformation that accelerates the model-space convergence of many-body calculations. Three-nucleon effects, which are mandatory for the correct description of bulk properties of nuclei, are included in our calculations by using the normal-ordered two-body approximation, which has been shown to be sufficient to capture the main effects of the three-nucleon interaction.

Using these interactions, we analyze energies of ground and excited states in the carbon and oxygen isotopic chains, where conventional NCSM calculations are still feasible and provide an important benchmark. Furthermore, we study the Hoyle state in ^{12}C—a three-alpha cluster state that cannot be converged in standard NCSM calculations. Moreover, we explore island-of-inversion physics in magnesium isotopes, where the shell-model magic numbers vanish and new ones appear.

Due to our implementation of the IM-NCSM method, we are restricted to nuclei with even mass numbers. We propose and benchmark a simple and straightforward idea for the extension to odd nuclei within the framework of IM-NCSM using a particle-attached or particle-removed scheme.

Zusammenfassung

In dieser Arbeit kombinieren wir zwei in der Kernstrukturphysik erfolgreiche *ab initio* Vielteilchenmethoden, das No-Core Schalenmodell (NCSM) und die Multireferenz In-Medium Similarity Renormalization Group (IM-SRG) Transformation. Dies ermöglicht einen neuen Zugang zur umfassenden Beschreibung von Grund- und Anregungszuständen mittelschwerer Kerne mit offener und geschlossener Schale.

Ausgehend von den Hauptvorteilen beider Methoden – der Entkopplung der Anregungen auf Vielteilchenlevel in der IM-SRG und der exakten Diagonalisierung im NCSM für leichte bis mittelschwere Kerne – ermöglicht ihre Kombination vollständig konvergierte no-core Rechnungen für einen noch nie erreichten Bereich der Kerne und Observablen mit moderatem Rechenaufwand. Aufgrund ihrer Effizienz und rapiden Modelraumkonvergenz eignet sich die neue Methode ideal für *ab initio* Studien von Grundzuständen und tiefliegenden angeregten Zuständen von Kernen bis ins mittelschwere Regime.

Wechselwirkungen aus der chiralen effektiven Feldtheorie bieten eine hervorragende Möglichkeit, Eigenschaften von Kernen ausgehend von den Grundprinzipien der Physik verankert in der Quantenchromodynamik zu beschreiben und die mangelnde Vorhersagekraft von phänomenologischen Wechselwirkungen zu überwinden. Die starke, kurzreichweitige Abstoßung der Wechselwirkungen ruft starke, kurzreichweitige Korrelationen hervor, die wir mithilfe der Similarity-Renormalization-Group Transformation, die die Modelraumkonvergenz der Vielteilchenrechnungen beschleunigt, abmildern. Dreinukleonen-Effekte, die für die korrekte Beschreibung der Masseneigenschaften der Kerne zwingend erforderlich sind, werden in unseren Rechnungen mittels der normalgeordneten Zweiteilchenapproximation behandelt, die ausreichend ist, um die Hauptwirkung der Dreiteilchenbeiträge zu erfassen.

Mit diesen Wechselwirkungen analysieren wir Grund- und Anregungsenergien in Kohlenstoff- und Sauerstoffketten, in denen traditionelle NCSM Rechnungen noch machbar sind und einen wichtigen Richtwert zum Vergleich bieten. Weiterhin studieren wir den Hoyle-Zustand in ^{12}C, einen Clusterzustand aus drei Alphateilchen, der in traditionellen NCSM Rechnungen nicht konvergiert werden kann. Weiterhin untersuchen wir die Physik der sogenannten „Island of Inversion“ in Magnesiumisotopen, bei denen die magischen Zahlen aus dem Schalenmodell verschwinden und Neue entstehen.

Aufgrund unserer Implementation der IM-NCSM Methode sind wir auf Kerne mit gerader Massenzahl beschränkt. Wir schlagen eine einfache Idee für die Erweiterung auf ungerade Kerne mittels des „particle-attached particle-removed“ Schemas vor und analysieren diese.

Contents

Introduction 1

I. Basics

Introduction to Part I 5

1. Similarity Renormalization Group 7

2. Hartree-Fock Method 11

3. Normal Ordering and Wick's Theorem 15

3.1. Vacuum Case . . . 16
3.2. Single-Reference Case . . . 18
3.3. Multi-Reference Case . . . 21
3.3.1. Problem and Guiding Principle . . . 21
3.3.2. Wick's Theorem . . . 22
3.3.3. Vacuum and Reference-State Representation . . . 26
3.3.4. Multi-Reference Two-Body Approximation for Three-Body Operators 28
3.3.5. Generalized Wick's Theorem . . . 28
3.3.6. Relevant Commutators . . . 30

II. In-Medium No-Core Shell Model

Introduction to Part II 35

4. Multi-Reference In-Medium Similarity Renormalization Group 37

4.1. Basic Concepts . . . 38
4.2. m-Scheme Flow Equations . . . 41
4.2.1. Commutator of the Generator and Hamiltonian . . . 41
4.2.2. Flow Equations . . . 43
4.2.3. Flow Equations in Natural Orbitals . . . 45
4.3. J-Coupled Flow Equations in Natural Orbitals . . . 47
4.3.1. Angular-Momentum-Coupling Coefficients and Pandya Transformation 47

4.3.2. Performing J-Coupling . . . 50
4.3.3. Summary of the J-Coupled Flow Equations in Natural Orbitals . . . 55
4.4. Implementation of the J-Coupled Flow Equations . . . 56
4.4.1. Bases, Matrix Products and Traces . . . 56
4.4.2. BLAS Compliant J-Coupled Flow Equations . . . 58
4.4.3. Summary of BLAS Compliant Flow Equations . . . 64
4.5. Generalized A-Particle A-Hole Basis . . . 67
4.5.1. General Considerations . . . 67
4.5.2. Generalized One-Particle One-Hole States . . . 73
4.5.3. Generalized Two-Particle Two-Hole States . . . 74
4.5.4. Algorithm and Two-Body System As Case Study . . . 77
4.6. Generators . . . 81
4.6.1. Basic Idea . . . 81
4.6.2. Wegner Generator . . . 84
4.6.3. White and Imaginary-Time Generator . . . 84
4.6.4. Brillouin Generator . . . 86
4.6.5. Decay Scales . . . 88
4.7. Observables . . . 91
4.7.1. General Idea . . . 91
4.7.2. Radii . . . 92
4.7.3. Electromagnetic Monopole Transition . . . 94

5. No-Core Shell Model and Importance Truncation 99
5.1. No-Core Shell Model . . . 99
5.2. Importance Truncation . . . 103

6. Merging In-Medium Similarity Renormalization Group and No-Core Shell Model 105
6.1. Motivation . . . 105
6.2. In-Medium No-Core Shell Model . . . 106
6.3. Decoupling of the Hamiltonian Matrix in Many-Body Basis . . . 108

III. Results

Introduction to Part III 117

7. Ground-State Energy 119
7.1. Parameter Dependences . . . 120
7.1.1. Model-Space Convergence . . . 120
7.1.2. Oscillator Frequency . . . 126
7.1.3. Impact of the Generators . . . 128
7.1.4. Reference-Space Size . . . 135
7.2. Carbon and Oxygen Isotopes . . . 136

7.3. Magnesium and Sodium Isotopes . . . 138

8. Excitation Spectra **141**
8.1. Carbon and Oxygen Isotopes . . . 141
8.2. Analysis of the Hoyle State in ^{12}C . . . 145
8.3. Island of Inversion: Magnesium and Sodium Isotopes . . . 152

9. Radii and Electric Monopole Transitions for the Hoyle State in ^{12}C **159**

10. Particle-Attached Particle-Removed Extension of IM-NCSM **163**

IV. Summary and Outlook

V. Appendices

A. Normal Ordering—Derivations **179**
A.1. Products of Normal-Ordered Operators . . . 179
A.2. Commutators of Normal-Ordered Operators . . . 183
A.2.1. Without Contraction . . . 183
A.2.2. Partially Contracted . . . 185
A.2.3. Fully Contracted . . . 189
A.3. Expectation Values . . . 202
A.3.1. Expectation Values of Products—Partially Contracted . . . 202
A.3.2. Expectation Values of Commutators—Partially Contracted . . . 202
A.3.3. Expectation Values of Commutators—Fully Contracted . . . 203

B. Multi-Reference In-Medium SRG—Derivations **205**
B.1. J-Coupling of the Flow Equations in Natural Orbitals . . . 205
B.1.1. J-Coupling of the Two-Body Terms . . . 205
B.1.2. J-Coupling of the One-Body Terms . . . 208
B.1.3. J-Coupling of the Zero-Body Terms . . . 214
B.2. Properties of n-Particle n-Hole Excitations . . . 216
B.3. Epstein-Nesbet Energy Differences . . . 221

C. Spherical-Tensor Decomposition **225**
C.1. Spherical Tensor Operators . . . 225
C.2. Wigner-Eckart Theorem . . . 227
C.3. Spherical Density Operators . . . 227

Glossary **233**

List of Figures **236**

Bibliography 245

List of Publications and Conferences 247

Introduction

The goal of physics, in general, is the understanding of nature. In particular, theoretical nuclear structure physicists aim at a consistent theoretical description of the atomic nucleus in the low-energy regime based on the fundamental laws of nature.

The nucleus is a compound of protons and neutrons, both called nucleons. As a first approximation, we describe the nucleus as a complex non-relativistic many-body quantum system made of point-like fermionic nucleons. The complexity of this system is rooted, amongst others, in the fact that the nucleons can interact with each other via the nuclear force that is deduced from the three fundamental forces of the standard model of physics [PS95; Ram99]. Furthermore, the nucleons themselves are not point-like particles as we treat them, but they are composed of quarks confined in colorless baryons. However, the quarks carry not only color charge, but also electric charge, and they can convert into each other. Furthermore, they can interact with each other via the electromagnetic and weak force, unified in the electroweak theory [Gla61; Wei67], as well as the strong force formulated in quantum chromodynamics (QCD) [PS95]. Consequently, the nuclear force among the nucleons is the residual force the nucleons in the nucleus feel derived from these fundamental forces.

Tackling the quantum system built of nucleons poses two key challenges: It is neither clear how to construct a nuclear interaction based on the fundamental theories nor how to solve the nuclear many-body problem associated with the Schrödinger equation.

Concerning the first point, there are different philosophies since the construction of a nuclear interaction is not unique. They can be roughly classified into phenomenological and QCD-motivated realistic interactions. It is desirable to derive the nuclear interaction from QCD, which contains quarks and gluons, where the latter mediates the strong force, as fundamental degrees of freedom. Unfortunately, QCD exhibits a non-perturbative character in the low-energy regime relevant for nuclear physics. Therefore, an effective description of the nucleus is used, where nucleons and pions, instead of quarks and gluons, are the effective degrees of freedom. The coupling between nucleons and pions is described consistently with respect to the symmetries of QCD in the framework of chiral effective field theory [ME11; EHM09].

Once an interaction is given, it is still extremely difficult to solve the Schrödinger equation. One of the most active areas in nuclear structure theory nowadays is the development of *ab initio* many-body methods for the comprehensive description of nuclei. The term *ab initio* ensures that the many-body technique is completely converged with respect to all truncations

that have to be introduced in order to make the Schrödinger equation numerically tractable. A special focus is put on the ground states, low-lying excitations and spectroscopic observables. Traditionally, nuclear spectroscopy is the domain of shell-model-type approaches, both the valence-space shell model [Cau+05] and the *ab initio* no-core shell model (NCSM) [Nav+07; Bro01; BNV13]. These methods solve a large-scale eigenvalue problem of the Hamiltonian in a truncated model space and address ground and excited states on equal footing, but they are limited by the basis dimension [Var+09]. Because of that, these methods are typically limited to nuclei in the p-shell.

Several other methods have been developed that tackle the many-body problem from a different angle, among them the coupled-cluster (CC) approach [Bin+14; Bin+13; Coe58; Wło+05; Hag+08; Hag+07] and the in-medium similarity renormalization group (IM-SRG) [TBS11; TBS12; Her+16; Her17]. Instead of solving the eigenvalue problem directly, these methods use a similarity transformation of the Hamiltonian to decouple a given reference state, representing the ground state, from all particle-hole excitations. This concept of decoupling is very powerful and complementary to a direct NCSM-type diagonalization. Generally, CC and IM-SRG have different computational characteristics and a much better scaling with particle number, but their basic formulation is limited to ground states. The complementarity with NCSM suggests that a combination of both philosophies, direct diagonalization and many-body decoupling, could be advantageous. First steps along these lines are the effective interactions for the valence-space shell model extracted from CC and IM-SRG calculations presented recently [Bog+14; Str+16; Jan+14; Str+17; Jan+16].

In contrast to valence-space methods, we propose an *ab initio* no-core approach, where convergence with respect to all model-space truncations is demonstrated explicitly. For the calculations presented here, we use a chiral nucleon-nucleon (NN) plus three-nucleon (3N) Hamiltonian softened via the free-space similarity-renormalization-group (SRG) transformation to accelerate model-space convergence. Since the complete inclusion of 3N interactions in the many-body method is associated with significantly increased computational cost, we rely on the multi-reference normal-ordered two-body approximation which has been justified to be sufficient to capture the main effects of the 3N interaction [GCR16].

This work is organized as follows: In part I, we summarize the basics of the (free-space) SRG transformation, the Hartree-Fock method and the concept of normal ordering. In particular, the normal-ordering technique is crucial for the formulation of the multi-reference IM-SRG. In part II, we extensively discuss the framework of the multi-reference IM-SRG and briefly introduce the NCSM. Subsequently, we describe why and how we merge them into a consistent *ab initio* many-body tool that we call in-medium no-core shell model (IM-NCSM). In part III, we present results of IM-NCSM calculations for ground and excited states of open-shell nuclei and benchmark them against large-scale NCSM calculations. We propose a simple and straightforward extension of the IM-NCSM using a particle-attached or particle-removed formalism to tackle odd nuclei. To test how well this extension works, we present results for selected nitrogen isotopes. In part IV, we provide a brief summary and outlook on remaining challenges for forthcoming investigations.

I.

Basics

Introduction to Part I

In this part, we present the basic tools necessary to formulate the in-medium no-core shell model that will be introduced in the next part.

In chapter 1, we start with the basic concepts of the (free-space) similarity-renormalization-group (SRG) method which is a powerful technique to soften an interaction, i.e., to pre-diagonalize its matrix representation. Furthermore, we derive the so-called operator flow equation, which is an essential ingredient for the in-medium similarity-renormalization-group (IM-SRG) transformation.

In chapter 2, we recap the Hartree-Fock (HF) method which is a simple approximate many-body method. It provides a simple and efficient way to optimize a single-particle basis, which can be used as a starting point for a more sophisticated many-body methods like IM-SRG or no-core shell model.

Finally, in chapter 3, we discuss the concept of normal ordering and Wick's theorem, which are crucial to include three-body interactions in an approximate way. Since, in particular, the whole IM-SRG framework is formulated in terms of normal-ordered operators, we illustrate the generalized Wick's theorem which is a mandatory technique for calculating products of normal-ordered operators. The concept of normal ordering is always based on a given A-body state that we call the reference state. We discuss three different classes of reference states: the physical vacuum $|0\rangle$, a single Slater determinant $|\Phi\rangle$, or a linear combination of Slater determinants $|\Psi\rangle$, respectively. The latter one is the most significant case for this work.

Chapter 1

Similarity Renormalization Group

The similarity-renormalization-group (SRG) transformation is a well established method to soften an interaction, i.e., to pre-diagonalize its matrix representation. The basic idea is to apply a unitary transformation to the initial Hamiltonian such that its matrix representation changes into band- or block-diagonal form in a specific basis, or in other words, to suppress matrix elements between high- and low-lying basis states. As a consequence, the convergence behavior of many-body calculations, such as the no-core shell model, is improved. Since a unitary transformation does not change the eigenvalues of an operator, the solution of the many-body problem using a unitarily transformed Hamiltonian is identical to the solution the eigenvalue problem of the initial Hamiltonian.

Let $\boldsymbol{U}_\alpha$ be a unitary operator depending continuously on the SRG flow parameter α. Hence, the SRG transformation on the initial Hamiltonian $\boldsymbol{H}$ is given by

$$\boldsymbol{H}_\alpha \coloneqq \boldsymbol{U}_\alpha^\dagger \boldsymbol{H} \boldsymbol{U}_\alpha, \tag{1.1}$$

where $\boldsymbol{H}_\alpha$ is called the SRG-transformed or SRG-evolved Hamiltonian. Taking the total derivative of that expression with respect to SRG flow parameter α yields

$$\frac{\mathrm{d}\boldsymbol{H}_\alpha}{\mathrm{d}\alpha} = \frac{\mathrm{d}\boldsymbol{U}_\alpha^\dagger}{\mathrm{d}\alpha} \boldsymbol{H} \boldsymbol{U}_\alpha + \boldsymbol{U}_\alpha^\dagger \boldsymbol{H} \frac{\mathrm{d}\boldsymbol{U}_\alpha}{\mathrm{d}\alpha}. \tag{1.2}$$

Since the transformation operator $\boldsymbol{U}_\alpha$ is unitary, i.e., $\boldsymbol{U}_\alpha \boldsymbol{U}_\alpha^\dagger = \mathbb{1}$, we obtain by differentiating this expression with respect to α

$$\frac{\mathrm{d}\boldsymbol{U}_\alpha^\dagger}{\mathrm{d}\alpha} = -\boldsymbol{U}_\alpha^\dagger \frac{\mathrm{d}\boldsymbol{U}_\alpha}{\mathrm{d}\alpha} \boldsymbol{U}_\alpha^\dagger. \tag{1.3}$$

With the aid of this relation and the unitarity of $\boldsymbol{U}_\alpha$, we can rewrite (1.2) in the following form

$$\frac{\mathrm{d}\boldsymbol{H}_\alpha}{\mathrm{d}\alpha} = -\boldsymbol{U}_\alpha^\dagger \frac{\mathrm{d}\boldsymbol{U}_\alpha}{\mathrm{d}\alpha} \boldsymbol{U}_\alpha^\dagger \boldsymbol{H} \boldsymbol{U}_\alpha + \boldsymbol{U}_\alpha^\dagger \boldsymbol{H} \boldsymbol{U}_\alpha \boldsymbol{U}_\alpha^\dagger \frac{\mathrm{d}\boldsymbol{U}_\alpha}{\mathrm{d}\alpha} \tag{1.4}$$

$$= -\boldsymbol{U}_\alpha^\dagger \frac{\mathrm{d}\boldsymbol{U}_\alpha}{\mathrm{d}\alpha} \boldsymbol{H}_\alpha + \boldsymbol{H}_\alpha \boldsymbol{U}_\alpha^\dagger \frac{\mathrm{d}\boldsymbol{U}_\alpha}{\mathrm{d}\alpha} \tag{1.5}$$

$$= \Big(-\boldsymbol{U}_\alpha^\dagger \frac{\mathrm{d}\boldsymbol{U}_\alpha}{\mathrm{d}\alpha} \Big) \boldsymbol{H}_\alpha - \boldsymbol{H}_\alpha \Big(-\boldsymbol{U}_\alpha^\dagger \frac{\mathrm{d}\boldsymbol{U}_\alpha}{\mathrm{d}\alpha} \Big) \tag{1.6}$$

$$= [-\boldsymbol{U}_\alpha^\dagger \frac{\mathrm{d}\boldsymbol{U}_\alpha}{\mathrm{d}\alpha}, \boldsymbol{H}_\alpha]. \tag{1.7}$$

In the last step, we introduced the commutator of two operators that is defined by $[\boldsymbol{A}, \boldsymbol{B}] \coloneqq \boldsymbol{A}\boldsymbol{B} - \boldsymbol{B}\boldsymbol{A}$ for arbitrary operators $\boldsymbol{A}$ and $\boldsymbol{B}$. The generator of the transformation is defined as

$$\boldsymbol{\eta}_\alpha \coloneqq -\boldsymbol{U}_\alpha^\dagger \frac{\mathrm{d}\boldsymbol{U}_\alpha}{\mathrm{d}\alpha}. \tag{1.8}$$

Hence, we have to solve an initial-value problem with the initial condition $\boldsymbol{H}_{\alpha=0} = \boldsymbol{H}$ in order to find the SRG-evolved Hamiltonian $\boldsymbol{H}_\alpha$. Using this definition, the *operator flow equation* for the SRG-evolved Hamiltonian $\boldsymbol{H}_\alpha$ is given by

$$\frac{\mathrm{d}\boldsymbol{H}_\alpha}{\mathrm{d}\alpha} = [\boldsymbol{\eta}_\alpha, \boldsymbol{H}_\alpha]. \tag{1.9}$$

The generator of the transformation $\boldsymbol{\eta}_\alpha$ is anti-Hermitian, i.e., $\boldsymbol{\eta}_\alpha^\dagger = -\boldsymbol{\eta}_\alpha$, which can be shown as follows

$$\boldsymbol{\eta}_\alpha + \boldsymbol{\eta}_\alpha^\dagger = -\boldsymbol{U}_\alpha^\dagger \frac{\mathrm{d}\boldsymbol{U}_\alpha}{\mathrm{d}\alpha} - \frac{\mathrm{d}\boldsymbol{U}_\alpha^\dagger}{\mathrm{d}\alpha} \boldsymbol{U}_\alpha = -\frac{\mathrm{d}(\boldsymbol{U}_\alpha^\dagger \boldsymbol{U}_\alpha)}{\mathrm{d}\alpha} = -\frac{\mathrm{d}\mathbb{1}}{\mathrm{d}\alpha} = 0. \tag{1.10}$$

There are many possibilities for the choice of the generator $\boldsymbol{\eta}_\alpha$, for instance the Wegner generator [Weg94]. Typically, the generator is chosen as a commutator of a Hermitian operator and the SRG-evolved Hamiltonian $\boldsymbol{H}_\alpha$, since this ensures anti-Hermiticity of the generator. In this work, the generator of the SRG transformation is chosen as the commutator of the intrinsic kinetic energy $\boldsymbol{T}_{\mathrm{int}}$ and the SRG-evolved Hamiltonian $\boldsymbol{H}_\alpha$ [BFP07], i.e.,

$$\boldsymbol{\eta}_\alpha \coloneqq m_N^2 [\boldsymbol{T}_{\mathrm{int}}, \boldsymbol{H}_\alpha], \tag{1.11}$$

where m_N is the nucleon mass, and the intrinsic kinetic energy is defined as

$$\boldsymbol{T}_{\mathrm{int}} \coloneqq \boldsymbol{T} - \boldsymbol{T}_{\mathrm{cm}}. \tag{1.12}$$

Here, $\boldsymbol{T}$ and $\boldsymbol{T}_{\mathrm{cm}}$ denote the total and the center-of-mass kinetic energy, respectively. This generator drives the Hamiltonian towards a diagonal form in a basis of eigenstates of the intrinsic kinetic energy, i.e., momentum eigenstates. For this specific choice of the generator, a dimensional analysis of the units yields that the SRG flow parameter α has the dimension of length to the power of four.

The SRG transformation of any n-body operator within an A-body system induces irreducible many-body operators up to the A-body level due to the commutator structure of the operator flow equation. Starting with a Hamiltonian $\boldsymbol{H}$ containing the intrinsic kinetic

energy $\boldsymbol{T}_{\mathrm{int}}$ and two- and three-nucleon interactions, $\boldsymbol{V}_{\mathrm{NN}}$ and $\boldsymbol{V}_{\mathrm{3N}}$, the SRG transformation yields

$$\begin{aligned}\boldsymbol{U}_\alpha^\dagger \boldsymbol{H} \boldsymbol{U}_\alpha &= \boldsymbol{U}_\alpha^\dagger \left(\boldsymbol{T}_{\mathrm{int}} + \boldsymbol{V}_{\mathrm{NN}} + \boldsymbol{V}_{\mathrm{3N}}\right) \boldsymbol{U}_\alpha \qquad (1.13)\\ &= \left(\boldsymbol{T}^{[2]}_{\mathrm{int},\alpha} + \boldsymbol{V}^{[2]}_{\mathrm{NN},\alpha}\right)\\ &\quad + \left(\boldsymbol{T}^{[3]}_{\mathrm{int},\alpha} + \boldsymbol{V}^{[3]}_{\mathrm{NN},\alpha} + \boldsymbol{V}^{[3]}_{\mathrm{3N},\alpha}\right)\\ &\quad \vdots\\ &\quad + \left(\boldsymbol{T}^{[A]}_{\mathrm{int},\alpha} + \boldsymbol{V}^{[A]}_{\mathrm{NN},\alpha} + \boldsymbol{V}^{[A]}_{\mathrm{3N},\alpha}\right) . \qquad (1.14)\end{aligned}$$

The number within the bracket denotes the particle rank. Note that there is no one-body term since we use the two-body form of the kinetic energy operator. Formally, only if all the induced terms up to the A-body level are kept, the SRG transformation is unitary and the spectrum of the Hamiltonian in an exact A-body calculation is preserved and independent of the SRG flow parameter α. In practice, the SRG transformation has to be truncated at a particle rank $m < A$, which formally violates the unitarity of the SRG transformation. Hence, the SRG flow parameter α is used as a diagnostic tool to quantify the relevance of omitted beyond-m-body terms.

Throughout this work, we stick to the NN+3N-full Hamiltonian starting with the initial chiral NN+3N Hamiltonian and retain all terms up to the three-body level in the SRG transformation with $\alpha = 0.08\,\mathrm{fm}^4$ [Rot+11], i.e.,

$$\boldsymbol{H}_\alpha = \left(\boldsymbol{T}^{[2]}_{\mathrm{int},\alpha} + \boldsymbol{V}^{[2]}_{\mathrm{NN},\alpha}\right) + \left(\boldsymbol{T}^{[3]}_{\mathrm{int},\alpha} + \boldsymbol{V}^{[3]}_{\mathrm{NN},\alpha} + \boldsymbol{V}^{[3]}_{\mathrm{3N},\alpha}\right) . \qquad (1.15)$$

Chapter 2

Hartree-Fock Method

In this chapter, we briefly recap the ideas of the Hartree-Fock (HF) method, which is widely used in atomic and nuclear physics, as well as quantum chemistry. The HF method has two scopes of application: On the one hand, it is used to approximate the ground state of the Hamiltonian on a self-consistent mean-field level, i.e., the nucleons move independently from each other without accounting for the correlation among the particles. On the other hand, it provides a simple and efficient way to optimize a single-particle basis, which can be used as a starting point for a more sophisticated many-body methods as the in-medium similarity renormalization group or the no-core shell model to account for missing correlations. The latter is the purpose of our usage.

Hamiltonian in Second Quantization

For the following discussion, it is convenient to formulate the Hamiltonian $\boldsymbol{H}$ in second quantization. To that end, we introduce the creation operator for a single-particle state $|p\rangle$ as $\boldsymbol{a}^p \coloneqq \boldsymbol{a}_p^\dagger$ and the annihilation operator as $\boldsymbol{a}_q$, respectively. Furthermore, we use a tensor-like notation to write products of creation and annihilation operators in a compact form

$$\boldsymbol{a}_q^p \coloneqq \boldsymbol{a}^p \boldsymbol{a}_q \tag{2.1a}$$

$$\boldsymbol{a}_{qs}^{pr} \coloneqq \boldsymbol{a}^p \boldsymbol{a}^r \boldsymbol{a}_s \boldsymbol{a}_q \tag{2.1b}$$

$$\boldsymbol{a}_{qsu}^{prt} \coloneqq \boldsymbol{a}^p \boldsymbol{a}^r \boldsymbol{a}^t \boldsymbol{a}_u \boldsymbol{a}_s \boldsymbol{a}_q. \tag{2.1c}$$

We refer to these operators as (basic) one-, two-, three-body operators. Note the reversed order of the lower indices.

Finally, using these operators, we can write the Hamiltonian in second quantization as

$$\boldsymbol{H} = h + \sum_{\substack{p \\ q}} h_q^p \boldsymbol{a}_q^p + \frac{1}{4} \sum_{\substack{pr \\ qs}} h_{qs}^{pr} \boldsymbol{a}_{qs}^{pr} + \frac{1}{36} \sum_{\substack{prt \\ qsu}} h_{qsu}^{prt} \boldsymbol{a}_{qsu}^{prt} \tag{2.2}$$

with the zero-body term h, one-body matrix elements h_q^p and the antisymmetrized two- and

three-body matrix elements defined as

$$h_{qs}^{pr} \coloneqq \langle pr| \left(\boldsymbol{T}_{\mathrm{int},\alpha}^{[2]} + \boldsymbol{V}_{\mathrm{NN},\alpha}^{[2]} \right) |qs\rangle \tag{2.3a}$$

$$h_{qsu}^{prt} \coloneqq \langle prt| \left(\boldsymbol{T}_{\mathrm{int},\alpha}^{[3]} + \boldsymbol{V}_{\mathrm{NN},\alpha}^{[3]} + \boldsymbol{V}_{\mathrm{3N},\alpha}^{[3]} \right) |qsu\rangle \,. \tag{2.3b}$$

Here, we add h and the one-body matrix elements h_q^p for a general treatment of the Hamiltonian, which are zero in our case since the Hamiltonian contains just two- and three-body operators (1.15). Note that we suppress the SRG flow parameter α for brevity since it is fixed to $\alpha = 0.08\,\mathrm{fm}^4$ throughout this work.

Closed-Shell Systems

Let us first discuss the HF method for closed-shell nuclei, i.e., the nucleons fill complete (sub-) shells. This case is well covered in the literature, and a standard treatment of this matter can be found in [Suh07; RS80; SO96]. Since the nucleons move independently from each other, the energetically favored configuration is where all nucleons occupy the energetically lowest single-particle states taking into account the Pauli exclusion principle. Therefore, we can choose a single Slater determinant $|\Phi_{\mathrm{HF}}\rangle$, an antisymmetrized A-body product state built of single-particle states, as first approximation to the many-body ground state of the system under consideration. Assuming that $|\Phi_{\mathrm{HF}}\rangle$ is normalized, we obtain the optimized single-particle states in the HF framework by minimizing the energy functional

$$\mathcal{E} \coloneqq \langle \Phi_{\mathrm{HF}} | \boldsymbol{H} | \Phi_{\mathrm{HF}} \rangle \tag{2.4}$$

$$= h + \sum_{\substack{p \\ q}} h_q^p \langle \Phi_{\mathrm{HF}} | \boldsymbol{a}_q^p | \Phi_{\mathrm{HF}} \rangle + \frac{1}{4} \sum_{\substack{pr \\ qs}} h_{qs}^{pr} \langle \Phi_{\mathrm{HF}} | \boldsymbol{a}_{qs}^{pr} | \Phi_{\mathrm{HF}} \rangle + \frac{1}{36} \sum_{\substack{prt \\ qsu}} h_{qsu}^{prt} \langle \Phi_{\mathrm{HF}} | \boldsymbol{a}_{qsu}^{prt} | \Phi_{\mathrm{HF}} \rangle \tag{2.5}$$

with respect to the single-particle states serving as optimization parameters. Introducing the one-, two- and three-body density matrix elements with respect to the HF Slater determinant

$$\rho_q^p \coloneqq \langle \Phi_{\mathrm{HF}} | \boldsymbol{a}_q^p | \Phi_{\mathrm{HF}} \rangle \tag{2.6a}$$

$$\rho_{qs}^{pr} \coloneqq \langle \Phi_{\mathrm{HF}} | \boldsymbol{a}_{qs}^{pr} | \Phi_{\mathrm{HF}} \rangle \tag{2.6b}$$

$$\rho_{qsu}^{prt} \coloneqq \langle \Phi_{\mathrm{HF}} | \boldsymbol{a}_{qsu}^{prt} | \Phi_{\mathrm{HF}} \rangle \tag{2.6c}$$

and making use of the fact that the higher-body density matrices factorize into products of one-body density matrices

$$\rho_{qs}^{pr} = \rho_q^p \rho_s^r - \rho_s^p \rho_q^r \tag{2.7a}$$

$$\rho_{qsu}^{prt} = \rho_q^p \rho_s^r \rho_u^t + \rho_u^p \rho_q^r \rho_s^t + \rho_s^p \rho_u^r \rho_q^t - \rho_u^p \rho_s^r \rho_q^t - \rho_s^p \rho_q^r \rho_u^t - \rho_q^p \rho_u^r \rho_s^t, \tag{2.7b}$$

which is characteristic for a single Slater determinant, we can simplify the energy functional to

$$\mathcal{E} = h + \sum_{\substack{p \\ q}} h_q^p \rho_q^p + \frac{1}{2} \sum_{\substack{pr \\ qs}} h_{qs}^{pr} \rho_q^p \rho_s^r + \frac{1}{6} \sum_{\substack{prt \\ qsu}} h_{qsu}^{prt} \rho_q^p \rho_s^r \rho_u^t. \tag{2.8}$$

The HF single-particle states have to be determined in a self-consistent way because the occupied states themselves generate the mean-field that the nucleons feel, which again fixes the single-particle states in which the nucleons move.

Open-Shell Systems

Going to open-shell systems while preserving the spherical symmetry of the basis, we face the problem that multiple configurations yield the same mean-field energy. Put differently, there are many allowed configurations associated with the same total energy on the mean-field level because the valence nucleons can occupy any of the states in the partially occupied shells. The equal-filling approximation is one possible solution to this problem, where we assume projection-number-independent fractional occupation numbers and the factorization of the higher-body densities as formulated in (2.7). With these requirements, the energy functional to be minimized is analogous to the original HF problem (2.8).

The most general case is given by doubly open-shell nuclei, i.e., the A_v^π protons and A_v^ν neutrons partially occupy states of the valence shells corresponding to an angular momentum j_v^π and j_v^ν, respectively. Obviously, $2j_v^\pi + 1$ must be strictly greater than A_v^π. The same must hold for the neutrons as well. We make the following ansatz for the one-body density matrix elements in the case where all indices correspond to one of the state in the valence shell, which is the non-trivial case

$$\rho_y^x = \delta_y^x \times \begin{cases} \frac{A_v^\pi}{2j_v^\pi+1} & \text{if } x \text{ refers to a proton valence state} \\ \frac{A_v^\nu}{2j_v^\nu+1} & \text{if } x \text{ refers to a neutron valence state.} \end{cases} \tag{2.9}$$

Obviously, this ansatz respects the requirement that the occupation numbers are independent of the magnetic quantum number.

Chapter 3

Normal Ordering and Wick's Theorem

Normal ordering is a powerful technique for the evaluation of expectation values of products of operators with respect to an arbitrary A-body state. The in-medium similarity renormalization group that will be subject of chapter 4 is formulated in terms of the so-called normal-ordered operators. Moreover, normal ordering with respect to non-trivial reference states is useful to systematically derive approximations to operators beyond the two-body rank, which are computationally and conceptually demanding to include in many-body calculations.

The concept of normal ordering is built on a given A-body state that we call the reference state. We discuss three different types of reference states: the physical vacuum $|0\rangle$, a single Slater determinant $|\Phi\rangle$ (single-reference case), or a linear combination of Slater determinants $|\Psi\rangle$ (multi-reference case). The latter one is the most significant case for this work. Note that the vacuum case is a special case of the single-reference one which in turn is a special case of the multi-reference one.

This chapter is organized as follows: We briefly discuss the concept of normal ordering with respect to the vacuum (section 3.1). Furthermore, we generalize this concept to a single-reference state with the aid of the particle-hole formalism and formulate Wick's theorem (section 3.2). Finally, we point out the problems we are facing when considering the multi-reference state, and formulate the extended Wick's theorem introduced by Kutzelnigg and Mukherjee (section 3.3). With the aid of this Wick's theorem, we derive formulae for changing from the so-called vacuum representation to the reference-state representation (section 3.3.3). Based on these results we show how to derive approximations for any three-body operator (section 3.3.4). Furthermore, we introduce the generalized Wick's theorem, which applies to products of normal-ordered operators (section 3.3.5). Finally, making use of the generalized Wick's theorem we summarize the results for commutators of normal-ordered operators in section 3.3.6, which are the main ingredient for the multi-reference in-medium similarity renormalization group. The detailed derivation can be found in appendix A.

3.1. Vacuum Case

The starting point is the following definition:

Definition 3.1. A product of fermionic operators is in normal order with respect to the vacuum $|0\rangle$ if all creation operators are to the left of all annihilation operators.

A product of operators fulfilling this condition is in vacuum normal order, briefly *operator in V-NO*. Alternatively, we refer to this product as vacuum normal-ordered operator (V-NO operator). Obviously, any single creation operator $\boldsymbol{a}^p = \boldsymbol{a}_p^\dagger$, and annihilation operator $\boldsymbol{a}_q$ is an operator in V-NO. To give more examples, the one-, two-, three-body operators from (2.1)

$$\boldsymbol{a}_q^p = \boldsymbol{a}^p \boldsymbol{a}_q \tag{3.1a}$$

$$\boldsymbol{a}_{qs}^{pr} = \boldsymbol{a}^p \boldsymbol{a}^r \boldsymbol{a}_s \boldsymbol{a}_q \tag{3.1b}$$

$$\boldsymbol{a}_{qsu}^{prt} = \boldsymbol{a}^p \boldsymbol{a}^r \boldsymbol{a}^t \boldsymbol{a}_u \boldsymbol{a}_s \boldsymbol{a}_q \tag{3.1c}$$

are operators in V-NO, too.

For the mathematical description of the normal ordering, we define an operator $\boldsymbol{\mathcal{N}}_{|0\rangle}$ that brings a product of operators into V-NO, taking into account a sign factor. Let $\boldsymbol{A}_1, \boldsymbol{A}_2, \ldots, \boldsymbol{A}_n$ be pairwise distinct fermionic operators each of them representing either a creation operator $\boldsymbol{a}^p$ or an annihilation operator $\boldsymbol{a}_q$. Using this requirement, we define the normal-ordering operator $\boldsymbol{\mathcal{N}}_{|0\rangle}$ as follows:

Definition 3.2. The normal-ordering (super)operator $\boldsymbol{\mathcal{N}}_{|0\rangle}$ is defined by

$$\boldsymbol{\mathcal{N}}_{|0\rangle}\{\boldsymbol{A}_1 \boldsymbol{A}_2 \ldots \boldsymbol{A}_n\} \coloneqq \operatorname{sgn}(\pi)\ \boldsymbol{A}_{\pi(1)} \boldsymbol{A}_{\pi(2)} \ldots \boldsymbol{A}_{\pi(n)}, \tag{3.2}$$

where $\operatorname{sgn}(\pi)$ is the sign of the permutation $\pi \in \mathcal{S}_n$ needed to bring the product $\boldsymbol{A}_1 \boldsymbol{A}_2 \ldots \boldsymbol{A}_n$ into normal order with respect to the vacuum. The product $\boldsymbol{A}_{\pi(1)} \boldsymbol{A}_{\pi(2)} \ldots \boldsymbol{A}_{\pi(n)}$ is then called an operator in V-NO. Here, $\mathcal{S}_n$ denotes the set of all permutations of $(1, 2, \ldots, n)$.

In general, this prescription is not unique, because two different creation operators anti-commute. The same applies to the annihilation operators. Additionally, we require that the normal-ordering operator is linear and maps the identity operator of the antisymmetric Fock space $\mathbf{1}$ onto itself, i.e., $\boldsymbol{\mathcal{N}}_{|0\rangle}\{\mathbf{1}\} = \mathbf{1}$. Linearity means

$$\begin{aligned} \boldsymbol{\mathcal{N}}_{|0\rangle}\{\boldsymbol{A}_1 \boldsymbol{A}_2 \ldots \boldsymbol{A}_j (\mu \boldsymbol{C} + \boldsymbol{D}) \boldsymbol{A}_{j+1} \ldots \boldsymbol{A}_n\} &= \mu \boldsymbol{\mathcal{N}}_{|0\rangle}\{\boldsymbol{A}_1 \boldsymbol{A}_2 \ldots \boldsymbol{A}_j \boldsymbol{C} \boldsymbol{A}_{j+1} \ldots \boldsymbol{A}_n\} \\ &\quad + \boldsymbol{\mathcal{N}}_{|0\rangle}\{\boldsymbol{A}_1 \boldsymbol{A}_2 \ldots \boldsymbol{A}_j \boldsymbol{D} \boldsymbol{A}_{j+1} \ldots \boldsymbol{A}_n\} \end{aligned} \tag{3.3}$$

for any complex number μ and any two operators $\boldsymbol{C}$ and $\boldsymbol{D}$.

By construction, the normal-ordering operator has the following property

$$\boldsymbol{\mathcal{N}}_{|0\rangle}\{\boldsymbol{A}_1 \boldsymbol{A}_2 \ldots \boldsymbol{A}_i \ldots \boldsymbol{A}_j \ldots \boldsymbol{A}_n\} = -\boldsymbol{\mathcal{N}}_{|0\rangle}\{\boldsymbol{A}_1 \boldsymbol{A}_2 \ldots \boldsymbol{A}_j \ldots \boldsymbol{A}_i \ldots \boldsymbol{A}_n\}, \tag{3.4}$$

which we simply call antisymmetric under transposition of any two different operators. This is related to the property of the signum function $\mathrm{sgn}(\pi\pi') = \mathrm{sgn}(\pi)\mathrm{sgn}(\pi')$, and that the sign of any transposition is negative.

We illustrate the action of the normal-ordering operator $\boldsymbol{\mathcal{N}}_{|0\rangle}$ by means of some simple examples

$$\boldsymbol{\mathcal{N}}_{|0\rangle}\{\boldsymbol{a}_q\boldsymbol{a}^p\} = -\boldsymbol{\mathcal{N}}_{|0\rangle}\{\boldsymbol{a}^p\boldsymbol{a}_q\} = -\boldsymbol{a}^p\boldsymbol{a}_q \tag{3.5}$$

$$\boldsymbol{\mathcal{N}}_{|0\rangle}\{\boldsymbol{a}_q\boldsymbol{a}_s\boldsymbol{a}^p\} = (-1)^2\,\boldsymbol{a}^p\boldsymbol{a}_q\boldsymbol{a}_s. \tag{3.6}$$

These simple examples demonstrate that acting with the normal-ordering operator $\boldsymbol{\mathcal{N}}_{|0\rangle}$ on a given product of operators, in general, generates a different operator compared to the initial one, i.e.,

$$\boldsymbol{A}_1\boldsymbol{A}_2\ldots\boldsymbol{A}_n \neq \boldsymbol{\mathcal{N}}_{|0\rangle}\{\boldsymbol{A}_1\boldsymbol{A}_2\ldots\boldsymbol{A}_n\}. \tag{3.7}$$

The question is how to transform a product of operators into normal order with respect to the vacuum while retaining an operator identity. Put differently, what are the missing terms on the right hand side to have an equal sign. We are looking for an operator identity that expresses the given product as a linear combination of operators in V-NO. We refer to this procedure as the *normal-ordering transformation*.

The straight-forward way is to put creation operators to the left of all annihilation operators using the anticommutation relations, given by

$$\{\boldsymbol{a}_q, \boldsymbol{a}_p\} = \{\boldsymbol{a}^q, \boldsymbol{a}^p\} = 0 \tag{3.8}$$

$$\{\boldsymbol{a}_q, \boldsymbol{a}^p\} = \delta_q^p, \tag{3.9}$$

where the brackets denote the anticommutator defined as $\{\boldsymbol{A}_1, \boldsymbol{A}_2\} := \boldsymbol{A}_1\boldsymbol{A}_2 + \boldsymbol{A}_2\boldsymbol{A}_1$. By means of the anticommutation relations, e.g., the product of $\boldsymbol{a}_q\boldsymbol{a}_s\boldsymbol{a}^p$ can be transformed to

$$\boldsymbol{a}_q\boldsymbol{a}_s\boldsymbol{a}^p \quad \longrightarrow \quad \boldsymbol{a}_q\boldsymbol{a}_s\boldsymbol{a}^p = \boldsymbol{a}^p\boldsymbol{a}_q\boldsymbol{a}_s + \delta_s^p\boldsymbol{a}_q - \delta_q^p\boldsymbol{a}_s. \tag{3.10}$$

We observe that the first term in (3.10) can be identified with the term obtained in (3.6), namely $\boldsymbol{\mathcal{N}}_{|0\rangle}\{\boldsymbol{a}_q\boldsymbol{a}_s\boldsymbol{a}^p\}$, and the two additional terms are operators in V-NO, too. Hence, the given product is expressed as a sum of operators in V-NO. Since we used only equivalence transformations, (3.10) is an operator identity.

The normal-ordering transformation can be very exhausting, especially if the number of operators is large. A more systematic approach to this problem is the use of Wick's theorem, where the normal-ordering operator $\boldsymbol{\mathcal{N}}_{|0\rangle}$ plays an important role. But before formulating the Wick's theorem, we generalize the concept of normal ordering to a single Slater determinant.

3.2. Single-Reference Case

We describe how to generalize the concept of normal ordering to a single Slater determinant based on the particle-hole formalism. Let $|\Phi\rangle$ be an A-body single-reference state[1], i.e., a single Slater determinant

$$|\Phi\rangle = \prod_{i=1}^{A} \boldsymbol{a}^i \, |0\rangle \, . \tag{3.11}$$

Furthermore, let the *occupied* single-particle states

$$\boldsymbol{a}^i \, |0\rangle \quad \text{with} \quad i = 1, 2, \ldots, A \tag{3.12}$$

and the *unoccupied* single-particle states

$$\boldsymbol{a}^b \, |0\rangle \quad \text{with} \quad b > A \tag{3.13}$$

form an orthonormal basis $\{\boldsymbol{a}^p \, |0\rangle : p = 1, 2, \ldots\}$ of the one-body Hilbert space. Conventionally, we refer to the indices $i, j, k, \ldots$ and $b, c, d, \ldots$ as *hole* and *particle* indices, respectively. The indices $p, q, r, \ldots$ can refer to both.

Acting with the operator $\boldsymbol{a}^i$ for a hole index on the reference state $|\Phi\rangle$ yields

$$\boldsymbol{a}^i \, |\Phi\rangle = 0 \tag{3.14}$$

due to Pauli exclusion principle. Moreover, annihilating the unoccupied single-particle state $|b\rangle$ from the reference state $|\Phi\rangle$ vanishes

$$\boldsymbol{a}_b \, |\Phi\rangle = 0 \tag{3.15}$$

due to the definition of annihilation operators. Since both types of operators act like annihilation operators with respect to the reference state $|\Phi\rangle$, we redefine them to be *quasiparticle annihilators*. Analogously, the operators $\boldsymbol{a}_i$ and $\boldsymbol{a}^b$ are redefined to be *quasiparticle creators* relative to the reference state, since they create a hole and a particle, respectively. Based on this reinterpretation, we can define normal ordering with respect to a single-reference state $|\Phi\rangle$ in analogy to the vacuum case.

Definition 3.3. A product of operators is in normal order with respect to a single-reference state $|\Phi\rangle$, if all quasiparticle creators are to the left of all quasiparticle annihilators.

A product of operators fulfilling this condition is in single-reference normal order, briefly an *operator in SR-NO*. Alternatively, we refer to it as single-reference normal-ordered operator (*SR-NO operator*). Note in both terms, we do not exactly specify the reference state $|\Phi\rangle$. Hence, care should be taken if different reference states are involved.

[1] The rigorous correct terminology is single-reference single-determinant reference state.

For the mathematical formulation, we introduce a normal-ordering operator $\boldsymbol{\mathcal{N}}_{|\Phi\rangle}$ with respect to the reference state $|\Phi\rangle$ that is linear and antisymmetric analogously to the vacuum case. Note that we recover the vacuum case if the reference state does not contain any particles. For illustration purposes, we consider the action of the normal-ordering operator $\boldsymbol{\mathcal{N}}_{|\Phi\rangle}$ on a product of quasiparticle operators

$$\boldsymbol{\mathcal{N}}_{|\Phi\rangle}\{\boldsymbol{a}^i\boldsymbol{a}_j\} = -\boldsymbol{a}_j\boldsymbol{a}^i\,, \qquad \boldsymbol{\mathcal{N}}_{|\Phi\rangle}\{\boldsymbol{a}^i\boldsymbol{a}_b\} = \boldsymbol{a}^i\boldsymbol{a}_b \tag{3.16}$$

$$\boldsymbol{\mathcal{N}}_{|\Phi\rangle}\{\boldsymbol{a}_b\boldsymbol{a}^c\} = -\boldsymbol{a}^c\boldsymbol{a}_b\,, \qquad \boldsymbol{\mathcal{N}}_{|\Phi\rangle}\{\boldsymbol{a}_b\boldsymbol{a}_j\} = -\boldsymbol{a}_j\boldsymbol{a}_b. \tag{3.17}$$

A key property of the operators in SR-NO is that their expectation value with respect to the state they are normal ordered to vanishes, i.e.,

$$\langle\Phi|\,\boldsymbol{\mathcal{N}}_{|\Phi\rangle}\{\boldsymbol{A}_1\boldsymbol{A}_2\dots\boldsymbol{A}_n\}\,|\Phi\rangle = 0. \tag{3.18}$$

This holds also for the vacuum case.

In practical calculations, we need to write a given product of operators as sum of operators in SR-NO. As a reminder, we refer to this procedure as normal-ordering transformation. One possible way to perform this transformation could be to make use of the anticommutation relations for the quasiparticle operators analogously to the vacuum case. This procedure might get cumbersome. A more sophisticated and systematic approach represents the Wick's theorem with respect to a given single-reference state $|\Phi\rangle$ stating:

Theorem 3.1. *A product of n operators $\boldsymbol{A}_1, \boldsymbol{A}_2, \dots, \boldsymbol{A}_n$ can be expressed as a sum of its SR-NO product and all possible normal-ordered contractions with respect to $|\Phi\rangle$ [Wic50]*

$$\boldsymbol{A}_1\boldsymbol{A}_2\dots\boldsymbol{A}_n = \boldsymbol{\mathcal{N}}_{|\Phi\rangle}\{\boldsymbol{A}_1\boldsymbol{A}_2\dots\boldsymbol{A}_n\} + \sum_{\substack{\text{all contractions}\\ \text{w.r.t.}|\Phi\rangle}} \boldsymbol{\mathcal{N}}_{|\Phi\rangle}\{\boldsymbol{A}_1\boldsymbol{A}_2\dots\boldsymbol{A}_n\}. \tag{3.19}$$

A contraction with respect to $|\Phi\rangle$ between $\boldsymbol{A}_1$ and $\boldsymbol{A}_2$ is indicated by

$$\overbracket{\boldsymbol{A}_1\boldsymbol{A}_2}, \tag{3.20}$$

and denotes a complex number. A normal-ordered contraction indicates normal ordering combined with a contraction between the operators $\boldsymbol{A}_i$ and $\boldsymbol{A}_j$, which has to be evaluated in the following way

$$\begin{aligned}&\boldsymbol{\mathcal{N}}_{|\Phi\rangle}\{\boldsymbol{A}_1\boldsymbol{A}_2\dots\boldsymbol{A}_{i-1}\overbracket{\boldsymbol{A}_i\boldsymbol{A}_{i+1}\dots\boldsymbol{A}_{j-1}\boldsymbol{A}_j}\boldsymbol{A}_{j+1}\dots\boldsymbol{A}_n\}\\ &= \operatorname{sgn}(\pi)\,\overbracket{\boldsymbol{A}_i\boldsymbol{A}_j}\,\boldsymbol{\mathcal{N}}_{|\Phi\rangle}\{\boldsymbol{A}_1\boldsymbol{A}_2\dots\boldsymbol{A}_{i-1}\boldsymbol{A}_{i+1}\dots\boldsymbol{A}_{j-1}\boldsymbol{A}_{j+1}\dots\boldsymbol{A}_n\},\end{aligned} \tag{3.21}$$

where π is a permutation that brings the two corresponding operators adjacent without changing their original order. This is because the contraction $\overbracket{\boldsymbol{A}_1\boldsymbol{A}_2}$ is not identical to $\overbracket{\boldsymbol{A}_2\boldsymbol{A}_1}$ as we will see later.

Theorem 3.1 is pointless without a formula for the contraction. For that purpose, we apply

it to a product of two operators $\boldsymbol{A}_1$ and $\boldsymbol{A}_2$ yielding

$$\boldsymbol{A}_1\boldsymbol{A}_2 = \boldsymbol{\mathcal{N}}_{|\Phi\rangle}\{\boldsymbol{A}_1\boldsymbol{A}_2\} + \boldsymbol{\mathcal{N}}_{|\Phi\rangle}\{\overbracket{\boldsymbol{A}_1\boldsymbol{A}_2}\} = \boldsymbol{\mathcal{N}}_{|\Phi\rangle}\{\boldsymbol{A}_1\boldsymbol{A}_2\} + \overbracket{\boldsymbol{A}_1\boldsymbol{A}_2}. \tag{3.22}$$

Since the expectation value of an operator in SR-NO with respect to $|\Phi\rangle$ vanishes according to (3.18), we obtain for the contraction with respect to the reference state

$$\overbracket{\boldsymbol{A}_1\boldsymbol{A}_2} = \langle\Phi|\,\boldsymbol{A}_1\boldsymbol{A}_2\,|\Phi\rangle\,, \tag{3.23}$$

which is equal to the expectation value of the product with respect to the reference state itself. We define a *hole contraction* as the contraction between an creator and annihilator

$$\overbracket{\boldsymbol{a}^p\boldsymbol{a}_q} = \langle\Phi|\,\boldsymbol{a}^p\boldsymbol{a}_q\,|\Phi\rangle =: \gamma_q^p \tag{3.24}$$

which is identical to a *one-particle* density matrix element γ_q^p with respect to the reference state. Furthermore, a *particle contraction* is given by

$$\overbracket{\boldsymbol{a}_q\boldsymbol{a}^p} = \langle\Phi|\,\boldsymbol{a}_q\boldsymbol{a}^p\,|\Phi\rangle =: \bar{\gamma}_q^p \tag{3.25}$$

which in this case corresponds to a *one-hole* density matrix element $\bar{\gamma}_q^p$. All other combinations vanish

$$\overbracket{\boldsymbol{a}^p\boldsymbol{a}^q} = \overbracket{\boldsymbol{a}_p\boldsymbol{a}_q} = 0. \tag{3.26}$$

Especially for a single-reference state, the one-particle and one-hole density matrix elements can be simplified to

$$\gamma_q^p = \delta_q^p n_q, \tag{3.27}$$

$$\bar{\gamma}_q^p = \delta_q^p(1 - n_q) = \delta_q^p - \gamma_q^p. \tag{3.28}$$

Here, we introduced the *particle occupation number* n_q which is just one or zero depending on whether this corresponding single-particle state is occupied in $|\Phi\rangle$ or not, i.e.,

$$n_q := \begin{cases} 1, & \text{if } q \text{ occupied in } |\Phi\rangle, \\ 0, & \text{else.} \end{cases} \tag{3.29}$$

The naming convention for the two non-vanishing types of contractions is rooted in the following observation. A hole contraction has non-vanishing contributions only if both indices, p and q, are hole indices (i, j, ...). Similarly, a particle contraction does not vanish only if both indices, p and q, are particle indices (b, c, ...). In other words, any mixing of particle and hole indices always leads to vanishing contractions.

In order to clarify the statement of theorem 3.1, we consider the one- and two–body operators, $\boldsymbol{a}_q^p$ and $\boldsymbol{a}_{qs}^{pr}$, which are, by definition, normal ordered with respect to the vacuum.

The aim is to express them as a sum of the operators in SR-NO. From (3.22) we immediately obtain

$$\boldsymbol{a}_q^p = \boldsymbol{a}^p \boldsymbol{a}_q = \boldsymbol{\mathcal{N}}_{|\Phi\rangle}\{\boldsymbol{a}_q^p\} + \gamma_q^p. \tag{3.30}$$

For the two-body operator, the application of theorem 3.1 yields

$$\begin{aligned} \boldsymbol{a}_{qs}^{pr} &= \boldsymbol{a}^p \boldsymbol{a}^r \boldsymbol{a}_s \boldsymbol{a}_q && (3.31)\\ &= \boldsymbol{\mathcal{N}}_{|\Phi\rangle}\{\boldsymbol{a}_{qs}^{pr}\} + \gamma_q^p \boldsymbol{\mathcal{N}}_{|\Phi\rangle}\{\boldsymbol{a}_s^r\} + \gamma_s^r \boldsymbol{\mathcal{N}}_{|\Phi\rangle}\{\boldsymbol{a}_q^p\} - \gamma_s^p \boldsymbol{\mathcal{N}}_{|\Phi\rangle}\{\boldsymbol{a}_q^r\} - \gamma_q^r \boldsymbol{\mathcal{N}}_{|\Phi\rangle}\{\boldsymbol{a}_s^p\} \\ &\quad + \gamma_q^p \gamma_s^r - \gamma_s^p \gamma_q^r. && (3.32) \end{aligned}$$

3.3. Multi-Reference Case

Since the normal ordering with respect to a single-reference state is limited to closed-shell nuclei, i.e., the nucleons fill complete (sub-) shells, it is desirable to extend the normal-ordering concept to linear combination of Slater determinants, called multi-reference case[2]. This will enable us to target open-shell systems.

In the whole section the following requirements are made: Let $\mathcal{H}_n$ be a finite-dimensional subspace of the A-body Hilbert space $\mathcal{H}$, and $\{|\phi_i\rangle : i = 1, \ldots, n\}$ be a complete orthonormal basis of $\mathcal{H}_n$. Furthermore, let $|\Psi\rangle \in \mathcal{H}_n$ be a normalized A-body state

$$|\Psi\rangle := \sum_{i=1}^{n} c_i |\phi_i\rangle , \tag{3.33}$$

with complex numbers c_i and single Slater determinants $|\phi_i\rangle$.

3.3.1. Problem and Guiding Principle

The "traditional" definition of normal ordering says that a product of operators is in normal order with respect to a reference state, if all (quasiparticle) creation operators are to the left of all (quasiparticle) annihilation operators. This statement is no longer useful for a multi-reference state $|\Psi\rangle$ since there is no well-defined particle-hole picture, i.e., for all i and $j \neq i$ there is a single-particle state $|p\rangle$ occupied in the i-th single Slater determinant and unoccupied in the j-th single Slater determinant

$$\boldsymbol{a}^p |\phi_i\rangle = 0, \tag{3.34}$$

$$\boldsymbol{a}^p |\phi_j\rangle \neq 0. \tag{3.35}$$

Consequently, the operator $\boldsymbol{a}^p$ is a (quasiparticle) annihilation operator with respect to $|\phi_i\rangle$ and (quasiparticle) creation operator with respect to $|\phi_j\rangle$. Hence, it is not obvious how to define normal ordering with respect to $|\Psi\rangle$. This simple observation implies that one has

[2]The rigorous correct terminology is single-reference multi-determinant reference state.

to give up the "traditional" definition of normal ordering. Therefore, the normal-ordering transformation is defined only in the framework of a Wick-like theorem. For the generalization of Wick's theorem with respect to a multi-reference state $|\Psi\rangle$ two basic requirements have to be fulfilled:

(I) *If an operator $\boldsymbol{X} \neq \mathbf{1}$ is in normal order with respect to $|\Psi\rangle$, briefly an operator in MR-NO, then the expectation value of $\boldsymbol{X}$ with respect to $|\Psi\rangle$ vanishes, i.e.,*

$$\langle\Psi|\,\boldsymbol{X}\,|\Psi\rangle = 0. \tag{3.36}$$

The opposite direction of this statement is in general wrong.

(II) *For the special case that $|\Psi\rangle$ consists only of a single Slater determinant, the well-known normal-ordering framework with respect to a single-reference state must be recovered.*

A generalization fulfilling both requirements was proposed and proven by Mukherjee and Kutzelnigg [Muk97; KM97], and formulated in form of a Wick-like theorem with respect to a multi-reference state.

3.3.2. Wick's Theorem

For the mathematical formulation of the normal ordering with respect to a multi-reference state $|\Psi\rangle$, we introduce a normal-ordering operator $\boldsymbol{\mathcal{N}} := \boldsymbol{\mathcal{N}}_{|\Psi\rangle}$ omitting the subscript from now on. This definition is more abstract, i.e., it does not correspond to a reordering of creation operators to the left of all annihilation operators. But the normal-ordering operator $\boldsymbol{\mathcal{N}}$ is required to be linear, antisymmetric and maps the identity operator $\mathbf{1}$ onto itself. The action of the normal-ordering operator on a product of operators leads to an operator in multi-reference normal order, briefly an operator in MR-NO. Alternatively, we say (reference-state) normal-ordered operator if it is clear which reference state we mean.

Analogously to the single-reference case, we can perform the normal-ordering transformation with the aid of Wick's theorem with respect to a multi-reference state $|\Psi\rangle$ stating:

Theorem 3.2. *A product of n operators $\boldsymbol{A}_1, \boldsymbol{A}_2, \ldots, \boldsymbol{A}_n$ can be expressed as a sum of its MR-NO product and all possible normal-ordered contractions with respect to $|\Psi\rangle$ [KM97; Muk97]*

$$\boldsymbol{A}_1\boldsymbol{A}_2\ldots\boldsymbol{A}_n = \boldsymbol{\mathcal{N}}\{\boldsymbol{A}_1\boldsymbol{A}_2\ldots\boldsymbol{A}_n\} + \sum_{\substack{\text{all contractions}\\ \text{w.r.t.}|\Psi\rangle}} \boldsymbol{\mathcal{N}}\{\boldsymbol{A}_1\boldsymbol{A}_2\ldots\boldsymbol{A}_n\}. \tag{3.37}$$

A contraction with respect to $|\Psi\rangle$ between $\boldsymbol{A}_1$ and $\boldsymbol{A}_2$ denoted by

$$\overline{\boldsymbol{A}_1\boldsymbol{A}_2} \tag{3.38}$$

yields a complex number. This type of contractions, called 2-tuple contraction, is comparable to the one introduced for the single-reference case (3.20). The new ingredient of theorem 3.2

is that additional contractions between more than two operators have to be considered which are denoted as

$$\overline{\boldsymbol{A}_1 \boldsymbol{A}_2 \dots \boldsymbol{A}_l} \quad \text{with } 3 \leq l \leq n. \tag{3.39}$$

We refer to these types of contractions as l-tuple contractions, which are also complex number only if all operators to be contracted are adjacent.

Normal ordering in combination with contractions is evaluated in the same way as in the single-reference case, i.e.,

$$\begin{aligned} &\boldsymbol{\mathcal{N}}\{\boldsymbol{A}_1 \boldsymbol{A}_2 \dots \boldsymbol{A}_{i-1} \overline{\boldsymbol{A}_i} \boldsymbol{A}_{i+1} \dots \boldsymbol{A}_{j-1} \overline{\boldsymbol{A}_j} \boldsymbol{A}_{j+1} \dots \boldsymbol{A}_n\} \\ &= \operatorname{sgn}(\pi)\, \overline{\boldsymbol{A}_i \boldsymbol{A}_j}\, \boldsymbol{\mathcal{N}}\{\boldsymbol{A}_1 \boldsymbol{A}_2 \dots \boldsymbol{A}_{i-1} \boldsymbol{A}_{i+1} \dots \boldsymbol{A}_{j-1} \boldsymbol{A}_{j+1} \dots \boldsymbol{A}_n\}. \end{aligned} \tag{3.40}$$

The same applies for the l-tuple contractions with $l > 2$.

Finally, as a direct consequence of theorem 3.2 in combination with the property of the normal-ordering operator (3.36), we obtain a formula how to calculate the expectation value of a product of operators with respect to the reference state

$$\langle \Psi | \, \boldsymbol{A}_1 \boldsymbol{A}_2 \dots \boldsymbol{A}_n \, | \Psi \rangle = \sum_{\substack{\textbf{full contractions} \\ \text{w.r.t. } |\Psi\rangle}} \boldsymbol{\mathcal{N}}\{\boldsymbol{A}_1 \boldsymbol{A}_2 \dots \boldsymbol{A}_n\}. \tag{3.41}$$

A full contraction is understood as a product of several contractions where all operators within the normal-ordering operator are contracted among each other. However, in order to make use of this formula and of theorem 3.2 in general, we need to derive formulae for these contractions.

Formulae for the Contractions

Applying theorem 3.2 to a product of two operators $\boldsymbol{A}_1$ and $\boldsymbol{A}_2$ leads to

$$\boldsymbol{A}_1 \boldsymbol{A}_2 = \boldsymbol{\mathcal{N}}\{\boldsymbol{A}_1 \boldsymbol{A}_2\} + \overline{\boldsymbol{A}_1 \boldsymbol{A}_2}. \tag{3.42}$$

Taking the expectation value with respect to the reference state $|\Psi\rangle$ and making use of requirement (3.36), we obtain a formula for the 2-tuple contraction with respect to $|\Psi\rangle$

$$\overline{\boldsymbol{A}_1 \boldsymbol{A}_2} = \langle \Psi | \, \boldsymbol{A}_1 \boldsymbol{A}_2 \, | \Psi \rangle \, . \tag{3.43}$$

We define a *hole contraction* as follows

$$\overline{\boldsymbol{a}^p \boldsymbol{a}_q} = \langle \Psi | \, \boldsymbol{a}^p \boldsymbol{a}_q \, | \Psi \rangle =: \gamma_q^p, \tag{3.44}$$

which is identical to a *one-particle density matrix element* with respect to $|\Psi\rangle$, denoted as γ_q^p. A *particle contraction* is given by

$$\overline{\boldsymbol{a}_q \boldsymbol{a}^p} = \langle\Psi|\, \boldsymbol{a}_q \boldsymbol{a}^p \,|\Psi\rangle =: \bar{\gamma}_q^p, \tag{3.45}$$

which is equal to a *one-hole density matrix element* with respect to $|\Psi\rangle$, denoted as $\bar{\gamma}_q^p$. All other combinations given by

$$\overline{\boldsymbol{a}^p \boldsymbol{a}^q} = \overline{\boldsymbol{a}_p \boldsymbol{a}_q} = 0 \tag{3.46}$$

vanish since the reference state has a fixed particle number.

Since the number of possible contractions can be very large due to the l-tuple contractions for $l > 2$, we summarize their main properties (see [Geb13] for more details). For this case, the l-tuple contraction vanishes if the number of creation and annihilation operators differ from each other, e.g.,

$$\overline{\boldsymbol{a}^p \boldsymbol{a}^r \boldsymbol{a}_q} = \overline{\boldsymbol{a}^p \boldsymbol{a}_s \boldsymbol{a}_q} = 0. \tag{3.47}$$

This implies that we have only l-tuple contraction with even l. In contrast to the 2-tuple contraction, the l-tuple contraction with $l > 2$ is antisymmetric with respect to exchange of any two different operators within the contraction

$$\overline{\boldsymbol{A}_1 \boldsymbol{A}_2 \dots \boldsymbol{A}_i \dots \boldsymbol{A}_j \dots \boldsymbol{A}_l} = -\overline{\boldsymbol{A}_1 \boldsymbol{A}_2 \dots \boldsymbol{A}_j \dots \boldsymbol{A}_i \dots \boldsymbol{A}_l}. \tag{3.48}$$

Combining both statements, all non-trivial l-tuple contractions with $l > 2$ are given by

$$\overline{\boldsymbol{a}^p \boldsymbol{a}^r \boldsymbol{a}_s \boldsymbol{a}_q} = \gamma_{qs}^{pr} - \mathbb{A}(\gamma_q^p \gamma_s^r) =: \lambda_{qs}^{pr} \tag{3.49a}$$

$$\overline{\boldsymbol{a}^p \boldsymbol{a}^r \boldsymbol{a}^t \boldsymbol{a}_u \boldsymbol{a}_s \boldsymbol{a}_q} = \gamma_{qsu}^{prt} - \mathbb{A}(\gamma_q^p \lambda_{su}^{rt}) - \mathbb{A}(\gamma_q^p \gamma_s^r \gamma_u^t) =: \lambda_{qsu}^{prt} \tag{3.49b}$$

$$\vdots$$

$$\overline{\boldsymbol{a}^{p_1} \boldsymbol{a}^{p_2} \dots \boldsymbol{a}^{p_n} \boldsymbol{a}_{q_n} \dots \boldsymbol{a}_{q_2} \boldsymbol{a}_{q_1}} = \lambda_{q_1 q_2 \dots q_n}^{p_1 p_2 \dots p_n} \tag{3.49c}$$

that are equal to the corresponding *irreducible* n-body density matrix element $\lambda_{q_1 q_2 \dots q_n}^{p_1 p_2 \dots p_n}$ describing genuine n-particle correlations. As expected, the l-tuple contractions with $l > 2$ do vanish for a single-reference state since it does not contain correlations. Hence, we do recover the single-reference case fulfilling the second requirement in section 3.3.1.

Here, we use the so-called index antisymmetrizer as introduced in [KNM10] defined as follows

$$\mathbb{A}(h_{q_1 \dots q_m}^{p_1 \dots p_m} g_{s_1 \dots s_n}^{r_1 \dots r_n}) := \frac{1}{(m!n!)^2 \mathcal{F}_{\text{sym}}} \sum_{\pi \in \mathcal{S}_{m+n}} \sum_{\sigma \in \mathcal{S}_{m+n}} \operatorname{sgn}(\pi\sigma) h_{q_{\pi(1)} \dots q_{\pi(m)}}^{p_{\sigma(1)} \dots p_{\sigma(m)}} g_{s_{\pi(1)} \dots s_{\pi(n)}}^{r_{\sigma(1)} \dots r_{\sigma(n)}} \tag{3.50}$$

with the symmetry factor

$$\mathcal{F}_{\mathrm{sym}} \coloneqq \begin{cases} \frac{1}{2!} & \text{if } m = n \text{ and } g \equiv h \\ 1 & \text{else,} \end{cases} \tag{3.51}$$

where both matrix elements $h^{p_1 \dots p_m}_{q_1 \dots q_m}$ and $g^{r_1 \dots r_n}_{s_1 \dots s_n}$ are assumed to be antisymmetric with respect to exchange among the upper and lower indices. The prefactor ensures that each unique permutation form appears with coefficient unity, and $\mathcal{S}_{m+n}$ denotes the set of all permutations of $(1, 2, \dots, m+n)$. We give some examples for the action of the index antisymmetrizer

$$\mathbb{A}(h^p_q g^r_s) = + h^p_q g^r_s + h^r_s g^p_q - h^p_s g^r_q - h^r_q g^p_s \tag{3.52}$$

$$\mathbb{A}(h^p_q h^r_s) = + h^p_q h^r_s - h^p_s h^r_q \tag{3.53}$$

$$\begin{aligned} \mathbb{A}(h^p_q g^{rt}_{su}) = &+ h^p_q g^{rt}_{su} - h^p_s g^{rt}_{qu} - h^p_u g^{rt}_{sq} \\ &- h^r_q g^{pt}_{su} + h^r_s g^{pt}_{qu} - h^r_u g^{pt}_{qs} \\ &- h^t_q g^{pr}_{us} - h^t_s g^{pr}_{qu} + h^t_u g^{pr}_{qs} \end{aligned} \tag{3.54}$$

$$\begin{aligned} \mathbb{A}(h^{pr}_{qs} g^t_u) = &+ h^{rt}_{su} g^p_q - h^{rt}_{qu} g^p_s - h^{rt}_{sq} g^p_u \\ &- h^{pt}_{su} g^r_q + h^{pt}_{qu} g^r_s - h^{pt}_{qs} g^r_u \\ &- h^{pr}_{us} g^t_q - h^{pr}_{qu} g^t_s + h^{pr}_{qs} g^t_u \end{aligned} \tag{3.55}$$

$$= \mathbb{A}(g^p_q h^{rt}_{su}). \tag{3.56}$$

Its action on a product of more than two multiply-indexed objects can be easily generalized by adjusting the symmetry factor properly. We show the simplest example where the symmetry factor is 3!

$$\begin{aligned} \mathbb{A}(h^p_q h^r_s h^t_u) = &+ h^p_q h^r_s h^t_u + h^p_u h^r_q h^t_s + h^p_s h^r_u h^t_q \\ &- h^p_u h^r_s h^t_q - h^p_s h^r_q h^t_u - h^p_q h^r_u h^t_s. \end{aligned} \tag{3.57}$$

Applications of the Wick's Theorem

We introduce a compact notation for the action of the normal-ordering operator $\boldsymbol{\mathcal{N}}$ on the one-, two-, three- and n-body operators in V-NO

$$\tilde{\boldsymbol{a}}^p_q \coloneqq \boldsymbol{\mathcal{N}}\{\boldsymbol{a}^p_q\} \tag{3.58a}$$

$$\tilde{\boldsymbol{a}}^{pr}_{qs} \coloneqq \boldsymbol{\mathcal{N}}\{\boldsymbol{a}^{pr}_{qs}\} \tag{3.58b}$$

$$\tilde{\boldsymbol{a}}^{prt}_{qsu} \coloneqq \boldsymbol{\mathcal{N}}\{\boldsymbol{a}^{prt}_{qsu}\} \tag{3.58c}$$

$$\vdots$$

$$\tilde{\boldsymbol{a}}^{p_1 p_2 \dots p_n}_{q_1 q_2 \dots q_n} \coloneqq \boldsymbol{\mathcal{N}}\{\boldsymbol{a}^{p_1 p_2 \dots p_n}_{q_1 q_2 \dots q_n}\}. \tag{3.58d}$$

We refer to them as the one-, two-, three- and n-body operators in MR-NO. Since the normal-ordering operator is antisymmetric with respect to exchange of any two different operators comparable to (3.4), these operators are antisymmetric with respect to exchange among the

upper and lower indices, respectively

$$\tilde{\boldsymbol{a}}^{p_1\dots p_i\dots p_j\dots p_n}_{q_1\dots q_i\dots q_j\dots q_n} = -\tilde{\boldsymbol{a}}^{p_1\dots p_j\dots p_i\dots p_n}_{q_1\dots q_i\dots q_j\dots q_n} = -\tilde{\boldsymbol{a}}^{p_1\dots p_i\dots p_j\dots p_n}_{q_1\dots q_j\dots q_i\dots q_n}. \tag{3.59}$$

Note that exchanging an upper index with a lower one does not make any sense. With the aid of theorem 3.2, we can express any n-body operator in V-NO as a sum of the one-, two-, up to n-body operators in MR-NO yielding

$$\begin{aligned}
\boldsymbol{a}^p_q &= \tilde{\boldsymbol{a}}^p_q + \gamma^p_q && \text{(3.60a)}\\
\boldsymbol{a}^{pr}_{qs} &= \tilde{\boldsymbol{a}}^{pr}_{qs} + \mathbb{A}(\gamma^p_q \tilde{\boldsymbol{a}}^r_s) + \gamma^{pr}_{qs} && \text{(3.60b)}\\
\boldsymbol{a}^{prt}_{qsu} &= \tilde{\boldsymbol{a}}^{prt}_{qsu} + \mathbb{A}(\gamma^p_q \tilde{\boldsymbol{a}}^{rt}_{su}) + \mathbb{A}(\gamma^{pr}_{qs} \tilde{\boldsymbol{a}}^t_u) + \gamma^{prt}_{qsu} && \text{(3.60c)}\\
&\vdots \\
\boldsymbol{a}^{p_1\dots p_n}_{q_1\dots q_n} &= \tilde{\boldsymbol{a}}^{p_1\dots p_n}_{q_1\dots q_n} + \sum_{i=1}^{n-1} \mathbb{A}(\gamma^{p_1\dots p_i}_{q_1\dots q_i} \tilde{\boldsymbol{a}}^{p_{i+1}\dots p_n}_{q_{i+1}\dots q_n}) + \gamma^{p_1\dots p_n}_{q_1\dots q_n}. && \text{(3.60d)}
\end{aligned}$$

3.3.3. Vacuum and Reference-State Representation

We can now change from vacuum to reference-state representation and back. Suppose we have an operator $\boldsymbol{O}$ that is a sum of general zero-, one-, two- and three-body contributions, i.e., written in second-quantized *vacuum representation* (where all creators are to left of all annihilators)

$$\boldsymbol{O} \coloneqq A + \sum_{\substack{p\\q}} B^p_q \boldsymbol{a}^p_q + \frac{1}{4}\sum_{\substack{pr\\qs}} C^{pr}_{qs} \boldsymbol{a}^{pr}_{qs} + \frac{1}{36}\sum_{\substack{prt\\qsu}} D^{prt}_{qsu} \boldsymbol{a}^{prt}_{qsu}. \tag{3.61}$$

Inserting relations (3.60a)–(3.60c) for the vacuum normal-ordered operators, we obtain

$$\begin{aligned}
\boldsymbol{O} =& A + \sum_{\substack{p\\q}} B^p_q \tilde{\boldsymbol{a}}^p_q + \sum_{\substack{p\\q}} B^p_q \gamma^p_q + \frac{1}{4}\sum_{\substack{pr\\qs}} C^{pr}_{qs} \tilde{\boldsymbol{a}}^{pr}_{qs} + \frac{4}{4}\sum_{\substack{pr\\qs}} C^{pr}_{qs} \gamma^p_q \tilde{\boldsymbol{a}}^r_s + \frac{1}{4}\sum_{\substack{pr\\qs}} C^{pr}_{qs} \gamma^{pr}_{qs}\\
&+ \frac{1}{36}\sum_{\substack{prt\\qsu}} D^{prt}_{qsu} \tilde{\boldsymbol{a}}^{prt}_{qsu} + \frac{1}{4}\sum_{\substack{prt\\qsu}} D^{prt}_{qsu} \gamma^p_q \tilde{\boldsymbol{a}}^{rt}_{su} + \frac{1}{4}\sum_{\substack{prt\\qsu}} D^{prt}_{qsu} \gamma^{pr}_{qs} \tilde{\boldsymbol{a}}^t_u + \frac{1}{36}\sum_{\substack{prt\\qsu}} D^{prt}_{qsu} \gamma^{prt}_{qsu} && \text{(3.62)}\\
=& A + \sum_{\substack{p\\q}} B^p_q \gamma^p_q + \frac{1}{4}\sum_{\substack{pr\\qs}} C^{pr}_{qs} \gamma^{pr}_{qs} + \frac{1}{36}\sum_{\substack{prt\\qsu}} D^{prt}_{qsu} \gamma^{prt}_{qsu}\\
&+ \sum_{\substack{p\\q}} \left(B^p_q + \sum_{\substack{r\\s}} C^{pr}_{qs} \gamma^r_s + \frac{1}{4}\sum_{\substack{rt\\su}} D^{prt}_{qsu} \gamma^{rt}_{su} \right) \tilde{\boldsymbol{a}}^p_q\\
&+ \frac{1}{4}\sum_{\substack{pr\\qs}} \left(C^{pr}_{qs} + \sum_{\substack{t\\u}} D^{prt}_{qsu} \gamma^t_u \right) \tilde{\boldsymbol{a}}^{pr}_{qs}\\
&+ \frac{1}{36}\sum_{\substack{prt\\qsu}} D^{prt}_{qsu} \tilde{\boldsymbol{a}}^{prt}_{qsu}. && \text{(3.63)}
\end{aligned}$$

where we renamed summation indices and organized the terms according to their particle rank in the last step. We can clearly see that the operator $\boldsymbol{O}$ is now expressed as a linear combination of the reference-state normal ordered operators $\mathbf{1}, \tilde{\boldsymbol{a}}^p_q, \tilde{\boldsymbol{a}}^{pr}_{qs}$ and $\tilde{\boldsymbol{a}}^{prt}_{qsu}$:

$$\boldsymbol{O} = X + \sum_{\substack{p\\q}} Y^p_q \tilde{\boldsymbol{a}}^p_q + \frac{1}{4} \sum_{\substack{pr\\qs}} Z^{pr}_{qs} \tilde{\boldsymbol{a}}^{pr}_{qs} + \frac{1}{36} \sum_{\substack{prt\\qsu}} W^{prt}_{qsu} \tilde{\boldsymbol{a}}^{prt}_{qsu} \tag{3.64}$$

and

$$X = A + \sum_{\substack{p\\q}} B^p_q \gamma^p_q + \frac{1}{4} \sum_{\substack{pr\\qs}} C^{pr}_{qs} \gamma^{pr}_{qs} + \frac{1}{36} \sum_{\substack{prt\\qsu}} D^{prt}_{qsu} \gamma^{prt}_{qsu} = \langle \Psi | \boldsymbol{O} | \Psi \rangle \tag{3.65a}$$

$$Y^p_q = B^p_q + \sum_{\substack{r\\s}} C^{pr}_{qs} \gamma^r_s + \frac{1}{4} \sum_{\substack{rt\\su}} D^{prt}_{qsu} \gamma^{rt}_{su} \tag{3.65b}$$

$$Z^{pr}_{qs} = C^{pr}_{qs} + \sum_{\substack{t\\u}} D^{prt}_{qsu} \gamma^t_u \tag{3.65c}$$

$$W^{prt}_{qsu} = D^{prt}_{qsu} \tag{3.65d}$$

we obtain the matrix elements in reference-state representation as a function of the original matrix elements in vacuum representation. It is noteworthy that the n-body matrix element in vacuum representation contribute to all lower particle ranks in reference-state representation. This observation is crucial to systematically define approximations of a given operator that are the subject of section 3.3.4. Furthermore, the zero-body part in reference-state representation X is identical to the expectation value of the considered operator $\boldsymbol{O}$ with respect the reference state $|\Psi\rangle$, which can be calculated more efficiently using Slater-Condon rules [Sla29; Con30] instead of performing the summation with the density matrix elements. Therefore, we do not need the three-particle density matrix explicitly; the one- and two-body density matrices can be easily computed using standard many-body technology.

Finally, for many-body approaches that do not naturally use a normal-ordered formulation, we give the inverse transformation, i.e., from reference-state to vacuum representation

$$A = X - \sum_{\substack{p\\q}} Y^p_q \gamma^p_q - \frac{1}{4} \sum_{\substack{pr\\qs}} Z^{pr}_{qs} (\gamma^{pr}_{qs} - 4\gamma^p_q \gamma^r_s) - \frac{1}{36} \sum_{\substack{prt\\qsu}} W^{prt}_{qsu} (\gamma^{prt}_{qsu} - 18\gamma^p_q \gamma^{rt}_{su} + 36\gamma^p_q \gamma^r_s \gamma^t_u) \tag{3.66a}$$

$$B^p_q = Y^p_q - \sum_{\substack{r\\s}} Z^{pr}_{qs} \gamma^r_s - \frac{1}{4} \sum_{\substack{rt\\su}} W^{prt}_{qsu} (\gamma^{rt}_{su} - 4\gamma^p_q \gamma^r_s) \tag{3.66b}$$

$$C^{pr}_{qs} = Z^{pr}_{qs} - \sum_{\substack{t\\u}} W^{prt}_{qsu} \gamma^t_u \tag{3.66c}$$

$$D^{prt}_{qsu} = W^{prt}_{qsu}. \tag{3.66d}$$

3.3.4. Multi-Reference Two-Body Approximation for Three-Body Operators

In practical calculations including operators beyond the two-body rank is, both, a computational and conceptual challenge. Hence, an approximate but systematic treatment in many-body methods is desired. The relations (3.65) are a proper starting point to derive such an approximation.

For instance, a pure three-body operator in vacuum representation

$$\boldsymbol{V}^{(3)} := \frac{1}{36} \sum_{\substack{prt \\ qsu}} V^{prt}_{qsu} \boldsymbol{a}^{prt}_{qsu} \tag{3.67}$$

can be transformed into reference-state representation via (3.65) while setting $A = B^p_q = C^{pr}_{qs} = 0$ and $D^{prt}_{qsu} = V^{prt}_{qsu}$ yielding

$$\boldsymbol{V}^{(3)} = \frac{1}{36} \sum_{\substack{prt \\ qsu}} V^{prt}_{qsu} \gamma^{prt}_{qsu} + \frac{1}{4} \sum_{\substack{prt \\ qsu}} V^{prt}_{qsu} \gamma^{pr}_{qs} \tilde{\boldsymbol{a}}^{t}_{u} + \frac{1}{4} \sum_{\substack{prt \\ qsu}} V^{prt}_{qsu} \gamma^{p}_{q} \tilde{\boldsymbol{a}}^{rt}_{su} + \frac{1}{36} \sum_{\substack{prt \\ qsu}} V^{prt}_{qsu} \tilde{\boldsymbol{a}}^{prt}_{qsu}. \tag{3.68}$$

By neglecting the reference-state normal-ordered three-body contribution, we obtain the so-called *multi-reference normal-ordered two-body (MR-NO2B) approximation*

$$\boldsymbol{V}^{(3)}_{\text{MR-NO2B}} := \frac{1}{36} \sum_{\substack{prt \\ qsu}} V^{prt}_{qsu} \gamma^{prt}_{qsu} + \frac{1}{4} \sum_{\substack{prt \\ qsu}} V^{prt}_{qsu} \gamma^{pr}_{qs} \tilde{\boldsymbol{a}}^{t}_{u} + \frac{1}{4} \sum_{\substack{prt \\ qsu}} V^{prt}_{qsu} \gamma^{p}_{q} \tilde{\boldsymbol{a}}^{rt}_{su}. \tag{3.69}$$

This approximation has been shown to be sufficient to capture the main effects of the three-nucleon interactions used in this work for the description of ground-state and excitation energies of closed and open-shell nuclei [Rot+12; GCR16]. To transform this operator into vacuum representation we can make use of the relations (3.66) while setting $W^{prt}_{qsu} = 0$.

3.3.5. Generalized Wick's Theorem

Various many-body techniques like in-medium similarity renormalization group or coupled-cluster approach are formulated in terms of the normal-ordered operators. Typically, we face the challenge to calculate the product or commutators of reference-state normal-ordered operators. The aim is to express this product again in terms of the normal-ordered operators. For illustration purposes, we consider the simplest non-trivial case, where a product of two one-body operators in MR-NO, $\boldsymbol{\mathcal{N}}\{\boldsymbol{A}_1\boldsymbol{A}_2\}$ and $\boldsymbol{\mathcal{N}}\{\boldsymbol{B}_1\boldsymbol{B}_2\}$, is given[3]. By means of (3.42), we can simplify this expression to

$$\boldsymbol{\mathcal{N}}\{\boldsymbol{A}_1\boldsymbol{A}_2\} \cdot \boldsymbol{\mathcal{N}}\{\boldsymbol{B}_1\boldsymbol{B}_2\} \tag{3.70}$$

$$= \left(\boldsymbol{A}_1\boldsymbol{A}_2 - \overline{\boldsymbol{A}_1\boldsymbol{A}_2}\right)\left(\boldsymbol{B}_1\boldsymbol{B}_2 - \overline{\boldsymbol{B}_1\boldsymbol{B}_2}\right) \tag{3.71}$$

$$= \boldsymbol{A}_1\boldsymbol{A}_2\boldsymbol{B}_1\boldsymbol{B}_2 - \boldsymbol{A}_1\boldsymbol{A}_2\overline{\boldsymbol{B}_1\boldsymbol{B}_2} - \overline{\boldsymbol{A}_1\boldsymbol{A}_2}\boldsymbol{B}_1\boldsymbol{B}_2 + \overline{\boldsymbol{A}_1\boldsymbol{A}_2}\ \overline{\boldsymbol{B}_1\boldsymbol{B}_2} \tag{3.72}$$

[3]The operators $\boldsymbol{B}_1$ and $\boldsymbol{B}_2$ has to be from the same set of second quantized operators as the $\boldsymbol{A}_i$.

$$
\begin{aligned}
&= \boldsymbol{A}_1\boldsymbol{A}_2\boldsymbol{B}_1\boldsymbol{B}_2 \\
&\quad - \left(\boldsymbol{\mathcal{N}}\{\boldsymbol{A}_1\boldsymbol{A}_2\} + \overline{\boldsymbol{A}_1\boldsymbol{A}_2}\right)\overline{\boldsymbol{B}_1\boldsymbol{B}_2} - \overline{\boldsymbol{A}_1\boldsymbol{A}_2}\left(\boldsymbol{\mathcal{N}}\{\boldsymbol{B}_1\boldsymbol{B}_2\} + \overline{\boldsymbol{B}_1\boldsymbol{B}_2}\right) + \overline{\boldsymbol{A}_1\boldsymbol{A}_2}\;\overline{\boldsymbol{B}_1\boldsymbol{B}_2}. \qquad (3.73)
\end{aligned}
$$

Furthermore, the first term can be expressed as sum of the normal-ordered operators with the aid of theorem 3.2 yielding

$$
\begin{aligned}
\boldsymbol{A}_1\boldsymbol{A}_2\boldsymbol{B}_1\boldsymbol{B}_2 = \boldsymbol{\mathcal{N}}\{&\boldsymbol{A}_1\boldsymbol{A}_2\boldsymbol{B}_1\boldsymbol{B}_2\} \\
&+ \overline{\boldsymbol{A}_1\boldsymbol{A}_2}\boldsymbol{\mathcal{N}}\{\boldsymbol{B}_1\boldsymbol{B}_2\} - \overline{\boldsymbol{A}_1\boldsymbol{B}_1}\boldsymbol{\mathcal{N}}\{\boldsymbol{A}_2\boldsymbol{B}_2\} + \overline{\boldsymbol{A}_1\boldsymbol{B}_2}\boldsymbol{\mathcal{N}}\{\boldsymbol{A}_2\boldsymbol{B}_1\} \\
&+ \overline{\boldsymbol{A}_2\boldsymbol{B}_1}\boldsymbol{\mathcal{N}}\{\boldsymbol{A}_1\boldsymbol{B}_2\} - \overline{\boldsymbol{A}_2\boldsymbol{B}_2}\boldsymbol{\mathcal{N}}\{\boldsymbol{A}_1\boldsymbol{B}_1\} + \overline{\boldsymbol{B}_1\boldsymbol{B}_2}\boldsymbol{\mathcal{N}}\{\boldsymbol{A}_1\boldsymbol{A}_2\} \\
&+ \overline{\boldsymbol{A}_1\boldsymbol{A}_2}\;\overline{\boldsymbol{B}_1\boldsymbol{B}_2} - \overline{\boldsymbol{A}_1\boldsymbol{B}_1}\;\overline{\boldsymbol{A}_2\boldsymbol{B}_2} + \overline{\boldsymbol{A}_1\boldsymbol{B}_2}\;\overline{\boldsymbol{A}_2\boldsymbol{B}_1} + \overline{\boldsymbol{A}_1\boldsymbol{A}_2\boldsymbol{B}_1\boldsymbol{B}_2}. \qquad (3.74)
\end{aligned}
$$

Hence, in total we obtain for the product of the given normal-ordered operators

$$
\begin{aligned}
&\boldsymbol{\mathcal{N}}\{\boldsymbol{A}_1\boldsymbol{A}_2\}\cdot\boldsymbol{\mathcal{N}}\{\boldsymbol{B}_1\boldsymbol{B}_2\} \\
&= \boldsymbol{\mathcal{N}}\{\boldsymbol{A}_1\boldsymbol{A}_2\boldsymbol{B}_1\boldsymbol{B}_2\} \\
&\quad - \overline{\boldsymbol{A}_1\boldsymbol{B}_1}\boldsymbol{\mathcal{N}}\{\boldsymbol{A}_2\boldsymbol{B}_2\} + \overline{\boldsymbol{A}_1\boldsymbol{B}_2}\boldsymbol{\mathcal{N}}\{\boldsymbol{A}_2\boldsymbol{B}_1\} + \overline{\boldsymbol{A}_2\boldsymbol{B}_1}\boldsymbol{\mathcal{N}}\{\boldsymbol{A}_1\boldsymbol{B}_2\} - \overline{\boldsymbol{A}_2\boldsymbol{B}_2}\boldsymbol{\mathcal{N}}\{\boldsymbol{A}_1\boldsymbol{B}_1\} \\
&\quad - \overline{\boldsymbol{A}_1\boldsymbol{B}_1}\;\overline{\boldsymbol{A}_2\boldsymbol{B}_2} + \overline{\boldsymbol{A}_1\boldsymbol{B}_2}\;\overline{\boldsymbol{A}_2\boldsymbol{B}_1} + \overline{\boldsymbol{A}_1\boldsymbol{A}_2\boldsymbol{B}_1\boldsymbol{B}_2}. \qquad (3.75)
\end{aligned}
$$

Taking a closer look, we observe that contractions including only $\boldsymbol{A}_1$ and $\boldsymbol{A}_2$ or only $\boldsymbol{B}_1$ and $\boldsymbol{B}_2$, called *self contractions*, do not appear anymore. Putting it in another way, we need only to consider contractions containing at least one $\boldsymbol{A}_i$ and at least one $\boldsymbol{B}_j$ operators. These kind of contractions are called *external contractions*.

This observation forms the basis of the *generalized Wick's theorem* with respect to a given reference state which generalizes this observation to any product of normal-ordered operators, and reads as follows:

Theorem 3.3. *A product of reference-state normal-ordered operators* $\boldsymbol{\mathcal{N}}\{\boldsymbol{A}_1, \boldsymbol{A}_2, \ldots, \boldsymbol{A}_n\}$ *and* $\boldsymbol{\mathcal{N}}\{\boldsymbol{B}_1, \boldsymbol{B}_2, \ldots, \boldsymbol{B}_m\}$ *can be expressed as a sum of operators in reference-state normal-ordered plus all external normal-ordered contractions [KM97; KNM10], i.e.,*

$$
\begin{aligned}
&\boldsymbol{\mathcal{N}}\{\boldsymbol{A}_1\boldsymbol{A}_2\ldots\boldsymbol{A}_n\}\cdot\boldsymbol{\mathcal{N}}\{\boldsymbol{B}_1\boldsymbol{B}_2\ldots\boldsymbol{B}_m\} \\
&= \boldsymbol{\mathcal{N}}\{\boldsymbol{A}_1\boldsymbol{A}_2\ldots\boldsymbol{A}_n\boldsymbol{B}_1\boldsymbol{B}_2\ldots\boldsymbol{B}_m\} + \sum_{\substack{\textbf{external}\\ \text{contractions}}} \boldsymbol{\mathcal{N}}\{\boldsymbol{A}_1\boldsymbol{A}_2\ldots\boldsymbol{A}_n\boldsymbol{B}_1\boldsymbol{B}_2\ldots\boldsymbol{B}_m\}. \qquad (3.76)
\end{aligned}
$$

Here, external contractions always involve at least one of the $\boldsymbol{A}_i$ *and one of* $\boldsymbol{B}_j$ *operators.*

For illustration purposes, we consider the product of two one-body operators in SR-NO yielding

$$
\begin{aligned}
\tilde{\boldsymbol{a}}^p_q\tilde{\boldsymbol{a}}^r_s &= \boldsymbol{\mathcal{N}}\{\boldsymbol{a}^p\boldsymbol{a}_q\}\cdot\boldsymbol{\mathcal{N}}\{\boldsymbol{a}^r\boldsymbol{a}_s\} && (3.77)\\
&= \boldsymbol{\mathcal{N}}\{\boldsymbol{a}^{pr}_{qs}\} - \overline{\boldsymbol{a}^p\boldsymbol{a}_s}\boldsymbol{\mathcal{N}}\{\boldsymbol{a}^r_q\} + \overline{\boldsymbol{a}_q\boldsymbol{a}^r}\boldsymbol{\mathcal{N}}\{\boldsymbol{a}^p_s\} + \overline{\boldsymbol{a}^p\boldsymbol{a}_s}\;\overline{\boldsymbol{a}_q\boldsymbol{a}^r} + \overline{\boldsymbol{a}^p\boldsymbol{a}_q\boldsymbol{a}^r\boldsymbol{a}_s} && (3.78)\\
&= \tilde{\boldsymbol{a}}^{pr}_{qs} - \gamma^p_s\tilde{\boldsymbol{a}}^r_q + \bar{\gamma}^r_q\tilde{\boldsymbol{a}}^p_s + \gamma^p_s\bar{\gamma}^r_q + \lambda^{pr}_{qs}. && (3.79)
\end{aligned}
$$

We note that the expectation value of a product of normal-ordered operators with respect to the reference state does not vanish in general, but it is equal to the fully-contracted terms, i.e., for the above example, we obtain

$$\langle\Psi|\tilde{\boldsymbol{a}}^p_q\tilde{\boldsymbol{a}}^r_s|\Psi\rangle = \gamma^p_s\bar{\gamma}^r_q + \lambda^{pr}_{qs} \tag{3.80}$$

Based on this results for the products of normal-ordered operators, we can calculate their commutators, e.g.,

$$\begin{aligned}
[\tilde{\boldsymbol{a}}^p_q, \tilde{\boldsymbol{a}}^r_s] =& \tilde{\boldsymbol{a}}^p_q\tilde{\boldsymbol{a}}^r_s - \tilde{\boldsymbol{a}}^r_s\tilde{\boldsymbol{a}}^p_q && (3.81)\\
=& \left(\tilde{\boldsymbol{a}}^{pr}_{qs} - \gamma^p_s\tilde{\boldsymbol{a}}^r_q + \bar{\gamma}^r_q\tilde{\boldsymbol{a}}^p_s + \gamma^p_s\bar{\gamma}^r_q + \lambda^{pr}_{qs}\right) - \left(\tilde{\boldsymbol{a}}^{rp}_{sq} - \gamma^r_q\tilde{\boldsymbol{a}}^p_s + \bar{\gamma}^p_s\tilde{\boldsymbol{a}}^r_q + \gamma^r_q\bar{\gamma}^p_s + \lambda^{rp}_{sq}\right) && (3.82)\\
=& 0 + (\bar{\gamma}^r_q + \gamma^r_q)\tilde{\boldsymbol{a}}^p_s - (\bar{\gamma}^p_s + \gamma^p_s)\tilde{\boldsymbol{a}}^r_q + \gamma^p_s\bar{\gamma}^r_q - \gamma^r_q\bar{\gamma}^p_s + 0 && (3.83)\\
=& \delta^r_q\tilde{\boldsymbol{a}}^p_s - \delta^p_s\tilde{\boldsymbol{a}}^r_q + \delta^r_q\gamma^p_s - \delta^p_s\gamma^r_q && (3.84)
\end{aligned}$$

where the normal-ordered two-body operators cancel each others. Further examples relevant for this work can be found in appendix A. We summarize the most important ones in the next section.

3.3.6. Relevant Commutators

In this section, we summarize the major results from appendix A for the derivation of commutators between the operators relevant for this work using theorem 3.3. Let us define the operators

$$\boldsymbol{A}^{(1)} \coloneqq \sum_{\substack{p\\q}} A^p_q\tilde{\boldsymbol{a}}^p_q\,, \qquad \boldsymbol{C}^{(2)} \coloneqq \frac{1}{4}\sum_{\substack{pr\\qs}} C^{pr}_{qs}\tilde{\boldsymbol{a}}^{pr}_{qs} \tag{3.85a}$$

$$\boldsymbol{B}^{(1)} \coloneqq \sum_{\substack{r\\s}} B^r_s\tilde{\boldsymbol{a}}^r_s\,, \qquad \boldsymbol{D}^{(2)} \coloneqq \frac{1}{4}\sum_{\substack{tv\\uw}} D^{tv}_{uw}\tilde{\boldsymbol{a}}^{tv}_{uw} \tag{3.85b}$$

that do not necessarily have to be Hermitian or anti-Hermitian. The matrix elements of the two-body operators C^{pr}_{qs} and D^{pr}_{qs} are assumed to be antisymmetric with respect to exchange among the upper and lower indices, respectively, i.e.,

$$C^{pr}_{qs} = -C^{rp}_{qs} = -C^{pr}_{sq} = +C^{rp}_{sq} \tag{3.86}$$

$$D^{pr}_{qs} = -D^{rp}_{qs} = -D^{pr}_{sq} = +D^{rp}_{sq}. \tag{3.87}$$

In (3.84), we have already observed that the commutator of two normal-ordered one-body operators does not contain a two-body part anymore. We generalize this observation to a commutator of any normal-ordered operators.

Proposition 3.1. *The commutator of a normal-ordered n-body and a normal-ordered m-body*

operator has a maximum rank of $n+m-1$*, i.e.,*

$$\left(\left[\tilde{\boldsymbol{a}}^{p_1p_2\ldots p_n}_{q_1q_2\ldots q_n}, \tilde{\boldsymbol{a}}^{r_1r_2\ldots r_m}_{s_1s_2\ldots s_m}\right]\right)^{[n+m]} = 0. \tag{3.88}$$

Proof. We need to show that the $n+m$-body part of the considered commutator vanishes

$$\begin{aligned}
\left(\left[\tilde{\boldsymbol{a}}^{p_1p_2\ldots p_n}_{q_1q_2\ldots q_n}, \tilde{\boldsymbol{a}}^{r_1r_2\ldots r_m}_{s_1s_2\ldots s_m}\right]\right)^{[n+m]} =& \left(\tilde{\boldsymbol{a}}^{p_1p_2\ldots p_n}_{q_1q_2\ldots q_n}\tilde{\boldsymbol{a}}^{r_1r_2\ldots r_m}_{s_1s_2\ldots s_m}\right)^{[n+m]} - \left(\tilde{\boldsymbol{a}}^{r_1r_2\ldots r_m}_{s_1s_2\ldots s_m}\tilde{\boldsymbol{a}}^{p_1p_2\ldots p_n}_{q_1q_2\ldots q_n}\right)^{[n+m]} && (3.89)\\
=& \tilde{\boldsymbol{a}}^{p_1p_2\ldots p_nr_1r_2\ldots r_m}_{q_1q_2\ldots q_ns_1s_2\ldots s_m} - \tilde{\boldsymbol{a}}^{r_1r_2\ldots r_mp_1p_2\ldots p_n}_{s_1s_2\ldots s_mq_1q_2\ldots q_n} && (3.90)\\
=& \tilde{\boldsymbol{a}}^{p_1p_2\ldots p_nr_1r_2\ldots r_m}_{q_1q_2\ldots q_ns_1s_2\ldots s_m} - (-)^{2(m\cdot n)}\tilde{\boldsymbol{a}}^{p_1p_2\ldots p_nr_1r_2\ldots r_m}_{q_1q_2\ldots q_ns_1s_2\ldots s_m} && (3.91)\\
=& 0, && (3.92)
\end{aligned}$$

where we made use of the antisymmetry with respect to exchange among the upper and lower indices of the normal-ordered operator, respectively. □

In accordance with the previous statement, we obtain

$$\begin{aligned}
[\boldsymbol{A}^{(1)}, \boldsymbol{B}^{(1)}] =& \sum_{\substack{p\\q}}\left(\sum_r (A^p_r B^r_q - B^p_r A^r_q)\right)\tilde{\boldsymbol{a}}^p_q\\
&+ \sum_{\substack{pr\\q}}(A^p_r B^r_q - B^p_r A^r_q)\gamma^p_q && (3.93a)\\
[\boldsymbol{C}^{(2)}, \boldsymbol{A}^{(1)}] =& \frac{1}{4}\sum_{\substack{pr\\qs}}\left(\sum_t (C^{pr}_{ts}A^t_q + C^{pr}_{qt}A^t_s - C^{tr}_{qs}A^p_t - C^{pt}_{qs}A^r_t)\right)\tilde{\boldsymbol{a}}^{pr}_{qs}\\
&+ \sum_{\substack{p\\q}}\left(\sum_{\substack{rt\\su}} C^{pr}_{qs}A^t_u(\delta^t_s\gamma^r_u - \gamma^t_s\delta^r_u)\right)\tilde{\boldsymbol{a}}^p_q\\
&+ \frac{1}{2}\sum_{\substack{prt\\qs}}(C^{pr}_{ts}A^t_q - C^{tr}_{qs}A^p_t)\lambda^{pr}_{qs} && (3.93b)\\
[\boldsymbol{A}^{(1)}, \boldsymbol{C}^{(2)}] =& -\left[\boldsymbol{C}^{(2)}, \boldsymbol{A}^{(1)}\right]\\
=& \frac{1}{4}\sum_{\substack{pr\\qs}}\left(\sum_t (-C^{pr}_{ts}A^t_q - C^{pr}_{qt}A^t_s + C^{tr}_{qs}A^p_t + C^{pt}_{qs}A^r_t)\right)\tilde{\boldsymbol{a}}^{pr}_{qs}\\
&+ \sum_{\substack{p\\q}}\left(\sum_{\substack{rt\\su}} C^{pr}_{qs}A^t_u(-\delta^t_s\gamma^r_u + \gamma^t_s\delta^r_u)\right)\tilde{\boldsymbol{a}}^p_q\\
&+ \frac{1}{2}\sum_{\substack{prt\\qs}}(-C^{pr}_{ts}A^t_q + C^{tr}_{qs}A^p_t)\lambda^{pr}_{qs} && (3.93c)
\end{aligned}$$

For the commutator between two two-body operators, we obtain

$$
\begin{aligned}
[\boldsymbol{C}^{(2)}, \boldsymbol{D}^{(2)}] =& \frac{1}{4} \sum_{\substack{prtv \\ qsuw}} G^{prtv}_{qsuw} \delta^t_q \tilde{\boldsymbol{a}}^{prv}_{usw} \\
&+ \frac{1}{4} \sum_{\substack{pr \\ qs}} \left(\frac{1}{2} \sum_{\substack{tv \\ uw}} G^{prtv}_{uwqs} (\delta^t_u \delta^v_w - 2\delta^t_u \gamma^v_w) \right) \tilde{\boldsymbol{a}}^{pr}_{qs} \\
&+ \frac{1}{4} \sum_{\substack{pr \\ qs}} \left(\sum_{\substack{tv \\ uw}} G^{ptvr}_{quws} (\gamma^t_w \delta^v_u - \gamma^v_u \delta^t_w) \right) \tilde{\boldsymbol{a}}^{pr}_{qs} \\
&+ \frac{1}{4} \sum_{\substack{pr \\ qs}} \left((-) \sum_{\substack{tv \\ uw}} G^{ptvr}_{suwq} (\gamma^t_w \delta^v_u - \gamma^v_u \delta^t_w) \right) \tilde{\boldsymbol{a}}^{pr}_{qs} \\
&+ \sum_{\substack{p \\ q}} \left(\frac{1}{2} \sum_{\substack{rtv \\ suw}} G^{prtv}_{usqw} (\bar{\gamma}^t_u \bar{\gamma}^v_s \gamma^r_w + \gamma^t_u \gamma^v_s \bar{\gamma}^r_w) \right) \tilde{\boldsymbol{a}}^{p}_{q} \\
&+ \sum_{\substack{p \\ q}} \left(\sum_{\substack{rtv \\ suw}} (\frac{1}{4} G^{ptrv}_{swqu} + G^{prtv}_{usqw} + \frac{1}{2} G^{prtv}_{qusw} - \frac{1}{2} G^{ptrv}_{qsuw}) \delta^t_u \lambda^{rv}_{sw} \right) \tilde{\boldsymbol{a}}^{p}_{q} \\
&+ \frac{1}{4} \sum_{\substack{prtv \\ qsuw}} G^{prtv}_{qsuw} \gamma^p_u \gamma^r_w \bar{\gamma}^t_q \bar{\gamma}^v_s \\
&+ \sum_{\substack{prtv \\ qsuw}} G^{ptrv}_{qusw} \gamma^t_w \bar{\gamma}^v_u \lambda^{pr}_{qs} \\
&+ \frac{1}{8} \sum_{\substack{prtv \\ qsuw}} G^{prtv}_{uwqs} (\bar{\gamma}^t_u \bar{\gamma}^v_w - \gamma^t_u \gamma^v_w) \lambda^{pr}_{qs} \\
&+ \frac{1}{4} \sum_{\substack{prtv \\ qsuw}} G^{prtv}_{qsuw} \delta^v_s \lambda^{ptr}_{quw}.
\end{aligned}
\tag{3.93d}
$$

Here, we used the abbreviation $G^{prtv}_{qsuw} := C^{pr}_{qs} D^{tv}_{uw} - D^{pr}_{qs} C^{tv}_{uw}$. A detailed derivation of these commutators can be found in appendix A.2. In contrast to the single-reference case, the commutator between two operators with different particle rank, e.g., one- and two-body operators, still contains a zero-body part, which is a peculiarity of the multi-reference case. This can be verified easily since the zero-body part of the commutator of the one- and two-body operators (3.93b) and (3.93c) is governed only by the irreducible two-body density matrix, which vanishes for the single-reference case.

II.

In-Medium No-Core Shell Model

Introduction to Part II

One of the most dynamic areas in nuclear structure theory today is the development of *ab initio* many-body methods that solve the stationary Schrödinger equation given by

$$\boldsymbol{H}\,|\Psi_n\rangle = E_n\,|\Psi_n\rangle\,, \tag{3.94}$$

where E_n denotes the eigenvalue associated to the eigenstate $|\Psi_n\rangle$ of the Hamiltonian $\boldsymbol{H}$. These *ab initio* many-body methods are crucial for modern nuclear structure theory, and provide a connection between QCD-based interactions and nuclear-structure observables. Furthermore, they establish ideal benchmark tool for approximate methods.

Ground states, low-lying excitations and spectroscopic observables are of essential importance. Traditionally, nuclear spectroscopy is the domain of shell-model-type approaches, both the valence-space shell model [Cau+05] and the *ab initio* no-core shell model (NCSM) [Nav+07; Bro01; BNV13]. These methods solve a large-scale eigenvalue problem of the Hamiltonian in a truncated model space, and address ground and excited states on equal footing, but they are limited by the basis dimension [Var+09].

In the last decade, other methods have been formulated that face the many-body problem with a different ansatz, among them the coupled-cluster (CC) approach and the in-medium similarity renormalization group (IM-SRG). These methods aim a decoupling of a given reference state from its excitations via a similarity transformation. Here, the reference state represents the ground state. This concept of decoupling is extremely powerful and complementary to a direct NCSM-type diagonalization, which solve the eigenvalue problem directly. Generally, CC and IM-SRG have a much polynomial scaling with particle number A. Unfortunately, their basic formulation is limited to ground states. Hence, their complementarity proposes that a combination of both formalism, many-body decoupling and direct diagonalization, could be advantageous. First steps along these lines are the effective interactions for the valence-space shell model extracted from CC and IM-SRG calculations presented recently [Bog+14; Str+16; Jan+14; Str+17; Jan+16].

This part is organized as follows: We discuss the multi-reference IM-SRG in detail in chapter 4. Furthermore, we recap the main ideas of NCSM in chapter 5. Subsequently, we merge them into a new *ab initio* many-body tool, called in-medium no-core shell model (IM-NCSM), to universally address ground and excited states of closed and open-shell nuclei up to medium masses, presented in chapter 6.

Chapter 4

Multi-Reference In-Medium Similarity Renormalization Group

The *multi-reference* in-medium similarity renormalization group (IM-SRG) is a very powerful and well established *ab initio* many-body method, especially in the medium-mass sector [Her+16; Her17]. It is based on the idea of a unitary transformation of the Hamiltonian, which preserves the spectrum, that decouples a given reference state $|\Psi\rangle$ from all states that are orthogonal to it. In its simplest version it is designed to extract ground-state observables.

This chapter is organized as follows: The basic concept of the multi-reference IM-SRG is described in detail in section 4.1. We derive the system of multi-reference IM-SRG flow equations in m-scheme, which are computationally very inefficient, in section 4.2. To improve on this, we exploit symmetries of the Hamiltonian and perform total-angular-momentum coupling (J-coupling) of these equations assuming scalar density matrices, which is given only if the reference state has vanishing total angular momentum (section 4.3). A more detailed explanation and a proof of this statement can be found in appendix C.3. Consequently, this assumption limits the investigation of this work to even nuclei and scalar operators. For a very efficient implementation of the J-coupled flow equations, we will rewrite them as matrix products to make use of highly-optimized implementations of the *Basic Linear Algebra Subprograms* (section 4.4). Based on the so-called generalized A-particle A-hole basis analyzed in detail in section 4.5, we will motivate the construction of the generators in section 4.6. Finally, we describe how to extract other observables beside ground-state energies in the framework of the multi-reference IM-SRG (section 4.7). Since we are limited to scalar operators, as aforementioned, we will focus on radii and electric monopole transitions.

4.1. Basic Concepts

The starting point is a Hamiltonian that typically contains operators up to three-body rank

$$\boldsymbol{H} = h + \sum_{\substack{p\\q}} h_q^p \boldsymbol{a}_q^p + \frac{1}{4} \sum_{\substack{pr\\qs}} h_{qs}^{pr} \boldsymbol{a}_{qs}^{pr} + \frac{1}{36} \sum_{\substack{prt\\qsu}} h_{qsu}^{prt} \boldsymbol{a}_{qsu}^{prt}, \tag{4.1}$$

where $\boldsymbol{a}_q^p$, $\boldsymbol{a}_{qs}^{pr}$ and $\boldsymbol{a}_{qsu}^{prt}$ denote the one-, two- and three-body operators (2.1), and h, h_q^p, h_{qs}^{pr} and h_{qsu}^{prt} are the zero-, one-, two- and three-body matrix elements of the Hamiltonian. In our calculations, we use the free-space SRG-evolved chiral Hamiltonian (2.2) which contains the intrinsic kinetic energy operator, nucleon-nucleon (NN) and three-nucleon (3N) interactions. We write this Hamiltonian in reference-state representation with respect to $|\Psi\rangle$ via normal ordering as given in (3.65)

$$\boldsymbol{H} = E + \sum_{\substack{p\\q}} f_q^p \tilde{\boldsymbol{a}}_q^p + \frac{1}{4} \sum_{\substack{pr\\qs}} \Gamma_{qs}^{pr} \tilde{\boldsymbol{a}}_{qs}^{pr} + \frac{1}{36} \sum_{\substack{prt\\qsu}} W_{qsu}^{prt} \tilde{\boldsymbol{a}}_{qsu}^{prt} \tag{4.2a}$$

with

$$E \coloneqq \langle\Psi| \boldsymbol{H} |\Psi\rangle = h + \sum_{\substack{p\\q}} h_q^p \gamma_q^p + \frac{1}{4} \sum_{\substack{pr\\qs}} h_{qs}^{pr} \gamma_{qs}^{pr} + \frac{1}{36} \sum_{\substack{prt\\qsu}} h_{qsu}^{prt} \gamma_{qsu}^{prt} \tag{4.2b}$$

$$f_q^p \coloneqq h_q^p + \sum_{\substack{r\\s}} h_{qs}^{pr} \gamma_s^r + \frac{1}{4} \sum_{\substack{rt\\su}} h_{qsu}^{prt} \gamma_{su}^{rt} \tag{4.2c}$$

$$\Gamma_{qs}^{pr} \coloneqq h_{qs}^{pr} + \sum_{\substack{t\\u}} h_{qsu}^{prt} \gamma_u^t \tag{4.2d}$$

$$W_{qsu}^{prt} \coloneqq h_{qsu}^{prt}. \tag{4.2e}$$

Here, $|\Psi\rangle$ denotes the reference state, which will be decoupled from the rest of the Hilbert space. Remarkably, the zero-, one- and two-body parts of the Hamiltonian in reference-state representation still contain information about the initial 3N interaction. We make use of the MR-NO2B approximation and omit the residual normal-ordered three-body contribution as explained in section 3.3.4. This approximation has been shown to be sufficient to capture the main effects of the 3N interactions used in this work for the description of ground-state and excitation energies of closed and open-shell nuclei [Rot+12; GCR16].

In contrast to the free-space SRG introduced in chapter 1, the fundamental goal here is to solve the many-body problem, which is an eigenvalue problem of the Hamiltonian. This is achieved via a *continuous unitary transformation* [Weg94]

$$\boldsymbol{H}(s) \coloneqq \boldsymbol{U}^\dagger(s) \boldsymbol{H}(0) \boldsymbol{U}(s), \tag{4.3}$$

which is parameterized by the real-valued *flow parameter* $s \geq 0$, and with the initial condition $\boldsymbol{H}(0) \coloneqq \boldsymbol{H}$. The main goal is to map the reference state on an eigenstate of the transformed

Hamiltonian with an associated energy $E(\infty)$ via the unitary transformation, i.e.,

$$\boldsymbol{H}(\infty)\,|\Psi\rangle = E(\infty)\,|\Psi\rangle\,. \tag{4.4}$$

Consequently, the reference state is decoupled from all other states orthogonal to it or decoupled from all excitations on top of it. The central idea is to suppress the so-called off-diagonal matrix elements of the Hamiltonian that couple the reference to other states orthogonal to it. The strategy will be explained in detail in section 4.6.

The major advantage of a unitary transformation is that the spectrum of the operator that is transformed is preserved. Additionally, the transformed operator remains Hermitian if the initial operator is Hermitian. Taking the derivative of (4.3) with respect to the flow parameter s, we obtain the so-called *operator flow equation*

$$\frac{\mathrm{d}\boldsymbol{H}(s)}{\mathrm{d}s} = [\boldsymbol{\eta}(s), \boldsymbol{H}(s)] \tag{4.5}$$

which is mathematically a first-order operator differential equation with a dynamical anti-Hermitian *generator* related to the unitary transformation via

$$\boldsymbol{\eta}(s) \coloneqq \frac{\mathrm{d}\boldsymbol{U}^\dagger(s)}{\mathrm{d}s}\boldsymbol{U}(s) = -\boldsymbol{\eta}^\dagger(s). \tag{4.6}$$

The exact steps how to derive the operator flow equation (4.5) starting from a general unitary transformation (4.3) can be found in chapter 1.

Since a commutator of n- and m-body operators is composed of operators up to the $(n+m-1)$-body level according to proposition 3.1, the commutator structure of the flow equation induces three- and higher-body contributions after an infinitesimal step even if we start with only two-body operators. After a finite evolution in the flow parameter s, the induced contribution can include up to A-body operators. To deal with this problem, we define states with respect to the reference state, this is where the normal-ordering procedure comes into play because all terms beyond two-body operators are too expensive to handle. If the reference state is a reasonable approximation of the true eigenstate of the Hamiltonian, which is unknown, then many-body terms are less important. This fact is encoded in the term "In-Medium" in the word IM-SRG.

Thus, we truncate $\boldsymbol{\eta}(s)$, $\boldsymbol{H}(s)$ and their commutator at a given particle rank $k \leq A$ in normal-ordered form, leading to the so-called multi-reference IM-SRG(k). In practical calculations, we stick to the multi-reference IM-SRG(2) truncation, in which the transformed Hamiltonian reads

$$\boldsymbol{H}(s) =: E(s) + \sum_{\substack{p\\q}} f_q^p(s)\tilde{\boldsymbol{a}}_q^p + \frac{1}{4}\sum_{\substack{pr\\qs}} \Gamma_{qs}^{pr}(s)\tilde{\boldsymbol{a}}_{qs}^{pr} \tag{4.7}$$

$$=: \boldsymbol{H}^{(0)}(s) + \boldsymbol{H}^{(1)}(s) + \boldsymbol{H}^{(2)}(s), \tag{4.8}$$

where the flow-parameter dependence is only given in the matrix elements of the Hamiltonian.

Pay attention to the ambiguity that the symbol s represents an index and the flow parameter written within the brackets. Consequently, the left-hand side of the operator flow equation is

$$\frac{\mathrm{d}\boldsymbol{H}(s)}{\mathrm{d}s} = \frac{\mathrm{d}E(s)}{\mathrm{d}s} + \sum_{\substack{p\\q}} \frac{\mathrm{d}f_q^p(s)}{\mathrm{d}s}\tilde{\boldsymbol{a}}_q^p + \frac{1}{4}\sum_{\substack{pr\\qs}} \frac{\mathrm{d}\Gamma_{qs}^{pr}(s)}{\mathrm{d}s}\tilde{\boldsymbol{a}}_{qs}^{pr}. \tag{4.9}$$

Analogously, we make the following ansatz for the generator

$$\boldsymbol{\eta}(s) = \sum_{\substack{p\\q}} \eta_q^p(s)\tilde{\boldsymbol{a}}_q^p + \frac{1}{4}\sum_{\substack{pr\\qs}} \eta_{qs}^{pr}(s)\tilde{\boldsymbol{a}}_{qs}^{pr} =: \boldsymbol{\eta}^{(1)}(s) + \boldsymbol{\eta}^{(2)}(s). \tag{4.10}$$

Note that the zero-body part of the generator $\boldsymbol{\eta}$—which is in general a pure imaginary number due to anti-Hermiticity—is set to zero since any value of this quantity would not affect the results due to the commutator structure of the flow equation. However, the matrix elements are assumed to be real-valued throughout this work. We leave the choice of the generator $\boldsymbol{\eta}$ unspecified and postpone the discussion of suitable choices to section 4.6.

In order to derive the system of multi-reference IM-SRG flow equations, we first have to work out the commutator on the right-hand side of the operator flow equation (4.5) by making use of Wick's theorem and then equating the coefficients to obtain a system of coupled first-order differential equations for the matrix elements of the Hamiltonian.

The method of equating the coefficients works as follows: Once the right-hand side has been expressed in terms of the normal-ordered operators $\mathbf{1}$, $\tilde{\boldsymbol{a}}_q^p$, $\tilde{\boldsymbol{a}}_{qs}^{pr}$, for instance

$$[\boldsymbol{\eta}(s), \boldsymbol{H}(s)] =: \kappa + \sum_{\substack{p\\q}} \kappa_q^p \tilde{\boldsymbol{a}}_q^p + \frac{1}{4}\sum_{\substack{pr\\qs}} \kappa_{qs}^{pr}\tilde{\boldsymbol{a}}_{qs}^{pr}, \tag{4.11a}$$

equating the coefficients yields the system of the multi-reference IM-SRG flow equations[1]

$$\frac{\mathrm{d}E(s)}{\mathrm{d}s} = \kappa \tag{4.11b}$$

$$\frac{\mathrm{d}f_q^p(s)}{\mathrm{d}s} = \kappa_q^p \tag{4.11c}$$

$$\frac{\mathrm{d}\Gamma_{qs}^{pr}(s)}{\mathrm{d}s} = \kappa_{qs}^{pr}. \tag{4.11d}$$

In order to work out the commutator on the right-hand side of the flow equation, we split it into several commutators using the linearity of the commutator and employ the results summarized in (3.93)

$$\begin{aligned}\frac{\mathrm{d}\boldsymbol{H}(s)}{\mathrm{d}s} &= [\boldsymbol{\eta}(s), \boldsymbol{H}(s)] = [\boldsymbol{\eta}^{(1)}(s) + \boldsymbol{\eta}^{(2)}(s), \boldsymbol{H}^{(0)}(s) + \boldsymbol{H}^{(1)}(s) + \boldsymbol{H}^{(2)}(s)] \qquad (4.12)\\ &= [\boldsymbol{\eta}^{(1)}(s), \boldsymbol{H}^{(1)}(s)] + [\boldsymbol{\eta}^{(1)}(s), \boldsymbol{H}^{(2)}(s)]\\ &\quad + [\boldsymbol{\eta}^{(2)}(s), \boldsymbol{H}^{(1)}(s)] + [\boldsymbol{\eta}^{(2)}(s), \boldsymbol{H}^{(2)}(s)]. \qquad (4.13)\end{aligned}$$

[1] The coefficients κ_{qs}^{pr} can be chosen such that they are antisymmetric with respect to exchange among the upper and lower indices, respectively.

Note that $\boldsymbol{H}^{(0)}$ does not contribute to the commutator since it is just a number.

4.2. m-Scheme Flow Equations

In this section, we derive the system of multi-reference IM-SRG flow equations in the so-called m-scheme version. First, we calculate the commutators on the right-hand side of the operator flow equation using the results of (3.93). Second, we make use of equating the coefficients to obtain a system of coupled first-order differential equations for the matrix elements of the Hamiltonian. Finally, we write the m-scheme flow equations in a specific single-particle basis, namely the so-called natural orbitals that will simplify the expressions enormously.

4.2.1. Commutator of the Generator and Hamiltonian

Suppressing the flow parameter s and making use of the relations (3.93), we obtain the commutator between the one- and two-body parts of the generator and Hamiltonian in any possible combinations. The complete commutator of the generator and Hamiltonian is then the sum of all sub-commutators due to linearity of the commutator.

The commutator between the one-body part of the generator and the one-body part of the Hamiltonian yields

$$\begin{aligned}[\boldsymbol{\eta}^{(1)}, \boldsymbol{H}^{(1)}] =& \sum_{\substack{p \\ q}} \left(\sum_{r} (\eta_r^p f_q^r - f_r^p \eta_q^r) \right) \tilde{\boldsymbol{a}}_q^p \\ &+ \sum_{\substack{pr \\ q}} (\eta_r^p f_q^r - f_r^p \eta_q^r) \gamma_q^p . \end{aligned} \tag{4.14}$$

Furthermore, for the one-body part of the generator with the two-body part of the Hamiltonian, we obtain

$$\begin{aligned}[\boldsymbol{\eta}^{(1)}, \boldsymbol{H}^{(2)}] =& \frac{1}{4} \sum_{\substack{pr \\ qs}} \left(\sum_{t} (-\Gamma_{ts}^{pr} \eta_q^t - \Gamma_{qt}^{pr} \eta_s^t + \Gamma_{qs}^{tr} \eta_t^p + \Gamma_{qs}^{pt} \eta_t^r) \right) \tilde{\boldsymbol{a}}_{qs}^{pr} \\ &+ \sum_{\substack{p \\ q}} \left(\sum_{\substack{rt \\ su}} \Gamma_{qs}^{pr} \eta_u^t (-\delta_s^t \gamma_u^r + \gamma_s^t \delta_u^r) \right) \tilde{\boldsymbol{a}}_q^p \\ &+ \frac{1}{2} \sum_{\substack{prt \\ qs}} (-\Gamma_{ts}^{pr} \eta_q^t + \Gamma_{qs}^{tr} \eta_t^p) \lambda_{qs}^{pr} . \end{aligned} \tag{4.15}$$

Analogously, we get for the two-body part of the generator with the one-body part of the

Hamiltonian

$$
\begin{aligned}
[\boldsymbol{\eta}^{(2)}, \boldsymbol{H}^{(1)}] =& \frac{1}{4} \sum_{\substack{pr \\ qs}} \left(\sum_{t} (\eta^{pr}_{ts} f^{t}_{q} + \eta^{pr}_{qt} f^{t}_{s} - \eta^{tr}_{qs} f^{p}_{t} - \eta^{pt}_{qs} f^{r}_{t}) \right) \tilde{\boldsymbol{a}}^{pr}_{qs} \\
&+ \sum_{\substack{p \\ q}} \left(\sum_{\substack{rt \\ su}} \eta^{pr}_{qs} f^{t}_{u} (\delta^{t}_{s} \gamma^{r}_{u} - \gamma^{t}_{s} \delta^{r}_{u}) \right) \tilde{\boldsymbol{a}}^{p}_{q} \\
&+ \frac{1}{2} \sum_{\substack{prt \\ qs}} (\eta^{pr}_{ts} f^{t}_{q} - \eta^{tr}_{qs} f^{p}_{t}) \lambda^{pr}_{qs}.
\end{aligned} \tag{4.16}
$$

Finally, for the commutator of the two-body parts of these operators we obtain

$$
\begin{aligned}
[\boldsymbol{\eta}^{(2)}, \boldsymbol{H}^{(2)}] =& \frac{1}{4} \sum_{\substack{prtv \\ qsuw}} G^{prtv}_{qsuw} \delta^{t}_{q} \tilde{\boldsymbol{a}}^{prv}_{usw} \\
&+ \frac{1}{4} \sum_{\substack{pr \\ qs}} \left(\frac{1}{2} \sum_{\substack{tv \\ uw}} G^{prtv}_{uwqs} (\delta^{t}_{u} \delta^{v}_{w} - 2\delta^{t}_{u} \gamma^{v}_{w}) \right) \tilde{\boldsymbol{a}}^{pr}_{qs} \\
&+ \frac{1}{4} \sum_{\substack{pr \\ qs}} \left(\sum_{\substack{tv \\ uw}} G^{ptvr}_{quws} (\gamma^{t}_{w} \delta^{v}_{u} - \gamma^{v}_{u} \delta^{t}_{w}) \right) \tilde{\boldsymbol{a}}^{pr}_{qs} \\
&- \frac{1}{4} \sum_{\substack{pr \\ qs}} \left(\sum_{\substack{tv \\ uw}} G^{ptvr}_{suwq} (\gamma^{t}_{w} \delta^{v}_{u} - \gamma^{v}_{u} \delta^{t}_{w}) \right) \tilde{\boldsymbol{a}}^{pr}_{qs} \\
&+ \sum_{\substack{p \\ q}} \left(\frac{1}{2} \sum_{\substack{rtv \\ suw}} G^{prtv}_{usqw} (\bar{\gamma}^{t}_{u} \bar{\gamma}^{v}_{s} \gamma^{r}_{w} + \gamma^{t}_{u} \gamma^{v}_{s} \bar{\gamma}^{r}_{w}) \right) \tilde{\boldsymbol{a}}^{p}_{q} \\
&+ \sum_{\substack{p \\ q}} \left(\sum_{\substack{rtv \\ suw}} (\frac{1}{4} G^{ptrv}_{swqu} + G^{prtv}_{usqw} + \frac{1}{2} G^{prtv}_{qusw} - \frac{1}{2} G^{ptrv}_{qsuw}) \delta^{t}_{u} \lambda^{rv}_{sw} \right) \tilde{\boldsymbol{a}}^{p}_{q} \\
&+ \frac{1}{4} \sum_{\substack{prtv \\ qsuw}} G^{prtv}_{qsuw} \gamma^{p}_{u} \gamma^{r}_{w} \bar{\gamma}^{t}_{q} \bar{\gamma}^{v}_{s} \\
&+ \sum_{\substack{prtv \\ qsuw}} G^{ptrv}_{qusw} \gamma^{t}_{w} \bar{\gamma}^{v}_{u} \lambda^{pr}_{qs} \\
&+ \frac{1}{8} \sum_{\substack{prtv \\ qsuw}} G^{prtv}_{uwqs} (\bar{\gamma}^{t}_{u} \bar{\gamma}^{v}_{w} - \gamma^{t}_{u} \gamma^{v}_{w}) \lambda^{pr}_{qs} \\
&+ \mathcal{O}(\lambda^{(3)}) \,,
\end{aligned} \tag{4.17}
$$

where terms involving three-body irreducible density matrices $\lambda^{(3)}$ are neglected since they contribute only by few keV's to the ground-state energies[2] [Her16]. Here, we redefined $G^{prtv}_{qsuw} := \eta^{pr}_{qs} \Gamma^{tv}_{uw} - \Gamma^{pr}_{qs} \eta^{tv}_{uw}$.

[2] Excluding the lighter nuclei, typical binding energy per nucleon is about 8 MeV.

4.2.2. Flow Equations

Discarding the induced three- and higher-body contributions, we obtain the so-called multi-reference IM-SRG(2). Additionally, we neglect terms including three-body irreducible density matrices $\lambda^{(3)}$. Using the shorthand notation $G^{prtv}_{qsuw} := \eta^{pr}_{qs}\Gamma^{tv}_{uw} - \Gamma^{pr}_{qs}\eta^{tv}_{uw}$ the method of equating the coefficients yields the system of multi-reference IM-SRG(2) flow equations in the m-scheme:

$$\begin{aligned}
\frac{\mathrm{d}\Gamma^{pr}_{qs}}{\mathrm{d}s} =& + \sum_t (-\Gamma^{pr}_{ts}\eta^t_q - \Gamma^{pr}_{qt}\eta^t_s + \Gamma^{tr}_{qs}\eta^p_t + \Gamma^{pt}_{qs}\eta^r_t) \\
&+ \sum_t (\eta^{pr}_{ts} f^t_q + \eta^{pr}_{qt} f^t_s - \eta^{tr}_{qs} f^p_t - \eta^{pt}_{qs} f^r_t) \\
&+ \frac{1}{2} \sum_{\substack{tv \\ uw}} G^{prtv}_{uwqs} (\delta^t_u \delta^v_w - 2\delta^t_u \gamma^v_w) \\
&+ \sum_{\substack{tv \\ uw}} G^{ptvr}_{quws} (\gamma^t_w \delta^v_u - \gamma^v_u \delta^t_w) \\
&- \sum_{\substack{tv \\ uw}} G^{ptvr}_{suwq} (\gamma^t_w \delta^v_u - \gamma^v_u \delta^t_w) \qquad (4.18a) \\
\frac{\mathrm{d}f^p_q}{\mathrm{d}s} =& + \sum_{\substack{r \\ s}} (\eta^p_r f^r_q - f^p_r \eta^r_q) \\
&+ \sum_{\substack{rt \\ su}} \Gamma^{pr}_{qs} \eta^t_u (-\delta^t_s \gamma^r_u + \gamma^t_s \delta^r_u) \\
&+ \sum_{\substack{rt \\ su}} \eta^{pr}_{qs} f^t_u (\delta^t_s \gamma^r_u - \gamma^t_s \delta^r_u) \\
&+ \frac{1}{2} \sum_{\substack{rtv \\ suw}} G^{prtv}_{usqw} (\bar{\gamma}^t_u \bar{\gamma}^v_s \gamma^r_w + \gamma^t_u \gamma^v_s \bar{\gamma}^r_w) \\
&+ \sum_{\substack{rtv \\ suw}} (\frac{1}{4} G^{ptrv}_{swqu} + G^{prtv}_{usqw} + \frac{1}{2} G^{prtv}_{qusw} - \frac{1}{2} G^{ptrv}_{qsuw}) \delta^t_u \lambda^{rv}_{sw} \qquad (4.18b) \\
\frac{\mathrm{d}E}{\mathrm{d}s} =& + \sum_{\substack{pr \\ q}} (\eta^p_r f^r_q - f^p_r \eta^r_q) \gamma^p_q \\
&+ \frac{1}{4} \sum_{\substack{prtv \\ qsuw}} G^{prtv}_{qsuw} \gamma^p_u \gamma^r_w \bar{\gamma}^t_q \bar{\gamma}^v_s \\
&+ \frac{1}{4} \sum_{\substack{pr \\ qs}} \frac{\mathrm{d}\Gamma^{pr}_{qs}}{\mathrm{d}s} \lambda^{pr}_{qs} \\
&+ \mathcal{O}(\lambda^{(3)}). \qquad (4.18c)
\end{aligned}$$

Remarkably, all terms of the two-body part from (4.18a) reappear in the zero-body part (4.18c) just contracted with the irreducible two-body density matrix element, i.e.,

$$\begin{aligned}\frac{1}{4}\sum_{\substack{pr\\qs}}\frac{\mathrm{d}\Gamma^{pr}_{qs}}{\mathrm{d}s}\lambda^{pr}_{qs} = \frac{1}{2}\sum_{\substack{prt\\qs}}(-\Gamma^{pr}_{ts}\eta^{t}_{q}+\Gamma^{tr}_{qs}\eta^{p}_{t})\lambda^{pr}_{qs}\\ +\frac{1}{2}\sum_{\substack{prt\\qs}}(\eta^{pr}_{ts}f^{t}_{q}-\eta^{tr}_{qs}f^{p}_{t})\lambda^{pr}_{qs}\\ +\sum_{\substack{prtv\\qsuw}}G^{prtv}_{qusw}\gamma^{t}_{w}\bar{\gamma}^{v}_{u}\lambda^{pr}_{qs}\\ +\frac{1}{8}\sum_{\substack{prtv\\qsuw}}G^{prtv}_{uwqs}(\bar{\gamma}^{t}_{u}\bar{\gamma}^{v}_{w}-\gamma^{t}_{u}\gamma^{v}_{w})\lambda^{pr}_{qs}.\end{aligned} \tag{4.19}$$

This observation is very helpful for an efficient implementation of these equations. We leave this reshaping of the mathematical expression (4.19) to the reader.

It is notable that the system of the multi-reference IM-SRG(2) flow equations (4.18) does not depend on the irreducible four-body density matrix $\lambda^{(4)}$ and on non-linear powers of the irreducible two-body density matrix $\lambda^{(2)}$. Even though these contractions appear in the products of normal-ordered two-body operators, they cancel in the commutators (compare results obtained in appendices A.1 and A.2.3).

It is convenient to transform these equations into a suitable single-particle basis, the so-called natural orbitals, which will be discussed in the next section.

4.2.3. Flow Equations in Natural Orbitals

Up to now, we have not specified which single-particle basis we use, and, in principle, we can take any single-particle basis. We will stick to the so-called *natural-orbital basis*, which is the eigenbasis of the (scalar) one-particle density matrix $\gamma^{(1)}$, i.e., by diagonalizing this matrix we obtain

$$\gamma_q^p \quad \longrightarrow \quad \gamma_q^p = n_p \delta_q^p \,, \tag{4.20}$$

where the arrow indicates the transformation into the eigenbasis of this one-particle density matrix. Here, $n_p \in [0,1]$ indicates the eigenvalues of the one-particle density matrix called the *mean particle occupation numbers*, which can take any value between zero and one. Note that in the single-reference case, they can be either zero or one. Trivially, the one-hole density matrix is diagonal in this basis as well, i.e.,

$$\bar{\gamma}_q^p = \delta_q^p - \gamma_q^p \quad \longrightarrow \quad \bar{\gamma}_q^p = (1 - n_p)\delta_q^p =: \bar{n}_p \delta_q^p \tag{4.21}$$

with the *mean hole occupation number* $\bar{n}_p = 1 - n_p$.

The reason for choosing the natural-orbital basis is simply because the number of summations in the system of the flow equations can be reduced significantly. For instance, the number of summation indices appearing in term (4.18c)

$$\frac{\mathrm{d}E}{\mathrm{d}s} = \ldots + \frac{1}{4} \sum_{\substack{prtv \\ qsuw}} G^{prtv}_{qsuw} \gamma^p_u \gamma^r_w \bar{\gamma}^t_q \bar{\gamma}^v_s + \ldots \tag{4.22}$$

$$= \ldots + \frac{1}{4} \sum_{prtv} G^{prtv}_{tvpr} n_p n_r \bar{n}_t \bar{n}_v + \ldots \tag{4.23}$$

is halved, which increases computational efficiency tremendously, i.e., the computational effort can be reduced from $\mathcal{O}(N^8)$ to $\mathcal{O}(N^4)$, where N is the dimension of the one-body basis.

In practical calculations all matrix elements are given in a different basis $\{|\alpha\rangle\}$, e.g., harmonic-oscillator or Hartree-Fock basis. Consequently, we have to transform the matrix elements into the natural-orbital basis $\{|p\rangle\}$ according to

$$X^p_q = \sum_{\alpha\beta} C^\alpha_p C^\beta_q X^\alpha_\beta \tag{4.24a}$$

$$Y^{pr}_{qs} = \sum_{\substack{\alpha\gamma \\ \beta\delta}} C^\alpha_p C^\beta_q C^\gamma_r C^\beta_s Y^{\alpha\gamma}_{\beta\delta}. \tag{4.24b}$$

Here, C^α_p denotes the transformation coefficients

$$|p\rangle = \sum_\alpha C^\alpha_p |\alpha\rangle \,, \tag{4.25}$$

which are diagonal in the angular momentum l_p, total angular momentum j_p, its projection

m_p and the projection of the isospin m_{t_p} for a scalar density matrix, i.e.,

$$C_p^\alpha \sim \delta_{l_p}^{l_\alpha} \delta_{j_p}^{j_\alpha} \delta_{m_p}^{m_\alpha} \delta_{m_{t_p}}^{m_{t_\alpha}}. \tag{4.26}$$

While the transformation coefficients are independent of the projection quantum number m_p, they depend on the isospin projection m_{t_p} and total angular momentum j_p. Thus, the transformation can only connect the radial quantum numbers of $|p\rangle$ and $|\alpha\rangle$ with each other. Furthermore, this transformation is unitary since it is a transformation between two orthonormal bases, i.e.,

$$\sum_p C_p^\alpha C_\beta^p = \delta_\beta^\alpha. \tag{4.27}$$

Finally, using the shorthand notation introduced earlier, $G_{qsuw}^{prtv} := \eta_{qs}^{pr}\Gamma_{uw}^{tv} - \Gamma_{qs}^{pr}\eta_{uw}^{tv}$, we can write the system of multi-reference IM-SRG(2) flow equations in natural-orbital basis still in m-scheme as follows:

$$\begin{aligned}
\frac{\mathrm{d}\Gamma_{qs}^{pr}}{\mathrm{d}s} =& + \sum_t (-\Gamma_{ts}^{pr}\eta_q^t - \Gamma_{qt}^{pr}\eta_s^t + \Gamma_{qs}^{tr}\eta_t^p + \Gamma_{qs}^{pt}\eta_t^r) \\
&+ \sum_t (\eta_{ts}^{pr} f_q^t + \eta_{qt}^{pr} f_s^t - \eta_{qs}^{tr} f_t^p - \eta_{qs}^{pt} f_t^r) \\
&+ \frac{1}{2}\sum_{tv} G_{tvqs}^{prtv}(1 - n_t - n_v) \\
&+ \sum_{tv} G_{qvts}^{ptvr}(n_t - n_v) \\
&- \sum_{tv} G_{svtq}^{ptvr}(n_t - n_v) \qquad (4.28a) \\
\frac{\mathrm{d}f_q^p}{\mathrm{d}s} =& + \sum_r (\eta_r^p f_q^r - f_r^p \eta_q^r) \\
&+ \sum_{rt} \Gamma_{qt}^{pr}\eta_r^t(n_t - n_r) \\
&+ \sum_{rt} \eta_{qt}^{pr} f_r^t(n_r - n_t) \\
&+ \frac{1}{2}\sum_{rtv} G_{tvqr}^{prtv}(\bar{n}_t\bar{n}_v n_r + n_t n_v \bar{n}_r) \\
&+ \sum_{\substack{rtv \\ sw}} (\frac{1}{4} G_{swqt}^{ptrv} + G_{tsqw}^{prtv} + \frac{1}{2} G_{qtsw}^{prtv} - \frac{1}{2} G_{qstw}^{ptrv})\lambda_{sw}^{rv} \qquad (4.28b) \\
\frac{\mathrm{d}E}{\mathrm{d}s} =& + \sum_{pr} (\eta_r^p f_p^r - f_r^p \eta_p^r) n_p \\
&+ \frac{1}{4}\sum_{prtv} G_{tvpr}^{prtv} n_p n_r \bar{n}_t \bar{n}_v \\
&+ \frac{1}{4}\sum_{\substack{pr \\ qs}} \frac{\mathrm{d}\Gamma_{qs}^{pr}}{\mathrm{d}s}\lambda_{qs}^{pr} + \mathcal{O}(\lambda^{(3)}) \qquad (4.28c)
\end{aligned}$$

Remarkably, we observe that the two-body part has the same structure as for the single-reference case [Her+16; Her17]. But note that the particle occupation numbers n_p can take any values between zero and one, whereas for the single-reference case they can either be zero or one, as mentioned before. Hence, sums over the single-particle basis cannot be simply split into particle and hole sums as in the single-reference case. The multi-reference specific terms are those involving the irreducible two-body density matrix elements λ^{pr}_{qs}: the last line in the one-body part (4.28b), having three structurally different terms, and the last line in the zero-body part (4.28c). The single-reference case is recovered just by setting the irreducible two-body density matrix $\lambda^{(2)}$ to zero.

It is clear from (4.28) that the computational effort for solving the multi-reference IM-SRG(2) flow equations is dictated by the two-body part that scales like $\mathcal{O}(N^6)$ with the single-particle basis size N.

For an efficient implementation, we perform a total-angular-momentum coupling of the system of multi-reference IM-SRG flow equations to exploit rotational invariance of the Hamiltonian, and then rewrite them as matrix products in order to make use of extremely fast implementations of the *Basic Linear Algebra Subprograms* (BLAS) [BLA17]. First, let us start with total-angular-momentum coupling explained in the next section.

4.3. J-Coupled Flow Equations in Natural Orbitals

We introduce the essential quantities like Clebsch-Gordan coefficients, Wigner $3j$ and $6j$ symbols for the total-angular-momentum coupling (J-coupling). Furthermore, we recap the properties of scalar one-body and J-coupled two-body matrix elements that will be needed for the J-coupling of the system of flow equations (4.28). Finally, we discuss the so-called Pandya transformation, which will be very useful for the implementation of these equations.

4.3.1. Angular-Momentum-Coupling Coefficients and Pandya Transformation

The Clebsch-Gordan coefficients are defined as the overlap of the J-coupled two-body state $|(j_p j_q)JM\rangle$ and the two-body product state $|j_p m_p j_q m_q\rangle$

$$\left(\begin{matrix} j_p & j_q \\ m_p & m_q \end{matrix}\middle| \begin{matrix} J \\ M \end{matrix}\right) \coloneqq \langle j_p m_p j_q m_q | (j_p j_q) JM \rangle \,. \tag{4.29}$$

They fulfill the orthogonality and completeness relations

$$\sum_{m_p m_q} \left(\begin{matrix} j_p & j_q \\ m_p & m_q \end{matrix}\middle| \begin{matrix} J \\ M \end{matrix}\right) \left(\begin{matrix} j_p & j_q \\ m_p & m_q \end{matrix}\middle| \begin{matrix} J' \\ M' \end{matrix}\right) = \delta^J_{J'} \delta^M_{M'} \tag{4.30}$$

$$\sum_{JM} \left(\begin{matrix} j_p & j_q \\ m_p & m_q \end{matrix}\middle| \begin{matrix} J \\ M \end{matrix}\right) \left(\begin{matrix} j_p & j_q \\ m'_p & m'_q \end{matrix}\middle| \begin{matrix} J \\ M \end{matrix}\right) = \delta^{m_p}_{m'_p} \delta^{m_q}_{m'_q} \tag{4.31}$$

and behave under exchange of the first two or second and third columns as follows:

$$\left(\begin{array}{cc|c} j_p & j_q & J \\ m_p & m_q & M \end{array}\right) = (-)^{J-j_p-j_q}\left(\begin{array}{cc|c} j_q & j_p & J \\ m_q & m_p & M \end{array}\right) \tag{4.32}$$

$$\left(\begin{array}{cc|c} j_p & j_q & J \\ m_p & m_q & M \end{array}\right) = (-)^{j_q-m_q}\frac{\hat{J}}{\hat{j}_q}\left(\begin{array}{cc|c} j_p & J & j_q \\ m_p & -M & -m_q \end{array}\right) \tag{4.33}$$

with the multiplicity $\hat{J} := 2J+1$. Making use of the symmetry, we can easily derive the following relation

$$\begin{aligned}\sum_{m_p M}\left(\begin{array}{cc|c} j_p & j_1 & J \\ m_p & m_1 & M \end{array}\right)\left(\begin{array}{cc|c} j_p & j_2 & J \\ m_p & m_2 & M \end{array}\right) &= \sum_{m_p M}(-)^{j_1-j_2}\left(\begin{array}{cc|c} j_1 & j_p & J \\ m_1 & m_p & M \end{array}\right)\left(\begin{array}{cc|c} j_2 & j_p & J \\ m_2 & m_p & M \end{array}\right) \\ &= \frac{\hat{J}^2}{\hat{j}_1^2}\delta^{j_1}_{j_2}\delta^{m_1}_{m_2}.\end{aligned} \tag{4.34}$$

The Wigner $3j$ symbols are defined as

$$\left(\begin{array}{ccc} j_1 & j_2 & j_3 \\ m_1 & m_2 & m_3 \end{array}\right) := \frac{(-1)^{j_1-j_2-m_3}}{\hat{j}_3}\left(\begin{array}{cc|c} j_1 & j_2 & j_3 \\ m_1 & m_2 & -m_3 \end{array}\right), \tag{4.35}$$

where the inverse relation yields

$$\left(\begin{array}{cc|c} j_1 & j_2 & j_3 \\ m_1 & m_2 & m_3 \end{array}\right) = \hat{j}_3(-1)^{j_1-j_2+m_3}\left(\begin{array}{ccc} j_1 & j_2 & j_3 \\ m_1 & m_2 & -m_3 \end{array}\right). \tag{4.36}$$

Furthermore, they fulfill a (modified) orthogonality relation as well, i.e.,

$$\hat{J}^2\sum_{m_1 m_2}\left(\begin{array}{ccc} j_1 & j_2 & J \\ m_1 & m_2 & M \end{array}\right)\left(\begin{array}{ccc} j_1 & j_2 & J' \\ m_1 & m_2 & M' \end{array}\right) = \delta^J_{J'}\delta^M_{M'} \tag{4.37}$$

$$\sum_{JM}\hat{J}^2\left(\begin{array}{ccc} j_1 & j_2 & J \\ m_1 & m_2 & M \end{array}\right)\left(\begin{array}{ccc} j_1 & j_2 & J \\ m_1' & m_2' & M \end{array}\right) = \delta^{m_1}_{m_1'}\delta^{m_2}_{m_2'}. \tag{4.38}$$

The Wigner $6j$ symbols are defined as a sum over products of four Wigner $3j$ symbols

$$\begin{aligned}\left\{\begin{array}{cc} j_1\, j_2\, J \\ j_3\, j_4\, J' \end{array}\right\} := \sum_{m_1 m_2 m_3 m_4 M M'} &(-1)^{(j_1-m_1)+(j_2-m_2)+(j_3-m_3)+(j_4-m_4)+(J-M)+(J'-M')} \\ &\times\left(\begin{array}{ccc} j_1 & j_2 & J \\ -m_1 & -m_2 & -M \end{array}\right)\left(\begin{array}{ccc} j_1 & j_4 & J' \\ m_1 & -m_4 & M' \end{array}\right) \\ &\times\left(\begin{array}{ccc} j_3 & j_2 & J' \\ m_3 & m_2 & -M' \end{array}\right)\left(\begin{array}{ccc} j_3 & j_4 & J \\ -m_3 & m_4 & M \end{array}\right)\end{aligned} \tag{4.39}$$

and fulfill the orthogonality relation given by

$$\sum_J \hat{J}^2 \begin{Bmatrix} j_1\, j_2\, J \\ j_3\, j_4\, J' \end{Bmatrix} \begin{Bmatrix} j_1\, j_2\, J \\ j_3\, j_4\, J'' \end{Bmatrix} = \frac{\delta^{J'}_{J''}}{\hat{J'}^2} \Delta_{\{j_1 j_4 J'\}} \Delta_{\{j_3 j_2 J'\}} \tag{4.40}$$

where

$$\Delta_{\{j_1 j_4 J'\}} \coloneqq \begin{cases} 1 & \text{if } J' \in \{|j_1 - j_4|, |j_1 - j_4| + 1, \ldots, j_1 + j_4\} \\ 0 & \text{else.} \end{cases} \tag{4.41}$$

Furthermore, they obey the symmetry relation given by

$$\begin{Bmatrix} j_1\, j_2\, J \\ j_3\, j_4\, J' \end{Bmatrix} = \begin{Bmatrix} j_3\, j_4\, J \\ j_1\, j_2\, J' \end{Bmatrix}. \tag{4.42}$$

The matrix elements of a scalar one-body operator can be expressed as[3]

$$O^{p m_p}_{q m_q} = O^p_q \delta^{m_p}_{m_q} = O^p_q \delta^{j_p}_{j_q} \delta^{m_p}_{m_q}. \tag{4.43}$$

Here, the projection quantum number m_p is written explicitly and the label p does not contain it anymore. By averaging over the projection quantum numbers, we obtain

$$O^p_q = \frac{1}{\hat{j}^2_p} \sum_{m_p m_q} O^{p m_p}_{q m_q}. \tag{4.44}$$

Furthermore, the matrix elements of a scalar two-body operator are given as function of the J-coupled matrix elements as follows

$$O^{p m_p r m_r}_{q m_q s m_s} = \sum_{JM} \left(\begin{matrix} j_p & j_r \\ m_p & m_r \end{matrix} \middle| \begin{matrix} J \\ M \end{matrix} \right) \left(\begin{matrix} j_q & j_s \\ m_q & m_s \end{matrix} \middle| \begin{matrix} J \\ M \end{matrix} \right) {}^J O^{pr}_{qs}. \tag{4.45}$$

Note that the J-coupled two-body matrix elements are not normalized because they lack a factor $(1 + \delta^p_q)^{-1/2}$. The inverse relation yields

$${}^J O^{pr}_{qs} = \sum_{\substack{m_p m_r \\ m_q m_q}} \left(\begin{matrix} j_p & j_r \\ m_p & m_r \end{matrix} \middle| \begin{matrix} J \\ M \end{matrix} \right) \left(\begin{matrix} j_q & j_s \\ m_q & m_s \end{matrix} \middle| \begin{matrix} J \\ M \end{matrix} \right) O^{p m_p r m_r}_{q m_q s m_s}. \tag{4.46}$$

Assuming antisymmetric two-body matrix elements

$$O^{p m_p r m_r}_{q m_q s m_s} = -O^{r m_r p m_p}_{q m_q s m_s} = -O^{p m_p r m_r}_{s m_s q m_q} \tag{4.47}$$

[3] See appendix C.1 for the exact definition of a scalar operator.

the J-coupled matrix elements behaves under exchange among the upper and lower indices like

$$ {}^{J}O^{pr}_{qs} = -(-)^{J-j_p-j_r}\, {}^{J}O^{rp}_{qs} = -(-)^{J-j_q-j_s}\, {}^{J}O^{pr}_{sq}, \tag{4.48} $$

which is a direct consequence of (4.32) and (4.47).

The definition of the Pandya transformation of J-coupled two-body matrix elements reads

$$ {}^{J}\overline{O}^{1\bar{2}}_{3\bar{4}} \coloneqq -\sum_{J'} \hat{J}'^2 \begin{Bmatrix} j_1 & j_2 & J \\ j_3 & j_4 & J' \end{Bmatrix} {}^{J'}O^{14}_{32}. \tag{4.49} $$

The inverse Pandya transformation looks quite similar

$$ {}^{J'}O^{14}_{32} = -\sum_{J} \hat{J}^2 \begin{Bmatrix} j_1 & j_2 & J \\ j_3 & j_4 & J' \end{Bmatrix} {}^{J}\overline{O}^{1\bar{2}}_{3\bar{4}} \tag{4.50} $$

since Wigner $6j$ symbols fulfill the orthogonality relation (4.40). Furthermore, if the initial matrix elements are (anti-)Hermitian then the Pandya-transformed matrix elements are (anti-)Hermitian, i.e.,

$$ {}^{J}O^{14}_{32} = \pm\, {}^{J}O^{32}_{14} \quad \Rightarrow \quad {}^{J}\overline{O}^{1\bar{2}}_{3\bar{4}} = \pm\, {}^{J}\overline{O}^{3\bar{4}}_{1\bar{2}}. \tag{4.51} $$

This is a direct consequence of the symmetry of the Wigner $6j$ symbols (4.42). But in contrast to ${}^{J}O^{12}_{34}$, the Pandya-transformed matrix elements in general do not fulfill the relation given in (4.48), i.e.,

$$ {}^{J}\overline{O}^{1\bar{2}}_{3\bar{4}} \neq -(-)^{J-j_1-j_2}\, {}^{J}\overline{O}^{2\bar{1}}_{3\bar{4}} \neq -(-)^{J-j_3-j_4}\, {}^{J}\overline{O}^{1\bar{2}}_{4\bar{3}}. \tag{4.52} $$

4.3.2. Performing J-Coupling

Since the J-coupling is very technical, we do not show how to couple every individual term. Instead, we explicitly demonstrate J-coupling for some terms and discuss all assumptions we made to perform the J-coupling, which will limit the applicability of the formulae to even nuclei and additionally to scalar operators, i.e., spherical tensor operators of rank zero. For the definition of a spherical tensor operator see (C.1). A detailed derivation of all terms can be found in appendix B. The main outcome of the derivation is summarized in section 4.3.3.

For the J-coupling, we assume that the density matrices are scalar. This can only be guaranteed if the reference state has vanishing total angular momentum—a proof of this statement can be found in appendix C.3. However, this is mostly true for ground states of even-mass nuclei. This leads to mean occupation numbers that are independent of the projection quantum number m_p , i.e.,

$$ n_p = n_{pm_p} \tag{4.53} $$

$$ \bar{n}_p = \bar{n}_{pm_p}. \tag{4.54} $$

Note that the Hamiltonian is scalar and the generator must be constructed as a scalar operator. So far, the system of multi-reference IM-SRG(2) equations (4.28) are in principle valid for any operator. From now on, we assume a Hermitian operator $\boldsymbol{H}$ (unitary transformations preserve this property)

$$\boldsymbol{H}^\dagger(s) = \boldsymbol{H}(s) \tag{4.55}$$

and let the operator $\boldsymbol{\eta}$ be either Hermitian or anti-Hermitian captured by the symbol χ, i.e.,

$$\boldsymbol{\eta}^\dagger(s) = \chi\,\boldsymbol{\eta}(s) \quad \text{with} \quad \chi \coloneqq \begin{cases} 1 & \text{if } \boldsymbol{\eta} \text{ Hermitian} \\ -1 & \text{if } \boldsymbol{\eta} \text{ anti-Hermitian.} \end{cases} \tag{4.56}$$

This simple flexibility will enable us to derive the formulae for the commutator of an anti-Hermitian and Hermitian operator with a Hermitian operator simultaneously. This helps us to implement the so-called Wegner generator which is defined as the commutator between two specific Hermitian operators, and will be subject of section 4.6.2. Hence, let us analyze the symmetry of the commutator of a Hermitian operator $\boldsymbol{H}$ and an anti-Hermitian (Hermitian) operator $\boldsymbol{\eta}$ yielding

$$[\boldsymbol{\eta}, \boldsymbol{H}]^\dagger = (\boldsymbol{\eta}\boldsymbol{H} - \boldsymbol{H}\boldsymbol{\eta})^\dagger = \chi\boldsymbol{H}\boldsymbol{\eta} - \chi\boldsymbol{\eta}\boldsymbol{H} = \chi[\boldsymbol{H}, \boldsymbol{\eta}] = -\chi[\boldsymbol{\eta}, \boldsymbol{H}] \tag{4.57}$$

which implies that the commutator between $\boldsymbol{\eta}$ and $\boldsymbol{H}$ is Hermitian (anti-Hermitian).

Having this statement in mind, the strategy for the J-coupling looks as follows. In order to emphasize external indices, we will enumerate them with arabic numbers $1, 2, \ldots$ and $m_1, m_2, \ldots$ for the projection quantum numbers. Each subterm in (4.28a)–(4.28c) will be enumerated with Roman numerals. Furthermore, it will be written in compact form using the following abbreviation for terms obtained by permutations

$$[1m_1 \leftrightarrow 2m_2] \coloneqq \text{interchange the indices 1 with 2 and } m_1 \text{ with } m_2 \tag{4.58}$$

$$[1m_1 2m_2 \leftrightarrow 3m_3 4m_4] \coloneqq [1m_1 \leftrightarrow 3m_3] \wedge [2m_2 \leftrightarrow 4m_4]. \tag{4.59}$$

For instance, these abbreviations for the permutation would generate the following expressions

$$A^{1m_1}_{2m_2} - [1m_1 \leftrightarrow 2m_2] = A^{1m_1}_{2m_2} - A^{2m_2}_{1m_1} \tag{4.60}$$

$$B^{1m_1 2m_2}_{3m_3 4m_4} - [1m_1 2m_2 \leftrightarrow 3m_3 4m_4] = B^{1m_1 2m_2}_{3m_3 4m_4} - B^{3m_3 4m_4}_{1m_1 2m_2} \tag{4.61}$$

where $A^{1m_1}_{2m_2}$ and $B^{1m_1 2m_2}_{3m_3 4m_4}$ can represent long and complicated terms depending on the indices $1m_1$, $2m_2$ and so on. Using this shorthand notation it is convenient to write (4.28a) and (4.28b) in fully symmetrized form in the following sense

$$X^{1m_1}_{2m_2} \coloneqq A^{1m_1}_{2m_2} - \chi[1m_1 \leftrightarrow 2m_2] \tag{4.62}$$

$$Y^{1m_1 2m_2}_{3m_3 4m_4} := \Big(\Big(B^{1m_1 2m_2}_{3m_3 4m_4} - [1m_1 \leftrightarrow 2m_2] \Big) - [3m_3 \leftrightarrow 4m_4] \Big) - \chi[1m_1 2m_2 \leftrightarrow 3m_3 4m_4]. \tag{4.63}$$

In this form it is obvious that these matrix elements obey the relations

$$X^{1m_1}_{2m_2} = -\chi X^{2m_2}_{1m_1} \tag{4.64}$$

$$Y^{1m_1 2m_2}_{3m_3 4m_4} = -\chi Y^{3m_3 4m_4}_{1m_1 2m_2} \tag{4.65}$$

and

$$Y^{1m_1 2m_2}_{3m_3 4m_4} = -Y^{2m_2 1m_1}_{3m_3 4m_4} = Y^{1m_1 2m_2}_{4m_4 3m_3}, \tag{4.66}$$

which is manifestly (anti-) Hermitian, according to (4.57). We perform J-coupling of the two-body part (4.28a) according to (4.46). For extracting the J-coupled one-body part (4.28b) we reshape the M-scheme equations to compare with (4.43), or—when necessary—use the averaging procedure as formulated in (4.44). It follows immediately from the symmetry relations of the Clebsch-Gordan coefficients (4.32) that the one- and two-body parts in the J-coupled version take the following form

$$X^1_2 = A^1_2 - \chi[1 \leftrightarrow 2] \tag{4.67}$$

$${}^J Y^{12}_{34} = \Big(\Big({}^J B^{12}_{34} - (-)^{J-j_1-j_2}[1 \leftrightarrow 2] \Big) - (-)^{J-j_3-j_4}[3 \leftrightarrow 4] \Big) - \chi[12 \leftrightarrow 34]. \tag{4.68}$$

Finally, we write the zero-body part (4.28c) such that it is proportional to $(1-\chi)$ to ensure (4.57) for the zero-body part.

J-Coupling of a Specific Two-Body Term as Demonstration

Let us consider a specific two-body part defined by the first two lines of (4.28a) that we enumerate with Roman I

$$\begin{aligned} \left(\frac{\mathrm{d}\Gamma^{1m_1 2m_2}_{3m_3 4m_4}}{\mathrm{d}s} \right)_{\mathrm{I}} := &+ \sum_t \sum_{m_t} (-\Gamma^{1m_1 2m_2}_{tm_t 4m_4} \eta^{tm_t}_{3m_3} - \Gamma^{1m_1 2m_2}_{3m_3 tm_t} \eta^{tm_t}_{4m_4} + \Gamma^{tm_t 2m_2}_{3m_3 4m_4} \eta^{1m_1}_{tm_t} + \Gamma^{1m_1 tm_t}_{3m_3 4m_4} \eta^{2m_2}_{tm_t}) \\ &+ \sum_t \sum_{m_t} (\eta^{1m_1 2m_2}_{tm_t 4m_4} f^{tm_t}_{3m_3} + \eta^{1m_1 2m_2}_{3m_3 tm_t} f^{tm_t}_{4m_4} - \eta^{tm_t 2m_2}_{3m_3 4m_4} f^{1m_1}_{tm_t} - \eta^{1m_1 tm_t}_{3m_3 4m_4} f^{2m_2}_{tm_t}). \end{aligned} \tag{4.69}$$

Since all other terms are particular permutations of the external indices, we take two specific terms as representative

$$\begin{aligned} = &\left(\sum_t \sum_{m_t} (\Gamma^{tm_t 2m_2}_{3m_3 4m_4} \eta^{1m_1}_{tm_t} - \eta^{tm_t 2m_2}_{3m_3 4m_4} f^{1m_1}_{tm_t}) - [1m_1 \leftrightarrow 2m_2] \right) \\ &- \chi[1m_1 2m_2 \leftrightarrow 3m_3 4m_4]. \end{aligned} \tag{4.70}$$

Using the antisymmetry of the matrix elements with respect to exchange among the lower indices, we arrive at a fully symmetrized form

$$\begin{aligned}=&\Bigg(\Bigg(\frac{1}{2}\sum_t\sum_{m_t}(\Gamma^{tm_t2m_2}_{3m_34m_4}\eta^{1m_1}_{tm_t}-\eta^{tm_t2m_2}_{3m_34m_4}f^{1m_1}_{tm_t})-[1m_1\leftrightarrow 2m_2]\Bigg)\\&-[3m_3\leftrightarrow 4m_4]\Bigg)-\chi[1m_12m_2\leftrightarrow 3m_34m_4].\end{aligned}\tag{4.71}$$

The permutation $[1m_12m_2\leftrightarrow 3m_34m_4]$ multiplied with factor $-\chi$ guarantees (4.57). The permutations $[1m_1\leftrightarrow 2m_2]$ and $[3m_3\leftrightarrow 4m_4]$ take care of the symmetry with respect to exchange among the upper and lower indices as expressed in (4.47), respectively.

The J-coupling procedure according to (4.46) yields

$$\left(\frac{\mathrm{d}\,{}^J\Gamma^{12}_{34}}{\mathrm{d}s}\right)_{\mathrm{I}}=\sum_{\substack{m_1m_2\\m_3m_4}}\begin{pmatrix}j_1&j_2\\m_1&m_2\end{vmatrix}\begin{matrix}J\\M\end{pmatrix}\begin{pmatrix}j_3&j_4\\m_3&m_4\end{vmatrix}\begin{matrix}J\\M\end{pmatrix}\left(\frac{\mathrm{d}\Gamma^{1m_12m_2}_{3m_34m_4}}{\mathrm{d}s}\right)_{\mathrm{I}}\tag{4.72}$$

$$\begin{aligned}=&\sum_{\substack{m_1m_2\\m_3m_4}}\begin{pmatrix}j_1&j_2\\m_1&m_2\end{vmatrix}\begin{matrix}J\\M\end{pmatrix}\begin{pmatrix}j_3&j_4\\m_3&m_4\end{vmatrix}\begin{matrix}J\\M\end{pmatrix}\\&\times\Bigg(\Bigg(\Bigg(\frac{1}{2}\sum_t\sum_{m_t}(\Gamma^{tm_t2m_2}_{3m_34m_4}\eta^{1m_1}_{tm_t}-\eta^{tm_t2m_2}_{3m_34m_4}f^{1m_1}_{tm_t})-[1m_1\leftrightarrow 2m_2]\Bigg)\\&-[3m_3\leftrightarrow 4m_4]\Bigg)-\chi[1m_12m_2\leftrightarrow 3m_34m_4]\Bigg)\end{aligned}\tag{4.73}$$

making use of the symmetry relation of the Clebsch-Gordan coefficients (4.32) yields

$$\begin{aligned}=&\Bigg(\Bigg(\frac{1}{2}\sum_t\sum_{m_t}\sum_{\substack{m_1m_2\\m_3m_4}}\begin{pmatrix}j_1&j_2\\m_1&m_2\end{vmatrix}\begin{matrix}J\\M\end{pmatrix}\begin{pmatrix}j_3&j_4\\m_3&m_4\end{vmatrix}\begin{matrix}J\\M\end{pmatrix}\\&\times(\Gamma^{tm_t2m_2}_{3m_34m_4}\eta^{1m_1}_{tm_t}-\eta^{tm_t2m_2}_{3m_34m_4}f^{1m_1}_{tm_t})-(-)^{J-j_1-j_2}[1\leftrightarrow 2]\Bigg)\\&-(-)^{J-j_3-j_4}[3\leftrightarrow 4]\Bigg)-\chi[12\leftrightarrow 34].\end{aligned}\tag{4.74}$$

Expressing the one- and two-body matrix elements in terms of the J-coupled matrix elements as given in (4.43) and (4.45), respectively, we obtain

$$\begin{aligned}=&\Bigg(\Bigg(\frac{1}{2}\sum_t\sum_{m_t}\sum_{\substack{m_1m_2\\m_3m_4}}\sum_{J'M'}\begin{pmatrix}j_1&j_2\\m_1&m_2\end{vmatrix}\begin{matrix}J\\M\end{pmatrix}\begin{pmatrix}j_3&j_4\\m_3&m_4\end{vmatrix}\begin{matrix}J\\M\end{pmatrix}\\&\times\begin{pmatrix}j_t&j_2\\m_t&m_2\end{vmatrix}\begin{matrix}J'\\M'\end{pmatrix}\begin{pmatrix}j_3&j_4\\m_3&m_4\end{vmatrix}\begin{matrix}J'\\M'\end{pmatrix}\delta^{j_1}_{j_t}\delta^{m_1}_{m_t}({}^{J'}\Gamma^{t2}_{34}\eta^1_t-{}^{J'}\eta^{t2}_{34}f^1_t)\\&-(-)^{J-j_1-j_2}[1\leftrightarrow 2]\Bigg)-(-)^{J-j_3-j_4}[3\leftrightarrow 4]\Bigg)-\chi[12\leftrightarrow 34]\end{aligned}\tag{4.75}$$

$$
\begin{aligned}
=&\Bigg(\Bigg(\frac{1}{2}\sum_t\sum_{m_t}\sum_{\substack{m_1m_2\\m_3m_4}}\sum_{J'M'}\begin{pmatrix}j_1 & j_2\\ m_1 & m_2\end{vmatrix}\begin{matrix}J\\M\end{matrix}\end{pmatrix}\begin{pmatrix}j_3 & j_4\\ m_3 & m_4\end{vmatrix}\begin{matrix}J\\M\end{matrix}\end{pmatrix}\\
&\times\begin{pmatrix}j_t & j_2\\ m_t & m_2\end{vmatrix}\begin{matrix}J'\\M'\end{matrix}\end{pmatrix}\begin{pmatrix}j_3 & j_4\\ m_3 & m_4\end{vmatrix}\begin{matrix}J'\\M'\end{matrix}\end{pmatrix}\delta^{j_1}_{j_t}\delta^{m_1}_{m_t}({}^{J'}\Gamma^{t2}_{34}\eta^1_t-{}^{J'}\eta^{t2}_{34}f^1_t)\\
&-(-)^{J-j_1-j_2}[1\leftrightarrow 2]\Bigg)-(-)^{J-j_3-j_4}[3\leftrightarrow 4]\Bigg)-\chi[12\leftrightarrow 34] \qquad (4.76)
\end{aligned}
$$

which can be simplified using the orthogonality relation (4.30) to

$$
\begin{aligned}
=&\Bigg(\Bigg(\frac{1}{2}\sum_t\sum_{J'M'}\delta^{J'}_J\delta^M_{M'}({}^{J'}\Gamma^{t2}_{34}\eta^1_t-{}^{J'}\eta^{t2}_{34}f^1_t)-(-)^{J-j_1-j_2}[1\leftrightarrow 2]\Bigg) \qquad (4.77)\\
&-(-)^{J-j_3-j_4}[3\leftrightarrow 4]\Bigg)-\chi[12\leftrightarrow 34] \qquad (4.78)\\
=&\Bigg(\Bigg(\frac{1}{2}\sum_t({}^{J}\Gamma^{t2}_{34}\eta^1_t-{}^{J}\eta^{t2}_{34}f^1_t)-(-)^{J-j_1-j_2}[1\leftrightarrow 2]\Bigg)\\
&-(-)^{J-j_3-j_4}[3\leftrightarrow 4]\Bigg)-\chi[12\leftrightarrow 34] \qquad (4.79)
\end{aligned}
$$

which is finally expressed in terms of the J-coupled two-body and m-independent one-body matrix elements.

J-Coupling of a Specific One-Body Term as Demonstration

Let us start with the first line in (4.28b) defining

$$
\begin{aligned}
\left(\frac{\mathrm{d}f^{1m_1}_{2m_2}}{\mathrm{d}s}\right)_{\mathrm{I}}&:=\sum_r\sum_{m_r}(\eta^{1m_1}_{rm_r}f^{rm_r}_{2m_2}-f^{1m_1}_{rm_r}\eta^{rm_r}_{2m_2}) && (4.80)\\
&=\sum_r\sum_{m_r}\eta^{1m_1}_{rm_r}f^{rm_r}_{2m_2}-\chi[1m_1\leftrightarrow 2m_2] && (4.81)\\
&=\sum_r\sum_{m_r}\eta^1_rf^r_2\delta^{j_1}_{j_r}\delta^{j_r}_{j_2}\delta^{m_1}_{m_r}\delta^{m_r}_{m_2}-\chi[1m_1\leftrightarrow 2m_2] && (4.82)\\
&=\delta^{j_1}_{j_2}\delta^{m_1}_{m_2}\sum_r\eta^1_rf^r_2-\chi[1m_1\leftrightarrow 2m_2]. && (4.83)
\end{aligned}
$$

Hence, we can read off the projection quantum number independent part

$$
\left(\frac{\mathrm{d}f^1_2}{\mathrm{d}s}\right)_{\mathrm{I}}=\sum_r\eta^1_rf^r_2-\chi[1\leftrightarrow 2]. \qquad (4.84)
$$

J-Coupling of a Specific Zero-Body Term as Demonstration

As a final demonstration, let us consider the first line in (4.28c)

$$
\left(\frac{\mathrm{d}E}{\mathrm{d}s}\right)_{\mathrm{I}}:=\sum_{pr}\sum_{m_pm_r}(\eta^{pm_p}_{rm_r}f^{rm_r}_{pm_p}-f^{pm_p}_{rm_r}\eta^{rm_r}_{pm_p})n_p \qquad (4.85)
$$

$$= (1-\chi) \sum_{pr} \sum_{m_p m_r} \eta^{p m_p}_{r m_r} f^{r m_r}_{p m_p} n_p \tag{4.86}$$

$$= (1-\chi) \sum_{pr} \eta^p_r f^r_p n_p \sum_{m_p m_r} \delta^{m_p}_{m_r} \delta^{j_p}_{j_r} \tag{4.87}$$

$$= (1-\chi) \sum_{pr} \hat{j}_p^2 \eta^p_r f^r_p n_p \tag{4.88}$$

which is completely determined by the projection number independent matrix elements.

4.3.3. Summary of the J-Coupled Flow Equations in Natural Orbitals

In summary, we get

$$\begin{aligned}
\frac{\mathrm{d}\, {}^J\Gamma^{12}_{34}}{\mathrm{d}s} =& \Bigg[\Bigg(\frac{1}{2} \sum_t \Big({}^J\Gamma^{t2}_{34} \eta^1_t - {}^J\eta^{t2}_{34} f^1_t \Big) \\
&+ \frac{1}{8} \sum_{tv} {}^J\eta^{12}_{tv} {}^J\Gamma^{tv}_{34} (1 - n_t - n_v) \\
&- \frac{1}{2} \sum_{tv} \sum_{J'} \hat{J'}^2 \begin{Bmatrix} J & j_1 & j_2 \\ J' & j_3 & j_4 \end{Bmatrix} {}^{J'}\overline{\eta}^{1\bar{4}}_{v\bar{t}} {}^{J'}\overline{\Gamma}^{v\bar{t}}_{3\bar{2}} (n_t - n_v) \\
&- (-)^{J-j_1-j_2} [1 \leftrightarrow 2] \Bigg) - (-)^{J-j_3-j_4} [3 \leftrightarrow 4] \Bigg] - \chi[12 \leftrightarrow 34]
\end{aligned} \tag{4.89a}$$

$$\begin{aligned}
\frac{\mathrm{d}f^1_2}{\mathrm{d}s} =& \Bigg[\sum_r \eta^1_r f^r_2 \\
&+ \frac{1}{\hat{j}_1^2} \sum_J \sum_{rt} \hat{J}^2 \Big({}^J\Gamma^{r1}_{t2} \eta^t_r - {}^J\eta^{r1}_{t2} f^t_r \Big) n_t \\
&+ \frac{1}{2\hat{j}_1^2} \sum_J \sum_{rtv} \hat{J}^2 \, {}^J\eta^{1r}_{tv} {}^J\Gamma^{tv}_{2r} (\bar{n}_t \bar{n}_v n_r + n_t n_v \bar{n}_r) \\
&+ \frac{1}{4} \frac{1}{\hat{j}_1^2} \sum_J \sum_{tswrv} \hat{J}^2 \, {}^J\eta^{1t}_{sw} {}^J\Gamma^{rv}_{2t} {}^J\lambda^{rv}_{sw} \\
&+ \frac{1}{\hat{j}_1^2} \sum_J \sum_{tsrvw} \hat{J}^2 \, {}^J\overline{\eta}^{1\bar{t}}_{s\bar{r}} {}^J\overline{\lambda}^{s\bar{r}}_{v\bar{w}} {}^J\overline{\Gamma}^{v\bar{w}}_{2\bar{t}} \\
&- \frac{1}{2} \frac{1}{\hat{j}_1^2} \sum_{J_1 J_2} \sum_{tsrvw} \hat{J}_1^2 \hat{J}_2^2 \frac{1}{\hat{j}_t^2} \delta^{j_t}_{j_s} \Big({}^{J_1}\eta^{1t}_{2s} {}^{J_2}\lambda^{sw}_{rv} {}^{J_2}\Gamma^{rv}_{tw} - [\, \eta \leftrightarrow \Gamma] \Big) \Bigg] \\
&- \chi[1 \leftrightarrow 2]
\end{aligned} \tag{4.89b}$$

$$\begin{aligned}
\frac{\mathrm{d}E}{\mathrm{d}s} =& + (1-\chi) \sum_{pr} \hat{j}_p^2 \eta^p_r f^r_p n_p \\
&+ \frac{1}{4} (1-\chi) \sum_J \sum_{prtv} \hat{J}^2 \, {}^J\eta^{pr}_{tv} {}^J\Gamma^{tv}_{pr} n_p n_r \bar{n}_t \bar{n}_v \\
&+ \frac{1}{4} \cdot \frac{(1-\chi)}{2} \sum_J \sum_{prqs} \hat{J}^2 \frac{\mathrm{d}\, {}^J\Gamma^{pr}_{qs}}{\mathrm{d}s} {}^J\lambda^{pr}_{qs} \\
&+ \mathcal{O}(\lambda^{(3)}).
\end{aligned} \tag{4.89c}$$

Given that all matrix elements are real-valued, the zero-body part vanishes completely as expected if we assume a Hermitian operator $\boldsymbol{\eta}$ by setting $\chi = 1$, since the commutator is then anti-Hermitian according to (4.57). The terms obtained by the permutations basically guarantee the (anti-)Hermiticity of the operator defined by the commutator, and the symmetry with respect to exchange among the upper and lower indices in the sense of (4.48).

4.4. Implementation of the J-Coupled Flow Equations

The main goal of this section is to rewrite the system of J-coupled flow equations (4.89) in a convenient form for an efficient implementation. The basic idea is to express these flow equations as matrix products to accelerate the evaluation of the right-hand side by using the *Basic Linear Algebra Subprograms* (BLAS) [BLA17] which are much faster than a straightforward implementation of the summation loops appearing in the flow equations.

4.4.1. Bases, Matrix Products and Traces

First, we introduce the one-body and two-body bases used to represent the operators taking into account their symmetries. Since the one-body operators used in this work are rotationally invariant, i.e., diagonal in the projection quantum number m_p and independent of it, we introduce a spherical one-body basis

$$\mathcal{B}^{(1)} \coloneqq \left\{ |p\, m_p\rangle = |\tilde{n}_p (l_p \tfrac{1}{2}) j_p m_p; \tfrac{1}{2} m_{t_p}\rangle \;:\; 2\tilde{n}_p + l_p \leq e_{\max} \;\wedge\; m_p = \tfrac{1}{2} \right\}. \tag{4.90}$$

truncated with respect to the maximum single-particle energy quantum number $e_{\max}$ to have a finite basis of dimension $d_1 := \dim(\mathcal{B}^{(1)})$. Here, $\tilde{n}_p \in \{0, 1, \ldots\}$ is the radial quantum number[4], the angular-momentum $l_p \in \{0, 1, \ldots\}$ and spin-$\frac{1}{2}$ quantum number are coupled to the total angular momentum $j_p \in \{\, |l_p - \frac{1}{2}|,\, |l_p - \frac{1}{2}| + 1,\, \ldots,\, l_p + \frac{1}{2}\}$ with its projection quantum number $m_p \in \{\, -j_p,\, -j_p + 1,\, \ldots,\, j_p\}$. Moreover, the z-component of the isospin-$\frac{1}{2}$ quantum number encodes whether this single-particle state belongs to a neutron $m_{t_p} = -\frac{1}{2}$ or a proton $m_{t_p} = +\frac{1}{2}$.

We denote the matrix representation of a given spherical one-body operator $\boldsymbol{A}$ as follows

$$\underline{\underline{A}} \coloneqq (A^p_q)^{p\in(1,\ldots,d_1)}_{q\in(1,\ldots,d_1)} = \begin{pmatrix} A^1_1 & A^1_2 & \ldots & A^1_{d_1} \\ A^2_1 & A^2_2 & \ldots & A^2_{d_1} \\ \vdots & \vdots & \ddots & \vdots \\ A^{d_1}_1 & A^{d_1}_2 & \ldots & A^{d_1}_{d_1} \end{pmatrix}, \tag{4.91}$$

where the upper and lower indices correspond to the row and column indices, respectively. This notation is generic and independent whether A^p_q refers to a matrix element of the operator $\boldsymbol{A}$ in vacuum or reference-state representation.

[4] To avoid confusion with the mean occupation number n_p, we put a tilde ˜ on top it.

Analogously, the diagonality in the coupled two-body angular momentum J and the independence of its projection M motivates the following definition for the two-body basis in each subspace spanned by two-body states with total angular momentum J, i.e.,

$$ {}^{J}\mathcal{B}^{(2)} \coloneqq \left\{ |(pr)JM\rangle \;:\; M = 0 \;\wedge\; \Delta_{\{j_p j_r J\}} \;\wedge\; 2\tilde{n}_p + l_p + 2\tilde{n}_r + l_r \leq E_{\max} \right\} \tag{4.92} $$

with the maximum two-body energy quantum number $E_{\max}$ and $\Delta_{\{j_p j_r J\}}$ being true if and only if the single-particle total angular momentum j_p and j_r can couple to the two-body total angular momentum J. Here, we can take the specific projection quantum number $M = 0$ since the quantum number J is an integer because j_p and j_r are half-integer. The complete two-body basis is the union of ${}^{J}\mathcal{B}^{(2)}$ over all possible values of J, which is finite since the one-body basis is finite. In this basis the matrix notation of a given rotationally invariant two-body operator $\boldsymbol{C}$ is given by

$$ {}^{J}\underline{\underline{C}} \coloneqq ({}^{J}C^{pr}_{qs})^{pr\in(1,\ldots,d_2^J)}_{qs\in(1,\ldots,d_2^J)} = \begin{pmatrix} {}^{J}C^{1}_{1} & {}^{J}C^{1}_{2} & \ldots & {}^{J}C^{1}_{d_2^J} \\ {}^{J}C^{2}_{1} & {}^{J}C^{2}_{2} & \ldots & {}^{J}C^{2}_{d_2^J} \\ \vdots & \vdots & \ddots & \vdots \\ {}^{J}C^{d_2^J}_{1} & {}^{J}C^{d_2^J}_{2} & \ldots & {}^{J}C^{d_2^J}_{d_2^J} \end{pmatrix}. \tag{4.93} $$

Here, the indices pr and qs can be seen as collective indices for the J-coupled two-body basis running from 1 to the dimension of the J-coupled two-body basis $d_2^J \coloneqq \dim({}^{J}\mathcal{B}^{(2)})$.

Using this matrix notation, we can write matrix products of the two given one-body matrices

$$ (\underline{\underline{A}} \cdot \underline{\underline{B}})^{p}_{q} \coloneqq \sum_{r} A^{p}_{r} B^{r}_{q} \tag{4.94} $$

and two-body matrices

$$ ({}^{J}\underline{\underline{X}} \cdot {}^{J}\underline{\underline{Y}})^{pr}_{qs} \coloneqq \sum_{tv} {}^{J}X^{pr}_{tv}\, {}^{J}Y^{tv}_{qs} \tag{4.95} $$

which can be implemented in a much more efficient way using BLAS operations than straightforward summation loops. For matrix products, we have to make sure that both matrices are given either in vacuum or reference-state representation, otherwise the product does not make sense. Moreover, the trace of a given one- or two-body matrix is defined as

$$ \mathrm{tr}(\underline{\underline{A}}) \coloneqq \sum_{p} A^{p}_{p} \tag{4.96} $$

$$ \mathrm{tr}({}^{J}\underline{\underline{C}}) \coloneqq \sum_{pr} {}^{J}C^{pr}_{pr}. \tag{4.97} $$

Finally, for an efficient implementation of the first term in two-body part (4.89a) and second term of the one-body part (4.89b), we embed any one-body matrix elements A^{p}_{q} into the

J-coupled two-body basis using the following prescription

$$ {}^{J}(\Omega_A)^{pr}_{qs} := A^p_q \delta^r_s = A^p_q \delta^r_s \Delta_{\{j_p j_r J\}} \Delta_{\{j_q j_s J\}} \tag{4.98} $$

where we implicitly assume that j_p and j_r couple to the total angular momentum J; the same applies for j_q and j_s. These embedded matrix elements are Hermitian (anti-Hermitian) if and only if the operator $\boldsymbol{A}$ is Hermitian (anti-Hermitian). But they are not necessarily antisymmetric with respect to exchange among the upper and lower indices in the following sense

$$ {}^{J}(\Omega_A)^{pr}_{qs} \neq (-)^{J-j_p-j_r} {}^{J}(\Omega_A)^{rp}_{qs} \neq (-)^{J-j_q-j_s} {}^{J}(\Omega_A)^{pr}_{sq}. \tag{4.99} $$

With the aid of this definition (4.98), we can write

$$ \sum_t A^1_t \, {}^{J}B^{t2}_{34} = \sum_{tu} A^1_t \delta^2_u \, {}^{J}B^{tu}_{34} = \sum_{tu} {}^{J}(\Omega_A)^{12}_{tu} \, {}^{J}B^{tu}_{34} = \Big({}^{J}\underline{\underline{\Omega_A}} \cdot {}^{J}\underline{\underline{B}} \Big)^{12}_{34}. \tag{4.100} $$

Even though we generate many trivial zero entries in the matrix ${}^{J}\underline{\underline{\Omega_A}}$, the right-hand side of this expression can be implemented using BLAS operations in a much more efficient way than a straightforward implementation of the summation loops.

4.4.2. BLAS Compliant J-Coupled Flow Equations

Our starting point is the system of multi-reference IM-SRG(2) flow equations (4.89). We will suppress the terms obtained by permutations for brevity. These terms basically guarantee the symmetry of the operator defined by the commutator according to (4.57), and the antisymmetry with respect to exchange among the upper and lower indices, respectively, as formulated in (4.48).

Two-Body Part

By embedding the one-body matrix elements into the J-coupled two-body basis according to (4.98), we obtain for the first term

$$ \left(\frac{\mathrm{d}\, {}^{J}\Gamma^{12}_{34}}{\mathrm{d}s} \right)_{\mathrm{I}} = \frac{1}{2} \sum_t \big({}^{J}\Gamma^{t2}_{34} \eta^1_t - {}^{J}\eta^{t2}_{34} f^1_t \big) \tag{4.101} $$

$$ = \frac{1}{2} \Big({}^{J}\underline{\underline{\Omega_\eta}} \cdot {}^{J}\underline{\underline{\Gamma}} - {}^{J}\underline{\underline{\Omega_f}} \cdot {}^{J}\underline{\underline{\eta}} \Big)^{12}_{34} \tag{4.102} $$

where we used (4.100). With the following definition

$$ {}^{J}F^{tv}_{uw} := (1 - n_t - n_v) \delta^{tv}_{uw} \tag{4.103} $$

which is a diagonal matrix in the two-body basis, we can recast the second term to

$$\left(\frac{\mathrm{d}\,{}^{J}\Gamma^{12}_{34}}{\mathrm{d}s}\right)_{\mathrm{II}} = +\frac{1}{8}\sum_{tv} {}^{J}\eta^{12}_{tv}\,{}^{J}\Gamma^{tv}_{34}(1-n_t-n_v) \tag{4.104}$$

$$= +\frac{1}{8}\sum_{\substack{tv\\uw}} {}^{J}\eta^{12}_{tv}\,{}^{J}F^{tv}_{uw}\,{}^{J}\Gamma^{uw}_{34} \tag{4.105}$$

$$= +\frac{1}{8}\left({}^{J}\underline{\underline{\eta}}\cdot{}^{J}\underline{\underline{F}}\cdot{}^{J}\underline{\underline{\Gamma}}\right)^{12}_{34}. \tag{4.106}$$

We define the two-body matrix element

$${}^{J'}D^{vu}_{wt} := -(n_v-n_t)\delta^{vu}_{wt}\Delta_{\{j_v j_u J'\}} \tag{4.107}$$

where we implicitly assume that j_v and j_t couple to J' on the right hand side, and performing its Pandya transformation (4.49) using relation (1) in [VMK88, p. 305] yields

$${}^{J}\overline{D}^{v\bar{t}}_{w\bar{u}} = -\sum_{J'}\begin{Bmatrix} j_v & j_t & J\\ j_w & j_u & J'\end{Bmatrix}{}^{J'}D^{vu}_{wt} \tag{4.108}$$

$$= +(n_v-n_t)\delta^{vu}_{wt}\sum_{J'}\begin{Bmatrix} j_v & j_t & J\\ j_v & j_t & J'\end{Bmatrix}\Delta_{\{j_v j_u J'\}} \tag{4.109}$$

$$= +(n_v-n_t)\delta^{vt}_{wu}\Delta_{\{j_v j_t J'\}} \tag{4.110}$$

$$= -\,{}^{J'}D^{vu}_{wt} = -\,{}^{J'}D^{vt}_{wu}. \tag{4.111}$$

This implies that the Pandya transformation of ${}^{J'}D^{vu}_{wt}$ is proportional to the identity transformation in this case. Introducing the abbreviation for the product of three Pandya-transformed matrices

$${}^{J'}\overline{B}^{1\bar{4}}_{3\bar{2}} := \sum_{\substack{tv\\uw}} {}^{J'}\overline{\eta}^{1\bar{4}}_{v\bar{t}}\,{}^{J'}\overline{D}^{v\bar{t}}_{w\bar{u}}\,{}^{J'}\overline{\Gamma}^{w\bar{u}}_{3\bar{2}} = \left({}^{J'}\underline{\underline{\overline{\eta}}}\cdot{}^{J'}\underline{\underline{\overline{D}}}\cdot{}^{J'}\underline{\underline{\overline{\Gamma}}}\right)^{1\bar{4}}_{3\bar{2}}. \tag{4.112}$$

we can recast the third term to

$$\left(\frac{\mathrm{d}\,{}^{J}\Gamma^{12}_{34}}{\mathrm{d}s}\right)_{\mathrm{III}} = -\frac{1}{2}\sum_{tv}\sum_{J'}\hat{J'}^2\begin{Bmatrix} J & j_1 & j_2\\ J' & j_3 & j_4\end{Bmatrix}{}^{J'}\overline{\eta}^{1\bar{4}}_{v\bar{t}}\,{}^{J'}\overline{\Gamma}^{v\bar{t}}_{3\bar{2}}(n_t-n_v) \tag{4.113}$$

identifying the Pandya-transformed two-body matrix element ${}^{J}\overline{D}^{v\bar{t}}_{w\bar{u}}$ since j_t and j_v couple to J' because of ${}^{J'}\overline{\Gamma}^{v\bar{t}}_{3\bar{2}}$, we get

$$= +\frac{1}{2}\sum_{\substack{tv\\uw}}\sum_{J'}\hat{J'}^2\begin{Bmatrix} J & j_1 & j_2\\ J' & j_3 & j_4\end{Bmatrix}{}^{J'}\overline{\eta}^{1\bar{4}}_{v\bar{t}}\,{}^{J'}\overline{D}^{v\bar{t}}_{w\bar{u}}\,{}^{J'}\overline{\Gamma}^{w\bar{u}}_{3\bar{2}} \tag{4.114}$$

$$= +\frac{1}{2}\sum_{J'}\hat{J'}^2\begin{Bmatrix} J & j_1 & j_2\\ J' & j_3 & j_4\end{Bmatrix}{}^{J'}\overline{B}^{1\bar{4}}_{3\bar{2}} \tag{4.115}$$

$$= -\frac{1}{2}\,{}^{J}B^{12}_{34}. \tag{4.116}$$

In the last step, we identified the inverse Pandya transformation (4.50) of ${}^{J'}\overline{B}^{1\bar{4}}_{3\bar{2}}$ and used an appropriate shorthand notation for the transformed matrix elements.

One-Body Part

The first term of the one-body part is simply a matrix product

$$\left(\frac{\mathrm{d}f_2^1}{\mathrm{d}s}\right)_{\mathrm{I}} = \sum_r \eta_r^1 f_2^r = \left(\underline{\underline{\eta}} \cdot \underline{\underline{f}}\right)_2^1. \tag{4.117}$$

The second term of the one-body part is analogous to first term of the two-body part

$$\begin{aligned}
\left(\frac{\mathrm{d}f_2^1}{\mathrm{d}s}\right)_{\mathrm{II}} =& \frac{1}{\hat{j}_1^2} \sum_J \sum_{rt} \hat{J}^2 n_t \left({}^J\Gamma^{r1}_{t2}\eta^t_r - {}^J\eta^{r1}_{t2} f^t_r \right) && (4.118)\\
=& \frac{1}{\hat{j}_1^2} \sum_J \sum_t \hat{J}^2 n_t \sum_r \left({}^J\Gamma^{r1}_{t2}\eta^t_r - {}^J\eta^{r1}_{t2} f^t_r \right) && (4.119)\\
=& \frac{1}{\hat{j}_1^2} \sum_J \sum_t \hat{J}^2 n_t \left({}^J\underline{\underline{\Omega}}_\eta \cdot {}^J\underline{\underline{\Gamma}} - {}^J\underline{\underline{\Omega}}_f \cdot {}^J\underline{\underline{\eta}} \right)^{t1}_{t2}. && (4.120)
\end{aligned}$$

With the aid of the diagonal matrices

$$\begin{aligned}
{}^J M^{tv}_{uw} :=& \bar{n}_t \bar{n}_v \delta^{tv}_{uw} && (4.121)\\
{}^J N^{tv}_{uw} :=& n_t n_v \delta^{tv}_{uw} && (4.122)
\end{aligned}$$

we can express the third term of the one-body part as matrix products

$$\begin{aligned}
\left(\frac{\mathrm{d}f_2^1}{\mathrm{d}s}\right)_{\mathrm{III}} =& \frac{1}{2\hat{j}_1^2} \sum_J \sum_{rtv} \hat{J}^2 \, {}^J\eta^{1r}_{tv} \, {}^J\Gamma^{tv}_{2r} (\bar{n}_t \bar{n}_v n_r + n_t n_v \bar{n}_r) && (4.123)\\
=& \frac{1}{2\hat{j}_1^2} \sum_J \sum_r \hat{J}^2 \left(n_r \sum_{\substack{tv\\uw}} {}^J\eta^{1r}_{tv} \, {}^J M^{tv}_{uw} \, {}^J\Gamma^{uw}_{2r} + \bar{n}_r \sum_{\substack{tv\\uw}} {}^J\eta^{1r}_{tv} \, N^{tv}_{uw} \, {}^J\Gamma^{uw}_{2r} \right) && (4.124)\\
=& \frac{1}{2\hat{j}_1^2} \sum_J \sum_r \hat{J}^2 \left(n_r \left({}^J\underline{\underline{\eta}} \cdot {}^J\underline{\underline{M}} \cdot {}^J\underline{\underline{\Gamma}} \right)^{1r}_{2r} + \bar{n}_r \left({}^J\underline{\underline{\eta}} \cdot {}^J\underline{\underline{N}} \cdot {}^J\underline{\underline{\Gamma}} \right)^{1r}_{2r} \right). && (4.125)
\end{aligned}$$

The fourth term is simply a product of three matrices

$$\begin{aligned}
\left(\frac{\mathrm{d}f_2^1}{\mathrm{d}s}\right)_{\mathrm{IV}} =& \frac{1}{4}\frac{1}{\hat{j}_1^2} \sum_J \sum_{tswrv} \hat{J}^2 \, {}^J\eta^{1t}_{sw} \, {}^J\Gamma^{rv}_{2t} \, {}^J\lambda^{rv}_{sw} && (4.126)\\
=& \frac{1}{4}\frac{1}{\hat{j}_1^2} \sum_J \sum_t \hat{J}^2 \left({}^J\underline{\underline{\eta}} \cdot {}^J\underline{\underline{\lambda}} \cdot {}^J\underline{\underline{\Gamma}} \right)^{1t}_{2t}. && (4.127)
\end{aligned}$$

Analogously, the fifth term is a product of three Pandya-transformed matrices

$$\left(\frac{\mathrm{d}f_2^1}{\mathrm{d}s}\right)_{\mathrm{V}} = \frac{1}{\hat{j}_1^2} \sum_J \sum_{rtswv} \hat{J}^2 \, {}^J\overline{\eta}^{1\bar{t}}_{s\bar{r}} \, {}^J\overline{\Gamma}^{v\bar{w}}_{2\bar{t}} \, {}^J\overline{\lambda}^{s\bar{r}}_{v\bar{w}} \tag{4.128}$$

$$= \frac{1}{\hat{j}_1^2} \sum_J \sum_t \hat{J}^2 \Big({}^J\underline{\overline{\eta}} \cdot {}^J\underline{\overline{\lambda}} \cdot {}^J\underline{\overline{\Gamma}} \Big)^{1\bar{t}}_{2\bar{t}}. \tag{4.129}$$

With the aid of the following abbreviation for a product of two matrices

$${}^{J_2}(\lambda\Gamma)^{pr}_{qs} := \sum_{tu} {}^{J_2}\lambda^{pr}_{tu}\, {}^{J_2}\Gamma^{tu}_{qs} = \Big({}^{J_2}\underline{\overline{\lambda}} \cdot {}^{J_2}\underline{\overline{\Gamma}} \Big)^{pr}_{qs} \tag{4.130}$$

$${}^{J_2}(\lambda\eta)^{pr}_{qs} := \sum_{tu} {}^{J_2}\lambda^{pr}_{tu}\, {}^{J_2}\eta^{tu}_{qs} = \Big({}^{J_2}\underline{\overline{\lambda}} \cdot {}^{J_2}\underline{\overline{\eta}} \Big)^{pr}_{qs} \tag{4.131}$$

we can reshape the last term as follows

$$\left(\frac{\mathrm{d} f_2^1}{\mathrm{d}s} \right)_{\mathrm{VI}} = -\frac{1}{2} \frac{1}{\hat{j}_1^2} \delta^{j_1}_{j_2} \sum_{J_1 J_2} \sum_{tsrv} \hat{J}_1^2 \hat{J}_2^2 \frac{1}{\hat{j}_t^2} \delta^{j_t}_{j_s} \Big({}^{J_1}\eta^{1t}_{2s}\, {}^{J_2}\lambda^{sw}_{rv}\, {}^{J_2}\Gamma^{rv}_{tw} - [\, \eta \leftrightarrow \Gamma] \Big) \tag{4.132}$$

$$= -\frac{1}{2} \frac{1}{\hat{j}_1^2} \delta^{j_1}_{j_2} \sum_{J_1 J_2} \sum_{tsw} \hat{J}_1^2 \hat{J}_2^2 \frac{1}{\hat{j}_t^2} \delta^{j_t}_{j_s} \Big({}^{J_1}\eta^{1t}_{2s}\, {}^{J_2}(\lambda\Gamma)^{sw}_{tw} - {}^{J_1}\Gamma^{1t}_{2s}\, {}^{J_2}(\lambda\eta)^{sw}_{tw} \Big) \tag{4.133}$$

which can be further simplified by means of a Pandya transformation. For that purpose, let us consider the first term of the previous expression

$$-\frac{1}{2} \frac{1}{\hat{j}_1^2} \delta^{j_1}_{j_2} \sum_{J_1 J_2} \sum_{tsw} \hat{J}_1^2 \hat{J}_2^2 \frac{1}{\hat{j}_t^2} \delta^{j_t}_{j_s}\, {}^{J_1}\eta^{1t}_{2s}\, {}^{J_2}(\lambda\Gamma)^{sw}_{tw} \tag{4.134}$$

$$= -\frac{1}{2} \frac{1}{\hat{j}_1^2} \delta^{j_1}_{j_2} \sum_{J_1 J_2} \sum_{tsw} (-)^{J_1 - J_2 - j_1 + j_w} \hat{J}_1^2 \hat{J}_2^2 \frac{1}{\hat{j}_t^2} \delta^{j_t}_{j_s}\, {}^{J_1}\eta^{1t}_{s2}\, {}^{J_2}(\lambda\Gamma)^{sw}_{wt} \tag{4.135}$$

$$= -\frac{1}{2} \frac{1}{\hat{j}_1^2} \delta^{j_1}_{j_2} \sum_{J_1 J_2} \sum_{tsw} (-)^{J_1 - J_2 - j_1 + j_w} \hat{J}_1^2 \hat{J}_2^2 \frac{1}{\hat{j}_t^2} \delta^{j_t}_{j_s}\, {}^{J_1}\eta^{1t}_{s2}\, {}^{J_2}(\lambda\Gamma)^{sw}_{wt} \tag{4.136}$$

$$= -(-)^2 \frac{1}{2} \frac{1}{\hat{j}_1^2} \delta^{j_1}_{j_2} \sum_{J_3 J_4} \sum_{J_1 J_2} \sum_{tsw} (-)^{J_1 - J_2 - j_1 + j_w} \hat{J}_1^2 \hat{J}_2^2 \hat{J}_3^2 \hat{J}_4^2 \frac{1}{\hat{j}_t^2} \delta^{j_t}_{j_s}\, {}^{J_3}\overline{\eta}^{1\bar{2}}_{s\bar{t}}\, {}^{J_4}\overline{(\lambda\Gamma)}^{s\bar{t}}_{w\bar{w}}$$
$$\times \begin{Bmatrix} j_1 & j_t & J_1 \\ j_t & j_1 & J_3 \end{Bmatrix} \begin{Bmatrix} j_t & j_w & J_2 \\ j_w & j_t & J_4 \end{Bmatrix} \tag{4.137}$$

$$= -\frac{1}{2} \frac{1}{\hat{j}_1^2} \delta^{j_1}_{j_2} \sum_{J_3 J_4} \sum_{J_1 J_2} \sum_{tsw} (-)^{J_1 - J_2 - j_1 + j_w} \hat{J}_1^2 \hat{J}_2^2 \hat{J}_3^2 \hat{J}_4^2 \frac{1}{\hat{j}_t^2} \delta^{j_t}_{j_s}\, {}^{J_3}\overline{\eta}^{1\bar{2}}_{s\bar{t}}\, {}^{J_4}\overline{(\lambda\Gamma)}^{s\bar{t}}_{w\bar{w}}$$
$$\times \begin{Bmatrix} j_1 & j_t & J_1 \\ j_t & j_1 & J_3 \end{Bmatrix} \begin{Bmatrix} j_t & j_w & J_2 \\ j_w & j_t & J_4 \end{Bmatrix} \tag{4.138}$$

$$= -\frac{1}{2} \frac{1}{\hat{j}_1^2} \delta^{j_1}_{j_2} \sum_{J_3 J_4} \sum_{tsw} (-)^{j_1 + j_t - (j_t + j_w) - j_1 + j_w} \hat{J}_3^2 \hat{J}_4^2 \hat{j}_1 \hat{j}_t \hat{j}_t \hat{j}_w \frac{1}{\hat{j}_t^2} \delta^{j_t}_{j_s} \delta^{J_3}_0 \delta^{J_4}_0\, {}^{J_3}\overline{\eta}^{1\bar{2}}_{s\bar{t}}\, {}^{J_4}\overline{(\lambda\Gamma)}^{s\bar{t}}_{w\bar{w}} \tag{4.139}$$

$$= -\frac{1}{2} \frac{\hat{j}_1}{\hat{j}_1^2} \delta^{j_1}_{j_2} \sum_{J_3 J_4} \sum_{tsw} \hat{J}_3^2 \hat{J}_4^2 \hat{j}_w \delta^{j_t}_{j_s} \delta^{J_3}_0 \delta^{J_4}_0\, {}^{J_3}\overline{\eta}^{1\bar{2}}_{s\bar{t}}\, {}^{J_4}\overline{(\lambda\Gamma)}^{s\bar{t}}_{w\bar{w}} \tag{4.140}$$

$$= -\frac{1}{2} \frac{1}{\hat{j}_1} \delta^{j_1}_{j_2} \sum_{tsw} \hat{j}_w \delta^{j_t}_{j_s}\, {}^{0}\overline{\eta}^{1\bar{2}}_{s\bar{t}}\, {}^{0}\overline{(\lambda\Gamma)}^{s\bar{t}}_{w\bar{w}} \tag{4.141}$$

$$= -\frac{1}{2} \frac{1}{\hat{j}_1} \delta^{j_1}_{j_2} \sum_{tsw} \hat{j}_w \delta^{j_t}_{j_s}\, {}^{0^+}\overline{\eta}^{1\bar{2}}_{s\bar{t}}\, {}^{0^+}\overline{(\lambda\Gamma)}^{s\bar{t}}_{w\bar{w}}. \tag{4.142}$$

Note that only the $J = 0$ block with positive parity, i.e., $+1$, is needed since the J-coupled two-body state $|(w\bar{w})JM\rangle$ always has positive parity. The reason is that the parity depends on the angular momentum l_w as follows $(-1)^{l_w+l_{\bar{w}}} = (-1)^{l_w+l_w} = (-1)^{2l_w} = +1$, which holds since l_w is an integer. The derivation of the second term is analogous. Hence, we obtain

$$\left(\frac{\mathrm{d}f_2^1}{\mathrm{d}s}\right)_{\mathrm{VI}} = -\frac{1}{2}\frac{1}{\hat{j}_1^2}\delta_{j_2}^{j_1}\sum_{J_1J_2}\sum_{tsrvw}\hat{J}_1^2\hat{J}_2^2\frac{1}{\hat{j}_t^2}\delta_{j_s}^{j_t}\left({}^{J_1}\eta_{2s}^{1t}\,{}^{J_2}\lambda_{rv}^{sw}\,{}^{J_2}\Gamma_{tw}^{rv} - [\,\eta \leftrightarrow \Gamma]\right) \tag{4.143}$$

$$= -\frac{1}{2}\frac{1}{\hat{j}_1}\delta_{j_2}^{j_1}\sum_{tsw}\hat{j}_w\left({}^{0}\overline{\eta}_{s\bar{t}}^{1\bar{2}}\,{}^{0^+}\overline{(\lambda\Gamma)}_{w\bar{w}}^{s\bar{t}} - {}^{0^+}\overline{\Gamma}_{s\bar{t}}^{1\bar{2}}\,{}^{0^+}\overline{(\lambda\eta)}_{w\bar{w}}^{s\bar{t}}\right) \tag{4.144}$$

$$= -\frac{1}{2}\frac{1}{\hat{j}_1}\delta_{j_2}^{j_1}\sum_{w}\hat{j}_w\left({}^{0^+}\underline{\overline{\eta}}\cdot{}^{0^+}\underline{\underline{\overline{(\lambda\Gamma)}}} - {}^{0^+}\underline{\overline{\Gamma}}\cdot{}^{0^+}\underline{\underline{\overline{(\lambda\eta)}}}\right)_{w\bar{w}}^{1\bar{2}} \tag{4.145}$$

with ${}^{0^+}\underline{\underline{\overline{(\lambda\Gamma)}}}$ and ${}^{0^+}\underline{\underline{\overline{(\lambda\eta)}}}$ being the $J = 0$ block of the Pandya-transformed matrices with positive parity of

$${}^{J'}\underline{\underline{(\lambda\Gamma)}} := {}^{J'}\underline{\lambda}\cdot{}^{J'}\underline{\Gamma} \tag{4.146}$$

$${}^{J'}\underline{\underline{(\lambda\eta)}} := {}^{J'}\underline{\lambda}\cdot{}^{J'}\underline{\eta}. \tag{4.147}$$

Note that all J' blocks of these matrices are needed for the calculation of ${}^{0^+}\underline{\underline{\overline{(\lambda\Gamma)}}}$ and ${}^{0^+}\underline{\underline{\overline{(\lambda\eta)}}}$ because of the sum over all J' in the definition of the Pandya transformation (4.49), i.e.,

$${}^{0^+}\overline{(\lambda\Gamma)}_{3\bar{4}}^{1\bar{2}} := \delta_{+}^{\pi_{\bar{2}}^1}\delta_{\pi_{\bar{4}}^3}^{+}\,{}^{0}\overline{(\lambda\Gamma)}_{3\bar{4}}^{1\bar{2}} = -\delta_{+}^{\pi_{\bar{2}}^1}\delta_{\pi_{\bar{4}}^3}^{+}\sum_{J'}\hat{J'}^2\begin{Bmatrix} j_1 & j_2 & 0 \\ j_3 & j_4 & J' \end{Bmatrix}{}^{J'}(\lambda\Gamma)_{32}^{14} \tag{4.148}$$

$${}^{0^+}\overline{(\lambda\eta)}_{3\bar{4}}^{1\bar{2}} := \delta_{+}^{\pi_{\bar{2}}^1}\delta_{\pi_{\bar{4}}^3}^{+}\,{}^{0}\overline{(\lambda\eta)}_{3\bar{4}}^{1\bar{2}} = -\delta_{+}^{\pi_{\bar{2}}^1}\delta_{\pi_{\bar{4}}^3}^{+}\sum_{J'}\hat{J'}^2\begin{Bmatrix} j_1 & j_2 & 0 \\ j_3 & j_4 & J' \end{Bmatrix}{}^{J'}(\lambda\eta)_{32}^{14} \tag{4.149}$$

with the parity $\pi_{\bar{q}}^{p} := (-1)^{l_p+l_{\bar{q}}} = (-1)^{l_p+l_q}$.

Zero-Body Part

The first term of the zero-body part is simply a matrix product that has already been calculated in the first term of the one-body part

$$\left(\frac{\mathrm{d}E}{\mathrm{d}s}\right)_{\mathrm{I}} = +(1-\chi)\sum_{pr}\hat{j}_p^2\eta_r^p f_p^r n_p \tag{4.150}$$

$$= +(1-\chi)\sum_{p}\hat{j}_p^2 n_p\left(\underline{\eta}\cdot\underline{f}\right)_p^p. \tag{4.151}$$

With the aid of the previously-defined diagonal matrices, the second term can be expressed as the trace of a product of four matrices

$$\left(\frac{\mathrm{d}E}{\mathrm{d}s}\right)_{\mathrm{II}} = +\frac{1}{4}(1-\chi)\sum_{J}\sum_{prtv}\hat{J}^2\,{}^{J}\eta_{tv}^{pr}\,{}^{J}\Gamma_{pr}^{tv}n_p n_r\bar{n}_t\bar{n}_v \tag{4.152}$$

$$= + \frac{1}{4}(1-\chi) \sum_J \sum_{\substack{prtv \\ qsuw}} \hat{J}^2 n_p n_r \delta_{qs}^{pr} \, {}^J\eta_{uw}^{qs} \bar{n}_u \bar{n}_w \delta_{tv}^{uw} \, {}^J\Gamma_{pr}^{tv} \tag{4.153}$$

$$= + \frac{1}{4}(1-\chi) \sum_J \sum_{\substack{prtv \\ qsuw}} \hat{J}^2 \, {}^J N_{qs}^{pr} \, {}^J\eta_{uw}^{qs} \, {}^J M_{tv}^{uw} \, {}^J\Gamma_{pr}^{tv} \tag{4.154}$$

$$= + \frac{1}{4}(1-\chi) \sum_J \hat{J}^2 \mathrm{tr} \left({}^J\underline{\underline{N}} \cdot {}^J\underline{\underline{\eta}} \cdot {}^J\underline{\underline{M}} \cdot {}^J\underline{\underline{\Gamma}} \right), \tag{4.155}$$

where we used the definition of the trace from (4.97). The last term is simply

$$\left(\frac{\mathrm{d}E}{\mathrm{d}s} \right)_{\mathrm{III}} = \frac{1}{4} \cdot \frac{1-\chi}{2} \sum_J \sum_{prqs} \hat{J}^2 \frac{\mathrm{d} \, {}^J\Gamma_{qs}^{pr}}{\mathrm{d}s} \, {}^J\lambda_{qs}^{pr} \tag{4.156}$$

$$= \frac{1}{4} \cdot \frac{1-\chi}{2} \sum_J \hat{J}^2 \, \mathrm{tr} \left(\frac{\mathrm{d}^J\underline{\underline{\Gamma}}}{\mathrm{d}s} \cdot {}^J\underline{\underline{\lambda}} \right). \tag{4.157}$$

4.4.3. Summary of BLAS Compliant Flow Equations

In summary, we obtain the system of J-coupled multi-reference IM-SRG(2) flow equations in natural orbitals rewritten in BLAS compliant form

$$
\begin{aligned}
\frac{\mathrm{d}\,{}^{J}\Gamma^{12}_{34}}{\mathrm{d}s} =& \Bigg[\Bigg(\frac{1}{2}\Big(\,{}^{J}\underline{\underline{\Omega_\eta}}\cdot{}^{J}\underline{\underline{\Gamma}} - \,{}^{J}\underline{\underline{\Omega_f}}\cdot{}^{J}\underline{\underline{\eta}}\Big)^{12}_{34} \\
&+ \frac{1}{8}\Big({}^{J}\underline{\underline{\eta}}\cdot{}^{J}\underline{\underline{F}}\cdot{}^{J}\underline{\underline{\Gamma}}\Big)^{12}_{34} \\
&- \frac{1}{2}\,{}^{J}B^{12}_{34}\Bigg) \\
&- (-)^{J-j_1-j_2}[1\leftrightarrow 2]\Bigg) - (-)^{J-j_3-j_4}[3\leftrightarrow 4]\Bigg] - \chi[12\leftrightarrow 34] \qquad (4.158a)\\
\frac{\mathrm{d}f^{1}_{2}}{\mathrm{d}s} =& \Big[\Big(\underline{\underline{\eta}}\cdot\underline{\underline{f}}\Big)^{1}_{2} \\
&+ \frac{1}{\hat{j}_1^2}\sum_J\sum_t \hat{J}^2 n_t\Big(\,{}^{J}\underline{\underline{\Omega_\eta}}\cdot{}^{J}\underline{\underline{\Gamma}} - \,{}^{J}\underline{\underline{\Omega_f}}\cdot{}^{J}\underline{\underline{\eta}}\Big)^{t1}_{t2} \\
&+ \frac{1}{2\hat{j}_1^2}\sum_J\sum_r \hat{J}^2\left(n_r\Big({}^{J}\underline{\underline{\eta}}\cdot{}^{J}\underline{\underline{M}}\cdot{}^{J}\underline{\underline{\Gamma}}\Big)^{1r}_{2r} + \bar{n}_r\Big({}^{J}\underline{\underline{\eta}}\cdot{}^{J}\underline{\underline{N}}\cdot{}^{J}\underline{\underline{\Gamma}}\Big)^{1r}_{2r}\right) \\
&+ \frac{1}{4}\frac{1}{\hat{j}_1^2}\sum_J\sum_t \hat{J}^2\Big({}^{J}\underline{\underline{\eta}}\cdot{}^{J}\underline{\underline{\lambda}}\cdot{}^{J}\underline{\underline{\Gamma}}\Big)^{1t}_{2t} \\
&+ \frac{1}{\hat{j}_1^2}\sum_J\sum_t \hat{J}^2\Big({}^{J}\underline{\underline{\overline{\eta}}}\cdot{}^{J}\underline{\underline{\overline{\lambda}}}\cdot{}^{J}\underline{\underline{\overline{\Gamma}}}\Big)^{1\bar{t}}_{2\bar{t}} \\
&- \frac{1}{2}\frac{1}{\hat{j}_1}\sum_w \hat{j}_w\Big({}^{0^+}\underline{\underline{\overline{\eta}}}\cdot{}^{0^+}\underline{\underline{\overline{(\lambda\Gamma)}}} - {}^{0^+}\underline{\underline{\overline{\Gamma}}}\cdot{}^{0^+}\underline{\underline{\overline{(\lambda\eta)}}}\Big)^{1\bar{2}}_{w\bar{w}}\Big] - \chi[1\leftrightarrow 2] \qquad (4.158b)\\
\frac{\mathrm{d}E}{\mathrm{d}s} =& (1-\chi)\sum_p \hat{j}_p^2 n_p\Big(\underline{\underline{\eta}}\cdot\underline{\underline{f}}\Big)^{p}_{p} \\
&+ \frac{1}{4}(1-\chi)\sum_J \hat{J}^2\mathrm{tr}\Big({}^{J}\underline{\underline{N}}\cdot{}^{J}\underline{\underline{\eta}}\cdot{}^{J}\underline{\underline{M}}\cdot{}^{J}\underline{\underline{\Gamma}}\Big) \\
&+ \frac{1}{4}\cdot\frac{1-\chi}{2}\sum_J \hat{J}^2\,\mathrm{tr}\left(\frac{\mathrm{d}\,{}^{J}\underline{\underline{\Gamma}}}{\mathrm{d}s}\cdot{}^{J}\underline{\underline{\lambda}}\right) \\
&+ \mathcal{O}(\lambda^{(3)}). \qquad (4.158c)
\end{aligned}
$$

For an efficient implementation, we make use of intermediate results. For instance, the second term in the one-body part is basically a partial trace of the first sub-expression in the two-body part. Furthermore, the Pandya-transformed matrix ${}^{J}\underline{\underline{\overline{\eta}}}$ calculated in the third term of the two-body part can be used to implement the fifth and sixth term of the one-body part. Finally, the matrix products $\underline{\underline{\eta}}\cdot\underline{\underline{f}}$ and ${}^{J}\underline{\underline{\eta}}\cdot{}^{J}\underline{\underline{M}}\cdot{}^{J}\underline{\underline{\Gamma}}$ appearing in the one-body part also occur in the first and second term of the zero-body part, respectively.

As a reminder, these are the definitions used to write these equations in compact form:

$$
\begin{aligned}
{}^{J}(\Omega_\eta)^{pr}_{qs} &:= \eta^p_q \delta^r_s && \text{(4.159a)}\\
{}^{J}(\Omega_f)^{pr}_{qs} &:= f^p_q \delta^r_s && \text{(4.159b)}\\
{}^{J}F^{tv}_{uw} &:= (1 - n_t - n_v)\delta^{tv}_{uw} && \text{(4.159c)}\\
{}^{J}\overline{D}^{v\bar{t}}_{w\bar{u}} &:= (n_v - n_t)\delta^{vt}_{wu} && \text{(4.159d)}\\
{}^{J'}\underline{\underline{\overline{B}}} &:= {}^{J'}\underline{\underline{\overline{\eta}}} \cdot {}^{J'}\underline{\underline{\overline{D}}} \cdot {}^{J'}\underline{\underline{\overline{\Gamma}}} && \text{(4.159e)}\\
{}^{J'}B^{12}_{34} &:= -\sum_J \hat{J}^2 \begin{Bmatrix} j_1 & j_4 & J \\ j_3 & j_2 & J' \end{Bmatrix} {}^{J}\overline{B}^{1\bar{4}}_{3\bar{2}} && \text{(4.159f)}\\
{}^{J}M^{tv}_{uw} &:= \bar{n}_t \bar{n}_v \delta^{tv}_{uw} && \text{(4.159g)}\\
{}^{J}N^{tv}_{uw} &:= n_t n_v \delta^{tv}_{uw} && \text{(4.159h)}\\
{}^{J'}\underline{\underline{(\lambda\Gamma)}} &:= {}^{J'}\underline{\underline{\lambda}} \cdot {}^{J'}\underline{\underline{\Gamma}} && \text{(4.159i)}\\
{}^{J'}\underline{\underline{(\lambda\eta)}} &:= {}^{J'}\underline{\underline{\lambda}} \cdot {}^{J'}\underline{\underline{\eta}} && \text{(4.159j)}\\
\pi^p_{\bar{q}} &:= (-1)^{l_p + l_q} && \text{(4.159k)}\\
{}^{0^+}\overline{(\lambda\Gamma)}^{1\bar{2}}_{3\bar{4}} &:= -\delta^{\pi^1_{\bar{2}}}_{+}\delta^{+}_{\pi^3_{\bar{4}}} \sum_{J'} \hat{J'}^2 \begin{Bmatrix} j_1 & j_2 & 0 \\ j_3 & j_4 & J' \end{Bmatrix} {}^{J'}(\lambda\Gamma)^{14}_{32} && \text{(4.159l)}\\
{}^{0^+}\overline{(\lambda\eta)}^{1\bar{2}}_{3\bar{4}} &:= -\delta^{\pi^1_{\bar{2}}}_{+}\delta^{+}_{\pi^3_{\bar{4}}} \sum_{J'} \hat{J'}^2 \begin{Bmatrix} j_1 & j_2 & 0 \\ j_3 & j_4 & J' \end{Bmatrix} {}^{J'}(\lambda\eta)^{14}_{32} && \text{(4.159m)}\\
\left(\frac{\mathrm{d}^J\underline{\underline{\Gamma}}}{\mathrm{d}s}\right)^{12}_{34} &:= \frac{\mathrm{d}\,{}^{J}\Gamma^{12}_{34}}{\mathrm{d}s} && \text{(4.159n)}
\end{aligned}
$$

Finally, we give an overview of the most important symbols used here.

$n_p, \bar{n}_p$	mean particle and hole occupation numbers
λ^{pr}_{qs}	irreducible two-body density matrix element
${}^J\lambda^{pr}_{qs}$	J-coupled irreducible two-body density matrix element
${}^J\overline{\lambda}^{p\bar{r}}_{q\bar{s}}$	Pandya-transformed J-coupled irreducible 2-body density matrix elem.
${}^J\underline{\underline{\lambda}}$	matrix representation of ${}^J\lambda^{pr}_{qs}$
${}^J\underline{\underline{\overline{\lambda}}}$	matrix representation of ${}^J\overline{\lambda}^{p\bar{r}}_{q\bar{s}}$
$\boldsymbol{H}$	Hamiltonian
$E, f^p_q, \Gamma^{pr}_{qs}, W^{prt}_{qsu}$	0-, 1-, 2-, 3-body matrix elements of $\boldsymbol{H}$ in reference-state repr.
${}^J\Gamma^{pr}_{qs}$	J-coupled two-body matrix elements of $\boldsymbol{H}$ in reference-state repr.
${}^J\overline{\Gamma}^{p\bar{r}}_{q\bar{s}}$	Pandya-transformed J-coupled two-body matrix elements of ${}^J\Gamma^{pr}_{qs}$
$\underline{\underline{f}}$	matrix representation of f^p_q
${}^J\underline{\underline{\Gamma}}$	matrix representation of ${}^J\Gamma^{pr}_{qs}$
${}^J\underline{\underline{\overline{\Gamma}}}$	matrix representation of ${}^J\overline{\Gamma}^{p\bar{r}}_{q\bar{s}}$
${}^J(\Omega_f)^{pr}_{qs}$	embedded J-coupled two-body matrix elements ${}^J(\Omega_f)^{pr}_{qs} \coloneqq f^p_q\delta^r_s$
${}^J\underline{\underline{\Omega_f}}$	matrix representation of ${}^J(\Omega_f)^{pr}_{qs}$
$\boldsymbol{\eta}$	generator of the multi-reference IM-SRG evolution
η^p_q, η^{pr}_{qs}	one- and two-body matrix elements of $\boldsymbol{\eta}$ in reference-state repr.
${}^J\eta^{pr}_{qs}$	J-coupled two-body matrix elements of $\boldsymbol{\eta}$ in reference-state repr.
${}^J\overline{\eta}^{p\bar{r}}_{q\bar{s}}$	Pandya-transformed J-coupled two-body matrix elements of ${}^J\eta^{pr}_{qs}$
$\underline{\underline{\eta}}$	matrix representation of η^p_q
${}^J\underline{\underline{\eta}}$	matrix representation of ${}^J\eta^{pr}_{qs}$
${}^J\underline{\underline{\overline{\eta}}}$	matrix representation of ${}^J\overline{\eta}^{p\bar{r}}_{q\bar{s}}$
${}^J(\Omega_\eta)^{pr}_{qs}$	embedded J-coupled two-body matrix elements ${}^J(\Omega_\eta)^{pr}_{qs} \coloneqq \eta^p_q\delta^r_s$
${}^J\underline{\underline{\Omega_\eta}}$	matrix representation of ${}^J(\Omega_\eta)^{pr}_{qs}$

4.5. Generalized A-Particle A-Hole Basis

In this section, we introduce a specific many-body basis of the A-body Hilbert space, called A-particle A-hole basis, based on a given A-body reference state (section 4.5.1). The concept of this basis is footed in the normal-ordering technique introduced in chapter 3, and is a crucial point for the construction of the generators for the IM-SRG evolution discussed in section 4.6. For illustration purposes, we focus on specific basis states (sections 4.5.2 and 4.5.3). It turns out that the A-particle A-hole basis is overcomplete. We propose an algorithm that gives at least the right number of basis states, and demonstrate its usage on a two-body system as a test case (section 4.5.4). But the linear independence of the states generated by this algorithm still remains to prove, which is highly non-trivial. However, we emphasize that the overcompleteness does not cause any problems in IM-SRG.

4.5.1. General Considerations

Suppose the reference state can be expressed as a linear combination of Slater determinants $|\Phi_n\rangle$, which are antisymmetrized A-body states, as follows

$$|\Psi\rangle = \sum_n c_n |\Phi_n\rangle . \tag{4.160}$$

Based on the reference state the single-particle basis can be classified in three disjoint sets which are schematically depicted in figure 4.1:

- A *core* state corresponds to a single-particle state occupied in all Slater determinants of the reference state. These single-particle states will be indicated by the indices $i, j, \ldots$, and the corresponding set of all core indices is abbreviated by $\mathcal{C}$.
- An *active* state is a single-particle state occupied in at least one, but not in all of these Slater determinants. These single-particle states will be indicated by the indices $x, y, \ldots$, and a shorthand notation for the set of all active indices is $\mathcal{A}$. Note that these states do not exist in the single-reference case.
- A *virtual* state is a single-particle state *unoccupied* in all of these Slater determinants. These single-particle states will be indicated by the indices $b, c, \ldots$, and the set containing all virtual indices is denoted by $\mathcal{V}$.

Conventionally, the indices p, r, q, s,... can refer to all of these types of indices. Due to Pauli exclusion principle, creating a core state or annihilating a virtual state on top of the reference state leads to

$$\boldsymbol{a}^i |\Psi\rangle = \langle\Psi| \boldsymbol{a}_i = 0 \tag{4.161}$$

$$\boldsymbol{a}_b |\Psi\rangle = \langle\Psi| \boldsymbol{a}^b = 0. \tag{4.162}$$

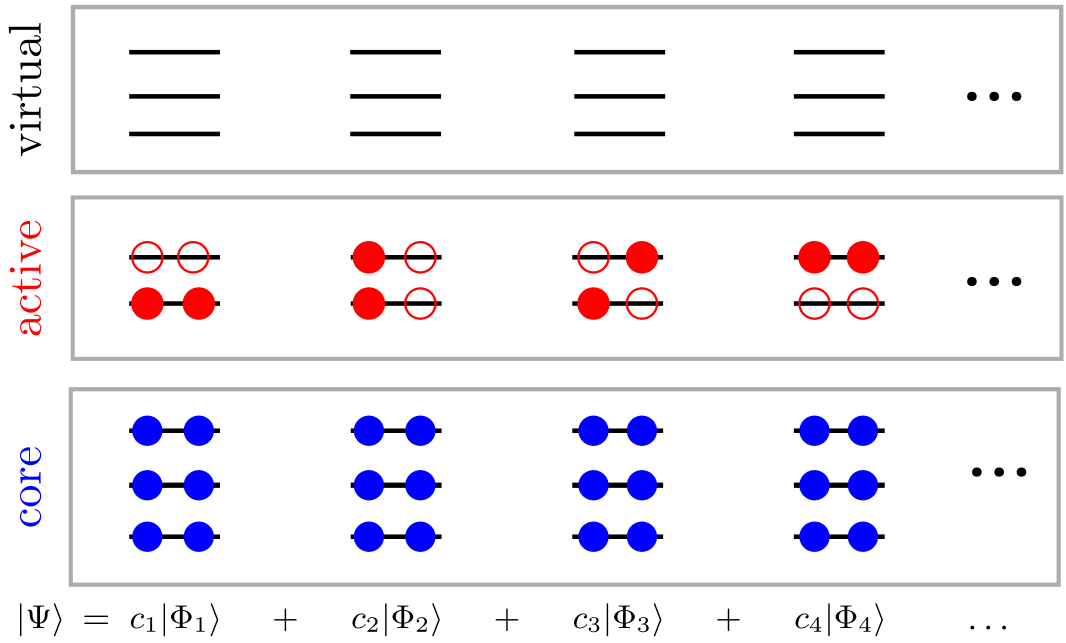

Figure 4.1.: A schematic depiction for the classification of the single-particle basis based on a reference state $|\Psi\rangle$ containing eight identical fermions. Core states (blue solid circles) are single-particle states occupied in all Slater determinants $|\Phi_n\rangle$, whereas the virtual states are occupied in none of them. The remaining single-particle states, called active states, are occupied (red solid circles) and unoccupied (red open circles) in some of them. The vertical ordering of the states has no meaning.

Consequently, the n-body density matrix element vanishes

$$\gamma^{p_1\ldots p_n}_{q_1\ldots q_n} = \langle\Psi|\boldsymbol{a}^{p_1\ldots p_n}_{q_1\ldots q_n}|\Psi\rangle = 0 \tag{4.163}$$

for different scenarios:

- If any index is virtual, i.e., $p_i \in \mathcal{V}$ or $q_i \in \mathcal{V}$ for any $i \in \{1, 2, \ldots, n\}$.
- If the number of the core, active and virtual indices in the upper and lower indices is different, e.g., if there are exactly two and three active orbitals in the upper and lower indices, respectively.

If one of the upper indices belongs to the core then the action of the n-body operator on the reference state is reducible in the sense that can be expressed as a linear combination of the action of $(n-1)$-body operators

$$\boldsymbol{a}^{i\,p_2p_3\ldots p_n}_{q_1q_2q_3\ldots q_n}|\Psi\rangle = (\delta^i_{q_1}\boldsymbol{a}^{p_2p_3\ldots p_n}_{q_2q_3\ldots q_n} - \delta^i_{q_2}\boldsymbol{a}^{p_2p_3\ldots p_n}_{q_1q_3\ldots q_n} + \ldots + (-1)^{n-1}\delta^i_{q_n}\boldsymbol{a}^{p_2p_3\ldots p_n}_{q_1q_2\ldots q_{n-1}})|\Psi\rangle \tag{4.164}$$

$$= \frac{1}{(n-1)!}\sum_{\pi\in\mathcal{S}_n}\mathrm{sgn}(\pi)\delta^i_{q_{\pi(1)}}\boldsymbol{a}^{p_2p_3\ldots p_n}_{q_{\pi(2)}q_{\pi(3)}\ldots q_{\pi(n)}}|\Psi\rangle\,. \tag{4.165}$$

Here, $\mathcal{S}_n$ denotes the set of all permutations of (1, 2, ..., n). By projecting (4.165) on the reference state, i.e., multiplying with $\langle\Psi|$ from the left, we can identify the one-body density

matrix elements that has the same form in this case

$$\gamma^{i\,p_2p_3\dots p_n}_{q_1q_2q_3\dots q_n} = \delta^i_{q_1}\gamma^{p_2p_3\dots p_n}_{q_2q_3\dots q_n} - \delta^i_{q_2}\gamma^{p_2p_3\dots p_n}_{q_1q_3\dots q_n} + \dots + (-1)^{n-1}\delta^i_{q_n}\gamma^{p_2p_3\dots p_n}_{q_1q_2\dots q_{n-1}} \tag{4.166}$$

$$= \frac{1}{(n-1)!}\sum_{\pi\in\mathcal{S}_n}\operatorname{sgn}(\pi)\delta^i_{q_{\pi(1)}}\gamma^{p_2p_3\dots p_n}_{q_{\pi(2)}q_{\pi(3)}\dots q_{\pi(n)}}. \tag{4.167}$$

Hence, if all upper indices correspond to the core then the density matrix element is trivially diagonal

$$\gamma^{i_1i_2\dots i_n}_{q_1q_2\dots q_n} = \mathbb{A}(\delta^{i_1}_{q_1}\delta^{i_2}_{q_2}\cdots\delta^{i_n}_{q_n}) \tag{4.168}$$

which looks like the single-reference case.

Based on the reference state $|\Psi\rangle$, we generate A-body states by acting with the normal-ordered n-body operator on this reference state

$$|\Psi^{p_1\dots p_n}_{q_1\dots q_n}\rangle := \tilde{\boldsymbol{a}}^{p_1\dots p_n}_{q_1\dots q_n}|\Psi\rangle \tag{4.169}$$

$$= (\boldsymbol{a}^{p_1\dots p_n}_{q_1\dots q_n} - \gamma^{p_1\dots p_n}_{q_1\dots q_n})|\Psi\rangle - \sum_{j=1}^{n-1}\mathbb{A}(\gamma^{p_1\dots p_j}_{q_1\dots q_j}|\Psi^{p_{j+1}\dots p_n}_{q_{j+1}\dots q_n}\rangle) \tag{4.170}$$

which we call the *generalized n-particle n-hole state* or *n-particle n-hole excitation*.

Obviously, these n-particle n-hole excitations are antisymmetric with respect to exchange among the upper and lower indices, respectively:

$$|\Psi^{p_1\dots p_i\dots p_j\dots p_n}_{q_1\dots q_i\dots q_j\dots q_n}\rangle = -|\Psi^{p_1\dots p_j\dots p_i\dots p_n}_{q_1\dots q_i\dots q_j\dots q_n}\rangle = -|\Psi^{p_1\dots p_i\dots p_j\dots p_n}_{q_1\dots q_j\dots q_i\dots q_n}\rangle \tag{4.171}$$

for all $i,j\in\{1,2,\dots n\}$ with $i\neq j$ because the (reference-state) normal-ordered operators do have this property (3.59). Let us analyze the scenarios where these n-particle n-hole excitations vanish.

Proposition 4.1. *Any n-particle n-hole excitation vanishes*

$$|\Psi^{p_1\dots p_n}_{q_1\dots q_n}\rangle = 0 \tag{4.172}$$

- *if at least one of the lower indices is a virtual index, i.e., $q_k\in\mathcal{V}$ for any $k\in\{1,2,\dots,n\}$,*
- *if at least one of the upper indices is a core index, i.e., $p_k\in\mathcal{C}$ for any $k\in\{1,2,\dots,n\}$.*

Since the proof of this proposition is extremely technical, we postpone it to appendix B.2. With the aid of the reference state and generalized n-particle n-hole excitations up to particle rank A, we can define a nucleus-specific many-body basis of the A-body Hilbert space, which

we call the *generalized A-particle A-hole basis*

$$\mathcal{B}_{\text{IM-SRG}} \coloneqq \Big\{ |\Psi\rangle \Big\} \bigcup \left\{ \bigcup_{n=1}^{A} \left\{ \bigcup_{\substack{p_1<p_2<\ldots<p_n \\ q_1<q_2<\ldots<q_n}} \{ |\Psi^{p_1 p_2 \ldots p_n}_{q_1 q_2 \ldots q_n}\rangle : p_1, p_2, \ldots p_n \notin \mathcal{C},\, q_1, q_2, \ldots, q_n \notin \mathcal{V} \} \right\} \right\} \tag{4.173}$$

$$\begin{aligned} =& \{ |\Psi\rangle \} \bigcup \{ |\Psi^{p_1}_{q_1}\rangle : p_1 \notin \mathcal{C},\, q_1 \notin \mathcal{V} \} \\ & \bigcup \{ |\Psi^{p_1 p_2}_{q_1 q_2}\rangle : p_1, p_2 \notin \mathcal{C},\, q_1, q_2 \notin \mathcal{V},\, p_1 < p_2, q_1 < q_2 \} \\ & \vdots \\ & \bigcup \{ |\Psi^{p_1 p_2 \ldots p_A}_{q_1 q_2 \ldots q_A}\rangle : p_1, p_2, \ldots p_A \notin \mathcal{C},\, q_1, q_2, \ldots, q_A \notin \mathcal{V}, \\ & \qquad p_1 < p_2 < \ldots < p_A, q_1 < q_2 < \ldots < q_A \} \end{aligned} \tag{4.174}$$

Here, we restricted the indices in order to get rid of trivial zero vectors as analyzed in proposition 4.1 and linear dependencies (4.171), but this basis still remains overcomplete in general. We propose an algorithm how to choose a proper number of basis states from the overcomplete A-particle A-hole basis, and explicitly demonstrate its usage on a simple problem in section 4.5.4. A general proof of the linear independence of the set of basis states generated by this algorithm has yet to be provided. Luckily, it does not cause any problem for our discussion. In multi-reference coupled cluster, for instance, this is a problematic point and one has to calculate the many-body overlap matrix. After diagonalizing this matrix, one can eliminate the overcompleteness by discarding all basis states related to zero eigenvalue of the overlap matrix.

Furthermore, this basis is not orthogonal because, e.g., the generalized one-particle one-hole states are in general not orthogonal to each other due to the irreducible two-body density matrix element, which does not vanish for the multi-reference case:

$$\langle \Psi^p_q | \Psi^r_s \rangle = n_p \bar{n}_q \delta^p_s \delta^r_q + \lambda^{pr}_{qs} \neq \delta^p_s \delta^r_q. \tag{4.175}$$

But it remains true that the reference state $|\Psi\rangle$ is orthogonal to all other states by construction due to normal ordering, i.e.,

$$\langle \Psi | \Psi^p_q \rangle = \langle \Psi | \tilde{\boldsymbol{a}}^p_q | \Psi \rangle = 0 \tag{4.176a}$$

$$\langle \Psi | \Psi^{pr}_{qs} \rangle = \langle \Psi | \tilde{\boldsymbol{a}}^{pr}_{qs} | \Psi \rangle = 0 \tag{4.176b}$$

$$\vdots$$

$$\langle \Psi | \Psi^{p_1 \ldots p_A}_{q_1 \ldots q_A} \rangle = \langle \Psi | \tilde{\boldsymbol{a}}^{p_1 \ldots p_A}_{q_1 \ldots q_A} | \Psi \rangle = 0. \tag{4.176c}$$

Thus, all states besides the reference state span a subspace of the A-body Hilbert space orthogonal to the subspace spanned by the reference state only (see figure 4.2).

Let us analyze the n-particle n-hole excitations for the case $n > A$. Obviously, this case does not contribute for the single-reference case, where the reference state is just a single

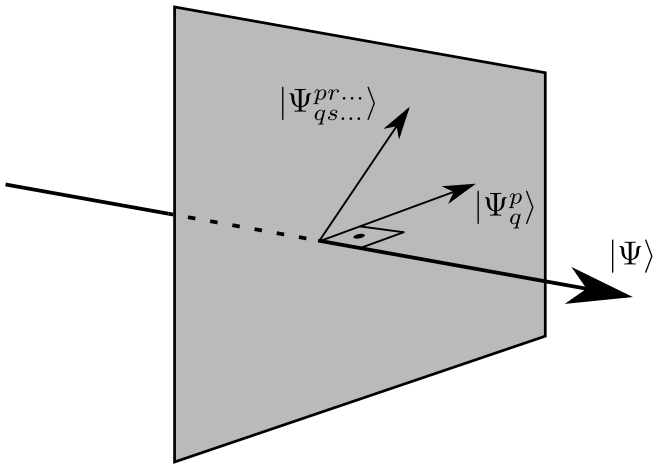

Figure 4.2.: Schematic depiction that all n-particle n-hole excitations are orthogonal to the reference state. Whereas the n-particle n-hole excitations are either orthogonal to each other nor normalized.

Slater determinant. But for the multi-reference case, taking a closer look at the definition of the n-particle n-hole excitations given in (4.169), we can clearly see that these basis states do not vanish since they contain contribution from lower-particle rank excitations. This is related to the existence of the active space. However, a natural question that arises is whether they can be expressed as linear combination of i-particle i-hole excitations with $i \leq A$.

Proposition 4.2. *Any n-particle n-hole excitation on top of the A-body reference state $|\Psi\rangle$ with $n > A$ can be written as linear combination of all generalized i-particle i-hole excitations with $i \leq A$*

$$|\Psi^{p_1\ldots p_n}_{q_1\ldots q_n}\rangle = \sum_{i=1}^{A} \left(\sum_{\substack{r_1\ldots r_i \\ s_1\ldots s_i}} c^{r_1\ldots r_i}_{s_1\ldots s_i} |\Psi^{r_1\ldots r_i}_{s_1\ldots s_i}\rangle \right). \tag{4.177}$$

Thus, excitations beyond A-body rank do not necessarily vanish, but are superposition of lower-particle rank excitations.

Proof. First step is to show that the generalized n-particle n-hole excited state is orthogonal to $|\Psi\rangle$

$$\langle\Psi|\Psi^{p_1\ldots p_n}_{q_1\ldots q_n}\rangle = \langle\Psi|\tilde{\boldsymbol{a}}^{p_1\ldots p_n}_{q_1\ldots q_n}|\Psi\rangle = 0, \tag{4.178}$$

which is guaranteed due to the construction of normal ordering. Introducing the shorthand notation for the vacuum normal-ordered n-body operator

$$\boldsymbol{a}^{[n]} := \boldsymbol{a}^{p_1\ldots p_n}_{q_1\ldots q_n} \tag{4.179}$$

we can convince ourselves that the *full* n-particle density matrix with respect to the reference

state vanishes for $n > A$

$$\gamma^{[n]} := \langle \Psi | \boldsymbol{a}^{[n]} | \Psi \rangle = 0 \tag{4.180}$$

since we cannot annihilate more than A particles occupied in the reference state $|\Psi\rangle$. The vacuum normal-ordered n-body operator can be expressed as a linear combination of the reference-state normal-ordered operators (3.60d). On the one hand, since all *full* l-particle density matrices for $l > A$ vanish, expression (3.60d) for the case $n > A$ can be formulated structurally as

$$\boldsymbol{a}^{[n]} = \tilde{\boldsymbol{a}}^{[n]} + \mathcal{F}(\gamma^{[1]}, \ldots, \gamma^{[A]}, \tilde{\boldsymbol{a}}^{[n-1]}, \ldots, \tilde{\boldsymbol{a}}^{[n-A]}) \tag{4.181}$$

with a properly defined function $\mathcal{F}$ which is a linear combination of the normal-ordered i-body operators with $n - A \leq i \leq n - 1$. On the other hand, by writing all normal-ordered operators in terms of the vacuum normal-ordered operators by a recursive treatment, we can recast this expression to

$$\tilde{\boldsymbol{a}}^{[n]} = \boldsymbol{a}^{[n]} - \mathcal{G}(\gamma^{[1]}, \ldots, \gamma^{[A]}, \boldsymbol{a}^{[n-1]}, \ldots, \boldsymbol{a}^{[A+1]}, \boldsymbol{a}^{[A]}, \ldots, \boldsymbol{a}^{[1]}) \tag{4.182}$$

with a properly defined function $\mathcal{G}$ which is still a linear combination of the vacuum normal-ordered j-body operators with $1 \leq j \leq n-1$. Note, in contrast to $\mathcal{F}$, the function $\mathcal{G}$ depends on all particle ranks down to one. The proof is closed by applying the normal-ordered n-body operator on the reference state $|\Psi\rangle$

$$\begin{aligned}
|\Psi^{[n]}\rangle :=& \tilde{\boldsymbol{a}}^{[n]} |\Psi\rangle && (4.183)\\
=& \underbrace{\boldsymbol{a}^{[n]} |\Psi\rangle}_{=0} - \mathcal{G}(\gamma^{[1]}, \ldots, \gamma^{[A]}, \boldsymbol{a}^{[n-1]}, \ldots, \boldsymbol{a}^{[A+1]}, \boldsymbol{a}^{[A]}, \ldots, \boldsymbol{a}^{[1]}) |\Psi\rangle && (4.184)\\
=& - \mathcal{G}_n(\gamma^{[1]}, \ldots, \gamma^{[A]}, \boldsymbol{a}^{[A]}, \ldots, \boldsymbol{a}^{[1]}) |\Psi\rangle && (4.185)
\end{aligned}$$

with a new function $\mathcal{G}_n$ for each rank n which does not depend on operators beyond particle rank A, since $g(\boldsymbol{a}^{[i]}) |\Psi\rangle = 0$ for all $i > A$ and any function g. By reexpressing the vacuum normal-ordered one- to A-body operators in terms of the reference-state normal-ordered one- to A-body operators, we can rewrite the above expression to

$$|\Psi^{[n]}\rangle = -\mathcal{H}_n(\gamma^{[1]}, \ldots, \gamma^{[A]}, \tilde{\boldsymbol{a}}^{[A]}, \ldots, \tilde{\boldsymbol{a}}^{[1]}) |\Psi\rangle \,. \tag{4.186}$$

with a properly defined function $\mathcal{H}_n$ which is still a linear combination of the reference-state normal-ordered operators up to particle rank A. This means that $|\Psi^{p_1 \ldots p_n}_{q_1 \ldots q_n}\rangle = |\Psi^{[n]}\rangle$ lives in the subspace spanned by all basis states $\{|\Psi^{r_1 \ldots r_i}_{s_1 \ldots s_i}\rangle\}$ with $i = 1, \ldots, A$. Consequently, it can be expressed as a linear combination of these states, which was the statement to be proven.

□

4.5.2. Generalized One-Particle One-Hole States

Since the definition of the generalized one-particle one-hole state, also called one-particle one-hole excitation, given in (4.169) contains the one-body density matrix elements, let us construct these

$$\gamma_q^p = \begin{cases} \delta_q^p & \text{if } p \in \mathcal{C} \text{ or } q \in \mathcal{C} \\ \gamma_q^p & \text{if } p, q \in \mathcal{A} \\ 0 & \text{else .} \end{cases} \tag{4.187}$$

Hence, the generalized one-particle one-hole excitation is given by

$$|\Psi_q^p\rangle = \tilde{\boldsymbol{a}}_q^p |\Psi\rangle = (\boldsymbol{a}_q^p - \gamma_q^p) |\Psi\rangle . \tag{4.188}$$

Let us consider different scenarios depending on the indices. For the case where the upper index belongs to the core, $p = i$, we obtain using the relations (4.165) and (4.167)

$$|\Psi_q^i\rangle = \boldsymbol{a}_q^i |\Psi\rangle - \gamma_q^i |\Psi\rangle = \delta_q^i |\Psi\rangle - \delta_q^i |\Psi\rangle = 0 \tag{4.189}$$

which is in accordance with proposition 4.1. The case where the upper index is a virtual one, $p = x$, we have to consider two non trivial cases depending on the type of the lower index

$$|\Psi_q^x\rangle = \begin{cases} \boldsymbol{a}_q^x |\Psi\rangle & \text{if } q \in \mathcal{C} \\ (\boldsymbol{a}_q^x - \gamma_q^x) |\Psi\rangle & \text{if } q \in \mathcal{A} \\ 0 & \text{else.} \end{cases} \tag{4.190}$$

The last case is given by an upper virtual index, $p = b$, yielding

$$|\Psi_q^b\rangle = \begin{cases} \boldsymbol{a}_q^b |\Psi\rangle & \text{if } q \in \mathcal{C} \cup \mathcal{A} \\ 0 & \text{else.} \end{cases} \tag{4.191}$$

All non-vanishing one-particle one-hole excitations can be classified into four different scenarios depicted in figure 4.3. The blue and red shaded areas correspond to core and active orbitals, respectively. In the first scenario, we can annihilate a core state in the reference state and create a virtual state, which is the only non-vanishing combination appearing in the single-reference case. Analogously, we can annihilate a core or active state and create an active or virtual state, respectively. In the latter scenario, we can even annihilate an active and create another (or the same) active state. Additionally, we have to subtract a multiple of the reference state to construct the one-particle one-hole excitation, which makes this scenario special compared to the other cases.

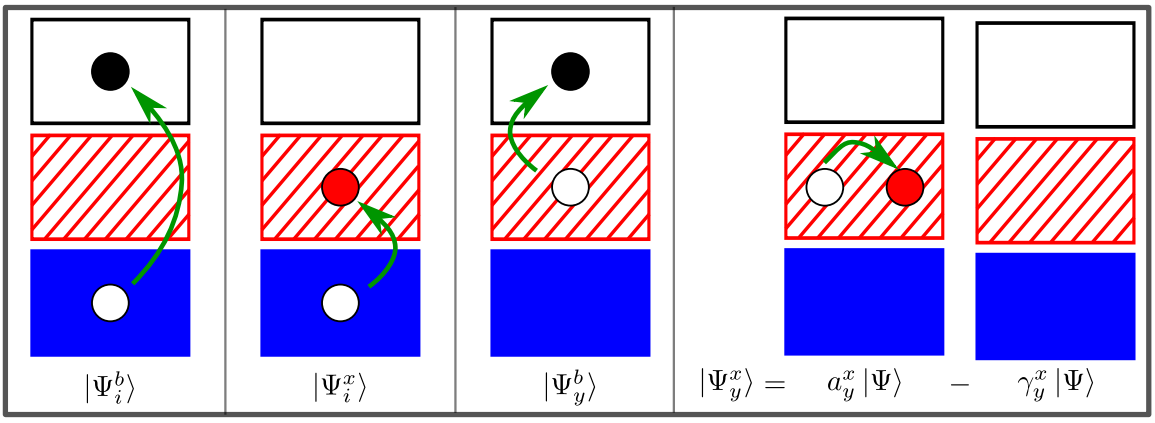

Figure 4.3.: Depicted are the non-vanishing generalized one-particle one-hole excitations. The blue and red shaded area correspond to core and active orbitals, respectively. In the first case, we can annihilate a core state in the reference state and create a virtual state which is the only circumstance appearing in the single-reference case. All other cases are specific for the multi-reference case.

4.5.3. Generalized Two-Particle Two-Hole States

In analogy to the generalized one-particle one-hole state, let us start with the construction of the two-body density matrix elements. If one of the upper indices belongs to the core, $p = i$, the two-body density matrix can be simplified with the aid of (4.167) to

$$\gamma_{qs}^{ir} = \langle\Psi|\boldsymbol{a}_{qs}^{ir}|\Psi\rangle = \delta_q^i\gamma_s^r - \delta_s^i\gamma_q^r. \tag{4.192}$$

Hence, for the general case we obtain

$$\gamma_{qs}^{pr} = \begin{cases} \delta_q^p\delta_s^r - \delta_s^p\delta_q^r & \text{if } p,r \in \mathcal{C} \\ \delta_q^p\gamma_s^r - \delta_s^p\gamma_q^r & \text{if } p \in \mathcal{C}, r \in \mathcal{A} \\ \delta_s^r\gamma_q^p - \delta_q^r\gamma_s^p & \text{if } p \in \mathcal{A}, r \in \mathcal{C} \\ \gamma_{qs}^{pr} & \text{if } p,r,q,s \in \mathcal{A} \\ 0 & \text{else ,} \end{cases} \tag{4.193}$$

where we made use of the statement in (4.163) to write down the non-trivial cases.

Let us consider the generalized two-particle two-hole state given by

$$|\Psi_{qs}^{pr}\rangle = \tilde{\boldsymbol{a}}_{qs}^{pr}|\Psi\rangle = (\boldsymbol{a}_{qs}^{pr} - \gamma_{qs}^{pr})|\Psi\rangle - \mathbb{A}(\gamma_q^p|\Psi_s^r\rangle). \tag{4.194}$$

for different scenarios. If one of the upper index corresponds to the core, for instance $p = i$, then the generalized two-particle two-hole excitation vanishes

$$|\Psi_{qs}^{ir}\rangle = (\boldsymbol{a}_{qs}^{ir} - \gamma_{qs}^{ir})|\Psi\rangle - \mathbb{A}(\gamma_q^i|\Psi_s^r\rangle) \tag{4.195}$$

$$= \delta_q^i(\boldsymbol{a}_s^r - \gamma_s^r)|\Psi\rangle - \delta_s^i(\boldsymbol{a}_q^r - \gamma_q^r)|\Psi\rangle - (\gamma_q^i|\Psi_s^r\rangle - \gamma_s^i|\Psi_q^r\rangle + 0 - 0) \tag{4.196}$$

$$=\delta_q^i \tilde{\boldsymbol{a}}_s^r \left|\Psi\right\rangle - \delta_s^i \tilde{\boldsymbol{a}}_q^r \left|\Psi\right\rangle - \delta_q^i \left|\Psi_s^r\right\rangle + \delta_s^i \left|\Psi_q^r\right\rangle + 0 - 0 \tag{4.197}$$

$$=0 \tag{4.198}$$

which is in accordance with the proposition 4.1. If all upper indices belongs to the active space, $p = x$ and $r = y$, then there are two non-trivial scenarios

$$\left|\Psi_{qs}^{xy}\right\rangle = \begin{cases} \boldsymbol{a}_{qs}^{xy} \left|\Psi\right\rangle & \text{if } q \in \mathcal{C}, s \notin \mathcal{V} \text{ or } q \notin \mathcal{V}, s \in \mathcal{C} \\ (\boldsymbol{a}_{qs}^{xy} - \gamma_{qs}^{xy}) \left|\Psi\right\rangle - \mathbb{A}(\gamma_q^x \left|\Psi_s^x\right\rangle) & \text{if } q, s \in \mathcal{A} \\ 0 & \text{else .} \end{cases} \tag{4.199}$$

If one index belongs to the active space and the other one to the virtual space, $p = x$ and $r = b$, we can simplify the two-particle two-hole excitation making use of the fact that the one-body density vanish if the upper index corresponds to the virtual space

$$\left|\Psi_{qs}^{xb}\right\rangle = \boldsymbol{a}_{qs}^{xb} \left|\Psi\right\rangle + \gamma_s^x \left|\Psi_q^b\right\rangle - \gamma_q^x \left|\Psi_s^b\right\rangle . \tag{4.200}$$

Based on this expression we can write down all non-trivial cases

$$\left|\Psi_{qs}^{xb}\right\rangle = \begin{cases} \boldsymbol{a}_{qs}^{xb} \left|\Psi\right\rangle & \text{if } q \in \mathcal{C}, s \in \mathcal{C} \\ \boldsymbol{a}_{qs}^{xb} \left|\Psi\right\rangle + \gamma_s^x \left|\Psi_q^b\right\rangle & \text{if } q \in \mathcal{C}, s \in \mathcal{A} \\ \boldsymbol{a}_{qs}^{xb} \left|\Psi\right\rangle - \gamma_q^x \left|\Psi_s^b\right\rangle & \text{if } q \in \mathcal{A}, s \in \mathcal{C} \\ \boldsymbol{a}_{qs}^{xb} \left|\Psi\right\rangle + \gamma_s^x \left|\Psi_q^b\right\rangle - \gamma_q^x \left|\Psi_s^b\right\rangle & \text{if } q \in \mathcal{A}, s \in \mathcal{A} \\ 0 & \text{else .} \end{cases} \tag{4.201}$$

The last scenario assumes both upper indices to be elements of the virtual space, i.e., $p = b$ and $r = c$, yielding

$$\left|\Psi_{qs}^{bc}\right\rangle = (\boldsymbol{a}_{qs}^{bc} - 0) \left|\Psi\right\rangle - 0 \tag{4.202}$$

$$= \begin{cases} \boldsymbol{a}_{qs}^{bc} \left|\Psi\right\rangle & \text{if } q, s \in \mathcal{C} \cup \mathcal{A} \\ 0 & \text{else ,} \end{cases} \tag{4.203}$$

which is the only case appearing in the single-reference case keeping in mind that $\mathcal{A}$ is empty. All non-vanishing two-particle two-hole excitations are depicted in figure 4.4.

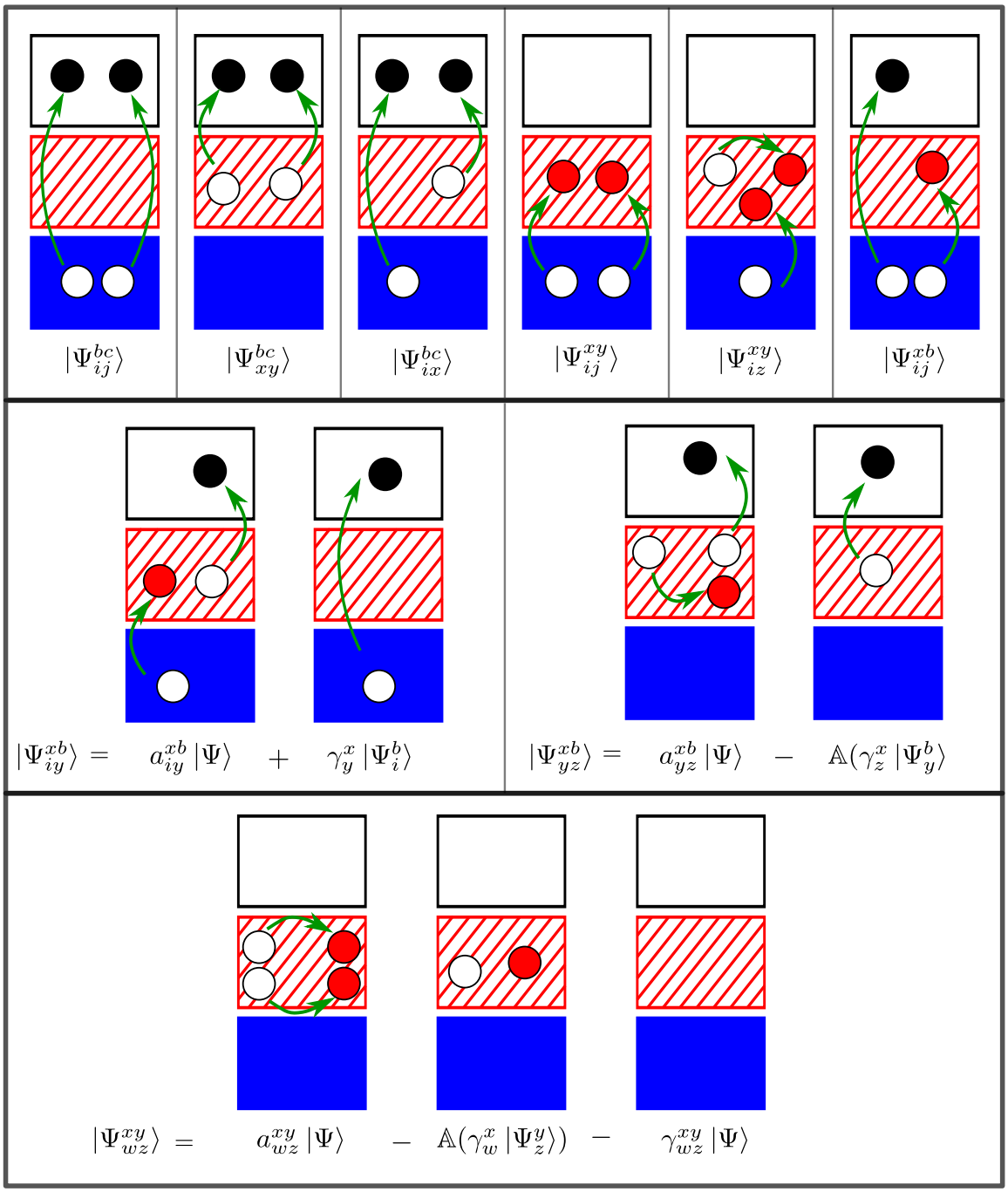

Figure 4.4.: Depicted are the non-vanishing generalized two-particle two-hole excitations. The blue and red shaded area correspond to core and active orbitals, respectively.

4.5.4. Algorithm and Two-Body System As Case Study

In this section, we propose an algorithm that yields a proper basis dimension of the antisymmetrized A-body Hilbert space, which is $\binom{d_1}{A}$ with $d_1 \geq A$ being the dimension of the single-particle basis. Since the overcompleteness is directly related to multiple counting of equivalent configurations, we propose an algorithm to avoid this multiple counting:

- For a given reference state $|\Psi\rangle$, define a set of A single-particle indices as follows

$$\mathcal{D} \coloneqq \{\underbrace{1, 2, \ldots, |\mathcal{C}|}_{\in \mathcal{C}}, \underbrace{|\mathcal{C}|+1, \ldots, A}_{\in \mathcal{A}}\} \tag{4.204}$$

  where $|\mathcal{C}|$ denotes the number of core states. Additionally, we require that the Slater determinant $|\Phi_{\mathcal{D}}\rangle := |12\ldots A\rangle$ constructed with these single-particle states is non-orthogonal to the reference state, i.e.,

$$\langle \Phi_{\mathcal{D}} | \Psi \rangle \neq 0. \tag{4.205}$$

  Note that we have freedom in the choice of the $A - |\mathcal{C}|$ indices from the active space $\mathcal{A}$.

- Use these A single-particle indices from $\mathcal{D}$ in the lower n slots and the remaining ones in the upper n slots of the n-particle n-hole excitation.

$$\left\{ |\Psi^{p_1 p_2 \ldots p_n}_{q_1 q_2 \ldots q_n}\rangle \ : \ q_1, q_2, \ldots, q_n \in \mathcal{D}, p_1, p_2, \ldots, p_n \in (\mathcal{A} \cup \mathcal{V}) \backslash \mathcal{D} \right\}. \tag{4.206}$$

- The total number of all n-particle n-hole excitations generated in this way for $n = 1$, $2, \ldots, \min\{A, d_1 - A\}$ plus one—for the reference state—is identical to the dimension of the antisymmetrized A-body Hilbert space, which is $\binom{d_1}{A}$.

We give a proof of the last statement. According to the algorithm, we have $\binom{A}{n}$ physically distinct possibilities to assign n of the first A single-particle indices to the lower slots of the n-particle n-hole excitation. Analogously, we have $\binom{d_1 - A}{n}$ combinations to distribute the $d_1 - A$ remaining indices on the n upper slots of the n-particle n-hole excitation. Supposing that $A = \min\{A, d_1 - A\}$, the total number is given by

$$1 + \sum_{n=1}^{A} \binom{A}{n}\binom{d_1 - A}{n} = \sum_{k=0}^{A} \binom{A}{k}\binom{d_1 - A}{k} \tag{4.207}$$

$$= \sum_{k=0}^{A} \binom{A}{A-k}\binom{d_1 - A}{k} = \binom{A + (d_1 - A)}{(A-k) + k} = \binom{d_1}{A}. \tag{4.208}$$

The case, $d_1 - A = \min\{A, d_1 - A\}$, is similar and yields the same result.

Let us consider a simple example of a two-particle fermionic quantum system, i.e., $A = 2$. We use this example to demonstrate the usage of the algorithm and to illustrate the overcompleteness of the generalized A-particle A-hole basis. Suppose we have a four dimensional orthonormal single-particle basis $\{|1\rangle, |2\rangle, |3\rangle, |4\rangle\}$, i.e., $\langle i|j\rangle = \delta^i_j$. Based on this single-particle

basis we can generate a basis of the (antisymmetrized) two-body Hilbert space, consisting of antisymmetrized two-body Slater determinants (configurations). This Hilbert space is 6 $(= \binom{4}{2} = \frac{4!}{2!\cdot 2!})$ dimensional, and all configurations are

$$\Big\{ |\Phi_1\rangle := |12\rangle\,, |\Phi_2\rangle := |13\rangle\,, |\Phi_3\rangle := |14\rangle\,, |\Phi_4\rangle := |24\rangle\,, |\Phi_5\rangle := |34\rangle\,, |\Phi_6\rangle := |23\rangle \Big\}. \tag{4.209}$$

This two-body basis is obviously orthonormal, i.e., $\langle \Phi_l | \Phi_k \rangle = \delta^l_k$. Now, let us define the reference state as follows

$$|\Psi\rangle := c\,|\Phi_1\rangle + d\,|\Phi_2\rangle = c\,|12\rangle + d\,|13\rangle \tag{4.210}$$

with non-zero real-valued coefficients c and d fulfilling $c^2 + d^2 = 1$ that ensures that the norm of the reference state is $\langle \Psi | \Psi \rangle = 1$. Based on this reference state we can classify the single-particle basis according to core, active and virtual states

$$\mathcal{C} = \{1\} \tag{4.211}$$
$$\mathcal{A} = \{2, 3\} \tag{4.212}$$
$$\mathcal{V} = \{4\} \tag{4.213}$$

which is shown schematically in figure 4.5. To apply the algorithm described above, we define the first $A = 2$ indices as follows

$$\mathcal{D} = \{1, 2\}. \tag{4.214}$$

Alternatively, we could have used $\{1, 3\}$. In both cases, the overlap $\langle \Phi_{\mathcal{D}} | \Psi \rangle \neq 0$ does not vanish, as required. According to the algorithm, the basis states that need to be considered are

$$\Big\{ |\Psi\rangle \Big\} \bigcup \Big\{ |\Psi^3_1\rangle\,, |\Psi^4_1\rangle\,, |\Psi^3_2\rangle\,, |\Psi^4_2\rangle \Big\} \bigcup \Big\{ |\Psi^{34}_{12}\rangle \Big\}, \tag{4.215}$$

which has the proper number of basis states. At this point, we emphasize that it is not clear whether these basis states are linearly independent or not. Let us write them out explicitly using their definitions (4.169) or the results derived in sections 4.5.2 and 4.5.3. For that

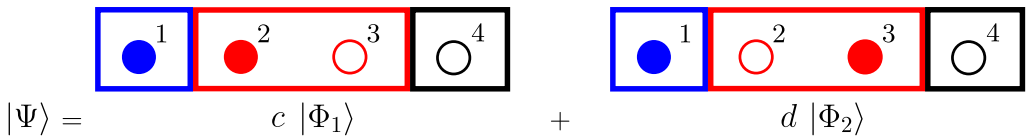

Figure 4.5.: Classification of the single-particle basis based on the given reference state (4.210). Filled (open) symbol correspond to occupied (unoccupied) single-particle states. Blue, red and black colors indicate core, active and virtual states, respectively.

purpose, let us first calculate the one-body density matrix with the aid of (4.187)

$$\underline{\underline{\gamma}}^{(1)} = \begin{pmatrix} 1 & 0 & 0 & 0 \\ 0 & c^2 & cd & 0 \\ 0 & cd & d^2 & 0 \\ 0 & 0 & 0 & 0 \end{pmatrix}. \tag{4.216}$$

Hence, we obtain for the n-particle n-hole states with $n \leq 2$

$$|\Psi_1^3\rangle = -c\,|23\rangle \tag{4.217a}$$
$$|\Psi_1^4\rangle = -c\,|24\rangle - d\,|34\rangle \tag{4.217b}$$
$$|\Psi_2^3\rangle = c\,|13\rangle - cd\,|\Psi\rangle = (c - cd^2)\,|13\rangle - c^2 d\,|12\rangle \tag{4.217c}$$
$$|\Psi_2^4\rangle = c\,|14\rangle \tag{4.217d}$$
$$|\Psi_{12}^{34}\rangle = c\,|34\rangle + cd\,|\Psi_2^4\rangle = c\,|34\rangle + c^2 d\,|14\rangle\,. \tag{4.217e}$$

As expected, some basis states are superposition of Slater determinants, non-normalized and non-orthogonal to each other. The determinant of the overlap matrix between these n-particle n-hole excitations from (4.215) and the configurations from (4.209) yields

$$\det \begin{pmatrix} \langle\Phi_1|\Psi\rangle & \langle\Phi_1|\Psi_1^3\rangle & \langle\Phi_1|\Psi_1^4\rangle & \langle\Phi_1|\Psi_2^3\rangle & \langle\Phi_1|\Psi_2^4\rangle & \langle\Phi_1|\Psi_{12}^{34}\rangle \\ \langle\Phi_2|\Psi\rangle & \langle\Phi_2|\Psi_1^3\rangle & \langle\Phi_2|\Psi_1^4\rangle & \langle\Phi_2|\Psi_2^3\rangle & \langle\Phi_2|\Psi_2^4\rangle & \langle\Phi_2|\Psi_{12}^{34}\rangle \\ \langle\Phi_3|\Psi\rangle & \langle\Phi_3|\Psi_1^3\rangle & \langle\Phi_3|\Psi_1^4\rangle & \langle\Phi_3|\Psi_2^3\rangle & \langle\Phi_3|\Psi_2^4\rangle & \langle\Phi_3|\Psi_{12}^{34}\rangle \\ \langle\Phi_4|\Psi\rangle & \langle\Phi_4|\Psi_1^3\rangle & \langle\Phi_4|\Psi_1^4\rangle & \langle\Phi_4|\Psi_4^3\rangle & \langle\Phi_4|\Psi_4^4\rangle & \langle\Phi_4|\Psi_{14}^{34}\rangle \\ \langle\Phi_5|\Psi\rangle & \langle\Phi_5|\Psi_1^3\rangle & \langle\Phi_5|\Psi_1^4\rangle & \langle\Phi_5|\Psi_2^3\rangle & \langle\Phi_5|\Psi_2^4\rangle & \langle\Phi_5|\Psi_{12}^{34}\rangle \\ \langle\Phi_6|\Psi\rangle & \langle\Phi_6|\Psi_1^3\rangle & \langle\Phi_6|\Psi_1^4\rangle & \langle\Phi_6|\Psi_2^3\rangle & \langle\Phi_6|\Psi_2^4\rangle & \langle\Phi_6|\Psi_{12}^{34}\rangle \end{pmatrix} \tag{4.218}$$
$$= c^6 \tag{4.219}$$
$$= \langle\Phi_{\mathcal{D}}|\Psi\rangle^{\binom{d_1}{A}} \neq 0, \tag{4.220}$$

which is non-vanishing. Here, we see the impact of the additional constraint (4.205) in the algorithm. If we do not fulfill this requirement, the overlap matrix vanishes and the set of the states from (4.215) is obviously linearly dependent. However, the algorithm generates a complete set basis states of the A-body Hilbert space in this case study—a general proof of the linear independence still remains. Consequently, all other n-particle n-hole states can be expressed as linear combination of the basis states from (4.215), e.g.,

$$|\Psi_1^2\rangle = d\,|23\rangle = -\frac{d}{c}\,|\Psi_1^3\rangle \tag{4.221}$$
$$|\Psi_2^2\rangle = c\,|12\rangle - c^2\,|\Psi\rangle = 2\,|\Psi\rangle - \frac{d}{c}\,|\Psi_2^3\rangle \tag{4.222}$$
$$|\Psi_3^3\rangle = d\,|13\rangle - d^2\,|\Psi\rangle = \frac{d}{c}\,|\Psi_2^3\rangle \tag{4.223}$$
$$|\Psi_{12}^{24}\rangle = c\,|24\rangle + c^2\,|\Psi_1^4\rangle = -\frac{1}{c}\,|\Psi_1^4\rangle - \frac{d}{c^2}\,|\Psi_{12}^{34}\rangle + \frac{d^2}{c}\,|\Psi_2^4\rangle\,. \tag{4.224}$$

The three-particle three-hole states are superposition of these basis states as well, i.e.,

$$|\Psi^{prt}_{qsu}\rangle = (\boldsymbol{a}^{prt}_{qsu} - \gamma^{prt}_{qsu})\,|\Psi\rangle - \mathbb{A}(\gamma^{p}_{q}\,|\Psi^{rt}_{su}\rangle) - \mathbb{A}(\gamma^{pr}_{qs}\,|\Psi^{t}_{u}\rangle) \tag{4.225}$$

$$= -\mathbb{A}(\gamma^{p}_{q}\,|\Psi^{rt}_{su}\rangle) - \mathbb{A}(\gamma^{pr}_{qs}\,|\Psi^{t}_{u}\rangle). \tag{4.226}$$

Here, the first term vanishes since our reference state contains only two particles. This result is in accordance with proposition 4.2.

To demonstrate the importance of the additional constraint (4.205) in the algorithm, let us consider a different reference state given by

$$|\Psi\rangle := c_1\,|13\rangle + c_2\,|23\rangle + c_3\,|24\rangle\,. \tag{4.227}$$

Obviously, the core and virtual space are empty in this case, i.e., the complete single-particle states belong the active space. Without the additional constraint, $|\Phi_{\mathcal{D}}\rangle := |12\rangle$, which is orthogonal to the given reference state, would be a possible choice, generating the basis states given in (4.215). But in this case the one-particle one-hole state $|\Psi^{3}_{1}\rangle = 0$ vanishes, leading to linear dependent set of basis states. This problem is solved if we choose a Slater determinant, for instance, $|\Phi_{\mathcal{D}}\rangle := |13\rangle$ that is non-orthogonal to the given reference state. The A-particle A-hole basis based on this reference is then given by

$$\Big\{\,|\Psi\rangle\,\Big\} \bigcup \Big\{\,|\Psi^{2}_{1}\rangle\,, |\Psi^{4}_{1}\rangle\,, |\Psi^{2}_{3}\rangle\,, |\Psi^{4}_{3}\rangle\,\Big\} \bigcup \Big\{\,|\Psi^{24}_{13}\rangle\,\Big\}, \tag{4.228}$$

which indeed is a basis, since the determinant of the overlap matrix $\langle\Phi_{\mathcal{D}}|\Psi\rangle^{6}$ does not vanish.

In summary, we have proposed a smart algorithm to pick up a set of basis states from the (overcomplete) generalized A-particle A-hole basis (4.173). This automatically yields at least a proper basis dimension of the antisymmetrized A-body Hilbert space, but linear independence still remains to be proved. Using a simple two-body system as case study, we have discussed the overcompleteness and the usage of the algorithm.

4.6. Generators

In this section, we explain the main idea for the proper construction of generators for multi-reference IM-SRG ground-state energy calculations, i.e., for the energetically lowest state. Furthermore, we give an overview of the generators used in practical calculations, and briefly analyze their decoupling properties, meaning how off-diagonal matrix elements are suppressed for large enough value of the flow parameter.

4.6.1. Basic Idea

We recapitulate that the main goal is to solve the many-body problem of the initial Hamiltonian $\boldsymbol{H}(0)$ by means of a continuous unitary transformation such that

$$\boldsymbol{H}(\infty)\,|\Psi\rangle = E(\infty)\,|\Psi\rangle\,. \tag{4.229}$$

Then $E(\infty)$ is an eigenvalue of $\boldsymbol{H}(\infty)$ and $\boldsymbol{H}(0)$, as well, since a unitary transformation preserves the spectrum. In contrast to direct diagonalization methods, the main idea is to decouple a predefined reference state $|\Psi\rangle$, which is a physically motivated approximation of the ground state with the proper quantum numbers. This is achieved by splitting the flowing Hamiltonian into two pieces called *diagonal* and *off-diagonal* Hamiltonian

$$\boldsymbol{H}(s) = \boldsymbol{H}^{\mathrm{d}}(s) + \boldsymbol{H}^{\mathrm{od}}(s) \tag{4.230}$$

with the additional aim that the off-diagonal piece has to vanish in the limit, where the flow parameter s goes to infinity

$$\boldsymbol{H}^{\mathrm{od}}(s) \overset{s\to\infty}{\longrightarrow} 0. \tag{4.231}$$

The definition of the off-diagonal Hamiltonian $\boldsymbol{H}^{\mathrm{od}}$ can be specified based on the representation of the Hamiltonian in the generalized A-particle A-hole basis introduced in (4.173). By representing the initial or flowing Hamiltonian in this basis, it becomes clear which of the matrix elements need to be suppressed in order to decouple the reference state $|\Psi\rangle$ from other basis states, see figure 4.6. Once the following matrix elements

$$0 = \langle\Psi|\boldsymbol{H}(\infty)|\Psi_q^p\rangle \tag{4.232a}$$
$$0 = \langle\Psi|\boldsymbol{H}(\infty)|\Psi_{qs}^{pr}\rangle \tag{4.232b}$$
$$\vdots$$
$$0 = \langle\Psi|\boldsymbol{H}(\infty)|\Psi_{q_1\cdots q_A}^{p_1\cdots p_A}\rangle \tag{4.232c}$$

are suppressed by the unitary transformation, the reference state is decoupled from the generalized n-particle n-hole states with $n > A$ as well because these excitations are linearly dependent on the lower-particle rank excitations up to rank A according to proposition 4.2.

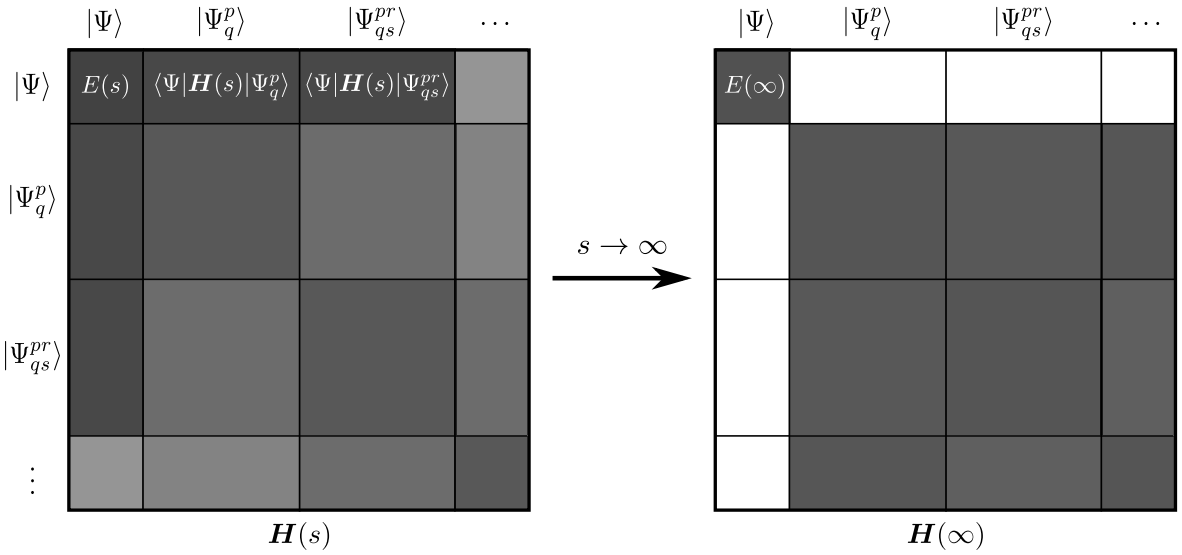

Figure 4.6.: Schematic depiction of the Hamiltonian evolved to a specific flow parameter s and to infinity, $\boldsymbol{H}(s)$ and $\boldsymbol{H}(\infty)$, respectively, represented in an A-body basis consisting of the reference state $|\Psi\rangle$ and generalized particle-hole excitations $|\Psi_q^p\rangle, |\Psi_{qs}^{pr}\rangle, \ldots$ of it. This illustrates and motivates how to define the off-diagonal Hamiltonian in order to have the reference state become an eigenstate of the final Hamiltonian. The desired eigenvalue of the initial and final Hamiltonian is then identical to $E(\infty) = \langle\Psi|\boldsymbol{H}(\infty)|\Psi\rangle$ since a unitary transformation preserves the spectrum.

Hence, it is sufficient to suppress excitations up to particle rank A, and then the reference state $|\Psi\rangle$ obviously becomes an eigenstate of the final Hamiltonian $\boldsymbol{H}(\infty)$.

The matrix elements that should be suppressed basically define the off-diagonal piece of the Hamiltonian written in second quantization for the multi-reference IM-SRG(2) truncation

$$\boldsymbol{H}^{\mathrm{od}}(s) = \sum_{\substack{p \\ q}} (f^{\mathrm{od}})_q^p(s)\tilde{\boldsymbol{a}}_q^p + \frac{1}{4}\sum_{\substack{pr \\ qs}} (\Gamma^{\mathrm{od}})_{qs}^{pr}(s)\tilde{\boldsymbol{a}}_{qs}^{pr} \tag{4.233}$$

with one- and two-body matrix elements given in m-scheme natural orbitals

$$\begin{aligned}
(f^{\mathrm{od}})_q^p(s) &\coloneqq \langle\Psi|\boldsymbol{H}(s)|\Psi_q^p\rangle + [p \leftrightarrow q] && \text{(4.234a)}\\
&= \bar{n}_p n_q f_q^p(s) + \mathcal{O}(\lambda^{(2)}) + [p \leftrightarrow q] && \text{(4.234b)}\\
(\Gamma^{\mathrm{od}})_{qs}^{pr}(s) &\coloneqq \langle\Psi|\boldsymbol{H}(s)|\Psi_{qs}^{pr}\rangle + [pr \leftrightarrow qs] && \text{(4.234c)}\\
&= \bar{n}_p\bar{n}_r n_q n_s \Gamma_{qs}^{pr}(s) + \mathcal{O}(\lambda^{(n\geq 2)}) + [pr \leftrightarrow qs]. && \text{(4.234d)}
\end{aligned}$$

The generalization to multi-reference IM-SRG(A) is obvious. In our implementation, we neglect terms depending on irreducible two- and higher-body density matrix elements due to computational efficiency. We note that the complete expressions can be deduced from appendix A.3.1 which might be interesting for forthcoming investigations.

Once a *decoupling pattern*, i.e., the definition of the off-diagonal Hamiltonian, is identified,

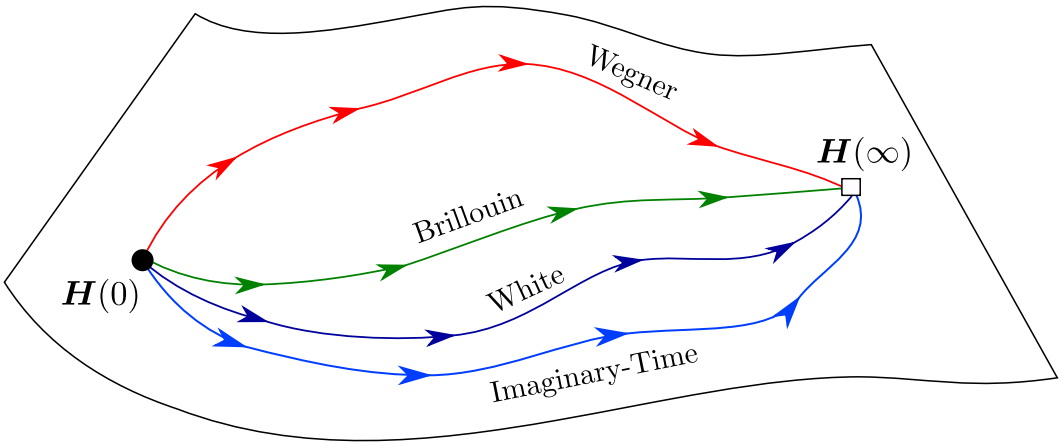

Figure 4.7.: We illustrate in a simplified picture the manifold of the unitarily equivalent Hamiltonians to the initial Hamiltonian $\boldsymbol{H}(0)$. Once the decoupling pattern is set by the off-diagonal Hamiltonian, the final Hamiltonian $\boldsymbol{H}(\infty)$ is fixed. There are still many paths going from the initial Hamiltonian to the final Hamiltonian. Which path on this manifold we take, or in other word decoupling scheme, depends on the choice of the generator. Wegner, White, Imaginary-Time and Brillouin are some well-established examples for generators in the literature. Neglecting truncation effects, all paths should lead to the same final Hamiltonian. Note that the Wegner generator can have other fixed points beside the final Hamiltonian (see section 4.6.2).

the fixed point of the evolution is given by $\boldsymbol{H}(\infty)$ (see figure 4.7). There are still infinitely many paths on the manifold of all unitary equivalent Hamiltonians going from $\boldsymbol{H}(0)$ to $\boldsymbol{H}(\infty)$. Which path or, in other words, which *decoupling scheme* we take depends on the choice of the generator. There are different choices for the generators which differ in how the off-diagonal matrix elements are suppressed, numerical efficiency, and how they induce many-body interactions in practical calculations. In multi-reference IM-SRG(A) without any truncation, all generators yield the same final result. The commonly used generators in the literature are the Wegner, White, Imaginary-Time and Brillouin generators, which will be introduced in sections 4.6.2–4.6.4.

Note that we cannot guarantee that the multi-reference IM-SRG, even the untruncated version, will necessarily extract the ground-state energy of the nucleus under consideration, but it will converge against one eigenvalue. However, we expect that the evolution will converge against the eigenstate that has the largest overlap with reference state, which is difficult to prove.

Other decoupling patterns to decouple the reference state and other eigenstates are also possible theoretically, but they have proved to be useless in practical calculations because of strong induced many-body interaction [Her+16].

4.6.2. Wegner Generator

After this brief motivation of the general idea, let us formulate the canonical choice for the multi-reference IM-SRG evolution proposed by Wegner [Weg94]

$$\boldsymbol{\eta}(s) \coloneqq [\boldsymbol{H}^{\mathrm{d}}, \boldsymbol{H}] = -[\boldsymbol{H}^{\mathrm{od}}, \boldsymbol{H}]. \tag{4.235}$$

Due to the similarity to the multi-reference IM-SRG operator flow equation, which is the commutator between $\boldsymbol{\eta}$ and $\boldsymbol{H}$, we can make use of the formulae (4.18a) and (4.18b), keeping the global minus sign in mind, and replace $\boldsymbol{\eta}$ by $\boldsymbol{H}^{\mathrm{od}}$, i.e., $\eta_q^p \to (f^{\mathrm{od}})_q^p$ and $\eta_{qs}^{pr} \to (\Gamma^{\mathrm{od}})_{qs}^{pr}$. Note that the zero-body part can be set to zero because of the commutator structure of the flow equation. Moreover, the matrix elements in practical calculations are real, anyway. The J-coupled version in natural orbitals can be obtained from formulae (4.89a) and (4.89b) with the corresponding replacement and by setting $\chi = 1$ since $\boldsymbol{H}^{\mathrm{od}}$ is Hermitian.

Since $\boldsymbol{\eta} = 0$ is a trivial fixed point of the multi-reference IM-SRG evolution, the Wegner generator has additional fixed points where $\boldsymbol{H}^{\mathrm{od}}$ commutes with $\boldsymbol{H}^{\mathrm{d}}$ even though $\boldsymbol{H}^{\mathrm{od}}$ is non-zero, e.g., due to a degeneracy in the spectrum of $\boldsymbol{H}(s)$ [Her+16]. A second type of fixed point exists when the flow parameter s goes to infinity, where $\boldsymbol{H}^{\mathrm{od}}(s)$ vanishes as required.

The Wegner generator is inefficient in practical applications. The reason is that the flow equations become extremely stiff which is related to the fact that third powers of the matrix elements f_q^p and Γ_{qs}^{pr} appear in the flow equations. In practical calculations, it is known that solver for ordinary differential equations for stiff problems have higher storage and computing time requirements than for non-stiff or weakly-stiff cases [Her+16] which is the case for the White or Imaginary-Time generators, which will be introduced in the next section.

The SRG with the Wegner generator is a true renormalization-group transformation, i.e., it preferentially suppresses matrix elements of states with large energy differences (see also the discussion about decay scales in section 4.6.5).

4.6.3. White and Imaginary-Time Generator

In second quantization consistent with the multi-reference IM-SRG(2) truncation, the generator in general has the following form

$$\boldsymbol{\eta} = \sum_{\substack{p \\ q}} \eta_q^p \tilde{\boldsymbol{a}}_q^p + \frac{1}{4} \sum_{\substack{pr \\ qs}} \eta_{qs}^{pr} \tilde{\boldsymbol{a}}_{qs}^{pr}. \tag{4.236}$$

The matrix elements of the *White* and *Imaginary-Time generator* are defined with the aid of the matrix elements of the off-diagonal Hamiltonian (4.234) [Whi02; TBS11; Her+16]

$$\eta_q^p \coloneqq \mathcal{F}(\Delta_q^p)(f^{\mathrm{od}})_q^p - [p \leftrightarrow q] \tag{4.237a}$$

$$= \mathcal{F}(\Delta_q^p)(\bar{n}_p n_q f_q^p + \mathcal{O}(\lambda^{(2)})) - [p \leftrightarrow q] \tag{4.237b}$$

$$\eta_{qs}^{pr} \coloneqq \mathcal{F}(\Delta_{qs}^{pr})(\Gamma^{\mathrm{od}})_{qs}^{pr} - [pr \leftrightarrow qs] \tag{4.237c}$$

$$= \mathcal{F}(\Delta_{qs}^{pr})(\bar{n}_p \bar{n}_r n_q n_s \Gamma_{qs}^{pr} + \mathcal{O}(\lambda^{(n\geq 2)})) - [pr \leftrightarrow qs] \tag{4.237d}$$

with the following abbreviation

$$\mathcal{F}(\Delta) \coloneqq \begin{cases} \frac{1}{\Delta} & \text{for White generator} \\ \operatorname{sgn}(\Delta) & \text{for Imaginary-Time generator.} \end{cases} \tag{4.238}$$

The generalization to three-body or higher rank is obvious. The symbol Δ_q^p, called Epstein-Nesbet energy in the literature, indicates the difference between the expectation value of the evolved Hamiltonian with respect to a generalized one-particle one-hole excitations and the expectation value with respect to the reference state itself

$$\Delta_q^p(s) \coloneqq \langle \Psi | \, \tilde{\boldsymbol{a}}_p^q \, \boldsymbol{H}(s) \, \tilde{\boldsymbol{a}}_q^p \, | \Psi \rangle - \langle \Psi | \, \boldsymbol{H}(s) \, | \Psi \rangle \tag{4.239a}$$

$$= -\bar{n}_p^2 n_q^2 \Gamma_{pq}^{pq} + \bar{n}_p^2 n_q f_p^p - \bar{n}_p n_q^2 f_q^q + E\,(\bar{n}_p n_q - 1) + \mathcal{O}(\lambda^{(2)}) \tag{4.239b}$$

and analogously for the generalized two-particle two-hole excitation

$$\Delta_{qs}^{pr}(s) \coloneqq \langle \Psi | \, \tilde{\boldsymbol{a}}_{pr}^{qs} \, \boldsymbol{H}(s) \, \tilde{\boldsymbol{a}}_{qs}^{pr} \, | \Psi \rangle - \langle \Psi | \, \boldsymbol{H}(s) \, | \Psi \rangle \tag{4.239c}$$

$$\begin{aligned} = \Big(& \bar{n}_p \bar{n}_r n_q n_s (\tfrac{1}{2} \bar{n}_p \bar{n}_r \Gamma_{pr}^{pr} + \tfrac{1}{2} n_q n_s \Gamma_{qs}^{qs} - \bar{n}_p n_s \Gamma_{ps}^{ps} - \bar{n}_p n_q \Gamma_{pq}^{pq}) \\ & + \bar{n}_p \bar{n}_r n_q n_s (\bar{n}_p f_p^p - n_q f_q^q) + \tfrac{1}{2} E\,(\bar{n}_p \bar{n}_r n_q n_s - 1) + \mathcal{O}(\lambda^{(n\geq 2)}) \Big) + [pq \leftrightarrow rs] \end{aligned} \tag{4.239d}$$

where we suppressed the flow-parameter dependence of the matrix elements for brevity. Note that the Epstein-Nesbet energy differences also depend on the flow parameter s. In practical calculations, we have to truncate terms containing two- or higher-body irreducible two-body density matrices. For completeness, we give more precise formulae including $\lambda^{(2)}$ in appendix B.3. Furthermore, the energy differences are per definition symmetric with respect to exchange among the upper or lower indices, i.e., $\Delta_{qs}^{pr} = \Delta_{qs}^{rp} = \Delta_{sq}^{pr}$. But they are neither symmetric nor antisymmetric with respect to exchange of the upper with the lower indices, i.e., $\Delta_{qs}^{pr} \neq \pm \Delta_{pr}^{qs}$ and $\Delta_q^p \neq \pm \Delta_p^q$.

Finally, we remark that we make use of the following averaging

$$\Gamma_{pm_p qm_q}^{pm_p qm_q} \approx \frac{1}{\hat{j}_p^2 \hat{j}_q^2} \sum_{m_p m_q} \Gamma_{pm_p qm_q}^{pm_p qm_q} \tag{4.240}$$

$$= \frac{1}{\hat{j}_p^2 \hat{j}_q^2} \sum_{JM} {}^{J}\Gamma_{pq}^{pq} \sum_{m_p m_q} \begin{pmatrix} j_p & j_q \\ m_p & m_q \end{pmatrix} \Bigg| \begin{matrix} J \\ M \end{matrix} \Bigg) \begin{pmatrix} j_p & j_q \\ m_p & m_q \end{pmatrix} \Bigg| \begin{matrix} J \\ M \end{matrix} \Bigg) \tag{4.241}$$

$$= \frac{1}{\hat{j}_p^2 \hat{j}_q^2} \sum_{J} \hat{J}^2 {}^{J}\Gamma_{pq}^{pq} \tag{4.242}$$

in order to derive a J-coupled version of the matrix elements of the White and Imaginary-Time generator.

4.6.4. Brillouin Generator

The matrix elements of all generators introduced so far are constructed with the aid of the off-diagonal matrix elements (4.234), which include irreducible three- and four-body density matrices. While storage of the irreducible three-body density matrix might be feasible for specific choices of the reference state, the inclusion of four-body densities is computationally extremely expensive. Consequently, we have been forced to introduce truncations such that decoupling conditions given in (4.232) can no longer be guaranteed, in general. Thus, a different strategy is desired that avoids densities beyond the three-body rank and drives the Hamiltonian approximately into the desired shape formulated in the decoupling conditions.

For that purpose, let us split the decoupling conditions (4.232) into two terms as follows[5]

$$0 = \langle\Psi|\boldsymbol{H}(\infty)\tilde{\boldsymbol{a}}^p_q|\Psi\rangle = \tfrac{1}{2}\left(\langle\Psi|\big[\boldsymbol{H}(\infty),\tilde{\boldsymbol{a}}^p_q\big]|\Psi\rangle + \langle\Psi|\big\{\boldsymbol{H}(\infty),\tilde{\boldsymbol{a}}^p_q\big\}|\Psi\rangle\right) \tag{4.243a}$$

$$0 = \langle\Psi|\boldsymbol{H}(\infty)\tilde{\boldsymbol{a}}^{pr}_{qs}|\Psi\rangle = \tfrac{1}{2}\left(\langle\Psi|\big[\boldsymbol{H}(\infty),\tilde{\boldsymbol{a}}^{pr}_{qs}\big]|\Psi\rangle + \langle\Psi|\big\{\boldsymbol{H}(\infty),\tilde{\boldsymbol{a}}^{pr}_{qs}\big\}|\Psi\rangle\right) \tag{4.243b}$$

$$\vdots$$

We can easily show that if the decoupling conditions are fulfilled, then each term on the right-hand side, i.e., the expectation value of the commutator and the anticommutator with respect to the reference state, has to vanish separately due to the Hermiticity of the Hamiltonian.

The basic idea is now to suppress the expectation value of the commutator[6] with respect to the reference state in a controlled manner using IM-SRG by defining the matrix elements of the so-called *Brillouin generator* as [Her+16]

$$\eta^p_q \coloneqq \langle\Psi|\left[\boldsymbol{H},\tilde{\boldsymbol{a}}^p_q\right]|\Psi\rangle \tag{4.244a}$$

$$\eta^{pr}_{qs} \coloneqq \langle\Psi|\left[\boldsymbol{H},\tilde{\boldsymbol{a}}^{pr}_{qs}\right]|\Psi\rangle\,. \tag{4.244b}$$

A trivial fixed point of the IM-SRG evolution is reached when the generator vanishes, i.e., $\eta^p_q = 0$ and $\eta^{pr}_{qs} = 0$, which corresponds to the irreducible Brillouin conditions [MK01; KM02; KM04]—where the name of the generator comes from. Note that this does not ensure the decoupling conditions because of the remaining anticommutator. Since the irreducible Brillouin conditions are equivalent to the stationarity conditions of the energy functional $\mathcal{E}[|\Psi\rangle] \coloneqq \langle\Psi|\boldsymbol{H}(\infty)|\Psi\rangle$ through a unitary variation, we have good reasons to expect that the anticommutator is suppressed as well [Her+16]. There is empirical evidence for their reduction [Her+16].

However, we get rid of higher-rank densities as desired. We can see that by calculating the expectation value of the commutator with the aid of the formulae derived in appendix A.3.2

[5] This following relation $\boldsymbol{A}\boldsymbol{B} = \frac{1}{2}\left(\big[\boldsymbol{A},\boldsymbol{B}\big] + \big\{\boldsymbol{A},\boldsymbol{B}\big\}\right)$ holds for any operators $\boldsymbol{A}$ and $\boldsymbol{B}$.

[6] Note that the expectation value of the anticommutator cannot be used for the definition of the generator since it is invariant under exchange of the upper and lower indices.

yielding

$$\eta_q^p = \left[f_q^p n_q + \frac{1}{2} \sum_{rst} \Gamma_{st}^{rp} \lambda_{rq}^{st} \right] - [p \leftrightarrow q] \tag{4.245a}$$

$$\begin{aligned}
\eta_{qs}^{pr} = \Bigg[\Bigg(\Bigg(& \frac{1}{2} \sum_t f_t^p \lambda_{qs}^{tr} \\
& + \frac{1}{4} \Gamma_{qs}^{pr} \bar{n}_p \bar{n}_r n_q n_s \\
& + \frac{1}{8} (1 - n_p - n_r) \sum_{tu} \Gamma_{tu}^{pr} \lambda_{qs}^{tu} \\
& + \frac{1}{2} (n_p - n_s) \sum_{tu} \Gamma_{us}^{pt} \lambda_{qt}^{ur} \\
& + \frac{1}{4} \sum_{tuv} \Gamma_{uv}^{rt} \lambda_{tqs}^{uvp} \Bigg) \\
& - [p \leftrightarrow r] \Bigg) - [q \leftrightarrow s] \Bigg] - [pr \leftrightarrow qs].
\end{aligned} \tag{4.245b}$$

Like the multi-reference IM-SRG(2) flow equations (4.28), these expressions only depend linearly on irreducible two- and three-body density matrices, $\lambda^{(2)}$ and $\lambda^{(3)}$, which makes untruncated implementations feasible as desired. Finally, we give the J-coupled version in natural orbitals for an efficient implementation

$$\eta_q^p = \left[f_q^p n_q + \frac{1}{2} \frac{1}{\hat{j}_p^2} \sum_{rstJ} \hat{J}^2 \, {}^J\Gamma_{st}^{rp} \, {}^J\lambda_{rq}^{st} \right] - [p \leftrightarrow q] \tag{4.246a}$$

$$\begin{aligned}
{}^J\eta_{qs}^{pr} = \Bigg[\Bigg(\Bigg(& \frac{1}{2} \sum_t f_t^p \, {}^J\lambda_{qs}^{tr} \\
& + \frac{1}{4} \, {}^J\Gamma_{qs}^{pr} \bar{n}_p \bar{n}_r n_q n_s \\
& + \frac{1}{8} (1 - n_p - n_r) \sum_{tu} \, {}^J\Gamma_{tu}^{pr} \, {}^J\lambda_{qs}^{tu} \\
& + \frac{1}{2} (n_p - n_s) \sum_{tuJ'} \hat{J}'^2 \begin{Bmatrix} j_p & j_r & J \\ j_q & j_s & J' \end{Bmatrix} \, {}^{J'}\overline{\Gamma}_{u\bar{t}}^{p\bar{s}} \, {}^{J'}\overline{\lambda}_{q\bar{r}}^{u\bar{t}} \\
& + \frac{1}{4} \sum_{m_p m_r m_q m_s} \begin{pmatrix} j_p & j_r \\ m_p & m_r \end{pmatrix} \Bigg| \begin{matrix} J \\ 0 \end{matrix} \Bigg) \begin{pmatrix} j_q & j_s \\ m_q & m_s \end{pmatrix} \Bigg| \begin{matrix} J \\ 0 \end{matrix} \Bigg) \sum_{tuv} \sum_{m_t m_u m_v} \Gamma_{um_u \, vm_v}^{rm_r \, tm_t} \lambda_{tm_t \, qm_q \, sm_s}^{um_u \, vm_v \, pm_p} \Bigg) \\
& - (-)^{J-j_p-j_r} [p \leftrightarrow r] \Bigg) - (-)^{J-j_q-j_s} [q \leftrightarrow s] \Bigg] - [pr \leftrightarrow qs].
\end{aligned} \tag{4.246b}$$

Note that the last term has not been simplified. In order to obtain these J-coupled expressions, we made the same assumptions done for the derivation of J-coupled multi-reference IM-SRG(2) flow equations in section 4.3. As a reminder, the assumptions are that the one-particle density matrix as well as the irreducible two- and higher-body density matrices are scalar, i.e., spherical tensors of rank zero. This condition is only fulfilled if the reference state has vanishing total angular momentum (see appendix C.3).

4.6.5. Decay Scales

In this section, we derive the basic relation that motivates the construction of some generators, like the Wegner, White and Imaginary-Time. Furthermore, we study the decoupling properties of the generators, i.e., how they suppress the off-diagonal matrix elements for large enough values of the flow parameter s. We demonstrate how to derive the decay scales explicitly for the White generator.

We construct $\boldsymbol{H}^{\mathrm{d}}$ as a Hermitian operator by choosing an orthonormal basis

$$\{|\Psi\rangle, |\Psi_1\rangle, |\Psi_2\rangle, \ldots\} \tag{4.247}$$

and defining

$$\boldsymbol{H}^{\mathrm{d}}(s) \coloneqq E(s)\,|\Psi\rangle\langle\Psi| + \sum_i \tilde{E}_i(s)\,|\Psi_i\rangle\langle\Psi_i| \tag{4.248a}$$

with

$$E(s) = \langle\Psi|\boldsymbol{H}(s)|\Psi\rangle \tag{4.248b}$$

$$\tilde{E}_i(s) \coloneqq \langle\Psi_i|\boldsymbol{H}(s)|\Psi_i\rangle\,. \tag{4.248c}$$

Note that this basis is an eigenbasis of $\boldsymbol{H}^{\mathrm{d}}$ by construction and $|\Psi\rangle$ denotes the reference state. Furthermore, we emphasize that the energies $\tilde{E}_i$ are not the eigenvalues of the Hamiltonian $\boldsymbol{H}$. The states $\{|\Psi_1\rangle, |\Psi_2\rangle, \ldots\}$ span a subspace of the A-body Hilbert space that is orthogonal to the reference state, analogously to the subspace spanned by all basis states $|\Psi^{p_1\cdots}_{q_1\cdots}\rangle$ containing at least a one-particle one-hole excitation. The off-diagonal piece can simply be written as

$$\boldsymbol{H}^{\mathrm{od}}(s) = \boldsymbol{H}(s) - \boldsymbol{H}^{\mathrm{d}}(s). \tag{4.249}$$

For the matrix elements of the off-diagonal and diagonal Hamiltonian in this eigenbasis we obtain

$$\langle\Psi|\boldsymbol{H}^{\mathrm{d}}|\Psi_i\rangle = 0 \tag{4.250a}$$

$$\langle\Psi_i|\boldsymbol{H}^{\mathrm{d}}|\Psi_j\rangle = \tilde{E}_i\delta^i_j \tag{4.250b}$$

$$\langle\Psi|\boldsymbol{H}^{\mathrm{od}}|\Psi\rangle = \langle\Psi_i|\boldsymbol{H}^{\mathrm{od}}|\Psi_i\rangle = 0. \tag{4.250c}$$

Furthermore, the anti-Hermiticity of the generator implies

$$\langle\Psi|\boldsymbol{\eta}|\Psi\rangle = \langle\Psi_i|\boldsymbol{\eta}|\Psi_i\rangle = 0. \tag{4.251}$$

Inserting the identity operator in the eigenbasis of the diagonal Hamiltonian,

$$\mathbf{1} = |\Psi\rangle\langle\Psi| + \sum_k |\Psi_k\rangle\langle\Psi_k|\,, \tag{4.252}$$

and making use of the aforementioned expressions, we can determine the derivative of a

non-diagonal matrix element

$$\langle\Psi|\frac{\mathrm{d}\boldsymbol{H}}{\mathrm{d}s}|\Psi_i\rangle = \langle\Psi|[\boldsymbol{\eta},\boldsymbol{H}]|\Psi_i\rangle \tag{4.253}$$

$$= \langle\Psi|\boldsymbol{\eta}|\Psi\rangle\langle\Psi|\boldsymbol{H}|\Psi_i\rangle - \langle\Psi|\boldsymbol{H}|\Psi\rangle\langle\Psi|\boldsymbol{\eta}|\Psi_i\rangle + \sum_k(\langle\Psi|\boldsymbol{\eta}|\Psi_k\rangle\langle\Psi_k|\boldsymbol{H}|\Psi_i\rangle - \langle\Psi|\boldsymbol{H}|\Psi_k\rangle\langle\Psi_k|\boldsymbol{\eta}|\Psi_i\rangle) \tag{4.254}$$

$$= 0 - E\langle\Psi|\boldsymbol{\eta}|\Psi_i\rangle + \sum_k(\langle\Psi|\boldsymbol{\eta}|\Psi_k\rangle\tilde{E}_i\delta_i^k - \underbrace{\langle\Psi|\boldsymbol{H}^{\mathrm{d}}|\Psi_k\rangle}_{=0}\langle\Psi_k|\boldsymbol{\eta}|\Psi_i\rangle) + \sum_k(\langle\Psi|\boldsymbol{\eta}|\Psi_k\rangle\langle\Psi_k|\boldsymbol{H}^{\mathrm{od}}|\Psi_i\rangle - \langle\Psi|\boldsymbol{H}^{\mathrm{od}}|\Psi_k\rangle\langle\Psi_k|\boldsymbol{\eta}|\Psi_i\rangle) \tag{4.255}$$

$$= -\langle\Psi|\boldsymbol{\eta}|\Psi_i\rangle(E-\tilde{E}_i) + \sum_k(\langle\Psi|\boldsymbol{\eta}|\Psi_k\rangle\langle\Psi_k|\boldsymbol{H}^{\mathrm{od}}|\Psi_i\rangle - \langle\Psi|\boldsymbol{H}^{\mathrm{od}}|\Psi_k\rangle\langle\Psi_k|\boldsymbol{\eta}|\Psi_i\rangle). \tag{4.256}$$

This is a basic relation for the motivation of several generators and the analysis of their decay properties. We will explicitly demonstrate how this works for a White-type of generator. A natural choice based on the previous equation is given by

$$\langle\Psi|\boldsymbol{\eta}|\Psi_i\rangle := \frac{\langle\Psi|\boldsymbol{H}^{\mathrm{od}}|\Psi_i\rangle}{E-\tilde{E}_i} \tag{4.257a}$$

$$\langle\Psi_k|\boldsymbol{\eta}|\Psi_j\rangle := \frac{\langle\Psi_k|\boldsymbol{H}^{\mathrm{od}}|\Psi_j\rangle}{\tilde{E}_k-E_j}(1-\delta_j^k). \tag{4.257b}$$

Here, the denominator ensures the anti-Hermiticity of the generator. Note that the definition of the White generator from (4.237) is different from this White-type generator, but mimics its behavior for large values of the flow parameter, which is what we are interested in. Consider the following many-body matrix element of the derivative of the Hamiltonian

$$\langle\Psi|\frac{\mathrm{d}\boldsymbol{H}}{\mathrm{d}s}|\Psi_i\rangle = -\frac{\langle\Psi|\boldsymbol{H}^{\mathrm{od}}|\Psi_i\rangle}{E-\tilde{E}_i}(E-\tilde{E}_i) + \sum_{k\neq i}(\frac{1}{E-\tilde{E}_k}-\frac{1}{\tilde{E}_k-\tilde{E}_i})\langle\Psi|\boldsymbol{H}^{\mathrm{od}}|\Psi_k\rangle\langle\Psi_k|\boldsymbol{H}^{\mathrm{od}}|\Psi_i\rangle \tag{4.258}$$

$$= -\langle\Psi|\boldsymbol{H}^{\mathrm{od}}|\Psi_i\rangle + \sum_{k\neq i}\frac{2\tilde{E}_k-\tilde{E}_i-E}{(E-\tilde{E}_k)(\tilde{E}_k-\tilde{E}_i)}\langle\Psi|\boldsymbol{H}^{\mathrm{od}}|\Psi_k\rangle\langle\Psi_k|\boldsymbol{H}^{\mathrm{od}}|\Psi_i\rangle\,. \tag{4.259}$$

Assuming that the evolved Hamiltonian is sufficiently close to an attractive fixed point for $s \geq s_0$, we can show that the second term is negligible compared to the first one. For that purpose let us first consider the (Frobenius) norm of the off-diagonal piece, which is expected to go to zero. Hence, we can suppress it below an arbitrarily given positive number $\epsilon^2 > 0$:

$$||\boldsymbol{H}^{\mathrm{od}}||^2 = \mathrm{tr}((\boldsymbol{H}^{\mathrm{od}})^\dagger\boldsymbol{H}^{\mathrm{od}}) \tag{4.260}$$

$$= \langle\Psi|\boldsymbol{H}^{\mathrm{od}}\boldsymbol{H}^{\mathrm{od}}|\Psi\rangle + \sum_i\langle\Psi_i|\boldsymbol{H}^{\mathrm{od}}\boldsymbol{H}^{\mathrm{od}}|\Psi_i\rangle \tag{4.261}$$

$$= \langle\Psi|\boldsymbol{H}^{\mathrm{od}}|\Psi\rangle \langle\Psi|\boldsymbol{H}^{\mathrm{od}}|\Psi\rangle + \sum_k \langle\Psi|\boldsymbol{H}^{\mathrm{od}}|\Psi_k\rangle \langle\Psi_k|\boldsymbol{H}^{\mathrm{od}}|\Psi\rangle$$
$$+ \sum_i \langle\Psi_i|\boldsymbol{H}^{\mathrm{od}}|\Psi\rangle \langle\Psi|\boldsymbol{H}^{\mathrm{od}}|\Psi_i\rangle + \sum_{ik} \langle\Psi_i|\boldsymbol{H}^{\mathrm{od}}|\Psi_k\rangle \langle\Psi_k|\boldsymbol{H}^{\mathrm{od}}|\Psi_i\rangle \tag{4.262}$$
$$= 0 + 2\sum_i |\langle\Psi_i|\boldsymbol{H}^{\mathrm{od}}|\Psi\rangle|^2 + \sum_{ik} |\langle\Psi_i|\boldsymbol{H}^{\mathrm{od}}|\Psi_k\rangle|^2 < \epsilon^2. \tag{4.263}$$

Since all summands are positive, each term has to smaller than ϵ^2 separately

$$|\langle\Psi_i|\boldsymbol{H}^{\mathrm{od}}|\Psi\rangle|^2 < \epsilon^2 \tag{4.264}$$
$$|\langle\Psi_i|\boldsymbol{H}^{\mathrm{od}}|\Psi_k\rangle|^2 < \epsilon^2. \tag{4.265}$$

Assuming that the energies E and $\tilde{E}_i$ are approximately constant for sufficiently large flow parameter $s > s_0$, we can conclude that the second term in (4.259) goes faster to zero than the first one. This is because the second term goes like ϵ^2 while the first one goes like ϵ^1. Thus, neglecting these terms in (4.259), we obtain a first-order differential equation for the off-diagonal piece

$$\langle\Psi|\frac{\mathrm{d}\boldsymbol{H}}{\mathrm{d}s}|\Psi_i\rangle = \underbrace{\frac{\mathrm{d}\langle\Psi|\boldsymbol{H}^{\mathrm{d}}|\Psi_i\rangle}{\mathrm{d}s}}_{=0} + \frac{\mathrm{d}\langle\Psi|\boldsymbol{H}^{\mathrm{od}}(s)|\Psi_i\rangle}{\mathrm{d}s} \overset{!}{\approx} -\langle\Psi|\boldsymbol{H}^{\mathrm{od}}(s)|\Psi_i\rangle\,. \tag{4.266}$$

The solution for $s > s_0$ is given by

$$\langle\Psi|\boldsymbol{H}^{\mathrm{od}}(s)|\Psi_i\rangle \approx \langle\Psi|\boldsymbol{H}^{\mathrm{od}}(s_0)|\Psi_i\rangle \cdot \exp\left[-(s-s_0)\right]. \tag{4.267a}$$

Similar analysis for the other generators, Wegner and Imaginary-Time, that can be found in [Her17], yields

$$\langle\Psi|\boldsymbol{H}^{\mathrm{od}}(s)|\Psi_i\rangle \approx \langle\Psi|\boldsymbol{H}^{\mathrm{od}}(s_0)|\Psi_i\rangle \cdot \exp\left[-(E-\tilde{E}_i)^2(s-s_0)\right] \tag{4.267b}$$
$$\langle\Psi|\boldsymbol{H}^{\mathrm{od}}(s)|\Psi_i\rangle \approx \langle\Psi|\boldsymbol{H}^{\mathrm{od}}(s_0)|\Psi_i\rangle \cdot \exp\left[-|E-\tilde{E}_i|(s-s_0)\right], \tag{4.267c}$$

respectively. Thus, we see that the Wegner and Imaginary-Time generators yield proper renormalization-group transformations, in the sense that matrix elements of states with large energy differences to the ground state $|E-\tilde{E}_i|$ decay exponentially at smaller flow parameters s than states with small $|E-\tilde{E}_i|$. The White generator, on the other hand, acts on all matrix elements simultaneously. If we are only interested in the limit $s \to \infty$, this should not make a difference. For the Brillouin generator, we could not find its behavior in literature so far.

4.7. Observables

In this section, we discuss how to extract observables beside the ground-state energy within the framework of multi-reference IM-SRG.

4.7.1. General Idea

Suppose we have a Hermitian operator $\boldsymbol{O}$ associated to an observable. The aim is to calculate the expectation value of this operator with respect to an eigenstate $|\Psi_i\rangle$ of the Hamiltonian $\boldsymbol{H}$, that can be rewritten with the aid of the unitary transformation $\boldsymbol{U}(s)$ to

$$\langle\Psi_i|\boldsymbol{O}|\Psi_i\rangle = \langle\Psi_i|\boldsymbol{U}(s)\boldsymbol{U}^\dagger(s)\boldsymbol{O}(s)\boldsymbol{U}(s)\boldsymbol{U}^\dagger(s)|\Psi_i\rangle = \langle\Psi_i(s)|\boldsymbol{O}(s)|\Psi_i(s)\rangle \tag{4.268}$$

with the unitarily transformed operator

$$\boldsymbol{O}(s) \coloneqq \boldsymbol{U}^\dagger(s)\boldsymbol{O}\boldsymbol{U}(s) \tag{4.269}$$

and the transformed state

$$|\Psi_i(s)\rangle \coloneqq \boldsymbol{U}^\dagger(s)\,|\Psi_i\rangle \tag{4.270}$$

which is an eigenstate of the transformed Hamiltonian $\boldsymbol{H}(s) = \boldsymbol{U}^\dagger(s)\boldsymbol{H}(0)\boldsymbol{U}(s)$. The latter statement can be proved easily

$$\boldsymbol{H}(s)\,|\Psi_i(s)\rangle = \boldsymbol{U}^\dagger(s)\boldsymbol{H}(0)\underbrace{\boldsymbol{U}(s)\boldsymbol{U}^\dagger(s)}_{=\mathbf{1}}|\Psi_i\rangle = E_i\boldsymbol{U}^\dagger(s)\,|\Psi_i\rangle = E_i\,|\Psi_i(s)\rangle \tag{4.271}$$

where $|\Psi_i\rangle$ is an eigenstate of the initial Hamiltonian with the corresponding eigenvalue E_i.

Now, the key point is that in multi-reference IM-SRG(A) evolution the reference state $|\Psi\rangle$ becomes an eigenstate of the evolved Hamiltonian if the flow parameter s goes to infinity, i.e.,

$$\langle\Psi_i|\boldsymbol{O}|\Psi_i\rangle = \lim_{s\to\infty}\langle\Psi|\boldsymbol{O}(s)|\Psi\rangle\,. \tag{4.272}$$

Consequently, we are forced to consistently evolve the operator in order to extract observables associated with this operator within the multi-reference IM-SRG(A) framework according to the right-hand side of (4.268). But note that we cannot exactly control which eigenstate we target in multi-reference IM-SRG, as aforementioned.

In practical calculations of multi-reference IM-SRG, we do not explicitly construct the unitary transformation, instead, we use the flow-equation approach which can be formulated for this operator as well

$$\frac{\mathrm{d}\boldsymbol{O}(s)}{\mathrm{d}s} = [\boldsymbol{\eta}(s), \boldsymbol{O}(s)] \tag{4.273}$$

where the dynamical anti-Hermitian generator $\boldsymbol{\eta}(s)$, obtained from the evolution of the Hamiltonian, governs the unitary transformation. Thus, we have to solve the flow equation for the operator and the Hamiltonian (4.5) simultaneously. In contrast, the Magnus formulation of the (multi-reference) IM-SRG is an alternative way to construct the unitary transformation directly [Bla+09; MPB15].

Finally, we give an overview of the procedure how to extract observables in numerical calculations in multi-reference IM-SRG(2). Assuming that the operator written in second-quantized form in vacuum representation has a maximum particle rank of two

$$\boldsymbol{O} = A + \sum_{\substack{\alpha \\ \beta}} B_\beta^\alpha \boldsymbol{a}_\beta^\alpha + \frac{1}{4} \sum_{\substack{\alpha\gamma \\ \beta\delta}} C_{\beta\delta}^{\alpha\gamma} \boldsymbol{a}_{\beta\delta}^{\alpha\gamma} \tag{4.274}$$

with known zero, one- and two-body matrix elements A, B_β^α and $C_{\beta\delta}^{\alpha\gamma}$, we transform it into reference-state representation using the same reference state $|\Psi\rangle$ as for the Hamiltonian according to (3.65). If the operator also contains three-body pieces, their effects can be included using the MR-NO2B approximation as described in section 3.3.4. The matrix elements of this operator need to be transformed to the natural-orbital basis as given in (4.24) to use the formulae derived in this chapter. Afterwards, we work out the commutators yielding the same results as for the Hamiltonian. The m-scheme results in natural orbitals are basically given in (4.28) which are valid for any kind of operator. The J-scheme results in natural orbitals from formulae (4.89) are computationally very efficient, but only valid for scalar operators, i.e., spherical tensors of rank zero. Hence, we are limited to scalar operators, which include, for instance, the mean-square-radius operator and the electric monopole transition operator that will be the subject of sections 4.7.2 and 4.7.3. For non-zero rank tensors, the J-scheme formulation must be generalized.

4.7.2. Radii

The definition of *mean-square-radius* operator in particle-number-conserving theories[7], which is the case here, is defined as

$$\boldsymbol{r}_{\mathrm{ms}} := \frac{1}{A} \sum_{i=1}^{A} \left(\vec{\boldsymbol{r}}(i) - \vec{\boldsymbol{R}} \right)^2 \tag{4.275}$$

with the absolute coordinate vector operator of the i-th particle acting non-trivially only in the i-th subspace of the A-body Hilbert space

$$\vec{\boldsymbol{r}}(i) = \underbrace{\mathbf{1} \otimes \ldots \otimes \mathbf{1} \otimes \underbrace{\vec{\boldsymbol{r}}}_{i\text{-th place}} \otimes \mathbf{1} \otimes \ldots \otimes \mathbf{1}}_{A} \tag{4.276}$$

[7] In particle-number non-conserving theories the prefactor $\frac{1}{A}$ need to be raised to a Hermitian operator $\boldsymbol{A}^{-1}$.

and the center-of-mass vector operator for A nucleons with the same mass

$$\vec{\boldsymbol{R}} \coloneqq \frac{1}{A} \sum_{i=1}^{A} \vec{\boldsymbol{r}}(i). \tag{4.277}$$

With the abbreviation of the two-body relative distance vector operator between the j-th and i-th particle

$$\vec{\boldsymbol{r}}(ij) \coloneqq \vec{\boldsymbol{r}}(i) - \vec{\boldsymbol{r}}(j), \tag{4.278}$$

we obtain after some basic simplification steps for the mean-square-radius operator

$$\boldsymbol{r}_{\mathrm{ms}} = \frac{1}{A^2} \sum_{i<j}^{A} \vec{\boldsymbol{r}}^2(ij), \tag{4.279}$$

which is a quasi two-body operator that depends on the total number of particles A. Hence, it can be rewritten in second quantization

$$\boldsymbol{r}_{\mathrm{ms}} = \frac{1}{4} \sum_{\substack{pr \\ qs}} \frac{1}{A^2} \langle pr| \, \vec{\boldsymbol{r}}^2(12) \, |qs\rangle \, \boldsymbol{a}^{pr}_{qs}. \tag{4.280}$$

Note that this operator contains zero-, one-, two-body pieces in reference-state representation.

The *point-proton* and *point-neutron mean-square radius* are defined as

$$\boldsymbol{r}_{\pi\mathrm{ms}} \coloneqq \frac{1}{Z} \sum_{i=1}^{A} \left(\vec{\boldsymbol{r}}(i) - \vec{\boldsymbol{R}} \right)^2 \boldsymbol{\Pi}_{\pi}(i) \tag{4.281a}$$

$$\boldsymbol{r}_{\nu\mathrm{ms}} \coloneqq \frac{1}{N} \sum_{i=1}^{A} \left(\vec{\boldsymbol{r}}(i) - \vec{\boldsymbol{R}} \right)^2 \boldsymbol{\Pi}_{\nu}(i) \tag{4.281b}$$

where Z and N denote the number of protons (π) or neutrons (ν), respectively. Furthermore, $\boldsymbol{\Pi}_{\pi}(i)$ and $\boldsymbol{\Pi}_{\nu}(i)$ represent the one-body projection operator on the corresponding particle species

$$\boldsymbol{\Pi}_{\pi}(i) \coloneqq \tfrac{1}{2} + \boldsymbol{\tau}_z(i) \tag{4.282a}$$

$$\boldsymbol{\Pi}_{\nu}(i) \coloneqq \tfrac{1}{2} - \boldsymbol{\tau}_z(i) \tag{4.282b}$$

where $\boldsymbol{\tau}_z(i)$ is the z-component of isospin operator of the i-th particle.

After some simplification steps, we obtain for the point-proton and point-neutron mean-square-radius operator

$$\boldsymbol{r}_{\pi\mathrm{ms}} = \frac{1}{A^2} \sum_{i<j}^{A} \vec{\boldsymbol{r}}^2(ij) \left(\tfrac{2A}{Z} \boldsymbol{\Pi}_{\pi\pi}(ij) + \tfrac{A}{Z} \left(\boldsymbol{\Pi}_{\pi\nu}(ij) + \boldsymbol{\Pi}_{\nu\pi}(ij) \right) \right) - \boldsymbol{r}_{\mathrm{ms}} \tag{4.283a}$$

$$\boldsymbol{r}_{\nu\mathrm{ms}} = \frac{1}{A^2} \sum_{i<j}^{A} \vec{\boldsymbol{r}}^2(ij) \left(\tfrac{2A}{N} \boldsymbol{\Pi}_{\nu\nu}(ij) + \tfrac{A}{N} \left(\boldsymbol{\Pi}_{\nu\pi}(ij) - \boldsymbol{\Pi}_{\pi\nu}(ij) \right) \right) - \boldsymbol{r}_{\mathrm{ms}} \tag{4.283b}$$

with the two-body projection operator $\mathbf{\Pi}_{\alpha\beta}(ij) := \mathbf{\Pi}_{\alpha}(i)\mathbf{\Pi}_{\beta}(j)$ and $\alpha, \beta \in \{\pi, \nu\}$. Hence, both the point-proton and point-neutron mean-square radius are quasi two-body operators like the mean-square-radius operator.

Using these operators, we can define several associated observables, for instance, the *root-mean-square radius*—also called *point mass radius*—of a nucleus in an eigenstate $|\Psi_i\rangle$, given by

$$R_{\mathrm{rms}} \coloneqq \sqrt{\langle \Psi_i | \boldsymbol{r}_{\mathrm{ms}} | \Psi_i \rangle}, \tag{4.284}$$

and analogously for the *point-proton* and *point-neutron root-mean-square* radii

$$R_{\pi\mathrm{rms}} \coloneqq \sqrt{\langle \Psi_i | \boldsymbol{r}_{\pi\mathrm{ms}} | \Psi_i \rangle} \tag{4.285}$$

$$R_{\nu\mathrm{rms}} \coloneqq \sqrt{\langle \Psi_i | \boldsymbol{r}_{\nu\mathrm{ms}} | \Psi_i \rangle}. \tag{4.286}$$

Note that these quantities do not carry the index i of the eigenstate $|\Psi_i\rangle$, for brevity.

We obtain the *charge radius* of the nucleus in an eigenstate $|\Psi_i\rangle$ by applying the corrections due to the mean-square charge radii of the proton r_π^2 and neutron r_ν^2 [Kam97]

$$R_{\mathrm{ch}} \coloneqq \sqrt{R_{\pi\mathrm{rms}}^2 + r_\pi^2 + \frac{N}{Z} r_\nu^2} = \sqrt{R_{\pi\mathrm{rms}}^2 + 0.743\,\mathrm{fm}^2 - \frac{N}{Z} 0.116\,\mathrm{fm}^2}, \tag{4.287}$$

where we took the experimental data from [Ber+12]. The Darwin-Foldy term, which is a relativistic correction, is neglected since it is one order of magnitude smaller than r_π^2 and r_ν^2.

4.7.3. Electromagnetic Monopole Transition

Electromagnetic transitions are the response of a nucleus to an external electromagnetic field, where the field is assumed to be weak such that non-linear effects can be neglected. The strategy is to decompose the external electromagnetic field into multipoles, and the total response of the nucleus can be viewed as the superposition of the responses due to each multipole. Electromagnetic transition operators are classified into electric and magnetic transitions based on the angular momentum L of the photon, being the particle dual of the electromagnetic field, and the parity given by $(-)^L$ for electric and $(-)^{L+1}$ for magnetic type of transitions. Note that the distinction between electric and magnetic types might be misleading since transitions are neither purely electric nor magnetic.

Since we are limited to scalar operators, i.e., spherical tensors of rank zero, due to our current implementation of the IM-SRG evolution, we can only study electromagnetic monopole transitions that cannot change the total angular momentum and parity between the initial and final state. In contrast to electric monopole transitions, which are possible via internal conversion where the nucleus de-excites by emitting an electron from the atomic shell [RS80], magnetic monopole transitions are fundamentally forbidden because there are no magnetic monopoles in nature.

Expressions for the transition operators are usually derived by first-order time-dependent

perturbation theory and in a *long wavelength limit*, i.e., the wavelength of the electromagnetic field λ_γ is large compared to the nuclear radius r_{nucl}. The validity of this approximation can be analyzed based on the following consideration: On the one hand, the wavelength of the electromagnetic field is related to its energy E_γ via

$$\lambda_\gamma = \frac{2\pi\hbar c}{E_\gamma} \tag{4.288}$$

with c denoting the speed of light and $\hbar$ the Planck's constant. On the other hand, a stable nucleus has approximately a constant density and, therefore, the nuclear radius r_{nucl} can be approximated by the following empirical formula

$$r_{\text{nucl}} = 1.25\,\text{fm} \cdot A^{1/3}. \tag{4.289}$$

Hence, the condition $\lambda_\gamma \gg r_{\text{nucl}}$ leads to

$$E_\gamma \ll \frac{2\pi\hbar c}{1.25\,\text{fm}} \cdot A^{-1/3} = 991.2\,\text{MeV} \cdot A^{-1/3}. \tag{4.290}$$

Thus, the larger the number of nucleons, the smaller the range of photon energies where this condition can be justified. For systems up 40 nucleons, that is a particular interest of this work, this condition reads as $E_\gamma \ll 290\,\text{MeV}$ which is fulfilled for the typical spectroscopy of low-lying states in sd-shell nuclei we are interested in.

In this subsection, we derive the formulae widely used in the literature for the electric transition operator $\boldsymbol{Q}_{LM_L}$ with M_L being the z-component of the total angular momentum L of the photon. The starting point is the formula for the *electric multipole moment* given by [RS80]

$$E_{LM_L} \coloneqq \frac{(2L+1)!!}{q^L(L+1)} \int \mathrm{d}^3r\ \rho(\vec{r}) \frac{\partial}{\partial r}\Big[r j_L(qr)\Big] Y_{LM_L}(\vartheta,\varphi) \tag{4.291}$$

$$+ \frac{\mathbb{i}(2L+1)!!}{cq^{L-1}(L+1)} \int \mathrm{d}^3r\ \vec{r}\cdot\vec{j}(\vec{r})\ j_L(qr) Y_{LM_L}(\vartheta,\varphi) \tag{4.292}$$

which is not an operator type of expression. Here, q denotes the momentum transfer, j_L the spherical Bessel function of order L, Y_{LM_L} spherical harmonics and ρ is the electric charge density. In the second term, $\vec{j}$, c and $\mathbb{i}$ denote the electric current density, speed of light, and the imaginary unit, respectively. Lastly, the symbol $(2L+1)!! \coloneqq (2L+1)\cdot(2L-1)\cdot\ldots\cdot 3\cdot 1$ is the so-called double factorial.

We note that the second term is neglected in the long-wavelength limit, i.e., $qr \ll 1$, since the leading term goes like $(qr)^{L+1}$, whereas the leading term of the first term goes like $(qr)^L$. This can be seen once we expand the spherical Bessel function. For that purpose, let us expand the ordinary Bessel function for small arguments as

$$J_\alpha(x) = \sum_{j=0}^{\infty} \frac{(-)^j}{j!\,\Gamma(j+\alpha+1)} \left(\frac{x}{2}\right)^{2j+\alpha}, \tag{4.293}$$

with Γ being the Euler's gamma function and writing out the first two summands, we get

$$= \frac{1}{\Gamma(\alpha+1)} \left(\frac{x}{2}\right)^{\alpha} - \frac{1}{\Gamma(\alpha+2)} \left(\frac{x}{2}\right)^{2+\alpha} \pm \dots \tag{4.294}$$

$$= \frac{1}{\Gamma(\alpha+1)} \left(\frac{x}{2}\right)^{\alpha} \left(1 - \frac{\Gamma(\alpha+1)}{4\Gamma(\alpha+2)} x^2 \pm \dots\right). \tag{4.295}$$

Making use of $\Gamma(z+1) = z\Gamma(z)$ for any real number z, we obtain

$$= \frac{1}{\alpha\Gamma(\alpha)} \left(\frac{x}{2}\right)^{\alpha} \left(1 - \frac{1}{4(\alpha+1)} x^2 \pm \dots\right). \tag{4.296}$$

With these results we can expand the spherical Bessel function for a non-negative integer $L \in \{0, 1, \dots\}$

$$j_L(qr) \coloneqq \sqrt{\frac{\pi}{2qr}} J_{L+\frac{1}{2}}(qr) \tag{4.297}$$

$$= \sqrt{\frac{\pi}{2qr}} \frac{1}{(L+\frac{1}{2})\Gamma(L+\frac{1}{2})} \left(\frac{qr}{2}\right)^{L+\frac{1}{2}} \left(1 - \frac{1}{4(L+\frac{3}{2})} (qr)^2 \pm \dots\right) \tag{4.298}$$

since L is integer it follows $\Gamma(L+\frac{1}{2}) = \frac{(2L-1)!!\sqrt{\pi}}{2^L}$

$$= \sqrt{\frac{\pi}{2qr}} \frac{2^L}{(L+\frac{1}{2})(2L-1)!!\sqrt{\pi}} \left(\frac{qr}{2}\right)^{L+\frac{1}{2}} \left(1 - \frac{1}{4(L+\frac{3}{2})} (qr)^2 \pm \dots\right) \tag{4.299}$$

$$= \frac{(qr)^L}{(2L+1)(2L-1)!!} \left(1 - \frac{1}{2(2L+3)} (qr)^2 \pm \dots\right), \tag{4.300}$$

making use that $(2L+1)(2L-1)!! = (2L+1)!!$

$$= \frac{(qr)^L}{(2L+1)!!} \left(1 - \frac{1}{2(2L+3)} (qr)^2 \pm \dots\right). \tag{4.301}$$

Plugging this result into (4.291) yields

$$E_{LM_L} = \frac{(2L+1)!!}{q^L(L+1)} \int \mathrm{d}^3r\, \rho(\vec{r}) \frac{\partial}{\partial r} \left[r \frac{(qr)^L}{(2L+1)!!} \left(1 - \frac{1}{2(2L+3)} (qr)^2 \pm \dots\right)\right] Y_{LM_L}(\vartheta, \varphi) \tag{4.302}$$

$$= \int \mathrm{d}^3r\, \rho(\vec{r}) r^L Y_{LM_L}(\vartheta, \varphi) - \frac{(L+3)}{2q^L(L+1)(2L+3)} \int \mathrm{d}^3r\, \rho(\vec{r}) (qr)^{L+2} Y_{LM_L}(\vartheta, \varphi) \pm \dots. \tag{4.303}$$

Let us consider the monopole term, i.e., $L = M_L = 0$, leading to

$$E_{00} = \int \mathrm{d}^3r\, \rho(\vec{r}) Y_{00}(\vartheta, \varphi) - \frac{1}{2} \int \mathrm{d}^3r\, \rho(\vec{r})\, (qr)^2 Y_{00}(\vartheta, \varphi) \tag{4.304}$$

$$= \frac{1}{\sqrt{4\pi}} \int \mathrm{d}^3r\, \rho(\vec{r}) - \frac{q^2}{2\sqrt{4\pi}} \int \mathrm{d}^3r\, \rho(\vec{r})\, r^2 \tag{4.305}$$

$$= \frac{1}{\sqrt{4\pi}} Ze - \frac{q^2}{2\sqrt{4\pi}} \int \mathrm{d}^3 r \; \rho(\vec{r}) r^2 \tag{4.306}$$

where we made use that $Y_{00}(\vartheta, \varphi) = \frac{1}{\sqrt{4\pi}}$ and the integral over the electric charge density gives the total charge of the nucleus Ze since we have Z protons carrying the elementary charge e.

For non-relativistic point-like nucleons, we can raise this expression to operators by introducing the electric charge density operator

$$\boldsymbol{\rho}(\vec{r}\,') = e \sum_{i=1}^{A} \mathbf{\Pi}_\pi(i) \delta\left(\vec{r}\,' - \vec{\boldsymbol{r}}\,'(i)\right) \tag{4.307}$$

with

$$\vec{\boldsymbol{r}}\,'(i) \coloneqq \vec{\boldsymbol{r}}(i) - \vec{\boldsymbol{R}}. \tag{4.308}$$

Here, δ is the delta distribution, $\vec{\boldsymbol{r}}(i)$ is the absolute coordinate vector operator of the i-th particle (4.276), and $\vec{\boldsymbol{R}}$ is the center-of-mass vector operator (4.277), and $\mathbf{\Pi}_\pi(i)$ denotes the one-body projection operator on the protons (4.282a). The presence of the center-of-mass coordinate ensures translational invariance of the electromagnetic transition operators.

Finally, inserting the electric charge density in the expression (4.306) and integrating yields

$$\boldsymbol{E}_{00} = \frac{1}{\sqrt{4\pi}} Ze\mathbf{1} - \frac{q^2 e}{2\sqrt{4\pi}} \sum_{i=1}^{A} \mathbf{\Pi}_\pi(i) \left(\vec{\boldsymbol{r}}(i) - \vec{\boldsymbol{R}}\right)^2. \tag{4.309}$$

Since the first term of the electric monopole transition is proportional to the identity operator, it cannot induce transitions between two different states. Furthermore, we separate the nuclear-physics part from the kinematics of the virtual photon (which determines q^2) and define the *electric monopole transition operator* as

$$\boldsymbol{Q}_{00} \coloneqq e \sum_{i=1}^{A} \mathbf{\Pi}_\pi(i) \left(\vec{\boldsymbol{r}}(i) - \vec{\boldsymbol{R}}\right)^2 = e \sum_{i=1}^{A} \left(\vec{\boldsymbol{r}}(i) - \vec{\boldsymbol{R}}\right)^2 \mathbf{\Pi}_\pi(i) = eZ\boldsymbol{r}_{\pi\mathrm{ms}} \tag{4.310}$$

which is proportional to the point-proton mean-square radius (4.281a). Note that the prefactor $\frac{1}{2\sqrt{4\pi}}$ is missing in our definition of electric monopole transition operator which is only important if we want to compare our results to other calculations.

Chapter 5

No-Core Shell Model and Importance Truncation

In this chapter, we present the no-core shell model (NCSM) as a many-body method. Afterwards, we briefly describe the importance-truncated NCSM which is an extension of the NCSM.

5.1. No-Core Shell Model

The NCSM is one of the most powerful and universal *ab initio* many-body methods that belongs to the class of configuration-interaction approaches [BNV13; Nav+09]. All nucleons are considered active in contrast to typical shell-model-type of approaches. NCSM is variational for a given Hamiltonian, i.e., it provides an upper bound for all absolute energies of the exact eigenstates.

It is built on a representation of the Schrödinger equation as a large-scale matrix eigenvalue problem, using an expansion of the eigenstates in an orthonormal basis of A-body states $|\Phi_i\rangle$,

$$|\Psi_n\rangle = \sum_i c_i^{(n)} |\Phi_i\rangle \tag{5.1}$$

with the expansion coefficient $c_i^{(n)}$.

Inserting this into to the stationary Schrödinger equation (3.94), and multiplying by $\langle\Phi_j|$ from the left, we obtain

$$\sum_j \langle\Phi_j| \boldsymbol{H} |\Phi_i\rangle c_i^{(n)} = E_n c_i^{(n)}, \tag{5.2}$$

which is an eigenvalue problem for the matrix representation of the Hamiltonian $H_{ji} := \langle\Phi_j| \boldsymbol{H} |\Phi_i\rangle$. Since the Hilbert space is infinite dimensional in general, we need to introduce some truncations.

The basis states $|\Phi_i\rangle$ are antisymmetrized A-body product states, also called Slater determinants or *configurations*

$$|\Phi_i\rangle \coloneqq |p_1 p_2 \dots p_A\rangle_i \tag{5.3}$$

built from single-particle states $|p\rangle$. A typical choice of the single-particle basis is the harmonic oscillator (HO)

$$\mathcal{B}_1 \coloneqq \left\{ |p\rangle \coloneqq |\tilde{n}_p (l_p \tfrac{1}{2}) j_p m_p \tfrac{1}{2} m_{t_p}\rangle \,:\, p \in \{1, 2, \dots\} \right\} \tag{5.4}$$

which is orthonormal. Here, $\tilde{n}_p \in \{0, 1, \dots\}$ is the radial quantum number, the angular-momentum $l_p \in \{0, 1, \dots\}$ and spin-$\frac{1}{2}$ quantum number are coupled to the total angular momentum $j_p \in \{|l_p - \frac{1}{2}|,\ |l_p - \frac{1}{2}| + 1,\ \dots,\ l_p + \frac{1}{2}\}$ with its projection quantum number $m_p \in \{-j_p, -j_p + 1, \dots, j_p\}$, and the z-component of the isospin-$\frac{1}{2}$ quantum number encodes whether this single-particle state belongs to a neutron $m_{t_p} = -\frac{1}{2}$ or a proton $m_{t_p} = +\frac{1}{2}$. Other single-particle bases, for instance Hartree Fock (HF) discussed in chapter 2 or natural orbitals [CMV12], can be used as well—which are all orthonormal bases, too. In this work, we will exploit the HO and HF single-particle bases.

The many-body basis must be truncated to render the problem numerically tractable, as aforementioned. For that purpose, we introduce the *single-particle energy quantum number*[1]

$$e_p \coloneqq 2\tilde{n}_p + l_p. \tag{5.5}$$

Furthermore, we assign each configuration $|\Phi_i\rangle$ an *energy quantum number* by simply adding the single-particle energy quantum numbers of all states occupied in this configuration, i.e.,

$$e(|\Phi_i\rangle) \coloneqq \sum_{\substack{p \in \mathcal{B}_1 \\ (a_p |\Phi_i\rangle \neq 0)}} e_p. \tag{5.6}$$

Obviously, there is at least one configuration $|\Phi_{\min}\rangle$ with the lowest energy quantum number that we call *base determinant*

$$e(|\Phi_{\min}\rangle) \leq e(|\Phi_i\rangle) \quad \text{for all } i. \tag{5.7}$$

Note that the base determinant is not unique in open-shell systems. However, we can define for a given configuration a new quantity called *number of excitation quanta*

$$N(|\Phi_i\rangle) \coloneqq e(|\Phi_i\rangle) - e(|\Phi_{\min}\rangle) \tag{5.8}$$

which is a non-negative integer. The truncation on the many-body level then may be realized

[1] For the single-particle basis HF and natural orbitals, this is an artificial quantity.

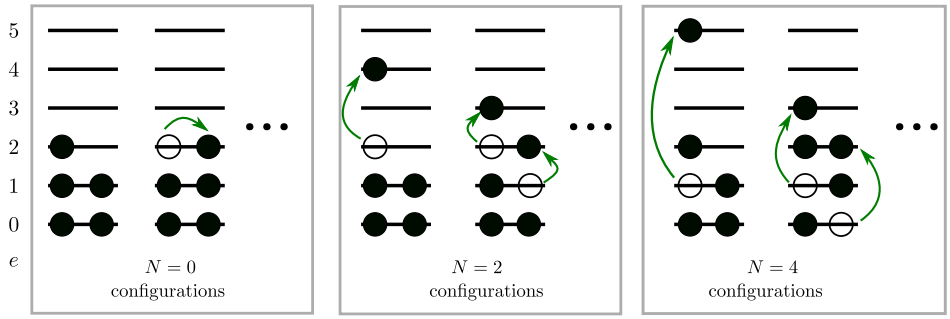

Figure 5.1.: We schematically illustrate the truncations of the many-body basis for the NCSM calculations. Starting from an energetically lowest configuration, called base determinant, which is not unique in open-shell systems, we construct the model space by exciting particles to unoccupied states. If one or more of the newly-occupied states belong to energetically higher orbitals, we associate the total number of excitation quanta N with the configuration formed this way. The model space is truncated for a given $N_{\max}$ by including only those states with $N \leq N_{\max}$. A configuration with $N = 0$ is formed by permuting particles among states belonging to the same orbit (left panel). Configurations with $N = 2$ can be constructed for instance by either exciting one particle by two orbitals or two particles by one orbit each (middle panel).

using $N_{\max}$ giving the maximum number of allowed excitation quanta

$$\mathcal{B}_{\text{NCSM}}^{(N_{\max})} := \{|\Phi_i\rangle \,:\, N(|\Phi_i\rangle) \leq N_{\max}\}. \tag{5.9}$$

A graphical illustration is shown in figure 5.1.

Additionally, we can reduce the number of basis states based on the symmetry of the Hamiltonian of the nuclear system: On the one hand, since the Hamiltonian is rotationally invariant, the nuclear energy levels are degenerate with respect to the angular momentum projection which is an additive quantum number

$$M_J(|\Phi_i\rangle) = \sum_{\substack{p\in\mathcal{B}_1 \\ (\boldsymbol{a}_p|\Phi_i\rangle\neq 0)}} m_p \tag{5.10}$$

and we can restrict the space to a specific M_J—typically the smallest allowed value $M_J = 0$ ($M_J = +\frac{1}{2}$) for even (odd) number of particles. On the other hand, using the parity conservation of the Hamiltonian

$$\pi(|\Phi_i\rangle) = \prod_{\substack{p\in\mathcal{B}_1 \\ (\boldsymbol{a}_p|\Phi_i\rangle\neq 0)}} (-1)^{l_p} \tag{5.11}$$

we also restrict the model space to basis states of either natural or unnatural parity. Here, natural-parity states has the same parity as the parity of the uncorrelated ground state predicted by the naive shell model, while unnatural-parity states do not. If we are only

interested in natural (unnatural) parity eigenstates, we need only to consider configurations with even (odd) number of excitation quanta N.

In conventional NCSM calculations, the HO basis in combination with the $N_{\max}$-truncation is used. The main advantages of this choice are the computational efficiency and the exact factorization of the eigenstates $|\Psi_n\rangle$ in intrinsic $|\Psi_{n,\text{int.}}\rangle$ and center-of-mass (CM) $|\Psi_{n,\text{cm}}\rangle$ parts

$$|\Psi_n\rangle = |\Psi_{n,\text{int.}}\rangle \otimes |\Psi_{n,\text{cm}}\rangle \tag{5.12}$$

avoiding mixing CM and intrinsic excitations. To get rid of CM excitations in the spectrum, we add a CM Hamiltonian of the form [RGP09]

$$\boldsymbol{H}_{\text{cm}} = \frac{1}{2mA}\vec{\boldsymbol{P}}^2 + \frac{mA\Omega^2}{2}\vec{\boldsymbol{R}}^2 - \frac{3}{2}\hbar\Omega \tag{5.13}$$

with

$$\vec{\boldsymbol{P}} := \sum_{i=1}^{A} \vec{\boldsymbol{p}}(i) \tag{5.14}$$

$$\vec{\boldsymbol{R}} := \frac{1}{A}\sum_{i=1}^{A} \vec{\boldsymbol{r}}(i), \tag{5.15}$$

acting on the CM momentum $\vec{\boldsymbol{P}}^2$ and CM coordinates $\vec{\boldsymbol{R}}^2$ of A particles with the same mass m to the intrinsic one. Hence, the total Hamiltonian in our calculations is given by

$$\boldsymbol{H} = \boldsymbol{H}_{\text{int}} + \beta\boldsymbol{H}_{\text{cm}}, \tag{5.16}$$

where the parameter β controls the strength of the CM part. Consequently, states with a CM components different from the harmonic-oscillator ground state are shifted to higher energies and removed from the part of the spectrum we are interested in.

NCSM calculations are limited by the dimension of the model space that grows factorially with increasing the number of nucleons A, and the model-space size $N_{\max}$ that needs to be increased in order to reach convergence. Nowadays, linear dimensions of 10^{10} are the upper limit of tractable matrices during the computations, such that NCSM calculations for ^{16}O can practically be performed only in relatively small model spaces ($N_{\max} \leq 8$) where convergence has not yet been reached [Var+09; Rot09]. In the next step, the importance-truncated NCSM, in which the NCSM model space can be reduced with guidance of the multi-configuration many-body perturbation theory, will be introduced.

We solve the eigenvalue problem of the finite matrix for a few low-lying eigenstates using the Lanczos-type algorithms [Lan50; SN69; Whi72], yielding energies and eigenvectors that can be used to compute any secondary observable. The truncations of the many-body space establish the crucial departure from an exact treatment of the Schrödinger equation. Hence, in practically calculation, we have to demonstrate that the truncations do not affect the observables of interest. This convergence is the critical condition for determining the

uncertainties of the method and also the limiting factor in practical applications. Several tools are being used to extend reach of the NCSM, e.g., through additional truncations of the many-body model space [RN07; Rot09] or through a pre-diagonalization of the Hamiltonian by a unitary transformation [Rot+11; JNF09; Ôku54; SL80]. Without these extensions, the NCSM is typically limited to ^{4}He [Rot+14; JNF11].

5.2. Importance Truncation

The importance-truncated NCSM reduces the NCSM model space to a tractable size without losing precision of the eigenvalues and eigenstates compared to an NCSM calculation [Rot09]. The starting point is an NCSM model space

$$\mathcal{M} := \mathrm{span}\left(\mathcal{B}_{\mathrm{NCSM}}^{(N_{\max})}\right) \tag{5.17}$$

and so-called *reference states*[2] $|\Psi'_n\rangle \in \mathcal{M}' \subseteq \mathcal{M}$. The reference states $|\Psi'_n\rangle$ are approximations of the target states, which will be calculated later, to have the correct angular momentum. To ensure this requirement, $|\Psi'_n\rangle$ are determined in NCSM-type calculation in $\mathcal{M}'$.

In order to quantify the importance of the basis states which are included in $\mathcal{M}$, but excluded from $\mathcal{M}'$, the first perturbative correction of $|\Psi'_n\rangle$

$$|\Psi'^{(1)}_n\rangle = -\sum_{|\Phi_i\rangle \notin \mathcal{M}'} \frac{\langle\Phi_i|\,\boldsymbol{H}\,|\Psi'_n\rangle}{\epsilon_i - \epsilon'_n}\,|\Phi_i\rangle \tag{5.18}$$

is considered, where ϵ_i is the unperturbed energy of the basis states $|\Phi_i\rangle \notin \mathcal{M}'$, and ϵ'_n is the expectation value with respect to $|\Psi'_n\rangle$ of the Hamiltonian $\boldsymbol{H}$.

Afterwards, the coefficient

$$\kappa_i^{(n)} := -\frac{\langle\Phi_i|\,\boldsymbol{H}\,|\Psi'_n\rangle}{\epsilon_i - \epsilon'_n} \tag{5.19}$$

is used as an *a priori* importance measure of the basis state $|\Phi_i\rangle \notin \mathcal{M}'$. Only basis states with an importance measure $|\kappa_i^{(n)}|$ above a threshold $\kappa_{\min}$ for at least one reference state are retained in the model space. Hence, diagonalization of the matrix can be carried out in this smaller space. A variation of the threshold $\kappa_{\min}$ allows an *a posteriori* extrapolation of $\kappa_{\min}$ towards zero to recover the contribution of the discarded basis states.

The procedure for the importance truncation of the model space can be extended to an iterative method: We start with a particular model space and the reference states calculated in an NCSM-tractable model space, and reduce the model space by means of the importance measure (5.19). By diagonalizing the Hamiltonian matrix within the importance-truncated model space, a set of eigenstates are obtained that can be used for the next larger model space. This procedure is iterated while making progress to larger model spaces. The reduc-

[2] Do not be confused with the reference state $|\Psi\rangle$ introduced in previous chapters which does not enter the consideration in this chapter.

tion of the model space facilitates calculations in ranges that are not manageable in NCSM. For instance, calculations for ^{16}O in the model space $N_{\max} = 10$—not tractable in the framework of NCSM—are computationally possible in importance-truncated NCSM because of the tremendous reduction of the model-space size. Even calculations within a model space up to $N_{\max} = 22$ and beyond are tractable in importance-truncated NCSM while this limit is set by the available two-body matrix elements and not by the importance-truncated NCSM calculation itself [Rot09].

Chapter 6

Merging In-Medium Similarity Renormalization Group and No-Core Shell Model

In this chapter, we merge the *multi-reference* in-medium similarity renormalization group (IM-SRG) and the no-core shell model (NCSM) introduced in the previous chapters to define the in-medium no-core shell model (IM-NCSM). In section 6.1, we give a brief motivation why we merge them. Furthermore, we give a prescription how to merge them discussed in section 6.2. Finally, in section 6.3, we show the Hamiltonian matrix in a many-body basis in order to illustrate how well the IM-NCSM works.

6.1. Motivation

We motivate combining the two many-body methods, IM-SRG and NCSM, by confronting the advantages and limitations of each method. The complementarity of both approaches makes it ideal for merging these techniques.

Let us start with the NCSM, which is limited to light nuclei due to the factorial growth of the model space. It is computationally very demanding to obtain model-space convergence. For larger systems the model-space sizes needed are beyond the reach of current computers. In contrast to that, using the IM-SRG, we can easily access heavy nuclei due to the soft computational scaling with particle number A of the nucleus. A very nice feature of the IM-SRG is that the Hamiltonian is decoupled in the A-body basis, which will be explicitly demonstrated later on.

However, the IM-SRG is not an exact *ab initio* method due to additional truncations and is not variational. As explained in detail in section 4.7, it is designed for ground-state observables only. The description of excited states and spectroscopic observables are not straightforward. Moreover, it is limited to even nuclei due to the J-coupled implementation for scalar operators. On the other hand, the NCSM is a (quasi)-exact method enabling easy

access to excited states, and, therefore, spectroscopy does not incur significant additional computational cost since we get also the eigenstates of the Hamiltonian from the diagonalization. Finally, it is not limited to even nuclei as the IM-SRG.

By merging these two techniques we get a powerful method which exploits the advantages of both techniques, and we can overcome some limitations.

6.2. In-Medium No-Core Shell Model

In this section, we describe how to merge the multi-reference IM-SRG and the NCSM to define the IM-NCSM approach. This procedure consists of three major steps as depicted schematically in figure 6.1:

1. We perform an NCSM calculation to obtain a reference state $|\Psi\rangle$ for the specific nucleus of interest in a small model space with truncation parameter $N_{\max}^{\text{ref}}$, called the *reference-space size*. We choose $N_{\max}^{\text{ref}} = 0$ model spaces unless otherwise stated, which are multidimensional in open-shell nuclei. The lowest eigenstate with the appropriate quantum numbers serves as reference state.

2. We normal order the Hamiltonian with respect to the reference state $|\Psi\rangle$, which is multi-determinantal in general, and solve the J-coupled multi-reference IM-SRG flow equations (4.89). For each value of the flow parameter s, the flow equations yield a normal-ordered Hamiltonian $\boldsymbol{H}(s)$. Thus, we generate a family of Hamiltonians in which multi-particle multi-hole excitations are successively decoupled from the reference state.

3. The IM-SRG-evolved Hamiltonians are used in NCSM calculations for a range of truncation parameters $N_{\max}$. These calculations provide ground- and excited-state energies, as well as the respective eigenvectors. The eigenvectors can be used to evaluate other observables that have been transformed consistently in an IM-SRG evolution.

For simplicity, we refer to this scheme as *in-medium no-core shell model* (IM-NCSM), because the key point is the use of an in-medium decoupled Hamiltonian in the NCSM. The IM-NCSM scheme has a number of important advantages over simple IM-SRG or NCSM calculations. The initial NCSM calculation can be performed for arbitrary open-shell systems and we can control the complexity of the reference state $|\Psi\rangle$ via the parameter $N_{\max}^{\text{ref}}$. The entire $N_{\max}^{\text{ref}}$ space is decoupled from the rest of the model space, and remaining couplings within that space, caused by the IM-SRG truncations, are handled by the subsequent NCSM diagonalization. The decoupling dramatically accelerates the convergence of the subsequent NCSM calculation, which will be demonstrated in the next section. Furthermore, we obtain ground- and excited-state wave functions that can be used for calculating observables. Since we have a continuous mapping between the initial and the decoupled Hamiltonian, we can probe and quantify the effects of the truncations of the IM-SRG flow equations by varying the flow parameter s.

Figure 6.1.: Schematic overview of the merging procedure of the IM-NCSM. We diagonalize the Hamiltonian in small model space in NCSM and the ground state basically defines the reference state which enters the evolution of the Hamiltonian and—if requested—other operators. This step serves as a pre-diagonalization in A-body space. Finally, we diagonalize the IM-SRG evolved Hamiltonian, obtain the eigenstates and then extract observables.

In the interest of clarity, we compare the IM-NCSM with the so-called valence-space IM-SRG [Str+16]. Both methods are two-stage approaches where an IM-SRG evolution is used to adapt the Hamiltonian for a subsequent diagonalization in a truncated space. Furthermore, they inherit advantages and problems from this second step, the valence-space shell model or no-core shell model, respectively. Therefore, the step from IM-SRG for valence-space interaction to IM-NCSM is of similar importance and impact as the step from the phenomenological shell model to the no-core shell model in the early 1990s.

More specifically, there are several unresolved problems in the valence-space IM-SRG, which by construction cannot occur in the IM-NCSM. For instance, the ground-state energies obtained in the initial IM-SRG for valence-space interaction applications show a systematic overbinding as the number of valence nucleons increases. This problem has been addressed recently though a heuristic modification of the density matrix entering the normal-ordering procedure [Str+17]. This modification is meant to circumvent a rigorous multi-determinantal reference state for the nucleus under consideration. In the IM-NCSM, we start with a multi-determinantal reference state from an NCSM calculation and perform a full multi-reference IM-SRG evolution in a strict *ab initio* sense. Furthermore, the valence-space IM-SRG has only been applied successfully to valence spaces covering a single major shell thus far. Attempts to extend the valence space to multiple shells have failed due to uncontrolled behavior in the IM-SRG evolution. Therefore, many interesting phenomena, e.g., the physics of intruder configurations, cannot be described in the valence-space IM-SRG at present. In addition, the presence of a core and the current issues with extending the valence space inhibits a systematic study of the model-space convergence that is mandatory for a stringent *ab initio* approach. The IM-NCSM is a no-core method using the total number of excitation quanta, $N_{\max}$, as the only model-space truncation parameter. The convergence of all observables with increasing $N_{\max}$ is investigated explicitly in each calculation, providing model-space uncertainty estimates for all results.

6.3. Decoupling of the Hamiltonian Matrix in Many-Body Basis

In order to gain an intuitive understanding of the IM-NCSM, let us consider the Hamiltonian matrix in a many-body basis (5.9), for instance one constructed for ^{12}C. In this section, we limit ourselves to natural parity eigenstates of the Hamiltonian in an $N_{\max} = 4$ model space, and total angular momentum projection of $M_J = 0$. Because of the parity conservation of the Hamiltonian, we need to include only configurations with even number of excitation quanta $N = 0, 2$ and 4. Hence, the many-body basis of this subspace, schematically shown in figure 6.2, sorted with respect to their number of excitation quanta is given by

$$\mathcal{B}^{(4)}_{\text{NCSM}} = \bigcup_{N\in(0,2,4)} \left(\bigcup_{i\in(0,1,\dots)} \left(|\Phi_i^{(N)}\rangle \right) \right) \tag{6.1}$$

$$= \Big(|\Phi_0^{(0)}\rangle, |\Phi_1^{(0)}\rangle, \dots, |\Phi_0^{(2)}\rangle, |\Phi_1^{(2)}\rangle, \dots, |\Phi_0^{(4)}\rangle, |\Phi_1^{(4)}\rangle, \dots \Big), \tag{6.2}$$

where the upper index of the basis states indicates the exact number of excitation quanta N with respect to the energetically lowest configurations, and the lower index enumerates them. The single-particle energy truncation is set to $e_{\max} = 12$. As mentioned before, this basis is orthonormal, i.e., $\langle \Phi_i^{(N)} | \Phi_j^{(N')} \rangle = \delta_j^i \delta_{N'}^N$. The number of natural parity configurations with total angular momentum projection $M_J = 0$ for ^{12}C with exactly zero, two and four excitation quanta is 51, 17 674 and 1 101 201, respectively. In general, the $N_{\max} = 0$ model space for open-shell nuclei is multidimensional, here 51 for ^{12}C, but one dimensional in closed-shell nuclei.

Since the $N_{\max} = 4$ model space is 1 118 926 (=51+17 674+1 101 201) dimensional, for a graphical illustration of the Hamiltonian matrix we have to restrict ourselves to those configurations with the strongest coupling to the $N = 0$ configurations. One possible way to

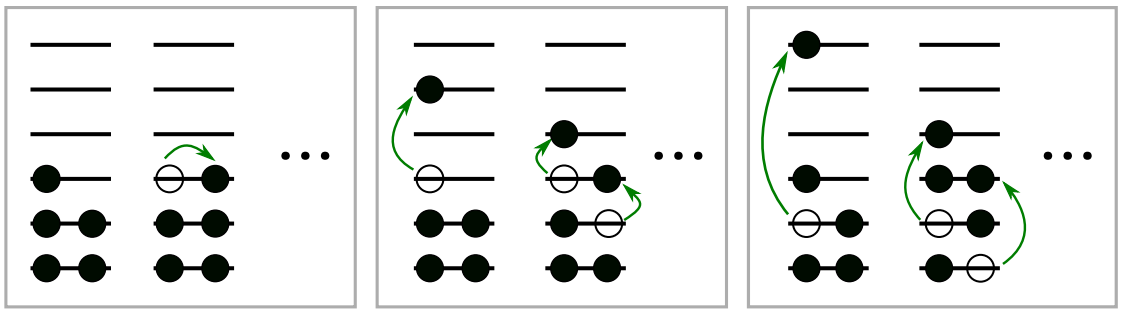

Figure 6.2.: Schematic illustration of the many-body basis $\mathcal{B}^{(4)}_{\text{NCSM}}$ containing up to four excitation quanta. Note that odd number of excitation quanta N are not necessary, if we are interested only in natural parity states of ^{12}C which is the case here.

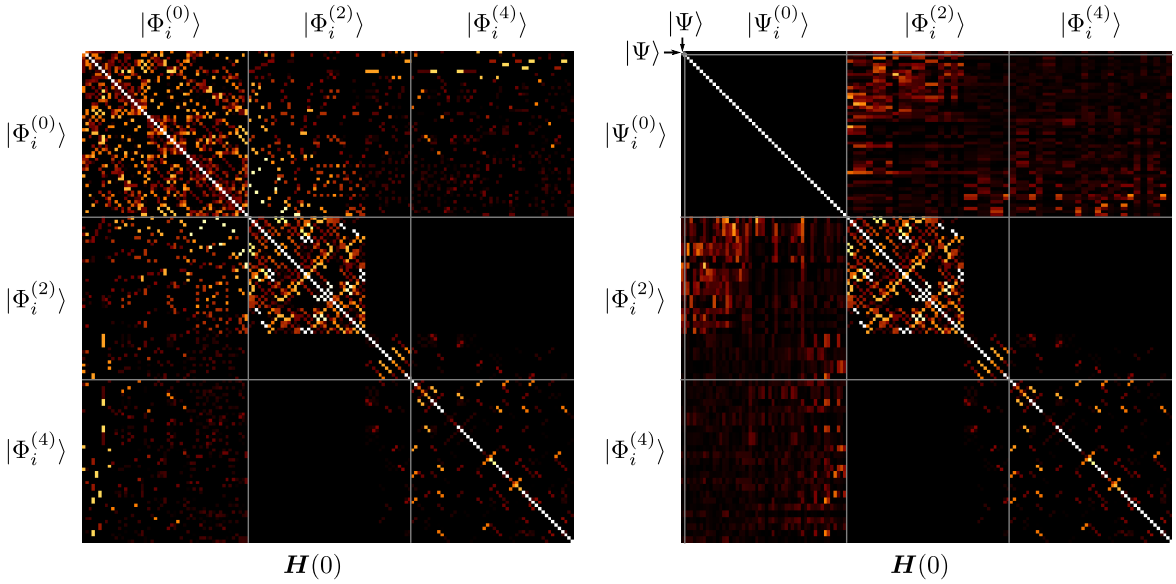

Figure 6.3.: Illustration of the initial Hamiltonian in the many-body basis containing exactly 0, 2 and 4 excitations quanta (left panel), and in a many-body basis where the $N = 0$ configurations, $|\Phi_i^{(0)}\rangle$, are replaced with the $N_{\max} = 0$ eigenstates, $|\Psi_i^{(0)}\rangle$, of the initial Hamiltonian (right panel), where the reference state is the first basis state $|\Psi\rangle = |\Psi_0^{(0)}\rangle$. We take all $N = 0$ configurations and those each fifty $N = 2$ and $N = 4$ configurations that have the largest coupling to the $N = 0$ configurations measured by (6.3). The absolute values are encoded in colors: the brighter the color the larger its value, where black indicates vanishing absolute value. Obviously, the $N_{\max} = 0$ block of the initial Hamiltonian is diagonal in the basis containing the $N_{\max} = 0$ eigenstates. The other blocks have been transformed as well.

quantify this coupling is

$$c_i^{(N)} := \sum_j |\langle \Phi_j^{(0)} | \boldsymbol{H} | \Phi_i^{(N)} \rangle|. \tag{6.3}$$

We take those fifty configurations with the largest value of $c_i^{(N)}$ for each $N > 0$. In the left panel of figure 6.3 we show the absolute value of the initial Hamiltonian matrix elements in this truncated many-body basis with up to four excitation quanta. The absolute values are encoded in colors: the brighter the color the larger its value, where black indicates vanishing absolute value.

In order to bring the reference state into the game, we replace the $N = 0$ configurations by $N_{\max} = 0$ eigenstates. For that purpose, we diagonalize the initial Hamiltonian in the $N_{\max} = 0$ model space, i.e.,

$$\boldsymbol{\Pi}^{(0)} \, \boldsymbol{H} \, \boldsymbol{\Pi}^{(0)} \, |\Psi_i^{(0)}\rangle = E_i^{(0)} \, |\Psi_i^{(0)}\rangle \, . \tag{6.4}$$

Here $\boldsymbol{\Pi}^{(0)}$ denotes the projection operator on the $N_{\max} = 0$ subspace, and $E_i^{(0)}$ is the eigen-

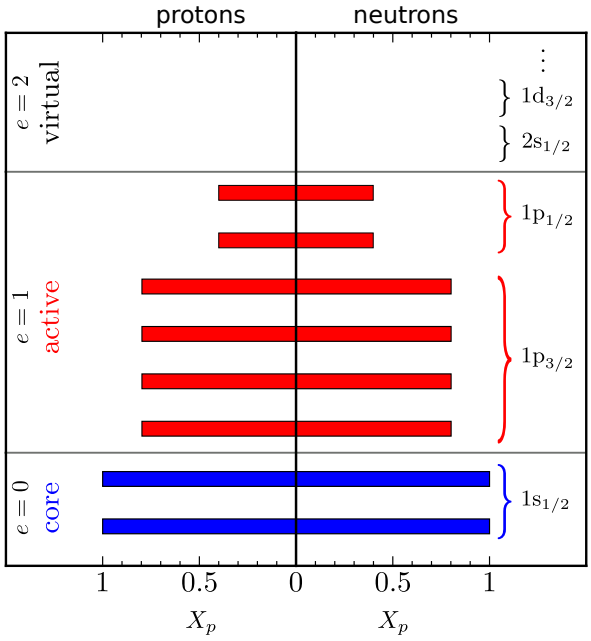

Figure 6.4.: We analyze the reference state for ^{12}C constructed in $N_{\max} = 0$ subspace to emphasize its multi-determinantal character. On the x-axis is depicted the quantity X_p from (6.7) for protons (left panel) and neutrons (right panel) separately. This quantity is exactly one and zero for core (blue) and virtual states, respectively, while it is something in between for active (red) ones. Since the p-shell is partially occupied, the reference state is indeed multi determinantal. We used the spectroscopic notation "$(\tilde{n}_p + 1)L_{j_p}$" where $\tilde{n}_p \in \{0, 1, \ldots\}$ is the radial quantum number, j_p the total-angular-momentum quantum number, and $L \in (s, p, d, \ldots)$ encodes the angular momentum quantum number $l_p \in (0, 1, 2, \ldots)$ of the state $|p\rangle$. On the left side is additionally depicted the energy quantum number $e_p = 2\tilde{n}_p + l_p$.

value associated to the eigenstate $|\Psi_i^{(0)}\rangle$ of the Hamiltonian in the $N_{\max} = 0$ subspace. Replacing the $N = 0$ configurations $|\Phi_i^{(0)}\rangle$ from above with these $N = 0$ eigenstates yields

$$\mathcal{B}'^{(4)}_{\text{NCSM}} := \left(|\Psi_0^{(0)}\rangle, |\Psi_1^{(0)}\rangle, \ldots, |\Phi_0^{(2)}\rangle, |\Phi_1^{(2)}\rangle, \ldots, |\Phi_0^{(4)}\rangle, |\Phi_1^{(4)}\rangle, \ldots \right) \tag{6.5}$$

which is still an orthonormal basis since Hermitian operators have an orthonormal eigenbasis.

The reference state $|\Psi\rangle$ for the IM-SRG evolution is chosen as the lowest eigenstate in the $N_{\max} = 0$ subspace with the appropriate quantum numbers; let us assume

$$|\Psi\rangle := |\Psi_0^{(0)}\rangle . \tag{6.6}$$

We emphasize once again that the reference state is a multi-determinantal state with this choice. To confirm this statement, we show in figure 6.4 the quantity

$$X_p := \sum_{\substack{i \\ (a_p | \Phi_i^{(0)}\rangle \neq 0)}} |\langle \Phi_i^{(0)} | \Psi \rangle|^2 \tag{6.7}$$

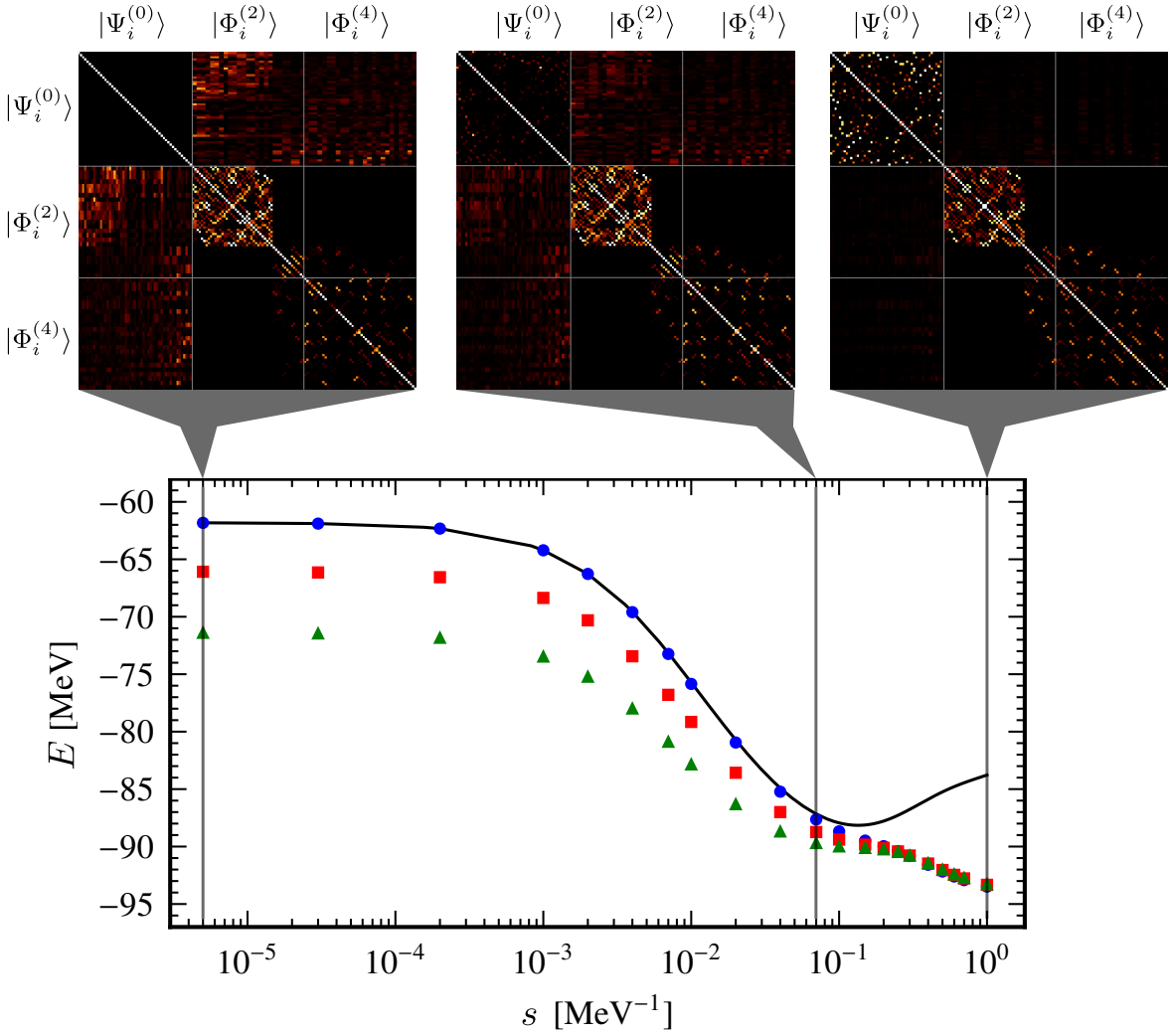

Figure 6.5.: The lower panel shows the zero-body part of the flowing Hamiltonian $E(s)$ (black solid line) and the lowest eigenvalue of $\boldsymbol{H}(s)$ obtained in IM-NCSM calculations in an $N_{\max}$=0 (●), 2 (■) and 4 (▲) model space. The upper panels show the flowing Hamiltonian in a truncated many-body basis for different values of s. All calculations use a Hartree-Fock basis with $e_{\max} = 12$ and $\hbar\Omega = 20\,\mathrm{MeV}$.

where the sum runs over all configurations in which the given single-particle state $|p\rangle$ is occupied. Obviously, this quantity is exactly one and zero for core and virtual states, respectively, while it is something in between for active ones. The multi-determinantal character of the reference state is manifested in partially occupied p-shell.

Not surprisingly, the Hamiltonian matrix represented in the basis (6.5) is diagonal in $N_{\max} = 0$ subspace, the other blocks need to be transformed as well. A representation of the initial Hamiltonian in this basis is given on the right panel of figure 6.3.

While performing the IM-SRG evolution, let us track some important characteristics of this matrix as a function of the flow parameter s on a logarithmic scale (see lower panel in figure 6.5). First, the expectation value of the evolved Hamiltonian with respect to the reference state $|\Psi\rangle$, which is identical to the zero-body part of the Hamiltonian in reference-

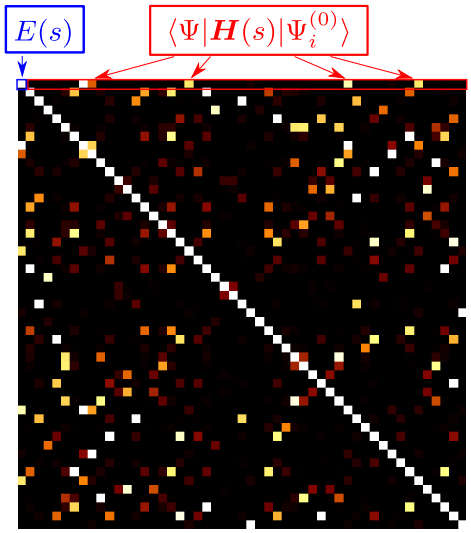

Figure 6.6.: Zoom into the $N_{\max} = 0$ block of the evolved Hamiltonian matrix to a specific value of the flow parameter $s = 1.0\,\mathrm{MeV}^{-1}$. The first line of the Hamiltonian matrix indicates those matrix elements that couple the reference state to other $N_{\max} = 0$ eigenstates.

state representation, i.e.,

$$E(s) = \langle\Psi|\boldsymbol{H}(s)|\Psi\rangle\,, \tag{6.8}$$

which is the first entry in the Hamiltonian matrix by construction. Second, the smallest eigenvalue in $N_{\max} = 0$ subspace, which coincides with $E(s)$ for small flow parameters since the reference state is already an eigenstate obtained in $N_{\max} = 0$ subspace according to (6.6). Third, the lowest eigenvalue obtained in the $N_{\max} = 2$ and 4 model spaces, spanned by states up to two and four excitation quanta, respectively.

Taking a closer look at matrix elements that couple the reference state to $N = 2$ and 4 configurations, we can clearly see that these matrix elements are suppressed and that strength is shifted into the $N_{\max} = 0$ subspace (see upper panels in figure 6.5). Hence, for sufficiently large flow-parameter values the lowest eigenvalue obtained in the $N_{\max} = 0$, 2 and 4 model spaces is practically the same. However, these quantities do not stabilize as a function of the flow parameter due to induced many-body contributions. Nevertheless, this is proof that IM-SRG successfully decouples the reference state from states with $N > 0$, here 2 and 4, i.e.,

$$\langle\Psi|\,\boldsymbol{H}(s)\,|\Phi_i^{(2)}\rangle \approx 0 \tag{6.9}$$

$$\langle\Psi|\,\boldsymbol{H}(s)\,|\Phi_i^{(4)}\rangle \approx 0 \tag{6.10}$$

for sufficiently large flow parameter s. Similarly, we observe that other eigenstates obtained in the $N_{\max} = 0$ subspace are also decoupled from states with $N > 0$, which we believe is a useful by-product of the IM-SRG(2) truncation.

Furthermore, we observe from figure 6.5 that the expectation value of the evolved Hamil-

tonian, $E(s)$, and the lowest $N_{\max} = 0$ eigenvalue differ from each other for large flow parameters. To investigate this issue, let us zoom into the $N_{\max} = 0$ subspace of the evolved Hamiltonian at $s = 1\,\mathrm{MeV}^{-1}$ (see figure 6.6). Keeping in mind that the reference state is the first basis state by construction, we can clearly see that several of the $N_{\max} = 0$ eigenstates of the initial Hamiltonian couple to the reference state. In other words, the initial reference state $|\Psi\rangle$ is not an eigenstate of the final Hamiltonian anymore. Therefore, $E(s)$ loses its interpretation as ground-state energy and we have to explicitly diagonalize $\boldsymbol{H}(s)$. The coupling of the reference state to other $N_{\max} = 0$ basis states is related to the IM-SRG(2) truncation that neglects the induced many-body contributions.

We remark that these coupling matrix elements should be suppressed in IM-SRG(A), i.e., $\langle\Psi|\,\boldsymbol{H}(s)\,|\Psi_j^{(0)}\rangle \overset{s\to\infty}{\longrightarrow} 0$ for $j \geq 1$. In this case, there is nice connection to the decoupling pattern depicted in figure 4.6 stating that the reference state has to be decoupled from the generalized n-particle n-hole states in order to have the reference state become an eigenstate of the final Hamiltonian. We know that the generalized n-particle n-hole states with $1 \leq n \leq A$ span the same subspace as the basis states from $\mathcal{B}'^{(N_{\max})}_{\mathrm{NCSM}} \backslash \{|\Psi\rangle\}$ in the limit that $N_{\max}$ goes to infinity (see figure 6.7). Therefore, we can express any generalized n-particle n-hole states with $1 \leq n \leq A$ as a linear combination of all states from $\mathcal{B}'^{(N_{\max})}_{\mathrm{NCSM}} \backslash \{|\Psi\rangle\}$ in the above-mentioned limit, and vice versa. Consequently, the coupling matrix elements of the reference state to other basis states from $\mathcal{B}'^{(N_{\max})}_{\mathrm{NCSM}} \backslash \{|\Psi\rangle\}$ would be suppressed in the limit that $N_{\max}$ goes to infinity if and only if the conditions (4.232) are fulfilled.

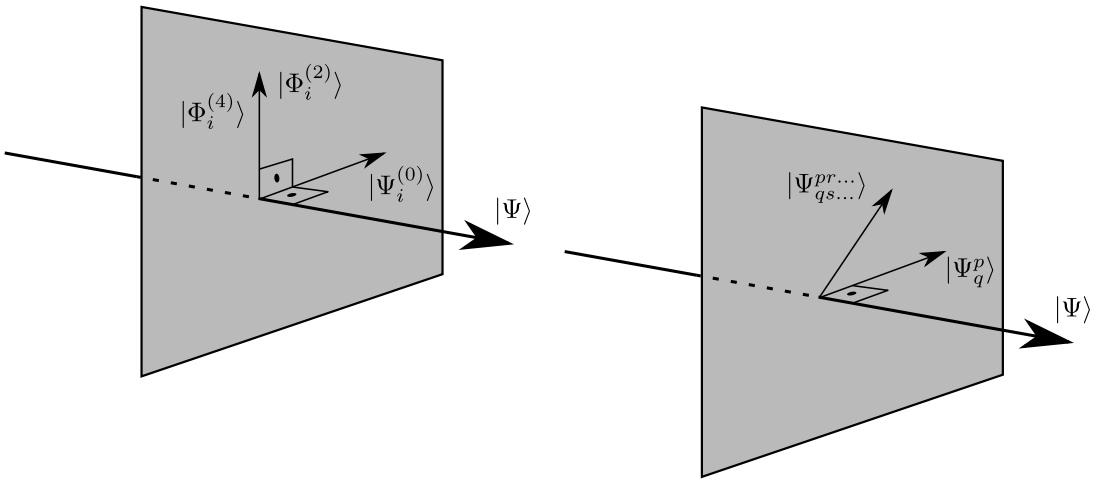

Figure 6.7.: We compare the many-body bases from (4.173) (right panel) and (6.1) (left panel) to make the connection to the schematic decoupling pattern of figure 4.6. See text for details.

III.

Results

Introduction to Part III

In this part, we present ground-state and excitation energies as well as radii and electric monopole transitions obtained within the framework of the in-medium no-core shell model (IM-NCSM) introduced in chapter 6.

We study the dependence of the IM-NCSM ground-state energies on several parameters in chapter 7, e.g., model-space truncations, oscillator frequency, choice of the generator and reference-space size. Afterward, we benchmark our results by comparing to other many-body methods like the NCSM. We also consider some selected magnesium and sodium isotopes.

In chapter 8, we investigate the IM-NCSM excitation energies of the carbon and oxygen isotopes. An interesting effect is found for the second 0^+ state in ^{12}C known to be a cluster state and called the Hoyle state. Moreover, we consider the excitation energies of the magnesium and sodium isotopes to address island-of-inversion physics.

We turn back our focus on the Hoyle state in ^{12}C and analyze radii and electric-monopole-transition properties to the ground state in chapter 9.

For reasons of efficiency, we use a J-coupled formulation of the multi-reference in-medium similarity renormalization group (IM-SRG) that requires a reference state with vanishing total angular momentum, our discussions up to now are limited to nuclei with even particle numbers. However, the theoretical framework is completely generic and a generalization to odd-mass nuclei is possible via an implementation of the IM-SRG for non-scalar tensor operators. We introduce the particle-attached particle-removed extension of the IM-NCSM and show results for some selected nitrogen isotopes in chapter 10.

Chapter 7

Ground-State Energy

In this chapter, we focus on the ground-state energies of several nuclei in the framework of the in-medium no-core shell model (IM-NCSM).

In section 7.1, we study the dependence of IM-NCSM ground-state energies on several parameters, like the model-space truncations, oscillator frequency, choice of the generators and the reference-space size. Furthermore, we benchmark our results throughout the even carbon and oxygen isotopic chain against exact results from the large-scale no-core shell model (NCSM) in section 7.2. We also compare the ground-state energies with results obtained in the multi-reference IM-SRG using spherical particle-number projected Hartree-Fock-Bogoliubov reference states [Her+13a]. Moreover, we study the island-of-inversion region in neutron-rich sodium and magnesium isotopes (see section 7.3).

All calculations in this work use the chiral nucleon-nucleon (NN) interaction at next-to-next-to-next-to-leading order by Entem and Machleidt with cutoff $\Lambda_{\mathrm{NN}} = 500\,\mathrm{MeV/c}$ [EM03] and local three-nucleon (3N) interaction at next-to-next-to-leading order with $\Lambda_{\mathrm{3N}} = 400\,\mathrm{MeV/c}$ [Nav07; Rot+14]. This interaction together with the kinetic-energy operator building the Hamiltonian are softened by a free-space similarity-renormalization-group (SRG) evolution at the three-body level to $\alpha = 0.08\,\mathrm{fm}^4$ [Rot+11; BFP07; JNF09; Rot+14; Heb12; Wen13]. Details on the SRG evolution and the treatment of the 3N contributions can be found in [Rot+14]. We truncate the initial three-body matrix elements in the total HO energy quantum number $E_{3\,\mathrm{max}} = 14$ in order to control the memory requirements [Rot+12; Her+13a; Her+13b; Bin+13; Bin+14]. This Hamiltonian has been used in numerous applications with great success [Her+13a; Bin+14]. However, it is known to significantly underestimate nuclear charge radii. This has remained a puzzle [Lap+16] and motivated researcher to develop new interactions, e.g., $\mathrm{N^2LO_{sat}}$ interaction [Eks+15].

7.1. Parameter Dependences

In order to extract the ground-state energy of a given nucleus in an *ab initio* manner, we have to explicitly demonstrate the convergence with respect to all model-space truncations. In the framework of the IM-NCSM, these are the single-particle energy truncation $e_{\max}$ and the largest allowed excitation quanta $N_{\max}$ serving as a truncation on a many-body level.

Furthermore, since both single-particle bases, HO and HF, depend intrinsically on the oscillator frequency $\hbar\Omega$, we have to demonstrate the robustness of the ground-state energy with respect to variation of this parameter.

Typically, we use a reference state for the multi-reference IM-SRG evolution obtained by diagonalizing the initial Hamiltonian in a feasible model space truncated with $N_{\max}^{\text{ref}}$. In section 7.1.4, we check if the results are independent of the choice of $N_{\max}^{\text{ref}}$.

Moreover, the multi-reference IM-SRG evolution can be performed using different generators. The specific choices determine the path on the manifold of the unitarily equivalent Hamiltonians to the initial one during the IM-SRG evolution, as shown graphically in figure 4.7. We analyze if the results are indeed independent of the choice of the generator as expected from theory (see section 7.1.3).

7.1.1. Model-Space Convergence

$N_{\max}$-Convergence during the IM-SRG Evolution

We start by investigating the model-space convergence of the lowest eigenvalue of the evolved Hamiltonian for selected open-shell nuclei. In figure 7.1, the ground-state energies of ^{12}C and ^{20}O obtained in IM-NCSM calculations using the HF basis are shown as a function of the flow parameter s for several values of $N_{\max}$ and a fixed value of the single-particle energy truncation $e_{\max} = 12$. Furthermore, we use the Imaginary-Time generator for the IM-SRG evolution. For comparison, we also show the zero-body piece of the flowing Hamiltonian, i.e., the expectation value $E(s) = \langle\Psi|\boldsymbol{H}(s)|\Psi\rangle$ that should converge against an eigenvalue of the Hamiltonian in standard applications of the IM-SRG in the limit of $s \to \infty$.

Let us consider the convergence with respect to the model-space truncation $N_{\max}$ of the subsequent NCSM calculations. For small flow parameters, we recover the results of a direct NCSM calculation with the initial normal-ordered Hamiltonian in HF basis. The ground-state energies exhibit extremely slow $N_{\max}$-convergence, which makes an extrapolation challenging. Since the energy quantum numbers (5.5) of the HF single-particle basis do not correspond to the HF single-particle energies, they are artificial. Thus, the $N_{\max}$-truncated model space, where these artificial energy quantum numbers enter, might not include the relevant many-body configurations.

We conclude that the $N_{\max}$-truncation, which has been motivated by the HO level scheme, is incompatible with the HF single-particle basis. However, increasing the flow parameter leads to extremely enhanced $N_{\max}$-convergence of the subsequent NCSM calculation. This even reaches a point where all model-space truncations, including $N_{\max} = 0$, yield the same

energy eigenvalue. In particular, this is the case for $s > 0.2\,\mathrm{MeV}^{-1}$ and $s > 0.15\,\mathrm{MeV}^{-1}$ for ^{12}C and ^{20}O, respectively. This is related to the fact that the IM-SRG decouples the reference state from all basis states at higher $N_{\max}$ (cf. figure 6.5).

Let us focus on the role of the expectation value $E(s)$ of the IM-SRG evolved Hamiltonian $\boldsymbol{H}(s)$ with respect to the reference state, which is the energetically lowest eigenstate obtained in $N_{\max}^{\mathrm{ref}} = 0$ model space at $s = 0\,\mathrm{MeV}^{-1}$. In the initial stages of the evolution, this quantity agrees with the lowest eigenvalue of the evolved Hamiltonian. This means that the reference state remains an eigenstate of $\boldsymbol{H}(s)$ in $N_{\max} = 0$ to a good approximation. However, in some cases, the lowest eigenvalue of the evolved Hamiltonian is below $E(s)$ in the later stages of the flow, i.e., the reference state is not an $N_{\max} = 0$ eigenstate anymore. This is not surprising since the IM-SRG transformation changes the structure of the $N_{\max} = 0$ block of the Hamiltonian such that the reference state still couples to other $N_{\max} = 0$ eigenstates, as already illustrated in figure 6.6. Therefore, $E(s)$ loses its interpretation as ground-state energy and we have to explicitly diagonalize $\boldsymbol{H}(s)$. The effect on the energies is much stronger for the ground-state energy of ^{12}C than for ^{20}O.

Let us consider the many-body contributions that are discarded due to the truncation of the IM-SRG flow equations at the normal-ordered two-body level. Their effect can be estimated by comparing to importance-truncated NCSM results in the HO basis that include explicit 3N interactions, i.e., without the NO2B approximation. For ^{20}O, we find a deviation of less than 2.3 MeV (2%), which is in line with previous multi-reference IM-SRG calculations [Her+13a]. For ^{12}C, which is a special case, the deviations are larger, slightly above 4%, and we observe a distinctive drop for $s > 0.3\,\mathrm{MeV}^{-1}$ after a plateau of stable and well-converged energies, signaling a systematic growth of induced many-body contributions. Note that the discrepancies in the energy include the discarded residual normal-ordered three-body contribution at the initial Hamiltonian as well as the neglected induced many-body contributions due to the IM-SRG(2) truncation that violates the unitarity of the evolution in the A-body system. Earlier studies have shown that the truncation of the initial Hamiltonian in NO2B approximation alone causes a deviation of approximately 1% [Rot+12; GCR16].

To extract the final ground-state energy in the framework of the IM-NCSM, we select a maximum flow parameter $s_{\max}$ within the plateau for which stable convergence is observed at sufficiently small $N_{\max}$. Additionally, we consider the energy much earlier in the evolution, i.e., at $s_{\max}/2$. The range from $s_{\max}/2$ to $s_{\max}$ in the IM-SRG flow (cf. figure 7.1) provides an uncertainty estimate for the energy at a given $N_{\max}$. If the evolution is stable and saturates, this uncertainty is very small. Only if the evolution fails to stabilize or the $N_{\max}$-convergence is incomplete, the uncertainty will be non-negligible. We will use this uncertainty quantification protocol for all observables.

We explicitly stress that the variational principle with respect to $N_{\max}$ applies at each value of the flow parameter s separately. But because of the IM-SRG(2) truncation that violates the unitarity in the A-body system, as aforementioned, we observe discrepancies between $N_{\max}$-converged results at different values of the flow parameters. Furthermore, we note that ^{20}O is representative for the majority of nuclei discussed here, while ^{12}C is the most

challenging case considered in this work.

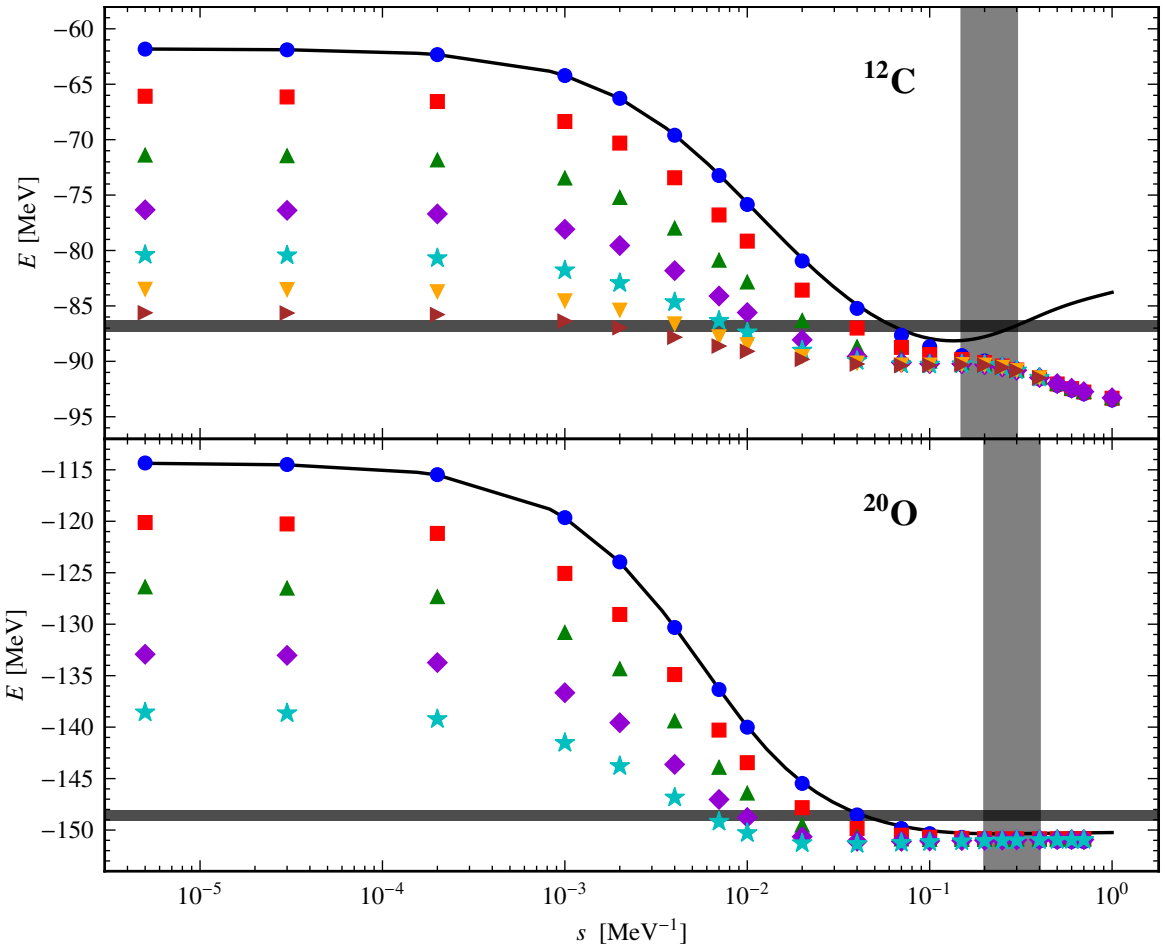

Figure 7.1.: We analyze the $N_{\max}$-convergence of the IM-NCSM ground-state energy in ^{12}C and ^{20}O as a function of the flow parameter s while fixing the single-particle energy truncation to $e_{\max} = 12$. The different symbols represent the ground-state energy obtained in various model spaces: $N_{\max}$=0 (●), 2 (■), 4 (▲), 6 (◆), 8 (★), 10 (▼) and 12 (►). The black solid line indicates the expectation value of the evolved Hamiltonian $\boldsymbol{H}(s)$ with respect to the reference state, $E(s)$. The horizontal gray line represents the $N_{\max}$-extrapolated ground-state energy using the importance-truncated NCSM with the explicit 3N interaction, i.e., without the NO2B approximation. The vertical gray band represents the range of flow parameters $s_{\max}/2$ to $s_{\max}$ for the quantification of uncertainties (see text). We use an HF basis and the Imaginary-Time generator. (published in [Geb+17])

Finally, we present the IM-NCSM ground-state energies in a slightly different way to emphasize the tremendous acceleration of the $N_{\max}$-convergence due to the IM-SRG evolution. In figure 7.2, the ground-state energies of ^{12}C and ^{20}O are shown as a function of the model-space size $N_{\max}$ for a set of values for the flow parameter s.

The $N_{\max}$-convergence is extremely slow for small values of the flow parameter s making an $N_{\max}$-extrapolation difficult, which is related to the incompatibility of an HF single-particle basis with the $N_{\max}$-truncation, as aforementioned. This problem does not occur in the HO basis, but the HO basis shows a disadvantageous behavior with respect to variation of the oscillator frequency, which will be analyzed in section 7.1.2. However, the $N_{\max}$-convergence is drastically enhanced with increasing value of the flow parameter, as already seen in figure 7.1.

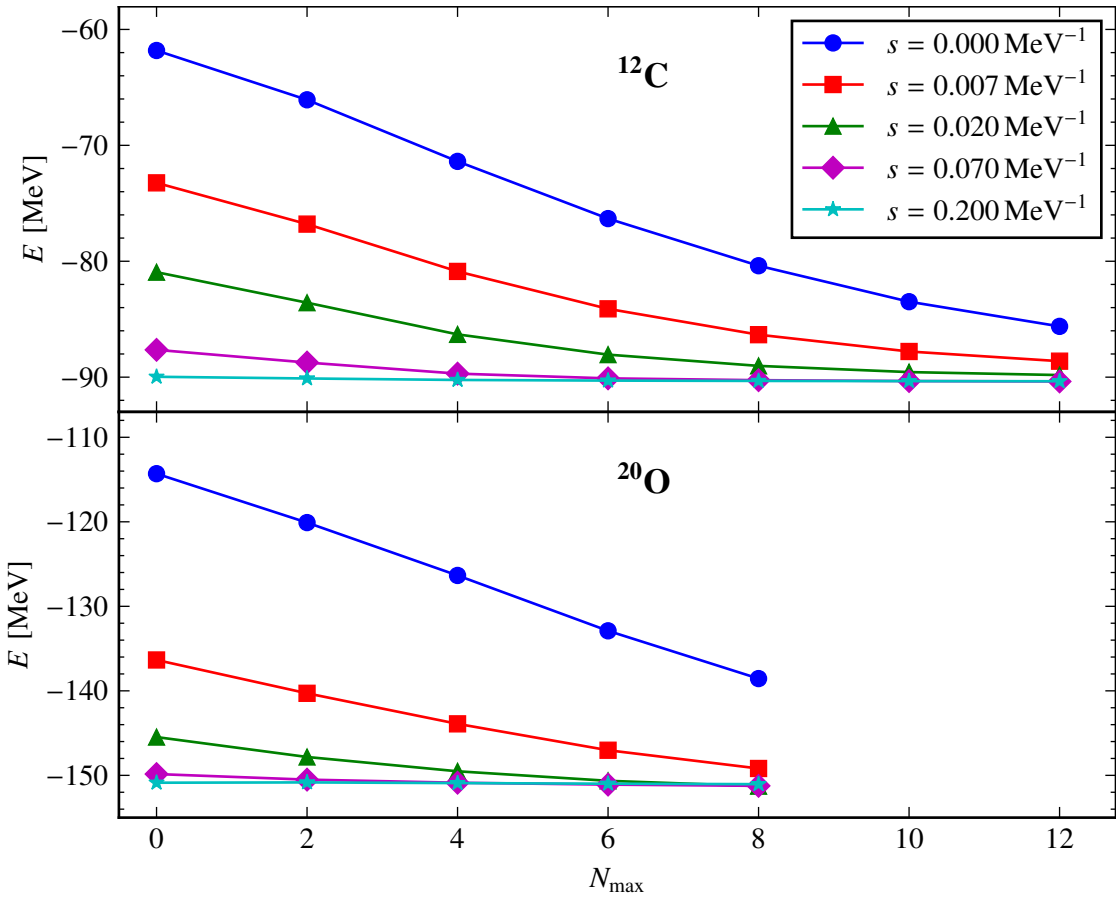

Figure 7.2.: We analyze the $N_{\max}$-convergence of the IM-NCSM ground-state energy for $e_{\max} = 12$ at different values of the flow parameter s. Increasing the flow parameter leads to enhanced $N_{\max}$-convergence. At $s = 0\,\mathrm{MeV}^{-1}$, the $N_{\max}$-convergence is extremely slow such that $N_{\max}$-extrapolation is difficult. In contrast to that, for $s = 0.2\,\mathrm{MeV}^{-1}$ all results including the one obtained in $N_{\max} = 0$ yield the same value. We use an HF basis and the Imaginary-Time generator.

$e_{\max}$-Convergence at different stages of the IM-SRG Evolution

So far, we have analyzed the $N_{\max}$-convergence at a fixed value of the single-particle energy truncation $e_{\max} = 12$. To extract ground-state energies in the sense of an *ab initio* calculation, we have to explicitly demonstrate the convergence with respect to the single-particle energy truncation $e_{\max}$ as well. For that purpose, we analyze the ground-state energy as a function of the single-particle energy truncation $e_{\max}$ for different values of the many-body truncation $N_{\max}$ at two different values of the flow parameter as shown in figure 7.3. We consider the $e_{\max}$-convergence for the ground-state energies of the initial input Hamiltonian corresponding to the flow parameter $s = 0\,\mathrm{MeV}^{-1}$ (left-hand panels). Additionally, we consider the IM-SRG evolved Hamiltonian for the flow parameter $s = 0.2\,\mathrm{MeV}^{-1}$ (right-hand panels). In this case, the IM-SRG evolution has already reached the decoupled regime, i.e., the reference state is sufficiently decoupled from the other basis states orthogonal to it.

We observe that the ground-state energy obtained in an $N_{\max} = 0$ model space is nearly independent of $e_{\max}$ for the initial Hamiltonian. This is a clear indication that the low-lying HF single-particle states relevant for the construction of the $N_{\max} = 0$ model space in ^{12}C, i.e., the lowest s- and p-shells for protons and neutrons, are converged. This leads to stable HF energy on a mean-field level of $-49.7408\,\mathrm{MeV}$, $-50.5058\,\mathrm{MeV}$ and $-50.9082\,\mathrm{MeV}$ for $e_{\max} = 4, 6$ and 12, respectively.

For the initial Hamiltonian, we observe that the ground-state energies systematically increase for fixed value of $N_{\max} > 0$ as a function of $e_{\max}$ signaling that higher-lying HO single-particle states still contribute to the low-lying HF single-particle states beyond the already converged lowest s- and p-orbitals. Based on this observation, we conclude that the many-body truncation $N_{\max}$ is not well suited for the many-body basis built of HF single-particle states, as discussed before.

However, there is no fundamental reason not to use the $N_{\max}$-truncation for a many-body basis composed of HF single-particle states as long as we can demonstrate the convergence with respect to all truncations, which is the case once we perform the IM-SRG evolution. In this case, we observe a perfectly monotonic convergence with respect to the single-particle energy truncation $e_{\max}$. The results for all $N_{\max}$ are identical for $e_{\max} \geq 10$, as already seen in figures 7.1 and 7.2 for $e_{\max} = 12$. We emphasize that this convergence is not related to the variational principle with respect to single-particle energy truncation $e_{\max}$, since the HF basis and, thus, the input Hamiltonian change for different single-particle energy truncations $e_{\max}$.

Based on this analysis, we conclude that $e_{\max} = 12$ is sufficient to extract converged ground-state energies of carbon and oxygen isotopes. Care should be taken when going to heavier systems, where $e_{\max} = 12$ might not be sufficient. In this case, the $e_{\max}$-convergence needs to be revisited.

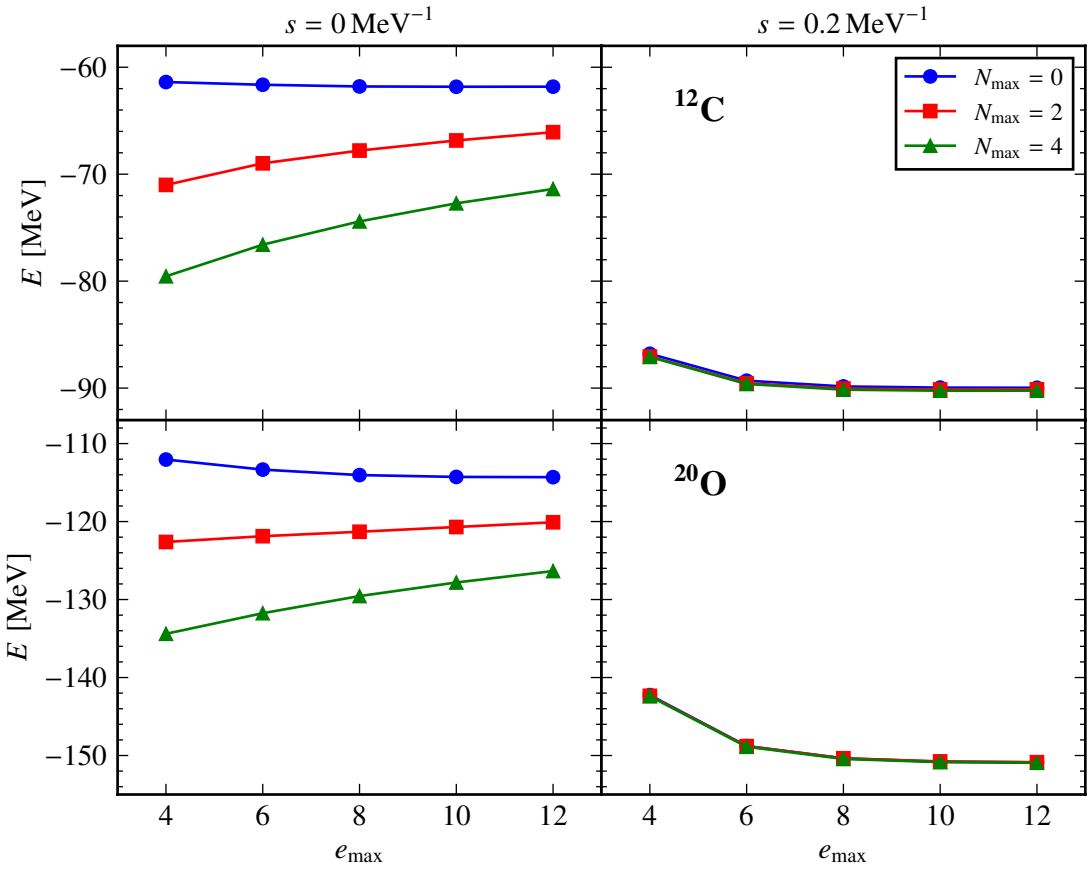

Figure 7.3.: We analyze the $e_{\max}$-convergence of the IM-NCSM ground-state energies of the initial Hamiltonian (left panel) obtained in different model spaces $N_{\max} = 0, 2, 4$. Additional, we consider the evolved Hamiltonian to a specific flow parameter $0.2\,\mathrm{MeV}^{-1}$ (right panel). The upper and lower panels correspond to ^{12}C and ^{20}O nuclei, respectively. We use an HF basis and the Imaginary-Time generator.

7.1.2. Oscillator Frequency

So far, we have applied an HF single-particle basis. To justify this choice, we analyze the ground-state energy of ^{12}C as a function of the oscillator frequency $\hbar\Omega$ for different model-space truncations $(e_{\max}, N_{\max})$ at three different stages of the IM-SRG evolution in HF and HO basis, which is depicted in figure 7.4.

The ground-state energies—and other observables—exhibit a dependence on the model-space truncations $(e_{\max}, N_{\max})$ and, in particular, the oscillator frequency $\hbar\Omega$, which is expected to vanish once complete model-space convergence is reached. In traditional NCSM calculations, which employ the HO basis without $e_{\max}$-truncation, we search for regions with the fastest $N_{\max}$-convergence and the smallest dependence on $\hbar\Omega$. For the ground-state energy in the range of the so-called optimal frequency, we observe a minimum as a function of the oscillator frequency $\hbar\Omega$ [Rot09; Bin+13]. However, we note that the optimal frequency range can vary for different observables and isotopes. An exact HF calculation would completely eliminate the $\hbar\Omega$-dependence, but due to the $e_{\max}$-truncation there is a residual dependence on the oscillator frequency, which is expected to be smaller than in HO case. Consequently, an HF basis has an enlarged region of optimal frequency as already seen in [Her+16].

HF Basis

Let us start with the investigations of the IM-NCSM results for ground state of ^{12}C using an HF basis shown in the upper panels of figure 7.4. At all stages of the IM-SRG evolution, the $\hbar\Omega$-dependence in $N_{\max} = 0$ is very weak for sufficiently large value of the single-particle energy truncation $e_{\max} \geq 6$. This is related to the converged low-lying single-particle states relevant for the construction of the $N_{\max} = 0$ model spaces. But the $\hbar\Omega$-variation in $N_{\max} = 2$ space—at the initial stage of the IM-SRG evolution—does not have a minimum in this $\hbar\Omega$ region. In the intermediate stage the ground-state energy is lowered for all parameters compared to the initial stage. Furthermore, $e_{\max}$-dependence becomes apparent in $N_{\max} = 0$ leading to a spreading of the ground-state energies. In the final stage of the IM-SRG evolution the ground-state energy is independent of the oscillator frequency $\hbar\Omega$ for sufficiently large value of single-particle energy truncation $e_{\max} \geq 8$ and all $N_{\max}$ as expected.

HO Basis

Let us turn our investigations to the $\hbar\Omega$-dependence using the HO basis shown in the lower panels of figure 7.4. In the initial stage, we observe that all $e_{\max}$ results for fixed $N_{\max}$ are identical since the $e_{\max}$-truncation is inactive in the HO basis in contrast to an HF basis. More importantly, there is a minimum at $\hbar\Omega = 20\,\text{MeV}$ for the ground-state energies obtained in all $N_{\max}$ model space. The ground-state energy in an $N_{\max} = 0$ model space in HO basis is above the one obtained when using the HF basis because an HF basis provides an optimized single-particle basis (see chapter 2 for more details). This is not true anymore for the ground-state energies obtained in an $N_{\max} = 2$ model space, which are lower in the HO case compared to HF. This is a consequence of the already mentioned incompatibility of the $N_{\max}$-truncation

with HF basis. In contrast to this, the $N_{\max}$-convergence for the HO basis is much better than for the HF case in the initial stage. In the intermediate stage, the minimum is still at $\hbar\Omega = 20\,\mathrm{MeV}$. Moreover, we observe that the $e_{\max}$-truncation, which was inactive in the initial stage, becomes apparent. This is because the IM-SRG evolution is different in each model space defined by $e_{\max}$ leading to ground-state energies obtained in $N_{\max}$ that depend on $e_{\max}$. In the final stage, the energy minimum at $\hbar\Omega = 20\,\mathrm{MeV}$ disappears in this $\hbar\Omega$ region. This indicates an incompatibility of the IM-SRG(2) truncation with the HO basis, in the sense that neglected many-body contribution have different signs depending on the oscillator frequency leading to the disappearance of the minimum. Therefore, we use an HF basis for further investigations.

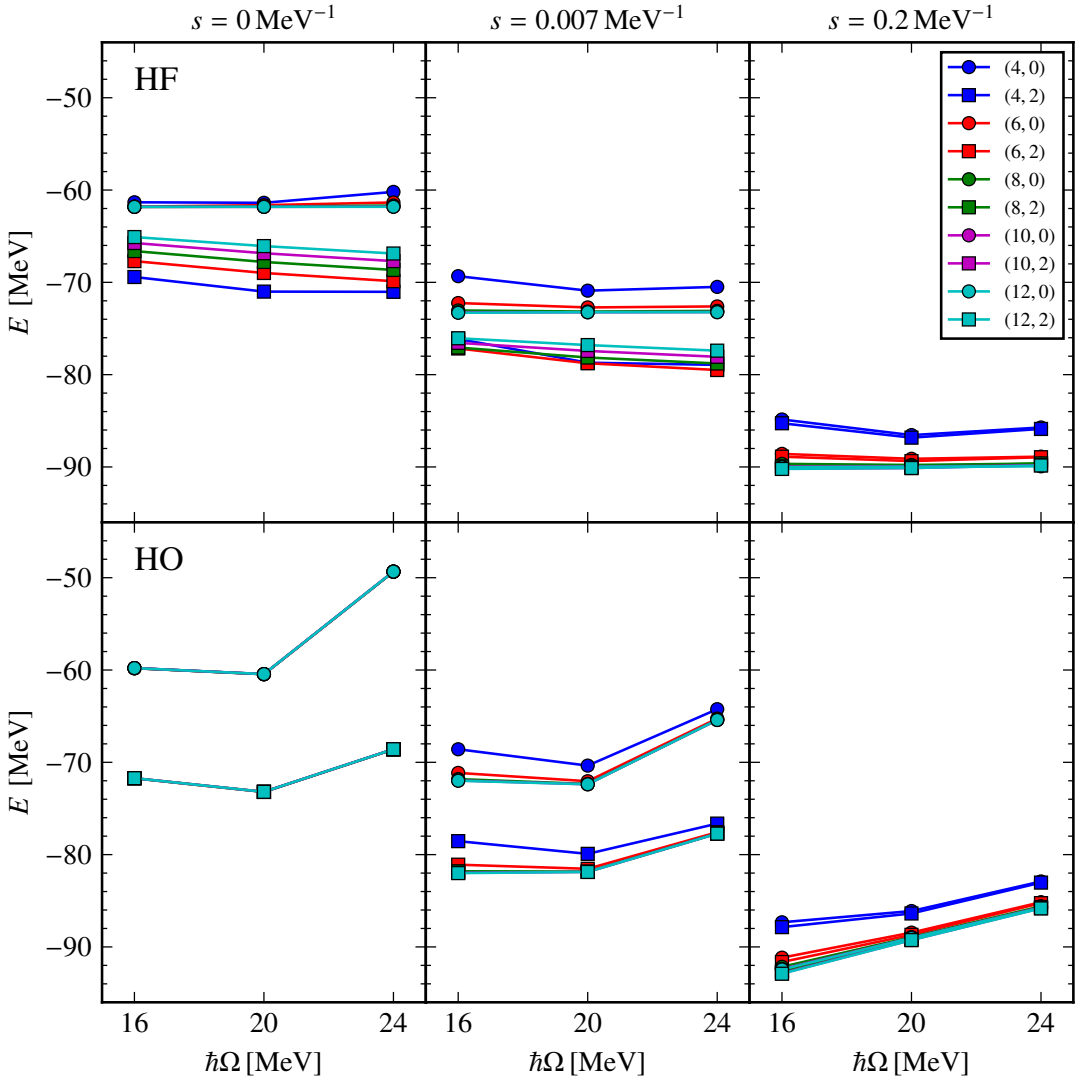

Figure 7.4.: We analyze the robustness of the IM-NCSM ground-state energy in ^{12}C with respect to variation of the oscillator frequency $\hbar\Omega$ for different model-space parameters $(e_{\max}, N_{\max})$ at three different stages of the IM-SRG evolution in HF (upper panels) and HO (lower panels) basis. We use the Imaginary-Time generator.

7.1.3. Impact of the Generators

We also analyze the impact of using different generators in the IM-SRG evolution on the ground-state energy. For this analysis, we fix the single-particle energy truncation to $e_{\max} = 6$ in order to reduce the computational cost, but the model space is sufficiently large to capture the main effects.

A many-body basis constructed from HF single-particle states in combination with the $N_{\max}$-truncation breaks translational invariance, i.e., the total wavefunction does not factorize into an intrinsic and center-of-mass (CM) part. To investigate this effect, we analyze the expectation value of the CM Hamiltonian (5.13), which measures the degree of CM contaminations [RGP09]. According to the Hellmann-Feyman theorem [Fey39], stating that the derivative of the expectation value of the Hamiltonian with respect to β is equal to the expectation value of the Hamiltonian derived with respect to β, i.e.,

$$\frac{\mathrm{d}}{\mathrm{d}\beta} \langle \Psi(\beta) | \boldsymbol{H}(\beta) | \Psi(\beta) \rangle = \langle \Psi(\beta) | \frac{\mathrm{d}}{\mathrm{d}\beta} \boldsymbol{H}(\beta) | \Psi(\beta) \rangle \,. \tag{7.1}$$

Here, the expectation value is understood with respect an eigenstate of the Hamiltonian, which implicitly depends on β. In our case, the derivative of the Hamiltonian (5.16) with respect to β is equal to the CM Hamiltonian. Since the expectation value of this Hamiltonian should be independent of β, states with small CM contaminations yield small expectation values.

The evolution of the CM Hamiltonian is shown in the four lower panels of figure 7.5 for ^{12}C. To analyze the generators in more detail, we show the zero-body part of the Hamiltonian $E(s)$ and the step size as well as the total number of steps of the ordinary-differential-equation (ODE) solver as a function of the flow parameter in figure 7.6 for ^{12}C. We use an explicit Runge-Kutta-Fehlberg (RKF45) algorithm with adaptive step-size control from the GNU Scientific Library [GSL17; Gou09], which is relevant to reduce the number of ODE steps and, thus, the computing time. Furthermore, the evolution of the CM Hamiltonian is shown in the four lower panels of figure 7.7 for ^{20}O.

The ground state in both nuclei, ^{12}C and ^{20}O, is experimentally found as well as predicted by our Hamiltonian to be a 0^+ state. The total angular momentum of the corresponding state in the framework of the IM-NCSM is calculated simply by taking the expectation value of the total-angular-momentum operator with respect to the eigenstates.

Analysis of ^{12}C

The four upper panels in figure 7.5 show the lowest eigenvalue of the evolved Hamiltonian obtained in $N_{\max} = 0, 2$ and 4 model spaces for ^{12}C and the expectation value of the IM-SRG evolved Hamiltonian with respect to the reference state $E(s)$. The ground-state energy converges against the same value within the plateau region of the energy flow for all generators except for the Brillouin one. The curve of the flow given by $E(s)$ varies for the different generators, and with it also the shape of the plateau. For the Brillouin generator, we can

hardly identify a plateau region. The largest plateau region can be seen for the Wegner generator, but it is difficult to compare the generators among each other since the units of the IM-SRG flow parameter s differ for each generator. For the Imaginary-Time and Brillouin generators it is MeV^{-1}. For the Wegner generator it is MeV^{-2} while for the White generator the flow parameter is dimensionless.

The Imaginary-Time and White generators show a similar behavior throughout the IM-SRG evolution, especially for flow parameters beyond the plateau region. This might be related to the fact that both generators have quite similar operator structure (see (4.237) for their definitions). For the Wegner generator, we observe a pronounced plateau region in the flow parameter, where the ground-state energy is perfectly converged with respect to $N_{\max}$. Going to larger flow parameters, the numerical instabilities grow rapidly, manifested in the abrupt drop in the ODE step size and large total number of ODE steps during the evolution. This leads to completely uncontrolled behavior where even the $N_{\max}$-convergence is no longer available.

Let us turn our focus to the four lower panels in figure 7.5 showing the expectation value of the consistently IM-SRG evolved CM Hamiltonian with respect to the eigenstate of the IM-SRG evolved Hamiltonian. The CM Hamiltonian is by construction a positive definite operator, i.e., the expectation value of this operator with respect to any normalized state is always positive. In the initial stage, this holds for all generators. However, the expectation value of the CM Hamiltonian becomes negative for large values of the flow parameter. This is due to the induced many-body contributions to the evolved CM Hamiltonian neglected during the IM-SRG evolution. These neglected contributions can have positive as well as negative sign.

However, the CM contaminations seem to be reduced with increasing $N_{\max}$ except in the flow-parameter region where the evolution is numerically unstable. This can be seen for the Wegner and Brillouin generators for very large values of the flow parameter.

The expectation value of the evolved CM Hamiltonian obtained for all generators is below 0.6 MeV, i.e., relatively small, in the well-behaved region of the IM-SRG evolution. We conclude that this quantity—in addition to the energies—can be taken as an indicator for the emergence of truncation artifacts in the IM-SRG evolution.

To analyze the performance of the generators in more detail, we analyze the following quantities as a function of the flow parameter depicted in figure 7.6 for ^{12}C:

- As a reference, we show again the IM-NCSM ground-state energies for different generators as well as the expectation value of the flowing Hamiltonian with respect to the reference state, $E(s)$, obtained in different model-spaces sizes $N_{\max}$.

- The second panel illustrates the squared norm of the one- and two-body part of the off-diagonal Hamiltonian for each generator defined as

$$\|f^{\mathrm{od}}\|^2 \coloneqq \mathrm{tr}\left(\underline{\underline{f}}^{\mathrm{od}} \cdot \underline{\underline{f}}^{\mathrm{od}\dagger}\right) = \sum_{\substack{p \\ q}} \left|\left(f^{\mathrm{od}}\right)_q^p\right|^2 \tag{7.2a}$$

$$\|\Gamma^{\mathrm{od}}\|^2 \coloneqq \mathrm{tr}\left(\underline{\underline{\Gamma^{\mathrm{od}}}} \cdot \underline{\underline{\Gamma^{\mathrm{od}\dagger}}}\right) = \sum_{\substack{pr \\ qs}} \left| \left(\Gamma^{\mathrm{od}}\right)^{pr}_{qs} \right|^2 \tag{7.2b}$$

where the definition of the matrices $\underline{\underline{f^{\mathrm{od}}}}$ and $\underline{\underline{\Gamma^{\mathrm{od}}}}$ can be found in (4.234).

- For each of the generators, the lower two panels show the step size of the ODE solver and the total number of evaluations of the commutator of the generator and the Hamiltonian, which corresponds to the right-hand side of the IM-SRG flow equation.

We remark that the latter quantities depend on several other parameters of the ODE solvers, which we do not discuss in detail here, since we are interested in a qualitative analysis.

For the Imaginary-Time and White generators, the squared norm of the two-body part of the off-diagonal Hamiltonian is suppressed by three orders of magnitude during to the IM-SRG evolution, and stabilizes below $10\,\mathrm{MeV}^2$. In contrast to that the one-body part remains nearly unchanged throughout the IM-SRG evolution. The Wegner generator is capable to suppress $\|f^{\mathrm{od}}\|^2$ and $\|\Gamma^{\mathrm{od}}\|^2$ slightly below $10\,\mathrm{MeV}^2$ and $10^2\,\mathrm{MeV}^2$, respectively. In untruncated IM-SRG(A), the off-diagonal matrix elements are supposed to converge against zero for these generators by construction. In practical calculations, this is not the case due to the IM-SRG(2) truncation and neglected higher-body densities in the definitions of the off-diagonal matrix elements (4.234), leading to incomplete generators. However, the remaining off-diagonal matrix elements, i.e., those not suppressed in the IM-SRG evolution, have negligibly low impact on the ground-state energies beyond $N_{\mathrm{max}} = 0$ space for sufficiently large flow parameters as depicted in the upper panel of figure 7.6. In other words, the remaining couplings matrix elements of the reference state to its excitations are treated through the subsequent NCSM diagonalization, yielding ground-state energies converged with respect to N_{max}, already in $N_{\mathrm{max}} = 0$, due to the IM-SRG evolution. This is a great success.

The Brillouin generator has to be considered differently regarding the suppression of the off-diagonal matrix elements. In contrast to the other generators, the Brillouin generator—even though we have not neglected irreducible three-body densities in the implementation (4.244)—is not directly constructed to suppress the off-diagonal matrix elements[1]. Hence, it not surprising that off-diagonal matrix elements cannot be suppressed, namely the squared norm of the two-body part $\|\Gamma^{\mathrm{od}}\|^2$ is even above $10^2\,\mathrm{MeV}^2$, while $\|f^{\mathrm{od}}\|^2$ stays almost constant. However, using the Brillouin generator—analogously to the other generators—we obtain converged ground-state energies. This is what really matters in practical calculations.

The step size h of the ODE solver changes during the IM-SRG evolution due to the adaptive character of the ODE solver. This quantity first increases and stabilizes during the IM-SRG evolution for Imaginary-Time and Brillouin generators. For the Wegner generator, we identify a kink in the step size h of the ODE solver at $s \geq 0.2\,\mathrm{MeV}^{-2}$ leading to decreased step sizes. This effect is much more significant for the Brillouin generator, where the step size drops down abruptly at $s \geq 0.7\,\mathrm{MeV}^{-1}$ and the number of ODE steps increases extremely at the

[1] There is the expectation value of the anticommutator that cannot be suppressed directly with the Brillouin generator. See section 4.6.4 for more details.

same time. These are clear signals that numerical instabilities affect the solutions.

However, the Brillouin generator does not destroy the $N_{\max}$-convergence contrary to the Wegner generator. Furthermore, the zero-body part of the evolved Hamiltonian, $E(s)$, throughout the IM-SRG evolution is identical to the ground-state energy obtained in the same model space as the reference state is constructed, i.e., $N_{\max} = N_{\max}^{\text{ref}} = 0$. This is a nice feature of the Brillouin generator, which might be related to its interpretation as the gradient of the energy with respect to the parameters of the unitary transformation at each step of the flow [Her+16]. Unfortunately, there is not a pronounced plateau region apparent since the eigenvalues obtained in an $N_{\max}$ model spaces fall creepingly with increasing flow parameter s.

Analysis of ^{20}O

In figure 7.7, we analyze the impact of the generators on the ground-state energy (upper panels) in ^{20}O and the expectation value of the consistently evolved CM Hamiltonian with respect to the eigenstates of the IM-SRG evolved Hamiltonian (lower panels).

The ground-state energy obtained with the Imaginary-Time, White and Brillouin generators are in perfect agreement within the plateau region.

As already seen in ^{12}C case, the expectation value of the Hamiltonian with respect to the reference state, $E(s)$, using the Brillouin generator is always identical to the ground-state energy of the IM-SRG evolved Hamiltonian. For the Imaginary-Time and White generators, we observe a small discrepancy of less than 1 MeV.

Contrary to the other generators, numerical instabilities appear in the IM-SRG evolution using the Wegner generator before $N_{\max}$-convergence can be reached. Again the expectation value of the CM Hamiltonian captures this uncontrolled behavior and blows up for $s \geq 2 \times 10^{-3}\,\text{MeV}^{-2}$.

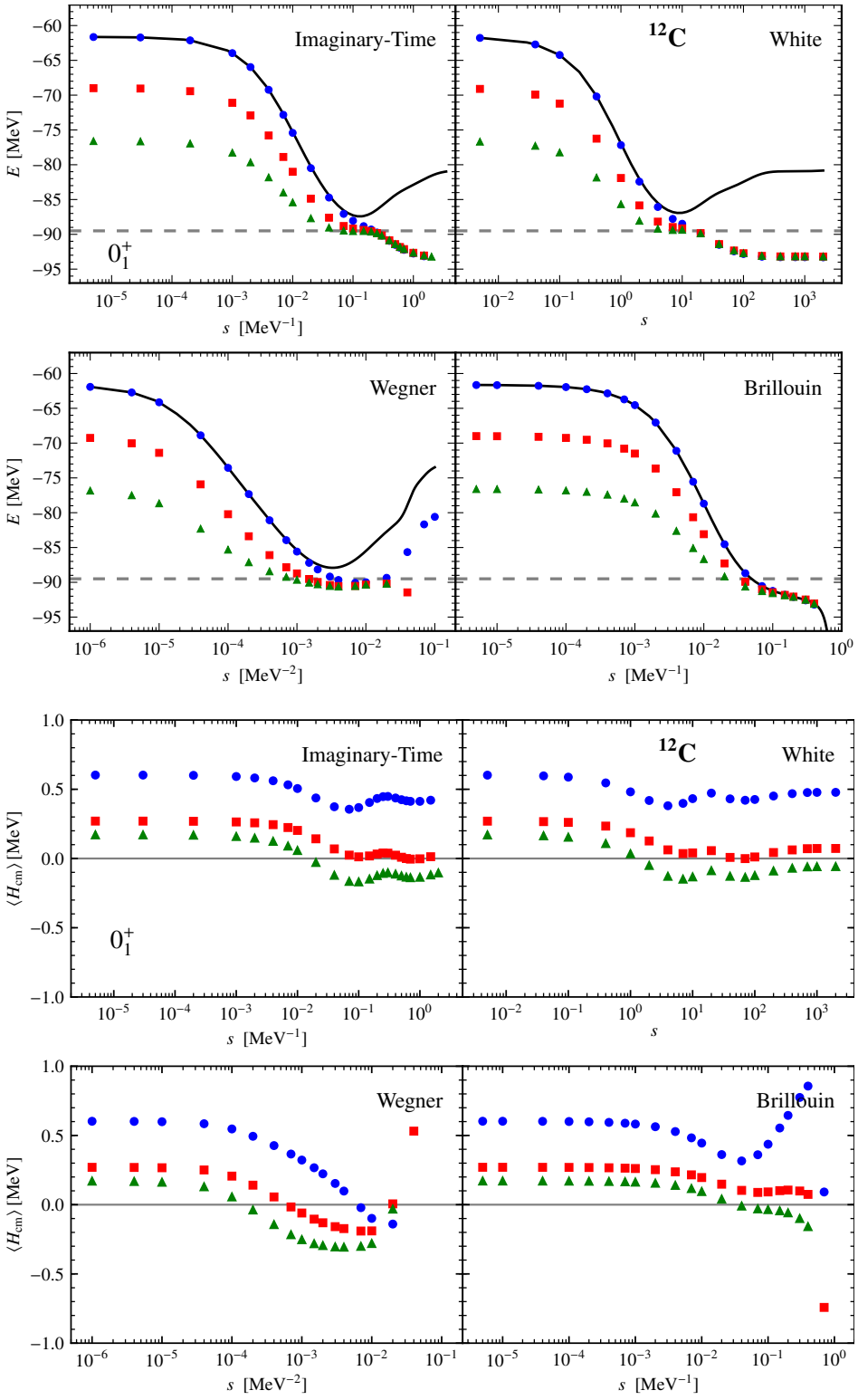

Figure 7.5.: We analyze the impact of the different generators on the IM-NCSM ground-state energies (upper four panels) and the expectation value of the CM Hamiltonian with respect to the eigenstate of the evolved Hamiltonian (lower four panels) for ^{12}C obtained in the model spaces $N_{\rm max}$=0 (●), 2 (■), 4 (▲). The horizontal dashed line indicates the converged energy obtained with the Imaginary-Time generator. We use an HF basis with $e_{\rm max} = 6$.

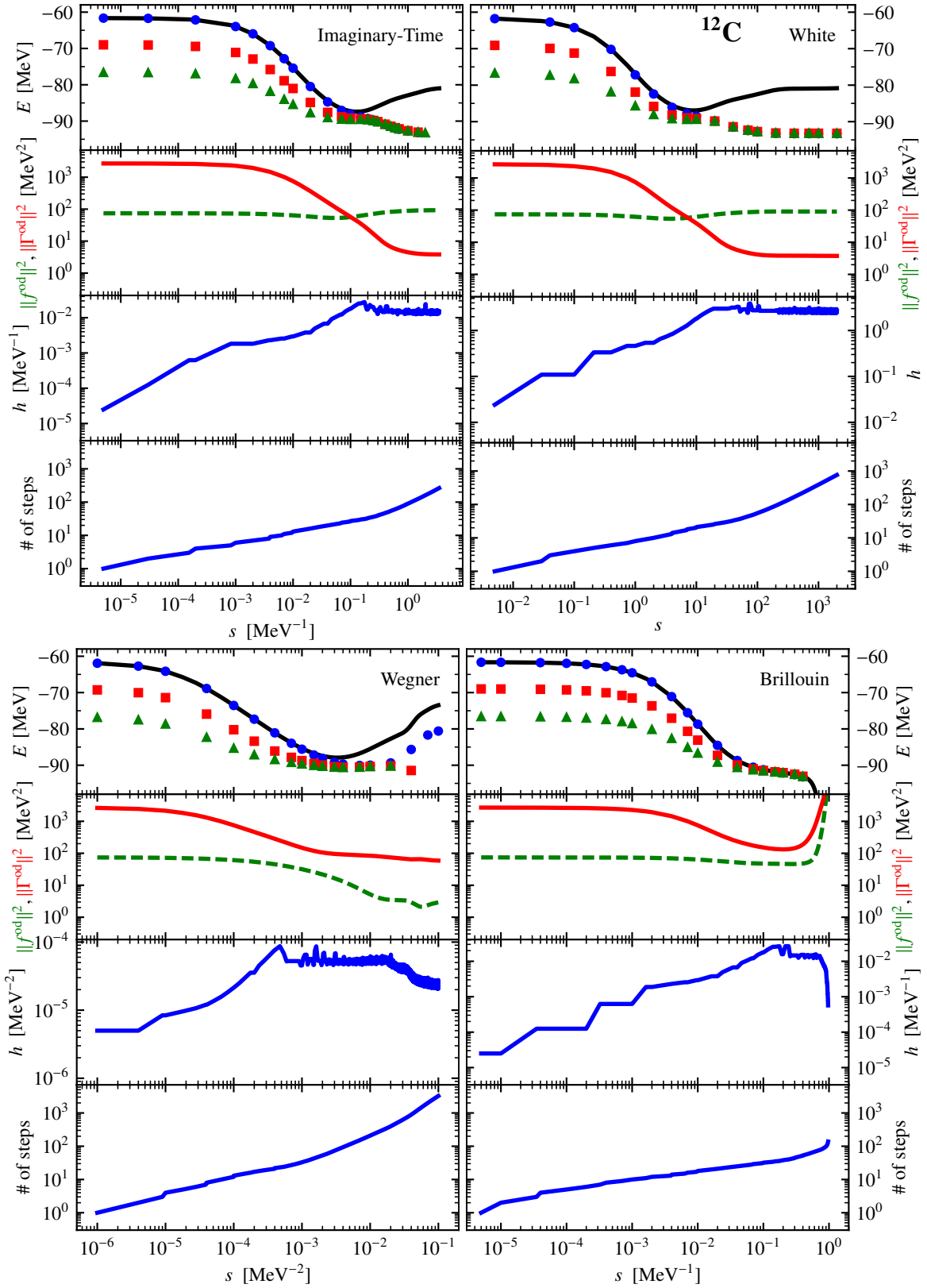

Figure 7.6.: Depicted are the ground-state energies (first panel) in $N_{\max}$=0 (●), 2 (■), 4 (▲) model spaces, squared norm of the one- (green dashed line) and two-body (red solid line) part of the off-diagonal Hamiltonian (7.2) (second panel), step size h (third panel) and the number of ODE steps (forth panel) for different generators.

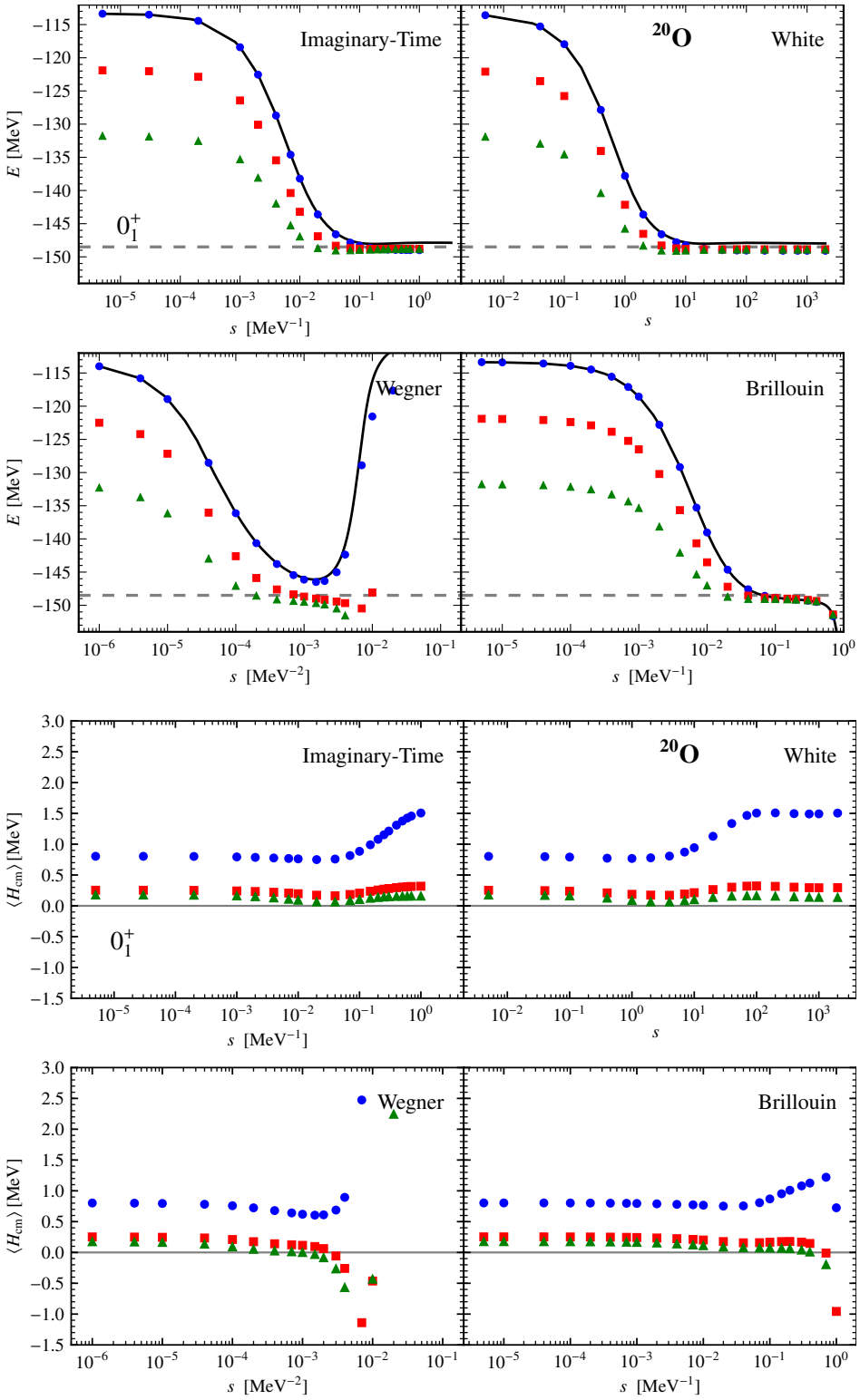

Figure 7.7.: We analyze the impact of the different generators on the IM-NCSM ground-state energies (upper four panels) and the expectation value of the CM Hamiltonian with respect to the eigenstate of the evolved Hamiltonian (lower four panels) in ^{20}O obtained in the model spaces $N_{\rm max}$=0 (●), 2 (■), 4 (▲). The horizontal dashed line indicates the converged energy obtained with the Imaginary-Time generator. We use an HF basis with $e_{\rm max} = 6$.

7.1.4. Reference-Space Size

We construct the reference state $|\Psi\rangle$, which enters the IM-SRG evolution, by diagonalizing the initial Hamiltonian within a small model space truncated with respect to the parameter $N_{\max}^{\mathrm{ref}}$, which we call the reference-space size. Up to now, we have chosen $N_{\max}^{\mathrm{ref}} = 0$ for the reference-space size. It is necessary to show that our results are independent of the parameter $N_{\max}^{\mathrm{ref}}$. For that purpose let us construct the reference state as the energetically lowest eigenstate of the initial Hamiltonian obtained in model spaces for different values of $N_{\max}^{\mathrm{ref}}$ and analyze the lowest eigenvalue of the IM-SRG evolved Hamiltonian in different model spaces $N_{\max} = 0, 2$ and 4. Furthermore, we depict the expectation value $E(s)$ of the IM-SRG evolved Hamiltonian with respect to the given reference state.

The results are shown in figure 7.8 using the Imaginary-Time generator for ^{12}C (upper panels) and ^{20}O (lower panels). In order to limit the computational cost, we set the single-particle energy truncation to $e_{\max} = 6$.

The main observation is that the ground-state energies obtained in different model spaces for $N_{\max} = 0, 2$ and 4 are extremely robust with respect to variation of the reference-space size $N_{\max}^{\mathrm{ref}}$.

We observe that the expectation value of the IM-SRG evolved Hamiltonian with respect to the reference state obtained in an $N_{\max}^{\mathrm{ref}}$ model space, $E(s)$, tracks the corresponding lowest eigenvalue obtained in $N_{\max}$ with the condition $N_{\max} = N_{\max}^{\mathrm{ref}}$. The reason is that the reference state is already an eigenstate of the initial Hamiltonian obtained in the same subspace where the subsequent diagonalization is performed. However, this statement holds up to a value for the flow parameter s where $E(s)$ and the corresponding lowest eigenvalue obtained in $N_{\max}^{\mathrm{ref}} = N_{\max}$ model space drift apart. The larger the reference-space size, the earlier this drifting in the IM-SRG evolution appears, e.g., for $N_{\max}^{\mathrm{ref}} = 0, 2$ and 4, the drifting starts for $s \geq 0.07\,\mathrm{MeV}^{-1}$, $0.04\,\mathrm{MeV}^{-1}$ and $0.02\,\mathrm{MeV}^{-1}$, respectively.

Note that increasing the reference-space size $N_{\max}^{\mathrm{ref}}$ leads to increased computational cost, such that we could not perform the calculation for ^{20}O using an $N_{\max}^{\mathrm{ref}} = 4$ reference state. The bottleneck was our J-coupled implementation of the multi-reference normal-ordered two-body approximation in HF basis. For instance, our code needed for $N_{\max}^{\mathrm{ref}} = 4$ reference state of ^{12}C using $e_{\max} = 6$ approximately two orders of magnitude more computing time compared to $N_{\max}^{\mathrm{ref}} = 0$ or 2. All calculations have been done on the same local computer architecture to guarantee comparability. Recently, we have parallelized our code using message passing interface, which decreases the computing wall time tremendously. However, all observations are in accordance with the ^{12}C case up to $N_{\max}^{\mathrm{ref}} = 2$. Hence, there is currently no necessity to perform the calculations for ^{20}O with $N_{\max}^{\mathrm{ref}} = 4$.

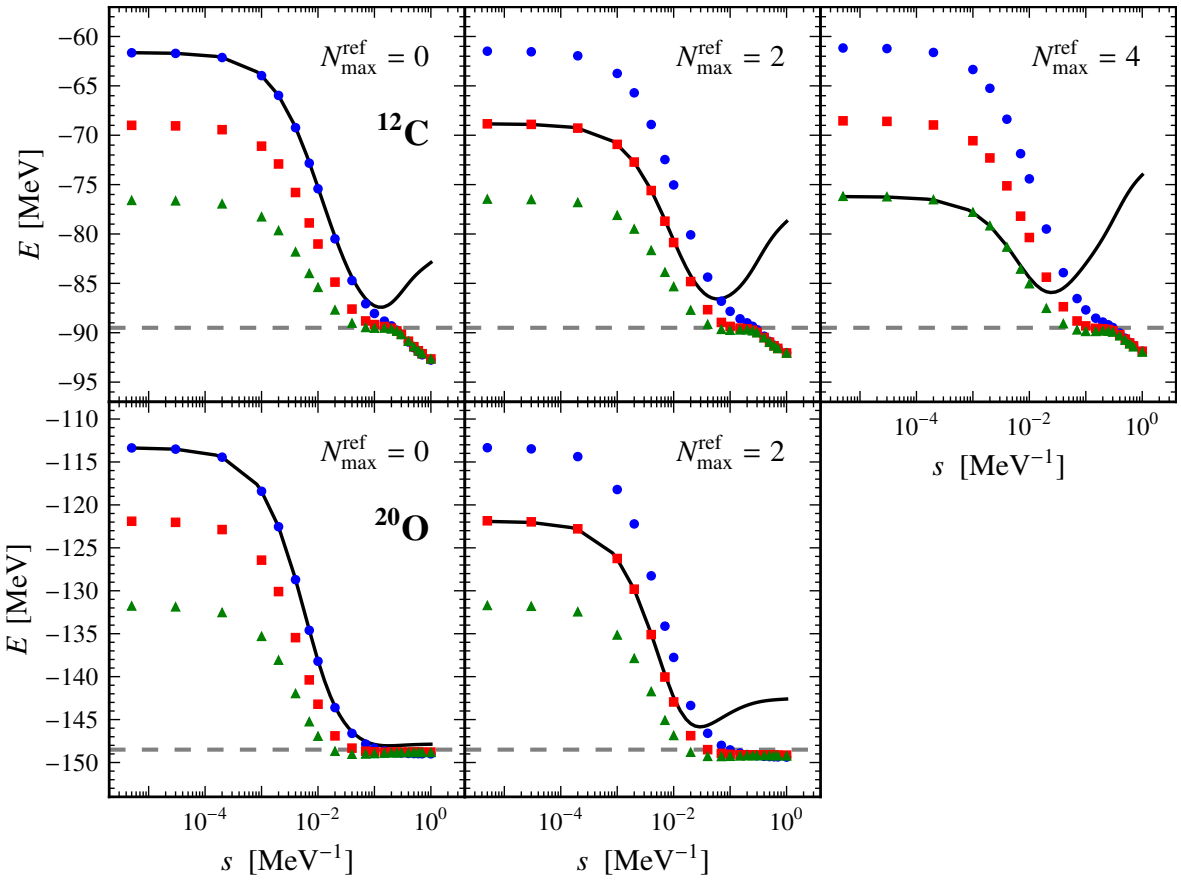

Figure 7.8.: We analyze the dependence of the IM-NCSM ground-state energy obtained in the model spaces N_{max}=0 (●), 2 (■), 4 (▲) for ^{12}C (upper panels) and ^{20}O (lower panels) on the reference-space size N_{max}^{ref} as a function of the flow parameter s using the Imaginary-Time generator. We use an HF basis with $e_{max} = 6$. The horizontal dashed line is shown to guide the eye.

7.2. Carbon and Oxygen Isotopes

In the previous section, we have studied in detail the dependence of IM-NCSM calculations on several parameters. In summary, we have found that the model-space sizes with $N_{max} = 4$ and $e_{max} = 12$ are sufficient to obtain converged ground-state energies for ^{12}C and ^{20}O nuclei. Furthermore, we conclude that an HF basis should be preferred to the HO basis, since it is robust with respect to variations of the oscillator frequency $\hbar\Omega$. Additionally, we have observed that the Imaginary-Time generator is the best compromise between robustness and efficiency, while the Wegner and Brillouin generators suffer from numerical instabilities.

With this in mind, we analyze the IM-NCSM ground-state energies of even carbon and oxygen isotopes using an HF single-particle basis with $\hbar\Omega = 20$ MeV and model-space truncation parameters $N_{max} = 4$ and $e_{max} = 12$. The results are summarized in figure 7.9 and compared to importance-truncated NCSM calculations up to $N_{max} = 12$ including all 3N contributions, i.e., without the use of the NO2B approximation. The latter use a simple exponential extrapolation with an uncertainty of up to 1 MeV for the most neutron-rich isotopes. We also show

multi-reference IM-SRG results obtained with spherical number-projected HF-Bogoliubov reference states [Her+13a].

Let us consider the carbon chain, where we observe relatively large deviations among the three methods. Here, the isotope ^{12}C appears as the most distinct case, where IM-NCSM and multi-reference IM-SRG with HF-Bogoliubov reference states already differ by roughly 6%. In contrast to that the methods agree perfectly for ^{14}C. Going to neutron rich systems, the relative deviation among the methods increases up to 5%. Also, the deviation to the experimental data increases. It is known that this Hamiltonian used in this work overbinds the ground-state energies for medium-mass nuclei. However, all many-body methods using the same input Hamiltonian underestimate the experimental ground-state energy.

In contrast to the carbon isotopes, the results for the oxygen isotopes of all three methods agree very well. The maximum deviations between IM-NCSM and NCSM is around 1.8% for the heaviest isotopes. Similar deviations have been observed with valence-space interactions obtained from the IM-SRG [Str+17]. All many-body methods correctly reproduce the neutron dripline at ^{24}O, i.e., oxygen isotopes with more than 16 neutrons are unstable with respect to neutron decay.

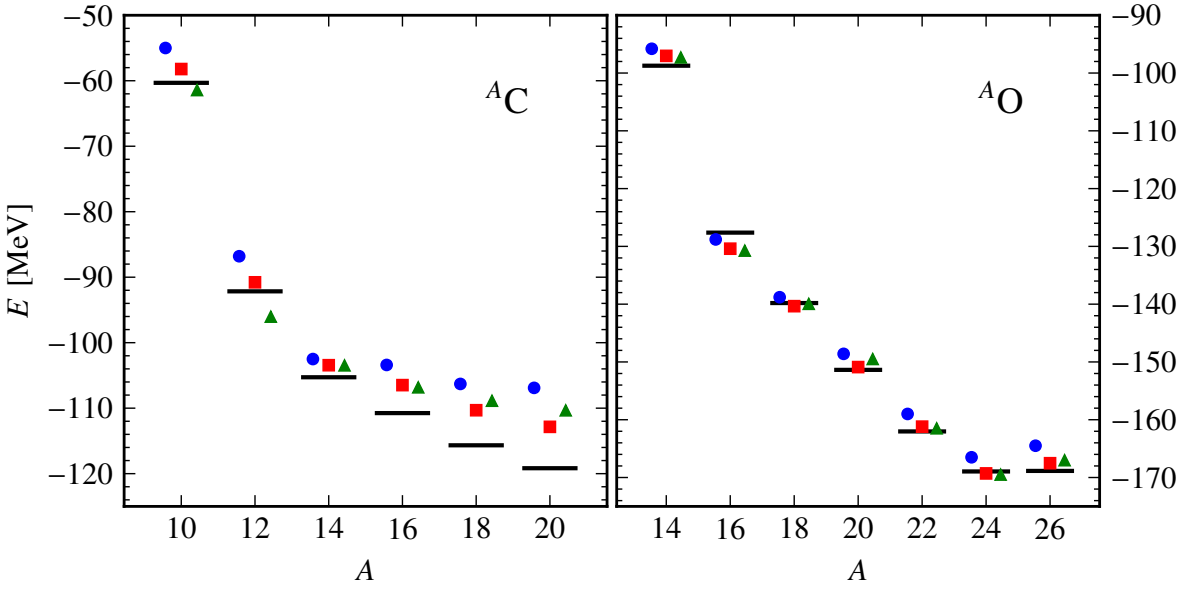

Figure 7.9.: Ground-state energies for even carbon and oxygen isotopes obtained from the IM-NCSM for $N_{\max} = 4$ and $e_{\max} = 12$ with $\hbar\Omega = 20\,\text{MeV}$ (■) in comparison to importance-truncated NCSM calculations with explicit 3N interactions (●) and the multi-reference IM-SRG with HF-Bogoliubov reference states (▲) [Her+13a]. Experimental values are indicated by black bars [KAE17]. The uncertainty for the IM-NCSM results due to flow-parameter dependence is negligible on this scale. (published in [Geb+17])

7.3. Magnesium and Sodium Isotopes

After benchmarking the IM-NCSM against the exact NCSM calculations and multi-reference IM-SRG using HF-Bogoliubov reference states, we can now access heavier systems, where exact diagonalizations are not available anymore. We consider some selected magnesium and sodium isotopes as a challenging case. Why these isotopes are of interest will become clear in section 8.3. We should keep in mind that the input Hamiltonian for heavier systems than oxygen overbinds with respect to experiment [Bin+14].

First, let us analyze the evolution of the IM-NCSM ground-state energies of ^{30,32}Mg shown in figure 7.10. The IM-SRG evolution is very robust and stabilizes for flow parameters between $0.2\,\mathrm{MeV}^{-1}$ and $0.4\,\mathrm{MeV}^{-1}$ for both nuclei. Our results overbind the experimental ground-state energies by $9\,\mathrm{MeV}(3.6\%)$ and $7\,\mathrm{MeV}(2.7\%)$ for ^{30}Mg and ^{32}Mg, respectively. Taking into account that the input Hamiltonian has been fixed to systems composed of up to three nucleons these are impressive results.

Let us focus our discussion on the sodium isotopes, where the situation is more complicated compared to all previous cases. The reason is that the experimental total-angular-momentum quantum numbers of the ground states are different from zero for ^{26,28,30}Na. Consequently, the reference state, which in our implementation of the IM-SRG evolution has to be a 0^+ state, is not the ground state of the nucleus under consideration.

In figure 7.11, we show the energetically *lowest* eigenvalue of the evolved Hamiltonian for ^{26,28,30}Na and the expectation value of the flowing Hamiltonian with respect to the reference state $E(s)$. For ^{26,28}Na, we can clearly observe that these two quantities, the lowest eigenvalue and $E(s)$, already differ in the initial stage of the IM-SRG evolution by about 2 MeV from each other. The reason is that the initial Hamiltonian does not produce a 0^+ ground state in $N_{\mathrm{max}}^{\mathrm{ref}} = 0$ for ^{26,28}Na, but our implementation of IM-SRG evolution requires a 0^+ reference state, as aforementioned (see chapters 4 and 6). Fortunately, we can find an excited 0^+ state in both cases, which we can use as a reference state. Hence, the lowest eigenvalue and $E(s)$ cannot be identical already at the beginning of the IM-SRG evolution. However, in all sodium isotopes we do not reproduce the ground state correctly (not shown in figure 7.11). We obtain 2^+ eigenstates for ^{26,28}Na and a 0^+ eigenstate for ^{30}Na, whereas the experimental values are 3^+, 1^+ and 2^+ for ^{26,28,30}Na, respectively. This issue will be revisited when discussing the excitation energies in section 8.3.

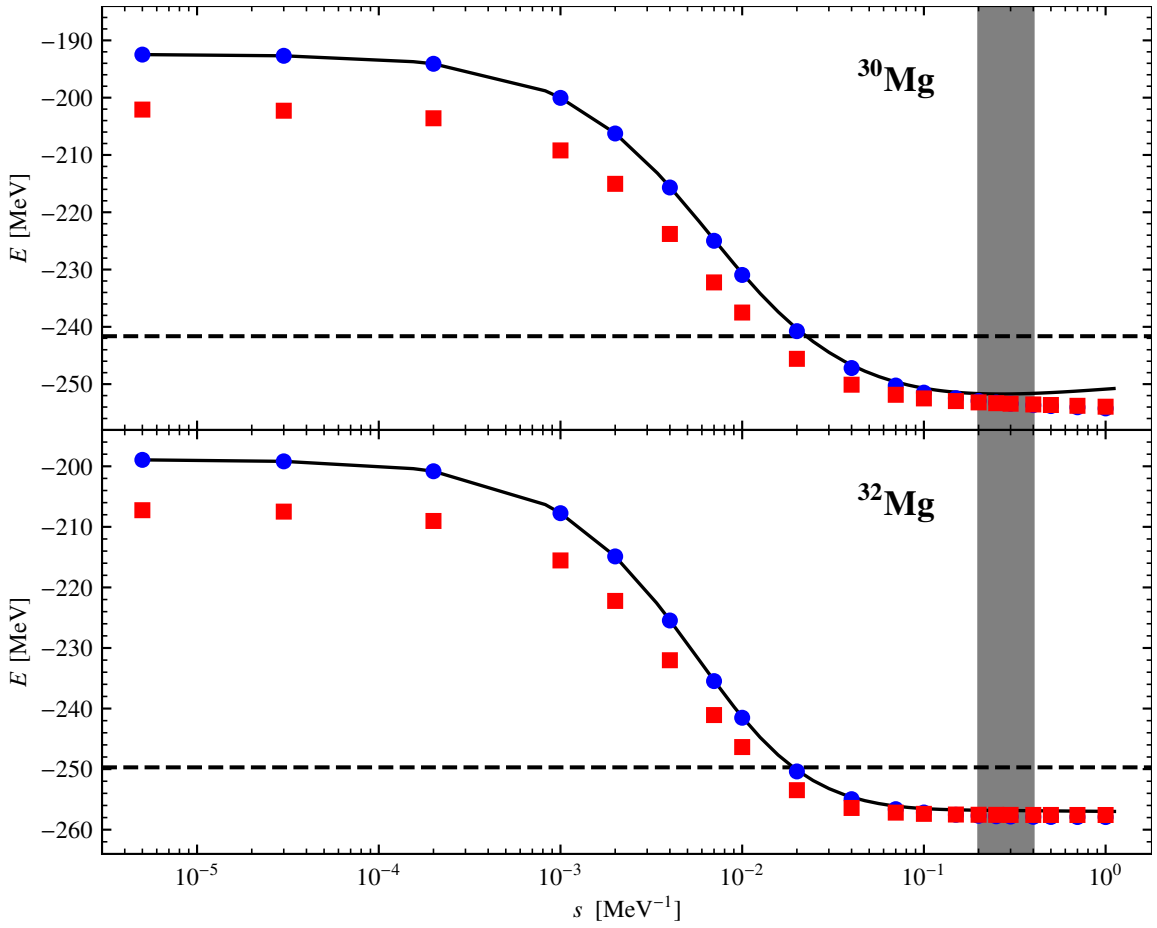

Figure 7.10.: We analyze the IM-NCSM ground-state energy of ^{30}Mg and ^{32}Mg as a function of the flow parameter s. The different symbols represent the ground-state energy obtained in various model spaces: $N_{\max}$=0 (●) and 2 (■). The black solid line indicates the expectation value of the evolved Hamiltonian $\boldsymbol{H}(s)$ with respect to the reference state, $E(s)$. The horizontal black dashed line illustrates the experiment ground-state energy. The vertical gray band represents the range of flow parameters $s_{\max}/2$ to $s_{\max}$ for the quantification of uncertainties as already discussed earlier. We use an HF basis with $e_{\max} = 12$.

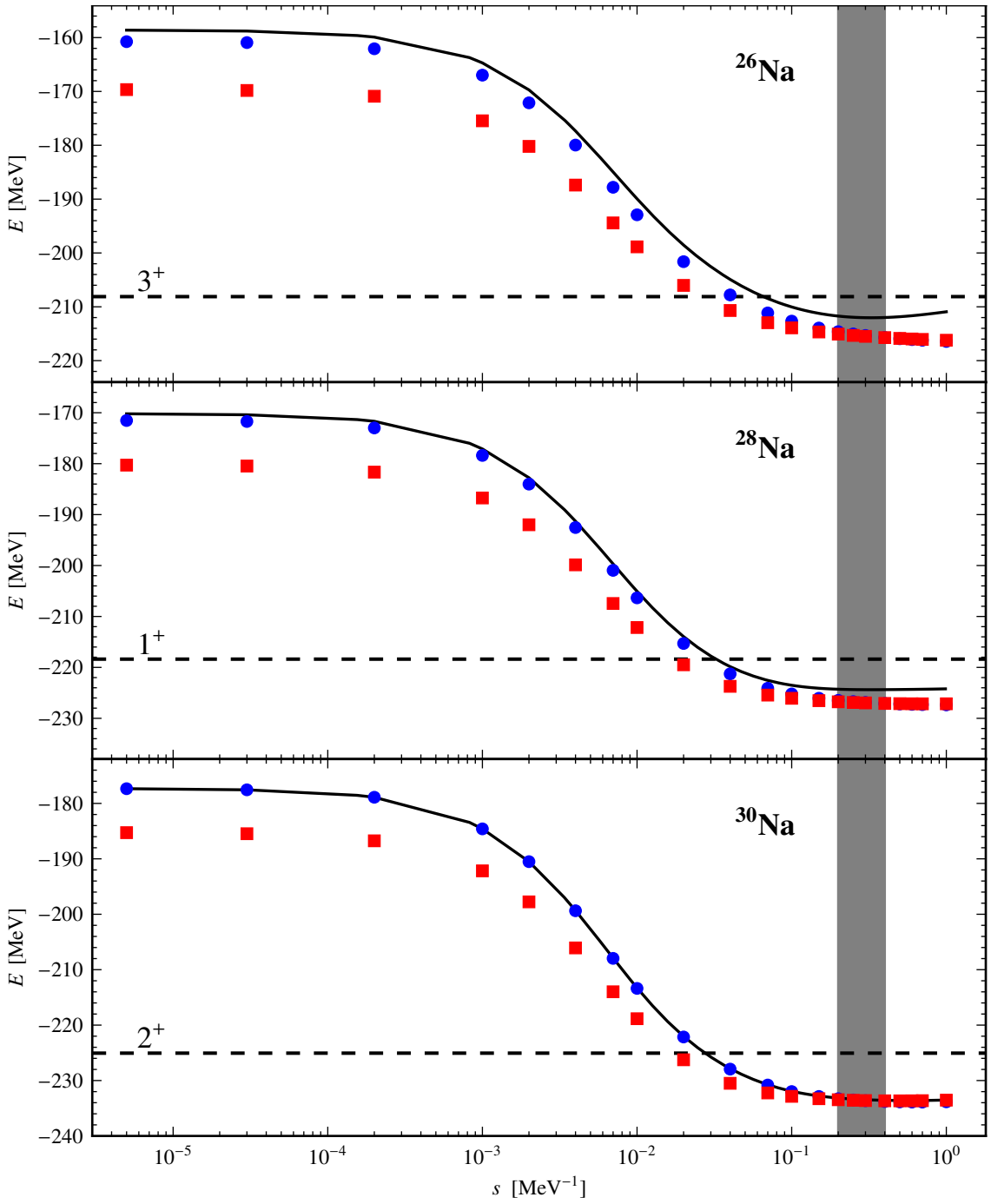

Figure 7.11.: Depicted is the energetically lowest eigenvalue of the IM-SRG evolved Hamiltonian for some selected sodium isotopes as a function of the flow parameter s. The different symbols represent the results obtained in various model spaces: $N_{\max}$=0 (●) and 2 (■). The black solid line indicates the expectation value of the evolved Hamiltonian $\boldsymbol{H}(s)$ with respect to the reference state, $E(s)$. The horizontal black dashed line illustrates the experiment ground-state energy. The vertical gray band represents the range of flow parameters $s_{\max}/2$ to $s_{\max}$ for the quantification of uncertainties as already discussed earlier. We use an HF basis with $e_{\max} = 12$.

Chapter 8

Excitation Spectra

So far, we have considered only ground-state energies, but the in-medium no-core shell-model (IM-NCSM) calculations produce excited states and excitation energies without need for additional calculations.

In this chapter, we first analyze the flow-parameter dependence and the $N_{\max}$-convergence of IM-NCSM excitation energies of ^{12}C and ^{20}O, and show as a benchmark typical excitation spectra for selected carbon and oxygen isotopes (see section 8.1). However, ^{12}C remains a very exciting case, where the second 0^+—the so-called Hoyle state [Bur+57], which is experimentally known to be a cluster state—shows very interesting behavior. We investigate this state in more detail in section 8.2. Finally, we explore the island-of-inversion physics for a few selected sodium and magnesium isotopes section 8.3.

8.1. Carbon and Oxygen Isotopes

In figure 8.1, the evolution of the excitation energies for the low-lying states of ^{12}C and ^{20}O are presented for different model-space truncations $N_{\max}$ and with a fixed, but sufficiently large, single-particle energy truncation $e_{\max} = 12$. In the subsequent NCSM calculation, we add the center-of-mass (CM) Hamiltonian (5.13), evolved consistently in the IM-SRG, to the intrinsic Hamiltonian in order to remove spurious CM excitations from the spectrum [GL74].

We observe that the rate of convergence of the excitation energies is not improved for most of the cases considered here. Moreover, the decoupling of the reference state from all excitations causes the excitation energies to converge monotonically from above for sufficiently large flow parameters. This is related to the fact that the variational principle with respect to $N_{\max}$ for a fixed given Hamiltonian always applies to absolute energies of all states. Once the ground-state energy is converged, excitation energies also become variational with respect to $N_{\max}$. This is not the case for the initial Hamiltonian in general.

The excitation energies in ^{20}O are almost independent of the flow parameter once we reach $N_{\max} = 4$, and show a perfect convergence in the same flow-parameter range as the ground-state energy indicated by the gray band in figure 7.1. The excitation energies in ^{12}C also

stabilize in the same range, but they start increasing as a consequence of the pronounced drop of the ground-state energy. The dependence of the excitation energies on the flow parameter is weak once we reach $N_{\max} = 4$—as long as we do not exceed $s_{\max}$ estimated from the evolution of the ground-state energy.

A remarkable exception is the first excited 0^+ state in ^{12}C, which falls from roughly 14 MeV to 8 MeV for flow parameters where the decoupling of the ground state happens. In contrast, the excitation energies of the other states remain relatively stable. This 0^+ state at 14 MeV is well known from standard NCSM calculations, and it cannot be converged in large-scale NCSM calculations [Mar+14]. Due to this extremely slow model-space convergence in standard NCSM calculations, it is believed to represent the Hoyle state, which has been proposed by Sir Fred Hoyle [Bur+57]. This state is crucial for the emergence of heavy elements in the universe, and is the resonance just above the triple-alpha threshold in ^{12}C.

Theoretical investigations made within the framework of fermionic molecular dynamics [Che+07; Nef12] and lattice effective field theories [Epe+11; Epe+12] successfully describe this state as a three-alpha cluster state. The latter one suffers from the artifacts of lattice spacing by the discretization of space and time.

However, in our calculations, the IM-SRG evolution seems to decouple multi-particle multi-hole excitations—needed to describe the Hoyle state—from the reference space, such that the $N_{\max} = 0$ result is already closer to experiment than the largest possible conventional NCSM calculations. Further investigations of this state are presented in section 8.2. We have also evaluated other signatures of the first excited 0^+ state, e.g., mass and charge radii as well as the electric monopole transition matrix element to the ground state discussed in chapter 9.

In figure 8.2, we study the excitation spectra of selected carbon and oxygen nuclei including their $N_{\max}$-convergence obtained in IM-NCSM and large-scale NCSM calculations. The bands in the IM-NCSM results from the uncertainty estimate determined in the range $s_{\max}/2$ to $s_{\max}$, where $s_{\max}$ is taken from the evolution of the ground-state energies. Both methods agree perfectly for the excitation energies of states that are robust and well converged. This shows that impact of all truncations on this quantity is small. As for ^{12}C, we find an excited 0^+ state in the IM-NCSM for ^{16}C which lies at higher energy in the conventional NCSM. Some higher lying states, however, show a slower $N_{\max}$-convergence indicating an intrinsic structure that probes pieces of the Hamiltonian that are not completely decoupled. This might be an interesting aspect for further optimizations of the IM-SRG generators.

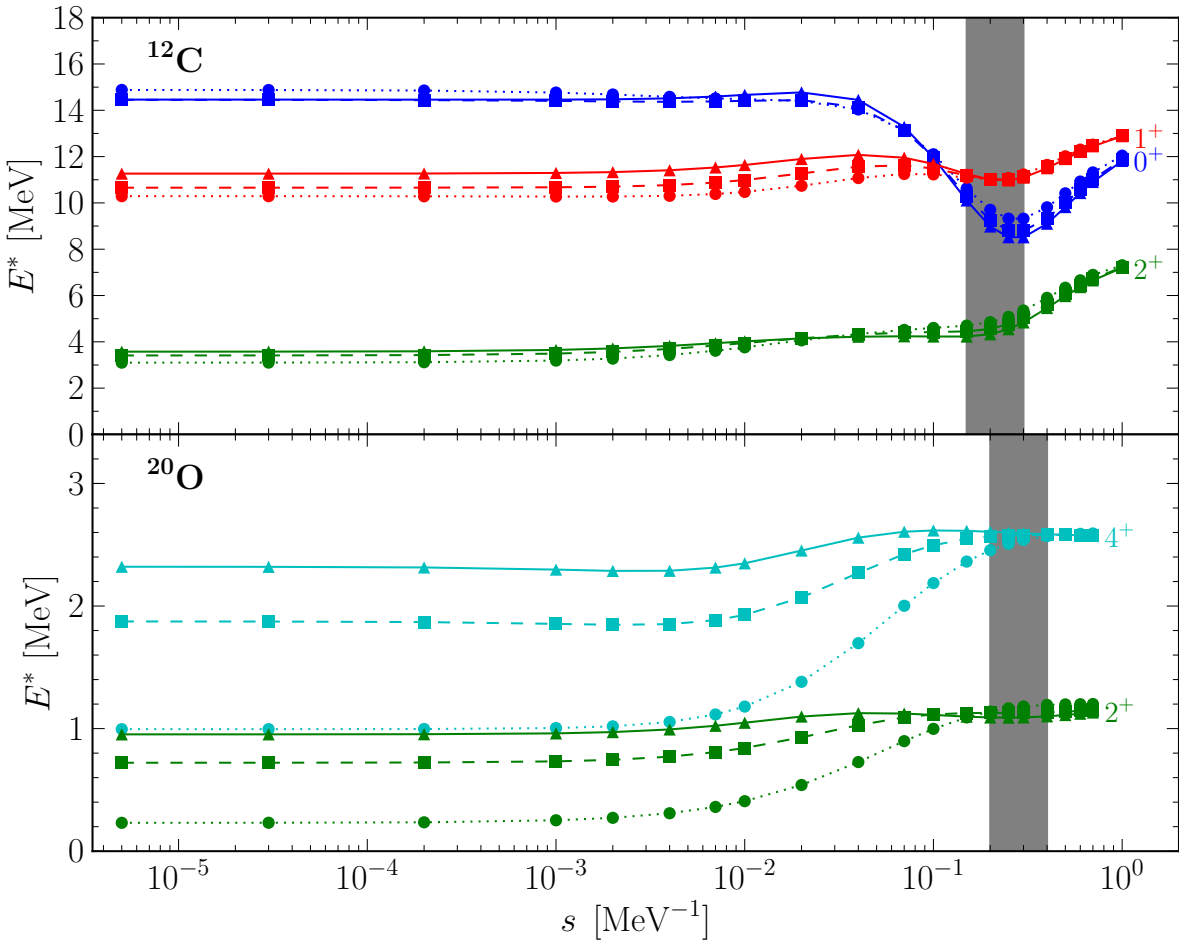

Figure 8.1.: Evolution of the excitation energies in ^{12}C and ^{20}O. Depicted are the low-lying eigenvalues of $\boldsymbol{H}(s)$ obtained in IM-NCSM calculations for $N_{\max} = 0$ (●, dotted line), 2 (■, dashed line), 4 (▲, solid line). All calculations use an HF basis with $e_{\max} = 12$ and $\hbar\Omega = 20\,\mathrm{MeV}$. The gray band represents the range of flow parameters for the uncertainty analysis. (published in [Geb+17])

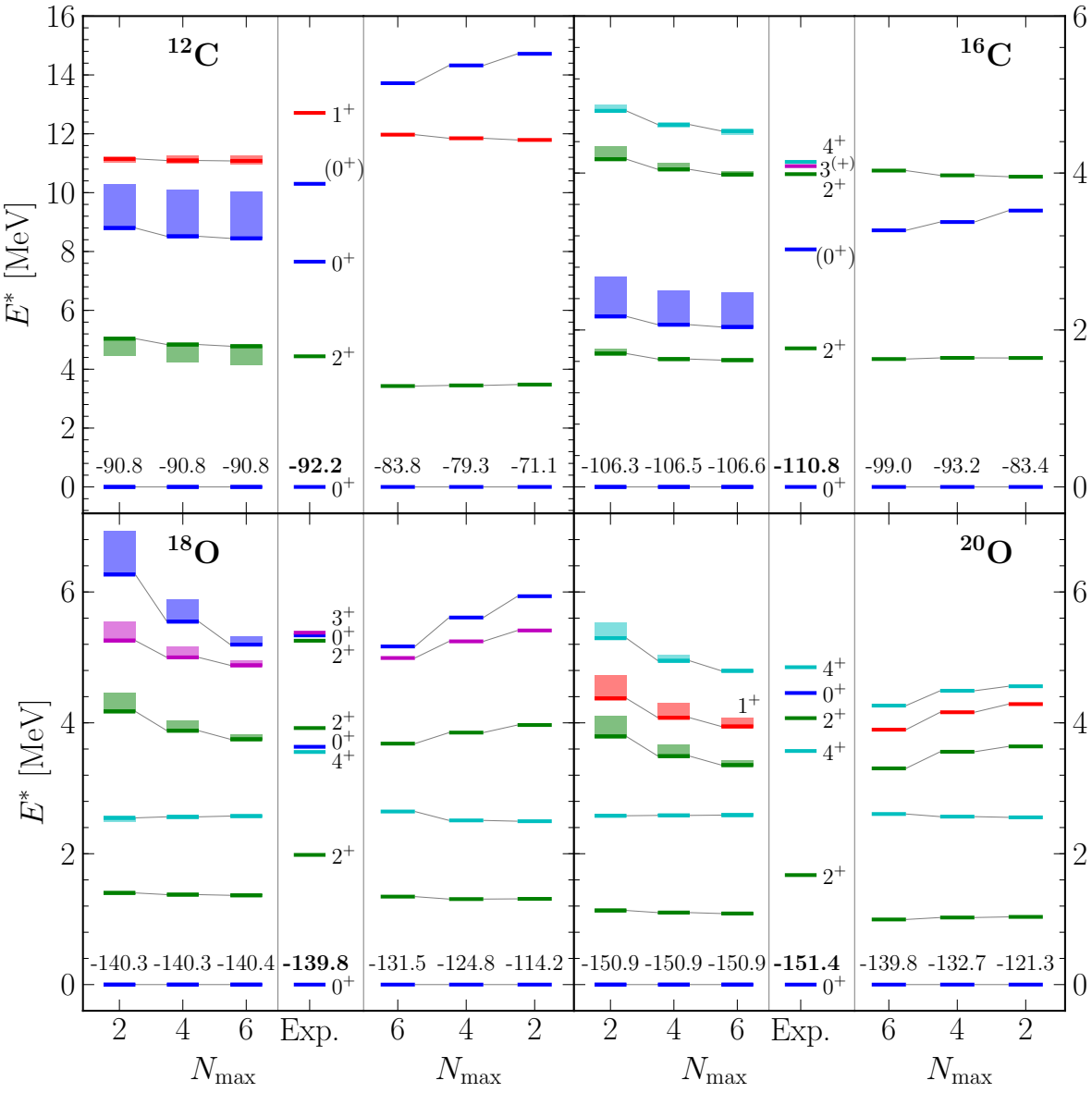

Figure 8.2.: Excitation spectra for selected isotopes obtained from the IM-NCSM (left-hand columns) and the importance-truncated NCSM (right-hand columns) in comparison to experiment (center columns) [NND17]. The bands indicate the residual flow-parameter dependence in the range from $s_{\max}/2$ to $s_{\max}$ with bars marking the latter. The importance-truncated NCSM results are obtained with explicit 3N interactions using the HO basis with $\hbar\Omega = 16\,\mathrm{MeV}$. (published in [Geb+17])

8.2. Analysis of the Hoyle State in ^{12}C

In the previous section, we have observed that the second 0^+ state in ^{12}C behaves differently as a function of the flow parameter compared to other low-lying states. As a reminder, this state drops down from approximately 14 MeV to 8 MeV during the IM-SRG evolution. This state is known to be the Hoyle state experimentally and is very problematic to converge in standard NCSM calculations [Mar+14].

In this section, we present a detailed analysis of this state. First, we confirm that the absolute and excitation energies of this state are not CM contaminated. This is done by testing the robustness of these quantities with respect to variation of the parameter β that controls the strength of CM Hamiltonian in the total Hamiltonian for the solution of the eigenvalue problem. Furthermore, we investigate the impact of the generators on this state. Finally, we explore the variation of the excitation energies as well as the absolute energy with the reference-space size $N_{\max}^{\text{ref}}$.

Center-of-Mass Contamination

In exact theories, the total many-body state $|\Psi\rangle$ of the nucleus factorizes into an intrinsic part $|\Psi_{\text{int}}\rangle$ and a CM part $|\Psi_{\text{cm}}\rangle$ describing the dynamics of the CM. This decoupling ensures that any intrinsic state of the nucleus is translationally invariant, as dictated by the symmetries of the Hamiltonian [RGP09]. Consequently, all intrinsic observables must be free of spuriousities caused by the CM component of the system.

In general, the exact factorization of the total many-body state as formulated in (5.12) is not fulfilled in truncated many-body calculations. The traditional NCSM, where we combine the HO single-particle basis with the $N_{\max}$-truncation, ensures this factorization [NKB00]. However, this is not the case for an HF basis. In order to quantify the CM contamination, we simultaneously evolve the intrinsic Hamiltonian $\boldsymbol{H}_{\text{int}}(s)$ as well as the CM Hamiltonian $\boldsymbol{H}_{\text{cm}}(s)$ (5.13) while only the intrinsic Hamiltonian enters the construction of the generator. Diagonalizing the total Hamiltonian given by

$$\boldsymbol{H}(s;\beta) = \boldsymbol{H}_{\text{int}}(s) + \beta \boldsymbol{H}_{\text{cm}}(s), \tag{8.1}$$

we obtain the eigenstates and eigenvalues

$$\boldsymbol{H}(s;\beta)\,|\Psi(s;\beta)\rangle = E_{\text{tot}}(s;\beta)\,|\Psi(s;\beta)\rangle\,. \tag{8.2}$$

The intrinsic energy is defined by

$$E_{\text{int}}(s;\beta) \coloneqq E_{\text{tot}}(s;\beta) - \beta\,\langle\Psi(s;\beta)|\boldsymbol{H}_{\text{cm}}(s)|\Psi(s;\beta)\rangle\,. \tag{8.3}$$

which should be independent of the parameter β if the condition (5.12) is fulfilled.

In order to test the second 0^+ state in ^{12}C for CM contamination, we analyze the following quantities obtained in various $N_{\max}$ model spaces at three different stages of the IM-SRG

evolution as a function of β shown in figure 8.3:

- its absolute (intrinsic) energy E, which is equivalent to $E_{\mathrm{int}}(s;\beta)$,
- its excitation energy E^*,
- the expectation value of the consistently evolved CM Hamiltonian with respect to the second 0^+ eigenstate of the total Hamiltonian, $\langle \boldsymbol{H}_{\mathrm{cm}} \rangle \coloneqq \langle \Psi(s;\beta) | \boldsymbol{H}_{\mathrm{cm}}(s) | \Psi(s;\beta) \rangle$,
- the difference of the intrinsic energies obtained with and without the CM Hamiltonian introduced in [RGP09], i.e.,

$$\Delta E_{\mathrm{int}} \coloneqq E_{\mathrm{int}}(s;\beta) - E_{\mathrm{int}}(s;0). \tag{8.4}$$

Let us analyze the results in the initial stage of the IM-SRG evolution depicted in the left-hand columns of figure 8.3. We observe that the absolute as well as the excitation energy of the second 0^+ state obtained in $N_{\mathrm{max}} = 0$ and 2 are completely independent of β. In contrast to that, the $N_{\mathrm{max}} = 4$ results show a modest dependence on β signaling spuriousity for small parameters $\beta \leq 0.1$, which is eliminated by increasing β. The same can also be seen for the expectation value of the CM Hamiltonian. Here, even the $N_{\mathrm{max}} = 2$ results have CM contaminations which also go to zero for sufficiently large values of β. Contrary to that, the quantity ΔE_{int} jumps from 0 MeV to 5 MeV in $N_{\mathrm{max}} = 4$ model space and stays relatively constant, while the results obtained in $N_{\mathrm{max}} = 0$ and 2 are not affected much.

However, performing the IM-SRG evolution drives ΔE_{int} to less than 200 keV for all values of N_{max} and $\beta \geq 0.1$ showing that the CM contamination is negligibly small (cf. right panels of figure 8.3). This confirms our observation for the expectation value of the CM Hamiltonian which is driven to zero. Moreover, it is in line with our interpretation that we can suppress CM contaminations by adding a consistently evolved HO Hamiltonian to the intrinsic one.

For further investigations, we recommend to set the parameter $\beta = 1.0$. All calculations including the ground-state energies up to this point have been performed with this recommended value for β.

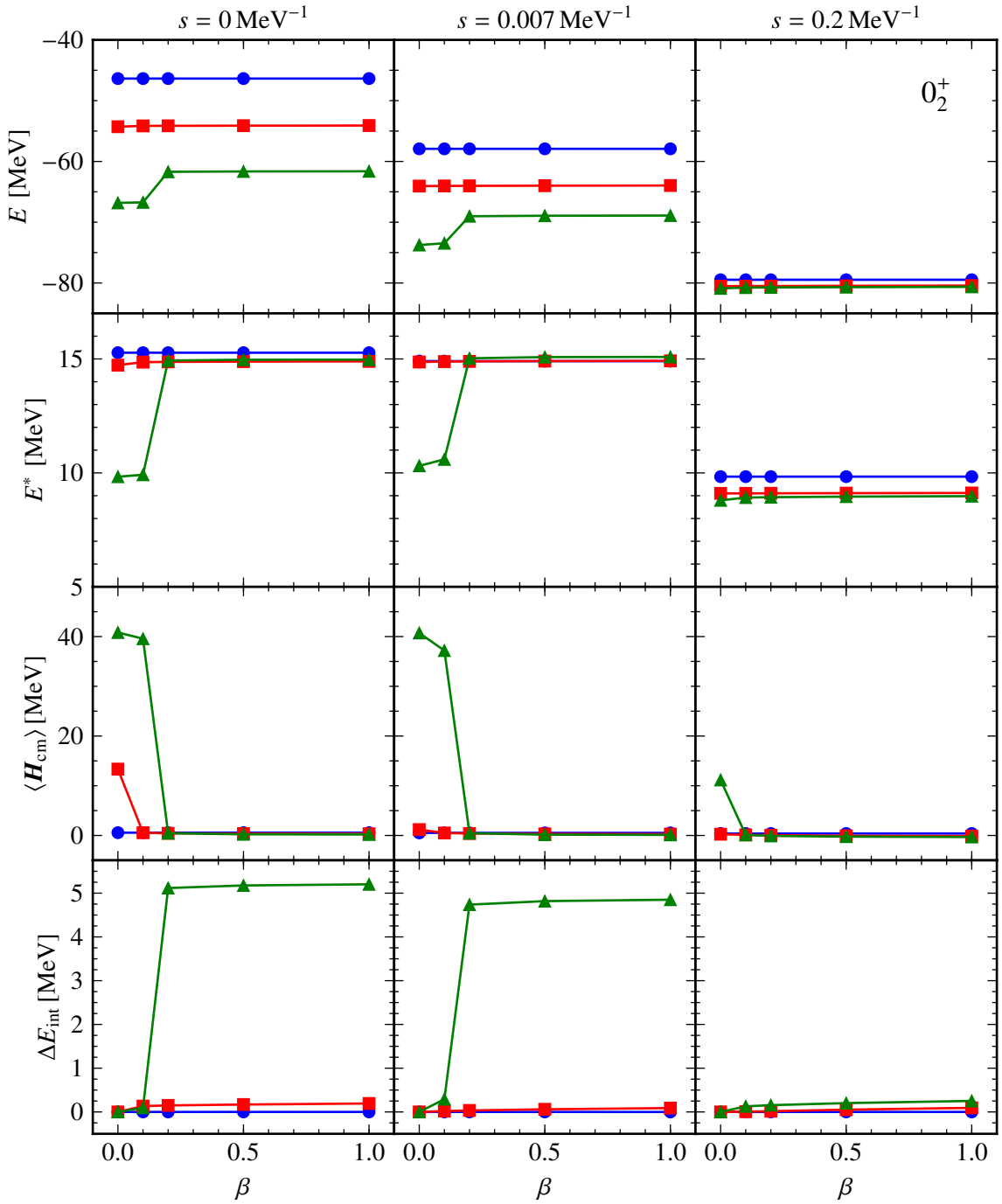

Figure 8.3.: We analyze the absolute and excitation energies of the second 0^+ state, expectation values of the CM Hamiltonian with respect to this state and $\Delta E_{\rm int}$ from (8.4) obtained in the model spaces $N_{\rm max}$=0 (●), 2 (■), 4 (▲) at three different stages of the IM-SRG evolution as a function of the parameter β. For more details see text. We use an HF basis with $e_{\rm max} = 6$ and $\hbar\Omega = 20\,$MeV.

Impact of the Choice of the Generator

Now that we have shown that the second 0^+ state in ^{12}C is free of CM contaminations, we investigate if there is a dependence on the generators.

We analyze the impact of the generators on the excitation energy of the second 0^+ state in ^{12}C in figure 8.4. The Imaginary-Time and White generators show the same behavior, the excitation energy of the second 0^+ state drops to 8 MeV. Going to larger values of the flow parameter increases the excitation energy. This is related to the fact that the ground-state energy decreases in energy after the plateau at the end of the IM-SRG evolution due to neglected induced many-body contributions, which become significant.

In contrast to that, the Wegner and Brillouin generators show a completely different behavior. They push the excitation energy to higher values. These results for the Wegner and Brillouin generators should be handled with caution, since the ground-state energy is not under control for ^{12}C as already seen in figure 7.5. Numerical instabilities for Wegner and induced-many body contribution for Brillouin complicate extracting converged ground-state energies before reaching stable results as discussed in section 7.1.3.

Let us turn our investigations to the absolute energy of the second 0^+ state and the expectation value of the CM Hamiltonian with respect to that state depicted in the four upper and lower panels of figure 8.5, respectively. Similarly to the excitation energies, the absolute energies obtained with the Imaginary-Time and White generators are consistent and stabilize at approximately -83 MeV, while the other two generators behave differently.

For the Wegner generator, the energies obtained in $N_{\max} = 4$ model space show a minimum around $s \approx 4 \times 10^{-4}\,\text{MeV}^{-2}$. This might be an indication that induced many-body contributions become apparent before the ground-state energy is stable. Hence, these results should be treated cautiously. However, the energies stabilize around -72 MeV which is higher compared to the results obtained with the Imaginary-Time and White generators. Using the Brillouin generator, the absolute energies of the second 0^+ state are not even converged with respect to $N_{\max}$, signaling that this state is not decoupled from other states. Consequently, these results should be considered with caution as well.

The expectation value of the CM Hamiltonian with respect to this second 0^+ state is relatively small indicating that our results do not suffer from CM contamination. As for ground-state energies, care should be taken if we go to large values of the flow parameter using the Wegner or Brillouin generator, where numerical instabilities become significant in the IM-SRG evolution.

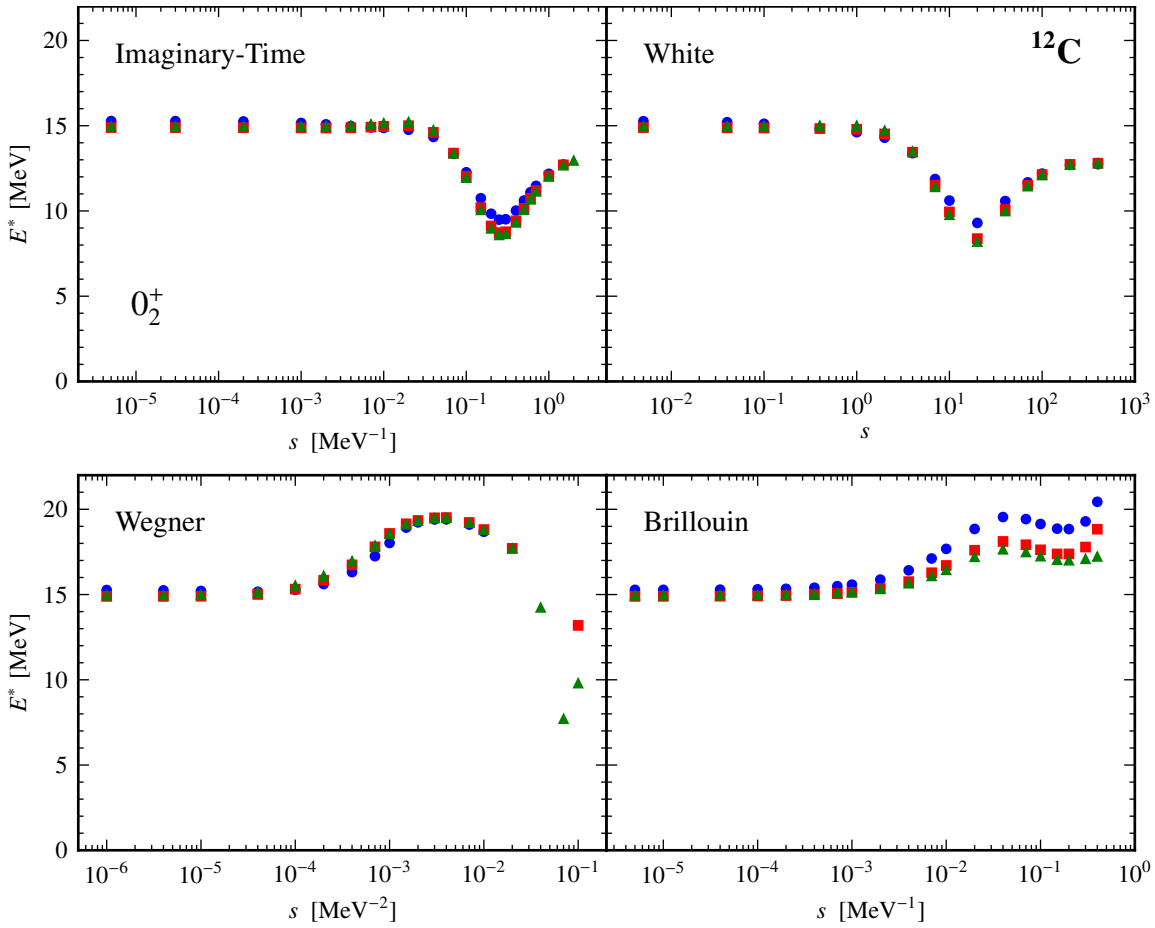

Figure 8.4.: We analyze the impact of the generators on the excitation energy of the second 0^+ state in ^{12}C obtained in the model spaces with $N_{\max}$=0 (●), 2 (■), 4 (▲). We use an HF basis with $e_{\max} = 6$ and $\hbar\Omega = 20\,\mathrm{MeV}$.

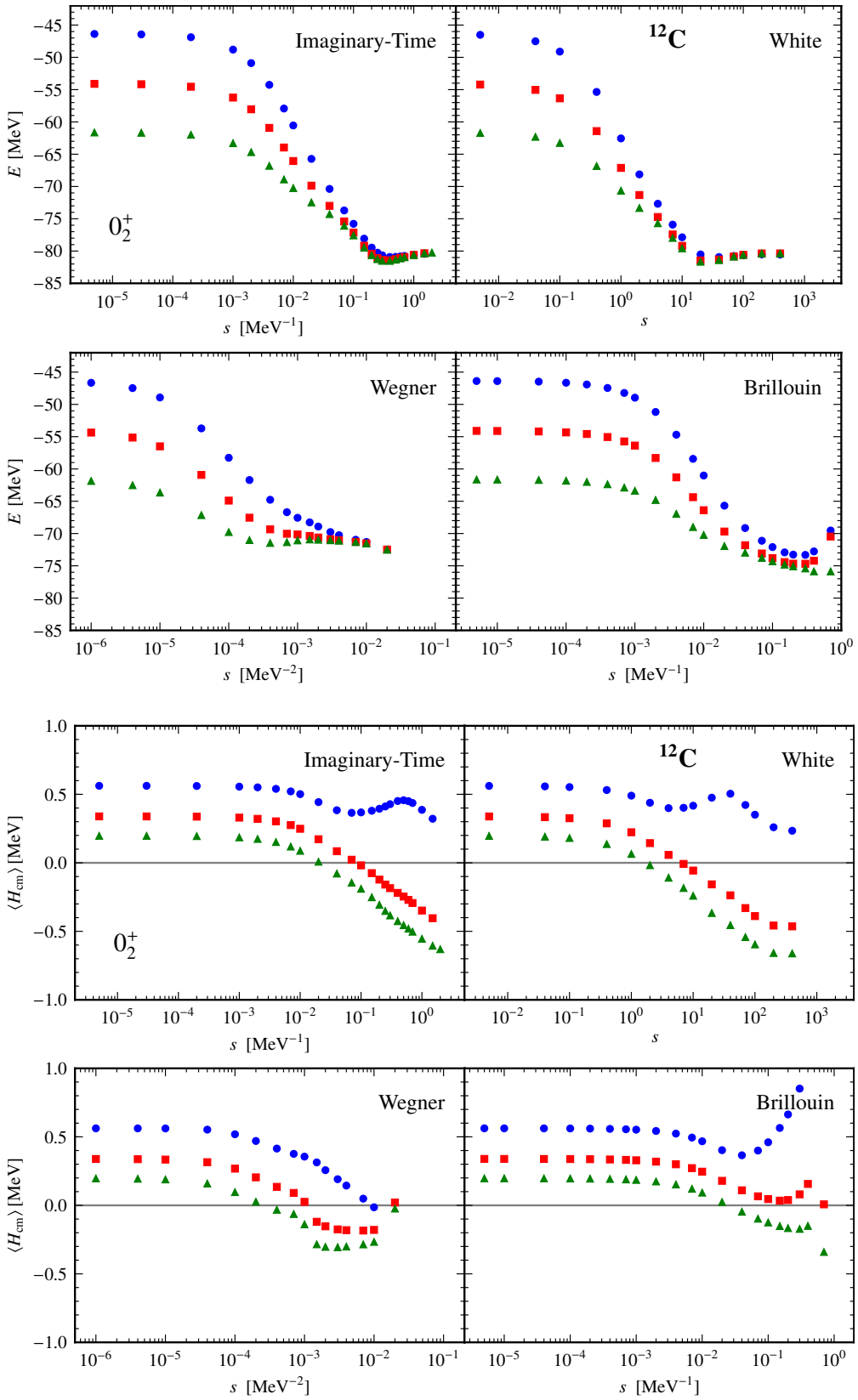

Figure 8.5.: We analyze the impact of the generators on the absolute energy (upper panels) and $\langle \boldsymbol{H}_{\rm cm} \rangle$ (lower panels) of the second 0^+ state in ^{12}C obtained in the model spaces with $N_{\rm max}$=0 (●), 2 (■), 4 (▲). We use an HF basis with $e_{\rm max} = 6$.

Variation of the Reference-Space Size

The reference state $|\Psi\rangle$ used for the IM-SRG evolution is the ground state of the initial Hamiltonian obtained in a model space with small $N_{\max}^{\text{ref}}$. In section 7.1.4, we have already confirmed that the IM-NCSM ground-state energies are independent of the choice of the reference-space size $N_{\max}^{\text{ref}}$. Now, it is interesting to study whether this parameter has an impact on the absolute energy of the second 0^+ state.

In figure 8.6, we analyze the absolute energy of the second 0^+ state in ^{12}C on the reference-space size $N_{\max}^{\text{ref}}$. These calculations were performed using the Imaginary-Time generator with a fixed single-particle energy truncation $e_{\max} = 6$ and oscillator frequency $\hbar\Omega = 20\,\text{MeV}$. Furthermore, we add a consistently evolved CM Hamiltonian with $\beta = 1.0$ to get rid of spuriousities.

We can clearly see that the absolute IM-NCSM energies of the second 0^+ state are independent of the reference-space size $N_{\max}^{\text{ref}}$. This result is compatible with the observation made for the ground-state energy in figure 7.8.

In chapter 9, we continue investigating this state by calculating its electric monopole transition to the ground state, which are more sensitive to the structure of nuclei compared to energies. Additionally, we consider the mass and charge radii of this state.

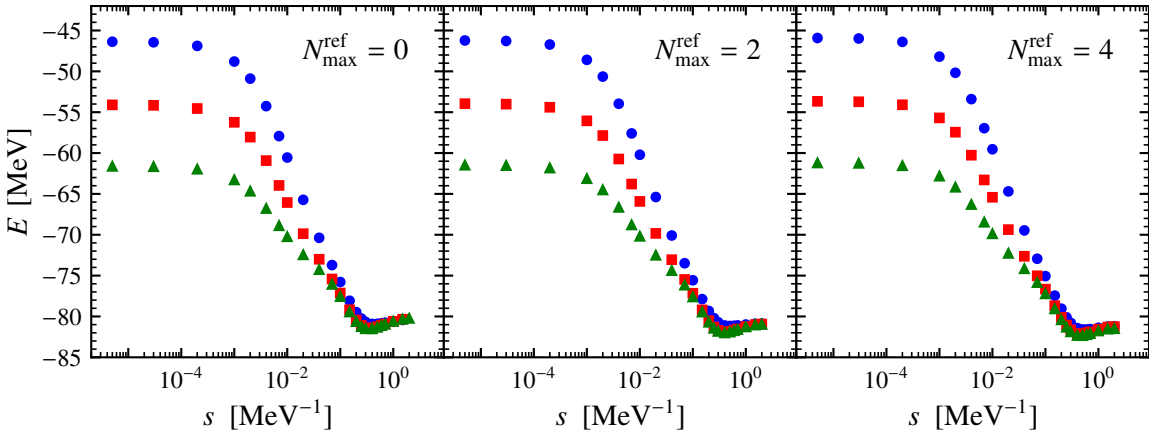

Figure 8.6.: We analyze the absolute energy of the second 0^+ state in ^{12}C on the model-space truncation parameter $N_{\max}^{\text{ref}}$ of the reference state which is the ground state. These calculations were performed using the Imaginary-Time generator with a fixed single-particle energy truncation $e_{\max} = 6$ and oscillator frequency $\hbar\Omega = 20\,\text{MeV}$. Furthermore, we add a consistently evolved CM Hamiltonian with $\beta = 1.0$ to get rid of spuriousities.

8.3. Island of Inversion: Magnesium and Sodium Isotopes

Introduction and Motivation

The well-known nuclear magic numbers are a very important and powerful concept in nuclear structure. They are derived from the nuclear shell model, which is the foundation for the appearance of energy gaps in the single-particle spectrum. They coincide with large energy gaps in the single-particle energy spectra near the Fermi energy, i.e., the single-particle states are fully occupied with protons or neutrons up to an energy just below these energy gaps. However, investigations showed that the magic numbers are not fixed throughout the nuclear chart [Sch11]. There are regions in the nuclear chart, called "island of inversion", where the shell-model magic numbers can vanish and new ones can appear.

We give some examples from the literature related to this nuclear phenomenon: The evidence for a new magic number $N = 34$ has been confirmed in ^{54}Ca [Ste$^+$13]. Another prominent example is the appearance of the magic shell gap in the neutron-rich oxygen isotopes at $N = 16$ (^{24}O) [Hof$^+$08; Kan$^+$09]. Finally, the magic number $N = 20$ disappears in very neutron rich neon, sodium and magnesium isotopes [Wim$^+$10]. We focus on the sodium and magnesium isotopes.

In figure 8.7, the nuclear chart is depicted where the valley of stable nuclei (black squares) and those predicted to lie inside the driplines (open blue symbols) can be seen. Outside the driplines nuclei become unstable to proton or neutron decay. The red shaded area depicts the region where the shell-model magic numbers (2, 8, 20, 28, ...) are broken. The nuclei ^{32,34}Mg and $^{31-33}$Na lie within this island-of-inversion region. Since we are limited to even nuclei, we decided to investigate the neutron-rich ^{32}Mg in our framework to explore island-of-inversion physics. To see the transition when going from 'standard' to 'island-of-inversion' nuclei we consider also ^{30}Mg. Additionally, we study the ^{26,28,30}Na isotopes.

Finally, let us complete our motivation for the island-of-inversion physics by considering the number of publications between 1970 and 2010 shown in figure 8.8. These numbers show the enormous interest that increased dramatically since the mid 90's. However, until today, for studying the structure of exotic nuclei, which is the case for very neutron-rich nuclei, one often needs to modify conventional nuclear models to account for intruder physics for instance [Zho17]. Therefore, it is of great interest to tackle those nuclei within an *ab initio* framework. The latter is exactly what we can do now after establishing the IM-NCSM.

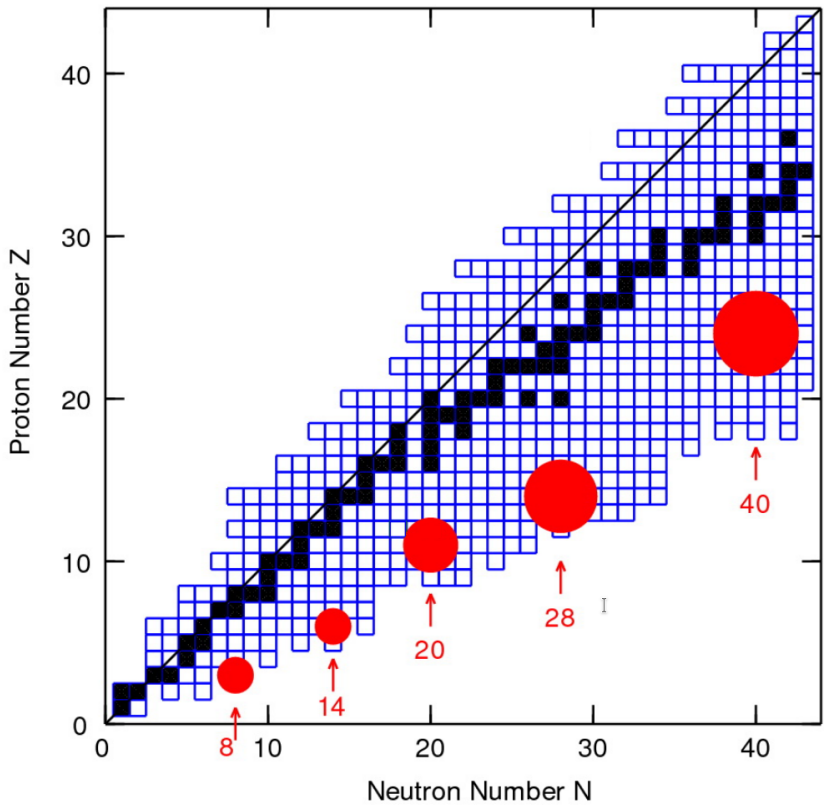

Figure 8.7.: Depicted is the nuclear chart: valley of stable nuclei (black squares) and those predicted to lie inside the proton and neutron drip lines (open blue symbols) The red shaded area depicts the region where the shell-model magic numbers are broken. This region is called island of inversion. (figure taken from [Bro10])

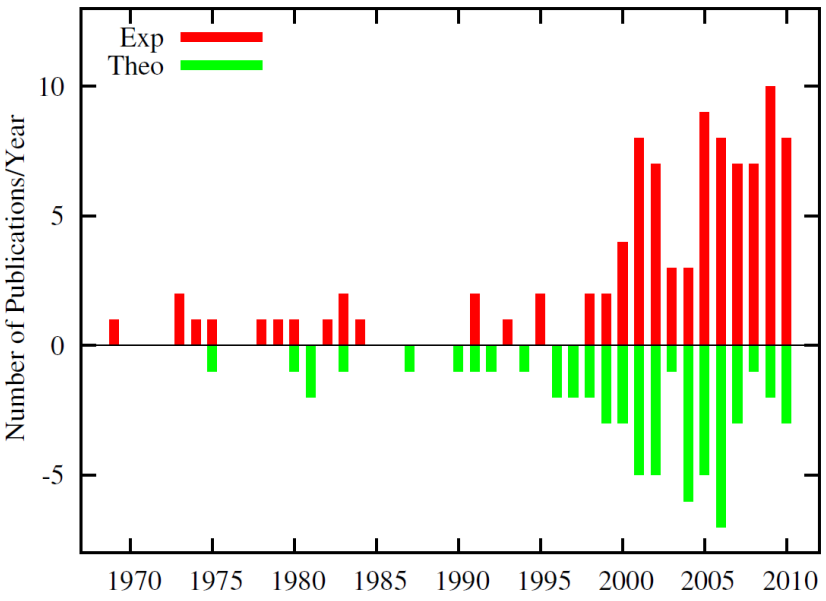

Figure 8.8.: Shown is the number of publications between 1970 and 2010 related to island-of-inversion physics. The interest on this subject increased dramatically since mid 90's. (figure taken from [Sch11])

As a reminder, we have already investigated the ground-state energies of the nuclei, ^{30,32}Mg and ^{26,28,30}Na, within the framework of IM-NCSM in section 7.3. For both magnesium isotopes, we can reproduce the ground-state energies with a reasonable accuracy. In particular, the quantum numbers of the ground states have been predicted by the input Hamiltonian in agreement with experiment. In contrast to this, the total angular quantum numbers of the ground states in the considered sodium isotopes could not be reproduced.

Magnesium Isotopes

The excitation energies of the low-lying states in ^{30,32}Mg as a function of the flow parameter are shown in figure 8.9. The experimental data are depicted in the right-hand panels. The states whose quantum numbers have not been identified uniquely so far are shown as gray horizontal bars.

We analyze the total angular momentum for the ground state predicted by the input Hamiltonian to be a 0^+ state which is in agreement with experiment.

The energy splitting between the first and second 4^+ states in ^{30}Mg is too high, whereas these states are degenerated experimentally. Moreover, the level ordering is not correct, e.g., the second 2^+ is above the first 4^+ which should be reversed actually.

We turn our discussion to ^{32}Mg, where the situation looks quite different. The whole spectrum is compressed to lower energies compared to ^{30}Mg. To be more quantitative, we consider the excitation energy of the first eigenstate—that is the first 2^+ state—which is a good indicator since it provides a very strong signature of shell evolution [CC08]. In experimental excitation energy decreases from 1.48 MeV to 0.89 MeV when going from ^{30}Mg to ^{32}Mg, which is in line with our results obtaining 1.24 MeV for ^{30}Mg and 0.86 MeV for ^{32}Mg. Keeping in mind that ^{32}Mg is magic nuclei, this effect is the opposite of what is expected for approaching a magic number. This reflects the fact that ^{32}Mg is an island-of-inversion nucleus.

Furthermore, the 2^+ and 4^+ states are in very good agreement with experiment, e.g., the 4^+ state is approximately 350 keV too low in energy compared to experiment while the 2^+ state is on top of the experimental value.

An interesting fact is that there are no other states below 5.6 MeV for ^{32}Mg predicted by the input Hamiltonian, but experimentally there is a bunch of states whose quantum numbers have not been determined uniquely. In particular, the experimentally observed second 0^+ has not been predicted by our Hamiltonian. The same holds for ^{30}Mg. For both isotopes, the reference state is the lowest eigenstate of the initial Hamiltonian obtained in $N_{\max}^{\text{ref}} = 0$ space. Consequently, we may miss intruder physics which is crucial to describe this missing state adequately. It is an open question whether a reference state from $N_{\max}^{\text{ref}} = 2$ space could solve this problem.

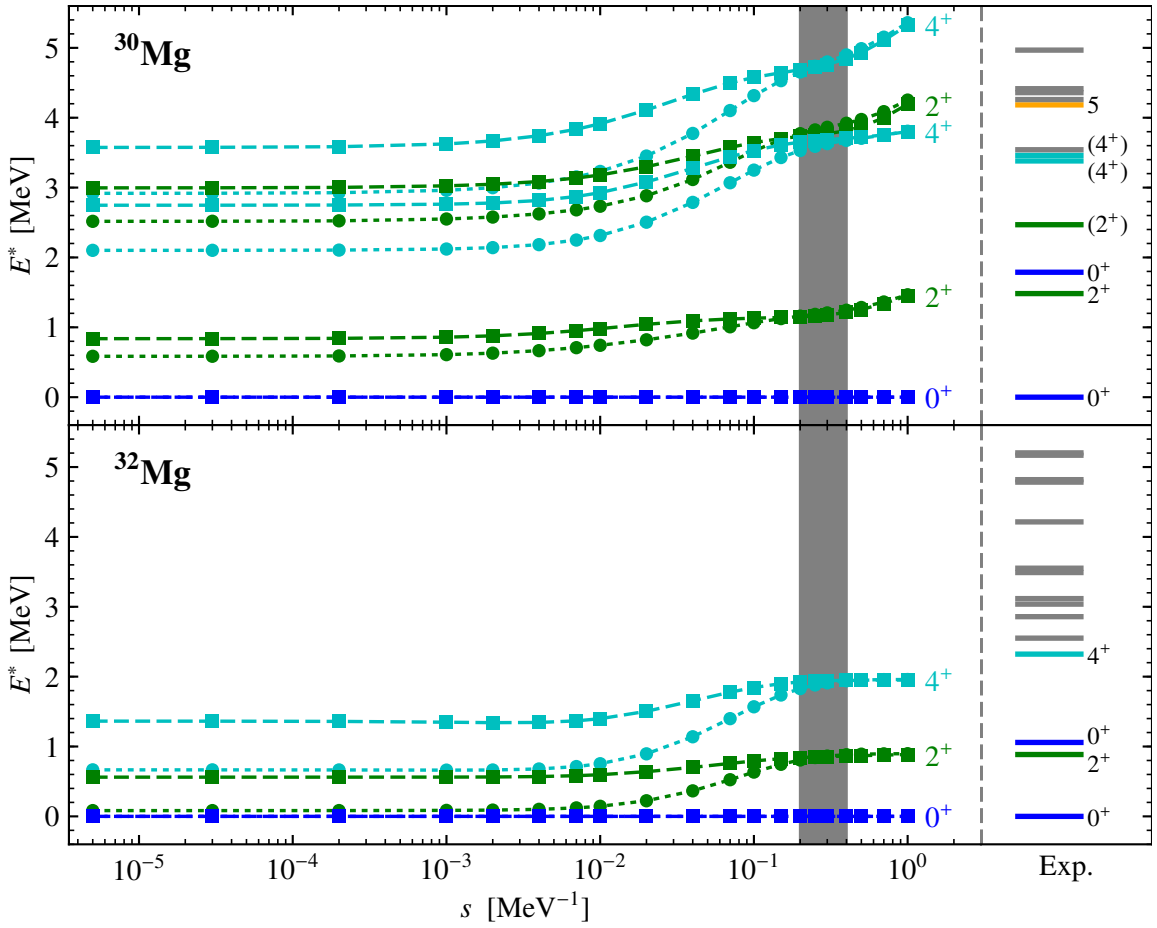

Figure 8.9.: The left panels show the IM-NCSM excitation energies of low-lying states in selected sodium isotopes as a function of the flow parameter obtained in the model spaces $N_{\max} = 0$ (●, dotted line) and 2 (■, dashed line). In both cases, the reference state is the lowest eigenstate of the initial Hamiltonian obtained in $N_{\max}^{\text{ref}} = 0$ space. Additionally, the experimental data are depicted in the right panels. The vertical gray band represents the range of flow parameters where the ground-state energy is already converged. The states whose quantum numbers are unknown are depicted in gray horizontal bars. We use an HF basis with $e_{\max} = 12$.

Sodium Isotopes

The left panels of figure 8.10 show the IM-NCSM excitation energies of the low-lying states with respect to the experimentally known ground states in selected sodium isotopes as a function of the flow parameter obtained in different model spaces $N_{\max}$. We emphasize that the excitation energies are depicted with respect to the state identified as the ground state in experiment. These are the $3^+, 1^+$ and 2^+ states for ^{26}Na, ^{28}Na and ^{30}Na, respectively. The experimental data are depicted in the right-hand columns. The states whose quantum numbers have not been identified are depicted in gray horizontal bars.

The excitation energies are less than 1 MeV which makes a reliable determination of the excitation energies basically impossible since the CM contamination quantified via the expectation value of the consistently evolved CM Hamiltonian is at the same order, in particular, 0.5 MeV which is significant here. In contrast to that, for the magnesium isotopes the CM contamination was negligible. We observe an enhanced dynamic, e.g., level crossings, in the IM-SRG evolution of the excitation energies in ^{26,30}Na. As aforementioned, we do not reproduce the ground states in any of the considered isotopes, i.e., there is always another lower lying state than the experimentally identified ground state. In ^{26}Na, we do at least observe all states that have been seen experimentally, but in a different order. For ^{30}Na, there is a 0^+ state below the true ground state that does not exist in experiment. We note that experimental data for ^{28}Na are very rare.

Conclusion

We have made first pilot studies to address island-of-inversion physics in magnesium and sodium isotopes within the IM-NCSM framework.

For the magnesium isotopes, we are able to reproduce the ground-state energies and low-lying 2^+ state in a good agreement with experiment. Based on the decreased excitation energy of 2^+ state in ^{32}Mg compared to ^{30}Mg, we could confirm the island-of-inversion character of the isotope ^{32}Mg observed experimentally. A remaining challenge is the second 0^+ state that cannot be seen in our calculations. This might be related to intruder physics, which is crucial to describe this state adequately. It is interesting to study whether a reference state from $N_{\max}^{\text{ref}} = 2$ space captures the intruder physics missing in our reference state.

The sodium isotopes considered here have extremely compressed spectra complicating an adequate description. The accuracy level needed to make accurate predictions for these systems go beyond our current capability. There are uncertainties originating from the Hamiltonian and the many-body techniques due to truncations. The excitation energies depend highly on the flow parameter signaling a difficult structure of these systems. Even the total angular momentum of the ground states have not been reproduced.

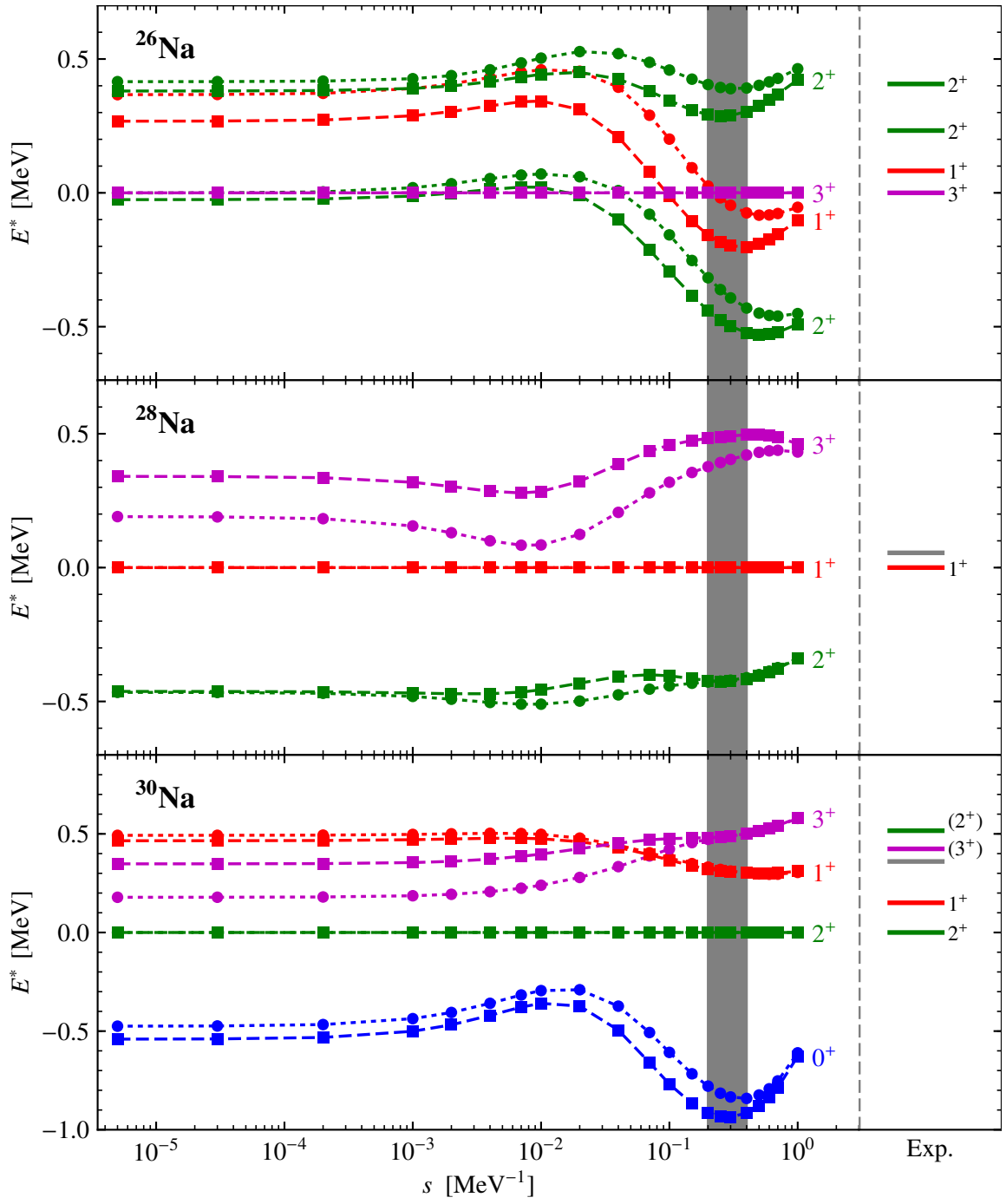

Figure 8.10.: The left panels show the IM-NCSM excitation energies of low-lying states with respect to the experimentally known ground state in selected sodium isotopes as a function of the flow parameter obtained in the model spaces $N_{\max} = 0$ (●, dotted line) and 2 (■, dashed line). The experimental data are depicted in the right panels. The states whose quantum numbers are unknown are depicted in gray horizontal bars. We use an HF basis with $e_{\max} = 12$.

Chapter 9

Radii and Electric Monopole Transitions for the Hoyle State in ^{12}C

Let us turn our focus to the second 0^+ state in ^{12}C, the Hoyle state. To extract more information on this state, we perform calculations for charge and mass radii as well as the monopole transition matrix elements from this state to the ground state in the framework of IM-NCSM, including a consistent multi-reference IM-SRG evolution of the relevant operators. We refer the reader to (4.284) and (4.287) for the exact expressions for charge and mass radii, respectively. The electric monopole transition matrix element is given by the transition matrix element of the operator defined in (4.310) with respect to the states of interest, i.e., in this case the Hoyle and the ground state

$$|\mathcal{M}(\mathrm{E0}; 0_2^+ \to 0_1^+)| := |\langle 0_1^+ | \boldsymbol{Q}_{00} | 0_2^+ \rangle|. \tag{9.1}$$

We remind that the electric monopole transition operator is Hermitian and scalar, i.e., it is a spherical tensor of rank zero.

The prime observables to identify the Hoyle state are radii and electric monopole transitions. Due to its triple-alpha structure, this state has a large spatial extent. From experiment we know that the charge radius of the Hoyle state is about 0.4 fm larger than the ground state [Dan+09]—even though it is controversial how to assign a radius to a resonance state. The electric monopole transition matrix element to the ground state is less controversial, which is around 5.5 e fm^2 [Ajz90]. Recent lattice effective field theory calculations at leading order obtain a radius which is about 0.2 fm larger than the ground state, and an electric monopole matrix element of around 3(1) e fm^2 [Epe+12]. Calculations in fermionic molecular dynamics yield a radius about 1.0 fm larger than the ground state and an electric monopole transition matrix element of 6.53 e fm^2 [Che+07].

The IM-NCSM results are summarized in figure 9.1. We show the dependence of the

excitation energy of the second 0^+ state, the point mass and the charge radii of both 0^+ states, as well as the electric monopole transition matrix element between them as a function of the flow parameter. The gray band indicates the range of flow parameters before truncation artifacts appear in the ground-state energy (cf. discussion on the ground-state energy in chapter 7).

The dependence of these observables on the flow parameter is astonishing. The mass R_{rms} and charge R_{ch} radii of the second 0^+ state start to increase quickly once the excitation energy starts to decrease. Similarly, the electric monopole transition matrix element increases rapidly. Before reaching the flow parameters where truncation artifacts appear, the radii have increased by 0.1 fm and the monopole transition matrix element by a factor of 2.5. Obviously, the IM-SRG decoupling efficiently maps the physics ingredients relevant for the description of the Hoyle state into a tiny $N_{\mathrm{max}} = 0$ space. Increasing the model space confirms the correct trend to enhanced mass and charge radii of the Hoyle state.

Unfortunately, we are currently unable to provide stable and converged results for these observables, since the IM-SRG truncation effects set in before these observables become independent of the flow parameter. The systematics indicate that radii and transition matrix elements would continue to increase with increasing flow parameter. We have confirmed that similar pictures emerge for the excitation energy with other choices for the single-particle basis as well as the Imaginary-Time and White generators. For the Wegner and Brillouin generators, we have problems with numerical instabilities as discussed in section 8.2. In order to make an accurate prediction for the properties of the Hoyle state, we need to improve on the truncation of the IM-SRG flow equations.

Nonetheless, the present calculations already indicate that the IM-NCSM has the potential to quantitatively describe the Hoyle state. They provide a strong motivation to continue the investigation of this and related states in the IM-NCSM and to develop efficient corrections for the omitted many-body terms in the flow equations.

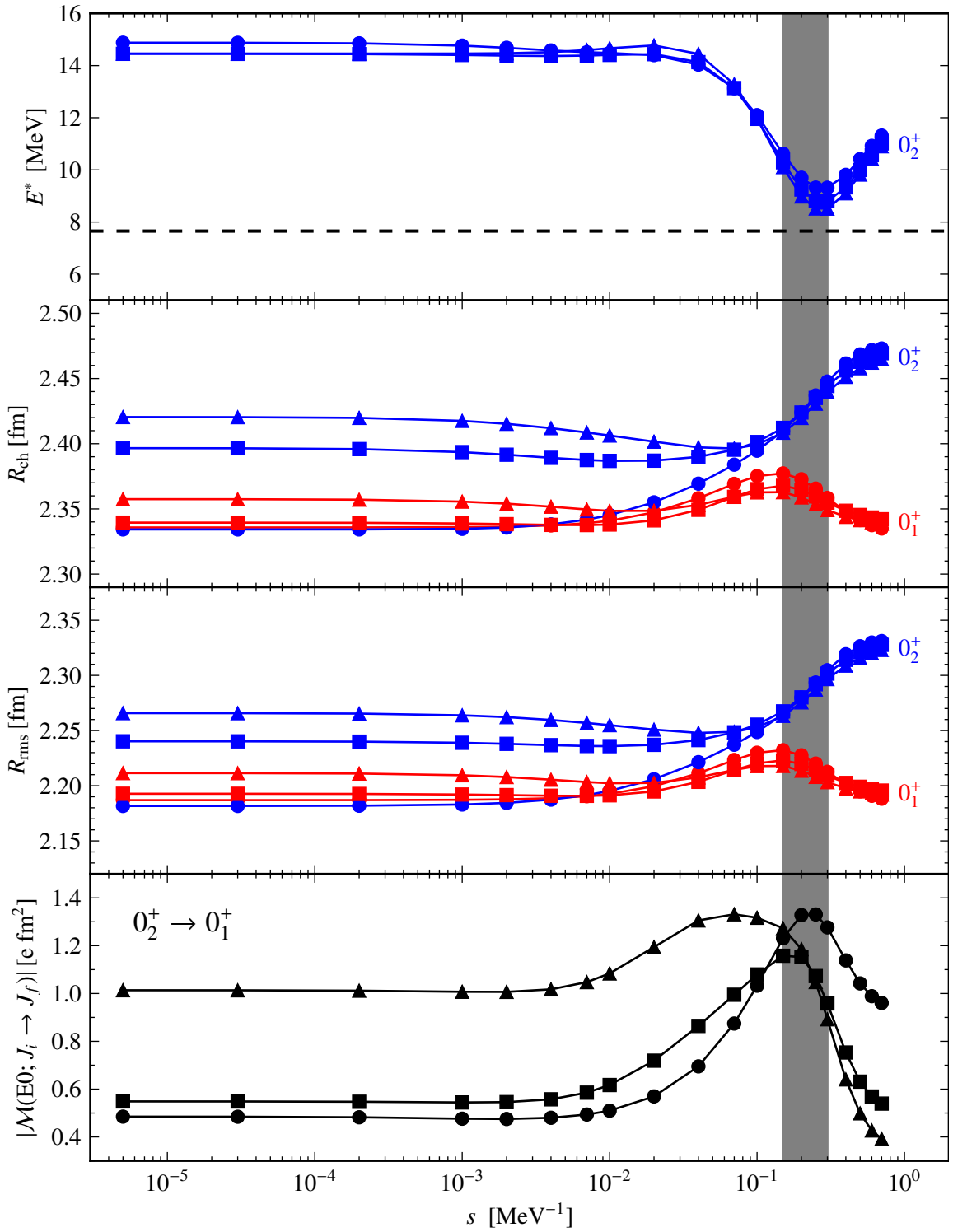

Figure 9.1.: Depicted is the excitation energy of the 0_2^+ state and the mass $R_{\rm rms}$ and charge $R_{\rm ch}$ radii of the first two 0^+ states. The dashed black line indicates the experimental excitation energy of the Hoyle state. The lowest panel shows the electric monopole transition matrix element $|\mathcal{M}(\mathrm{E0}; 0_2^+ \to 0_1^+)|$. All results have been obtained from an $N_{\rm max} = 0$ (circle), 2 (square) and 4 (triangular) diagonalization using an $N_{\rm max}^{\rm ref} = 0$ reference state. We use an HF basis with $e_{\rm max} = 12$.

Chapter 10

Particle-Attached Particle-Removed Extension of IM-NCSM

In this chapter, we introduce a simple and straightforward formalism to extend the IM-NCSM to odd nuclei, i.e., nuclei that have a odd total number of particles A. Firstly, we describe the idea and general strategy of the particle-attached particle-removed extension of IM-NCSM abbreviated as pp̸-IM-NCSM. Afterwards, we benchmark the pp̸-IM-NCSM calculations in some selected even nitrogen isotopes that can be also addressed in the 'standard' IM-NCSM framework serving as a reference point. Finally, we show results for the ground-state as well as excitation energies for those isotopes.

General Strategy

Let us recall where the limitation of the IM-NCSM framework to even nuclei originates from. For reasons of efficiency, we use a J-coupled formulation of the multi-reference IM-SRG that assumes a reference state with vanishing total angular momentum, as discussed in chapter 4. We stick to this type of reference states, which imply a restriction of the IM-NCSM calculations to even particle numbers A. However, we emphasize that the theoretical framework is completely general and we would only need a more general implementation of the IM-SRG evolution for non-scalar tensors, which is a tough task.

The question is how we can overcome the restriction to even nuclei with less effort. One simple and straightforward answer results from the following idea. Since the IM-SRG evolution is a unitary transformation, the IM-SRG evolved Hamiltonian for a given nucleus, the parent nucleus, can be used to target any other nucleus, the target nucleus. Note that the unitarity is violated in practical calculations due to omitted many-body contribution which must be quantified in some way.

We refer to this extension as the pp̸-IM-NCSM whose strategy is schematically shown in figure 10.1. We generate a family of IM-SRG evolved Hamiltonians using a reference state of a specific even parent nucleus and, subsequently, target nuclei that differ only by few

nucleons from this parent nucleus. Thus, we perform an NCSM calculation for the target nucleus using the IM-SRG evolved Hamiltonians of the parent nucleus to extract ground-state and excitation energies of the target nucleus. A great advantage compared to the coupled-cluster approach is that the IM-SRG evolved Hamiltonians are Hermitian such that they can be fed directly into subsequent many-body methods like NCSM. The philosophy we pursue here is comparable to the particle-attached or particle-removed equations-of-motion coupled-cluster approach [Jan+11; PGW09] or the equation-of-motion extension of the IM-SRG [PMB17; Par+17]. Nevertheless, our framework is extremely simple from a conceptional and computational point of view.

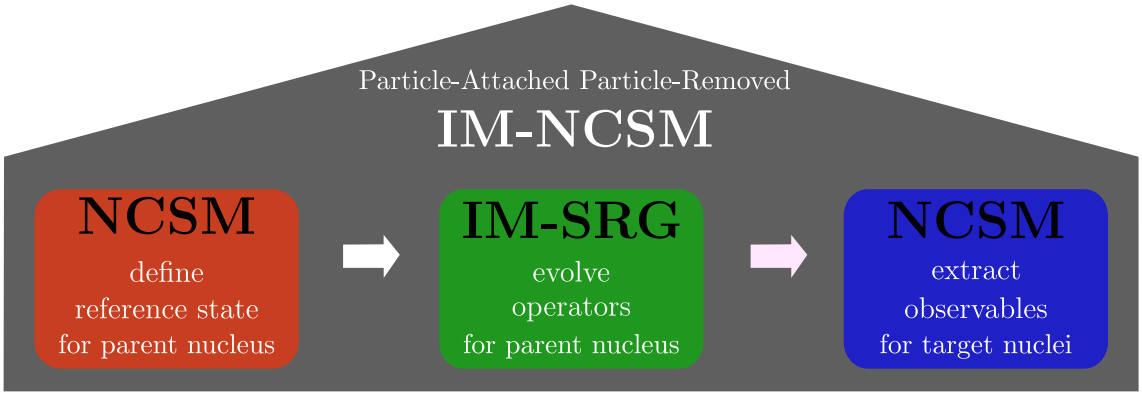

Figure 10.1.: Schematic overview of the particle-attached particle-removed extension of the IM-NCSM. We diagonalize the Hamiltonian using NCSM for the parent nucleus, and its ground state defines the reference state which enters the IM-SRG evolution of the Hamiltonian in the parent nucleus. This step is a unitarity transformation in an A-body system. Hence, we can diagonalize the IM-SRG evolved Hamiltonian in the target nuclei of interest, and can extract observables.

Benchmarking Ground-State Energies of Even Nitrogen

To benchmark the pp-IM-NCSM formalism, we target odd-odd nuclei that can be also targeted directly in the IM-NCSM since these nuclei have even number of total particle number A. Furthermore, let us restrict ourselves to neighboring isobars as parent nuclei to avoid complication with the choice of the particle number A in the kinetic-energy operator, which has a direct dependence on A.

Since we have already demonstrated that the IM-NCSM calculations for the carbon and oxygen isotopes are robust and well converged (see section 7.2), let us target the ground-state as well as excitation energies of the nitrogen isotopes ^{16,18,20}N starting from the neighboring isobars ^{16,18,20}C and ^{16,18,20}O shown schematically in figure 10.2. For example, to target ^{16}N we perform the IM-SRG evolution using the ground-states of the nuclei ^{16}C as well as ^{16}O as reference states obtained in $N_{\max}^{\text{ref}} = 0$ model spaces to generate a family of IM-SRG evolved Hamiltonians. These calculations correspond to a proton-attached neutron-removed and a neutron-attached proton-removed formalism in case of ^{16}C and ^{16}O, respectively. Since the

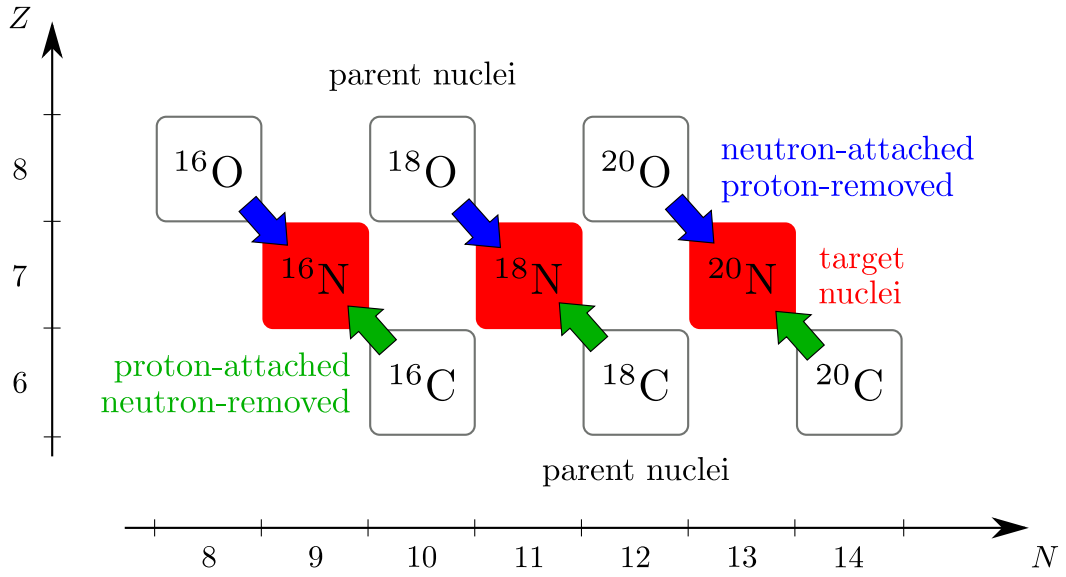

Figure 10.2.: Schematic overview how we tackle the target nitrogen isotopes starting from the carbon and oxygen isobars in the framework of the pp̸-IM-NCSM. In the cases of the carbon (green arrow) and oxygen (blue arrow) isobars as parent nuclei, we have the proton-attached neutron-removed and neutron-attached proton-removed formalism, respectively. Note that we can directly address ^{16,18,20}N isotopes in the IM-NCSM framework without the extension, while these results serve as a reference point to benchmark pp̸-IM-NCSM.

nitrogen isotopes ^{16,18,20}N have odd number of protons and neutrons $Z = 7$ and $N = 9, 11, 13$, respectively, we can additionally target them directly in the framework of IM-NCSM which serves as a reference point for our results.

In figure 10.3, the lowest eigenvalues of the IM-SRG evolved Hamiltonian are depicted for ^{16,18,20}N using isobaric carbon and oxygen as well as nitrogen as parent nuclei. The notation written in the upper right corner of the each sub-figure, e.g., $^{16}\text{C} \rightarrow {}^{16}\text{N}$, means that we tackle the target nucleus ^{16}N using ^{16}C as parent nucleus. For all calculations we use an HF basis with $e_{\max} = 6$ for convenience and $\hbar\Omega = 20\,\text{MeV}$.

In the initial stage of the IM-SRG evolution, i.e., $s \leq 10^{-4}\,\text{MeV}^{-1}$, the ground-state energies of the target nuclei in a fixed model space $N_{\max}$ are independent of the choice of the parent nuclei. This implies that we can even use reference states where a proton is replaced by a neutron or vice versa, and the results for the target nuclei remain unchanged. This goes beyond the observation made for the robustness of the multi-reference normal-ordered two-body approximation with respect to variation of the parameter $N_{\max}^{\text{ref}}$ as demonstrated in [GCR16].

Performing the IM-SRG evolution, we obtain perfectly $N_{\max}$-converged IM-NCSM ground-state energies (middle panels) using the corresponding nitrogen nuclei as parent nuclei which is the standard way how we extract ground-state energies in the IM-NCSM framework. Even the zero-body part of the Hamiltonian in reference-state representation (black line) which is identical to the expectation value of the Hamiltonian with respect to the reference state, $E(s)$,

is very robust even though the reference state is not the energetically lowest eigenstate of the initial Hamiltonian. This is the second excited eigenstate for ^{16}N, and the forth eigenstates for ^{18}N and ^{20}N, that are 0^- states in all cases. This is also the reason why the zero-body part of the Hamiltonian in reference-state representation, $E(s)$, slightly deviates from the lowest eigenvalues obtained in $N_{\max} = 0$ model space for ^{18,20}N even throughout the IM-SRG evolution, but especially for small flow parameter.

The neutron-attached proton-removed IM-NCSM ground-state energies using the corresponding carbon isobars as parent nuclei do agree perfectly with the results obtained with the 'standard' way. In contrast to that, the proton-attached and neutron removed IM-NCSM ground-state energies, i.e., using the IM-SRG evolved Hamiltonian in the corresponding oxygen parent nucleus, do not produce $N_{\max}$-converged results even though the IM-NCSM results stabilize for large enough value of the flow parameter s. This might be related to fact that the oxygen isotopes have a pronounced proton shell closure, which is inappropriate for the decoupling pattern of the nitrogen isotopes.

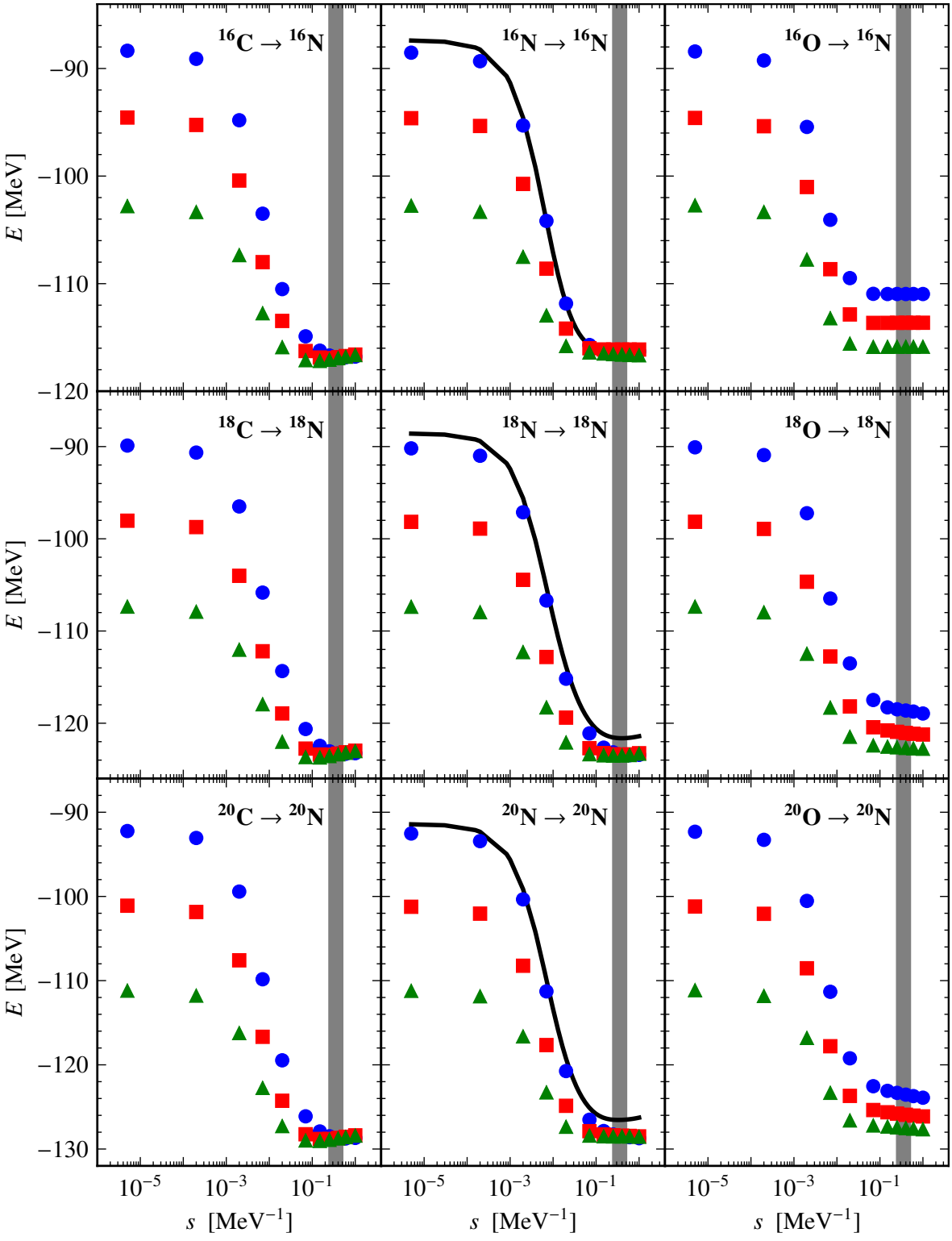

Figure 10.3.: The lowest eigenvalue the IM-SRG evolved Hamiltonian for ^{16,18,20}N within the particle-attached particle-removed IM-NCSM obtained in various model spaces $N_{\max}$=0 (●), 2 (■), 4 (▲). The parent nuclei are the carbon (left panels) and oxygen (right panels) isobars. In the case where the parent and target nuclei are identical, we additionally show the zero-body part of the Hamiltonian $E(s)$ (middle panels). We use an HF basis with $e_{\max} = 6$ and $\hbar\Omega = 20\,\mathrm{MeV}$.

Benchmarking Excitation Spectra in Even Nitrogen

We benchmark the excitation energies of the even nitrogen isotopes. In figure 10.4, we show the excitation energies of ^{16,18,20}N using carbon (left-hand panels) and oxygen (right-hand panels) isobars and the target nuclei itself (middle panels) as parent nuclei. Let us emphasize that ground and excited states are obtained on equal footing. The bands indicate the residual flow-parameter dependence in the range from $s_{\max}/2$ to $s_{\max}$ with bars, indicated by gray band in figure 10.3. The flow parameter is chosen in the region where the ground-state energy is relatively stable with respect to the flow parameter $s_{\max} = 0.5\,\mathrm{MeV}^{-1}$ for all cases. Additionally, we analyze the total angular momentum of the states.

First, let us focus on the ground states, which are correctly reproduced in comparison to experiment in all considered nitrogen isotopes for all parent nuclei—at least if the model space $N_{\max}$ is sufficiently large. The total angular momentum of the ground state of ^{16}N using ^{16}N itself as parent nucleus obtained in $N_{\max} = 0$ and 2—which is 1^-—is not in agreement with the results using ^{16}C and ^{16}O as parent nuclei predicting both a 2^- ground state. But once we go to a larger model space, e.g., $N_{\max} = 4$, the 2^- state drops down in excitation energy such that it becomes the ground state. These results are also consistent to the available experimental data in [NND17] measuring 2^- and 1^- for ^{16}N and ^{18}N, respectively. Unfortunately, there is no experimental data available for ^{20}N. In this case, we predict a 2^- ground state independent of the choice of the parent nucleus.

Let us turn our focus on the low-lying excited states. On the one hand, all states are reproduced consistently to each other independent of the choice of the parent nucleus. On the other hand, extracting the value of the excitation energies is extremely difficult due to induced many-body contributions and the scale of the excitation energies that is currently beyond our accuracy.

Remarkably, the carbon isobars as parents nuclei produce quite stable and $N_{\max}$-converged results. In contrast to that the results obtained with the oxygen show large flow-parameter dependence for the target nuclei ^{18,20}N. This is not really surprising since the ground-state energies are not converged yet with respect to $N_{\max}$ as already seen in figure 10.3.

The excitation spectra for ^{16}N and ^{18}N obtained with the various parent nuclei are in quite good agreement regarding the level ordering if the model space is large enough, but the energy splitting between the states is not consistent.

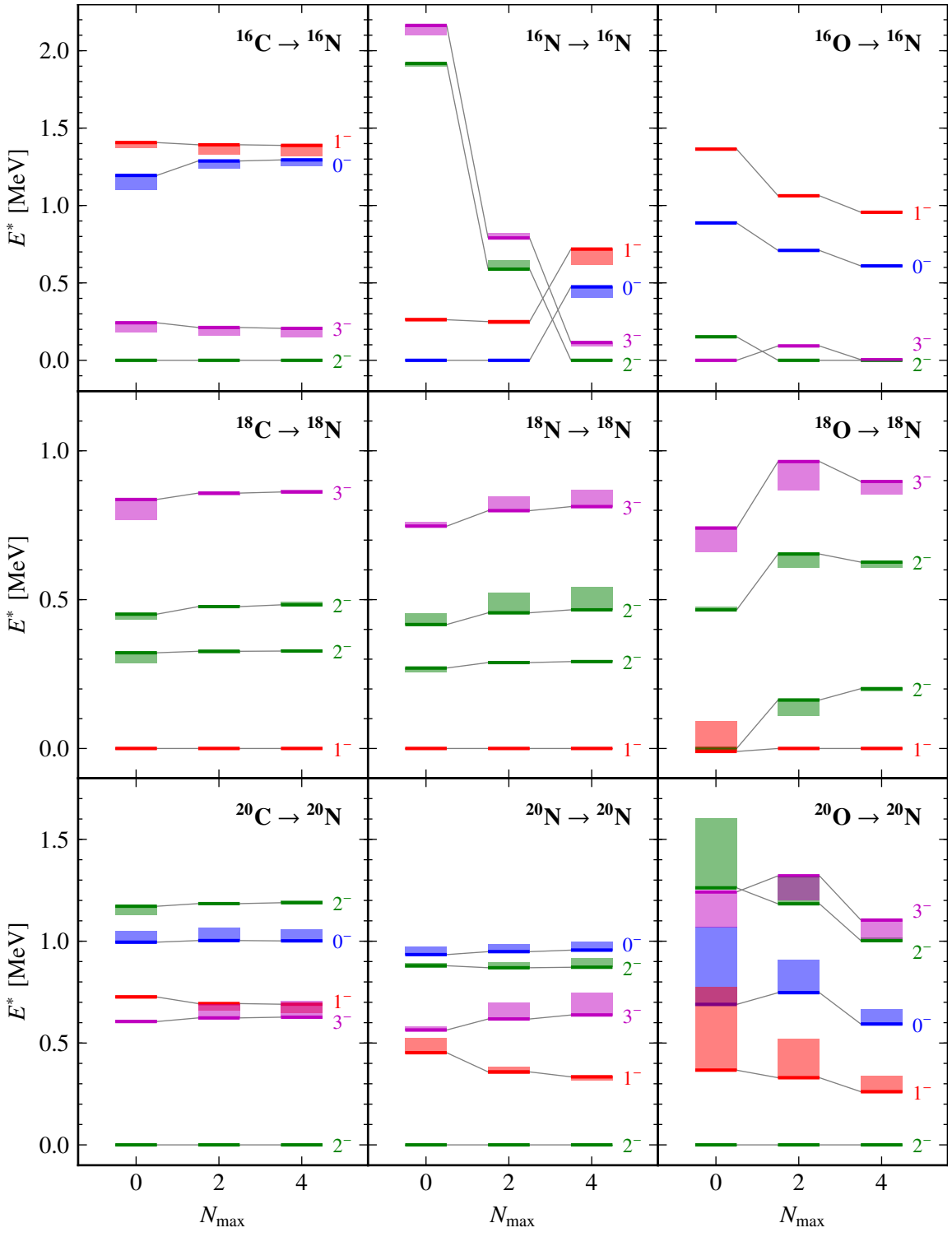

Figure 10.4.: Depicted are the low-lying excitation spectra of ^{16,18,20}N target using carbon (left) and oxygen (right) isobars, as well as the nucleus itself (middle panels) as parent nuclei. The bands indicate the residual flow-parameter dependence in the range from $s_{\max}/2$ to $s_{\max}$ with bars where we set $s_{\max} = 0.5\,\mathrm{MeV}^{-1}$ in all cases. We use an HF basis with $e_{\max} = 6$ and $\hbar\Omega = 20\,\mathrm{MeV}$.

IV.

Summary and Outlook

Summary and Outlook

In this work, we have established the *in-medium no-core shell model* (IM-NCSM) for nuclear-structure calculations. This method merges the multi-reference in-medium similarity renormalization group (IM-SRG) and the no-core shell model (NCSM) in a consistent manner. The basic idea is to transform the Hamiltonian via the IM-SRG to decouple a given reference state obtained from an initial NCSM calculation from its excitations. This Hamiltonian is then used in subsequent NCSM calculations.

In a first step, we have analyzed the sensitivity of the IM-NCSM ground-state energies on several parameters such as the model-space truncations, oscillator frequency, choice of the generators as well as the reference-space size. We have explicitly demonstrated that relatively small model spaces are sufficient in the subsequent NCSM calculations to extract converged ground-state energies. The convergence acceleration in these calculations is attributed to the IM-SRG evolution that decouples the reference state from its excitations. We have analyzed a Hartree-Fock (HF) and the harmonic-oscillator (HO) single-particle bases. An HF basis reduces the dependence of the IM-NCSM ground-state energies on the oscillator frequency dramatically, as expected. In contrast to this, the HO basis seems to be incompatible with the IM-SRG(2) truncations leading to disappearance of the minimum in the energies as a function of the oscillator frequency. Moreover, we have examined the impact of the generators. The Imaginary-Time and White generators show similar behavior during the IM-SRG evolution, which can be related to their similar operator structure. For the Wegner generator, numerical instabilities can appear complicating reliable extraction of converged ground-state energies. Analogously, for the Brillouin generator we can hardly identify a plateau region for the flow parameters, which is related to the creeping induced many-body contributions. The dependence on the reference-space size has been found to be negligibly low such that the smallest value is sufficient.

Based on this analysis, we have fixed the parameters to systematically analyze ground-state energies in carbon and oxygen chains. We have compared our results against large-scale NCSM calculations and multi-reference IM-SRG calculations using spherical number-projected HF-Bogoliubov reference states. For the oxygen isotopes, we have obtained perfect agreement among the three methods. Furthermore, the neutron dripline in the oxygen isotopes has been reproduced consistently to experiment. In contrast to that, we have observed relatively large deviations in the carbon isotopes. The largest deviation at the level of 10 % has been found for ^{12}C, which is the most distinct case.

After benchmarking and establishing the IM-NCSM framework, we have explored ground-state energies of magnesium and sodium isotopes, where exact diagonalizations are not available anymore. Our results for ^{30,32}Mg overbind by less than 4 % relative to experiment. Furthermore, the total-angular-momentum quantum numbers of the ground states could be reproduced correctly, while it is not the case for the sodium isotopes. By considering the excitation spectra of the sodium isotopes, we have observed that the accuracy requirements needed to describe these systems adequately are beyond our current reach. Inaccuracies in our calculations are rooted both in the many-body methods and the input Hamiltonian itself, which make reliable determination difficult.

We have studied excitation energies for the low-lying states of ^{12}C and ^{20}O, where the rate of convergence is not enhanced in general, but the excitation energies converge monotonically since the ground-state energies are converged. An interesting effect has been found for the second 0^+ state in ^{12}C, known to be a cluster state and called the Hoyle state, that cannot be converged in standard NCSM calculations. A remarkable outcome of this work is that the excitation energy of this state drops during the IM-SRG evolution from about 14 MeV to 8 MeV in good agreement to experiment, while the other excitation energies remain stable. We have calculated key signatures of this state, e.g., mass and charge radii as well as the electric monopole transition to the ground state. The present calculations already indicate that the IM-NCSM has the potential to quantitatively describe the Hoyle state. They provide a strong motivation to continue the investigation of this and related states in the IM-NCSM and to develop efficient corrections for the omitted many-body terms in the flow equations.

To explore island-of-inversion physics, we have investigated the magnesium isotope ^{32}Mg which is known to lie inside the island-of-inversion region. The ground-state energy has been reproduced with a reasonable accuracy with respect to experiment, and its total angular momentum is consistent to experiment, too. Furthermore, the low-lying states have been reproduced correctly whereas the excited 0^+ state, that has been seen in experiment, could not be reproduced in our calculations. An outstanding issue is whether this state can be seen when we use a reference state containing information about higher-lying orbitals. In this way, we could include intruder physics which might help to solve this problem.

The results for the sodium isotopes imply that the input Hamiltonian is not adequate to describe these systems accurately. It might be interesting to investigate these sodium isotopes using other interactions. One is provided by the Low Energy Nuclear Physics International Collaboration (LENPIC) [Bin+16] enabling an order-by-order analysis of effective-field-theory uncertainties. Another interesting choice is given by the next-to-next-to-leading order saturated (N^2LO_{sat}) interactions [Eks+15] that contain heavier systems in the fitting procedure.

However, the analysis regarding the island of inversion must be done systematically, which has not been done in this work. Our investigations included only ground and excitation energies, it is also of great interest to calculate and analyze other observables related to island-of-inversion physics, e.g., dipole or quadrupole electromagnetic transitions. This requires the IM-SRG evolution of non-scalar operators.

We have introduced and tested a simple and straightforward way how to extend the IM-

NCSM to odd-mass nuclei using the particle-attached particle-removed formalism. The reason for this limitation is that we used a J-coupled formulation of the multi-reference IM-SRG for reasons of efficiency, which assumes a reference state with vanishing total angular momentum. This implies a restriction of the IM-NCSM calculations to even particle numbers. As a benchmark, we targeted the odd-odd nitrogen isotopes using carbon and oxygen isobars as parent nuclei. These nitrogen isotopes are ideal since we could additionally target them directly in the framework of IM-NCSM. The ground-state energies of the nitrogen isotopes agree well when using the carbon and nitrogen nuclei as parent nuclei, which is not the case for the oxygen isotopes. A possible reason might be the strong proton shell closure in the oxygen isotopes, which is inappropriate for the decoupling of the ground states of the nitrogen isotopes.

It would be also very interesting to tackle a given nuclei using an isotope as parent nuclei that correspond to particle-attached or particle-removed only procedure, i.e., targeting ^{15}C using ^{14}C or ^{16}C. Alternatively, we could extend the applicability of IM-NCSM to odd nuclei by allowing a reference state that does not have a vanishing total angular momentum. For that purpose, the whole framework including the angular-momentum-coupling of the IM-SRG flow equations needs to be revisited. This requires the implementation of the IM-SRG evolution for non-scalar operators. Alternatively, we can use the existing formulation and implementation by decomposing the density matrices into spherical tensors and neglecting all non-scalar parts (see appendix C more details).

Finally, a parallelization of the IM-SRG code via message passing interface is recommended to increase the applicability of the IM-NCSM, especially for the evolution of non-scalar operators using non-scalar density operators in order to investigate electromagnetic transitions in open-shell nuclei.

V.

Appendices

Appendix A

Normal Ordering—Derivations

A.1. Products of Normal-Ordered Operators

Throughout this section, we derive the expressions for products of normal-ordered operators with the aid of the theorem 3.3, called generalized Wick's theorem. The results obtained here will be needed in appendix A.2 for calculating the commutator between those operators which are relevant for the multi-reference in-medium similarity renormalization group method discussed in chapter 4. We make use of the following relations:

$$\bar{\gamma}^p_q + \gamma^p_q = \delta^p_q - \gamma^p_q + \gamma^p_q = \delta^p_q \tag{A.1}$$

$$\bar{\gamma}^p_q \gamma^r_s - \gamma^p_q \bar{\gamma}^r_s = \delta^p_q \gamma^r_s - \gamma^p_q \delta^r_s \tag{A.2}$$

$$\bar{\gamma}^p_q \bar{\gamma}^r_s - \gamma^p_q \gamma^r_s = \delta^p_q \delta^r_s - \delta^p_q \gamma^r_s - \gamma^p_q \delta^r_s \tag{A.3}$$

$$\bar{\gamma}^{tv}_{us} \gamma^r_w + \gamma^{tv}_{us} \bar{\gamma}^r_w = (\bar{\gamma}^t_u \bar{\gamma}^v_s - \bar{\gamma}^t_s \bar{\gamma}^v_u)\gamma^r_w + (\gamma^t_u \gamma^v_s - \gamma^t_s \gamma^v_u)\bar{\gamma}^r_w + \lambda^{tv}_{us} \delta^r_w \tag{A.4}$$

and the antisymmetry with respect to exchange among the upper and lower indices of the normal-ordered two-body operator and of the irreducible two-body density matrix element, respectively,

$$\tilde{\boldsymbol{a}}^{pr}_{qs} = -\tilde{\boldsymbol{a}}^{rp}_{qs} = -\tilde{\boldsymbol{a}}^{pr}_{sq} = +\tilde{\boldsymbol{a}}^{rp}_{sq} \tag{A.5}$$

$$\lambda^{pr}_{qs} = -\lambda^{rp}_{qs} = -\lambda^{pr}_{sq} = +\lambda^{rp}_{sq} \tag{A.6}$$

and the Hermiticity of the irreducible two-body density matrix element

$$\lambda^{pr}_{qs} = \lambda^{sq}_{pr}. \tag{A.7}$$

Product of 1B and 1B

The product of two normal-ordered one-body operator yields

$$\tilde{\boldsymbol{a}}^p_q \tilde{\boldsymbol{a}}^r_s = \tilde{\boldsymbol{a}}^{pr}_{qs} - \gamma^p_s \tilde{\boldsymbol{a}}^r_q + \bar{\gamma}^r_q \tilde{\boldsymbol{a}}^p_s + \gamma^p_s \bar{\gamma}^r_q + \lambda^{pr}_{qs}. \tag{A.8}$$

Product of 2B and 1B

According to the generalized Wick's theorem for this case only terms containing 3-, 2-, 1- and 0-body operators can appear, denoted in the upper square brackets:

$$\tilde{\boldsymbol{a}}^{pr}_{qs}\tilde{\boldsymbol{a}}^{t}_{u} = (\tilde{\boldsymbol{a}}^{pr}_{qs}\tilde{\boldsymbol{a}}^{t}_{u})^{[3]} + (\tilde{\boldsymbol{a}}^{pr}_{qs}\tilde{\boldsymbol{a}}^{t}_{u})^{[2]} + (\tilde{\boldsymbol{a}}^{pr}_{qs}\tilde{\boldsymbol{a}}^{t}_{u})^{[1]} + (\tilde{\boldsymbol{a}}^{pr}_{qs}\tilde{\boldsymbol{a}}^{t}_{u})^{[0]} \tag{A.9}$$

with

$$(\tilde{\boldsymbol{a}}^{pr}_{qs}\tilde{\boldsymbol{a}}^{t}_{u})^{[3]} := \tilde{\boldsymbol{a}}^{prt}_{qsu} \tag{A.10}$$

$$(\tilde{\boldsymbol{a}}^{pr}_{qs}\tilde{\boldsymbol{a}}^{t}_{u})^{[2]} := \bar{\gamma}^{t}_{q}\tilde{\boldsymbol{a}}^{pr}_{us} + \bar{\gamma}^{t}_{s}\tilde{\boldsymbol{a}}^{pr}_{qu} - \gamma^{p}_{u}\tilde{\boldsymbol{a}}^{tr}_{qs} - \gamma^{r}_{u}\tilde{\boldsymbol{a}}^{pt}_{qs} \tag{A.11}$$

$$\begin{aligned}(\tilde{\boldsymbol{a}}^{pr}_{qs}\tilde{\boldsymbol{a}}^{t}_{u})^{[1]} := &+ (\bar{\gamma}^{t}_{s}\gamma^{r}_{u} + \lambda^{rt}_{su})\tilde{\boldsymbol{a}}^{p}_{q} - (\bar{\gamma}^{t}_{s}\gamma^{p}_{u} + \lambda^{pt}_{su})\tilde{\boldsymbol{a}}^{r}_{q} \\ &+ (\bar{\gamma}^{t}_{q}\gamma^{p}_{u} + \lambda^{pt}_{qu})\tilde{\boldsymbol{a}}^{r}_{s} - (\bar{\gamma}^{t}_{q}\gamma^{r}_{u} + \lambda^{rt}_{qu})\tilde{\boldsymbol{a}}^{p}_{s} \\ &- \lambda^{rt}_{sq}\tilde{\boldsymbol{a}}^{p}_{u} - \lambda^{pt}_{qs}\tilde{\boldsymbol{a}}^{r}_{u} - \lambda^{pr}_{us}\tilde{\boldsymbol{a}}^{t}_{q} - \lambda^{pr}_{qu}\tilde{\boldsymbol{a}}^{t}_{s}\end{aligned} \tag{A.12}$$

$$(\tilde{\boldsymbol{a}}^{pr}_{qs}\tilde{\boldsymbol{a}}^{t}_{u})^{[0]} := \bar{\gamma}^{t}_{q}\lambda^{pr}_{us} + \bar{\gamma}^{t}_{s}\lambda^{pr}_{qu} - \gamma^{p}_{u}\lambda^{rt}_{sq} - \gamma^{r}_{u}\lambda^{pt}_{qs} + \lambda^{prt}_{qsu}. \tag{A.13}$$

Finally, we get

$$\begin{aligned}\tilde{\boldsymbol{a}}^{pr}_{qs}\tilde{\boldsymbol{a}}^{t}_{u} = &+ \tilde{\boldsymbol{a}}^{prt}_{qsu} \\ &+ \bar{\gamma}^{t}_{q}\tilde{\boldsymbol{a}}^{pr}_{us} + \bar{\gamma}^{t}_{s}\tilde{\boldsymbol{a}}^{pr}_{qu} - \gamma^{p}_{u}\tilde{\boldsymbol{a}}^{tr}_{qs} - \gamma^{r}_{u}\tilde{\boldsymbol{a}}^{pt}_{qs} \\ &+ (\bar{\gamma}^{t}_{s}\gamma^{r}_{u} + \lambda^{rt}_{su})\tilde{\boldsymbol{a}}^{p}_{q} - (\bar{\gamma}^{t}_{s}\gamma^{p}_{u} + \lambda^{pt}_{su})\tilde{\boldsymbol{a}}^{r}_{q} \\ &+ (\bar{\gamma}^{t}_{q}\gamma^{p}_{u} + \lambda^{pt}_{qu})\tilde{\boldsymbol{a}}^{r}_{s} - (\bar{\gamma}^{t}_{q}\gamma^{r}_{u} + \lambda^{rt}_{qu})\tilde{\boldsymbol{a}}^{p}_{s} \\ &- \lambda^{rt}_{sq}\tilde{\boldsymbol{a}}^{p}_{u} - \lambda^{pt}_{qs}\tilde{\boldsymbol{a}}^{r}_{u} - \lambda^{pr}_{us}\tilde{\boldsymbol{a}}^{t}_{q} - \lambda^{pr}_{qu}\tilde{\boldsymbol{a}}^{t}_{s} \\ &+ \bar{\gamma}^{t}_{q}\lambda^{pr}_{us} + \bar{\gamma}^{t}_{s}\lambda^{pr}_{qu} - \gamma^{p}_{u}\lambda^{rt}_{sq} - \gamma^{r}_{u}\lambda^{pt}_{qs} + \lambda^{prt}_{qsu}\end{aligned} \tag{A.14}$$

Product of 1B and 2B

Analogously, we can write this product as

$$\tilde{\boldsymbol{a}}^{t}_{u}\tilde{\boldsymbol{a}}^{pr}_{qs} = (\tilde{\boldsymbol{a}}^{t}_{u}\tilde{\boldsymbol{a}}^{pr}_{qs})^{[3]} + (\tilde{\boldsymbol{a}}^{t}_{u}\tilde{\boldsymbol{a}}^{pr}_{qs})^{[2]} + (\tilde{\boldsymbol{a}}^{t}_{u}\tilde{\boldsymbol{a}}^{pr}_{qs})^{[1]} + (\tilde{\boldsymbol{a}}^{t}_{u}\tilde{\boldsymbol{a}}^{pr}_{qs})^{[0]} \tag{A.15}$$

with

$$(\tilde{\boldsymbol{a}}^{t}_{u}\tilde{\boldsymbol{a}}^{pr}_{qs})^{[3]} := \tilde{\boldsymbol{a}}^{tpr}_{uqs} \tag{A.16}$$

$$(\tilde{\boldsymbol{a}}^{t}_{u}\tilde{\boldsymbol{a}}^{pr}_{qs})^{[2]} := \bar{\gamma}^{p}_{u}\tilde{\boldsymbol{a}}^{tr}_{qs} + \bar{\gamma}^{r}_{u}\tilde{\boldsymbol{a}}^{pt}_{qs} - \gamma^{t}_{q}\tilde{\boldsymbol{a}}^{pr}_{us} - \gamma^{t}_{s}\tilde{\boldsymbol{a}}^{pr}_{qu} \tag{A.17}$$

$$\begin{aligned}(\tilde{\boldsymbol{a}}^{t}_{u}\tilde{\boldsymbol{a}}^{pr}_{qs})^{[1]} := &+ (\gamma^{t}_{s}\bar{\gamma}^{r}_{u} + \lambda^{rt}_{su})\tilde{\boldsymbol{a}}^{p}_{q} - (\gamma^{t}_{s}\bar{\gamma}^{p}_{u} + \lambda^{pt}_{su})\tilde{\boldsymbol{a}}^{r}_{q} \\ &+ (\gamma^{t}_{q}\bar{\gamma}^{p}_{u} + \lambda^{pt}_{qu})\tilde{\boldsymbol{a}}^{r}_{s} - (\gamma^{t}_{q}\bar{\gamma}^{r}_{u} + \lambda^{rt}_{qu})\tilde{\boldsymbol{a}}^{p}_{s} \\ &- \lambda^{rt}_{sq}\tilde{\boldsymbol{a}}^{p}_{u} - \lambda^{pt}_{qs}\tilde{\boldsymbol{a}}^{r}_{u} - \lambda^{pr}_{us}\tilde{\boldsymbol{a}}^{t}_{q} - \lambda^{pr}_{qu}\tilde{\boldsymbol{a}}^{t}_{s}\end{aligned} \tag{A.18}$$

$$(\tilde{\boldsymbol{a}}^{t}_{u}\tilde{\boldsymbol{a}}^{pr}_{qs})^{[0]} := -\gamma^{t}_{q}\lambda^{pr}_{us} - \gamma^{t}_{s}\lambda^{pr}_{qu} + \bar{\gamma}^{p}_{u}\lambda^{rt}_{sq} + \bar{\gamma}^{r}_{u}\lambda^{pt}_{qs} + \lambda^{tpr}_{uqs}. \tag{A.19}$$

Finally, we get

$$\begin{aligned}\tilde{\boldsymbol{a}}^t_u \tilde{\boldsymbol{a}}^{pr}_{qs} =& \tilde{\boldsymbol{a}}^{tpr}_{uqs} \\ &+ \bar{\gamma}^p_u \tilde{\boldsymbol{a}}^{tr}_{qs} + \bar{\gamma}^r_u \tilde{\boldsymbol{a}}^{pt}_{qs} - \gamma^t_q \tilde{\boldsymbol{a}}^{pr}_{us} - \gamma^t_s \tilde{\boldsymbol{a}}^{pr}_{qu} \\ &+ (\gamma^t_s \bar{\gamma}^r_u + \lambda^{rt}_{su}) \tilde{\boldsymbol{a}}^p_q - (\gamma^t_s \bar{\gamma}^p_u + \lambda^{pt}_{su}) \tilde{\boldsymbol{a}}^r_q \\ &+ (\gamma^t_q \bar{\gamma}^p_u + \lambda^{pt}_{qu}) \tilde{\boldsymbol{a}}^r_s - (\gamma^t_q \bar{\gamma}^r_u + \lambda^{rt}_{qu}) \tilde{\boldsymbol{a}}^p_s \\ &- \lambda^{rt}_{sq} \tilde{\boldsymbol{a}}^p_u - \lambda^{pt}_{qs} \tilde{\boldsymbol{a}}^r_u - \lambda^{pr}_{us} \tilde{\boldsymbol{a}}^t_q - \lambda^{pr}_{qu} \tilde{\boldsymbol{a}}^t_s \\ &- \gamma^t_q \lambda^{pr}_{us} - \gamma^t_s \lambda^{pr}_{qu} + \bar{\gamma}^p_u \lambda^{rt}_{sq} + \bar{\gamma}^r_u \lambda^{pt}_{qs} + \lambda^{tpr}_{uqs} \end{aligned} \tag{A.20}$$

Product of 2B and 2B

It is useful to separate the terms in subterms according to the particle rank

$$\tilde{\boldsymbol{a}}^{pr}_{qs} \tilde{\boldsymbol{a}}^{tv}_{uw} = (\tilde{\boldsymbol{a}}^{pr}_{qs} \tilde{\boldsymbol{a}}^{tv}_{uw})^{[4]} + (\tilde{\boldsymbol{a}}^{pr}_{qs} \tilde{\boldsymbol{a}}^{tv}_{uw})^{[3]} + (\tilde{\boldsymbol{a}}^{pr}_{qs} \tilde{\boldsymbol{a}}^{tv}_{uw})^{[2]} + (\tilde{\boldsymbol{a}}^{pr}_{qs} \tilde{\boldsymbol{a}}^{tv}_{uw})^{[1]} + (\tilde{\boldsymbol{a}}^{pr}_{qs} \tilde{\boldsymbol{a}}^{tv}_{uw})^{[0]}. \tag{A.21}$$

The four-body piece is simply

$$(\tilde{\boldsymbol{a}}^{pr}_{qs} \tilde{\boldsymbol{a}}^{tv}_{uw})^{[4]} := \tilde{\boldsymbol{a}}^{prtv}_{qsuw}, \tag{A.22}$$

the three-body piece is given by

$$\begin{aligned}(\tilde{\boldsymbol{a}}^{pr}_{qs} \tilde{\boldsymbol{a}}^{tv}_{uw})^{[3]} :=& + \bar{\gamma}^t_q \tilde{\boldsymbol{a}}^{prv}_{usw} + \bar{\gamma}^t_s \tilde{\boldsymbol{a}}^{prv}_{quw} + \bar{\gamma}^v_s \tilde{\boldsymbol{a}}^{prt}_{qwu} + \bar{\gamma}^v_q \tilde{\boldsymbol{a}}^{prt}_{wsu} \\ &- \gamma^p_u \tilde{\boldsymbol{a}}^{rtv}_{sqw} - \gamma^p_w \tilde{\boldsymbol{a}}^{rtv}_{suq} - \gamma^r_u \tilde{\boldsymbol{a}}^{ptv}_{qsw} - \gamma^r_w \tilde{\boldsymbol{a}}^{ptv}_{qus}. \end{aligned} \tag{A.23}$$

The two-body piece will be separated into further subterms

$$(\tilde{\boldsymbol{a}}^{pr}_{qs} \tilde{\boldsymbol{a}}^{tv}_{uw})^{[2]} := (\tilde{\boldsymbol{a}}^{pr}_{qs} \tilde{\boldsymbol{a}}^{tv}_{uw})^{[2,\mathrm{I}]} + (\tilde{\boldsymbol{a}}^{pr}_{qs} \tilde{\boldsymbol{a}}^{tv}_{uw})^{[2,\mathrm{II}]} + (\tilde{\boldsymbol{a}}^{pr}_{qs} \tilde{\boldsymbol{a}}^{tv}_{uw})^{[2,\mathrm{III}]} \tag{A.24}$$

$$\begin{aligned}(\tilde{\boldsymbol{a}}^{pr}_{qs} \tilde{\boldsymbol{a}}^{tv}_{uw})^{[2,\mathrm{I}]} :=& + (\bar{\gamma}^t_q \bar{\gamma}^v_s - \bar{\gamma}^t_s \bar{\gamma}^v_q + \lambda^{tv}_{qs}) \tilde{\boldsymbol{a}}^{pr}_{uw} \\ &+ (\gamma^p_u \gamma^r_w - \gamma^p_w \gamma^r_u + \lambda^{pr}_{uw}) \tilde{\boldsymbol{a}}^{tv}_{qs} \end{aligned} \tag{A.25}$$

$$\begin{aligned}(\tilde{\boldsymbol{a}}^{pr}_{qs} \tilde{\boldsymbol{a}}^{tv}_{uw})^{[2,\mathrm{II}]} :=& + (\gamma^p_w \bar{\gamma}^v_q + \lambda^{pv}_{qw}) \tilde{\boldsymbol{a}}^{rt}_{su} + (\gamma^p_u \bar{\gamma}^t_q + \lambda^{pt}_{qu}) \tilde{\boldsymbol{a}}^{rv}_{sw} \\ &+ (\gamma^p_u \bar{\gamma}^v_s + \lambda^{pv}_{su}) \tilde{\boldsymbol{a}}^{rt}_{qw} + (\gamma^p_w \bar{\gamma}^t_s + \lambda^{pt}_{sw}) \tilde{\boldsymbol{a}}^{rv}_{qu} \\ &+ (\gamma^r_w \bar{\gamma}^v_s + \lambda^{rv}_{sw}) \tilde{\boldsymbol{a}}^{pt}_{qu} + (\gamma^r_u \bar{\gamma}^t_s + \lambda^{rt}_{su}) \tilde{\boldsymbol{a}}^{pv}_{qw} \\ &+ (\gamma^r_u \bar{\gamma}^v_q + \lambda^{rv}_{qu}) \tilde{\boldsymbol{a}}^{pt}_{sw} + (\gamma^r_w \bar{\gamma}^t_q + \lambda^{rt}_{qw}) \tilde{\boldsymbol{a}}^{pv}_{su} \\ &- (\gamma^p_u \bar{\gamma}^v_q + \lambda^{pv}_{qu}) \tilde{\boldsymbol{a}}^{rt}_{sw} - (\gamma^p_w \bar{\gamma}^t_q + \lambda^{pt}_{qw}) \tilde{\boldsymbol{a}}^{rv}_{su} \\ &- (\gamma^p_w \bar{\gamma}^v_s + \lambda^{pv}_{sw}) \tilde{\boldsymbol{a}}^{rt}_{qu} - (\gamma^p_u \bar{\gamma}^t_s + \lambda^{pt}_{su}) \tilde{\boldsymbol{a}}^{rv}_{qw} \\ &- (\gamma^r_u \bar{\gamma}^v_s + \lambda^{rv}_{su}) \tilde{\boldsymbol{a}}^{pt}_{qw} - (\gamma^r_w \bar{\gamma}^t_s + \lambda^{rt}_{sw}) \tilde{\boldsymbol{a}}^{pv}_{qu} \\ &- (\gamma^r_w \bar{\gamma}^v_q + \lambda^{rv}_{qw}) \tilde{\boldsymbol{a}}^{pt}_{su} - (\gamma^r_u \bar{\gamma}^t_q + \lambda^{rt}_{qu}) \tilde{\boldsymbol{a}}^{pv}_{sw} \end{aligned} \tag{A.26}$$

$$
\begin{aligned}
(\tilde{\boldsymbol{a}}^{pr}_{qs}\tilde{\boldsymbol{a}}^{tv}_{uw})^{[2,\mathrm{III}]} \coloneqq &- \lambda^{tv}_{sw}\tilde{\boldsymbol{a}}^{pr}_{qu} - \lambda^{tv}_{us}\tilde{\boldsymbol{a}}^{pr}_{qw} - \lambda^{tv}_{qw}\tilde{\boldsymbol{a}}^{pr}_{us} - \lambda^{tv}_{uq}\tilde{\boldsymbol{a}}^{pr}_{ws} \\
&- \lambda^{rv}_{uw}\tilde{\boldsymbol{a}}^{pt}_{qs} - \lambda^{rt}_{wu}\tilde{\boldsymbol{a}}^{pv}_{qs} - \lambda^{pv}_{uw}\tilde{\boldsymbol{a}}^{rt}_{qs} - \lambda^{pt}_{wu}\tilde{\boldsymbol{a}}^{rv}_{qs} \\
&- \lambda^{rv}_{sq}\tilde{\boldsymbol{a}}^{tp}_{uw} - \lambda^{rt}_{sq}\tilde{\boldsymbol{a}}^{pv}_{uw} - \lambda^{pv}_{qs}\tilde{\boldsymbol{a}}^{tr}_{uw} - \lambda^{pt}_{qs}\tilde{\boldsymbol{a}}^{rv}_{uw} \\
&- \lambda^{pr}_{ws}\tilde{\boldsymbol{a}}^{tv}_{uq} - \lambda^{pr}_{us}\tilde{\boldsymbol{a}}^{tv}_{qw} - \lambda^{pr}_{qw}\tilde{\boldsymbol{a}}^{tv}_{us} - \lambda^{pr}_{qu}\tilde{\boldsymbol{a}}^{tv}_{sw}.
\end{aligned} \tag{A.27}
$$

Analogously, the one-body piece will be separated into

$$
\begin{aligned}
(\tilde{\boldsymbol{a}}^{pr}_{qs}\tilde{\boldsymbol{a}}^{tv}_{uw})^{[1]} \coloneqq &+ (\tilde{\boldsymbol{a}}^{pr}_{qs}\tilde{\boldsymbol{a}}^{tv}_{uw})^{[1,\mathrm{I}]} + (\tilde{\boldsymbol{a}}^{pr}_{qs}\tilde{\boldsymbol{a}}^{tv}_{uw})^{[1,\mathrm{II}]} + (\tilde{\boldsymbol{a}}^{pr}_{qs}\tilde{\boldsymbol{a}}^{tv}_{uw})^{[1,\mathrm{III}]} \\
&+ (\tilde{\boldsymbol{a}}^{pr}_{qs}\tilde{\boldsymbol{a}}^{tv}_{uw})^{[1,\mathrm{IV}]} + (\tilde{\boldsymbol{a}}^{pr}_{qs}\tilde{\boldsymbol{a}}^{tv}_{uw})^{[1,\mathrm{V}]},
\end{aligned} \tag{A.28}
$$

where the subterm IV and V do not contribute to $\left[\boldsymbol{C}^{(2)}, \boldsymbol{D}^{(2)}\right]$ in appendix A.2.3

$$
(\tilde{\boldsymbol{a}}^{pr}_{qs}\tilde{\boldsymbol{a}}^{tv}_{uw})^{[1,\mathrm{I}]} \coloneqq \bar{\gamma}^{tv}_{qs}\mathbb{A}(\gamma^{r}_{w}\tilde{\boldsymbol{a}}^{p}_{u}) + \gamma^{pr}_{uw}\mathbb{A}(\bar{\gamma}^{t}_{s}\tilde{\boldsymbol{a}}^{v}_{q}) \tag{A.29}
$$

with two-hole and two-particle density matrix elements $\bar{\gamma}^{tv}_{qs}$ and γ^{pr}_{uw}, respectively. The other terms are

$$
\begin{aligned}
(\tilde{\boldsymbol{a}}^{pr}_{qs}\tilde{\boldsymbol{a}}^{tv}_{uw})^{[1,\mathrm{II}]} \coloneqq &+ (+\bar{\gamma}^{v}_{s}\lambda^{rt}_{qw} + \bar{\gamma}^{t}_{q}\lambda^{rv}_{sw} - \bar{\gamma}^{v}_{q}\lambda^{rt}_{sw} - \bar{\gamma}^{t}_{s}\lambda^{rv}_{qw})\tilde{\boldsymbol{a}}^{p}_{u} \\
&+ (-\bar{\gamma}^{v}_{s}\lambda^{rt}_{qu} - \bar{\gamma}^{t}_{q}\lambda^{rv}_{su} + \bar{\gamma}^{v}_{q}\lambda^{rt}_{su} + \bar{\gamma}^{t}_{s}\lambda^{rv}_{qu})\tilde{\boldsymbol{a}}^{p}_{w} \\
&+ (-\bar{\gamma}^{v}_{s}\lambda^{pt}_{qw} - \bar{\gamma}^{t}_{q}\lambda^{pv}_{sw} + \bar{\gamma}^{v}_{q}\lambda^{pt}_{sw} + \bar{\gamma}^{t}_{s}\lambda^{pv}_{qw})\tilde{\boldsymbol{a}}^{r}_{u} \\
&+ (+\bar{\gamma}^{v}_{s}\lambda^{pt}_{qu} + \bar{\gamma}^{t}_{q}\lambda^{pv}_{su} - \bar{\gamma}^{v}_{q}\lambda^{pt}_{su} - \bar{\gamma}^{t}_{s}\lambda^{pv}_{qu})\tilde{\boldsymbol{a}}^{r}_{w} \\
&+ (+\gamma^{r}_{u}\lambda^{pv}_{sw} + \gamma^{p}_{w}\lambda^{rv}_{su} - \gamma^{r}_{w}\lambda^{pv}_{su} - \gamma^{p}_{u}\lambda^{rv}_{sw})\tilde{\boldsymbol{a}}^{t}_{q} \\
&+ (-\gamma^{r}_{u}\lambda^{pv}_{qw} - \gamma^{p}_{w}\lambda^{rv}_{qu} + \gamma^{r}_{w}\lambda^{pv}_{qu} + \gamma^{p}_{u}\lambda^{rv}_{qw})\tilde{\boldsymbol{a}}^{t}_{s} \\
&+ (-\gamma^{r}_{u}\lambda^{pt}_{sw} - \gamma^{p}_{w}\lambda^{rt}_{su} + \gamma^{r}_{w}\lambda^{pt}_{su} + \gamma^{p}_{u}\lambda^{rt}_{sw})\tilde{\boldsymbol{a}}^{v}_{q} \\
&+ (+\gamma^{r}_{u}\lambda^{pt}_{qw} + \gamma^{p}_{w}\lambda^{rt}_{qu} - \gamma^{r}_{w}\lambda^{pt}_{qu} - \gamma^{p}_{u}\lambda^{rt}_{qw})\tilde{\boldsymbol{a}}^{v}_{s}
\end{aligned} \tag{A.30}
$$

$$
\begin{aligned}
(\tilde{\boldsymbol{a}}^{pr}_{qs}\tilde{\boldsymbol{a}}^{tv}_{uw})^{[1,\mathrm{III}]} \coloneqq &+ (\bar{\gamma}^{t}_{s}\lambda^{vr}_{wu} + \bar{\gamma}^{v}_{s}\lambda^{tr}_{uw})\tilde{\boldsymbol{a}}^{p}_{q} + (\bar{\gamma}^{t}_{q}\lambda^{vp}_{wu} + \bar{\gamma}^{v}_{q}\lambda^{tp}_{uw})\tilde{\boldsymbol{a}}^{r}_{s} \\
&- (\bar{\gamma}^{t}_{q}\lambda^{vr}_{wu} + \bar{\gamma}^{v}_{q}\lambda^{tr}_{uw})\tilde{\boldsymbol{a}}^{p}_{s} - (\bar{\gamma}^{t}_{s}\lambda^{vp}_{wu} + \bar{\gamma}^{v}_{s}\lambda^{tp}_{uw})\tilde{\boldsymbol{a}}^{r}_{q} \\
&+ (\gamma^{p}_{u}\lambda^{rv}_{sq} + \gamma^{r}_{u}\lambda^{pv}_{qs})\tilde{\boldsymbol{a}}^{t}_{w} + (\gamma^{p}_{w}\lambda^{rt}_{sq} + \gamma^{r}_{w}\lambda^{pt}_{qs})\tilde{\boldsymbol{a}}^{v}_{u} \\
&- (\gamma^{p}_{w}\lambda^{rv}_{sq} + \gamma^{r}_{w}\lambda^{pv}_{qs})\tilde{\boldsymbol{a}}^{t}_{u} - (\gamma^{p}_{u}\lambda^{rt}_{sq} + \gamma^{r}_{u}\lambda^{pt}_{qs})\tilde{\boldsymbol{a}}^{v}_{w} \\
&+ (\bar{\gamma}^{v}_{q}\lambda^{rp}_{sw} + \bar{\gamma}^{v}_{s}\lambda^{pr}_{qw})\tilde{\boldsymbol{a}}^{t}_{u} + (\bar{\gamma}^{t}_{q}\lambda^{rp}_{su} + \bar{\gamma}^{t}_{s}\lambda^{pr}_{qu})\tilde{\boldsymbol{a}}^{v}_{w} \\
&- (\bar{\gamma}^{t}_{q}\lambda^{rp}_{sw} + \bar{\gamma}^{t}_{s}\lambda^{pr}_{qw})\tilde{\boldsymbol{a}}^{v}_{u} - (\bar{\gamma}^{v}_{q}\lambda^{rp}_{su} + \bar{\gamma}^{v}_{s}\lambda^{pr}_{qu})\tilde{\boldsymbol{a}}^{t}_{w} \\
&+ (\gamma^{p}_{u}\lambda^{vt}_{ws} + \gamma^{p}_{w}\lambda^{tv}_{us})\tilde{\boldsymbol{a}}^{r}_{q} + (\gamma^{r}_{u}\lambda^{vt}_{wq} + \gamma^{r}_{w}\lambda^{tv}_{uq})\tilde{\boldsymbol{a}}^{p}_{s} \\
&- (\gamma^{r}_{u}\lambda^{vt}_{ws} + \gamma^{r}_{w}\lambda^{tv}_{us})\tilde{\boldsymbol{a}}^{p}_{q} - (\gamma^{p}_{u}\lambda^{vt}_{wq} + \gamma^{p}_{w}\lambda^{tv}_{uq})\tilde{\boldsymbol{a}}^{r}_{s}
\end{aligned} \tag{A.31}
$$

$$
\begin{aligned}
(\tilde{\boldsymbol{a}}^{pr}_{qs}\tilde{\boldsymbol{a}}^{tv}_{uw})^{[1,\mathrm{IV}]} \coloneqq &- \lambda^{rtv}_{sqw}\tilde{\boldsymbol{a}}^{p}_{u} - \lambda^{rtv}_{suq}\tilde{\boldsymbol{a}}^{p}_{w} - \lambda^{ptv}_{qsw}\tilde{\boldsymbol{a}}^{r}_{u} - \lambda^{pvt}_{qsu}\tilde{\boldsymbol{a}}^{r}_{w} \\
&- \lambda^{prv}_{usw}\tilde{\boldsymbol{a}}^{t}_{q} - \lambda^{prv}_{quw}\tilde{\boldsymbol{a}}^{t}_{s} - \lambda^{prt}_{wsu}\tilde{\boldsymbol{a}}^{v}_{q} - \lambda^{prt}_{qwu}\tilde{\boldsymbol{a}}^{v}_{s}
\end{aligned} \tag{A.32}
$$

$$
\begin{aligned}
(\tilde{\boldsymbol{a}}^{pr}_{qs}\tilde{\boldsymbol{a}}^{tv}_{uw})^{[1,\mathrm{V}]} \coloneqq &- \lambda^{tvp}_{uws}\tilde{\boldsymbol{a}}^{r}_{q} - \lambda^{tvp}_{uwq}\tilde{\boldsymbol{a}}^{p}_{s} + \lambda^{rtv}_{suw}\tilde{\boldsymbol{a}}^{p}_{q} + \lambda^{ptv}_{quw}\tilde{\boldsymbol{a}}^{r}_{s} \\
&- \lambda^{prt}_{qsw}\tilde{\boldsymbol{a}}^{v}_{u} - \lambda^{prv}_{qsu}\tilde{\boldsymbol{a}}^{t}_{w} + \lambda^{prv}_{qsw}\tilde{\boldsymbol{a}}^{t}_{u} + \lambda^{prt}_{qsu}\tilde{\boldsymbol{a}}^{v}_{w}.
\end{aligned} \tag{A.33}
$$

The zero-body piece is separated in

$$\begin{aligned}(\tilde{\boldsymbol{a}}^{pr}_{qs}\tilde{\boldsymbol{a}}^{tv}_{uw})^{[0]} :=& + (\tilde{\boldsymbol{a}}^{pr}_{qs}\tilde{\boldsymbol{a}}^{tv}_{uw})^{[0,\mathrm{I}]} + (\tilde{\boldsymbol{a}}^{pr}_{qs}\tilde{\boldsymbol{a}}^{tv}_{uw})^{[0,\mathrm{II}]} + (\tilde{\boldsymbol{a}}^{pr}_{qs}\tilde{\boldsymbol{a}}^{tv}_{uw})^{[0,\mathrm{III}]} \\ &+ (\tilde{\boldsymbol{a}}^{pr}_{qs}\tilde{\boldsymbol{a}}^{tv}_{uw})^{[0,\mathrm{IV}]} + (\tilde{\boldsymbol{a}}^{pr}_{qs}\tilde{\boldsymbol{a}}^{tv}_{uw})^{[0,\mathrm{V}]} + (\tilde{\boldsymbol{a}}^{pr}_{qs}\tilde{\boldsymbol{a}}^{tv}_{uw})^{[0,\mathrm{VI}]} \end{aligned} \tag{A.34}$$

where the subterms III, IV and VI do not contribute to the commutator of $[\boldsymbol{C}^{(2)}, \boldsymbol{D}^{(2)}]$. The subterms read

$$(\tilde{\boldsymbol{a}}^{pr}_{qs}\tilde{\boldsymbol{a}}^{tv}_{uw})^{[0,\mathrm{I}]} := + \gamma^p_u\gamma^r_w\bar{\gamma}^t_q\bar{\gamma}^v_s + \gamma^p_w\gamma^r_u\bar{\gamma}^v_q\bar{\gamma}^t_s - \gamma^p_w\gamma^r_u\bar{\gamma}^t_q\bar{\gamma}^v_s - \gamma^p_u\gamma^r_w\bar{\gamma}^t_s\bar{\gamma}^v_q \tag{A.35}$$

$$\begin{aligned}(\tilde{\boldsymbol{a}}^{pr}_{qs}\tilde{\boldsymbol{a}}^{tv}_{uw})^{[0,\mathrm{II}]} :=& + \gamma^p_u\bar{\gamma}^t_q\lambda^{rv}_{sw} + \gamma^r_w\bar{\gamma}^v_s\lambda^{pt}_{qu} + \gamma^p_w\bar{\gamma}^v_q\lambda^{rt}_{su} + \gamma^r_u\bar{\gamma}^t_s\lambda^{pv}_{qw} \\ &- \gamma^p_w\bar{\gamma}^t_q\lambda^{rv}_{su} - \gamma^r_u\bar{\gamma}^v_s\lambda^{pt}_{qw} - \gamma^p_w\bar{\gamma}^v_s\lambda^{tr}_{uq} - \gamma^r_u\bar{\gamma}^t_q\lambda^{vp}_{ws} \\ &- \gamma^p_u\bar{\gamma}^v_q\lambda^{rt}_{sw} - \gamma^r_w\bar{\gamma}^t_s\lambda^{pv}_{qu} - \gamma^r_w\bar{\gamma}^v_q\lambda^{tp}_{us} - \gamma^p_u\bar{\gamma}^t_s\lambda^{vr}_{wq} \\ &- \gamma^r_w\bar{\gamma}^t_q\lambda^{pv}_{us} - \gamma^r_u\bar{\gamma}^v_q\lambda^{pt}_{ws} - \gamma^p_u\bar{\gamma}^v_s\lambda^{tr}_{qw} - \gamma^p_w\bar{\gamma}^t_s\lambda^{rv}_{uq} \\ &+ \bar{\gamma}^t_q\bar{\gamma}^v_s\lambda^{pr}_{uw} + \bar{\gamma}^v_q\bar{\gamma}^t_s\lambda^{pr}_{wu} + \gamma^p_u\gamma^r_w\lambda^{tv}_{qs} + \gamma^r_u\gamma^p_w\lambda^{tv}_{sq} \end{aligned} \tag{A.36}$$

$$\begin{aligned}(\tilde{\boldsymbol{a}}^{pr}_{qs}\tilde{\boldsymbol{a}}^{tv}_{uw})^{[0,\mathrm{III}]} :=& + \lambda^{pt}_{qu}\lambda^{rv}_{sw} + \lambda^{pv}_{qw}\lambda^{rt}_{su} \\ &- \lambda^{pt}_{qw}\lambda^{rv}_{su} - \lambda^{pv}_{qu}\lambda^{rt}_{sw} - \lambda^{vp}_{ws}\lambda^{tr}_{uq} - \lambda^{tp}_{us}\lambda^{vr}_{wq} \\ &+ \lambda^{tv}_{qs}\lambda^{pr}_{uw} + \lambda^{tp}_{sw}\lambda^{rv}_{uq} + \lambda^{tr}_{qw}\lambda^{pv}_{us} \end{aligned} \tag{A.37}$$

$$\begin{aligned}(\tilde{\boldsymbol{a}}^{pr}_{qs}\tilde{\boldsymbol{a}}^{tv}_{uw})^{[0,\mathrm{IV}]} :=& - \lambda^{tp}_{uw}\lambda^{rv}_{sq} - \lambda^{tv}_{uq}\lambda^{rp}_{sw} - \lambda^{pt}_{qs}\lambda^{vr}_{wu} - \lambda^{pr}_{qu}\lambda^{vt}_{ws} \\ &- \lambda^{vp}_{wu}\lambda^{rt}_{sq} - \lambda^{vt}_{wq}\lambda^{rp}_{su} - \lambda^{pv}_{qs}\lambda^{tr}_{uw} - \lambda^{pr}_{qw}\lambda^{tv}_{us} \end{aligned} \tag{A.38}$$

$$\begin{aligned}(\tilde{\boldsymbol{a}}^{pr}_{qs}\tilde{\boldsymbol{a}}^{tv}_{uw})^{[0,\mathrm{V}]} :=& + \bar{\gamma}^v_s\lambda^{ptr}_{quw} + \bar{\gamma}^t_s\lambda^{pvr}_{qwu} + \bar{\gamma}^t_q\lambda^{rvp}_{swu} + \bar{\gamma}^v_q\lambda^{rtp}_{suw} \\ &- \gamma^r_w\lambda^{ptv}_{qus} - \gamma^r_u\lambda^{pvt}_{qws} - \gamma^p_u\lambda^{rvt}_{swq} - \gamma^p_w\lambda^{rtv}_{suq} \end{aligned} \tag{A.39}$$

$$(\tilde{\boldsymbol{a}}^{pr}_{qs}\tilde{\boldsymbol{a}}^{tv}_{uw})^{[0,\mathrm{VI}]} := \lambda^{prtv}_{qsuw}. \tag{A.40}$$

A.2. Commutators of Normal-Ordered Operators

A.2.1. Without Contraction

Commutator of 1B and 1B

$$[\tilde{\boldsymbol{a}}^p_q, \tilde{\boldsymbol{a}}^r_s] = \tilde{\boldsymbol{a}}^p_q\tilde{\boldsymbol{a}}^r_s - \tilde{\boldsymbol{a}}^r_s\tilde{\boldsymbol{a}}^p_q \tag{A.41}$$

$$= \tilde{\boldsymbol{a}}^p_q\tilde{\boldsymbol{a}}^r_s - [pq \leftrightarrow rs] \tag{A.42}$$

$$\begin{aligned} =& \quad \tilde{\boldsymbol{a}}^{pr}_{qs} - \gamma^p_s\tilde{\boldsymbol{a}}^r_q + \bar{\gamma}^r_q\tilde{\boldsymbol{a}}^p_s + \gamma^p_s\bar{\gamma}^r_q + \lambda^{pr}_{qs} \\ &- \left(\tilde{\boldsymbol{a}}^{rp}_{sq} - \gamma^r_q\tilde{\boldsymbol{a}}^p_s + \bar{\gamma}^p_s\tilde{\boldsymbol{a}}^r_q + \gamma^r_q\bar{\gamma}^p_s + \lambda^{rp}_{sq}\right) \end{aligned} \tag{A.43}$$

$$= 0 + (\bar{\gamma}^r_q + \gamma^r_q)\tilde{\boldsymbol{a}}^p_s - (\bar{\gamma}^p_s + \gamma^p_s)\tilde{\boldsymbol{a}}^r_q + \gamma^p_s\bar{\gamma}^r_q - \gamma^r_q\bar{\gamma}^p_s + 0 \tag{A.44}$$

$$= \delta^r_q\tilde{\boldsymbol{a}}^p_s - \delta^p_s\tilde{\boldsymbol{a}}^r_q + \delta^r_q\gamma^p_s - \delta^p_s\gamma^r_q \tag{A.45}$$

Commutator of 2B and 1B

Defining

$$\left(\left[\tilde{\boldsymbol{a}}^{pr}_{qs}, \tilde{\boldsymbol{a}}^{t}_{u}\right]\right)^{[i]} \coloneqq \left(\tilde{\boldsymbol{a}}^{pr}_{qs}\tilde{\boldsymbol{a}}^{t}_{u}\right)^{[i]} - \left(\tilde{\boldsymbol{a}}^{t}_{u}\tilde{\boldsymbol{a}}^{pr}_{qs}\right)^{[i]} \tag{A.46}$$

we can write

$$\begin{aligned}
\left[\tilde{\boldsymbol{a}}^{pr}_{qs}, \tilde{\boldsymbol{a}}^{t}_{u}\right] =& \tilde{\boldsymbol{a}}^{pr}_{qs}\tilde{\boldsymbol{a}}^{t}_{u} - \tilde{\boldsymbol{a}}^{t}_{u}\tilde{\boldsymbol{a}}^{pr}_{qs} && \text{(A.47)}\\
=& \left(\left[\tilde{\boldsymbol{a}}^{pr}_{qs}, \tilde{\boldsymbol{a}}^{t}_{u}\right]\right)^{[2]} + \left(\left[\tilde{\boldsymbol{a}}^{pr}_{qs}, \tilde{\boldsymbol{a}}^{t}_{u}\right]\right)^{[1]} + \left(\left[\tilde{\boldsymbol{a}}^{pr}_{qs}, \tilde{\boldsymbol{a}}^{t}_{u}\right]\right)^{[0]}. && \text{(A.48)}
\end{aligned}$$

We obtain

$$\begin{aligned}
\left(\left[\tilde{\boldsymbol{a}}^{pr}_{qs}, \tilde{\boldsymbol{a}}^{t}_{u}\right]\right)^{[2]} =& + \bar{\gamma}^{t}_{q}\tilde{\boldsymbol{a}}^{pr}_{us} + \bar{\gamma}^{t}_{s}\tilde{\boldsymbol{a}}^{pr}_{qu} - \gamma^{p}_{u}\tilde{\boldsymbol{a}}^{tr}_{qs} - \gamma^{r}_{u}\tilde{\boldsymbol{a}}^{pt}_{qs}\\
& - \left(\bar{\gamma}^{p}_{u}\tilde{\boldsymbol{a}}^{tr}_{qs} + \bar{\gamma}^{r}_{u}\tilde{\boldsymbol{a}}^{pt}_{qs} - \gamma^{t}_{q}\tilde{\boldsymbol{a}}^{pr}_{us} - \gamma^{t}_{s}\tilde{\boldsymbol{a}}^{pr}_{qu}\right) && \text{(A.49)}\\
=& (\bar{\gamma}^{t}_{q} + \gamma^{t}_{q})\tilde{\boldsymbol{a}}^{pr}_{us} + (\bar{\gamma}^{t}_{s} + \gamma^{t}_{s})\tilde{\boldsymbol{a}}^{pr}_{qu} - (\gamma^{p}_{u} + \bar{\gamma}^{p}_{u})\tilde{\boldsymbol{a}}^{tr}_{qs} - (\gamma^{r}_{u} + \bar{\gamma}^{r}_{u})\tilde{\boldsymbol{a}}^{pt}_{qs} && \text{(A.50)}\\
=& \delta^{t}_{q}\tilde{\boldsymbol{a}}^{pr}_{us} + \delta^{t}_{s}\tilde{\boldsymbol{a}}^{pr}_{qu} - \delta^{p}_{u}\tilde{\boldsymbol{a}}^{tr}_{qs} - \delta^{r}_{u}\tilde{\boldsymbol{a}}^{pt}_{qs} && \text{(A.51)}\\
\left(\left[\tilde{\boldsymbol{a}}^{pr}_{qs}, \tilde{\boldsymbol{a}}^{t}_{u}\right]\right)^{[1]} =& + (\bar{\gamma}^{t}_{s}\gamma^{r}_{u} + \lambda^{rt}_{su})\tilde{\boldsymbol{a}}^{p}_{q} - (\bar{\gamma}^{t}_{s}\gamma^{p}_{u} + \lambda^{pt}_{su})\tilde{\boldsymbol{a}}^{r}_{q}\\
& + (\bar{\gamma}^{t}_{q}\gamma^{p}_{u} + \lambda^{pt}_{qu})\tilde{\boldsymbol{a}}^{r}_{s} - (\bar{\gamma}^{t}_{q}\gamma^{r}_{u} + \lambda^{rt}_{qu})\tilde{\boldsymbol{a}}^{p}_{s}\\
& - \lambda^{rt}_{sq}\tilde{\boldsymbol{a}}^{p}_{u} - \lambda^{pt}_{qs}\tilde{\boldsymbol{a}}^{r}_{u} - \lambda^{pr}_{us}\tilde{\boldsymbol{a}}^{t}_{q} - \lambda^{pr}_{qu}\tilde{\boldsymbol{a}}^{t}_{s}\\
& - \Big(+ (\gamma^{t}_{s}\bar{\gamma}^{r}_{u} + \lambda^{rt}_{su})\tilde{\boldsymbol{a}}^{p}_{q} - (\gamma^{t}_{s}\bar{\gamma}^{p}_{u} + \lambda^{pt}_{su})\tilde{\boldsymbol{a}}^{r}_{q}\\
& + (\gamma^{t}_{q}\bar{\gamma}^{p}_{u} + \lambda^{pt}_{qu})\tilde{\boldsymbol{a}}^{r}_{s} - (\gamma^{t}_{q}\bar{\gamma}^{r}_{u} + \lambda^{rt}_{qu})\tilde{\boldsymbol{a}}^{p}_{s}\\
& - \lambda^{rt}_{sq}\tilde{\boldsymbol{a}}^{p}_{u} - \lambda^{pt}_{qs}\tilde{\boldsymbol{a}}^{r}_{u} - \lambda^{pr}_{us}\tilde{\boldsymbol{a}}^{t}_{q} - \lambda^{pr}_{qu}\tilde{\boldsymbol{a}}^{t}_{s}\Big) && \text{(A.52)}\\
=& + (\bar{\gamma}^{t}_{s}\gamma^{r}_{u} - \gamma^{t}_{s}\bar{\gamma}^{r}_{u})\tilde{\boldsymbol{a}}^{p}_{q} - (\bar{\gamma}^{t}_{s}\gamma^{p}_{u} - \gamma^{t}_{s}\bar{\gamma}^{p}_{u})\tilde{\boldsymbol{a}}^{r}_{q}\\
& + (\bar{\gamma}^{t}_{q}\gamma^{p}_{u} - \gamma^{t}_{q}\bar{\gamma}^{p}_{u})\tilde{\boldsymbol{a}}^{r}_{s} - (\bar{\gamma}^{t}_{q}\gamma^{r}_{u} - \gamma^{t}_{q}\bar{\gamma}^{r}_{u})\tilde{\boldsymbol{a}}^{p}_{s} && \text{(A.53)}\\
=& + (\delta^{t}_{s}\gamma^{r}_{u} - \gamma^{t}_{s}\delta^{r}_{u})\tilde{\boldsymbol{a}}^{p}_{q} - (\delta^{t}_{s}\gamma^{p}_{u} - \gamma^{t}_{s}\delta^{p}_{u})\tilde{\boldsymbol{a}}^{r}_{q}\\
& + (\delta^{t}_{q}\gamma^{p}_{u} - \gamma^{t}_{q}\delta^{p}_{u})\tilde{\boldsymbol{a}}^{r}_{s} - (\delta^{t}_{q}\gamma^{r}_{u} - \gamma^{t}_{q}\delta^{r}_{u})\tilde{\boldsymbol{a}}^{p}_{s} && \text{(A.54)}\\
\left(\left[\tilde{\boldsymbol{a}}^{pr}_{qs}, \tilde{\boldsymbol{a}}^{t}_{u}\right]\right)^{[0]} =& \quad + \bar{\gamma}^{t}_{q}\lambda^{pr}_{us} + \bar{\gamma}^{t}_{s}\lambda^{pr}_{qu} - \gamma^{p}_{u}\lambda^{rt}_{sq} - \gamma^{r}_{u}\lambda^{pt}_{qs} + \lambda^{prt}_{qsu}\\
& - (-\gamma^{t}_{q}\lambda^{pr}_{us} - \gamma^{t}_{s}\lambda^{pr}_{qu} + \bar{\gamma}^{p}_{u}\lambda^{rt}_{sq} + \bar{\gamma}^{r}_{u}\lambda^{pt}_{qs} + \lambda^{tpr}_{uqs}) && \text{(A.55)}\\
=& (\bar{\gamma}^{t}_{q} + \gamma^{t}_{q})\lambda^{pr}_{us} + (\bar{\gamma}^{t}_{s} + \gamma^{t}_{s})\lambda^{pr}_{qu} - (\gamma^{p}_{u} + \bar{\gamma}^{p}_{u})\lambda^{rt}_{sq} - (\gamma^{r}_{u} + \bar{\gamma}^{r}_{u})\lambda^{pt}_{qs} && \text{(A.56)}\\
=& \delta^{t}_{q}\lambda^{pr}_{us} + \delta^{t}_{s}\lambda^{pr}_{qu} - \delta^{p}_{u}\lambda^{rt}_{sq} - \delta^{r}_{u}\lambda^{pt}_{qs}. && \text{(A.57)}
\end{aligned}$$

Finally, we obtain

$$\begin{aligned}[\tilde{\boldsymbol{a}}^{pr}_{qs}, \tilde{\boldsymbol{a}}^{t}_{u}] = &+ \delta^t_q \tilde{\boldsymbol{a}}^{pr}_{us} + \delta^t_s \tilde{\boldsymbol{a}}^{pr}_{qu} - \delta^p_u \tilde{\boldsymbol{a}}^{tr}_{qs} - \delta^r_u \tilde{\boldsymbol{a}}^{pt}_{qs} \\ &+ (\delta^t_s \gamma^r_u - \gamma^t_s \delta^r_u) \tilde{\boldsymbol{a}}^{p}_{q} - (\delta^t_s \gamma^p_u - \gamma^t_s \delta^p_u) \tilde{\boldsymbol{a}}^{r}_{q} \\ &+ (\delta^t_q \gamma^p_u - \gamma^t_q \delta^p_u) \tilde{\boldsymbol{a}}^{r}_{s} - (\delta^t_q \gamma^r_u - \gamma^t_q \delta^r_u) \tilde{\boldsymbol{a}}^{p}_{s} \\ &+ \delta^t_q \lambda^{pr}_{us} + \delta^t_s \lambda^{pr}_{qu} - \delta^p_u \lambda^{rt}_{sq} - \delta^r_u \lambda^{pt}_{qs}. \end{aligned} \tag{A.58}$$

Commutator of 1B and 2B

Making use of the antisymmetry of the commutator, we find

$$[\tilde{\boldsymbol{a}}^{t}_{u}, \tilde{\boldsymbol{a}}^{pr}_{qs}] = - [\tilde{\boldsymbol{a}}^{pr}_{qs}, \tilde{\boldsymbol{a}}^{t}_{u}] \tag{A.59}$$

$$\begin{aligned} = &- \delta^t_q \tilde{\boldsymbol{a}}^{pr}_{us} - \delta^t_s \tilde{\boldsymbol{a}}^{pr}_{qu} + \delta^p_u \tilde{\boldsymbol{a}}^{tr}_{qs} + \delta^r_u \tilde{\boldsymbol{a}}^{pt}_{qs} \\ &- (\delta^t_s \gamma^r_u - \gamma^t_s \delta^r_u) \tilde{\boldsymbol{a}}^{p}_{q} + (\delta^t_s \gamma^p_u - \gamma^t_s \delta^p_u) \tilde{\boldsymbol{a}}^{r}_{q} \\ &- (\delta^t_q \gamma^p_u - \gamma^t_q \delta^p_u) \tilde{\boldsymbol{a}}^{r}_{s} + (\delta^t_q \gamma^r_u - \gamma^t_q \delta^r_u) \tilde{\boldsymbol{a}}^{p}_{s} \\ &- \delta^t_q \lambda^{pr}_{us} - \delta^t_s \lambda^{pr}_{qu} + \delta^p_u \lambda^{rt}_{sq} + \delta^r_u \lambda^{pt}_{qs}. \end{aligned} \tag{A.60}$$

Commutator of 2B and 2B

In principle, this commutator can be derived using the result obtained above

$$\begin{aligned}[\tilde{\boldsymbol{a}}^{pr}_{qs}, \tilde{\boldsymbol{a}}^{tv}_{uw}] &= \sum_{i=0}^{3} \left([\tilde{\boldsymbol{a}}^{pr}_{qs}, \tilde{\boldsymbol{a}}^{tv}_{uw}] \right)^{[i]} \\ &= \sum_{i=0}^{3} (\tilde{\boldsymbol{a}}^{pr}_{qs} \tilde{\boldsymbol{a}}^{tv}_{uw})^{[i]} - [prqs \leftrightarrow tvuw], \end{aligned} \tag{A.61}$$

but we won't write it out completely because of the large number of terms.

A.2.2. Partially Contracted

Let's define the operators

$$\boldsymbol{A}^{(1)} \coloneqq \sum_{\substack{p \\ q}} A^p_q \tilde{\boldsymbol{a}}^p_q \tag{A.62}$$

$$\boldsymbol{B}^{(1)} \coloneqq \sum_{\substack{r \\ s}} B^r_s \tilde{\boldsymbol{a}}^r_s \tag{A.63}$$

$$\boldsymbol{C}^{(2)} \coloneqq \sum_{\substack{pr \\ qs}} C^{pr}_{qs} \tilde{\boldsymbol{a}}^{pr}_{qs} \tag{A.64}$$

$$\boldsymbol{D}^{(2)} \coloneqq \sum_{\substack{tv \\ uw}} D^{tv}_{uw} \tilde{\boldsymbol{a}}^{tv}_{uw} \tag{A.65}$$

that do not necessarily have to be Hermitian or anti-Hermitian. Matrix elements of the two-body operators C^{pr}_{qs} and D^{pr}_{qs} are assumed to be antisymmetric with respect to exchange

among the upper and lower indices, respectively, i.e.

$$C^{pr}_{qs} = -C^{rp}_{qs} = -C^{pr}_{sq} = +C^{rp}_{sq} \tag{A.66}$$

$$D^{pr}_{qs} = -D^{rp}_{qs} = -D^{pr}_{sq} = +D^{rp}_{sq} \tag{A.67}$$

Commutator of 1B and 1B—Partially Contracted

$$[\boldsymbol{A}^{(1)}, \tilde{\boldsymbol{a}}^r_s] = \sum_{\substack{p\\q}} A^p_q [\tilde{\boldsymbol{a}}^p_q, \tilde{\boldsymbol{a}}^r_s] \tag{A.68}$$

$$= \sum_{\substack{p\\q}} A^p_q (\delta^r_q \tilde{\boldsymbol{a}}^p_s - \delta^p_s \tilde{\boldsymbol{a}}^r_q + \delta^r_q \gamma^p_s - \delta^p_s \gamma^r_q) \tag{A.69}$$

$$= \sum_p A^p_r \tilde{\boldsymbol{a}}^p_s - \sum_q A^s_q \tilde{\boldsymbol{a}}^r_q + \sum_p A^p_r \gamma^p_s - \sum_q A^s_q \gamma^r_q \tag{A.70}$$

Commutator of 1B and 2B—Partially Contracted

$$([\tilde{\boldsymbol{a}}^p_q, \tilde{\boldsymbol{a}}^{rt}_{su}])^{[2]} = -\delta^p_s \tilde{\boldsymbol{a}}^{rt}_{qu} - \delta^p_u \tilde{\boldsymbol{a}}^{rt}_{sq} + \delta^r_q \tilde{\boldsymbol{a}}^{pt}_{su} + \delta^t_q \tilde{\boldsymbol{a}}^{rp}_{su} \tag{A.71}$$

$$\begin{aligned}([\tilde{\boldsymbol{a}}^p_q, \tilde{\boldsymbol{a}}^{rt}_{su}])^{[1]} = &-(\delta^p_u \gamma^t_q - \gamma^p_u \delta^t_q)\tilde{\boldsymbol{a}}^r_s + (\delta^p_u \gamma^r_q - \gamma^p_u \delta^r_q)\tilde{\boldsymbol{a}}^t_s \\ &-(\delta^p_s \gamma^r_q - \gamma^p_s \delta^r_q)\tilde{\boldsymbol{a}}^t_u + (\delta^p_s \gamma^t_q - \gamma^p_s \delta^t_q)\tilde{\boldsymbol{a}}^r_u\end{aligned} \tag{A.72}$$

$$([\tilde{\boldsymbol{a}}^p_q, \tilde{\boldsymbol{a}}^{rt}_{su}])^{[0]} = -\delta^p_s \lambda^{rt}_{qu} - \delta^p_u \lambda^{rt}_{sq} + \delta^r_q \lambda^{tp}_{us} + \delta^t_q \lambda^{rp}_{su} \tag{A.73}$$

$$\begin{aligned}\sum_{\substack{p\\q}} A^p_q ([\tilde{\boldsymbol{a}}^p_q, \tilde{\boldsymbol{a}}^{rt}_{su}])^{[2]} &= \sum_{\substack{p\\q}} A^p_q \left(-\delta^p_s \tilde{\boldsymbol{a}}^{rt}_{qu} - \delta^p_u \tilde{\boldsymbol{a}}^{rt}_{sq} + \delta^r_q \tilde{\boldsymbol{a}}^{pt}_{su} + \delta^t_q \tilde{\boldsymbol{a}}^{rp}_{su}\right) \\ &= -\sum_q (A^s_q \tilde{\boldsymbol{a}}^{rt}_{qu} + A^u_q \tilde{\boldsymbol{a}}^{rt}_{sq}) + \sum_p (A^p_r \tilde{\boldsymbol{a}}^{pt}_{su} + A^p_t \tilde{\boldsymbol{a}}^{rp}_{su})\end{aligned} \tag{A.74}$$

$$\begin{aligned}\sum_{\substack{p\\q}} A^p_q ([\tilde{\boldsymbol{a}}^p_q, \tilde{\boldsymbol{a}}^{rt}_{su}])^{[1]} = \sum_{\substack{p\\q}} A^p_q \Big(&-(\delta^p_u \gamma^t_q - \gamma^p_u \delta^t_q)\tilde{\boldsymbol{a}}^r_s + (\delta^p_u \gamma^r_q - \gamma^p_u \delta^r_q)\tilde{\boldsymbol{a}}^t_s \\ &-(\delta^p_s \gamma^r_q - \gamma^p_s \delta^r_q)\tilde{\boldsymbol{a}}^t_u + (\delta^p_s \gamma^t_q - \gamma^p_s \delta^t_q)\tilde{\boldsymbol{a}}^r_u\Big)\end{aligned} \tag{A.75}$$

$$\begin{aligned}= &-\left(\sum_q A^u_q \gamma^t_q - \sum_p A^p_t \gamma^p_u\right)\tilde{\boldsymbol{a}}^r_s + \left(\sum_q A^u_q \gamma^r_q - \sum_p A^p_r \gamma^p_u\right)\tilde{\boldsymbol{a}}^t_s \\ &-\left(\sum_q A^s_q \gamma^r_q - \sum_p A^p_r \gamma^p_s\right)\tilde{\boldsymbol{a}}^t_u + \left(\sum_q A^s_q \gamma^t_q - \sum_p A^p_t \gamma^p_s\right)\tilde{\boldsymbol{a}}^r_u\end{aligned} \tag{A.76}$$

$$\sum_{\substack{p\\q}} A_q^p([\tilde{\boldsymbol{a}}_q^p, \tilde{\boldsymbol{a}}_{su}^{rt}])^{[0]} = \sum_{\substack{p\\q}} A_q^p \left(-\delta_s^p \lambda_{qu}^{rt} - \delta_u^p \lambda_{sq}^{rt} + \delta_q^r \lambda_{us}^{tp} + \delta_q^t \lambda_{su}^{rp}\right) \tag{A.77}$$

$$= -\sum_q (A_q^s \lambda_{qu}^{rt} + A_q^u \lambda_{sq}^{rt}) + \sum_p (A_r^p \lambda_{us}^{tp} + A_t^p \lambda_{su}^{rp}) \tag{A.78}$$

Finally, we obtain

$$[\boldsymbol{A}^{(1)}, \tilde{\boldsymbol{a}}_{su}^{rt}] = \sum_{\substack{p\\q}} A_q^p [\tilde{\boldsymbol{a}}_q^p, \tilde{\boldsymbol{a}}_{su}^{rt}] \tag{A.79}$$

$$\begin{aligned} &= -\sum_q (A_q^s \tilde{\boldsymbol{a}}_{qu}^{rt} + A_q^u \tilde{\boldsymbol{a}}_{sq}^{rt}) + \sum_p (A_r^p \tilde{\boldsymbol{a}}_{su}^{pt} + A_t^p \tilde{\boldsymbol{a}}_{su}^{rp}) \\ &\quad - \left(\sum_q A_q^u \gamma_q^t - \sum_p A_t^p \gamma_u^p\right) \tilde{\boldsymbol{a}}_s^r + \left(\sum_q A_q^u \gamma_q^r - \sum_p A_r^p \gamma_u^p\right) \tilde{\boldsymbol{a}}_s^t \\ &\quad - \left(\sum_q A_q^s \gamma_q^r - \sum_p A_r^p \gamma_s^p\right) \tilde{\boldsymbol{a}}_u^t + \left(\sum_q A_q^s \gamma_q^t - \sum_p A_t^p \gamma_s^p\right) \tilde{\boldsymbol{a}}_u^r \\ &\quad - \sum_q (A_q^s \lambda_{qu}^{rt} + A_q^u \lambda_{sq}^{rt}) + \sum_p (A_r^p \lambda_{us}^{tp} + A_t^p \lambda_{su}^{rp}). \end{aligned} \tag{A.80}$$

Commutator of 2B and 1B—Partially Contracted

Let us consider now the commutator between a two-body operator that is a linear combination of normal-ordered two-body operators, and a normal-ordered one-body operator as follows

$$[\boldsymbol{C}^{(2)}, \tilde{\boldsymbol{a}}_u^t] = \frac{1}{4} \sum_{\substack{pr\\qs}} C_{qs}^{pr} [\tilde{\boldsymbol{a}}_{qs}^{pr}, \tilde{\boldsymbol{a}}_u^t] \tag{A.81}$$

$$= +\frac{1}{4} \sum_{\substack{pr\\qs}} C_{qs}^{pr} ([\tilde{\boldsymbol{a}}_{qs}^{pr}, \tilde{\boldsymbol{a}}_u^t])^{[2]} + \frac{1}{4} \sum_{\substack{pr\\qs}} C_{qs}^{pr} ([\tilde{\boldsymbol{a}}_{qs}^{pr}, \tilde{\boldsymbol{a}}_u^t])^{[1]} + \frac{1}{4} \sum_{\substack{pr\\qs}} C_{qs}^{pr} ([\tilde{\boldsymbol{a}}_{qs}^{pr}, \tilde{\boldsymbol{a}}_u^t])^{[0]}. \tag{A.82}$$

The two-body piece is

$$\begin{aligned} \frac{1}{4} \sum_{\substack{pr\\qs}} C_{qs}^{pr} ([\tilde{\boldsymbol{a}}_{qs}^{pr}, \tilde{\boldsymbol{a}}_u^t])^{[2]} &= \frac{1}{4} \sum_{\substack{pr\\qs}} C_{qs}^{pr} \left(\delta_q^t \tilde{\boldsymbol{a}}_{us}^{pr} + \delta_s^t \tilde{\boldsymbol{a}}_{qu}^{pr} - \delta_u^p \tilde{\boldsymbol{a}}_{qs}^{tr} - \delta_u^r \tilde{\boldsymbol{a}}_{qs}^{pt}\right) \\ &= \frac{1}{4} \left(\sum_{\substack{pr\\s}} C_{ts}^{pr} \tilde{\boldsymbol{a}}_{us}^{pr} + \sum_{\substack{pr\\q}} C_{qt}^{pr} \tilde{\boldsymbol{a}}_{qu}^{pr} - \sum_{\substack{r\\qs}} C_{qs}^{ur} \tilde{\boldsymbol{a}}_{qs}^{tr} - \sum_{\substack{p\\qs}} C_{qs}^{pu} \tilde{\boldsymbol{a}}_{qs}^{pt}\right) \\ &= \frac{1}{4} \left(\sum_{\substack{pr\\s}} C_{ts}^{pr} \tilde{\boldsymbol{a}}_{us}^{pr} + \sum_{\substack{pr\\s}} C_{st}^{pr} \tilde{\boldsymbol{a}}_{su}^{pr} - \sum_{\substack{r\\qs}} C_{qs}^{ur} \tilde{\boldsymbol{a}}_{qs}^{tr} - \sum_{\substack{r\\qs}} C_{qs}^{ru} \tilde{\boldsymbol{a}}_{qs}^{rt}\right) \\ &= \frac{1}{2} \left(\sum_{\substack{pr\\s}} C_{ts}^{pr} \tilde{\boldsymbol{a}}_{us}^{pr} - \sum_{\substack{r\\qs}} C_{qs}^{ur} \tilde{\boldsymbol{a}}_{qs}^{tr}\right) \\ &= \frac{1}{2} \sum_{\substack{pr\\q}} \left(C_{tq}^{pr} \tilde{\boldsymbol{a}}_{uq}^{pr} - C_{pr}^{uq} \tilde{\boldsymbol{a}}_{pr}^{tq}\right), \end{aligned} \tag{A.83}$$

the one-body piece reads

$$\frac{1}{4}\sum_{\substack{pr\\qs}} C^{pr}_{qs}([\tilde{\boldsymbol{a}}^{pr}_{qs},\tilde{\boldsymbol{a}}^{t}_{u}])^{[1]} = \frac{1}{4}\sum_{\substack{pr\\qs}} C^{pr}_{qs}\Big(+ (\delta^t_s\gamma^r_u - \gamma^t_s\delta^r_u)\tilde{\boldsymbol{a}}^p_q - (\delta^t_s\gamma^p_u - \gamma^t_s\delta^p_u)\tilde{\boldsymbol{a}}^r_q + (\delta^t_q\gamma^p_u - \gamma^t_q\delta^p_u)\tilde{\boldsymbol{a}}^r_s - (\delta^t_q\gamma^r_u - \gamma^t_q\delta^r_u)\tilde{\boldsymbol{a}}^p_s\Big) \tag{A.84}$$

$$= \frac{1}{4}\Big(+ \sum_{\substack{pr\\qs}} C^{pr}_{qs}(\delta^t_s\gamma^r_u - \gamma^t_s\delta^r_u)\tilde{\boldsymbol{a}}^p_q - \sum_{\substack{pr\\qs}} C^{rp}_{qs}(\delta^t_s\gamma^r_u - \gamma^t_s\delta^r_u)\tilde{\boldsymbol{a}}^p_q + \sum_{\substack{pr\\qs}} C^{rp}_{sq}(\delta^t_s\gamma^r_u - \gamma^t_s\delta^r_u)\tilde{\boldsymbol{a}}^p_q - \sum_{\substack{pr\\qs}} C^{pr}_{sq}(\delta^t_s\gamma^r_u - \gamma^t_s\delta^r_u)\tilde{\boldsymbol{a}}^p_q\Big) \tag{A.85}$$

$$= \sum_{\substack{pr\\qs}} C^{pr}_{qs}(\delta^t_s\gamma^r_u - \gamma^t_s\delta^r_u)\tilde{\boldsymbol{a}}^p_q \tag{A.86}$$

where we made use of the antisymmetry in the upper and lower indices, respectively, of the matrix elements C^{pr}_{qs}. The zero-body piece is

$$\frac{1}{4}\sum_{\substack{pr\\qs}} C^{pr}_{qs}([\tilde{\boldsymbol{a}}^{pr}_{qs},\tilde{\boldsymbol{a}}^{t}_{u}])^{[0]} = \frac{1}{4}\sum_{\substack{pr\\qs}} C^{pr}_{qs}\left(\delta^t_q\lambda^{pr}_{us} + \delta^t_s\lambda^{pr}_{qu} - \delta^p_u\lambda^{rt}_{sq} - \delta^r_u\lambda^{pt}_{qs}\right) \tag{A.87}$$

$$= \frac{1}{4}\left(\sum_{\substack{pr\\s}} C^{pr}_{ts}\lambda^{pr}_{us} + \sum_{\substack{pr\\q}} C^{pr}_{qt}\lambda^{pr}_{qu} - \sum_{\substack{r\\qs}} C^{ur}_{qs}\lambda^{rt}_{sq} - \sum_{\substack{p\\qs}} C^{pu}_{qs}\lambda^{pt}_{qs}\right) \tag{A.88}$$

$$= \frac{1}{4}\left(\sum_{\substack{pr\\q}} C^{pr}_{tq}\lambda^{pr}_{us} + \sum_{\substack{pr\\q}} C^{pr}_{qt}\lambda^{pr}_{qu} - \sum_{\substack{p\\qs}} C^{up}_{qs}\lambda^{pt}_{sq} - \sum_{\substack{p\\qs}} C^{pu}_{qs}\lambda^{pt}_{qs}\right) \tag{A.89}$$

$$= \frac{1}{4}\cdot 2\left(\sum_{\substack{pr\\q}} C^{pr}_{qt}\lambda^{pr}_{qu} - \sum_{\substack{p\\qs}} C^{pu}_{qs}\lambda^{pt}_{qs}\right) \tag{A.90}$$

$$= \frac{1}{2}\sum_{\substack{pr\\q}}\left(C^{pr}_{qt}\lambda^{pr}_{qu} - C^{qu}_{pr}\lambda^{qt}_{pr}\right). \tag{A.91}$$

Putting everything together yields

$$[\boldsymbol{C}^{(2)},\tilde{\boldsymbol{a}}^t_u] = \frac{1}{2}\sum_{\substack{pr\\q}}\left(C^{pr}_{tq}\tilde{\boldsymbol{a}}^{pr}_{uq} - C^{uq}_{pr}\tilde{\boldsymbol{a}}^{tq}_{pr}\right) + \sum_{\substack{pr\\qs}} C^{pr}_{qs}(\delta^t_s\gamma^r_u - \gamma^t_s\delta^r_u)\tilde{\boldsymbol{a}}^p_q + \frac{1}{2}\sum_{\substack{pr\\q}}\left(C^{pr}_{qt}\lambda^{pr}_{qu} - C^{qu}_{pr}\lambda^{qt}_{pr}\right). \tag{A.92}$$

Commutator of 2B and 2B—Partially Contracted

We skip this case for two reasons: On the one hand, this case is extremely expensive and not directly needed in this work. On the other hand, for the calculation of $[\boldsymbol{C}^{(2)}, \boldsymbol{D}^{(2)}]$ which is the relevant case for this work (discussed in appendix A.2.3), we can rely on the result of $\tilde{\boldsymbol{a}}^{pr}_{qs}\tilde{\boldsymbol{a}}^{tv}_{uw}$ that has already been elaborated in appendix A.1.

A.2.3. Fully Contracted

Note that the commutators $[\boldsymbol{C}^{(2)}, \boldsymbol{A}^{(1)}]$, $[\boldsymbol{A}^{(1)}, \boldsymbol{C}^{(2)}]$ and $[\boldsymbol{C}^{(2)}, \boldsymbol{D}^{(2)}]$—we refer to them as fully-contracted commutators since there is no external index left anymore—can be derived using the partially-contracted formulae obtained in appendix A.2.2. But for the method of equating the coefficients of the two-body part needed for the flow equation in (4.11) it is not recommended to rename particular indices among each other fixed by the left-hand side of the flow equation.

To be more concrete: Assuming the indices p, r, q and s are the ones fixed by the left-hand side of the flow equation, it useful not to exchange these indices among each other, e.g., p with r, q, s and the same for the index q which should not be renamed to p, r, s.

Otherwise, after the equating the coefficients, we might loose the symmetry of the operator defined by the considered commutator. This symmetry can be restored manually but it can be extremely costly. Not to do it manually, we prefer to go back to the commutators obtained in appendix A.2.1 and derive the following expressions from there on as done for the partially-contracted ones. This remark does not apply to the commutator of $[\boldsymbol{A}^{(1)}, \boldsymbol{B}^{(1)}]$ since it does not contain a two-body part. Furthermore, for the equating the coefficients the commutators need to be written in a convenient and suitable form, e.g., with a prefactor of $\frac{1}{4}$ in front of the two-body piece.

Putting it another way, the expressions, to which we have to apply the method of equating the coefficients, has the following form

$$\frac{1}{4}\sum_{\substack{pr\\qs}} c^{pr}_{qs}\tilde{\boldsymbol{a}}^{pr}_{qs} \stackrel{!}{=} \sum_{\substack{pr\\qs}} d^{pr}_{qs}\tilde{\boldsymbol{a}}^{pr}_{qs}, \tag{A.93}$$

where the coefficient c^{pr}_{qs} is antisymmetric with respect to exchange among the upper and lower indices, respectively, which is not the case for the coefficient d^{pr}_{qs}. The key point is that the normal-ordered operators are antisymmetric with respect to exchange among the upper and lower indices, respectively, which we need to take into account for the equating the coefficients. For that purpose, we rewrite the right-hand term in a complicated way

$$= \frac{1}{4}\sum_{\substack{pr\\qs}} (d^{pr}_{qs}\tilde{\boldsymbol{a}}^{pr}_{qs} + d^{rp}_{sq}\tilde{\boldsymbol{a}}^{rp}_{sq} + d^{rp}_{qs}\tilde{\boldsymbol{a}}^{rp}_{qs} + d^{pr}_{sq}\tilde{\boldsymbol{a}}^{pr}_{sq}) \tag{A.94}$$

and make use of the antisymmetry of the normal-ordered operator leading to

$$= \frac{1}{4} \sum_{\substack{pr \\ qs}} \left(d^{pr}_{qs} + d^{rp}_{sq} - d^{rp}_{qs} - d^{pr}_{sq} \right) \tilde{\boldsymbol{a}}^{pr}_{qs}. \tag{A.95}$$

Hence, the method of equating the coefficients yields $c^{pr}_{qs} = d^{pr}_{qs} + d^{rp}_{sq} - d^{rp}_{qs} - d^{pr}_{sq}$, which preserves the symmetry of the coefficients c^{pr}_{qs}. In this example, the coefficients c^{pr}_{qs} and d^{pr}_{qs} represent the two-body parts of the left- and right-hand side of operator flow equation (4.5), respectively.

Commutator of 1B and 1B—Fully Contracted

Using the results obtained above, and simplifying the term yields

$$\begin{aligned}
[\boldsymbol{A}^{(1)}, \boldsymbol{B}^{(1)}] &= \sum_{\substack{p \\ q}} A^p_q B^r_s [\tilde{\boldsymbol{a}}^p_q, \tilde{\boldsymbol{a}}^r_s] && \text{(A.96)} \\
&= \sum_{\substack{pr \\ qs}} A^p_q B^r_s \left(\delta^r_q \tilde{\boldsymbol{a}}^p_s - \delta^p_s \tilde{\boldsymbol{a}}^r_q + \delta^r_q \gamma^p_s - \delta^p_s \gamma^r_q \right) && \text{(A.97)} \\
&= \sum_{\substack{pr \\ qs}} \left(A^p_s B^r_q \delta^r_s \tilde{\boldsymbol{a}}^p_q - A^r_q B^p_s \delta^r_s \tilde{\boldsymbol{a}}^p_q \right) + \sum_{\substack{pr \\ qs}} \left(A^p_s B^r_q - A^r_q B^p_s \right) \delta^r_s \gamma^p_q && \text{(A.98)} \\
&= \sum_{\substack{p \\ q}} \left(\sum_r \left(A^p_r B^r_q - A^r_q B^p_r \right) \right) \tilde{\boldsymbol{a}}^p_q \\
&\quad + \sum_{\substack{pr \\ q}} \left(A^p_r B^r_q - A^r_q B^p_r \right) \gamma^p_q. && \text{(A.99)}
\end{aligned}$$

Commutator of 2B and 1B—Fully Contracted

Our goal is the calculation of the commutator

$$\begin{aligned}
[\boldsymbol{C}^{(2)}, \boldsymbol{A}^{(1)}] &= \frac{1}{4} \sum_{\substack{prt \\ qsu}} C^{pr}_{qs} A^t_u [\tilde{\boldsymbol{a}}^{pr}_{qs}, \tilde{\boldsymbol{a}}^t_u] && \text{(A.100)} \\
&= + \frac{1}{4} \sum_{\substack{prt \\ qsu}} C^{pr}_{qs} A^t_u ([\tilde{\boldsymbol{a}}^{pr}_{qs}, \tilde{\boldsymbol{a}}^t_u])^{[2]} \\
&\quad + \frac{1}{4} \sum_{\substack{prt \\ qsu}} C^{pr}_{qs} A^t_u ([\tilde{\boldsymbol{a}}^{pr}_{qs}, \tilde{\boldsymbol{a}}^t_u])^{[1]} \\
&\quad + \frac{1}{4} \sum_{\substack{prt \\ qsu}} C^{pr}_{qs} A^t_u ([\tilde{\boldsymbol{a}}^{pr}_{qs}, \tilde{\boldsymbol{a}}^t_u])^{[0]}. && \text{(A.101)}
\end{aligned}$$

Consider the two-body piece. By renaming the summation indices, we get

$$\frac{1}{4} \sum_{\substack{prt \\ qsu}} C^{pr}_{qs} A^t_u ([\tilde{\boldsymbol{a}}^{pr}_{qs}, \tilde{\boldsymbol{a}}^t_u])^{[2]} = \frac{1}{4} \sum_{\substack{prt \\ qsu}} C^{pr}_{qs} A^t_u (\delta^t_q \tilde{\boldsymbol{a}}^{pr}_{us} + \delta^t_s \tilde{\boldsymbol{a}}^{pr}_{qu} - \delta^p_u \tilde{\boldsymbol{a}}^{tr}_{qs} - \delta^r_u \tilde{\boldsymbol{a}}^{pt}_{qs}) \tag{A.102}$$

$$= \frac{1}{4} \sum_{\substack{pr \\ qs}} \left(\sum_{\substack{t \\ u}} (C^{pr}_{us} A^t_q + C^{pr}_{qu} A^t_s - C^{tr}_{qs} A^p_u - C^{pt}_{qs} A^r_u) \delta^t_u \right) \tilde{\boldsymbol{a}}^{pr}_{qs} \tag{A.103}$$

$$= \frac{1}{4} \sum_{\substack{pr \\ qs}} \left(\sum_{t} (C^{pr}_{ts} A^t_q + C^{pr}_{qt} A^t_s - C^{tr}_{qs} A^p_t - C^{pt}_{qs} A^r_t) \right) \tilde{\boldsymbol{a}}^{pr}_{qs}. \tag{A.104}$$

The one-body piece is given by

$$\frac{1}{4} \sum_{\substack{prt \\ qsu}} C^{pr}_{qs} A^t_u ([\tilde{\boldsymbol{a}}^{pr}_{qs}, \tilde{\boldsymbol{a}}^t_u])^{[1]} = \frac{1}{4} \sum_{\substack{prt \\ qsu}} C^{pr}_{qs} A^t_u \Big((\delta^t_s \gamma^r_u - \gamma^t_s \delta^r_u) \tilde{\boldsymbol{a}}^p_q - (\delta^t_s \gamma^p_u - \gamma^t_s \delta^p_u) \tilde{\boldsymbol{a}}^r_q + (\delta^t_q \gamma^p_u - \gamma^t_q \delta^p_u) \tilde{\boldsymbol{a}}^r_s - (\delta^t_q \gamma^r_u - \gamma^t_q \delta^r_u) \tilde{\boldsymbol{a}}^p_s \Big) \tag{A.105}$$

$$= \frac{1}{4} \cdot 4 \sum_{\substack{prt \\ qsu}} C^{pr}_{qs} A^t_u (\delta^t_s \gamma^r_u - \gamma^t_s \delta^r_u) \tilde{\boldsymbol{a}}^p_q \tag{A.106}$$

$$= \sum_{\substack{p \\ q}} \left(\sum_{\substack{rt \\ su}} C^{pr}_{qs} A^t_u (\delta^t_s \gamma^r_u - \gamma^t_s \delta^r_u) \right) \tilde{\boldsymbol{a}}^p_q. \tag{A.107}$$

Simplifying the zero-body piece yields

$$\frac{1}{4} \sum_{\substack{prt \\ qsu}} C^{pr}_{qs} A^t_u ([\tilde{\boldsymbol{a}}^{pr}_{qs}, \tilde{\boldsymbol{a}}^t_u])^{[0]}$$

$$= \frac{1}{4} \sum_{\substack{prt \\ qsu}} C^{pr}_{qs} A^t_u \left(\delta^t_q \lambda^{pr}_{us} + \delta^t_s \lambda^{pr}_{qu} - \delta^p_u \lambda^{rt}_{sq} - \delta^r_u \lambda^{pt}_{qs} \right) \tag{A.108}$$

$$= \frac{1}{4} \sum_{\substack{prt \\ qsu}} \left(C^{pr}_{qs} A^t_u \delta^t_q \lambda^{pr}_{us} + C^{pr}_{sq} A^t_u \delta^t_q \lambda^{pr}_{su} - C^{pr}_{qs} A^t_u \delta^p_u \lambda^{rt}_{sq} - C^{rp}_{qs} A^t_u \delta^p_u \lambda^{rt}_{qs} \right) \tag{A.109}$$

$$= \frac{1}{4} \sum_{\substack{prt \\ qsu}} \left(C^{pr}_{qs} A^t_u \delta^t_q \lambda^{pr}_{us} + (-)^2 C^{pr}_{qs} A^t_u \delta^t_q \lambda^{pr}_{us} - C^{pr}_{qs} A^t_u \delta^p_u \lambda^{rt}_{sq} - (-)^2 C^{pr}_{qs} A^t_u \delta^p_u \lambda^{rt}_{sq} \right) \tag{A.110}$$

$$= \frac{1}{2} \sum_{\substack{prt \\ qsu}} C^{pr}_{qs} A^t_u \left(\delta^t_q \lambda^{pr}_{us} - \delta^p_u \lambda^{tr}_{qs} \right) \tag{A.111}$$

$$= \frac{1}{2} \sum_{\substack{prt \\ qsu}} (C^{pr}_{us} A^t_q - C^{tr}_{qs} A^p_u) \delta^t_u \lambda^{pr}_{qs} \tag{A.112}$$

$$= \frac{1}{2} \sum_{\substack{prt \\ qs}} (C^{pr}_{ts} A^t_q - C^{tr}_{qs} A^p_t) \lambda^{pr}_{qs}. \tag{A.113}$$

Finally, we obtain

$$\begin{aligned}[\boldsymbol{C}^{(2)}, \boldsymbol{A}^{(1)}] =& \frac{1}{4} \sum_{\substack{pr \\ qs}} \left(\sum_{t} (C_{ts}^{pr} A_q^t + C_{qt}^{pr} A_s^t - C_{qs}^{tr} A_t^p - C_{qs}^{pt} A_t^r) \right) \tilde{\boldsymbol{a}}_{qs}^{pr} \\ &+ \sum_{\substack{p \\ q}} \left(\sum_{\substack{rt \\ su}} C_{qs}^{pr} A_u^t (\delta_s^t \gamma_u^r - \gamma_s^t \delta_u^r) \right) \tilde{\boldsymbol{a}}_q^p \\ &+ \frac{1}{2} \sum_{\substack{prt \\ qs}} (C_{ts}^{pr} A_q^t - C_{qs}^{tr} A_t^p) \lambda_{qs}^{pr}. \end{aligned} \tag{A.114}$$

Commutator of 1B and 2B—Fully Contracted

By means of the antisymmetry of the commutator, we can make use of the previous result yielding

$$[\boldsymbol{A}^{(1)}, \boldsymbol{C}^{(2)}] = -\left[\boldsymbol{C}^{(2)}, \boldsymbol{A}^{(1)}\right] \tag{A.115}$$

$$\begin{aligned} =& \frac{1}{4} \sum_{\substack{pr \\ qs}} \left(\sum_{t} (-C_{ts}^{pr} A_q^t - C_{qt}^{pr} A_s^t + C_{qs}^{tr} A_t^p + C_{qs}^{pt} A_t^r) \right) \tilde{\boldsymbol{a}}_{qs}^{pr} \\ &+ \sum_{\substack{p \\ q}} \left(\sum_{\substack{rt \\ su}} C_{qs}^{pr} A_u^t (-\delta_s^t \gamma_u^r + \gamma_s^t \delta_u^r) \right) \tilde{\boldsymbol{a}}_q^p \\ &+ \frac{1}{2} \sum_{\substack{prt \\ qs}} (-C_{ts}^{pr} A_q^t + C_{qs}^{tr} A_t^p) \lambda_{qs}^{pr}. \end{aligned} \tag{A.116}$$

Commutator of 2B and 2B—Fully Contracted

Here, we use a different technique:

$$[\boldsymbol{C}^{(2)}, \boldsymbol{D}^{(2)}] = \frac{1}{4^2} \sum_{\substack{prtv \\ qsuw}} C_{qs}^{pr} D_{uw}^{tv} [\tilde{\boldsymbol{a}}_{qs}^{pr}, \tilde{\boldsymbol{a}}_{uw}^{tv}] \tag{A.117}$$

$$= \frac{1}{16} \sum_{\substack{prtv \\ qsuw}} C_{qs}^{pr} D_{uw}^{tv} (\tilde{\boldsymbol{a}}_{qs}^{pr} \tilde{\boldsymbol{a}}_{uw}^{tv} - \tilde{\boldsymbol{a}}_{uw}^{tv} \tilde{\boldsymbol{a}}_{qs}^{pr}) \tag{A.118}$$

$$= \frac{1}{16} \sum_{\substack{prtv \\ qsuw}} (C_{qs}^{pr} D_{uw}^{tv} - C_{uw}^{tv} D_{qs}^{pr}) \tilde{\boldsymbol{a}}_{qs}^{pr} \tilde{\boldsymbol{a}}_{uw}^{tv} \tag{A.119}$$

$$= \sum_{i=0}^{4} \left(\frac{1}{16} \sum_{\substack{prtv \\ qsuw}} (C_{qs}^{pr} D_{uw}^{tv} - C_{uw}^{tv} D_{qs}^{pr}) (\tilde{\boldsymbol{a}}_{qs}^{pr} \tilde{\boldsymbol{a}}_{uw}^{tv})^{[i]} \right) \tag{A.120}$$

$$= \sum_{i=0}^{4} \left(\frac{1}{16} \sum_{\substack{prtv \\ qsuw}} G_{qsuw}^{prtv} (\tilde{\boldsymbol{a}}_{qs}^{pr} \tilde{\boldsymbol{a}}_{uw}^{tv})^{[i]} \right) \tag{A.121}$$

with the following definition

$$G^{prtv}_{qsuw} := C^{pr}_{qs} D^{tv}_{uw} - D^{pr}_{qs} C^{tv}_{uw}. \tag{A.122}$$

Obviously, the multiply-indexed object G^{prtv}_{qsuw} has the following properties

$$G^{prtv}_{qsuw} = -G^{rptv}_{qsuw} = -G^{prtv}_{squw} = -G^{prvt}_{qsuw} = -G^{prtv}_{qswu} \tag{A.123}$$

$$G^{prtv}_{qsuw} = -G^{tvpr}_{uwqs}\,. \tag{A.124}$$

Note that the four-body piece vanishes according to proposition 3.1.

Hence, consider the three-body piece

$$\begin{aligned}\frac{1}{16}\sum_{\substack{prtv\\qsuw}} G^{prtv}_{qsuw}(\tilde{\boldsymbol{a}}^{pr}_{qs}\tilde{\boldsymbol{a}}^{tv}_{uw})^{[3]} =& \frac{1}{16}\sum_{\substack{prtv\\qsuw}} G^{prtv}_{qsuw}\Big(+ \bar{\gamma}^{t}_{q}\tilde{\boldsymbol{a}}^{prv}_{usw} + \bar{\gamma}^{t}_{s}\tilde{\boldsymbol{a}}^{prv}_{quw} + \bar{\gamma}^{v}_{s}\tilde{\boldsymbol{a}}^{prt}_{qwu} + \bar{\gamma}^{v}_{q}\tilde{\boldsymbol{a}}^{prt}_{wsu} \\ & - \gamma^{p}_{u}\tilde{\boldsymbol{a}}^{rtv}_{sqw} - \gamma^{p}_{w}\tilde{\boldsymbol{a}}^{rtv}_{suq} - \gamma^{r}_{u}\tilde{\boldsymbol{a}}^{ptv}_{qsw} - \gamma^{r}_{w}\tilde{\boldsymbol{a}}^{ptv}_{qus}\Big)\end{aligned} \tag{A.125}$$

$$= \frac{1}{4}\sum_{\substack{prtv\\qsuw}} G^{prtv}_{qsuw}\delta^{t}_{q}\tilde{\boldsymbol{a}}^{prv}_{usw}. \tag{A.126}$$

The two-body piece is given by

$$\begin{aligned}\frac{1}{16}\sum_{\substack{prtv\\qsuw}} G^{prtv}_{qsuw}(\tilde{\boldsymbol{a}}^{pr}_{qs}\tilde{\boldsymbol{a}}^{tv}_{uw})^{[2]} =& + \frac{1}{16}\sum_{\substack{prtv\\qsuw}} G^{prtv}_{qsuw}(\tilde{\boldsymbol{a}}^{pr}_{qs}\tilde{\boldsymbol{a}}^{tv}_{uw})^{[2,\mathrm{I}]} \\ & + \frac{1}{16}\sum_{\substack{prtv\\qsuw}} G^{prtv}_{qsuw}(\tilde{\boldsymbol{a}}^{pr}_{qs}\tilde{\boldsymbol{a}}^{tv}_{uw})^{[2,\mathrm{II}]} \\ & + \frac{1}{16}\sum_{\substack{prtv\\qsuw}} G^{prtv}_{qsuw}(\tilde{\boldsymbol{a}}^{pr}_{qs}\tilde{\boldsymbol{a}}^{tv}_{uw})^{[2,\mathrm{III}]}.\end{aligned} \tag{A.127}$$

The first subterm yields

$$\begin{aligned}&\frac{1}{16}\sum_{\substack{prtv\\qsuw}} G^{prtv}_{qsuw}(\tilde{\boldsymbol{a}}^{pr}_{qs}\tilde{\boldsymbol{a}}^{tv}_{uw})^{[2,\mathrm{I}]} \\ =& \frac{1}{16}\sum_{\substack{prtv\\qsuw}} G^{prtv}_{qsuw}\Big(+ (\bar{\gamma}^{t}_{q}\bar{\gamma}^{v}_{s} - \bar{\gamma}^{t}_{s}\bar{\gamma}^{v}_{q} + \lambda^{tv}_{qs})\tilde{\boldsymbol{a}}^{pr}_{uw} \\ & + (\gamma^{p}_{u}\gamma^{r}_{w} - \gamma^{p}_{w}\gamma^{r}_{u} + \lambda^{pr}_{uw})\tilde{\boldsymbol{a}}^{tv}_{qs}\Big)\end{aligned} \tag{A.128}$$

$$= \frac{1}{16} \sum_{\substack{prtv \\ qsuw}} G^{prtv}_{uwqs} (\bar{\gamma}^t_u \bar{\gamma}^v_w - \bar{\gamma}^t_w \bar{\gamma}^v_u + \lambda^{tv}_{uw}) \tilde{\boldsymbol{a}}^{pr}_{qs}$$

$$+ \frac{1}{16} \sum_{\substack{prtv \\ qsuw}} G^{tvpr}_{qsuw} (\gamma^t_u \gamma^v_w - \gamma^t_w \gamma^v_u + \lambda^{tv}_{uw}) \tilde{\boldsymbol{a}}^{pr}_{qs} \tag{A.129}$$

$$\overset{A.123}{=} \frac{1}{16} \sum_{\substack{prtv \\ qsuw}} G^{prtv}_{uwqs} (2\bar{\gamma}^t_u \bar{\gamma}^v_w + \lambda^{tv}_{uw}) \tilde{\boldsymbol{a}}^{pr}_{qs} + \frac{1}{16} \sum_{\substack{prtv \\ qsuw}} G^{tvpr}_{qsuw} (2\gamma^t_u \gamma^v_w + \lambda^{tv}_{uw}) \tilde{\boldsymbol{a}}^{pr}_{qs} \tag{A.130}$$

$$\overset{A.124}{=} \frac{1}{16} \sum_{\substack{prtv \\ qsuw}} G^{prtv}_{uwqs} (2\bar{\gamma}^t_u \bar{\gamma}^v_w + \lambda^{tv}_{uw}) \tilde{\boldsymbol{a}}^{pr}_{qs} - \frac{1}{16} \sum_{\substack{prtv \\ qsuw}} G^{prtv}_{uwqs} (2\gamma^t_u \gamma^v_w + \lambda^{tv}_{uw}) \tilde{\boldsymbol{a}}^{pr}_{qs} \tag{A.131}$$

$$= \frac{1}{16} \cdot 2 \sum_{\substack{prtv \\ qsuw}} G^{prtv}_{uwqs} (\bar{\gamma}^t_u \bar{\gamma}^v_w - \gamma^t_u \gamma^v_w) \tilde{\boldsymbol{a}}^{pr}_{qs} + \frac{1}{16} \sum_{\substack{prtv \\ qsuw}} G^{prtv}_{uwqs} (\underbrace{\lambda^{tv}_{uw} - \lambda^{tv}_{uw}}_{=0}) \tilde{\boldsymbol{a}}^{pr}_{qs} \tag{A.132}$$

$$= \frac{1}{8} \sum_{\substack{prtv \\ qsuw}} G^{prtv}_{uwqs} (\bar{\gamma}^t_u \bar{\gamma}^v_w - \gamma^t_u \gamma^v_w) \tilde{\boldsymbol{a}}^{pr}_{qs} \tag{A.133}$$

$$= \frac{1}{8} \sum_{\substack{prtv \\ qsuw}} G^{prtv}_{uwqs} (\delta^t_u \delta^v_w - \delta^t_u \gamma^v_w - \gamma^t_u \delta^v_w) \tilde{\boldsymbol{a}}^{pr}_{qs} \tag{A.134}$$

$$\overset{A.123}{=} \frac{1}{4} \sum_{\substack{pr \\ qs}} \left(\frac{1}{2} \sum_{\substack{tv \\ uw}} G^{prtv}_{uwqs} (\delta^t_u \delta^v_w - 2\delta^t_u \gamma^v_w) \right) \tilde{\boldsymbol{a}}^{pr}_{qs}. \tag{A.135}$$

The second subterms is given by

$$
\begin{aligned}
&\frac{1}{16}\sum_{\substack{prtv\\qsuw}} G^{prtv}_{qsuw}(\tilde{\boldsymbol{a}}^{pr}_{qs}\tilde{\boldsymbol{a}}^{tv}_{uw})^{[2,\mathrm{II}]} \\
=&\frac{1}{16}\sum_{\substack{prtv\\qsuw}} G^{prtv}_{qsuw}\Big(+ (\gamma^p_w\bar{\gamma}^v_q + \lambda^{pv}_{qw})\tilde{\boldsymbol{a}}^{rt}_{su} + (\gamma^p_u\bar{\gamma}^t_q + \lambda^{pt}_{qu})\tilde{\boldsymbol{a}}^{rv}_{sw} \\
&\qquad + (\gamma^p_u\bar{\gamma}^v_s + \lambda^{pv}_{su})\tilde{\boldsymbol{a}}^{rt}_{qw} + (\gamma^p_w\bar{\gamma}^t_s + \lambda^{pt}_{sw})\tilde{\boldsymbol{a}}^{rv}_{qu} \\
&\qquad + (\gamma^r_w\bar{\gamma}^v_s + \lambda^{rv}_{sw})\tilde{\boldsymbol{a}}^{pt}_{qu} + (\gamma^r_u\bar{\gamma}^t_s + \lambda^{rt}_{su})\tilde{\boldsymbol{a}}^{pv}_{qw} \\
&\qquad + (\gamma^r_u\bar{\gamma}^v_q + \lambda^{rv}_{qu})\tilde{\boldsymbol{a}}^{pt}_{sw} + (\gamma^r_w\bar{\gamma}^t_q + \lambda^{rt}_{qw})\tilde{\boldsymbol{a}}^{pv}_{su} \\
&\qquad - (\gamma^p_u\bar{\gamma}^v_q + \lambda^{pv}_{qu})\tilde{\boldsymbol{a}}^{rt}_{sw} - (\gamma^p_w\bar{\gamma}^t_q + \lambda^{pt}_{qw})\tilde{\boldsymbol{a}}^{rv}_{su} \\
&\qquad - (\gamma^p_w\bar{\gamma}^v_s + \lambda^{pv}_{sw})\tilde{\boldsymbol{a}}^{rt}_{qu} - (\gamma^p_u\bar{\gamma}^t_s + \lambda^{pt}_{su})\tilde{\boldsymbol{a}}^{rv}_{qw} \\
&\qquad - (\gamma^r_u\bar{\gamma}^v_s + \lambda^{rv}_{su})\tilde{\boldsymbol{a}}^{pt}_{qw} - (\gamma^r_w\bar{\gamma}^t_s + \lambda^{rt}_{sw})\tilde{\boldsymbol{a}}^{pv}_{qu} \\
&\qquad - (\gamma^r_w\bar{\gamma}^v_q + \lambda^{rv}_{qw})\tilde{\boldsymbol{a}}^{pt}_{su} - (\gamma^r_u\bar{\gamma}^t_q + \lambda^{rt}_{qu})\tilde{\boldsymbol{a}}^{pv}_{sw}\Big),
\end{aligned}
\tag{A.136}
$$

after some simplification steps, we obtain

$$
\begin{aligned}
=&\frac{1}{4}\sum_{\substack{pr\\qs}}\left(\sum_{\substack{tv\\uw}} G^{ptvr}_{quws}(\gamma^t_w\delta^v_u - \gamma^v_u\delta^t_w)\right)\tilde{\boldsymbol{a}}^{pr}_{qs} \\
&+\frac{1}{4}\sum_{\substack{pr\\qs}}\left((-)\sum_{\substack{tv\\uw}} G^{ptvr}_{suwq}(\gamma^t_w\delta^v_u - \gamma^v_u\delta^t_w)\right)\tilde{\boldsymbol{a}}^{pr}_{qs}.
\end{aligned}
\tag{A.137}
$$

It is not recommended to rename the indices q and s among each other, as aforementioned, because they are indices fixed by the left-hand side of the flow equation per convention for equating the coefficients. Otherwise, the operator defined by $[\boldsymbol{C}^{(2)}, \boldsymbol{D}^{(2)}]$ would not have the right symmetry. These notes are relevant for equating the coefficients of the flow equations.

The following term vanishes:

$$\begin{aligned}
&\frac{1}{16}\sum_{\substack{prtv\\qsuw}} G^{prtv}_{qsuw}(\tilde{\boldsymbol{a}}^{pr}_{qs}\tilde{\boldsymbol{a}}^{tv}_{uw})^{[2,\mathrm{III}]}\\
&=\frac{1}{16}\sum_{\substack{prtv\\qsuw}} G^{prtv}_{qsuw}\Big(- \lambda^{tv}_{sw}\tilde{\boldsymbol{a}}^{pr}_{qu} - \lambda^{tv}_{us}\tilde{\boldsymbol{a}}^{pr}_{qw} - \lambda^{tv}_{qw}\tilde{\boldsymbol{a}}^{pr}_{us} - \lambda^{tv}_{uq}\tilde{\boldsymbol{a}}^{pr}_{ws}\\
&\qquad\qquad - \lambda^{rv}_{uw}\tilde{\boldsymbol{a}}^{pt}_{qs} - \lambda^{rt}_{wu}\tilde{\boldsymbol{a}}^{pv}_{qs} - \lambda^{pv}_{uw}\tilde{\boldsymbol{a}}^{rt}_{qs} - \lambda^{pt}_{wu}\tilde{\boldsymbol{a}}^{rv}_{qs}\\
&\qquad\qquad - \lambda^{rv}_{sq}\tilde{\boldsymbol{a}}^{tp}_{uw} - \lambda^{rt}_{sq}\tilde{\boldsymbol{a}}^{pv}_{uw} - \lambda^{pv}_{qs}\tilde{\boldsymbol{a}}^{tr}_{uw} - \lambda^{pt}_{qs}\tilde{\boldsymbol{a}}^{rv}_{uw}\\
&\qquad\qquad - \lambda^{pr}_{ws}\tilde{\boldsymbol{a}}^{tv}_{uq} - \lambda^{pr}_{us}\tilde{\boldsymbol{a}}^{tv}_{qw} - \lambda^{pr}_{qw}\tilde{\boldsymbol{a}}^{tv}_{us} - \lambda^{pr}_{qu}\tilde{\boldsymbol{a}}^{tv}_{sw}\Big) \qquad \text{(A.138)}\\
&= 0. \qquad \text{(A.139)}
\end{aligned}$$

The first subterm of the one-body piece can be simplified to

$$\begin{aligned}
\frac{1}{16}\sum_{\substack{prtv\\qsuw}} G^{prtv}_{qsuw}(\tilde{\boldsymbol{a}}^{pr}_{qs}\tilde{\boldsymbol{a}}^{tv}_{uw})^{[1,\mathrm{I}]} &= \frac{1}{16}\sum_{\substack{prtv\\qsuw}} G^{prtv}_{qsuw}\Big(\bar{\gamma}^{tv}_{qs}\mathbb{A}(\gamma^{r}_{w}\tilde{\boldsymbol{a}}^{p}_{u}) + \gamma^{pr}_{uw}\mathbb{A}(\bar{\gamma}^{t}_{s}\tilde{\boldsymbol{a}}^{v}_{q})\Big) && \text{(A.140)}\\
&= \frac{1}{16}\cdot 4\sum_{\substack{prtv\\qsuw}} G^{prtv}_{qsuw}\Big(\bar{\gamma}^{tv}_{qs}\gamma^{r}_{w}\tilde{\boldsymbol{a}}^{p}_{u} + \gamma^{pr}_{uw}\bar{\gamma}^{t}_{s}\tilde{\boldsymbol{a}}^{v}_{q}\Big) && \text{(A.141)}\\
&= \frac{1}{4}\sum_{\substack{prtv\\qsuw}} G^{prtv}_{usqw}\bar{\gamma}^{tv}_{us}\gamma^{r}_{w}\tilde{\boldsymbol{a}}^{p}_{q} + \frac{1}{4}\sum_{\substack{prtv\\qsuw}} G^{vrtp}_{qsuw}\gamma^{vr}_{uw}\bar{\gamma}^{t}_{s}\tilde{\boldsymbol{a}}^{p}_{q} && \text{(A.142)}\\
&= \frac{1}{4}\sum_{\substack{prtv\\qsuw}} G^{prtv}_{usqw}(\bar{\gamma}^{tv}_{us}\gamma^{r}_{w} + \gamma^{tv}_{us}\bar{\gamma}^{r}_{w})\tilde{\boldsymbol{a}}^{p}_{q} && \text{(A.143)}\\
&\overset{A.4}{=} \frac{1}{4}\sum_{\substack{prtv\\qsuw}} G^{prtv}_{usqw}\Big((\bar{\gamma}^{t}_{u}\bar{\gamma}^{v}_{s} - \bar{\gamma}^{t}_{s}\bar{\gamma}^{v}_{u})\gamma^{r}_{w} + (\gamma^{t}_{u}\gamma^{v}_{s} - \gamma^{t}_{s}\gamma^{v}_{u})\bar{\gamma}^{r}_{w}\Big)\tilde{\boldsymbol{a}}^{p}_{q}\\
&\quad + \frac{1}{4}\sum_{\substack{prtv\\qsuw}} G^{prtv}_{usqw}\lambda^{tv}_{us}\delta^{r}_{w}\tilde{\boldsymbol{a}}^{p}_{q} && \text{(A.144)}\\
&= \frac{1}{4}\sum_{\substack{prtv\\qsuw}} G^{prtv}_{usqw}\Big(2\bar{\gamma}^{t}_{u}\bar{\gamma}^{v}_{s}\gamma^{r}_{w} + 2\gamma^{t}_{u}\gamma^{v}_{s}\bar{\gamma}^{r}_{w}\Big)\tilde{\boldsymbol{a}}^{p}_{q}\\
&\quad + \frac{1}{4}\sum_{\substack{prtv\\qsuw}} G^{ptrv}_{wsqu}\lambda^{rv}_{ws}\delta^{t}_{u}\tilde{\boldsymbol{a}}^{p}_{q} && \text{(A.145)}\\
&= \sum_{\substack{p\\q}}\left(\frac{1}{2}\sum_{\substack{rtv\\suw}} G^{prtv}_{usqw}(\bar{\gamma}^{t}_{u}\bar{\gamma}^{v}_{s}\gamma^{r}_{w} + \gamma^{t}_{u}\gamma^{v}_{s}\bar{\gamma}^{r}_{w})\right)\tilde{\boldsymbol{a}}^{p}_{q}\\
&\quad + \sum_{\substack{p\\q}}\left(\frac{1}{4}\sum_{\substack{rtv\\suw}} G^{ptrv}_{wsqu}\lambda^{rv}_{ws}\delta^{t}_{u}\right)\tilde{\boldsymbol{a}}^{p}_{q}. && \text{(A.146)}
\end{aligned}$$

The second subterm of the one-body piece yields

$$
\begin{aligned}
&\frac{1}{16}\sum_{\substack{prtv\\qsuw}} G^{prtv}_{qsuw}(\tilde{\boldsymbol{a}}^{pr}_{qs}\tilde{\boldsymbol{a}}^{tv}_{uw})^{[1,\mathrm{II}]} \\
&=\frac{1}{16}\sum_{\substack{prtv\\qsuw}} G^{prtv}_{qsuw}\Big((+\bar{\gamma}^{v}_{s}\lambda^{rt}_{qw}+\bar{\gamma}^{t}_{q}\lambda^{rv}_{sw}-\bar{\gamma}^{v}_{q}\lambda^{rt}_{sw}-\bar{\gamma}^{t}_{s}\lambda^{rv}_{qw})\tilde{\boldsymbol{a}}^{p}_{u} \\
&\qquad\qquad +(-\bar{\gamma}^{v}_{s}\lambda^{rt}_{qu}-\bar{\gamma}^{t}_{q}\lambda^{rv}_{su}+\bar{\gamma}^{v}_{q}\lambda^{rt}_{su}+\bar{\gamma}^{t}_{s}\lambda^{rv}_{qu})\tilde{\boldsymbol{a}}^{p}_{w} \\
&\qquad\qquad +(-\bar{\gamma}^{v}_{s}\lambda^{pt}_{qw}-\bar{\gamma}^{t}_{q}\lambda^{pv}_{sw}+\bar{\gamma}^{v}_{q}\lambda^{pt}_{sw}+\bar{\gamma}^{t}_{s}\lambda^{pv}_{qw})\tilde{\boldsymbol{a}}^{r}_{u} \\
&\qquad\qquad +(+\bar{\gamma}^{v}_{s}\lambda^{pt}_{qu}+\bar{\gamma}^{t}_{q}\lambda^{pv}_{su}-\bar{\gamma}^{v}_{q}\lambda^{pt}_{su}-\bar{\gamma}^{t}_{s}\lambda^{pv}_{qu})\tilde{\boldsymbol{a}}^{r}_{w}\Big) \\
&\quad+\frac{1}{16}\sum_{\substack{prtv\\qsuw}} G^{prtv}_{qsuw}\Big((+\gamma^{r}_{u}\lambda^{pv}_{sw}+\gamma^{p}_{w}\lambda^{rv}_{su}-\gamma^{r}_{w}\lambda^{pv}_{su}-\gamma^{p}_{u}\lambda^{rv}_{sw})\tilde{\boldsymbol{a}}^{t}_{q} \\
&\qquad\qquad +(-\gamma^{r}_{u}\lambda^{pv}_{qw}-\gamma^{p}_{w}\lambda^{rv}_{qu}+\gamma^{r}_{w}\lambda^{pv}_{qu}+\gamma^{p}_{u}\lambda^{rv}_{qw})\tilde{\boldsymbol{a}}^{t}_{s} \\
&\qquad\qquad +(-\gamma^{r}_{u}\lambda^{pt}_{sw}-\gamma^{p}_{w}\lambda^{rt}_{su}+\gamma^{r}_{w}\lambda^{pt}_{su}+\gamma^{p}_{u}\lambda^{rt}_{sw})\tilde{\boldsymbol{a}}^{v}_{q} \\
&\qquad\qquad +(+\gamma^{r}_{u}\lambda^{pt}_{qw}+\gamma^{p}_{w}\lambda^{rt}_{qu}-\gamma^{r}_{w}\lambda^{pt}_{qu}-\gamma^{p}_{u}\lambda^{rt}_{qw})\tilde{\boldsymbol{a}}^{v}_{s}\Big) \qquad \text{(A.147)} \\
&=\frac{1}{16}\cdot 16\sum_{\substack{prtv\\qsuw}} G^{prtv}_{usqw}\bar{\gamma}^{t}_{u}\lambda^{rv}_{sw}\tilde{\boldsymbol{a}}^{p}_{q}+\frac{1}{16}\cdot 16\sum_{\substack{prtv\\qsuw}} G^{prtv}_{usqw}\gamma^{t}_{u}\lambda^{rv}_{sw}\tilde{\boldsymbol{a}}^{p}_{q} \qquad \text{(A.148)} \\
&=\sum_{\substack{prtv\\qsuw}} G^{prtv}_{usqw}(\bar{\gamma}^{t}_{u}+\gamma^{t}_{u})\lambda^{rv}_{sw}\tilde{\boldsymbol{a}}^{p}_{q} \qquad \text{(A.149)} \\
&=\sum_{\substack{p\\q}}\left(\sum_{\substack{rtv\\suw}} G^{prtv}_{usqw}\delta^{t}_{u}\lambda^{rv}_{sw}\right)\tilde{\boldsymbol{a}}^{p}_{q}. \qquad \text{(A.150)}
\end{aligned}
$$

The third subterm of the one-body piece is given by

$$
\begin{aligned}
&\frac{1}{16}\sum_{\substack{prtv\\qsuw}} G^{prtv}_{qsuw}(\tilde{\boldsymbol{a}}^{pr}_{qs}\tilde{\boldsymbol{a}}^{tv}_{uw})^{[1,\mathrm{III}]} \\
&=\frac{1}{16}\sum_{\substack{prtv\\qsuw}} G^{prtv}_{qsuw}\Big(+ (\bar{\gamma}^t_s\lambda^{vr}_{wu} + \bar{\gamma}^v_s\lambda^{tr}_{uw})\tilde{\boldsymbol{a}}^p_q + (\bar{\gamma}^t_q\lambda^{vp}_{wu} + \bar{\gamma}^v_q\lambda^{tp}_{uw})\tilde{\boldsymbol{a}}^r_s \\
&\qquad\qquad - (\bar{\gamma}^t_q\lambda^{vr}_{wu} + \bar{\gamma}^v_q\lambda^{tr}_{uw})\tilde{\boldsymbol{a}}^p_s - (\bar{\gamma}^t_s\lambda^{vp}_{wu} + \bar{\gamma}^v_s\lambda^{tp}_{uw})\tilde{\boldsymbol{a}}^r_q \\
&\qquad\qquad + (\gamma^p_u\lambda^{rv}_{sq} + \gamma^r_u\lambda^{pv}_{qs})\tilde{\boldsymbol{a}}^t_w + (\gamma^p_w\lambda^{rt}_{sq} + \gamma^r_w\lambda^{pt}_{qs})\tilde{\boldsymbol{a}}^v_u \\
&\qquad\qquad - (\gamma^p_w\lambda^{rv}_{sq} + \gamma^r_w\lambda^{pv}_{qs})\tilde{\boldsymbol{a}}^t_u - (\gamma^p_u\lambda^{rt}_{sq} + \gamma^r_u\lambda^{pt}_{qs})\tilde{\boldsymbol{a}}^v_w\Big) \\
&\quad + \frac{1}{16}\sum_{\substack{prtv\\qsuw}} G^{prtv}_{qsuw}\Big(+ (\bar{\gamma}^v_q\lambda^{rp}_{sw} + \bar{\gamma}^v_s\lambda^{pr}_{qw})\tilde{\boldsymbol{a}}^t_u + (\bar{\gamma}^t_q\lambda^{rp}_{su} + \bar{\gamma}^t_s\lambda^{pr}_{qu})\tilde{\boldsymbol{a}}^v_w \\
&\qquad\qquad - (\bar{\gamma}^t_q\lambda^{rp}_{sw} + \bar{\gamma}^t_s\lambda^{pr}_{qw})\tilde{\boldsymbol{a}}^v_u - (\bar{\gamma}^v_q\lambda^{rp}_{su} + \bar{\gamma}^v_s\lambda^{pr}_{qu})\tilde{\boldsymbol{a}}^t_w \\
&\qquad\qquad + (\gamma^p_u\lambda^{vt}_{ws} + \gamma^p_w\lambda^{tv}_{us})\tilde{\boldsymbol{a}}^r_q + (\gamma^r_u\lambda^{vt}_{wq} + \gamma^r_w\lambda^{tv}_{uq})\tilde{\boldsymbol{a}}^p_s \\
&\qquad\qquad - (\gamma^r_u\lambda^{vt}_{ws} + \gamma^r_w\lambda^{tv}_{us})\tilde{\boldsymbol{a}}^p_q - (\gamma^p_u\lambda^{vt}_{wq} + \gamma^p_w\lambda^{tv}_{uq})\tilde{\boldsymbol{a}}^r_s\Big) \qquad \text{(A.151)}
\end{aligned}
$$

$$
=\frac{1}{16}\cdot 8\sum_{\substack{prtv\\qsuw}} G^{ptrv}_{qsuw}(\bar{\gamma}^r_s + \gamma^r_s)\lambda^{tv}_{uw}\tilde{\boldsymbol{a}}^p_q + \frac{1}{16}\cdot 8\sum_{\substack{prtv\\qsuw}} G^{prtv}_{qusw}(-\bar{\gamma}^r_s - \gamma^r_s)\lambda^{tv}_{uw}\tilde{\boldsymbol{a}}^p_q \qquad \text{(A.152)}
$$

$$
=\frac{1}{2}\sum_{\substack{prtv\\qsuw}} G^{ptrv}_{qsuw}\delta^r_s\lambda^{tv}_{uw}\tilde{\boldsymbol{a}}^p_q + \frac{1}{2}\sum_{\substack{prtv\\qsuw}} G^{prtv}_{qusw}(-)\delta^r_s\lambda^{tv}_{uw}\tilde{\boldsymbol{a}}^p_q \qquad \text{(A.153)}
$$

$$
=\sum_{\substack{p\\q}}\left(\frac{1}{2}\sum_{\substack{rtv\\suw}} G^{prtv}_{qusw}\delta^t_u\lambda^{rv}_{sw}\right)\tilde{\boldsymbol{a}}^p_q + \sum_{\substack{p\\q}}\left(-\frac{1}{2}\sum_{\substack{rtv\\suw}} G^{ptrv}_{qsuw}\delta^t_u\lambda^{rv}_{sw}\right)\tilde{\boldsymbol{a}}^p_q \qquad \text{(A.154)}
$$

$$
=\sum_{\substack{p\\q}}\left(\frac{1}{2}\sum_{\substack{rtv\\suw}} G^{prtv}_{qusw}\delta^t_u\lambda^{rv}_{sw} - \frac{1}{2}\sum_{\substack{rtv\\suw}} G^{ptrv}_{qsuw}\delta^t_u\lambda^{rv}_{sw}\right)\tilde{\boldsymbol{a}}^p_q. \qquad \text{(A.155)}
$$

The fourth subterm of the one-body piece does not contribute to the commutator, namely

$$\begin{aligned}
&\frac{1}{16}\sum_{\substack{prtv\\qsuw}} G^{prtv}_{qsuw}(\tilde{\boldsymbol{a}}^{pr}_{qs}\tilde{\boldsymbol{a}}^{tv}_{uw})^{[1,\mathrm{IV}]}\\
&=\frac{1}{16}\sum_{\substack{prtv\\qsuw}} G^{prtv}_{qsuw}\Big(-\lambda^{rtv}_{sqw}\tilde{\boldsymbol{a}}^{p}_{u}-\lambda^{rtv}_{suq}\tilde{\boldsymbol{a}}^{p}_{w}-\lambda^{ptv}_{qsw}\tilde{\boldsymbol{a}}^{r}_{u}-\lambda^{pvt}_{qsu}\tilde{\boldsymbol{a}}^{r}_{w}\\
&\qquad\qquad -\lambda^{prv}_{usw}\tilde{\boldsymbol{a}}^{t}_{q}-\lambda^{prv}_{quw}\tilde{\boldsymbol{a}}^{t}_{s}-\lambda^{prt}_{wsu}\tilde{\boldsymbol{a}}^{v}_{q}-\lambda^{prt}_{qwu}\tilde{\boldsymbol{a}}^{v}_{s}\Big) &\text{(A.156)}\\
&=\frac{1}{16}\cdot 4\sum_{\substack{prtv\\qsuw}} G^{prtv}_{usqw}\lambda^{rtv}_{suw}\tilde{\boldsymbol{a}}^{p}_{q}-\frac{1}{16}\cdot 4\sum_{\substack{prtv\\qsuw}} G^{prtv}_{usqw}\lambda^{rtv}_{suw}\tilde{\boldsymbol{a}}^{p}_{q} &\text{(A.157)}\\
&=0. &\text{(A.158)}
\end{aligned}$$

The last term of the one-body piece vanishes as well

$$\begin{aligned}
&\frac{1}{16}\sum_{\substack{prtv\\qsuw}} G^{prtv}_{qsuw}(\tilde{\boldsymbol{a}}^{pr}_{qs}\tilde{\boldsymbol{a}}^{tv}_{uw})^{[1,\mathrm{V}]}\\
&=\frac{1}{16}\sum_{\substack{prtv\\qsuw}} G^{prtv}_{qsuw}\Big(-\lambda^{tvp}_{uws}\tilde{\boldsymbol{a}}^{r}_{q}-\lambda^{tvp}_{uwq}\tilde{\boldsymbol{a}}^{p}_{s}+\lambda^{rtv}_{suw}\tilde{\boldsymbol{a}}^{p}_{q}+\lambda^{ptv}_{quw}\tilde{\boldsymbol{a}}^{r}_{s}\\
&\qquad\qquad -\lambda^{prt}_{qsw}\tilde{\boldsymbol{a}}^{v}_{u}-\lambda^{prv}_{qsu}\tilde{\boldsymbol{a}}^{t}_{w}+\lambda^{prv}_{qsw}\tilde{\boldsymbol{a}}^{t}_{u}+\lambda^{prt}_{qsu}\tilde{\boldsymbol{a}}^{v}_{w}\Big) &\text{(A.159)}\\
&=\frac{1}{16}\cdot 4\sum_{\substack{prtv\\qsuw}} G^{prtv}_{qsuw}\lambda^{rtv}_{suw}\tilde{\boldsymbol{a}}^{p}_{q}-\frac{1}{16}\cdot 4\sum_{\substack{prtv\\qsuw}} G^{prtv}_{qsuw}\lambda^{rtv}_{suw}\tilde{\boldsymbol{a}}^{p}_{q} &\text{(A.160)}\\
&=0. &\text{(A.161)}
\end{aligned}$$

Let us consider the zero-body piece where the first subterms can be simplified to

$$\begin{aligned}
&\frac{1}{16}\sum_{\substack{prtv\\qsuw}} G^{prtv}_{qsuw}(\tilde{\boldsymbol{a}}^{pr}_{qs}\tilde{\boldsymbol{a}}^{tv}_{uw})^{[0,\mathrm{I}]}\\
&=\frac{1}{16}\sum_{\substack{prtv\\qsuw}} G^{prtv}_{qsuw}\Big(+\gamma^{p}_{u}\gamma^{r}_{w}\bar{\gamma}^{t}_{q}\bar{\gamma}^{v}_{s}+\gamma^{p}_{w}\gamma^{r}_{u}\bar{\gamma}^{v}_{q}\bar{\gamma}^{t}_{s}-\gamma^{p}_{w}\gamma^{r}_{u}\bar{\gamma}^{t}_{q}\bar{\gamma}^{v}_{s}-\gamma^{p}_{u}\gamma^{r}_{w}\bar{\gamma}^{t}_{s}\bar{\gamma}^{v}_{q}\Big) &\text{(A.162)}\\
&=\frac{1}{16}\cdot 4\sum_{\substack{prtv\\qsuw}} G^{prtv}_{qsuw}\gamma^{p}_{u}\gamma^{r}_{w}\bar{\gamma}^{t}_{q}\bar{\gamma}^{v}_{s} &\text{(A.163)}\\
&=\frac{1}{4}\sum_{\substack{prtv\\qsuw}} G^{prtv}_{qsuw}\gamma^{p}_{u}\gamma^{r}_{w}\bar{\gamma}^{t}_{q}\bar{\gamma}^{v}_{s}. &\text{(A.164)}
\end{aligned}$$

The second subterm of the zero-body piece reads

$$
\begin{aligned}
&\frac{1}{16}\sum_{\substack{prtv\\qsuw}} G^{prtv}_{qsuw}(\tilde{\boldsymbol{a}}^{pr}_{qs}\tilde{\boldsymbol{a}}^{tv}_{uw})^{[0,\mathrm{II}]}\\
=&\frac{1}{16}\sum_{\substack{prtv\\qsuw}} G^{prtv}_{qsuw}\Big(+ \gamma^p_u\bar{\gamma}^t_q\lambda^{rv}_{sw} + \gamma^r_w\bar{\gamma}^v_s\lambda^{pt}_{qu} + \gamma^p_w\bar{\gamma}^v_q\lambda^{rt}_{su} + \gamma^r_u\bar{\gamma}^t_s\lambda^{pv}_{qw}\\
&\qquad - \gamma^p_w\bar{\gamma}^t_q\lambda^{rv}_{su} - \gamma^r_u\bar{\gamma}^v_s\lambda^{pt}_{qw} - \gamma^p_w\bar{\gamma}^v_s\lambda^{tr}_{uq} - \gamma^r_u\bar{\gamma}^t_q\lambda^{vp}_{ws}\\
&\qquad - \gamma^p_u\bar{\gamma}^v_q\lambda^{rt}_{sw} - \gamma^r_w\bar{\gamma}^t_s\lambda^{pv}_{qu} - \gamma^r_w\bar{\gamma}^v_q\lambda^{tp}_{us} - \gamma^p_u\bar{\gamma}^t_s\lambda^{vr}_{wq}\\
&\qquad - \gamma^r_w\bar{\gamma}^t_q\lambda^{pv}_{us} - \gamma^r_u\bar{\gamma}^v_q\lambda^{pt}_{ws} - \gamma^p_u\bar{\gamma}^v_s\lambda^{tr}_{qw} - \gamma^p_w\bar{\gamma}^t_s\lambda^{rv}_{uq}\Big)\\
&+\frac{1}{16}\sum_{\substack{prtv\\qsuw}} G^{prtv}_{qsuw}\Big(+ \bar{\gamma}^t_q\bar{\gamma}^v_s\lambda^{pr}_{uw} + \bar{\gamma}^v_q\bar{\gamma}^t_s\lambda^{pr}_{wu} + \gamma^p_u\gamma^r_w\lambda^{tv}_{qs} + \gamma^r_u\gamma^p_w\lambda^{tv}_{sq}\Big) \qquad (A.165)\\
=&\sum_{\substack{prtv\\qsuw}} G^{ptrv}_{qusw}\gamma^t_w\bar{\gamma}^v_u\lambda^{pr}_{qs}\\
&+\frac{1}{8}\sum_{\substack{prtv\\qsuw}} G^{prtv}_{uwqs}(\bar{\gamma}^t_u\bar{\gamma}^v_w - \gamma^t_u\gamma^v_w)\lambda^{pr}_{qs}. \qquad (A.166)
\end{aligned}
$$

The third subterm of the zero-body piece vanishes

$$
\begin{aligned}
&\frac{1}{16}\sum_{\substack{prtv\\qsuw}} G^{prtv}_{qsuw}(\tilde{\boldsymbol{a}}^{pr}_{qs}\tilde{\boldsymbol{a}}^{tv}_{uw})^{[0,\mathrm{III}]}\\
=&\frac{1}{16}\sum_{\substack{prtv\\qsuw}} G^{prtv}_{qsuw}\Big(+ \lambda^{pt}_{qu}\lambda^{rv}_{sw} + \lambda^{pv}_{qw}\lambda^{rt}_{su} - \lambda^{pt}_{qw}\lambda^{rv}_{su} - \lambda^{pv}_{qu}\lambda^{rt}_{sw} - \lambda^{vp}_{ws}\lambda^{tr}_{uq} - \lambda^{tp}_{us}\lambda^{vr}_{wq}\Big)\\
&+\frac{1}{16}\sum_{\substack{prtv\\qsuw}} G^{prtv}_{qsuw}\Big(+ \lambda^{tv}_{qs}\lambda^{pr}_{uw} + \lambda^{tp}_{sw}\lambda^{rv}_{uq} + \lambda^{tr}_{qw}\lambda^{pv}_{us}\Big) \qquad (A.167)\\
=&\frac{1}{16}\cdot 6\sum_{\substack{prtv\\qsuw}} G^{ptrv}_{qusw}\lambda^{tv}_{uw}\lambda^{pr}_{qs}\\
&+\frac{1}{16}\sum_{\substack{prtv\\qsuw}} G^{prtv}_{uwqs}\lambda^{tv}_{uw}\lambda^{pr}_{qs} + \frac{1}{16}\cdot 2\sum_{\substack{prtv\\qsuw}} G^{ptrv}_{qusw}\lambda^{tv}_{uw}\lambda^{pr}_{qs} \qquad (A.168)\\
=&\frac{1}{2}\sum_{\substack{prtv\\qsuw}} G^{ptrv}_{qusw}\lambda^{tv}_{uw}\lambda^{pr}_{qs} + \frac{1}{16}\sum_{\substack{prtv\\qsuw}} G^{prtv}_{uwqs}\lambda^{tv}_{uw}\lambda^{pr}_{qs} \qquad (A.169)\\
=&\frac{1}{2}\sum_{\substack{prtv\\qsuw}} \tfrac{1}{2}(G^{ptrv}_{qusw} - G^{rvpt}_{swqu})\lambda^{tv}_{uw}\lambda^{pr}_{qs} + \frac{1}{16}\sum_{\substack{prtv\\qsuw}} \tfrac{1}{2}(G^{prtv}_{uwqs} - G^{tvpr}_{qsuw})\lambda^{tv}_{uw}\lambda^{pr}_{qs} \qquad (A.170)\\
=&0. \qquad (A.171)
\end{aligned}
$$

The same is true for the fourth term of the zero-body piece

$$\begin{aligned}
&\frac{1}{16}\sum_{\substack{prtv\\qsuw}} G^{prtv}_{qsuw}(\tilde{\boldsymbol{a}}^{pr}_{qs}\tilde{\boldsymbol{a}}^{tv}_{uw})^{[0,\mathrm{IV}]}\\
=&\frac{1}{16}\sum_{\substack{prtv\\qsuw}} G^{prtv}_{qsuw}\Big(-\lambda^{tp}_{uw}\lambda^{rv}_{sq}-\lambda^{tv}_{uq}\lambda^{rp}_{sw}-\lambda^{pt}_{qs}\lambda^{vr}_{wu}-\lambda^{pr}_{qu}\lambda^{vt}_{ws}\\
&\qquad -\lambda^{vp}_{wu}\lambda^{rt}_{sq}-\lambda^{vt}_{wq}\lambda^{rp}_{su}-\lambda^{pv}_{qs}\lambda^{tr}_{uw}-\lambda^{pr}_{qw}\lambda^{tv}_{us}\Big) \qquad (A.172)\\
=&-\frac{1}{8}\sum_{\substack{prtv\\qsuw}}(G^{vrtp}_{qsuw}+G^{prtv}_{wsuq}+G^{ptrv}_{qsuw}+G^{prtv}_{qusw})\lambda^{tv}_{uw}\lambda^{pr}_{qs} \qquad (A.173)
\end{aligned}$$

after some simplification steps, we obtain

$$=0. \qquad (A.174)$$

The fifth subterm of the zero-body piece can be written as

$$\begin{aligned}
&\frac{1}{16}\sum_{\substack{prtv\\qsuw}} G^{prtv}_{qsuw}(\tilde{\boldsymbol{a}}^{pr}_{qs}\tilde{\boldsymbol{a}}^{tv}_{uw})^{[0,\mathrm{V}]}\\
=&\frac{1}{16}\sum_{\substack{prtv\\qsuw}} G^{prtv}_{qsuw}\Big(+\bar{\gamma}^{v}_{s}\lambda^{ptr}_{quw}+\bar{\gamma}^{t}_{s}\lambda^{pvr}_{qwu}+\bar{\gamma}^{t}_{q}\lambda^{rvp}_{swu}+\bar{\gamma}^{v}_{q}\lambda^{rtp}_{suw}\\
&\qquad -\gamma^{r}_{w}\lambda^{ptv}_{qus}-\gamma^{r}_{u}\lambda^{pvt}_{qws}-\gamma^{p}_{u}\lambda^{rvt}_{swq}-\gamma^{p}_{w}\lambda^{rtv}_{suq}\Big) \qquad (A.175)\\
=&\frac{1}{16}\cdot 4\sum_{\substack{prtv\\qsuw}} G^{prtv}_{qsuw}(\bar{\gamma}^{v}_{s}+\gamma^{v}_{s})\lambda^{ptr}_{quw} \qquad (A.176)\\
=&\frac{1}{4}\sum_{\substack{prtv\\qsuw}} G^{prtv}_{qsuw}\delta^{v}_{s}\lambda^{ptr}_{quw}. \qquad (A.177)
\end{aligned}$$

The sixth subterm of the zero-body piece vanishes

$$\begin{aligned}
\frac{1}{16}\sum_{\substack{prtv\\qsuw}} G^{prtv}_{qsuw}(\tilde{\boldsymbol{a}}^{pr}_{qs}\tilde{\boldsymbol{a}}^{tv}_{uw})^{[0,\mathrm{VI}]} =&\frac{1}{16}\sum_{\substack{prtv\\qsuw}} G^{prtv}_{qsuw}\lambda^{prtv}_{qsuw} \qquad (A.178)\\
=&\frac{1}{16}\sum_{\substack{prtv\\qsuw}}\frac{1}{2}(G^{prtv}_{qsuw}\lambda^{prtv}_{qsuw}+G^{prtv}_{qsuw}\lambda^{prtv}_{qsuw}) \qquad (A.179)\\
\overset{A.124}{=}&\frac{1}{16}\sum_{\substack{prtv\\qsuw}}\frac{1}{2}(G^{prtv}_{qsuw}\lambda^{prtv}_{qsuw}-G^{tvpr}_{uwqs}\lambda^{prtv}_{qsuw}) \qquad (A.180)\\
=&\frac{1}{16}\sum_{\substack{prtv\\qsuw}}\frac{1}{2}(G^{prtv}_{qsuw}\lambda^{prtv}_{qsuw}-G^{tvpr}_{uwqs}\lambda^{tvpr}_{uwqs}) \qquad (A.181)\\
=&0. \qquad (A.182)
\end{aligned}$$

A.3. Expectation Values

In this section, we derive expectation values of products of reference-state normal-ordered operators with respect to a given many-body state $|\Psi\rangle$ which is the reference state used for the normal ordering. We introduce a shorthand notation for the expectation of an operator $\boldsymbol{X}$ with respect to the reference state

$$\langle \boldsymbol{X} \rangle \coloneqq \langle \Psi | \boldsymbol{X} | \Psi \rangle \,. \tag{A.183}$$

A.3.1. Expectation Values of Products—Partially Contracted

$$\langle \boldsymbol{A}^{(1)} \tilde{\boldsymbol{a}}^p_q \rangle = \sum_{\substack{r \\ s}} A^r_s \langle \tilde{\boldsymbol{a}}^r_s \tilde{\boldsymbol{a}}^p_q \rangle = \sum_{\substack{r \\ s}} A^r_s (\tilde{\boldsymbol{a}}^r_s \tilde{\boldsymbol{a}}^p_q)^{[0]} = \sum_{\substack{r \\ s}} A^r_s (\gamma^r_q \bar{\gamma}^p_s + \lambda^{rp}_{sq}) \tag{A.184}$$

$$\langle \boldsymbol{A}^{(1)} \tilde{\boldsymbol{a}}^{pr}_{qs} \rangle = \sum_{\substack{t \\ u}} A^t_u \langle \tilde{\boldsymbol{a}}^t_u \tilde{\boldsymbol{a}}^{pr}_{qs} \rangle \tag{A.185}$$

$$= \sum_{\substack{t \\ u}} A^t_u (-\gamma^t_q \lambda^{pr}_{us} - \gamma^t_s \lambda^{pr}_{qu} + \bar{\gamma}^p_u \lambda^{rt}_{sq} + \bar{\gamma}^r_u \lambda^{pt}_{qs} + \lambda^{tpr}_{uqs}) \tag{A.186}$$

$$= \sum_{\substack{t \\ u}} A^t_u (-2\gamma^t_q \lambda^{pr}_{us} + 2\bar{\gamma}^p_u \lambda^{rt}_{sq} + \lambda^{tpr}_{uqs}) \tag{A.187}$$

$$\langle \boldsymbol{C}^{(2)} \tilde{\boldsymbol{a}}^t_u \rangle = \frac{1}{4} \sum_{\substack{pr \\ qs}} C^{pr}_{qs} (2\bar{\gamma}^t_q \lambda^{pr}_{us} - 2\gamma^p_u \lambda^{rt}_{sq} + \lambda^{prt}_{qsu}) \tag{A.188}$$

$$\begin{aligned} \langle \boldsymbol{C}^{(2)} \tilde{\boldsymbol{a}}^{tv}_{uw} \rangle = \frac{1}{4} \sum_{\substack{pr \\ qs}} C^{pr}_{qs} (& 4\gamma^p_u \gamma^r_w \bar{\gamma}^t_q \bar{\gamma}^v_s \\ & + 4\gamma^p_u \bar{\gamma}^t_q \lambda^{rv}_{sw} + 4\gamma^r_w \bar{\gamma}^v_s \lambda^{pt}_{qu} - 4\gamma^p_w \bar{\gamma}^t_q \lambda^{rv}_{su} \\ & - 4\gamma^r_u \bar{\gamma}^v_s \lambda^{pt}_{qw} + 2\bar{\gamma}^t_q \bar{\gamma}^v_s \lambda^{pr}_{uw} + 2\gamma^p_u \gamma^r_w \lambda^{tv}_{qs} \\ & + 4\lambda^{pt}_{qu} \lambda^{rv}_{sw} - 4\lambda^{pt}_{qw} \lambda^{rv}_{su} + \lambda^{tv}_{qs} \lambda^{pr}_{uw} \\ & - 2\lambda^{tp}_{uw} \lambda^{rv}_{sq} - 2\lambda^{tv}_{uq} \lambda^{rp}_{sw} - 2\lambda^{pt}_{qs} \lambda^{vr}_{wu} - 2\lambda^{pr}_{qu} \lambda^{vt}_{ws} \\ & + 2\bar{\gamma}^v_s \lambda^{ptr}_{quw} + 2\bar{\gamma}^t_s \lambda^{pvr}_{qwu} - 2\gamma^r_w \lambda^{ptv}_{qus} - 2\gamma^r_u \lambda^{pvt}_{qws} \\ & + \lambda^{prtv}_{qsuw}) \end{aligned} \tag{A.189}$$

A.3.2. Expectation Values of Commutators—Partially Contracted

$$\langle [\boldsymbol{A}^{(1)}, \tilde{\boldsymbol{a}}^r_s] \rangle = \sum_p A^p_r \langle \tilde{\boldsymbol{a}}^p_s \rangle - \sum_q A^s_q \langle \tilde{\boldsymbol{a}}^r_q \rangle + \sum_p A^p_r \gamma^p_s - \sum_q A^s_q \gamma^r_q \tag{A.190}$$

$$= \sum_p A^p_r \gamma^p_s - \sum_q A^s_q \gamma^r_q \tag{A.191}$$

$$\langle [\boldsymbol{A}^{(1)}, \tilde{\boldsymbol{a}}^{rt}_{su}] \rangle = -\sum_{q} (A^{s}_{q}\lambda^{rt}_{qu} + A^{u}_{q}\lambda^{rt}_{sq}) + \sum_{p} (A^{p}_{r}\lambda^{tp}_{us} + A^{p}_{t}\lambda^{rp}_{su}) \tag{A.192}$$

$$\langle [\boldsymbol{C}^{(2)}, \tilde{\boldsymbol{a}}^{t}_{u}] \rangle = \frac{1}{4} \sum_{\substack{pr \\ qs}} C^{pr}_{qs} ([\tilde{\boldsymbol{a}}^{pr}_{qs}, \tilde{\boldsymbol{a}}^{t}_{u}])^{[0]} = \frac{1}{2} \sum_{\substack{pr \\ q}} \left(C^{pr}_{qt}\lambda^{pr}_{qu} - C^{qu}_{pr}\lambda^{qt}_{pr} \right) \tag{A.193}$$

$$\begin{aligned}
\langle [\boldsymbol{C}^{(2)}, \tilde{\boldsymbol{a}}^{tv}_{uw}] \rangle = & \sum_{\substack{pr \\ qs}} C^{pr}_{qs} (\gamma^{p}_{u}\gamma^{r}_{w}\bar{\gamma}^{t}_{q}\bar{\gamma}^{v}_{s} - \gamma^{t}_{q}\gamma^{v}_{s}\bar{\gamma}^{p}_{u}\bar{\gamma}^{r}_{w}) \\
& + \sum_{\substack{pr \\ qs}} C^{pr}_{qs} \Big((\gamma^{r}_{w}\bar{\gamma}^{v}_{s} - \gamma^{v}_{s}\bar{\gamma}^{r}_{w})\lambda^{pt}_{qu} - (\gamma^{r}_{u}\bar{\gamma}^{v}_{s} - \gamma^{v}_{s}\bar{\gamma}^{r}_{w})\lambda^{pt}_{qw} + \\
& \qquad + (\gamma^{r}_{u}\bar{\gamma}^{t}_{s} - \gamma^{t}_{s}\bar{\gamma}^{r}_{u})\lambda^{pv}_{qw} - (\gamma^{r}_{w}\bar{\gamma}^{t}_{s} - \gamma^{t}_{s}\bar{\gamma}^{r}_{w})\lambda^{pv}_{qu} \Big) \\
& + \frac{1}{2} \sum_{\substack{pr \\ qs}} C^{pr}_{qs} \Big((\bar{\gamma}^{t}_{q}\bar{\gamma}^{v}_{s} - \gamma^{t}_{q}\gamma^{v}_{s})\lambda^{pr}_{uw} - (\bar{\gamma}^{p}_{u}\bar{\gamma}^{r}_{w} - \gamma^{p}_{u}\gamma^{r}_{w})\lambda^{tv}_{qs} \Big) \\
& + \frac{1}{2} \sum_{\substack{pr \\ qs}} C^{pr}_{qs} \Big(\delta^{v}_{s}\lambda^{ptr}_{quw} - \delta^{r}_{w}\lambda^{ptv}_{qus} + \delta^{t}_{s}\lambda^{pvr}_{qwu} - \delta^{r}_{u}\lambda^{pvt}_{qws} \Big)
\end{aligned} \tag{A.194}$$

A.3.3. Expectation Values of Commutators—Fully Contracted

$$\langle [\boldsymbol{A}^{(1)}, \boldsymbol{B}^{(1)}] \rangle = \sum_{\substack{pr \\ q}} \left(A^{p}_{r}B^{r}_{q} - A^{r}_{q}B^{p}_{r} \right) \gamma^{p}_{q} \tag{A.195}$$

$$\langle [\boldsymbol{C}^{(2)}, \boldsymbol{A}^{(1)}] \rangle = \frac{1}{2} \sum_{\substack{prt \\ qs}} (C^{pr}_{ts}A^{t}_{q} - C^{tr}_{qs}A^{p}_{t})\lambda^{pr}_{qs} \tag{A.196}$$

$$\langle [\boldsymbol{A}^{(1)}, \boldsymbol{C}^{(2)}] \rangle = \frac{1}{2} \sum_{\substack{prt \\ qs}} (-C^{pr}_{ts}A^{t}_{q} + C^{tr}_{qs}A^{p}_{t})\lambda^{pr}_{qs} \tag{A.197}$$

$$\begin{aligned}
\langle [\boldsymbol{C}^{(2)}, \boldsymbol{D}^{(2)}] \rangle = & \frac{1}{4} \sum_{\substack{prtv \\ qsuw}} G^{prtv}_{qsuw}\gamma^{p}_{u}\gamma^{r}_{w}\bar{\gamma}^{t}_{q}\bar{\gamma}^{v}_{s} \\
& + \sum_{\substack{prtv \\ qsuw}} G^{ptrv}_{qusw}\gamma^{t}_{w}\bar{\gamma}^{v}_{u}\lambda^{pr}_{qs} \\
& + \frac{1}{8} \sum_{\substack{prtv \\ qsuw}} G^{prtv}_{uwqs}(\bar{\gamma}^{t}_{u}\bar{\gamma}^{v}_{w} - \gamma^{t}_{u}\gamma^{v}_{w})\lambda^{pr}_{qs} \\
& + \frac{1}{4} \sum_{\substack{prtv \\ qsuw}} G^{prtv}_{qsuw}\delta^{v}_{s}\lambda^{ptr}_{quw}
\end{aligned} \tag{A.198}$$

Appendix B

Multi-Reference In-Medium SRG—Derivations

B.1. J-Coupling of the Flow Equations in Natural Orbitals

B.1.1. J-Coupling of the Two-Body Terms

Let us start with two-body part. Since the first term has already been considered in section 4.3.2, we start with the second term.

The third line of (4.28a) defines the second term, and can be written in a compact and fully symmetrized form

$$\left(\frac{\mathrm{d}\Gamma^{1m_1 2m_2}_{3m_3 4m_4}}{\mathrm{d}\alpha}\right)_{\mathrm{II}} := \frac{1}{2}\sum_{tv}\sum_{m_t m_v} G^{1m_1 2m_2 t m_t v m_v}_{t m_t v m_v 3m_3 4m_4}(1-n_t-n_v) \tag{B.1}$$

$$= \frac{1}{2}\sum_{tv}\sum_{m_t m_v} \eta^{1m_1 2m_2}_{t m_t v m_v}\Gamma^{t m_t v m_v}_{3m_3 4m_4}(1-n_t-n_v) - \chi[1m_1 2m_2 \leftrightarrow 3m_3 4m_4] \tag{B.2}$$

$$= \Bigg(\left(\frac{1}{2}\cdot\frac{1}{2^2}\sum_{tv}\sum_{m_t m_v} \eta^{1m_1 2m_2}_{t m_t v m_v}\Gamma^{t m_t v m_v}_{3m_3 4m_4}(1-n_t-n_v) - [1m_1 \leftrightarrow 2m_2]\right) - [3m_3 \leftrightarrow 4m_4]\Bigg) - \chi[1m_1 2m_2 \leftrightarrow 3m_3 4m_4]. \tag{B.3}$$

Performing J-coupling yields

$$\begin{aligned}\left(\frac{\mathrm{d}\,{}^{J}\Gamma^{12}_{34}}{\mathrm{d}\alpha}\right)_{\mathrm{II}} = \Bigg(\Bigg(\frac{1}{8}\sum_{tv}\sum_{m_t m_v}\sum_{J'M'}\sum_{J''M''}\sum_{\substack{m_1 m_2\\ m_3 m_4}} {}^{J'}\eta^{12}_{tv}\,{}^{J''}\Gamma^{tv}_{34}(1-n_t-n_v)\\ \times \begin{pmatrix} j_1 & j_2 \\ m_1 & m_2 \end{pmatrix}\!\!\begin{matrix} J \\ M \end{matrix}\!\!\begin{pmatrix} j_3 & j_4 \\ m_3 & m_4 \end{pmatrix}\!\!\begin{matrix} J \\ M \end{matrix}\!\!\begin{pmatrix} j_1 & j_2 \\ m_1 & m_2 \end{pmatrix}\!\!\begin{matrix} J' \\ M' \end{matrix}\!\!\begin{pmatrix} j_t & j_v \\ m_t & m_v \end{pmatrix}\!\!\begin{matrix} J' \\ M' \end{matrix}\\ \times \begin{pmatrix} j_t & j_v \\ m_t & m_v \end{pmatrix}\!\!\begin{matrix} J'' \\ M'' \end{matrix}\!\!\begin{pmatrix} j_3 & j_4 \\ m_3 & m_4 \end{pmatrix}\!\!\begin{matrix} J'' \\ M'' \end{matrix} - (-)^{J-j_1-j_2}[1 \leftrightarrow 2]\Bigg)\\ - (-)^{J-j_3-j_4}[3 \leftrightarrow 4]\Bigg) - \chi[12 \leftrightarrow 34]\end{aligned} \tag{B.4}$$

$$\overset{(4.30)}{=}\Bigg(\Bigg(\frac{1}{8}\sum_{tv}{}^{J}\eta^{12}_{tv}\,{}^{J}\Gamma^{tv}_{34}(1-n_t-n_v)-(-)^{J-j_1-j_2}[1\leftrightarrow 2]\Bigg) \\ -(-)^{J-j_3-j_4}[3\leftrightarrow 4]\Bigg)-\chi[12\leftrightarrow 34]. \tag{B.5}$$

The remaining lines of (4.28a) define the last term

$$\left(\frac{\mathrm{d}\Gamma^{1m_1 2m_2}_{3m_3 4m_4}}{\mathrm{d}\alpha}\right)_{\mathrm{III}} \coloneqq \sum_{tv}\sum_{m_t m_v}\left(G^{1m_1 tm_t vm_v 2m_2}_{3m_3 vm_v tm_t 4m_4}-G^{1m_1 tm_t vm_v 2m_2}_{4m_4 vm_v tm_t 3m_3}\right)(n_t-n_v) \tag{B.6}$$

$$=\sum_{tv}\sum_{m_t m_v}\Bigg(\eta^{1m_1 tm_t}_{3m_3 vm_v}\Gamma^{vm_v 2m_2}_{tm_t 4m_4}-\Gamma^{1m_1 tm_t}_{3m_3 vm_v}\eta^{vm_v 2m_2}_{tm_t 4m_4} \\ -\eta^{1m_1 tm_t}_{4m_4 vm_v}\Gamma^{vm_v 2m_2}_{tm_t 3m_3}+\Gamma^{1m_1 tm_t}_{4m_4 vm_v}\eta^{vm_v 2m_2}_{tm_t 3m_3}\Bigg)(n_t-n_v) \tag{B.7}$$

$$=\Bigg(-\sum_{tv}\sum_{m_t m_v}\eta^{1m_1 tm_t}_{4m_4 vm_v}\Gamma^{vm_v 2m_2}_{tm_t 3m_3}(n_t-n_v)-[3m_3\leftrightarrow 4m_4]\Bigg) \\ -\chi[1m_1 2m_2\leftrightarrow 3m_3 4m_4] \tag{B.8}$$

$$=\Bigg(\Bigg(-\frac{1}{2}\sum_{tv}\sum_{m_t m_v}\eta^{1m_1 tm_t}_{4m_4 vm_v}\Gamma^{vm_v 2m_2}_{tm_t 3m_3}(n_t-n_v)-[1m_1\leftrightarrow 2m_2]\Bigg) \\ -[3m_3\leftrightarrow 4m_4]\Bigg)-\chi[1m_1 2m_2\leftrightarrow 3m_3 4m_4] \tag{B.9}$$

interchanging lower indices yields

$$=\Bigg(\Bigg(-(-)^2\frac{1}{2}\sum_{tv}\sum_{m_t m_v}\eta^{1m_1 tm_t}_{vm_v 4m_4}\Gamma^{vm_v 2m_2}_{3m_3 tm_t}(n_t-n_v)-[1m_1\leftrightarrow 2m_2]\Bigg) \\ -[3m_3\leftrightarrow 4m_4]\Bigg)-\chi[1m_1 2m_2\leftrightarrow 3m_3 4m_4]. \tag{B.10}$$

The J-coupling then yields

$$\left(\frac{\mathrm{d}\,{}^{J}\Gamma^{12}_{34}}{\mathrm{d}\alpha}\right)_{\mathrm{III}}=\sum_{\substack{m_1 m_2\\ m_3 m_4}}\left(\frac{\mathrm{d}\Gamma^{1m_1 2m_2}_{3m_3 4m_4}}{\mathrm{d}\alpha}\right)_{\mathrm{III}}\begin{pmatrix}j_1 & j_2\\ m_1 & m_2\end{pmatrix}\!\!\begin{vmatrix}J\\ M\end{vmatrix}\begin{pmatrix}j_3 & j_4\\ m_3 & m_4\end{pmatrix}\!\!\begin{vmatrix}J\\ M\end{vmatrix}. \tag{B.11}$$

Averaging over the M quantum number does not change the term and we get

$$=\sum_{M}\sum_{\substack{m_1 m_2\\ m_3 m_4}}\frac{1}{\hat{J}^2}\left(\frac{\mathrm{d}\Gamma^{1m_1 2m_2}_{3m_3 4m_4}}{\mathrm{d}\alpha}\right)_{\mathrm{III}}\begin{pmatrix}j_1 & j_2\\ m_1 & m_2\end{pmatrix}\!\!\begin{vmatrix}J\\ M\end{vmatrix}\begin{pmatrix}j_3 & j_4\\ m_3 & m_4\end{pmatrix}\!\!\begin{vmatrix}J\\ M\end{vmatrix} \tag{B.12}$$

$$=\Bigg(\Bigg(-\frac{1}{2}\sum_{M}\sum_{\substack{m_1 m_2\\ m_3 m_4}}\sum_{tv}\sum_{m_t m_v}\frac{1}{\hat{J}^2}\eta^{1m_1 tm_t}_{vm_v 4m_4}\Gamma^{vm_v 2m_2}_{3m_3 tm_t}(n_t-n_v) \\ \times\begin{pmatrix}j_1 & j_2\\ m_1 & m_2\end{pmatrix}\!\!\begin{vmatrix}J\\ M\end{vmatrix}\begin{pmatrix}j_3 & j_4\\ m_3 & m_4\end{pmatrix}\!\!\begin{vmatrix}J\\ M\end{vmatrix}-(-)^{J-j_1-j_2}[1\leftrightarrow 2]\Bigg) \\ -(-)^{J-j_3-j_4}[3\leftrightarrow 4]\Bigg)-\chi[12\leftrightarrow 34] \tag{B.13}$$

$$
\begin{aligned}
=\Bigg(\Bigg(&-\frac{1}{2}\sum_{M}\sum_{\substack{m_1m_2\\m_3m_4}}\sum_{tv}\sum_{m_tm_v}\sum_{J_1J_2}\sum_{M_1M_2}\frac{1}{\hat{J}^2}\,{}^{J_1}\eta_{v4}^{1t}\,{}^{J_2}\Gamma_{3t}^{v2}(n_t-n_v)\\
&\times\begin{pmatrix} j_1 & j_t \\ m_1 & m_t \end{pmatrix}\!\!\begin{vmatrix} J_1 \\ M_1 \end{vmatrix}\begin{pmatrix} j_v & j_4 \\ m_v & m_4 \end{pmatrix}\!\!\begin{vmatrix} J_1 \\ M_1 \end{vmatrix}\begin{pmatrix} j_v & j_2 \\ m_v & m_2 \end{pmatrix}\!\!\begin{vmatrix} J_2 \\ M_2 \end{vmatrix}\begin{pmatrix} j_3 & j_t \\ m_3 & m_t \end{pmatrix}\!\!\begin{vmatrix} J_2 \\ M_2 \end{vmatrix}\\
&\times\begin{pmatrix} j_1 & j_2 \\ m_1 & m_2 \end{pmatrix}\!\!\begin{vmatrix} J \\ M \end{vmatrix}\begin{pmatrix} j_3 & j_4 \\ m_3 & m_4 \end{pmatrix}\!\!\begin{vmatrix} J \\ M \end{vmatrix}-(-)^{J-j_1-j_2}[1\leftrightarrow 2]\Bigg)\\
&-(-)^{J-j_3-j_4}[3\leftrightarrow 4]\Bigg)-\chi[12\leftrightarrow 34].
\end{aligned}
\tag{B.14}
$$

Using (16) in [VMK88, p. 339] and inserting the inverse Pandya transformation (4.50) yields

$$
\begin{aligned}
=\Bigg(\Bigg(&-\frac{1}{2}\sum_{tv}\sum_{J_1J_2}\sum_{J_5J_6}\frac{1}{\hat{J}^2}\hat{J}_5^2\hat{J}_6^2\begin{Bmatrix} j_1 & j_4 & J_5 \\ j_v & j_t & J_1 \end{Bmatrix}\begin{Bmatrix} j_v & j_t & J_6 \\ j_3 & j_2 & J_2 \end{Bmatrix}{}^{J_5}\overline{\eta}_{v\bar{t}}^{1\bar{4}}\,{}^{J_6}\overline{\Gamma}_{3\bar{2}}^{v\bar{t}}(n_t-n_v)\\
&\times\hat{J}^2\hat{J}_1^2\hat{J}_2^2\begin{Bmatrix} J & j_1 & j_2 \\ j_3 & j_t & J_2 \\ j_4 & J_1 & j_v \end{Bmatrix}-(-)^{J-j_1-j_2}[1\leftrightarrow 2]\Bigg)\\
&-(-)^{J-j_3-j_4}[3\leftrightarrow 4]\Bigg)-\chi[12\leftrightarrow 34]
\end{aligned}
\tag{B.15}
$$

$$
\begin{aligned}
=\Bigg(\Bigg(&-\frac{1}{2}\sum_{tv}\sum_{J_1J_2}\sum_{J_5J_6}\frac{1}{\cancel{\hat{J}^2}}\hat{J}_5^2\hat{J}_6^2\begin{Bmatrix} j_1 & j_4 & J_5 \\ j_v & j_t & J_1 \end{Bmatrix}\begin{Bmatrix} j_v & j_t & J_6 \\ j_3 & j_2 & J_2 \end{Bmatrix}{}^{J_5}\overline{\eta}_{v\bar{t}}^{1\bar{4}}\,{}^{J_6}\overline{\Gamma}_{3\bar{2}}^{v\bar{t}}(n_t-n_v)\\
&\times\cancel{\hat{J}^2}\hat{J}_1^2\hat{J}_2^2\begin{Bmatrix} J & j_1 & j_2 \\ j_3 & j_t & J_2 \\ j_4 & J_1 & j_v \end{Bmatrix}-(-)^{J-j_1-j_2}[1\leftrightarrow 2]\Bigg)\\
&-(-)^{J-j_3-j_4}[3\leftrightarrow 4]\Bigg)-\chi[12\leftrightarrow 34].
\end{aligned}
\tag{B.16}
$$

The sum over J_1 and J_2 can be simplified using relation (25) on p. 467 in [VMK88]

$$
\begin{aligned}
=\Bigg(\Bigg(&-\frac{1}{2}\sum_{tv}\sum_{J_5J_6}\hat{J}_5^2\cancel{\hat{J}_6^2}\frac{1}{\cancel{\hat{J}_6^2}}\delta^{J_5}_{J_6}\begin{Bmatrix} J & j_1 & j_2 \\ J_6 & j_3 & j_4 \end{Bmatrix}{}^{J_5}\overline{\eta}_{v\bar{t}}^{1\bar{4}}\,{}^{J_6}\overline{\Gamma}_{3\bar{2}}^{v\bar{t}}(n_t-n_v) &\text{(B.17)}\\
&-(-)^{J-j_1-j_2}[1\leftrightarrow 2]\Bigg)-(-)^{J-j_3-j_4}[3\leftrightarrow 4]\Bigg)-\chi[12\leftrightarrow 34] &\text{(B.18)}\\
=\Bigg(\Bigg(&-\frac{1}{2}\sum_{tv}\sum_{J_5}\hat{J}_5^2\begin{Bmatrix} J & j_1 & j_2 \\ J_5 & j_3 & j_4 \end{Bmatrix}{}^{J_5}\overline{\eta}_{v\bar{t}}^{1\bar{4}}\,{}^{J_5}\overline{\Gamma}_{3\bar{2}}^{v\bar{t}}(n_t-n_v)\\
&-(-)^{J-j_1-j_2}[1\leftrightarrow 2]\Bigg)-(-)^{J-j_3-j_4}[3\leftrightarrow 4]\Bigg)-\chi[12\leftrightarrow 34] &\text{(B.19)}\\
=\Bigg(\Bigg(&-\frac{1}{2}\sum_{tv}\sum_{J'}\hat{J}'^2\begin{Bmatrix} J & j_1 & j_2 \\ J' & j_3 & j_4 \end{Bmatrix}{}^{J'}\overline{\eta}_{v\bar{t}}^{1\bar{4}}\,{}^{J'}\overline{\Gamma}_{3\bar{2}}^{v\bar{t}}(n_t-n_v)\\
&-(-)^{J-j_1-j_2}[1\leftrightarrow 2]\Bigg)-(-)^{J-j_3-j_4}[3\leftrightarrow 4]\Bigg)-\chi[12\leftrightarrow 34]. &\text{(B.20)}
\end{aligned}
$$

B.1.2. J-Coupling of the One-Body Terms

For the J-coupling of the one-body terms we will proceed as follows: We write each term in a way that is proportional to the factor $\delta^{j_1}_{j_2}\delta^{m_1}_{m_2}$. Consequently, the remaining term is the m-independent matrix element that we are looking for. Only for a specific term we will make use of the averaging procedure.

The first term has already been considered in section 4.3.2. The second and third lines in (4.28b) can be combined to

$$\left(\frac{\mathrm{d}f^{1m_1}_{2m_2}}{\mathrm{d}s}\right)_{\mathrm{II}} := \sum_{rt}\sum_{m_r m_t} \Gamma^{1m_1 rm_r}_{2m_2 tm_t}\eta^{tm_t}_{rm_r}(n_t-n_r) + \sum_{rt}\sum_{m_r m_t}\eta^{1m_1 rm_r}_{2m_2 tm_t} f^{tm_t}_{rm_r}(n_r-n_t) \tag{B.21}$$

$$= \sum_{rt}\sum_{m_r m_t}\left(\Gamma^{1m_1 rm_r}_{2m_2 tm_t}\eta^{tm_t}_{rm_r} - \eta^{1m_1 rm_r}_{2m_2 tm_t} f^{tm_t}_{rm_r}\right)(n_t-n_r) \tag{B.22}$$

$$= (-)^2\sum_{rt}\sum_{m_r m_t}\left(\Gamma^{rm_r 1m_1}_{tm_t 2m_2}\eta^{tm_t}_{rm_r} - \eta^{rm_r 1m_1}_{tm_t 2m_2} f^{tm_t}_{rm_r}\right) n_t - \chi[1m_1 \leftrightarrow 2m_2] \tag{B.23}$$

$$= \sum_{JM}\sum_{rt}\sum_{m_r m_t}\left({}^{J}\Gamma^{r1}_{t2}\eta^{t}_{r} - {}^{J}\eta^{r1}_{t2} f^{t}_{r}\right) n_t \begin{pmatrix} j_r & j_1 & J \\ m_r & m_1 & M \end{pmatrix}\begin{pmatrix} j_t & j_2 & J \\ m_t & m_2 & M \end{pmatrix}\delta^{j_t}_{j_r}\delta^{m_t}_{m_r} - \chi[1m_1 \leftrightarrow 2m_2] \tag{B.24}$$

$$\overset{(4.34)}{=} \frac{1}{\hat{j}_1^2}\delta^{j_1}_{j_2}\delta^{m_1}_{m_2}\sum_{J}\sum_{rt}\hat{J}^2\left({}^{J}\Gamma^{r1}_{t2}\eta^{t}_{r} - {}^{J}\eta^{r1}_{t2} f^{t}_{r}\right) n_t - \chi[1m_1 \leftrightarrow 2m_2], \tag{B.25}$$

where the projection-quantum-number independent part is given by

$$\left(\frac{\mathrm{d}f^{1}_{2}}{\mathrm{d}s}\right)_{\mathrm{II}} = \frac{1}{\hat{j}_1^2}\sum_{J}\sum_{rt}\hat{J}^2 n_t\left({}^{J}\Gamma^{r1}_{t2}\eta^{t}_{r} - {}^{J}\eta^{r1}_{t2} f^{t}_{r}\right) - \chi[1 \leftrightarrow 2]. \tag{B.26}$$

The expression in the fourth line of (4.28b) can be summarized to

$$\left(\frac{\mathrm{d}f^{1m_1}_{2m_2}}{\mathrm{d}s}\right)_{\mathrm{III}} := \frac{1}{2}\sum_{rtv}\sum_{m_r m_t m_v} G^{1m_1 rm_r tm_t vm_v}_{tm_t vm_v 2m_2 rm_r}(\bar{n}_t\bar{n}_v n_r + n_t n_v\bar{n}_r) \tag{B.27}$$

$$= \frac{1}{2}\sum_{rtv}\sum_{m_r m_t m_v}\left(\eta^{1m_1 rm_r}_{tm_t vm_v}\Gamma^{tm_t vm_v}_{2m_2 rm_r} - \Gamma^{1m_1 rm_r}_{tm_t vm_v}\eta^{tm_t vm_v}_{2m_2 rm_r}\right)(\bar{n}_t\bar{n}_v n_r + n_t n_v\bar{n}_r) \tag{B.28}$$

$$= \frac{1}{2}\sum_{rtv}\sum_{m_r m_t m_v}\eta^{1m_1 rm_r}_{tm_t vm_v}\Gamma^{tm_t vm_v}_{2m_2 rm_r}(\bar{n}_t\bar{n}_v n_r + n_t n_v\bar{n}_r) - \chi[1m_1 \leftrightarrow 2m_2] \tag{B.29}$$

$$= \frac{1}{2}\sum_{JM}\sum_{rtv}\sum_{m_r}{}^{J}\eta^{1r}_{tv}\,{}^{J}\Gamma^{tv}_{2r}\begin{pmatrix} j_1 & j_r & J \\ m_1 & m_r & M \end{pmatrix}\begin{pmatrix} j_2 & j_r & J \\ m_2 & m_r & M \end{pmatrix}(\bar{n}_t\bar{n}_v n_r + n_t n_v\bar{n}_r) - \chi[1m_1 \leftrightarrow 2m_2] \tag{B.30}$$

$$\overset{(4.34)}{=} \frac{1}{2}\frac{1}{\hat{j}_1^2}\delta^{j_1}_{j_2}\delta^{m_1}_{m_2}\sum_{J}\sum_{rtv}\hat{J}^2\,{}^{J}\eta^{1r}_{tv}\,{}^{J}\Gamma^{tv}_{2r}(\bar{n}_t\bar{n}_v n_r + n_t n_v\bar{n}_r) - \chi[1m_1 \leftrightarrow 2m_2], \tag{B.31}$$

yielding

$$\left(\frac{\mathrm{d}f_2^1}{\mathrm{d}s}\right)_{\mathrm{III}} = \frac{1}{2\hat{j}_1^2}\sum_J\sum_{rtv} \hat{J}^2\, {}^J\eta^{1r}_{tv}\, {}^J\Gamma^{tv}_{2r}(\bar{n}_t\bar{n}_v n_r + n_t n_v \bar{n}_r) - \chi[1 \leftrightarrow 2]. \tag{B.32}$$

The last line in (4.28b) contains three structurally different terms that are specific for the multi-reference case. The term IV is defined as the first subterm

$$\left(\frac{\mathrm{d}f_{2m_2}^{1m_1}}{\mathrm{d}s}\right)_{\mathrm{IV}} := \frac{1}{4}\sum_{tswrv}\sum_{m_t m_s m_w m_r m_v} G^{1m_1 tm_t rm_r vm_v}_{sm_s wm_w 2m_2 tm_t}\lambda^{rm_r vm_v}_{sm_s wm_w} \tag{B.33}$$

$$= \frac{1}{4}\sum_{tswrv}\sum_{m_t m_s m_w m_r m_v} \eta^{1m_1 tm_t}_{sm_s wm_w}\Gamma^{rm_r vm_v}_{2m_2 tm_t}\lambda^{rm_r vm_v}_{sm_s wm_w} - [\,\eta \leftrightarrow\ \Gamma] \tag{B.34}$$

$$= \frac{1}{4}\sum_{tswrv}\sum_{m_t m_s m_w m_r m_v} \eta^{1m_1 tm_t}_{sm_s wm_w}\Gamma^{rm_r vm_v}_{2m_2 tm_t}\lambda^{rm_r vm_v}_{sm_s wm_w} - \chi[1m_1 \leftrightarrow 2m_2] \tag{B.35}$$

$$= \frac{1}{4}\sum_{JM}\sum_{tswrv}\sum_{m_t} {}^J\eta^{1t}_{sw}\, {}^J\Gamma^{rv}_{2t}\, {}^J\lambda^{rv}_{sw}\begin{pmatrix} j_1 & j_t \\ m_1 & m_t \end{pmatrix}\!\Big| \begin{matrix} J \\ M \end{matrix}\!\Big)\begin{pmatrix} j_2 & j_t \\ m_2 & m_t \end{pmatrix}\!\Big| \begin{matrix} J \\ M \end{matrix}\!\Big) - \chi[1m_1 \leftrightarrow 2m_2] \tag{B.36}$$

$$\overset{(4.34)}{=} \frac{1}{4}\frac{1}{\hat{j}_1^2}\delta^{j_1}_{j_2}\delta^{m_1}_{m_2}\sum_J\sum_{tswrv} \hat{J}^2\, {}^J\eta^{1t}_{sw}\, {}^J\Gamma^{rv}_{2t}\, {}^J\lambda^{rv}_{sw} - \chi[1m_1 \leftrightarrow 2m_2], \tag{B.37}$$

where the m-independent part can be read off

$$\left(\frac{\mathrm{d}f_2^1}{\mathrm{d}s}\right)_{\mathrm{IV}} = \frac{1}{4}\frac{1}{\hat{j}_1^2}\sum_J\sum_{tswrv} \hat{J}^2\, {}^J\eta^{1t}_{sw}\, {}^J\Gamma^{rv}_{2t}\, {}^J\lambda^{rv}_{sw} - \chi[1 \leftrightarrow 2]. \tag{B.38}$$

The second subterm in last line of (4.28b) can be simplified to

$$\left(\frac{\mathrm{d}f_{2m_2}^{1m_1}}{\mathrm{d}s}\right)_{\mathrm{V}} := \sum_{rtswv}\sum_{m_r m_t m_s m_w m_v} G^{1m_1 rm_r tm_t vm_v}_{tm_t sm_s 2m_2 wm_w}\lambda^{rm_r vm_v}_{sm_s wm_w} \tag{B.39}$$

$$= \sum_{rtswv}\sum_{m_r m_t m_s m_w m_v} \eta^{1m_1 rm_r}_{tm_t sm_s}\Gamma^{tm_t vm_v}_{2m_2 wm_w}\lambda^{rm_r vm_v}_{sm_s wm_w} - [\,\eta \leftrightarrow\ \Gamma] \tag{B.40}$$

$$= -\sum_{rtswv}\sum_{m_r m_t m_s m_w m_v} \eta^{1m_1 rm_r}_{sm_s tm_t}\lambda^{sm_s wm_w}_{vm_v rm_r}\Gamma^{vm_v tm_t}_{2m_2 wm_w} - \chi[1m_1 \leftrightarrow 2m_2] \tag{B.41}$$

$$= -\sum_{rtswv}\sum_{m_r m_t m_s m_w m_v}\sum_{J_4 J_5 J_6}\sum_{M_4 M_5 M_6} {}^{J_4}\eta^{1r}_{st}\, {}^{J_5}\lambda^{sw}_{vr}\, {}^{J_6}\Gamma^{vt}_{2w}$$
$$\times \begin{pmatrix} j_1 & j_r \\ m_1 & m_r \end{pmatrix}\!\Big| \begin{matrix} J_4 \\ M_4 \end{matrix}\!\Big)\begin{pmatrix} j_s & j_t \\ m_s & m_t \end{pmatrix}\!\Big| \begin{matrix} J_4 \\ M_4 \end{matrix}\!\Big)\begin{pmatrix} j_s & j_w \\ m_s & m_w \end{pmatrix}\!\Big| \begin{matrix} J_5 \\ M_5 \end{matrix}\!\Big)$$
$$\times \begin{pmatrix} j_v & j_r \\ m_v & m_r \end{pmatrix}\!\Big| \begin{matrix} J_5 \\ M_5 \end{matrix}\!\Big)\begin{pmatrix} j_v & j_t \\ m_v & m_t \end{pmatrix}\!\Big| \begin{matrix} J_6 \\ M_6 \end{matrix}\!\Big)\begin{pmatrix} j_2 & j_w \\ m_2 & m_w \end{pmatrix}\!\Big| \begin{matrix} J_6 \\ M_6 \end{matrix}\!\Big) - \chi[1m_1 \leftrightarrow 2m_2] \tag{B.42}$$

$$
\begin{aligned}
&= -(-)^3 \sum_{rtswv} \sum_{m_r m_t m_s m_w m_v} \sum_{J_4 J_5 J_6} \sum_{M_4 M_5 M_6} \sum_{J_1 J_2 J_3} \hat{J}_1^2 \hat{J}_2^2 \hat{J}_3^2 \, {}^{J_1}\overline{\eta}^{1\bar{t}}_{s\bar{r}} \, {}^{J_2}\overline{\lambda}^{s\bar{r}}_{v\bar{w}} \, {}^{J_3}\overline{\Gamma}^{v\bar{w}}_{2\bar{t}} \\
&\quad \times \begin{Bmatrix} j_1 & j_r & J_4 \\ j_s & j_t & J_1 \end{Bmatrix} \begin{Bmatrix} j_s & j_w & J_5 \\ j_v & j_r & J_2 \end{Bmatrix} \begin{Bmatrix} j_v & j_t & J_6 \\ j_2 & j_w & J_3 \end{Bmatrix} \hat{J}_4^2 \hat{J}_5^2 \hat{J}_6^2 \, (-)^6 \\
&\quad \times \begin{pmatrix} j_1 & j_r & J_4 \\ m_1 & m_r & -M_4 \end{pmatrix} \begin{pmatrix} j_s & j_t & J_4 \\ m_s & m_t & -M_4 \end{pmatrix} \begin{pmatrix} j_s & j_w & J_5 \\ m_s & m_w & -M_5 \end{pmatrix} \\
&\quad \times \begin{pmatrix} j_v & j_r & J_5 \\ m_v & m_r & -M_5 \end{pmatrix} \begin{pmatrix} j_v & j_t & J_6 \\ m_v & m_t & -M_6 \end{pmatrix} \begin{pmatrix} j_2 & j_w & J_6 \\ m_2 & m_w & -M_6 \end{pmatrix} \\
&\quad - \chi[1 m_1 \leftrightarrow 2 m_2]. \qquad \text{(B.43)}
\end{aligned}
$$

For this case, we make use of the averaging procedure as formulated in (4.44) to extract the m-independent part

$$
\begin{aligned}
\left(\frac{\mathrm{d} f_2^1}{\mathrm{d}s}\right)_{\mathrm{V}} &= + \frac{1}{\hat{j}_1^2} \sum_{m_1 m_2} \delta^{m_1}_{m_2} \delta^{j_1}_{j_2} \\
&\quad \times \Bigg(\sum_{rtswv} \sum_{m_r m_t m_s m_w m_v} \sum_{J_4 J_5 J_6} \sum_{M_4 M_5 M_6} \sum_{J_1 J_2 J_3} \hat{J}_1^2 \hat{J}_2^2 \hat{J}_3^2 \, {}^{J_1}\overline{\eta}^{1\bar{t}}_{s\bar{r}} \, {}^{J_2}\overline{\lambda}^{s\bar{r}}_{v\bar{w}} \, {}^{J_3}\overline{\Gamma}^{v\bar{w}}_{2\bar{t}} \\
&\quad \times \begin{Bmatrix} j_1 & j_r & J_4 \\ j_s & j_t & J_1 \end{Bmatrix} \begin{Bmatrix} j_s & j_w & J_5 \\ j_v & j_r & J_2 \end{Bmatrix} \begin{Bmatrix} j_v & j_t & J_6 \\ j_2 & j_w & J_3 \end{Bmatrix} \hat{J}_4^2 \hat{J}_5^2 \hat{J}_6^2 \\
&\quad \times \begin{pmatrix} j_1 & j_r & J_4 \\ m_1 & m_r & -M_4 \end{pmatrix} \begin{pmatrix} j_s & j_t & J_4 \\ m_s & m_t & -M_4 \end{pmatrix} \begin{pmatrix} j_s & j_w & J_5 \\ m_s & m_w & -M_5 \end{pmatrix} \\
&\quad \times \begin{pmatrix} j_v & j_r & J_5 \\ m_v & m_r & -M_5 \end{pmatrix} \begin{pmatrix} j_v & j_t & J_6 \\ m_v & m_t & -M_6 \end{pmatrix} \begin{pmatrix} j_2 & j_w & J_6 \\ m_2 & m_w & -M_6 \end{pmatrix} \Bigg) - \chi[1 \leftrightarrow 2] \qquad \text{(B.44)} \\
&= + \frac{1}{\hat{j}_1^2} \delta^{j_1}_{j_2} \sum_{m_1} \sum_{rtswv} \sum_{m_r m_t m_s m_w m_v} \sum_{J_4 J_5 J_6} \sum_{M_4 M_5 M_6} \sum_{J_1 J_2 J_3} \hat{J}_1^2 \hat{J}_2^2 \hat{J}_3^2 \, {}^{J_1}\overline{\eta}^{1\bar{t}}_{s\bar{r}} \, {}^{J_2}\overline{\lambda}^{s\bar{r}}_{v\bar{w}} \, {}^{J_3}\overline{\Gamma}^{v\bar{w}}_{2\bar{t}} \\
&\quad \times \begin{Bmatrix} j_1 & j_r & J_4 \\ j_s & j_t & J_1 \end{Bmatrix} \begin{Bmatrix} j_s & j_w & J_5 \\ j_v & j_r & J_2 \end{Bmatrix} \begin{Bmatrix} j_v & j_t & J_6 \\ j_1 & j_w & J_3 \end{Bmatrix} \hat{J}_4^2 \hat{J}_5^2 \hat{J}_6^2 \\
&\quad \times \begin{pmatrix} j_1 & j_r & J_4 \\ m_1 & m_r & -M_4 \end{pmatrix} \begin{pmatrix} j_s & j_t & J_4 \\ m_s & m_t & -M_4 \end{pmatrix} \begin{pmatrix} j_s & j_w & J_5 \\ m_s & m_w & -M_5 \end{pmatrix} \\
&\quad \times \begin{pmatrix} j_v & j_r & J_5 \\ m_v & m_r & -M_5 \end{pmatrix} \begin{pmatrix} j_v & j_t & J_6 \\ m_v & m_t & -M_6 \end{pmatrix} \begin{pmatrix} j_1 & j_w & J_6 \\ m_1 & m_w & -M_6 \end{pmatrix} - \chi[1 \leftrightarrow 2]. \qquad \text{(B.45)}
\end{aligned}
$$

With the aid of proposition B.1, which will be proved later on, we obtain

$$
\begin{aligned}
&= \frac{1}{\hat{j}_1^2} \delta^{j_1}_{j_2} \sum_{rtswv} \sum_{J_1 J_2 J_3} {}^{J_1}\overline{\eta}^{1\bar{t}}_{s\bar{r}} \, {}^{J_2}\overline{\lambda}^{s\bar{r}}_{v\bar{w}} \, {}^{J_3}\overline{\Gamma}^{v\bar{w}}_{2\bar{t}} \, \hat{J}_1^2 \delta^{J_1}_{J_3} \delta^{J_2}_{J_3} - \chi[1 \leftrightarrow 2] \qquad \text{(B.46)} \\
&= \frac{1}{\hat{j}_1^2} \sum_{J} \sum_{rtswv} \hat{J}^2 \, {}^{J}\overline{\eta}^{1\bar{t}}_{s\bar{r}} \, {}^{J}\overline{\lambda}^{s\bar{r}}_{v\bar{w}} \, {}^{J}\overline{\Gamma}^{v\bar{w}}_{2\bar{t}} - \chi[1 \leftrightarrow 2]. \qquad \text{(B.47)}
\end{aligned}
$$

In the last step, we used the following identity that can be proved with the aid of some relations from [VMK88]:

Proposition B.1.

$$\begin{aligned}
&\sum_{m_1}\sum_{m_r m_t m_s m_w m_v}\sum_{J_4 J_5 J_6}\sum_{M_4 M_5 M_6} \hat{j}_1^2\hat{j}_2^2\hat{j}_3^2\hat{j}_4^2\hat{j}_5^2\hat{j}_6^2 \begin{Bmatrix} j_1 & j_r & J_4 \\ j_s & j_t & J_1 \end{Bmatrix}\begin{Bmatrix} j_s & j_w & J_5 \\ j_v & j_r & J_2 \end{Bmatrix}\begin{Bmatrix} j_v & j_t & J_6 \\ j_1 & j_w & J_3 \end{Bmatrix} \\
&\quad\times \begin{pmatrix} j_1 & j_r & J_4 \\ m_1 & m_r & -M_4 \end{pmatrix}\begin{pmatrix} j_s & j_t & J_4 \\ m_s & m_t & -M_4 \end{pmatrix}\begin{pmatrix} j_s & j_w & J_5 \\ m_s & m_w & -M_5 \end{pmatrix} \\
&\quad\times \begin{pmatrix} j_v & j_r & J_5 \\ m_v & m_r & -M_5 \end{pmatrix}\begin{pmatrix} j_v & j_t & J_6 \\ m_v & m_t & -M_6 \end{pmatrix}\begin{pmatrix} j_1 & j_w & J_6 \\ m_1 & m_w & -M_6 \end{pmatrix} \\
&= \hat{J}_1^2\delta_{J_3}^{J_1}\delta_{J_3}^{J_2}\Delta_{\{j_v j_w J_1\}}\Delta_{\{j_1 j_t J_1\}}\Delta_{\{j_r j_s J_1\}}
\end{aligned} \tag{B.48}$$

Proof. Since all relations necessary to prove this identity are taken from [VMK88], we note the page, equation number above the equal sign (=) to shorten the notation.

$$\begin{aligned}
&\sum_{m_1}\sum_{m_r m_t m_s m_w m_v}\sum_{J_4 J_5 J_6}\sum_{M_4 M_5 M_6} \hat{j}_1^2\hat{j}_2^2\hat{j}_3^2\hat{j}_4^2\hat{j}_5^2\hat{j}_6^2 \begin{Bmatrix} j_1 & j_r & J_4 \\ j_s & j_t & J_1 \end{Bmatrix}\begin{Bmatrix} j_s & j_w & J_5 \\ j_v & j_r & J_2 \end{Bmatrix}\begin{Bmatrix} j_v & j_t & J_6 \\ j_1 & j_w & J_3 \end{Bmatrix} \\
&\quad\times \begin{pmatrix} j_1 & j_r & J_4 \\ m_1 & m_r & -M_4 \end{pmatrix}\begin{pmatrix} j_s & j_t & J_4 \\ m_s & m_t & -M_4 \end{pmatrix}\begin{pmatrix} j_s & j_w & J_5 \\ m_s & m_w & -M_5 \end{pmatrix} \\
&\quad\times \begin{pmatrix} j_v & j_r & J_5 \\ m_v & m_r & -M_5 \end{pmatrix}\begin{pmatrix} j_v & j_t & J_6 \\ m_v & m_t & -M_6 \end{pmatrix}\begin{pmatrix} j_1 & j_w & J_6 \\ m_1 & m_w & -M_6 \end{pmatrix}
\end{aligned} \tag{B.49}$$

$$\begin{aligned}
&\overset{\text{p.455 (10)}}{=} \sum_{m_r m_t m_v}\sum_{J_4 J_5 J_6}\sum_{M_5 M_6}\sum_{J_7 M_7} \hat{J}_7^2\hat{j}_1^2\hat{j}_2^2\hat{j}_3^2\hat{j}_4^2\hat{j}_5^2\hat{j}_6^2 \begin{Bmatrix} j_1 & j_r & J_4 \\ j_s & j_t & J_1 \end{Bmatrix}\begin{Bmatrix} j_s & j_w & J_5 \\ j_v & j_r & J_2 \end{Bmatrix}\begin{Bmatrix} j_v & j_t & J_6 \\ j_1 & j_w & J_3 \end{Bmatrix} \\
&\quad\times \begin{pmatrix} J_5 & J_7 & J_6 \\ -M_5 & -M_7 & M_6 \end{pmatrix}\begin{pmatrix} j_t & J_7 & j_r \\ -m_t & M_7 & m_r \end{pmatrix}\begin{Bmatrix} j_1 & j_s & J_7 \\ J_5 & J_6 & j_w \end{Bmatrix}\begin{Bmatrix} j_1 & j_r & J_4 \\ j_t & j_s & J_7 \end{Bmatrix} \\
&\quad\times \begin{pmatrix} j_v & j_r & J_5 \\ m_v & m_r & -M_5 \end{pmatrix}\begin{pmatrix} j_v & j_t & J_6 \\ m_v & m_t & -M_6 \end{pmatrix} \\
&\quad\times (-)^{j_r+j_t+j_s+j_w+J_4+J_5+J_6+J_7+M_7+m_r+M_5+1}
\end{aligned} \tag{B.50}$$

$$\begin{aligned}
&= \sum_{m_r m_t m_v}\sum_{J_4 J_5 J_6}\sum_{M_5 M_6}\sum_{J_7 M_7} \hat{J}_7^2\hat{j}_1^2\hat{j}_2^2\hat{j}_3^2\hat{j}_4^2\hat{j}_5^2\hat{j}_6^2 \begin{Bmatrix} j_1 & j_r & J_4 \\ j_s & j_t & J_1 \end{Bmatrix}\begin{Bmatrix} j_s & j_w & J_5 \\ j_v & j_r & J_2 \end{Bmatrix}\begin{Bmatrix} j_v & j_t & J_6 \\ j_1 & j_w & J_3 \end{Bmatrix} \\
&\quad\times \begin{pmatrix} J_5 & J_7 & J_6 \\ -M_5 & -M_7 & M_6 \end{pmatrix}\begin{pmatrix} j_t & J_7 & j_r \\ -m_t & M_7 & m_r \end{pmatrix}\begin{Bmatrix} j_1 & j_s & J_7 \\ J_5 & J_6 & j_w \end{Bmatrix}\begin{Bmatrix} j_1 & j_r & J_4 \\ j_t & j_s & J_7 \end{Bmatrix} \\
&\quad\times \begin{pmatrix} j_v & j_r & J_5 \\ m_v & m_r & -M_5 \end{pmatrix}\begin{pmatrix} j_v & j_t & J_6 \\ m_v & m_t & -M_6 \end{pmatrix} \\
&\quad\times (-)^{j_r+j_t+j_s+j_w+J_4+J_5+J_6+J_7+M_7+m_r+M_5+1}
\end{aligned} \tag{B.51}$$

$$\overset{\text{p.454 (6)}}{=} \sum_{m_t m_v} \sum_{J_4 J_5 J_6} \sum_{M_6} \sum_{J_7} \hat{J}_7^2 \hat{J}_1^2 \hat{J}_2^2 \hat{J}_3^2 \hat{J}_4^2 \hat{J}_5^2 \hat{J}_6^2 \begin{Bmatrix} j_1 & j_r & J_4 \\ j_s & j_t & J_1 \end{Bmatrix} \begin{Bmatrix} j_s & j_w & J_5 \\ j_v & j_r & J_2 \end{Bmatrix} \begin{Bmatrix} j_v & j_t & J_6 \\ j_1 & j_w & J_3 \end{Bmatrix}$$
$$\times \begin{pmatrix} j_t & j_v & J_6 \\ m_t & m_v & -M_6 \end{pmatrix} \begin{Bmatrix} j_r & j_t & J_7 \\ J_6 & J_5 & j_v \end{Bmatrix} \begin{Bmatrix} j_1 & j_s & J_7 \\ J_5 & J_6 & j_w \end{Bmatrix} \begin{Bmatrix} j_1 & j_r & J_4 \\ j_t & j_s & J_7 \end{Bmatrix}$$
$$\times \begin{pmatrix} j_v & j_t & J_6 \\ m_v & m_t & -M_6 \end{pmatrix} (-)^{j_r+j_s+j_w+j_1+J_4+J_5} \tag{B.52}$$

$$= \sum_{m_t m_v} \sum_{J_4 J_5 J_6} \sum_{M_6} \sum_{J_7} \hat{J}_7^2 \hat{J}_1^2 \hat{J}_2^2 \hat{J}_3^2 \hat{J}_4^2 \hat{J}_5^2 \hat{J}_6^2 \begin{Bmatrix} j_1 & j_r & J_4 \\ j_s & j_t & J_1 \end{Bmatrix} \begin{Bmatrix} j_s & j_w & J_5 \\ j_v & j_r & J_2 \end{Bmatrix} \begin{Bmatrix} j_v & j_t & J_6 \\ j_1 & j_w & J_3 \end{Bmatrix}$$
$$\times \begin{pmatrix} j_t & j_v & J_6 \\ m_t & m_v & -M_6 \end{pmatrix} \begin{Bmatrix} j_r & j_t & J_7 \\ J_6 & J_5 & j_v \end{Bmatrix} \begin{Bmatrix} j_1 & j_s & J_7 \\ J_5 & J_6 & j_w \end{Bmatrix} \begin{Bmatrix} j_1 & j_r & J_4 \\ j_t & j_s & J_7 \end{Bmatrix}$$
$$\times \begin{pmatrix} j_v & j_t & J_6 \\ m_v & m_t & -M_6 \end{pmatrix} (-)^{j_r+j_s+j_w+j_1+J_4+J_5} \tag{B.53}$$

$$\overset{(4.37)}{=} \sum_{J_4 J_5 J_6} \sum_{M_6} \sum_{J_7} \hat{J}_7^2 \hat{J}_1^2 \hat{J}_2^2 \hat{J}_3^2 \hat{J}_4^2 \hat{J}_5^2 \begin{Bmatrix} j_1 & j_r & J_4 \\ j_s & j_t & J_1 \end{Bmatrix} \begin{Bmatrix} j_s & j_w & J_5 \\ j_v & j_r & J_2 \end{Bmatrix} \begin{Bmatrix} j_v & j_t & J_6 \\ j_1 & j_w & J_3 \end{Bmatrix}$$
$$\times \begin{Bmatrix} j_r & j_t & J_7 \\ J_6 & J_5 & j_v \end{Bmatrix} \begin{Bmatrix} j_1 & j_s & J_7 \\ J_5 & J_6 & j_w \end{Bmatrix} \begin{Bmatrix} j_1 & j_r & J_4 \\ j_t & j_s & J_7 \end{Bmatrix} (-)^{j_r+j_s+j_w+j_1+J_4+J_5+j_t+j_v+J_6} \tag{B.54}$$

$$= \sum_{J_4 J_5 J_6} \sum_{M_6} \sum_{J_7} \hat{J}_7^2 \hat{J}_1^2 \hat{J}_2^2 \hat{J}_3^2 \hat{J}_4^2 \hat{J}_5^2 \begin{Bmatrix} j_1 & j_r & J_4 \\ j_s & j_t & J_1 \end{Bmatrix} \begin{Bmatrix} j_s & j_w & J_5 \\ j_v & j_r & J_2 \end{Bmatrix} \begin{Bmatrix} j_v & j_t & J_6 \\ j_1 & j_w & J_3 \end{Bmatrix}$$
$$\times \begin{Bmatrix} j_r & j_t & J_7 \\ J_6 & J_5 & j_v \end{Bmatrix} \begin{Bmatrix} j_1 & j_s & J_7 \\ J_5 & J_6 & j_w \end{Bmatrix} \begin{Bmatrix} j_1 & j_r & J_4 \\ j_t & j_s & J_7 \end{Bmatrix} (-)^{j_r+j_s+j_w+j_1+J_4+J_5+j_t+j_v+J_6} \tag{B.55}$$

$$\overset{\text{p.463 (8)}}{=} \sum_{J_5 J_6} \sum_{M_6} \sum_{J_7} \hat{J}_7^2 \hat{J}_1^2 \hat{J}_2^2 \hat{J}_3^2 \hat{J}_5^2 \begin{Bmatrix} j_s & j_1 & J_7 \\ j_t & j_r & J_1 \end{Bmatrix} \begin{Bmatrix} j_s & j_w & J_5 \\ j_v & j_r & J_2 \end{Bmatrix} \begin{Bmatrix} j_v & j_t & J_6 \\ j_1 & j_w & J_3 \end{Bmatrix}$$
$$\times \begin{Bmatrix} j_r & j_t & J_7 \\ J_6 & J_5 & j_v \end{Bmatrix} \begin{Bmatrix} j_1 & j_s & J_7 \\ J_5 & J_6 & j_w \end{Bmatrix} (-)^{j_r+j_s+j_w+j_1+J_5+j_t+j_v+J_6+J_1+J_7} \tag{B.56}$$

$$= \sum_{J_5 J_6} \sum_{M_6} \sum_{J_7} \hat{J}_7^2 \hat{J}_1^2 \hat{J}_2^2 \hat{J}_3^2 \hat{J}_5^2 \begin{Bmatrix} j_s & j_1 & J_7 \\ j_t & j_r & J_1 \end{Bmatrix} \begin{Bmatrix} j_s & j_w & J_5 \\ j_v & j_r & J_2 \end{Bmatrix} \begin{Bmatrix} j_v & j_t & J_6 \\ j_1 & j_w & J_3 \end{Bmatrix}$$
$$\times \begin{Bmatrix} j_r & j_t & J_7 \\ J_6 & J_5 & j_v \end{Bmatrix} \begin{Bmatrix} j_1 & j_s & J_7 \\ J_5 & J_6 & j_w \end{Bmatrix} (-)^{j_r+j_s+j_w+j_1+J_5+j_t+j_v+J_6+J_1+J_7} \tag{B.57}$$

$$\overset{\text{p.466 (18)}}{=} \sum_{J_6} \sum_{M_6} \sum_{J_7} \hat{J}_7^2 \hat{J}_1^2 \hat{J}_2^2 \hat{J}_3^2 (-)^{J_1+J_2} \begin{Bmatrix} j_s & j_1 & J_7 \\ j_t & j_r & J_1 \end{Bmatrix} \begin{Bmatrix} J_2 & j_t & j_1 \\ J_6 & j_w & j_v \end{Bmatrix} \begin{Bmatrix} J_2 & j_t & j_1 \\ J_7 & j_s & j_r \end{Bmatrix} \begin{Bmatrix} j_v & j_t & J_6 \\ j_1 & j_w & J_3 \end{Bmatrix} \tag{B.58}$$

$$= \sum_{J_6} \sum_{M_6} \sum_{J_7} \hat{J}_7^2 \hat{J}_1^2 \hat{J}_2^2 \hat{J}_3^2 (-)^{J_1+J_2} \begin{Bmatrix} j_s & j_1 & J_7 \\ j_t & j_r & J_1 \end{Bmatrix} \begin{Bmatrix} J_2 & j_t & j_1 \\ J_6 & j_w & j_v \end{Bmatrix} \begin{Bmatrix} J_2 & j_t & j_1 \\ J_7 & j_s & j_r \end{Bmatrix} \begin{Bmatrix} j_v & j_t & J_6 \\ j_1 & j_w & J_3 \end{Bmatrix} \tag{B.59}$$

$$\overset{\text{p.463 (7)}}{=} \sum_{J_6} \sum_{M_6} \hat{J}_2^2 \hat{J}_3^2 (-)^{J_1+J_2} \delta^{J_1}_{J_2} \Delta_{\{j_1 j_t J_1\}} \Delta_{\{j_r j_s J_1\}} \begin{Bmatrix} J_2 & j_t & j_1 \\ J_6 & j_w & j_v \end{Bmatrix} \begin{Bmatrix} j_v & j_t & J_6 \\ j_1 & j_w & J_3 \end{Bmatrix} \tag{B.60}$$

$$= \sum_{J_6} \sum_{M_6} \hat{J}_2^2 \hat{J}_3^2 (-)^{J_1+J_2} \delta^{J_1}_{J_2} \Delta_{\{j_1 j_t J_1\}} \Delta_{\{j_r j_s J_1\}} \begin{Bmatrix} J_2 & j_t & j_1 \\ J_6 & j_w & j_v \end{Bmatrix} \begin{Bmatrix} j_v & j_t & J_6 \\ j_1 & j_w & J_3 \end{Bmatrix} \tag{B.61}$$

$$\overset{\text{p.463 (7)}}{=} \hat{J}_3^2 (-)^{J_1+J_2} \delta^{J_1}_{J_2} \delta^{J_2}_{J_3} \Delta_{\{j_1 j_t J_1\}} \Delta_{\{j_r j_s J_1\}} \Delta_{\{j_v j_w J_1\}} \Delta_{\{j_1 j_t J_1\}} \tag{B.62}$$

$$= \hat{J}_3^2 \delta^{J_1}_{J_2} \delta^{J_2}_{J_3} \Delta_{\{j_1 j_t J_1\}} \Delta_{\{j_r j_s J_1\}} \Delta_{\{j_v j_w J_1\}}. \tag{B.63}$$

□

The last two subterms in the last line of (4.28b) can be combined to

$$\left(\frac{\mathrm{d} f^{1m_1}_{2m_2}}{\mathrm{d}s}\right)_{\mathrm{VI}} := -\frac{1}{2} \sum_{tsrvw} \sum_{m_t m_s m_r m_v m_w} \left(G^{1m_1 t m_t r m_r v m_v}_{2m_2 s m_s t m_t w m_w} - G^{1m_1 r m_r t m_t v m_v}_{2m_2 t m_t s m_s w m_w} \right) \lambda^{r m_r v m_v}_{s m_s w m_w} \tag{B.64}$$

$$= -\frac{1}{2} \sum_{tsrvw} \sum_{m_t m_s m_r m_v m_w} \left(\eta^{1m_1 t m_t}_{2m_2 s m_s} \Gamma^{r m_r v m_v}_{t m_t w m_w} \lambda^{r m_r v m_v}_{s m_s w m_w} - [\,\eta \leftrightarrow \Gamma] \right)$$

$$- \chi[1m_1 \leftrightarrow 2m_2] \tag{B.65}$$

$$= -\frac{1}{2} \sum_{J_1 J_2 J_3} \sum_{M_1 M_2 M_3} \sum_{tsrvw} \sum_{m_t m_s m_r m_v m_w} \Bigg({}^{J_1}\eta^{1t\ J_2}_{2s}\Gamma^{rv\ J_3}_{tw} \lambda^{rv}_{sw}$$

$$\times \begin{pmatrix} j_1 & j_t \\ m_1 & m_t \end{pmatrix} \Big| \begin{matrix} J_1 \\ M_1 \end{matrix} \begin{pmatrix} j_2 & j_s \\ m_2 & m_s \end{pmatrix} \Big| \begin{matrix} J_1 \\ M_1 \end{matrix} \begin{pmatrix} j_r & j_v \\ m_r & m_v \end{pmatrix} \Big| \begin{matrix} J_2 \\ M_2 \end{matrix} \begin{pmatrix} j_t & j_w \\ m_t & m_w \end{pmatrix} \Big| \begin{matrix} J_2 \\ M_2 \end{matrix}$$

$$\times \begin{pmatrix} j_r & j_v \\ m_r & m_v \end{pmatrix} \Big| \begin{matrix} J_3 \\ M_3 \end{matrix} \begin{pmatrix} j_s & j_w \\ m_s & m_w \end{pmatrix} \Big| \begin{matrix} J_3 \\ M_3 \end{matrix} - [\,\eta \leftrightarrow \Gamma] \Bigg) - \chi[1m_1 \leftrightarrow 2m_2]. \tag{B.66}$$

Using proposition B.2 where its proof has been outsourced, we obtain

$$= -\frac{1}{2} \frac{1}{\hat{j}_1^2} \delta^{j_1}_{j_2} \delta^{m_1}_{m_2} \sum_{J_1 J_2 J_3} \sum_{tsrvw} \left(\hat{J}_1^2 \hat{J}_2^2 \delta^{J_2}_{J_3} \frac{1}{\hat{j}_t^2} \delta^{j_t}_{j_s} {}^{J_1}\eta^{1t\ J_2}_{2s} \Gamma^{rv\ J_3}_{tw} \lambda^{rv}_{sw} - [\,\eta \leftrightarrow \Gamma] \right)$$

$$- \chi[1m_1 \leftrightarrow 2m_2] \tag{B.67}$$

$$= -\frac{1}{2} \frac{1}{\hat{j}_1^2} \delta^{j_1}_{j_2} \delta^{m_1}_{m_2} \sum_{J_1 J_2 J_3} \sum_{tsrvw} \left(\hat{J}_1^2 \hat{J}_2^2 \delta^{J_2}_{J_3} \frac{1}{\hat{j}_t^2} \delta^{j_t}_{j_s} {}^{J_1}\eta^{1t\ J_2}_{2s} \Gamma^{rv\ J_3}_{tw} \lambda^{rv}_{sw} - [\,\eta \leftrightarrow \Gamma] \right)$$

$$- \chi[1m_1 \leftrightarrow 2m_2] \tag{B.68}$$

$$= -\frac{1}{2} \frac{1}{\hat{j}_1^2} \delta^{j_1}_{j_2} \delta^{m_1}_{m_2} \sum_{J_1 J_2} \sum_{tsrvw} \left(\hat{J}_1^2 \hat{J}_2^2 \frac{1}{\hat{j}_t^2} \delta^{j_t}_{j_s} {}^{J_1}\eta^{1t\ J_2}_{2s} \Gamma^{rv\ J_2}_{tw} \lambda^{rv}_{sw} - [\,\eta \leftrightarrow \Gamma] \right)$$

$$- \chi[1m_1 \leftrightarrow 2m_2]. \tag{B.69}$$

Hence, the m-independent is given by the following expression

$$\left(\frac{\mathrm{d} f^1_2}{\mathrm{d}s}\right)_{\mathrm{VI}} = -\frac{1}{2} \frac{1}{\hat{j}_1^2} \sum_{J_1 J_2} \sum_{tsrvw} \hat{J}_1^2 \hat{J}_2^2 \frac{1}{\hat{j}_t^2} \delta^{j_t}_{j_s} \left({}^{J_1}\eta^{1t\ J_2}_{2s} \Gamma^{rv\ J_2}_{tw} \lambda^{sw}_{rv} - [\,\eta \leftrightarrow \Gamma] \right) - \chi[1 \leftrightarrow 2]. \tag{B.70}$$

The crucial simplification step has been relocated to the following proposition:

Proposition B.2.

$$\begin{aligned}\sum_{M_1M_2M_3}\sum_{m_tm_sm_rm_vm_w}&\begin{pmatrix}j_1 & j_t\\ m_1 & m_t\end{pmatrix}\Big|\begin{matrix}J_1\\M_1\end{matrix}\Big)\begin{pmatrix}j_2 & j_s\\ m_2 & m_s\end{pmatrix}\Big|\begin{matrix}J_1\\M_1\end{matrix}\Big)\begin{pmatrix}j_r & j_v\\ m_r & m_v\end{pmatrix}\Big|\begin{matrix}J_2\\M_2\end{matrix}\Big)\\ &\times\begin{pmatrix}j_t & j_w\\ m_t & m_w\end{pmatrix}\Big|\begin{matrix}J_2\\M_2\end{matrix}\Big)\begin{pmatrix}j_r & j_v\\ m_r & m_v\end{pmatrix}\Big|\begin{matrix}J_3\\M_3\end{matrix}\Big)\begin{pmatrix}j_s & j_w\\ m_s & m_w\end{pmatrix}\Big|\begin{matrix}J_3\\M_3\end{matrix}\Big)\\ =&\frac{1}{\hat{j}_1^2}\delta^{j_1}_{j_2}\delta^{m_1}_{m_2}\hat{J}_1^2\hat{J}_2^2\delta^{J_2}_{J_3}\frac{1}{\hat{j}_t^2}\delta^{j_t}_{j_s}\end{aligned}\tag{B.71}$$

Proof.

$$\begin{aligned}&\sum_{M_1M_2M_3}\sum_{m_tm_sm_rm_vm_w}\begin{pmatrix}j_1 & j_t\\ m_1 & m_t\end{pmatrix}\Big|\begin{matrix}J_1\\M_1\end{matrix}\Big)\begin{pmatrix}j_2 & j_s\\ m_2 & m_s\end{pmatrix}\Big|\begin{matrix}J_1\\M_1\end{matrix}\Big)\begin{pmatrix}j_r & j_v\\ m_r & m_v\end{pmatrix}\Big|\begin{matrix}J_2\\M_2\end{matrix}\Big)\\ &\times\begin{pmatrix}j_t & j_w\\ m_t & m_w\end{pmatrix}\Big|\begin{matrix}J_2\\M_2\end{matrix}\Big)\begin{pmatrix}j_r & j_v\\ m_r & m_v\end{pmatrix}\Big|\begin{matrix}J_3\\M_3\end{matrix}\Big)\begin{pmatrix}j_s & j_w\\ m_s & m_w\end{pmatrix}\Big|\begin{matrix}J_3\\M_3\end{matrix}\Big)\end{aligned}\tag{B.72}$$

$$\begin{aligned}\overset{(4.30)}{=}&\sum_{M_1M_2M_3}\sum_{m_tm_sm_w}\delta^{J_2}_{J_3}\delta^{M_2}_{M_3}\begin{pmatrix}j_1 & j_t\\ m_1 & m_t\end{pmatrix}\Big|\begin{matrix}J_1\\M_1\end{matrix}\Big)\begin{pmatrix}j_2 & j_s\\ m_2 & m_s\end{pmatrix}\Big|\begin{matrix}J_1\\M_1\end{matrix}\Big)\\ &\times\begin{pmatrix}j_t & j_w\\ m_t & m_w\end{pmatrix}\Big|\begin{matrix}J_2\\M_2\end{matrix}\Big)\begin{pmatrix}j_s & j_w\\ m_s & m_w\end{pmatrix}\Big|\begin{matrix}J_3\\M_3\end{matrix}\Big)\end{aligned}\tag{B.73}$$

$$\begin{aligned}=&\sum_{M_1M_2M_3}\sum_{m_tm_sm_w}\delta^{J_2}_{J_3}\delta^{M_2}_{M_3}\begin{pmatrix}j_1 & j_t\\ m_1 & m_t\end{pmatrix}\Big|\begin{matrix}J_1\\M_1\end{matrix}\Big)\begin{pmatrix}j_2 & j_s\\ m_2 & m_s\end{pmatrix}\Big|\begin{matrix}J_1\\M_1\end{matrix}\Big)\\ &\times\begin{pmatrix}j_t & j_w\\ m_t & m_w\end{pmatrix}\Big|\begin{matrix}J_2\\M_2\end{matrix}\Big)\begin{pmatrix}j_s & j_w\\ m_s & m_w\end{pmatrix}\Big|\begin{matrix}J_3\\M_3\end{matrix}\Big)\end{aligned}\tag{B.74}$$

$$\overset{(4.34)}{=}\sum_{M_1}\sum_{m_tm_s}\hat{J}_2^2\delta^{J_2}_{J_3}\frac{1}{\hat{j}_t^2}\delta^{j_t}_{j_s}\delta^{m_t}_{m_s}\begin{pmatrix}j_1 & j_t\\ m_1 & m_t\end{pmatrix}\Big|\begin{matrix}J_1\\M_1\end{matrix}\Big)\begin{pmatrix}j_2 & j_s\\ m_2 & m_s\end{pmatrix}\Big|\begin{matrix}J_1\\M_1\end{matrix}\Big)\tag{B.75}$$

$$=\sum_{M_1}\sum_{m_tm_s}\hat{J}_2^2\delta^{J_2}_{J_3}\frac{1}{\hat{j}_t^2}\delta^{j_t}_{j_s}\delta^{m_t}_{m_s}\begin{pmatrix}j_1 & j_t\\ m_1 & m_t\end{pmatrix}\Big|\begin{matrix}J_1\\M_1\end{matrix}\Big)\begin{pmatrix}j_2 & j_s\\ m_2 & m_s\end{pmatrix}\Big|\begin{matrix}J_1\\M_1\end{matrix}\Big)\tag{B.76}$$

$$\overset{(4.34)}{=}\frac{1}{\hat{j}_1^2}\delta^{j_1}_{j_2}\delta^{m_1}_{m_2}\hat{J}_1^2\hat{J}_2^2\delta^{J_2}_{J_3}\frac{1}{\hat{j}_t^2}\delta^{j_t}_{j_s}\tag{B.77}$$

□

B.1.3. J-Coupling of the Zero-Body Terms

As a reminder, we note that the irreducible two-body density matrix is Hermitian, i.e.

$$\lambda^{pq}_{rs}=\lambda^{rs}_{pq}.\tag{B.78}$$

$$\left(\frac{\mathrm{d}E}{\mathrm{d}s}\right)_{\mathrm{II}}:=\frac{1}{4}\sum_{prtv}\sum_{m_pm_rm_tm_v}G^{pm_prm_rtm_tvm_v}_{tm_tvm_vpm_prm_r}n_pn_r\bar{n}_t\bar{n}_v\tag{B.79}$$

$$= \frac{1}{4} \sum_{prtv} \sum_{m_p m_r m_t m_v} (\eta^{pm_p rm_r}_{tm_t vm_v} \Gamma^{tm_t vm_v}_{pm_p rm_r} - \Gamma^{pm_p rm_r}_{tm_t vm_v} \eta^{tm_t v}_{pr}) n_p n_r \bar{n}_t \bar{n}_v \tag{B.80}$$

$$= \frac{1}{4}(1-\chi) \sum_{prtv} \sum_{m_p m_r m_t m_v} \eta^{pm_p rm_r}_{tm_t vm_v} \Gamma^{tm_t vm_v}_{pm_p rm_r} n_p n_r \bar{n}_t \bar{n}_v \tag{B.81}$$

$$= \frac{1}{4}(1-\chi) \sum_{prtv} \sum_{m_p m_r} \sum_{m_t m_v} \sum_{JM} \sum_{J'M'} {}^{J}\eta^{pr}_{tv} \, {}^{J'}\Gamma^{tv}_{pr} n_p n_r \bar{n}_t \bar{n}_v$$
$$\times \begin{pmatrix} j_p & j_r \\ m_p & m_r \end{pmatrix} \Big| \begin{matrix} J \\ M \end{matrix} \Big) \begin{pmatrix} j_t & j_v \\ m_t & m_v \end{pmatrix} \Big| \begin{matrix} J' \\ M' \end{matrix} \Big) \begin{pmatrix} j_t & j_v \\ m_t & m_v \end{pmatrix} \Big| \begin{matrix} J \\ M \end{matrix} \Big) \begin{pmatrix} j_p & j_r \\ m_p & m_r \end{pmatrix} \Big| \begin{matrix} J' \\ M' \end{matrix} \Big) \tag{B.82}$$

$$= \frac{1}{4}(1-\chi) \sum_{prtv} \sum_{JM} \sum_{J'M'} {}^{J}\eta^{pr}_{tv} \, {}^{J'}\Gamma^{tv}_{pr} n_p n_r \bar{n}_t \bar{n}_v \delta^{J}_{J'} \delta^{M}_{M'} \tag{B.83}$$

$$= \frac{1}{4}(1-\chi) \sum_{J} \sum_{prtv} \hat{J}^2 \, {}^{J}\eta^{pr}_{tv} \, {}^{J}\Gamma^{tv}_{pr} n_p n_r \bar{n}_t \bar{n}_v \tag{B.84}$$

$$\left(\frac{\mathrm{d}E}{\mathrm{d}s}\right)_{\mathrm{III}} := \frac{1}{4} \sum_{prqs} \sum_{\substack{m_p m_r \\ m_q m_s}} \frac{\mathrm{d}\Gamma^{pm_p rm_r}_{qm_q sm_s}}{\mathrm{d}s} \lambda^{pm_p rm_r}_{qm_q sm_s} \tag{B.85}$$

$$= \frac{1}{4} \sum_{J} \sum_{prqs} \hat{J}^2 \frac{\mathrm{d} \, {}^{J}\Gamma^{pr}_{qs}}{\mathrm{d}s} \, {}^{J}\lambda^{pr}_{qs} \tag{B.86}$$

$$= \frac{1}{4} \sum_{J} \sum_{prqs} \hat{J}^2 \frac{1}{2} \left(\frac{\mathrm{d} \, {}^{J}\Gamma^{pr}_{qs}}{\mathrm{d}s} + \frac{\mathrm{d} \, {}^{J}\Gamma^{pr}_{qs}}{\mathrm{d}s} \right) {}^{J}\lambda^{pr}_{qs}. \tag{B.87}$$

Renaming the indices in the second term yields

$$= \frac{1}{4} \cdot \frac{1}{2} \sum_{J} \sum_{prqs} \hat{J}^2 \left(\frac{\mathrm{d} \, {}^{J}\Gamma^{pr}_{qs}}{\mathrm{d}s} \, {}^{J}\lambda^{pr}_{qs} - \frac{\mathrm{d} \, {}^{J}\Gamma^{qs}_{pr}}{\mathrm{d}s} \, {}^{J}\lambda^{qs}_{pr} \right). \tag{B.88}$$

Making use of (4.57) and the Hermiticity of the irreducible density matrix (B.78) yields

$$= \frac{1}{4} \cdot \frac{1}{2} \sum_{J} \sum_{prqs} \hat{J}^2 \left(\frac{\mathrm{d} \, {}^{J}\Gamma^{pr}_{qs}}{\mathrm{d}s} \, {}^{J}\lambda^{pr}_{qs} - \chi \frac{\mathrm{d} \, {}^{J}\Gamma^{pr}_{qs}}{\mathrm{d}s} \, {}^{J}\lambda^{pr}_{qs} \right) \tag{B.89}$$

$$= \frac{1}{4} \cdot \frac{(1-\chi)}{2} \sum_{J} \sum_{prqs} \hat{J}^2 \frac{\mathrm{d} \, {}^{J}\Gamma^{pr}_{qs}}{\mathrm{d}s} \, {}^{J}\lambda^{pr}_{qs}. \tag{B.90}$$

B.2. Properties of n-Particle n-Hole Excitations

In this section, we give the proof for the statement of proposition 4.1. As a reminder, the statement reads as follows:
Any n-particle n-hole excitation vanishes

$$|\Psi^{p_1\dots p_n}_{q_1\dots q_n}\rangle = 0 \tag{B.91}$$

- if at least one of the lower indices is a virtual index, i.e., $q_k \in \mathcal{V}$ for any $k \in \{1, 2, \dots, n\}$,
- if at least one of the upper indices is a core index, i.e., $p_k \in \mathcal{C}$ for any $k \in \{1, 2, \dots, n\}$.

Proof. The first statement is based on the fact that all density matrix elements vanish (4.163) and the (vacuum normal-ordered) n-body operator annihilates the reference state (4.162) if one of the lower indices is a virtual index.

Before proving the second statement let us go through the basics of summing over the permutation set $\mathcal{S}_n$. For any function g depending on the composition of two permutations, π and σ, we know that the sum over one of the permutation can be written as

$$\sum_{\pi\in\mathcal{S}_n} g(\sigma\pi) = \sum_{\pi\in\mathcal{S}_n} g(\pi) \tag{B.92}$$

since the sum still runs over all elements of the permutation set $\mathcal{S}_n$. This implies immediately

$$\sum_{\pi\in\mathcal{S}_n}\sum_{\sigma\in\mathcal{S}_n} g(\sigma\pi) = n! \sum_{\pi\in\mathcal{S}_n} g(\pi) \tag{B.93}$$

due to the fact that $\mathcal{S}_n$ contains $n!$ different elements. Let us generalize this type of summations if the inner sum includes additional k different constraints of the following form

$$\sum_{\pi\in\mathcal{S}_n} \sum_{\substack{\sigma\in\mathcal{S}_n \\ \sigma\pi(l_1)=\pi(l_1) \\ \sigma\pi(l_2)=\pi(l_2) \\ \vdots \\ \sigma\pi(l_k)=\pi(l_k)}} g(\sigma\pi) = (n-k)! \sum_{\pi\in\mathcal{S}_n} g(\pi). \tag{B.94}$$

with $1 \leq k \leq n$ and pairwise different indices $l_1, l_2, \dots, l_k \in \{1, 2, \dots, n\}$. Finally, we can split the sum over the permutation in different ways. Once the permutation set $\mathcal{S}_n$ is expressed as a union of two disjoint subsets, i.e., $S_n = Q \bigcup T$, the sum over the permutation splits as follows

$$\sum_{\pi\in\mathcal{S}_n} g(\pi) = \sum_{\pi\in Q} g(\pi) + \sum_{\pi\in T} g(\pi). \tag{B.95}$$

Two examples of this type are

$$\sum_{\pi\in\mathcal{S}_n} g(\pi) = \sum_{\substack{\pi\in\mathcal{S}_n \\ \pi(1)=1}} g(\pi) + \sum_{\substack{\pi\in\mathcal{S}_n \\ \pi(1)\neq 1}} g(\pi) \tag{B.96}$$

$$\sum_{\pi\in\mathcal{S}_n g(\pi)} = \sum_{l=1}^{n} \sum_{\substack{\pi\in\mathcal{S}_n \\ \pi(l)=1}} g(\pi) \tag{B.97}$$

since the permutation set $\mathcal{S}_n$ can be expressed as a disjoint union $\mathcal{S}_n = \{\pi \in \mathcal{S}_n | \pi(1) = 1\} \bigcup \{\pi \in \mathcal{S}_n | \pi(1) \neq 1\}$ and $\mathcal{S}_n = \bigcup_{l=1}^{n} \{\pi \in \mathcal{S}_n | \pi(l) = 1\}$.

Now let us turn to the proof of the second statement that if one of the upper indices is a core index the n-particle n-hole excitations vanish. This statment will be proved inductively. The basis step for $n = 1$ follows immediately from (4.165) and (4.168)

$$|\Psi_q^i\rangle = \boldsymbol{a}_q^i |\Psi\rangle - \gamma_q^i |\Psi\rangle = \delta_q^i |\Psi\rangle - \delta_q^i |\Psi\rangle = 0. \tag{B.98}$$

Let us consider the induction step where we assume the induction hypothesis, saying that the j-particle j-hole excitations for $j \leq n-1$ vanish if one of the upper indices is a core, is true. The goal is then to show that the n-particle n-hole excitations vanish based on the induction hypothesis. Without loss of generality, let us assume that

$$p_1 \in \mathcal{C} \tag{B.99}$$

otherwise make use of the property (4.171) to bring the core index at the first place. Let us write the following expression in terms of sum over permutations using the definition of the index antisymmetrizer (3.50) and the basic formulae for the sum over permutations[1]

$$\mathbb{A}(\gamma_{q_1}^{p_1} |\Psi_{q_2\cdots q_n}^{p_2\cdots p_n}\rangle) = \frac{1}{(1!(n-1)!)^2} \sum_{\pi\in\mathcal{S}_n} \sum_{\pi'\in\mathcal{S}_n} \operatorname{sgn}(\pi\pi') \gamma_{q_{\pi(1)}}^{p_{\pi'(1)}} |\Psi_{q_{\pi(2)}\cdots q_{\pi(n)}}^{p_{\pi'(2)}\cdots p_{\pi'(n)}}\rangle \tag{B.100}$$

splitting the sum over π' into two disjoint summation according to (B.96)

$$\begin{aligned} = \frac{1}{(n-1)!^2} \sum_{\pi\in\mathcal{S}_n} \Bigg(& \sum_{\substack{\pi'\in\mathcal{S}_n \\ \pi'(1)=1}} \operatorname{sgn}(\pi\pi') \gamma_{q_{\pi(1)}}^{p_{\pi'(1)}} |\Psi_{q_{\pi(2)}\cdots q_{\pi(n)}}^{p_{\pi'(2)}\cdots p_{\pi'(n)}}\rangle \\ & + \sum_{\substack{\pi'\in\mathcal{S}_n \\ \pi'(1)\neq 1}} \operatorname{sgn}(\pi\pi') \gamma_{q_{\pi(1)}}^{p_{\pi'(1)}} |\Psi_{q_{\pi(2)}\cdots q_{\pi(n)}}^{p_{\pi'(2)}\cdots p_{\pi'(n)}}\rangle \Bigg) \end{aligned} \tag{B.101}$$

where the second term vanishes due to the induction hypothesis, yielding

$$= \frac{1}{(n-1)!^2} \sum_{\pi\in\mathcal{S}_n} \sum_{\substack{\pi'\in\mathcal{S}_n \\ \pi'(1)=1}} \operatorname{sgn}(\pi\pi') \gamma_{q_{\pi(1)}}^{p_{\pi'(1)}} |\Psi_{q_{\pi(2)}\cdots q_{\pi(n)}}^{p_{\pi'(2)}\cdots p_{\pi'(n)}}\rangle \tag{B.102}$$

[1] The symmetry factor from (3.50) is one in this case.

where the sum over π' gives just a factor $(n-1)!$ because the summand is symmetric under transposition of the last $n-1$ indices due to the sign of the permutation of π' and (4.171)

$$= \frac{1}{(n-1)!} \sum_{\pi \in \mathcal{S}_n} \operatorname{sgn}(\pi) \delta^{p_1}_{q_{\pi(1)}} \left| \Psi^{p_2 \dots p_n}_{q_{\pi(2)} \dots q_{\pi(n)}} \right\rangle . \tag{B.103}$$

Now, let us consider the n-particle n-hole excitation

$$\begin{aligned} &\left| \Psi^{p_1 p_2 \dots p_n}_{q_1 q_2 \dots q_n} \right\rangle \\ &= (\boldsymbol{a}^{p_1 p_2 \dots p_n}_{q_1 q_2 \dots q_n} - \gamma^{p_1 p_2 \dots p_n}_{q_1 q_2 \dots q_n}) \left| \Psi \right\rangle - \sum_{j=1}^{n-1} \mathbb{A}(\gamma^{p_1 p_2 \dots p_j}_{q_1 q_2 \dots q_j} \left| \Psi^{p_{j+1} \dots p_n}_{q_{j+1} \dots q_n} \right\rangle) \end{aligned} \tag{B.104}$$

writing the $j = 1$ summand of the second term explicitly

$$\begin{aligned} &= \frac{1}{(n-1)!} \sum_{\pi \in \mathcal{S}_n} \operatorname{sgn}(\pi) \delta^{p_1}_{q_{\pi(1)}} (\boldsymbol{a}^{p_2 p_3 \dots p_n}_{q_{\pi(2)} q_{\pi(3)} \dots q_{\pi(n)}} - \gamma^{p_2 p_3 \dots p_n}_{q_{\pi(2)} q_{\pi(3)} \dots q_{\pi(n)}}) \left| \Psi \right\rangle \\ &\quad - \mathbb{A}(\gamma^{p_1}_{q_1} \left| \Psi^{p_2 \dots p_n}_{q_2 \dots q_n} \right\rangle) - \sum_{j=2}^{n-1} \mathbb{A}(\gamma^{p_1 p_2 \dots p_j}_{q_1 q_2 \dots q_j} \left| \Psi^{p_{j+1} \dots p_n}_{q_{j+1} \dots q_n} \right\rangle). \end{aligned} \tag{B.105}$$

Substituting (B.103) for the first term on the second line and summarizing

$$\begin{aligned} &= \frac{1}{(n-1)!} \sum_{\pi \in \mathcal{S}_n} \operatorname{sgn}(\pi) \delta^{p_1}_{q_{\pi(1)}} \left((\boldsymbol{a}^{p_2 p_3 \dots p_n}_{q_{\pi(2)} q_{\pi(3)} \dots q_{\pi(n)}} - \gamma^{p_2 p_3 \dots p_n}_{q_{\pi(2)} q_{\pi(3)} \dots q_{\pi(n)}}) \left| \Psi \right\rangle - \left| \Psi^{p_2 \dots p_n}_{q_{\pi(2)} \dots q_{\pi(n)}} \right\rangle \right) \\ &\quad - \sum_{j=2}^{n-1} \mathbb{A}(\gamma^{p_1 p_2 \dots p_j}_{q_1 q_2 \dots q_j} \left| \Psi^{p_{j+1} \dots p_n}_{q_{j+1} \dots q_n} \right\rangle), \end{aligned} \tag{B.106}$$

where the first term can be rewritten with the aid of (4.170) to

$$\begin{aligned} &= \frac{1}{(n-1)!} \sum_{\pi \in \mathcal{S}_n} \operatorname{sgn}(\pi) \delta^{p_1}_{q_{\pi(1)}} \left(\sum_{j=2}^{n-1} \mathbb{A}(\gamma^{p_2 \dots p_j}_{q_{\pi(2)} \dots q_{\pi(j)}} \left| \Psi^{p_{j+1} \dots p_n}_{q_{\pi(j+1)} \dots q_{\pi(n)}} \right\rangle) \right) \\ &\quad - \sum_{j=2}^{n-1} \mathbb{A}(\gamma^{p_1 p_2 \dots p_j}_{q_1 q_2 \dots q_j} \left| \Psi^{p_{j+1} \dots p_n}_{q_{j+1} \dots q_n} \right\rangle) \end{aligned} \tag{B.107}$$

$$\begin{aligned} &= \sum_{j=2}^{n-1} \left(\frac{1}{(n-1)!} \sum_{\pi \in \mathcal{S}_n} \operatorname{sgn}(\pi) \delta^{p_1}_{q_{\pi(1)}} \mathbb{A}(\gamma^{p_2 \dots p_j}_{q_{\pi(2)} \dots q_{\pi(j)}} \left| \Psi^{p_{j+1} \dots p_n}_{q_{\pi(j+1)} \dots q_{\pi(n)}} \right\rangle) \right. \\ &\qquad \left. - \mathbb{A}(\gamma^{p_1 p_2 \dots p_j}_{q_1 q_2 \dots q_j} \left| \Psi^{p_{j+1} \dots p_n}_{q_{j+1} \dots q_n} \right\rangle) \right). \end{aligned} \tag{B.108}$$

We will bring these two terms in the same shape while neglecting the sum over j because they will cancel each other for each j. Considering only the first term without the sum over j and introducing two constraints on the permutations since the index antisymmetrizer does

not act on the lower and upper index of Kronecker's delta we obtain

$$\begin{aligned}
&\frac{1}{(n-1)!}\sum_{\pi\in\mathcal{S}_n}\operatorname{sgn}(\pi)\delta^{p_1}_{q_{\pi(1)}}\mathbb{A}(\gamma^{p_2\cdots p_j}_{q_{\pi(2)}\cdots q_{\pi(j)}}\,|\Psi^{p_{j+1}\cdots p_n}_{q_{\pi(j+1)}\cdots q_{\pi(n)}}\rangle\\
&=\frac{1}{(n-1)!((j-1)!(n-j)!)^2}\\
&\quad\times\sum_{\pi\in\mathcal{S}_n}\sum_{\substack{\pi'\in\mathcal{S}_n\\ \pi'(1)=1}}\sum_{\substack{\sigma\in\mathcal{S}_n\\ \sigma\pi(1)=\pi(1)}}\operatorname{sgn}(\sigma\pi\pi')\delta^{p_{\pi'(1)}}_{q_{\sigma\pi(1)}}\gamma^{p_{\pi'(2)}\cdots p_{\pi'(j)}}_{q_{\sigma\pi(2)}\cdots q_{\sigma\pi(j)}}\,|\Psi^{p_{\pi'(j+1)}\cdots p_{\pi'(n)}}_{q_{\sigma\pi(j+1)}\cdots q_{\sigma\pi(n)}}\rangle
\end{aligned}\tag{B.109}$$

where the sum over σ including one constraint yields a factor $(n-1)!$ according to (B.94)

$$=\frac{1}{((j-1)!(n-j)!)^2}\sum_{\pi\in\mathcal{S}_n}\sum_{\substack{\pi'\in\mathcal{S}_n\\ \pi'(1)=1}}\operatorname{sgn}(\pi\pi')\delta^{p_{\pi'(1)}}_{q_{\pi(1)}}\gamma^{p_{\pi'(2)}\cdots p_{\pi'(j)}}_{q_{\pi(2)}\cdots q_{\pi(j)}}\,|\Psi^{p_{\pi'(j+1)}\cdots p_{\pi'(n)}}_{q_{\pi(j+1)}\cdots q_{\pi(n)}}\rangle\,.\tag{B.110}$$

Let us simplify the second term in (B.108) without the sum over j

$$\begin{aligned}
&\mathbb{A}(\gamma^{p_1p_2\cdots p_j}_{q_1q_2\cdots q_j}\,|\Psi^{p_{j+1}\cdots p_n}_{q_{j+1}\cdots q_n}\rangle)\\
&=\frac{1}{(j!(n-j)!)^2}\sum_{\pi\in\mathcal{S}_n}\sum_{\pi'\in\mathcal{S}_n}\operatorname{sgn}(\pi\pi')\gamma^{p_{\pi'(1)}p_{\pi'(2)}\cdots p_{\pi'(j)}}_{q_{\pi(1)}q_{\pi(2)}\cdots q_{\pi(j)}}\,|\Psi^{p_{\pi'(j+1)}\cdots p_{\pi'(n)}}_{q_{\pi(j+1)}\cdots q_{\pi(n)}}\rangle\,.
\end{aligned}\tag{B.111}$$

Splitting the summation over π' into disjoint subsets of permutations (B.97) yields

$$\begin{aligned}
&=\frac{1}{(j!(n-j)!)^2}\sum_{\pi\in\mathcal{S}_n}\sum_{l=1}^{j}\sum_{\substack{\pi'\in\mathcal{S}_n\\ \pi'(l)=1}}\operatorname{sgn}(\pi\pi')\gamma^{p_{\pi'(1)}p_{\pi'(2)}\cdots p_{\pi'(j)}}_{q_{\pi(1)}q_{\pi(2)}\cdots q_{\pi(j)}}\,|\Psi^{p_{\pi'(j+1)}\cdots p_{\pi'(n)}}_{q_{\pi(j+1)}\cdots q_{\pi(n)}}\rangle\\
&\quad+\frac{1}{(j!(n-j)!)^2}\sum_{\pi\in\mathcal{S}_n}\sum_{l=j+1}^{n}\sum_{\substack{\pi'\in\mathcal{S}_n\\ \pi'(l)=1}}\operatorname{sgn}(\pi\pi')\gamma^{p_{\pi'(1)}p_{\pi'(2)}\cdots p_{\pi'(j)}}_{q_{\pi(1)}q_{\pi(2)}\cdots q_{\pi(j)}}\,|\Psi^{p_{\pi'(j+1)}\cdots p_{\pi'(n)}}_{q_{\pi(j+1)}\cdots q_{\pi(n)}}\rangle\,,
\end{aligned}\tag{B.112}$$

where the last term vanishes due to the induction hypothesis and the sum over l in the first term gives a factor j since the summand is symmetric under transposition of the first j upper indices

$$=\frac{j}{(j!(n-j)!)^2}\sum_{\pi\in\mathcal{S}_n}\sum_{\substack{\pi'\in\mathcal{S}_n\\ \pi'(1)=1}}\operatorname{sgn}(\pi\pi')\gamma^{p_{\pi'(1)}p_{\pi'(2)}\cdots p_{\pi'(j)}}_{q_{\pi(1)}q_{\pi(2)}\cdots q_{\pi(j)}}\,|\Psi^{p_{\pi'(j+1)}\cdots p_{\pi'(n)}}_{q_{\pi(j+1)}\cdots q_{\pi(n)}}\rangle\,.\tag{B.113}$$

Rewriting the j-particle density matrix element with one upper core index via (4.167) gives a factor $\frac{1}{(j-1)!}$ and introducing $(n-j)$ constraints not to permute the indices on the $(n-j)$-particle $(n-j)$-hole excitation yields

$$\begin{aligned}
&=\frac{j}{(j!(n-j)!)^2(j-1)!}\\
&\quad\times\sum_{\pi\in\mathcal{S}_n}\sum_{\substack{\pi'\in\mathcal{S}_n\\ \pi'(1)=1}}\sum_{\substack{\sigma\in\mathcal{S}_n\\ \sigma\pi(j+1)=\pi(j+1)\\ \vdots\\ \sigma\pi(n)=\pi(n)}}\operatorname{sgn}(\sigma\pi\pi')\delta^{p_{\pi'(1)}}_{q_{\sigma\pi(1)}}\gamma^{p_{\pi'(2)}\cdots p_{\pi'(j)}}_{q_{\sigma\pi(2)}\cdots q_{\sigma\pi(j)}}\,|\Psi^{p_{\pi'(j+1)}\cdots p_{\pi'(n)}}_{q_{\sigma\pi(j+1)}\cdots q_{\sigma\pi(n)}}\rangle\,,
\end{aligned}\tag{B.114}$$

where the sum over σ gives just a factor $j! = (n-(n-j))!$ according to (B.94)

$$= \frac{jj!}{(j!(n-j)!)^2(j-1)!} \sum_{\pi\in\mathcal{S}_n} \sum_{\substack{\pi'\in\mathcal{S}_n \\ \pi'(1)=1}} \operatorname{sgn}(\pi\pi') \delta^{p_{\pi'(1)}}_{q_{\pi(1)}} \gamma^{p_{\pi'(2)}\cdots p_{\pi'(j)}}_{q_{\pi(2)}\cdots q_{\pi(j)}} |\Psi^{p_{\pi'(j+1)}\cdots p_{\pi'(n)}}_{q_{\pi(j+1)}\cdots q_{\pi(n)}}\rangle \,. \tag{B.115}$$

Simplifying the prefactor, we have

$$= \frac{1}{((j-1)!(n-j)!)^2} \sum_{\pi\in\mathcal{S}_n} \sum_{\substack{\pi'\in\mathcal{S}_n \\ \pi'(1)=1}} \operatorname{sgn}(\pi\pi') \delta^{p_{\pi'(1)}}_{q_{\pi(1)}} \gamma^{p_{\pi'(2)}\cdots p_{\pi'(j)}}_{q_{\pi(2)}\cdots q_{\pi(j)}} |\Psi^{p_{\pi'(j+1)}\cdots p_{\pi'(n)}}_{q_{\pi(j+1)}\cdots q_{\pi(n)}}\rangle \tag{B.116}$$

which cancels the first term in (B.110) for each j.

□

B.3. Epstein-Nesbet Energy Differences

$$\Delta_2^1 \coloneqq \langle\Psi|\, \tilde{\boldsymbol{a}}_1^2 \boldsymbol{H} \tilde{\boldsymbol{a}}_2^1 \,|\Psi\rangle - \langle\Psi|\, \boldsymbol{H} \,|\Psi\rangle \tag{B.117}$$

$$= \frac{1}{4} \sum_{\substack{pq \\ rs}} \Gamma_{rs}^{pq} \langle\Psi|\, \tilde{\boldsymbol{a}}_1^2 \tilde{\boldsymbol{a}}_{rs}^{pq} \tilde{\boldsymbol{a}}_2^1 \,|\Psi\rangle + \sum_{pq} f_q^p \langle\Psi|\, \tilde{\boldsymbol{a}}_1^2 \tilde{\boldsymbol{a}}_q^p \tilde{\boldsymbol{a}}_2^1 \,|\Psi\rangle + E \left(\langle\Psi|\, \tilde{\boldsymbol{a}}_1^2 \tilde{\boldsymbol{a}}_2^1 \,|\Psi\rangle - 1 \right) \tag{B.118}$$

$$\langle\Psi|\, \tilde{\boldsymbol{a}}_1^2 \tilde{\boldsymbol{a}}_2^1 \,|\Psi\rangle = \bar{n}_1 n_2 - \lambda_{12}^{12} \tag{B.119}$$

$$\begin{aligned} \sum_{pq} f_q^p \langle\Psi|\, \tilde{\boldsymbol{a}}_1^2 \tilde{\boldsymbol{a}}_q^p \tilde{\boldsymbol{a}}_2^1 \,|\Psi\rangle = &+ \bar{n}_1 \bar{n}_1 n_2 f_1^1 - \bar{n}_1 n_2 n_2 f_2^2 \\ &- 2\bar{n}_1 \sum_p f_1^p \lambda_{12}^{p2} + 2 n_2 \sum_q f_q^2 \lambda_{q1}^{21} \\ &- n_2 \sum_{pq} f_q^p \lambda_{q1}^{p1} + \bar{n}_1 \sum_{pq} f_q^p \lambda_{q2}^{p2} \end{aligned} \tag{B.120}$$

$$\begin{aligned} \frac{1}{4} \sum_{\substack{pq \\ rs}} \Gamma_{rs}^{pq} \langle\Psi|\, \tilde{\boldsymbol{a}}_1^2 \tilde{\boldsymbol{a}}_{rs}^{pq} \tilde{\boldsymbol{a}}_2^1 \,|\Psi\rangle = &- \Gamma_{12}^{12} \bar{n}_1 \bar{n}_1 n_2 n_2 \\ &+ n_2 n_2 \sum_{pr} \Gamma_{r2}^{p2} \lambda_{r1}^{p1} + \bar{n}_1 \bar{n}_1 \sum_{pr} \Gamma_{r1}^{p1} \lambda_{r2}^{p2} \\ &+ \bar{n}_1 n_2 \sum_{pq} \Gamma_{12}^{pq} \lambda_{12}^{pq} + 2 \bar{n}_1 n_2 \sum_{pr} \Gamma_{r1}^{p2} \lambda_{r1}^{p2} \\ &- \bar{n}_1 n_2 \sum_{pqr} \left(\Gamma_{r1}^{pq} \lambda_{r1}^{pq} + \Gamma_{rs}^{p2} \lambda_{rs}^{p2} \right) \end{aligned} \tag{B.121}$$

$$\Delta_{34}^{12} \coloneqq \langle\Psi|\, \tilde{\boldsymbol{a}}_{12}^{34} \boldsymbol{H} \tilde{\boldsymbol{a}}_{34}^{12} \,|\Psi\rangle - \langle\Psi|\, \boldsymbol{H} \,|\Psi\rangle \tag{B.122}$$

$$= \frac{1}{4} \sum_{\substack{pq \\ rs}} \Gamma_{rs}^{pq} \langle\Psi|\, \tilde{\boldsymbol{a}}_{12}^{34} \tilde{\boldsymbol{a}}_{rs}^{pq} \tilde{\boldsymbol{a}}_{34}^{12} \,|\Psi\rangle + \sum_{pq} f_q^p \langle\Psi|\, \tilde{\boldsymbol{a}}_{12}^{34} \tilde{\boldsymbol{a}}_q^p \tilde{\boldsymbol{a}}_{34}^{12} \,|\Psi\rangle + E \left(\langle\Psi|\, \tilde{\boldsymbol{a}}_{12}^{34} \tilde{\boldsymbol{a}}_{34}^{12} \,|\Psi\rangle - 1 \right) \tag{B.123}$$

$$\begin{aligned} \langle\Psi|\, \tilde{\boldsymbol{a}}_{12}^{34} \tilde{\boldsymbol{a}}_{34}^{12} \,|\Psi\rangle = &+ \frac{1}{2} \bar{n}_1 \bar{n}_2 n_3 n_4 - \bar{n}_1 n_3 \lambda_{24}^{24} - \bar{n}_1 n_4 \lambda_{23}^{23} \\ &+ \frac{1}{2} \bar{n}_1 \bar{n}_2 \lambda_{34}^{34} + \frac{1}{2} n_3 n_4 \lambda_{12}^{12} \\ &+ [13 \leftrightarrow 24] \end{aligned} \tag{B.124}$$

$$
\begin{aligned}
\sum_{pq} f_q^p \left\langle \Psi \right| \tilde{\boldsymbol{a}}_{12}^{34} \tilde{\boldsymbol{a}}_q^p \tilde{\boldsymbol{a}}_{34}^{12} \left| \Psi \right\rangle = &+ \bar{n}_1 \bar{n}_2 n_3 n_4 (\bar{n}_1 f_1^1 - n_3 f_3^3) \\
&- \bar{n}_2 \bar{n}_2 n_4 \lambda_{13}^{13} f_2^2 + \bar{n}_2 n_4 n_4 \lambda_{13}^{13} f_4^4 \\
&+ \bar{n}_1 \bar{n}_2 \bar{n}_2 \lambda_{34}^{34} f_2^2 - \bar{n}_2 \bar{n}_2 n_3 \lambda_{14}^{14} f_2^2 \\
&+ \bar{n}_1 n_4 n_4 \lambda_{23}^{23} f_4^4 - n_3 n_4 n_4 \lambda_{12}^{12} f_4^4 \\
&- 2 \bar{n}_2 n_3 n_4 \lambda_{14}^{13} f_4^3 + 2 \bar{n}_1 \bar{n}_2 n_4 \lambda_{31}^{32} f_1^2 \\
&- 2 \bar{n}_1 \bar{n}_2 n_4 \sum_p \left(\lambda_{31}^{3p} f_1^p + \lambda_{32}^{3p} f_2^p + \lambda_{34}^{3p} f_4^p \right) \\
&+ 2 \bar{n}_2 n_3 n_4 \sum_q \left(\lambda_{1q}^{13} f_q^3 + \lambda_{1q}^{12} f_q^2 + \lambda_{1q}^{14} f_q^4 \right) \\
&- 2 \bar{n}_2 n_4 n_3 \left(\lambda_{14}^{12} f_4^2 + \lambda_{13}^{12} f_3^2 \right) \\
&+ 2 \bar{n}_1 \bar{n}_2 n_4 \left(\lambda_{34}^{32} f_4^2 + \lambda_{34}^{31} f_4^1 \right) \\
&+ \bar{n}_1 \bar{n}_2 n_4 \sum_{pq} \lambda_{q3}^{p3} f_q^p - \bar{n}_2 n_3 n_4 \sum_{pq} \lambda_{q1}^{p1} f_q^p \\
&+ [13 \leftrightarrow 24]
\end{aligned}
\tag{B.125}
$$

$$
\begin{aligned}
&\frac{1}{4}\sum_{\substack{pq\\rs}}\Gamma^{pq}_{rs}\left\langle\Psi\right|\tilde{\boldsymbol{a}}^{34}_{12}\tilde{\boldsymbol{a}}^{pq}_{rs}\tilde{\boldsymbol{a}}^{12}_{34}\left|\Psi\right\rangle\\
&=\Bigg(+\bar{n}_1\bar{n}_2n_3n_4(\frac{1}{2}\bar{n}_1\bar{n}_2\Gamma^{12}_{12}+\frac{1}{2}n_3n_4\Gamma^{34}_{34}-\bar{n}_1n_4\Gamma^{14}_{14}-\bar{n}_1n_3\Gamma^{13}_{13})\\
&\quad+\bar{n}_2\bar{n}_2n_4n_4\lambda^{13}_{13}\Gamma^{24}_{24}+\bar{n}_1\bar{n}_2n_3n_4\lambda^{14}_{23}\Gamma^{14}_{23}+\bar{n}_2\bar{n}_2n_3n_3\lambda^{14}_{14}\Gamma^{23}_{23}+\bar{n}_1\bar{n}_2n_3n_4\lambda^{13}_{24}\Gamma^{13}_{24}\\
&\quad+\frac{1}{2}\bar{n}_1\bar{n}_1\bar{n}_2\bar{n}_2\lambda^{34}_{34}\Gamma^{12}_{12}+\frac{1}{2}n_3n_3n_4n_4\lambda^{12}_{12}\Gamma^{34}_{34}\\
&\quad-2\bar{n}_2\bar{n}_2n_3n_4\lambda^{14}_{13}\Gamma^{24}_{23}-2\bar{n}_1\bar{n}_2n_4n_4\lambda^{31}_{32}\Gamma^{41}_{42}\\
&\quad+2\bar{n}_2n_3n_4n_4\lambda^{12}_{13}\Gamma^{42}_{43}+2\bar{n}_1n_4n_4n_3\lambda^{21}_{23}\Gamma^{41}_{43}+2\bar{n}_1\bar{n}_2\bar{n}_2n_4\lambda^{31}_{34}\Gamma^{21}_{24}+2\bar{n}_1\bar{n}_1\bar{n}_2n_4\lambda^{23}_{43}\Gamma^{12}_{14}\\
&\quad+2\bar{n}_1\bar{n}_2n_3n_4\sum_p\lambda^{1p}_{32}\Gamma^{p1}_{32}+2\bar{n}_1\bar{n}_2n_3n_4\sum_r\lambda^{14}_{3r}\Gamma^{14}_{r3}\\
&\quad-2\bar{n}_1n_3n_3n_4\sum_r\lambda^{21}_{2r}\Gamma^{13}_{r3}+2\bar{n}_1\bar{n}_1n_3n_4\sum_p\lambda^{2p}_{23}\Gamma^{p1}_{31}\\
&\quad+2\bar{n}_1\bar{n}_2n_3n_3\sum_r\lambda^{41}_{4r}\Gamma^{13}_{r3}-2\bar{n}_1\bar{n}_1\bar{n}_2n_3\sum_p\lambda^{4p}_{43}\Gamma^{p1}_{31}\\
&\quad+2\bar{n}_2\bar{n}_2n_3n_4\sum_p\lambda^{1p}_{13}\Gamma^{p2}_{32}-2\bar{n}_2n_3n_4n_4\sum_p\lambda^{1p}_{13}\Gamma^{p4}_{34}\\
&\quad-2\bar{n}_1\bar{n}_2\bar{n}_2n_4\sum_r\lambda^{31}_{3r}\Gamma^{12}_{r2}+2\bar{n}_1\bar{n}_2n_4n_4\sum_r\lambda^{31}_{3r}\Gamma^{14}_{r4}\\
&\quad+2\bar{n}_1\bar{n}_2n_3n_4\sum_p\lambda^{1p}_{42}\Gamma^{p1}_{42}-2\bar{n}_1n_3n_4n_4\sum_p\lambda^{2p}_{32}\Gamma^{p4}_{43}\\
&\quad-2\bar{n}_1\bar{n}_2\bar{n}_2n_3\sum_r\lambda^{14}_{4r}\Gamma^{21}_{r2}+2\bar{n}_1\bar{n}_2n_3n_4\sum_r\lambda^{24}_{3r}\Gamma^{24}_{r3}\\
&\quad-2\bar{n}_1n_3n_4n_4\sum_r\lambda^{21}_{2r}\Gamma^{14}_{r4}-2\bar{n}_1\bar{n}_2\bar{n}_2n_3\sum_p\lambda^{4p}_{43}\Gamma^{p2}_{32}\\
&\quad+2\bar{n}_1\bar{n}_2n_3n_4\sum_{pr}\left(\lambda^{3p}_{1r}\Gamma^{p3}_{r1}+\lambda^{4p}_{1r}\Gamma^{p4}_{r1}\right)\\
&\quad+\frac{1}{2}\bar{n}_1\bar{n}_2n_3n_4\left(\sum_{pq}\lambda^{pq}_{12}\Gamma^{pq}_{12}+\sum_{rs}\lambda^{34}_{rs}\Gamma^{34}_{rs}\right)\\
&\quad+2\bar{n}_1\bar{n}_2n_3n_4\left(\sum_p\lambda^{4p}_{12}\Gamma^{p4}_{12}+\sum_r\lambda^{34}_{2r}\Gamma^{34}_{r2}\right)\\
&\quad+\bar{n}_1\bar{n}_2\bar{n}_2n_3\sum_{qr}\lambda^{4q}_{4r}\Gamma^{2q}_{2r}+\bar{n}_1n_3n_4n_4\sum_{ps}\lambda^{2p}_{2s}\Gamma^{4p}_{4s}\\
&\quad+\bar{n}_1\bar{n}_2n_3n_4\left(\sum_{rs}\lambda^{24}_{rs}\Gamma^{24}_{rs}+\sum_{qr}\lambda^{3q}_{r4}\Gamma^{3q}_{r4}+\sum_{ps}\lambda^{p2}_{1s}\Gamma^{p2}_{1s}+\sum_{rs}\lambda^{23}_{rs}\Gamma^{23}_{rs}\right)\\
&\quad+\bar{n}_1\bar{n}_2n_4n_4\sum_{ps}\lambda^{p3}_{s3}\Gamma^{p4}_{4s}+\bar{n}_2\bar{n}_2n_3n_4\sum_{qr}\lambda^{1q}_{1r}\Gamma^{2q}_{r2}\\
&\quad-\bar{n}_2n_3n_4n_4\sum_{ps}\lambda^{1p}_{1s}\Gamma^{p4}_{4s}-\bar{n}_1\bar{n}_2\bar{n}_2n_4\sum_{qr}\lambda^{3q}_{3r}\Gamma^{2q}_{r2}\\
&\quad-\bar{n}_1\bar{n}_2n_3n_4\Big(\sum_{pqr}\lambda^{pq}_{r4}\Gamma^{pq}_{r4}+\sum_{pqr}\lambda^{p2}_{rs}\Gamma^{p2}_{rs}\Big)\Bigg)+[13\leftrightarrow 24]
\end{aligned}
\tag{B.126}
$$

Appendix C

Spherical-Tensor Decomposition

The main goal of this chapter is to decompose the density operators into spherical tensor components, i.e, to express them as a linear combination of spherical tensor operators. The next section gives a brief introduction to spherical tensor operators.

C.1. Spherical Tensor Operators

An operator $\boldsymbol{T}_K = (\boldsymbol{T}_{KQ})_{Q\in(-K,-K+1,\ldots,K)}$ is called a *spherical tensor operator* of rank K if all components of this operator fulfill the following conditions

$$[\boldsymbol{J}_z, \boldsymbol{T}_{KQ}] = \hbar Q \boldsymbol{T}_{KQ} \tag{C.1}$$

$$[\boldsymbol{J}_\pm, \boldsymbol{T}_{KQ}] = \hbar \zeta_\pm(K,Q) \boldsymbol{T}_{K,Q\pm1} \tag{C.2}$$

with

$$\zeta_\pm(K,Q) \coloneqq \sqrt{(K \pm Q + 1)(K \mp Q)}. \tag{C.3}$$

and $\boldsymbol{J}_z$ and $\boldsymbol{J}_\pm$ denote the z-component and ladder operator associated with total-angular-momentum vector operator $\vec{\boldsymbol{J}}$.

In second quantization, we can write the z-component and ladder operator

$$\boldsymbol{J}_z = \hbar \sum_{pm_p} m_p \boldsymbol{a}^\dagger_{pm_p} \boldsymbol{a}_{pm_p} \tag{C.4}$$

$$\boldsymbol{J}_\pm = \hbar \sum_{pm_p} \zeta_\mp(j_p, m_p) \boldsymbol{a}^\dagger_{pm_p} \boldsymbol{a}_{p,m_p\mp1}. \tag{C.5}$$

As an example let us consider the fermionic particle creation and annihilation operators.

Proposition C.1. *The fermionic particle creation $\boldsymbol{a}^\dagger_{rm_r}$ and (modified) annihilation operators $\overline{\boldsymbol{a}}_{rm_r} \coloneqq (-)^{j_r+m_r} \boldsymbol{a}_{r,-m_r}$ are spherical tensors of rank j_r. Note that the annihilation operator $\boldsymbol{a}_{rm_r}$ without the prefactor is not.*

Proof. We need to verfiy the relations (C.1) and (C.2) for both operators. Let us start with the creation operator, where the commutator with the z-component of the total-angular-momentum vector operator yields

$$[\boldsymbol{J}_z, \boldsymbol{a}^\dagger_{rm_r}] = \hbar \sum_{pm_p} m_p [\boldsymbol{a}^\dagger_{pm_p} \boldsymbol{a}_{pm_p}, \boldsymbol{a}^\dagger_{rm_r}] \tag{C.6}$$

$$= \hbar \sum_{pm_p} m_p (0 + \boldsymbol{a}^\dagger_{pm_p} \delta^p_r \delta^{m_p}_{m_r}) \tag{C.7}$$

$$= \hbar m_r \boldsymbol{a}^\dagger_{rm_r} \tag{C.8}$$

and with the ladder operator

$$[\boldsymbol{J}_\pm, \boldsymbol{a}^\dagger_{rm_r}] = \hbar \sum_{pm_p} \zeta_\mp(j_p, m_p) [\boldsymbol{a}^\dagger_{pm_p} \boldsymbol{a}_{p,m_p \mp 1}, \boldsymbol{a}^\dagger_{rm_r}] \tag{C.9}$$

$$= \hbar \sum_{pm_p} \zeta_\mp(j_p, m_p) (0 + \boldsymbol{a}^\dagger_{pm_p} \delta^r_p \delta^{m_p}_{m_r \pm 1}) \tag{C.10}$$

$$= \hbar \zeta_\mp(j_r, m_r \pm 1)\ \boldsymbol{a}^\dagger_{r,m_r \pm 1} \tag{C.11}$$

$$= \hbar \boldsymbol{a}^\dagger_{r,m_r \pm 1} \times \begin{cases} \sqrt{(j_r - (m_r + 1) + 1)(j_r + (m_r + 1))} \\ \sqrt{(j_r + (m_r - 1) + 1)(j_r - (m_r - 1))} \end{cases} \tag{C.12}$$

$$= \hbar \zeta_\pm(j_r, m_r \pm 1) \boldsymbol{a}^\dagger_{r,m_r \pm 1}. \tag{C.13}$$

Analogously, we obtain for the (modified) annihilation operator

$$[\boldsymbol{J}_z, \overline{\boldsymbol{a}}_{rm_r}] = \hbar \sum_{pm_p} m_p (-)^{j_r + m_r} [\boldsymbol{a}^\dagger_{pm_p} \boldsymbol{a}_{pm_p}, \boldsymbol{a}_{r,-m_r}] \tag{C.14}$$

$$= \hbar \sum_{pm_p} m_p (-)^{j_r + m_r} (-\delta^p_r \delta^{m_p}_{-m_r} \boldsymbol{a}_{pm_p} + 0) \tag{C.15}$$

$$= -\hbar (-m_r)(-)^{j_r + m_r} \boldsymbol{a}_{r,-m_r} \tag{C.16}$$

$$= +\hbar m_r \overline{\boldsymbol{a}}_{rm_r}. \tag{C.17}$$

Finally, the commutator with the ladder operator yields

$$[\boldsymbol{J}_\pm, \overline{\boldsymbol{a}}_{rm_r}] = \hbar \sum_{pm_p} \zeta_\mp(j_p, m_p) (-)^{j_r + m_r} [\boldsymbol{a}^\dagger_{pm_p} \boldsymbol{a}_{p,m_p \mp 1}, \boldsymbol{a}_{r,-m_r}] \tag{C.18}$$

$$= \hbar \sum_{pm_p} \zeta_\mp(j_p, m_p) (-)^{j_r + m_r} (-\delta^p_r \delta^{m_p}_{-m_r} \boldsymbol{a}_{p,m_p \mp 1} + 0) \tag{C.19}$$

$$= \hbar \zeta_\mp(j_r, -m_r) (-)^{j_r + (m_r \pm 1)} \boldsymbol{a}_{r,-(m_r \pm 1)} \tag{C.20}$$

$$= \hbar \overline{\boldsymbol{a}}_{r,m_r \pm 1} \times \begin{cases} \sqrt{(j_r - (-m_r) + 1)(j_r + (-m_r))} \\ \sqrt{(j_r + (-m_r) + 1)(j_r - (-m_r))} \end{cases} \tag{C.21}$$

$$= \hbar \zeta_\pm(j_r, m_r) \overline{\boldsymbol{a}}_{r,m_r \pm 1} \tag{C.22}$$

which proves the above statement. □

Finaly, we can construct an (irreducible) spherical tensor of rank K from two (irreducible) spherical tensors of rank K_1 and K_2 using the definition of the Clebsch-Gordan coefficient [VMK88, p. 63]:

$$[\boldsymbol{T}_{K_1} \otimes \boldsymbol{T}_{K_2}]_{KQ} \coloneqq \sum_{Q_1 Q_2} \begin{pmatrix} K_1 & K_2 \middle| K \\ Q_1 & Q_2 \middle| Q \end{pmatrix} \boldsymbol{T}_{K_1 Q_1} \boldsymbol{T}_{K_2 Q_2}. \tag{C.23}$$

C.2. Wigner-Eckart Theorem

The *Wigner–Eckart theorem* says that any matrix element for the Q-th component of a spherical tensor operator with rank K falls apart into a product of a geometrical factor, given by a Clebsch-Gordan coefficient, and a 'physical' factor, i.e., it reads in the convention given in [VMK88] as follows

$$\langle \phi j m | \boldsymbol{T}_{KQ} | \phi' j' m' \rangle = (-)^{2K} \frac{1}{\hat{j}} \begin{pmatrix} j' & K \middle| j \\ m' & Q \middle| m \end{pmatrix} (\phi j | \boldsymbol{T}_K | \phi' j') \tag{C.24}$$

$$= (-)^{2K+j'-m'} \frac{1}{\hat{K}} \begin{pmatrix} j' & j \middle| K \\ m' & -m \middle| -Q \end{pmatrix} (\phi j | \boldsymbol{T}_K | \phi' j') \tag{C.25}$$

where the 'physical' factor is indicated by the *reduced matrix element*

$$(\phi j | \boldsymbol{T}_K | \phi' j') \tag{C.26}$$

that is independent of the projection quantum numbers m, m' and Q. Here, ϕ denotes all quantum numbers of the corresponding state except for j and m.

A spherical tensor operator $\boldsymbol{T}_0 = (\boldsymbol{T}_{00})$ of rank zero is a called a *scalar* operator since it commutes with all components of the angular-momentum operator. The Wigner-Eckart theorem for a scalar operator yields

$$\langle \phi j m | \boldsymbol{T}_{00} | \phi' j' m' \rangle = \frac{1}{\hat{j}} \delta^j_{j'} \delta^m_{m'} (\phi j | \boldsymbol{T}_0 | \phi' j) \tag{C.27}$$

implying that the matrix elements of a scalar operator are diagonal in j and m, and independent of the projection quantum numbers m and m'.

C.3. Spherical Density Operators

Let us start with a generalized definition of the *(transition) one-body density matrix elements*

$$\gamma^{pm_p}_{qm_q}(jm, jm') \coloneqq \langle \Psi, jm | \boldsymbol{a}^\dagger_{pm_p} \boldsymbol{a}_{qm_q} | \Psi, jm' \rangle \tag{C.28}$$

with respect to given many-body states $|\Psi, jm\rangle$ with fixed total angular quantum number j, but considering all possible orientations of the projection quantum number

$$m \in \{-j, -j+1, \ldots, j\}. \tag{C.29}$$

In order to express the one-body density operator, which will be defined based on the generalized (transition) one-body density matrix elements, as a linear combination of spherical tensor operators which will become clear later on. However, these states are eigenstates of the squared and z-component total angular momentum with a fixed quantum number j, respectively, i.e.,

$$\vec{\boldsymbol{J}}^2 |\Psi, jm\rangle = \hbar j(j+1) |\Psi, jm\rangle \tag{C.30}$$

$$\boldsymbol{J}_z |\Psi, jm\rangle = \hbar m |\Psi, jm\rangle . \tag{C.31}$$

With the aid of the one-body density matrix elements, we can define a corresponding operator in second quantization which we call *one-body density operator*

$$\boldsymbol{\gamma}^{[1]}(jm, jm') \coloneqq \sum_{\substack{p \\ q}} \sum_{\substack{m_p \\ m_q}} \gamma_{qm_q}^{pm_p}(jm, jm') \boldsymbol{a}_{qm_q}^{pm_p} \tag{C.32}$$

$$= \sum_{\substack{p \\ q}} \sum_{\substack{m_p \\ m_q}} \langle \Psi, jm | \boldsymbol{a}_{pm_p}^\dagger \boldsymbol{a}_{qm_q} | \Psi, jm' \rangle \, \boldsymbol{a}_{pm_p}^\dagger \boldsymbol{a}_{qm_q} \tag{C.33}$$

$$= \sum_{\substack{p \\ q}} \sum_{KQ} \langle \Psi, jm | [\boldsymbol{a}_p^\dagger \otimes \overline{\boldsymbol{a}}_q]_{KQ} | \Psi, jm' \rangle \, [\boldsymbol{a}_p^\dagger \otimes \overline{\boldsymbol{a}}_q]_{KQ} \tag{C.34}$$

$$\overset{(C.25)}{=} \sum_{\substack{p \\ q}} \sum_{KQ} (-)^{2K+j-m'} \frac{1}{\hat{K}} \begin{pmatrix} j & j & K \\ m' & -m & -Q \end{pmatrix} (\Psi, j | [\boldsymbol{a}_p^\dagger \otimes \overline{\boldsymbol{a}}_q]_K | \Psi, j) \, [\boldsymbol{a}_p^\dagger \otimes \overline{\boldsymbol{a}}_q]_{KQ}. \tag{C.35}$$

This motivates the following definition of an operator called *spherical one-body density operator* of rank K

$$\boldsymbol{\gamma}_{KQ}^{[1]}(j) \coloneqq \frac{1}{\hat{j}^2} \sum_{mm'} (-)^{2K+j-m'} \begin{pmatrix} j & j & K \\ m' & -m & -Q \end{pmatrix} \boldsymbol{\gamma}^{[1]}(jm, jm') \tag{C.36}$$

which vanishes for $K > 2j$ because of the Clebsch-Gordan coefficient. Note that we have some freedom in the definition of this operator. It still remains to show that this definition indeed yields a spherical tensor operator of rank K. Let us first rewrite the above definition to

$$\boldsymbol{\gamma}_{KQ}^{[1]}(j) = \sum_{pq} \frac{1}{\hat{j}^2 \hat{K}} (\Psi, j | [\boldsymbol{a}_p^\dagger \otimes \overline{\boldsymbol{a}}_q]_K | \Psi, j) \, [\boldsymbol{a}_p^\dagger \otimes \overline{\boldsymbol{a}}_q]_{KQ}. \tag{C.37}$$

The commutators with the z-component of the total-angular-momentum operator yields

$$[\boldsymbol{J}_z, \boldsymbol{\gamma}^{[1]}_{KQ}(j)] = \sum_{pq} \frac{1}{\hat{j}^2 \hat{K}} (\Psi, j | [\boldsymbol{a}^\dagger_p \otimes \overline{\boldsymbol{a}}_q]_K | \Psi, j) [\boldsymbol{J}_z, [\boldsymbol{a}^\dagger_p \otimes \overline{\boldsymbol{a}}_q]_{KQ}] \tag{C.38}$$

$$= \sum_{pq} \frac{1}{\hat{j}^2 \hat{K}} (\Psi, j | [\boldsymbol{a}^\dagger_p \otimes \overline{\boldsymbol{a}}_q]_K | \Psi, j) \hbar Q [\boldsymbol{a}^\dagger_p \otimes \overline{\boldsymbol{a}}_q]_{KQ} \tag{C.39}$$

$$= \hbar Q \; \boldsymbol{\gamma}^{[1]}_{KQ}(j) \tag{C.40}$$

where we used that $[\boldsymbol{a}^\dagger_p \otimes \overline{\boldsymbol{a}}_q]_K$ is already a spherical tensor operator of rank K. Analogously, we obtain

$$[\boldsymbol{J}_\pm, \boldsymbol{\gamma}^{[1]}_{KQ}(j)] = \sum_{pq} \frac{1}{\hat{j}^2 \hat{K}} (\Psi, j | [\boldsymbol{a}^\dagger_p \otimes \overline{\boldsymbol{a}}_q]_K | \Psi, j) [\boldsymbol{J}_\pm, [\boldsymbol{a}^\dagger_p \otimes \overline{\boldsymbol{a}}_q]_{KQ}] \tag{C.41}$$

$$= \sum_{pq} \frac{1}{\hat{j}^2 \hat{K}} (\Psi, j | [\boldsymbol{a}^\dagger_p \otimes \overline{\boldsymbol{a}}_q]_K | \Psi, j) \hbar \zeta_\pm(K, Q) [\boldsymbol{a}^\dagger_p \otimes \overline{\boldsymbol{a}}_q]_{K, Q\pm1} \tag{C.42}$$

$$= \hbar \zeta_\pm(K, Q) \; \boldsymbol{\gamma}^{[1]}_{K, Q\pm1}(j) \tag{C.43}$$

which implies that the spherical one-body density operator is indeed a spherical tensor of rank K.

For practical calculations, we have to express the m-scheme matrix elements for the Q-th component of the spherical one-body density operator with rank K as a function of the one-body density matrix elements

$$\langle p m_p | \boldsymbol{\gamma}^{[1]}_{KQ}(j) | q m_q \rangle = \frac{1}{\hat{j}^2} \sum_{mm'} (-)^{2K+j-m'} \begin{pmatrix} j & j & K \\ m' & -m & -Q \end{pmatrix} \langle p m_p | \boldsymbol{\gamma}^{[1]}(jm, jm') | q m_q \rangle \tag{C.44}$$

$$= \frac{1}{\hat{j}^2} \sum_{mm'} (-)^{2K+j-m'} \begin{pmatrix} j & j & K \\ m' & -m & -Q \end{pmatrix} \gamma^{p m_p}_{q m_q}(jm, jm'). \tag{C.45}$$

The special case where the many-body state $|\Psi, jm\rangle$ has vanishing total angular momentum $j = 0$, yields

$$\langle p m_p | \boldsymbol{\gamma}^{[1]}_{KQ}(0) | q m_q \rangle = \delta^0_K \delta^0_Q \gamma^{p m_p}_{q m_q}(00, 00) \tag{C.46}$$

implying that the one-body density operator is a scalar operator, as expected. Finally, the scalar part of the spherical one-body density operator, i.e., $K = 0$, for any value of the total angular momentum j is given by

$$\langle p m_p | \boldsymbol{\gamma}^{[1]}_{00}(j) | q m_q \rangle = \frac{1}{\hat{j}^2} \sum_m \gamma^{p m_p}_{q m_q}(jm, jm) \tag{C.47}$$

which justifies the prefactor $\frac{1}{\hat{j}^2}$ in definition (C.36).

Finally, by writing down the inverse relation of (C.36)

$$\boldsymbol{\gamma}^{[1]}(jm,jm') = \hat{j}^2 \sum_{KQ} (-)^{2K+j-m'} \begin{pmatrix} j & j & K \\ m' & -m & -Q \end{pmatrix} \boldsymbol{\gamma}^{[1]}_{KQ}(j) \tag{C.48}$$

we can clearly see that the one-body density operator is decomposed in spherical tensor operators, i.e., it is expressed as a linear combination of a spherical tensor operators which was the goal of the chapter. Analogously, we can do the spherical-tensor decomposition for the two-body density operator which we are going to discuss next.

The *(transition) two-body density matrix elements* with respect to the states $|\Psi, jm\rangle$

$$\gamma^{pm_p rm_r}_{qm_q sm_s}(jm,jm') \coloneqq \langle \Psi, jm | \boldsymbol{a}^\dagger_{pm_p} \boldsymbol{a}^\dagger_{rm_r} \boldsymbol{a}_{qm_q} \boldsymbol{a}_{sm_s} | \Psi, jm' \rangle \,. \tag{C.49}$$

define the *(transition) two-body density operator*

$$\boldsymbol{\gamma}^{[2]}(jm,jm') \coloneqq \frac{1}{4} \sum_{\substack{pr \\ qs}} \sum_{\substack{m_p m_r \\ m_q m_s}} \gamma^{pm_p rm_r}_{qm_q sm_s}(jm,jm') \; \boldsymbol{a}^{pm_p rm_r}_{qm_q sm_s} \tag{C.50}$$

$$= \frac{1}{4} \sum_{\substack{pr \\ qs}} \sum_{\substack{m_p m_r \\ m_q m_s}} \langle \Psi, jm | \boldsymbol{a}^\dagger_{pm_p} \boldsymbol{a}^\dagger_{rm_r} \boldsymbol{a}_{sm_s} \boldsymbol{a}_{qm_q} | \Psi, jm' \rangle \; \boldsymbol{a}^\dagger_{pm_p} \boldsymbol{a}^\dagger_{rm_r} \boldsymbol{a}_{sm_s} \boldsymbol{a}_{qm_q} \tag{C.51}$$

$$= \frac{1}{4} \sum_{\substack{pr \\ qs}} \sum_{KQ} \sum_{J_1 J_2} \langle \Psi, jm | [[\boldsymbol{a}^\dagger_p \otimes \boldsymbol{a}^\dagger_r]_{J_1} \otimes [\overline{\boldsymbol{a}}^\dagger_s \otimes \overline{\boldsymbol{a}}^\dagger_q]_{J_2}]_{KQ} | \Psi, jm' \rangle$$
$$\times [[\boldsymbol{a}^\dagger_p \otimes \boldsymbol{a}^\dagger_r]_{J_1} \otimes [\overline{\boldsymbol{a}}^\dagger_s \otimes \overline{\boldsymbol{a}}^\dagger_q]_{J_2}]_{KQ} \tag{C.52}$$

$$= \frac{1}{4} \sum_{\substack{pr \\ qs}} \sum_{KQ} \sum_{J_1 J_2} (-)^{2K+j-m'} \frac{1}{\hat{K}} \begin{pmatrix} j & j & K \\ m' & -m & -Q \end{pmatrix}$$
$$\times (\Psi, j | [[\boldsymbol{a}^\dagger_p \otimes \boldsymbol{a}^\dagger_r]_{J_1} \otimes [\overline{\boldsymbol{a}}^\dagger_s \otimes \overline{\boldsymbol{a}}^\dagger_q]_{J_2}]_K | \Psi, j)$$
$$\times [[\boldsymbol{a}^\dagger_p \otimes \boldsymbol{a}^\dagger_r]_{J_1} \otimes [\overline{\boldsymbol{a}}^\dagger_s \otimes \overline{\boldsymbol{a}}^\dagger_q]_{J_2}]_{KQ}. \tag{C.53}$$

This motivates the following definition of the *spherical two-body density operator*

$$\boldsymbol{\gamma}^{[2]}_{KQ}(j) \coloneqq \frac{1}{\hat{j}^2} \sum_{mm'} (-)^{2K+j-m'} \begin{pmatrix} j & j & K \\ m' & -m & -Q \end{pmatrix} \boldsymbol{\gamma}^{[2]}(jm,jm') \tag{C.54}$$

which is indeed a spherical tensor operator of rank K.

Likewise, we can generalize this definition to the *spherical n-body density operator*

$$\boldsymbol{\gamma}^{[n]}_{KQ}(j) \coloneqq \frac{1}{\hat{j}^2} \sum_{mm'} (-)^{2K+j-m'} \begin{pmatrix} j & j & K \\ m' & -m & -Q \end{pmatrix} \boldsymbol{\gamma}^{[n]}(jm,jm'). \tag{C.55}$$

Here, we defined the *n-body density operator*

$$\boldsymbol{\gamma}^{[n]}(jm, jm') \coloneqq \frac{1}{(n!)^2} \sum_{\substack{p_1 \dots p_n \\ q_1 \dots q_n}} \sum_{\substack{m_{p_1} \dots m_{p_n} \\ m_{q_1} \dots m_{q_n}}} \gamma^{p_1 m_{p_1} \dots p_n m_{p_n}}_{q_1 m_{q_1} \dots q_n m_{q_n}}(jm, jm') \; \boldsymbol{a}^{p_1 m_{p_1} \dots p_n m_{p_n}}_{q_1 m_{q_1} \dots q_n m_{q_n}} \tag{C.56}$$

with the *n-body density matrix elements* of the state $|\Psi, jm\rangle$

$$\gamma^{p_1 m_{p_1} \dots p_n m_{p_n}}_{q_1 m_{q_1} \dots q_n m_{q_n}}(jm, jm') \coloneqq \langle \Psi, jm | \boldsymbol{a}^\dagger_{p_1 m_{p_1}} \dots \boldsymbol{a}^\dagger_{p_n m_{p_n}} \boldsymbol{a}_{q_n m_{q_n}} \dots \boldsymbol{a}_{q_1 m_{q_1}} | \Psi, jm' \rangle \,. \tag{C.57}$$

Glossary

Notations

$\boldsymbol{x}$	generic operator
$\vec{x}$	generic vector
$\vec{\boldsymbol{x}}$	generic vector operator
$\underline{\underline{X}}$	generic matrix
$\|0\rangle$	physical vacuum
$\|\Phi\rangle$	single-reference state
$\|\Psi\rangle$	multi-reference state
$\boldsymbol{\mathcal{N}}_{\|0\rangle}$	normal-ordering operator with respect to $\|0\rangle$
$\boldsymbol{\mathcal{N}}_{\|\Phi\rangle}$	normal-ordering operator with respect to $\|\Phi\rangle$
$\boldsymbol{\mathcal{N}}$	normal-ordering operator with respect to $\|\Psi\rangle$
$\gamma^{p_1 p_2 \ldots p_n}_{q_1 q_2 \ldots q_n}$	n-particle density matrix element
$\bar{\gamma}^{p_1 p_2 \ldots p_n}_{q_1 q_2 \ldots q_n}$	n-hole density matrix element
$\lambda^{p_1 p_2 \ldots p_n}_{q_1 q_2 \ldots q_n}$	irreducible n-body density matrix element
$\boldsymbol{a}^p$	creation operator
$\boldsymbol{a}_q$	annihilation operator
$\boldsymbol{a}^{pr\ldots}_{qs\ldots}$	vacuum normal-ordered operator
$\tilde{\boldsymbol{a}}^{pr\ldots}_{qs\ldots}$	reference-state normal-ordered operator
$[\boldsymbol{A}, \boldsymbol{B}]$	commutator of $\boldsymbol{A}$ and $\boldsymbol{B}$
$\{\boldsymbol{A}, \boldsymbol{B}\}$	anticommutator of $\boldsymbol{A}$ and $\boldsymbol{B}$
$\left(\begin{matrix} j_1 & j_2 \\ m_1 & m_2 \end{matrix}\middle\| \begin{matrix} J \\ M \end{matrix}\right)$	Clebsch-Gordan coefficient
$\begin{pmatrix} j_1 & j_2 & J \\ m_1 & m_2 & M \end{pmatrix}$	Wigner 3j-symbol
$\begin{Bmatrix} j_1 & j_2 & j_3 \\ j_4 & j_5 & j_6 \end{Bmatrix}$	Wigner 6j-symbol

Acronyms

QCD	quantum chromodynamics
NN	nucleon nucleon
3N	three nucleon
HF	Hartree Fock
HO	harmonic oscillator
CM	center of mass
CC	coupled cluster
SRG	similarity renormalization group
NCSM	no-core shell model
IM-SRG	(multi-reference) in-medium similarity renormalization group
IM-NCSM	in-medium no-core shell model
pp-IM-NCSM	particle-attached particle-removed IM-NCSM
V-NO	vacuum normal ordered
SR-NO	single-reference normal ordered
MR-NO	multi-reference normal ordered
MR-NO2B	multi-reference normal-ordered two-body
ODE	ordinary differential equation
RKF	Runge Kutta Fehlberg
BLAS	Basic Linear Algebra Subprograms
LENPIC	Low Energy Nuclear Physics International Collaboration
N^2LO_{sat}	next-to-next-to-leading order saturated

List of Figures

4.1. Classification of the single-particle states based on a general reference state . 68
4.2. The n-particle excitations span the subspace orthogonal to the reference state 71
4.3. All non-vanishing generalized one-particle one-hole states 74
4.4. All non-vanishing generalized two-particle two-hole states 76
4.5. Classification of the single-particle basis based on a specific reference state . . 78
4.6. Schematic depiction of the decoupling pattern for the ground state 82
4.7. Schematic picture of the manifold of unitarily equivalent Hamiltonians 83

5.1. The no-core shell-model configurations 101

6.1. Schematic overview of the merging procedure for the IM-NCSM 107
6.2. Many-body basis containing up to four excitation quanta 108
6.3. Initial Hamiltonian represented in two different many-body bases 109
6.4. Analysis of the reference state for ^{12}C 110
6.5. Characteristics of the flowing Hamiltonian 111
6.6. Zoom into the $N_{\max} = 0$ block of the evolved Hamiltonian 112
6.7. Comparison of the two specific many-body bases 113

7.1. Flow of ground-state energy in ^{12}C and ^{20}O, and comparison to NCSM . . . 122
7.2. $N_{\max}$-convergence of the ground-state energy in ^{12}C and ^{20}O 123
7.3. $e_{\max}$-dependence of the ground-state energy for ^{12}C and ^{20}O 125
7.4. $\hbar\Omega$-dependence of the IM-NCSM ground-state energy in ^{12}C 127
7.5. Impact of the generators on the ground-state energy in ^{12}C 132
7.6. Numerical quantities during the IM-SRG evolution for various generators . . 133
7.7. Impact of the generators on the ground-state energy in ^{20}O 134
7.8. Dependence of the ground-state energy on the reference-space size 136
7.9. IM-NCSM ground-state energies in comparison to other methods 137
7.10. Flow of ground-state energy in some selected magnesium isotopes 139
7.11. Flow of ground-state energy in some selected sodium isotopes 140

8.1. IM-SRG evolution of low-lying excitation energies in ^{12}C and ^{20}O 143
8.2. IM-NCSM excitation spectra in comparison with NCSM and experiment. . . 144
8.3. Center-of-mass contamination of the second 0^+ in ^{12}C 147

8.4. Generators' impact on the excitation energy of the 0_2^+ state in ^{12}C 149
8.5. Generators' impact on absolute energy and $\langle \boldsymbol{H}_{\mathrm{cm}} \rangle$ of the 0_2^+ state in ^{12}C . . . 150
8.6. Dependence of the absolute energy of the second 0^+ state in ^{12}C on $N_{\mathrm{max}}^{\mathrm{ref}}$ . . 151
8.7. Island-of-inversion region on the nuclear chart 153
8.8. Number of publications between 1970 and 2010 on island of inversion 153
8.9. Excitation energies of low-lying states in magnesium isotopes 155
8.10. Excitation energies of low-lying states in sodium isotopes 157

9.1. IM-NCSM radii and electric-monopole property of the second 0^+ in ^{12}C . . . 161

10.1. Strategy of the particle-attached particle-removed IM-NCSM 164
10.2. Schematic overview on how to tackle even nitrogen isotopes 165
10.3. Ground-state energies of ^{16,18,20}N obtained in pp-IM-NCSM 167
10.4. Excitation energies of ^{16,18,20}N obtained in pp-IM-NCSM 169

Bibliography

[Ajz90] F. Ajzenberg-Selove. "Energy levels of light nuclei $A = 11 - 12$". In: *Nuclear Physics A* 506.1 (1990), pp. 1–158. ISSN: 0375-9474. DOI: 10.1016/0375-9474(90)90271-M (cit. on p. 159).

[Ber+12] J. Beringer, J. F. Arguin, R. M. Barnett, et al. "Review of Particle Physics". In: *Phys. Rev. D* 86 (2012), p. 010001. DOI: 10.1103/PhysRevD.86.010001 (cit. on p. 94).

[BFP07] S. K. Bogner, R. J. Furnstahl, and R. J. Perry. "Similarity renormalization group for nucleon-nucleon interactions". In: *Phys. Rev. C* 75 (2007), p. 061001. DOI: 10.1103/PhysRevC.75.061001 (cit. on pp. 8, 119).

[Bin+13] S. Binder, J. Langhammer, A. Calci, et al. "*Ab initio* calculations of medium-mass nuclei with explicit chiral $3N$ interactions". In: *Phys. Rev. C* 87 (2013), p. 021303. DOI: 10.1103/PhysRevC.87.021303 (cit. on pp. 2, 119, 126).

[Bin+14] S. Binder, J. Langhammer, A. Calci, et al. "Ab initio path to heavy nuclei ". In: *Physics Letters B* 736 (2014), pp. 119–123. ISSN: 0370-2693. DOI: 10.1016/j.physletb.2014.07.010 (cit. on pp. 2, 119, 138).

[Bin+16] S. Binder, A. Calci, E. Epelbaum, et al. "Few-nucleon systems with state-of-the-art chiral nucleon-nucleon forces". In: *Phys. Rev. C* 93 (2016), p. 044002. DOI: 10.1103/PhysRevC.93.044002 (cit. on p. 174).

[Bla+09] S. Blanes, F. Casas, J. Oteo, et al. "The Magnus expansion and some of its applications". In: *Physics Reports* 470.5–6 (2009), pp. 151–238. ISSN: 0370-1573. DOI: https://doi.org/10.1016/j.physrep.2008.11.001 (cit. on p. 92).

[BLA17] BLAS. *Basic Linear Algebra Subprograms*. 2017. URL: http://www.netlib.org/blas/ (cit. on pp. 47, 56).

[BNV13] B. R. Barrett, P. Navrátil, and J. P. Vary. "Ab initio no core shell model". In: *Progress in Particle and Nuclear Physics* 69 (2013), pp. 131–181. ISSN: 0146-6410. DOI: /10.1016/j.ppnp.2012.10.003 (cit. on pp. 2, 35, 99).

[Bog+14] S. K. Bogner, H. Hergert, J. D. Holt, et al. "Nonperturbative Shell-Model Interactions from the In-Medium Similarity Renormalization Group". In: *Phys. Rev. Lett.* 113 (2014), p. 142501. DOI: 10.1103/PhysRevLett.113.142501 (cit. on pp. 2, 35).

[Bro01] B. Brown. "The nuclear shell model towards the drip lines". In: *Progress in Particle and Nuclear Physics* 47.2 (2001), pp. 517–599. ISSN: 0146-6410. DOI: /10.1016/S0146-6410(01)00159-4 (cit. on pp. 2, 35).

[Bro10] B. A. Brown. "Viewpoint: Islands of insight in the nuclear chart". In: *Physics 3* 104 (2010). URL: https://physics.aps.org/articles/v3/104 (cit. on p. 153).

[Bur+57] E. M. Burbidge, G. R. Burbidge, W. A. Fowler, et al. "Synthesis of the Elements in Stars". In: *Rev. Mod. Phys.* 29 (1957), pp. 547–650. DOI: 10.1103/RevModPhys.29.547 (cit. on pp. 141, 142).

[Cau+05] E. Caurier, G. Martínez-Pinedo, F. Nowacki, et al. "The shell model as a unified view of nuclear structure". In: *Rev. Mod. Phys.* 77 (2005), pp. 427–488. DOI: 10.1103/RevModPhys.77.427 (cit. on pp. 2, 35).

[CC08] R. B. Cakirli and R. F. Casten. "Empirical signature for shape transitions mediated by sub-shell changes". In: *Phys. Rev. C* 78 (2008), p. 041301. DOI: 10.1103/PhysRevC.78.041301 (cit. on p. 154).

[Che+07] M. Chernykh, H. Feldmeier, T. Neff, et al. "Structure of the Hoyle State in ^{12}C". In: *Phys. Rev. Lett.* 98 (2007), p. 032501. DOI: 10.1103/PhysRevLett.98.032501 (cit. on pp. 142, 159).

[CMV12] M. A. Caprio, P. Maris, and J. P. Vary. "The no-core shell model with general radial bases". In: *Journal of Physics: Conference Series* 403.1 (2012), p. 012014. URL: http://stacks.iop.org/1742-6596/403/i=1/a=012014 (cit. on p. 100).

[Coe58] F. Coester. "Bound states of a many-particle system". In: *Nuclear Physics* 7 (1958), pp. 421–424. ISSN: 0029-5582. DOI: doi:10.1016/0029-5582(58)90280-3 (cit. on p. 2).

[Con30] E. U. Condon. "The Theory of Complex Spectra". In: *Phys. Rev.* 36 (1930), pp. 1121–1133. DOI: 10.1103/PhysRev.36.1121 (cit. on p. 27).

[Dan+09] A. N. Danilov, T. L. Belyaeva, A. S. Demyanova, et al. "Determination of nuclear radii for unstable states in ^{12}C with diffraction inelastic scattering". In: *Phys. Rev. C* 80 (2009), p. 054603. DOI: 10.1103/PhysRevC.80.054603 (cit. on p. 159).

[EHM09] E. Epelbaum, H.-W. Hammer, and U.-G. Meißner. "Modern theory of nuclear forces". In: *Rev. Mod. Phys.* 81 (2009), pp. 1773–1825. DOI: 10.1103/RevModPhys.81.1773 (cit. on p. 1).

[Eks+15] A. Ekström, G. R. Jansen, K. A. Wendt, et al. "Accurate nuclear radii and binding energies from a chiral interaction". In: *Phys. Rev. C* 91 (2015), p. 051301. DOI: 10.1103/PhysRevC.91.051301 (cit. on pp. 119, 174).

[EM03] D. R. Entem and R. Machleidt. "Accurate charge-dependent nucleon-nucleon potential at fourth order of chiral perturbation theory". In: *Phys. Rev. C* 68 (2003), p. 041001. DOI: 10.1103/PhysRevC.68.041001 (cit. on p. 119).

[Epe+11] E. Epelbaum, H. Krebs, D. Lee, et al. “Ab Initio Calculation of the Hoyle State”. In: *Phys. Rev. Lett.* 106 (2011), p. 192501. DOI: 10.1103/PhysRevLett.106.192501 (cit. on p. 142).

[Epe+12] E. Epelbaum, H. Krebs, T. A. Lähde, et al. “Structure and Rotations of the Hoyle State”. In: *Phys. Rev. Lett.* 109 (2012), p. 252501. DOI: 10.1103/PhysRevLett.109.252501 (cit. on pp. 142, 159).

[Fey39] R. P. Feynman. “Forces in Molecules”. In: *Phys. Rev.* 56 (1939), pp. 340–343. DOI: 10.1103/PhysRev.56.340 (cit. on p. 128).

[GCR16] E. Gebrerufael, A. Calci, and R. Roth. “Open-shell nuclei and excited states from multireference normal-ordered Hamiltonians”. In: *Phys. Rev. C* 93 (2016), p. 031301. DOI: 10.1103/PhysRevC.93.031301 (cit. on pp. 2, 28, 38, 121, 165).

[Geb+17] E. Gebrerufael, K. Vobig, H. Hergert, et al. “*Ab Initio* Description of Open-Shell Nuclei: Merging No-Core Shell Model and In-Medium Similarity Renormalization Group”. In: *Phys. Rev. Lett.* 118 (2017), p. 152503. DOI: 10.1103/PhysRevLett.118.152503 (cit. on pp. 122, 137, 143, 144).

[Geb13] E. Gebrerufael. “Multi-Reference Normal Ordering for 3N Interactions”. Master’s thesis. Technische Universität Darmstadt, 2013. URL: http://crunch.ikp.physik.tu-darmstadt.de/tnp/pub/2013_gebrerufael_master.pdf (cit. on p. 24).

[GL74] D. H. Gloeckner and R. D. Lawson. “Spurious center-of-mass motion”. In: *Physics Letters B* 53.4 (1974), pp. 313–318. ISSN: 0370-2693. DOI: /10.1016/0370-2693(74)90390-6 (cit. on p. 141).

[Gla61] S. L. Glashow. “Partial Symmetries of Weak Interactions”. In: *Nucl. Phys.* 22 (1961), pp. 579–588. DOI: 10.1016/0029-5582(61)90469-2 (cit. on p. 1).

[Gou09] B. Gough. *GNU Scientific Library Reference Manual - Third Edition*. 3rd. Network Theory Ltd., 2009. ISBN: 0954612078, 9780954612078. URL: http://dl.acm.org/citation.cfm?id=1538674 (cit. on p. 128).

[GSL17] GSL. *GNU Scientific Library*. 2017. URL: https://www.gnu.org/software/gsl/ (cit. on p. 128).

[Hag+07] G. Hagen, T. Papenbrock, D. J. Dean, et al. “Coupled-cluster theory for three-body Hamiltonians”. In: *Phys. Rev. C* 76 (2007), p. 034302. DOI: 10.1103/PhysRevC.76.034302 (cit. on p. 2).

[Hag+08] G. Hagen, T. Papenbrock, D. J. Dean, et al. “Medium-Mass Nuclei from Chiral Nucleon-Nucleon Interactions”. In: *Phys. Rev. Lett.* 101 (2008), p. 092502. DOI: 10.1103/PhysRevLett.101.092502 (cit. on p. 2).

[Heb12] K. Hebeler. “Momentum-space evolution of chiral three-nucleon forces”. In: *Phys. Rev. C* 85 (2012), p. 021002. DOI: 10.1103/PhysRevC.85.021002 (cit. on p. 119).

[Her+13a] H. Hergert, S. Binder, A. Calci, et al. "*Ab Initio* Calculations of Even Oxygen Isotopes with Chiral Two-Plus-Three-Nucleon Interactions". In: *Phys. Rev. Lett.* 110 (2013), p. 242501. DOI: 10.1103/PhysRevLett.110.242501 (cit. on pp. 119, 121, 137).

[Her+13b] H. Hergert, S. K. Bogner, S. Binder, et al. "In-medium similarity renormalization group with chiral two- plus three-nucleon interactions". In: *Phys. Rev. C* 87 (2013), p. 034307. DOI: 10.1103/PhysRevC.87.034307 (cit. on p. 119).

[Her+16] H. Hergert, S. Bogner, T. Morris, et al. "The In-Medium Similarity Renormalization Group: A novel ab initio method for nuclei". In: *Physics Reports* 621 (2016). Memorial Volume in Honor of Gerald E. Brown, pp. 165–222. ISSN: 0370-1573. DOI: /10.1016/j.physrep.2015.12.007 (cit. on pp. 2, 37, 47, 83, 84, 86, 126, 131).

[Her16] H. Hergert. personal communication. 2016 (cit. on p. 42).

[Her17] H. Hergert. "In-medium similarity renormalization group for closed and open-shell nuclei". In: *Physica Scripta* 92.2 (2017), p. 023002. DOI: 10.1088/1402-4896/92/2/023002 (cit. on pp. 2, 37, 47, 90).

[Hof+08] C. R. Hoffman, T. Baumann, D. Bazin, et al. "Determination of the $N = 16$ Shell Closure at the Oxygen Drip Line". In: *Phys. Rev. Lett.* 100 (2008), p. 152502. DOI: 10.1103/PhysRevLett.100.152502 (cit. on p. 152).

[Jan+11] G. R. Jansen, M. Hjorth-Jensen, G. Hagen, et al. "Toward open-shell nuclei with coupled-cluster theory". In: *Phys. Rev. C* 83 (2011), p. 054306. DOI: 10.1103/PhysRevC.83.054306 (cit. on p. 164).

[Jan+14] G. R. Jansen, J. Engel, G. Hagen, et al. "*Ab Initio* Coupled-Cluster Effective Interactions for the Shell Model: Application to Neutron-Rich Oxygen and Carbon Isotopes". In: *Phys. Rev. Lett.* 113 (2014), p. 142502. DOI: 10.1103/PhysRevLett.113.142502 (cit. on pp. 2, 35).

[Jan+16] G. R. Jansen, M. D. Schuster, A. Signoracci, et al. "Open *sd*-shell nuclei from first principles". In: *Phys. Rev. C* 94 (2016), p. 011301. DOI: 10.1103/PhysRevC.94.011301 (cit. on pp. 2, 35).

[JNF09] E. D. Jurgenson, P. Navrátil, and R. J. Furnstahl. "Evolution of Nuclear Many-Body Forces with the Similarity Renormalization Group". In: *Phys. Rev. Lett.* 103 (2009), p. 082501. DOI: 10.1103/PhysRevLett.103.082501 (cit. on pp. 103, 119).

[JNF11] E. D. Jurgenson, P. Navrátil, and R. J. Furnstahl. "Evolving nuclear many-body forces with the similarity renormalization group". In: *Phys. Rev. C* 83 (2011), p. 034301. DOI: 10.1103/PhysRevC.83.034301 (cit. on p. 103).

[KAE17] KAERI. *Nuclear Data Center at KAERI*. 2017. URL: http://atom.kaeri.re.kr/ (cit. on p. 137).

[Kam97] G. P. Kamuntavičius. “Root-mean-square radii of light atomic nuclei: Neutron skin”. In: *Phys. Rev. C* 56 (1997), pp. 191–198. DOI: 10.1103/PhysRevC.56.191 (cit. on p. 94).

[Kan+09] R. Kanungo, C. Nociforo, A. Prochazka, et al. “One-Neutron Removal Measurement Reveals ^{24}**O** as a New Doubly Magic Nucleus”. In: *Phys. Rev. Lett.* 102 (2009), p. 152501. DOI: 10.1103/PhysRevLett.102.152501 (cit. on p. 152).

[KM02] W. Kutzelnigg and D. Mukherjee. “Irreducible Brillouin conditions and contracted Schrödinger equations for n-electron systems. II. Spin-free formulation”. In: *The Journal of Chemical Physics* 116.12 (2002), pp. 4787–4801. DOI: 10.1063/1.1448827 (cit. on p. 86).

[KM04] W. Kutzelnigg and D. Mukherjee. “Irreducible Brillouin conditions and contracted Schrödinger equations for n-electron systems. IV. Perturbative analysis”. In: *The Journal of Chemical Physics* 120.16 (2004), pp. 7350–7368. DOI: 10.1063/1.1652490 (cit. on p. 86).

[KM97] W. Kutzelnigg and D. Mukherjee. “Normal order and extended Wick theorem for a multiconfiguration reference wave function”. In: *The Journal of Chemical Physics* 107.2 (1997), pp. 432–449. DOI: 10.1063/1.474405 (cit. on pp. 22, 29).

[KNM10] L. Kong, M. Nooijen, and D. Mukherjee. “An algebraic proof of generalized Wick theorem”. In: *The Journal of Chemical Physics* 132.23, 234107 (2010), p. 234107. DOI: 10.1063/1.3439395 (cit. on pp. 24, 29).

[Lan50] C. Lanczos. “An iteration method for the solution of the eigenvalue problem of linear differential and integral operators”. In: *J. Res. Natl. Bur. Stand.* 45 (1950), p. 255. ISSN: 0091-0635. DOI: 10.6028/jres.045.026 (cit. on p. 102).

[Lap+16] V. Lapoux, V. Somà, C. Barbieri, et al. “Radii and Binding Energies in Oxygen Isotopes: A Challenge for Nuclear Forces”. In: *Phys. Rev. Lett.* 117 (2016), p. 052501. DOI: 10.1103/PhysRevLett.117.052501 (cit. on p. 119).

[Mar+14] P. Maris, J. P. Vary, A. Calci, et al. “^{12}C properties with evolved chiral three-nucleon interactions”. In: *Phys. Rev. C* 90 (2014), p. 014314. DOI: 10.1103/PhysRevC.90.014314 (cit. on pp. 142, 145).

[ME11] R. Machleidt and D. R. Entem. “Chiral effective field theory and nuclear forces”. In: *Physics Reports* 503.1 (2011), pp. 1–75. ISSN: 0370-1573. DOI: http://dx.doi.org/10.1016/j.physrep.2011.02.001 (cit. on p. 1).

[MK01] D. Mukherjee and W. Kutzelnigg. “Irreducible Brillouin conditions and contracted Schrödinger equations for n-electron systems. I. The equations satisfied by the density cumulants”. In: *The Journal of Chemical Physics* 114.5 (2001), pp. 2047–2061. DOI: 10.1063/1.1337058 (cit. on p. 86).

[MPB15] T. D. Morris, N. M. Parzuchowski, and S. K. Bogner. “Magnus expansion and in-medium similarity renormalization group”. In: *Phys. Rev. C* 92 (2015), p. 034331. DOI: 10.1103/PhysRevC.92.034331 (cit. on p. 92).

[Muk97] D. Mukherjee. “Normal ordering and a Wick-like reduction theorem for fermions with respect to a multi-determinantal reference state”. In: *Chemical Physics Letters* 274.5 (1997), pp. 561–566. ISSN: 0009-2614. DOI: 10.1016/S0009-2614(97)00714-8 (cit. on p. 22).

[Nav+07] P. Navrátil, V. G. Gueorguiev, J. P. Vary, et al. “Structure of $A = 10 - 13$ Nuclei with Two- Plus Three-Nucleon Interactions from Chiral Effective Field Theory”. In: *Phys. Rev. Lett.* 99 (2007), p. 042501. DOI: 10.1103/PhysRevLett.99.042501 (cit. on pp. 2, 35).

[Nav+09] P. Navrátil, S. Quaglioni, I. Stetcu, et al. “Recent developments in no-core shell-model calculations”. In: *Journal of Physics G: Nuclear and Particle Physics* 36.8 (2009), p. 083101. URL: http://stacks.iop.org/0954-3899/36/i=8/a=083101 (cit. on p. 99).

[Nav07] P. Navrátil. “Local three-nucleon interaction from chiral effective field theory”. In: *Few-Body Systems* 41.3 (2007), pp. 117–140. ISSN: 1432-5411. DOI: 10.1007/s00601-007-0193-3 (cit. on p. 119).

[Nef12] T. Neff. “Clusters and halos in light nuclei”. In: *Journal of Physics: Conference Series* 403.1 (2012), p. 012028. URL: http://stacks.iop.org/1742-6596/403/i=1/a=012028 (cit. on p. 142).

[NKB00] P. Navrátil, G. P. Kamuntavi čius, and B. R. Barrett. “Few-nucleon systems in a translationally invariant harmonic oscillator basis”. In: *Phys. Rev. C* 61 (2000), p. 044001. DOI: 10.1103/PhysRevC.61.044001 (cit. on p. 145).

[NND17] NNDC. *National Nuclear Data Center*. 2017. URL: http://www.nndc.bnl.gov/ensdf (cit. on pp. 144, 168).

[Ôku54] S. Ôkubo. “Diagonalization of Hamiltonian and Tamm-Dancoff Equation”. In: *Progress of Theoretical Physics* 12.5 (1954), pp. 603–622. DOI: 10.1143/PTP.12.603 (cit. on p. 103).

[Par+17] N. M. Parzuchowski, S. R. Stroberg, P. Navratil, et al. “Ab initio electromagnetic observables with the in-medium similarity renormalization group”. In: (2017). arXiv: 1705.05511 [nucl-th] (cit. on p. 164).

[PGW09] P. Piecuch, J. R. Gour, and M. Włoch. “Left-eigenstate completely renormalized equation-of-motion coupled-cluster methods: Review of key concepts, extension to excited states of open-shell systems, and comparison with electron-attached and ionized approaches”. In: *International Journal of Quantum Chemistry* 109.14 (2009), pp. 3268–3304. ISSN: 1097-461X. DOI: 10.1002/qua.22367 (cit. on p. 164).

[PMB17] N. M. Parzuchowski, T. D. Morris, and S. K. Bogner. "Ab initio excited states from the in-medium similarity renormalization group". In: *Phys. Rev. C* 95 (2017), p. 044304. DOI: 10.1103/PhysRevC.95.044304 (cit. on p. 164).

[PS95] M. E. Peskin and D. V. Schroeder. *An Introduction To Quantum Field Theory*. Westview Press, 1995. ISBN: 9780201503975. URL: https://westviewpress.com/books/an-introduction-to-quantum-field-theory/ (cit. on p. 1).

[Ram99] P. Ramond. *Journeys beyond the standard model*. Cambridge, Mass., 1999. ISBN: 0738201162. URL: https://catalog.hathitrust.org/Record/009390984 (cit. on p. 1).

[RGP09] R. Roth, J. R. Gour, and P. Piecuch. "Center-of-mass problem in truncated configuration interaction and coupled-cluster calculations". In: *Physics Letters B* 679.4 (2009), pp. 334–339. ISSN: 0370-2693. DOI: 10.1016/j.physletb.2009.07.071 (cit. on pp. 102, 128, 145, 146).

[RN07] R. Roth and P. Navrátil. "*Ab Initio* Study of ^{40}Ca with an Importance-Truncated No-Core Shell Model". In: *Phys. Rev. Lett.* 99 (2007), p. 092501. DOI: 10.1103/PhysRevLett.99.092501 (cit. on p. 103).

[Rot+11] R. Roth, J. Langhammer, A. Calci, et al. "Similarity-Transformed Chiral $NN+3N$ Interactions for the *Ab Initio* Description of ^{12}**C** and ^{16}**O**". In: *Phys. Rev. Lett.* 107 (2011), p. 072501. DOI: 10.1103/PhysRevLett.107.072501 (cit. on pp. 9, 103, 119).

[Rot+12] R. Roth, S. Binder, K. Vobig, et al. "Medium-Mass Nuclei with Normal-Ordered Chiral NN+3N Interactions". In: *Phys. Rev. Lett.* 109 (2012), p. 052501. DOI: 10.1103/PhysRevLett.109.052501 (cit. on pp. 28, 38, 119, 121).

[Rot+14] R. Roth, A. Calci, J. Langhammer, et al. "Evolved chiral $NN+3N$ Hamiltonians for *ab initio* nuclear structure calculations". In: *Phys. Rev. C* 90 (2014), p. 024325. DOI: 10.1103/PhysRevC.90.024325 (cit. on pp. 103, 119).

[Rot09] R. Roth. "Importance truncation for large-scale configuration interaction approaches". In: *Phys. Rev. C* 79 (2009), p. 064324. DOI: 10.1103/PhysRevC.79.064324 (cit. on pp. 102–104, 126).

[RS80] P. Ring and P. Schuck. *The Nuclear Many-Body Problem*. Springer, 1980. ISBN: 978-3-540-21206-5. URL: http://www.springer.com/us/book/9783540212065 (cit. on pp. 12, 94, 95).

[Sch11] H. Scheit. "Spectroscopy in and around the Island of Inversion". In: *Journal of Physics: Conference Series* 312.9 (2011), p. 092010. URL: http://stacks.iop.org/1742-6596/312/i=9/a=092010 (cit. on pp. 152, 153).

[SL80] K. Suzuki and S. Y. Lee. "Convergent Theory for Effective Interaction in Nuclei". In: *Progress of Theoretical Physics* 64.6 (1980), pp. 2091–2106. DOI: 10.1143/PTP.64.2091 (cit. on p. 103).

[Sla29] J. C. Slater. "The Theory of Complex Spectra". In: *Phys. Rev.* 34 (1929), pp. 1293–1322. DOI: 10.1103/PhysRev.34.1293 (cit. on p. 27).

[SN69] T. Sebe and J. Nachamkin. "Variational buildup of nuclear shell model bases". In: *Annals of Physics* 51.1 (1969), pp. 100–123. ISSN: 0003-4916. DOI: 10.1016/0003-4916(69)90348-0 (cit. on p. 102).

[SO96] A. Szabo and N. S. Ostlund. *Modern Quantum Chemistry: Introduction to Advanced Electronic Structure Theory*. Dover Publications, 1996. ISBN: 0-486-69186-1. URL: http://store.doverpublications.com/0486691861.html (cit. on p. 12).

[Ste+13] D. Steppenbeck et al. "Evidence for a new nuclear 'magic number' from the level structure of 54Ca". In: *Nature* 502.7470 (2013), pp. 207–210. DOI: 10.1038/nature12522 (cit. on p. 152).

[Str+16] S. R. Stroberg, H. Hergert, J. D. Holt, et al. "Ground and excited states of doubly open-shell nuclei from *ab initio* valence-space Hamiltonians". In: *Phys. Rev. C* 93 (2016), p. 051301. DOI: 10.1103/PhysRevC.93.051301 (cit. on pp. 2, 35, 107).

[Str+17] S. R. Stroberg, A. Calci, H. Hergert, et al. "Nucleus-Dependent Valence-Space Approach to Nuclear Structure". In: *Phys. Rev. Lett.* 118 (2017), p. 032502. DOI: 10.1103/PhysRevLett.118.032502 (cit. on pp. 2, 35, 107, 137).

[Suh07] J. Suhonen. *From Nucleons to Nucleus*. Springer, 2007. ISBN: 978-3-540-48859-0. DOI: 10.1007/978-3-540-48861-3 (cit. on p. 12).

[TBS11] K. Tsukiyama, S. K. Bogner, and A. Schwenk. "In-Medium Similarity Renormalization Group For Nuclei". In: *Phys. Rev. Lett.* 106 (2011), p. 222502. DOI: 10.1103/PhysRevLett.106.222502 (cit. on pp. 2, 84).

[TBS12] K. Tsukiyama, S. K. Bogner, and A. Schwenk. "In-medium similarity renormalization group for open-shell nuclei". In: *Phys. Rev. C* 85 (2012), p. 061304. DOI: 10.1103/PhysRevC.85.061304 (cit. on p. 2).

[Var+09] J. P. Vary, P. Maris, E. Ng, et al. "Ab initio nuclear structure – the large sparse matrix eigenvalue problem". In: *Journal of Physics: Conference Series* 180 (2009), p. 012083. ISSN: 1742-6596. DOI: 10.1088/1742-6596/180/1/012083 (cit. on pp. 2, 35, 102).

[VMK88] D. A. Varshalovich, A. N. Moskalev, and V. K. Khersonskii. *Quantum Theory of Angular Momentum*. Singapore: World Scientific, 1988. ISBN: 978-9971-5-0107-5 (cit. on pp. 59, 207, 211, 227).

[Weg94] F. Wegner. "Flow-equations for Hamiltonians". In: *Annalen der Physik* 506.2 (1994), pp. 77–91. ISSN: 1521-3889. DOI: 10.1002/andp.19945060203 (cit. on pp. 8, 38, 84).

[Wei67] S. Weinberg. “A Model of Leptons”. In: *Phys. Rev. Lett.* 19 (1967), pp. 1264–1266. DOI: 10.1103/PhysRevLett.19.1264 (cit. on p. 1).

[Wen13] K. A. Wendt. “Similarity renormalization group evolution of three-nucleon forces in a hyperspherical momentum representation”. In: *Phys. Rev. C* 87 (2013), p. 061001. DOI: 10.1103/PhysRevC.87.061001 (cit. on p. 119).

[Whi02] S. R. White. “Numerical canonical transformation approach to quantum many-body problems”. In: *The Journal of Chemical Physics* 117.16 (2002), pp. 7472–7482. DOI: 10.1063/1.1508370 (cit. on p. 84).

[Whi72] R. R. Whitehead. “A numerical approach to nuclear shell-model calculations”. In: *Nuclear Physics A* 182.2 (1972), pp. 290–300. ISSN: 0375-9474. DOI: 10.1016/0375-9474(72)90278-3 (cit. on p. 102).

[Wic50] G. C. Wick. “The Evaluation of the Collision Matrix”. In: *Phys. Rev.* 80 (1950), pp. 268–272. DOI: 10.1103/PhysRev.80.268 (cit. on p. 19).

[Wim+10] K. Wimmer, T. Kröll, R. Krücken, et al. “Discovery of the Shape Coexisting 0^+ State in ^{32}Mg by a Two Neutron Transfer Reaction”. In: *Phys. Rev. Lett.* 105 (2010), p. 252501. DOI: 10.1103/PhysRevLett.105.252501 (cit. on p. 152).

[Wło+05] M. Włoch, D. J. Dean, J. R. Gour, et al. “*Ab-Initio* Coupled-Cluster Study of ^{16}O”. In: *Phys. Rev. Lett.* 94 (2005), p. 212501. DOI: 10.1103/PhysRevLett.94.212501 (cit. on p. 2).

[Zho17] S.-G. Zhou. “Structure of Exotic Nuclei: A Theoretical Review”. In: *PoS* INPC2016 (2017), p. 373. arXiv: 1703.09045 [nucl-th] (cit. on p. 152).

List of Publications and Conferences

Publications in Peer-Reviewed Journals

1. E. Gebrerufael, K. Vobig, H. Hergert, and R. Roth

   "Ab Initio Description of Open-Shell Nuclei: Merging No-Core Shell Model and In-Medium Similarity Renormalization Group"

   In: *Physical Review Letters* 118, 152503,

   DOI: 10.1103/PhysRevLett.118.152503

2. A. Tichai, E. Gebrerufael, and R. Roth

   "Open-Shell Nuclei from No-Core Shell Model with Perturbative Improvement"

   submitted to *Physical Review Letters*

   URL: https://arxiv.org/abs/1703.05664v1

3. E. Gebrerufael, A. Calci, and R. Roth

   "Open-shell nuclei and excited states from multireference normal-ordered Hamiltonians"

   In: *Physical Review C* 93, 031301

   DOI: 10.1103/PhysRevC.93.031301

Conference Presentations

1. **Invited talk**, "Ab Initio Method: In-Medium No-Core Shell Model"

   ECT* Workshop 'Walk on the neutron-rich side'
   Trento, Italy

   April 10 - 13, 2017

   https://theorie.ikp.physik.tu-darmstadt.de/tnp/pres/2017_trento_gebrerufael.pdf

2. **Invited talk**, "Ab Initio Spectroscopy of Open-Shell Nuclei: Merging In-Medium Similarity Renormalization Group and No-Core Shell Model"

   Theory Seminar, Michigan State University and FRIB/NSCL
   East Lansing, USA

   October 18, 2016

   https://theorie.ikp.physik.tu-darmstadt.de/tnp/pres/2016_msu_gebrerufael.pdf

3. "Ab Initio Spectroscopy of Open-Shell Medium-Mass Nuclei: Merging NCSM and In-Medium SRG"

   80. Annual Meeting of the Deutsche Physikalische Gesellschaft (DPG) 2016
   Darmstadt, Germany

   March 14 - 18, 2016

   https://theorie.ikp.physik.tu-darmstadt.de/tnp/pres/2016_dpg_gebrerufael.pdf

4. **Invited talk**, "Ab Initio Spectroscopy of Open-Shell Medium-Mass Nuclei: Merging NCSM and In-Medium SRG"

   TRIUMF Workshop on Progress in Ab Initio Techniques in Nuclear Physics
   Vancouver, Canada

   February 23 - 26, 2016

   https://theorie.ikp.physik.tu-darmstadt.de/tnp/pres/2016_triumf_gebrerufael.pdf

5. "Multi-Reference In-Medium SRG"

   TRIUMF Workshop on Progress in Ab Initio Techniques in Nuclear Physics
   Vancouver, Canada

   February 17 - 20, 2015

   https://theorie.ikp.physik.tu-darmstadt.de/tnp/pres/2015_triumf_gebrerufael.pdf

Danksagung

In erster Linie danke ich Gott für die großartige Familie, Freunde und Mitmenschen, die er mir geschenkt hat, und für das Privileg unbesorgt an meiner Selbstverwirklichung arbeiten zu dürfen. Das sind keine Selbstverständlichkeiten im Leben und daher ehre und lobe ich Gott. Meine Dankliste ist ziemlich lang. Falls ich Jemanden vergessen haben sollte, bitte ich um Entschuldigung.

Diese spannende und erfolgreiche Doktorarbeit habe ich zu einem großen Teil meinem Doktorvater, Prof. Robert Roth, zu verdanken. Durch zahlreiche Diskussionen und zielführende Vorschläge hat er maßgeblich zum Gelingen dieser Arbeit beigetragen. Ich bedanke mich ebenfalls für die Möglichkeiten an verschiedenen Workshops in Vancouver und Trento teilnehmen zu dürfen. Weiterhin danke ich Prof. Jens Braun für die Übernahme des Zweitgutachtens dieser Arbeit. Außerdem bedanke ich mich bei meinem Kollaborator, Prof. Heiko Hergert, für die Einladung nach East Lansing an die Michigan State University und die Mühen, mich weiterhin in der Forschung als Postdoktorand zu behalten.

Anschließend danke ich Christina Stumpf, Richard Trippel, Roland Wirth und Alexander Tichai für die angenehme Arbeitsatmosphäre im Büro, den interessanten Gesprächen und der enormen Hilfsbereitschaft. Ganz besonders möchte ich mich bei Roland bedanken, der meine Arbeit durch zahlreiche programmiertechnische Tipps und fruchtbaren Diskussionen über Physik und Mathematik vorangetrieben hat. Für das intensive Korrekturlesen danke ich Stefan Schulz, Roland, Christina, Alexander und Klaus Vobig. Ich bin stolz und glücklich ein Teil der TNP++ Arbeitsgruppe gewesen zu sein.

Ein unheimlich großer Dank geht an meine wunderbaren Eltern, Gebrerufael Teweldebrahan und Slas Tekle, für die Liebe, Geduld und Unterstützung seit meiner Geburt:

„**Emey na Abey betami eye amesegenkum. Betami effetuwekum eye.**“

Schließlich danke ich vom ganzen Herzen meiner großartigen Frau, Adjam, die während des gesamten Studiums mit Rat und Tat an meiner Seite stand. Ich bin glücklich dich zu haben.

Großer Dank geht auch an: Frau Schöninger, Steven Arons, Adonias, Betty, Hevu, Heli, Teddy, Semi, Noel, Naomi, John, Eyerus, Nardu, Samanta, Zemam, Deborah, Stefanos, Nebiat, Freweni, Yodit, Hermon, Rahwa, Noah, Habteab, Geutom, Tiblez, Baba Isaak, Mama Haregu, Mikele, Biniam, Effraim, Biniam Yared, Jörg Berner, . . . :

„Ohne euch wäre mein Leben nicht mal halb so schön!“

Lebenslauf

Zur Person

Name	**Eskendr Gebrerufael**
Geburtsdatum	**13. April 1988**
Geburtsort	**Asmara, Eritrea**
Staatsangehörigkeit	**deutsch**
Eltern	**Gebrerufael Teweldebrahan**
	Slas Tekle

Bildungsweg

1998–2007	**Allgemeine Hochschulreife**, Dreieichschule Gymnasium, Langen
2007–2011	**Bachelor of Science** in Physik, TU Darmstadt
	Gesamtnote: gut (1.86)
2011–2013	**Master of Science** in Physik, TU Darmstadt
	Gesamtnote: sehr gut (1.15)
2013–2017	**Promotion** in Physik, TU Darmstadt
	Gesamtnote: mit Auszeichnung bestanden

Erklärung zur Eigenständigkeit

Hiermit versichere ich, die vorliegende Dissertation ohne Hilfe Dritter nur mit den angegebenen Quellen und Hilfsmitteln angefertigt zu haben. Alle Stellen, die aus diesen Quellen entnommen wurden, sind als solche kenntlich gemacht worden. Diese Arbeit hat in gleicher oder ähnlicher Form noch keiner Prüfungsbehörde vorgelegen.

Ort Datum Eskendr Gebrerufael